

AD\_\_\_\_\_

Award Number: W81XWH-05-1-0330

TITLE: A Biophysical-Computational Perspective of Breast Cancer Pathogenesis and Treatment Response

PRINCIPAL INVESTIGATOR: Valerie M. Weaver Ph.D.

CONTRACTING ORGANIZATION: University of California San Francisco  
San Francisco, CA 94143-0456

REPORT DATE: March 2008

TYPE OF REPORT: Annual

PREPARED FOR: U.S. Army Medical Research and Materiel Command  
Fort Detrick, Maryland 21702-5012

DISTRIBUTION STATEMENT: Approved for Public Release;  
Distribution Unlimited

The views, opinions and/or findings contained in this report are those of the author(s) and should not be construed as an official Department of the Army position, policy or decision unless so designated by other documentation.

REPORT DOCUMENTATION PAGE				Form Approved OMB No. 0704-0188	
Public reporting burden for this collection of information is estimated to average 1 hour per response, including the time for reviewing instructions, searching existing data sources, gathering and maintaining the data needed, and completing and reviewing this collection of information. Send comments regarding this burden estimate or any other aspect of this collection of information, including suggestions for reducing this burden to Department of Defense, Washington Headquarters Services, Directorate for Information Operations and Reports (0704-0188), 1215 Jefferson Davis Highway, Suite 1204, Arlington, VA 22202-4302. Respondents should be aware that notwithstanding any other provision of law, no person shall be subject to any penalty for failing to comply with a collection of information if it does not display a currently valid OMB control number. <b>PLEASE DO NOT RETURN YOUR FORM TO THE ABOVE ADDRESS.</b>					
1. REPORT DATE (DD-MM-YYYY) 01-03-2008		2. REPORT TYPE Annual		3. DATES COVERED (From - To) 1 MAR 2007 - 29 FEB 2008	
4. TITLE AND SUBTITLE  A Biophysical-Computational Perspective of Breast Cancer Pathogenesis and Treatment Response				5a. CONTRACT NUMBER	
				5b. GRANT NUMBER W81XWH-05-1-0330	
				5c. PROGRAM ELEMENT NUMBER	
6. AUTHOR(S) Valerie M. Weaver Ph.D.  E-Mail: valeriem.weaver@gmail.com				5d. PROJECT NUMBER	
				5e. TASK NUMBER	
				5f. WORK UNIT NUMBER	
7. PERFORMING ORGANIZATION NAME(S) AND ADDRESS(ES)  University of California San Francisco San Francisco, CA 94143-0456				8. PERFORMING ORGANIZATION REPORT NUMBER	
9. SPONSORING / MONITORING AGENCY NAME(S) AND ADDRESS(ES) U.S. Army Medical Research and Materiel Command Fort Detrick, Maryland 21702-5012				10. SPONSOR/MONITOR'S ACRONYM(S)	
				11. SPONSOR/MONITOR'S REPORT NUMBER(S)	
12. DISTRIBUTION / AVAILABILITY STATEMENT Approved for Public Release; Distribution Unlimited					
13. SUPPLEMENTARY NOTES					
14. ABSTRACT The extracellular matrix (ECM) and its integrin receptors modulate breast tissue homeostasis and are altered significantly during breast tumor progression. We found that the mammary gland ECM stiffens prior to and in association with malignant transformation of the breast. We showed that ECM stiffening is mediated by elevated collagen deposition, cross-linking and linearization. We determined that collagen stiffening via cross linking in culture and in vivo promotes breast tumor invasion and can modulate mammary epithelial cell survival and therapy responsiveness. ECM stiffness modulates breast cell behavior by altering integrin-dependent signaling through ERK, PI3kinase and JNK and by regulating the levels and activity of the tumor suppressor PTEN. We identified lysyl oxidase as a key regulator of ECM cross linking and matrix stiffening in the malignant breast and found that inhibiting lysyl oxidase activity substantially inhibited tumor progression in vivo. More recently we were able to successfully build a computational model of the integrin-ECM-cell membrane/cytoskeletal interface and by so doing identified a novel molecular regulator of integrin signaling whose significance we are now exploring. Finally, and most importantly the clinical relevance of our findings is now being explored.					
15. SUBJECT TERMS Extracellular matrix, stiffness, mechanical, force, apoptosis, resistance Bioengineering, invasion, computational, tumor progression					
16. SECURITY CLASSIFICATION OF:			17. LIMITATION OF ABSTRACT	18. NUMBER OF PAGES	19a. NAME OF RESPONSIBLE PERSON
a. REPORT	b. ABSTRACT	c. THIS PAGE			USAMRMC
U	U	U	UU	402	19b. TELEPHONE NUMBER (include area code)

---

## Table of Contents

<b>Introduction.....</b>	<b>4</b>
<b>Body.....</b>	<b>5-16</b>
<b>Key Research Accomplishments.....</b>	<b>5-16</b>
<b>Reportable Outcomes.....</b>	<b>16-21</b>
<b>Conclusions.....</b>	<b>21-22</b>
<b>References.....</b>	<b>23-24</b>
<b>Appendices.....</b>	<b>25-403</b>

**INTRODUCTION:**

Apoptosis resistance regulates the pathogenesis, and treatment response of breast tumors. Despite concerted effort towards understanding the molecular basis for apoptosis resistance in breast tumors, progress in this area has been frustratingly slow. Lack of advancement may be attributed in part to the current cell autonomous view of breast cancer etiology and treatment responsiveness. What we now appreciate is that the tissue microenvironment modifies the therapeutic responsiveness of tumors (Taylor et al., 2000; Zahir and Weaver, 2004), and the stroma itself regulates mammary development, homeostasis and transformation and metastasis (Unger and Weaver, 2003; Erler and Weaver 2008). Alterations in the mammary gland ECM correlate with changes in mammary differentiation, involution (apoptosis) and tumor progression, and culture experiments clearly show that the stromal ECM can modulate mammary epithelial cell (MEC) growth, differentiation and survival and alter apoptotic responsiveness (Lewis et al., 2002; Truong et al., 2003; Zahir and Weaver, 2004). **It is not known how the ECM alters mammary epithelial survival.**

My laboratory has been examining the role of integrin receptors in breast tissue morphology and behavior and malignant transformation and metastasis. Together we have begun to explore how the ECM via its major receptors the integrins modulates mammary tissue homeostasis, invasion and apoptosis responsiveness. We found that the expression of specific integrins including  $\alpha 5$ ,  $\alpha 6$  and  $\beta 1$  and  $\beta 4$  expression, organization and activity are consistently altered in primary and metastatic breast tumors and tumorigenic cell lines. Others and we have also determined that perturbing integrin expression and activity can drive malignant behavior of non-malignant and pre-malignant MECs, and that normalizing integrin activity represses expression of the malignant breast phenotype in culture and in vivo (Unger and Weaver, 2003; White et al., 2004). More specific to this proposal our data have shown that integrins including  $\alpha 6 \beta 4$  integrin can regulate cell survival and modulate the apoptotic responsiveness of mammary tissues to a diverse array of exogenous stimuli including various chemotherapies and immune receptor activators (Weaver et al., 2002; Zahir and Weaver, 2004). We found that integrin-dependent apoptosis resistance and survival are intimately linked to many of the biochemical pathways and mechanisms that regulate tissue organization and specifically tissue polarity. For example, we found that  $\alpha 6 \beta 4$  integrin directs mammary epithelial cells to assemble polarized mammary tissue structures that display apoptosis resistance to a wide spectrum of apoptotic insults. We are now exploring the underlying mechanisms whereby integrin expression and/or function becomes altered in breast tumors, how integrin modulate the survival of nonmalignant and transformed mammary epithelial cells, what the molecular link could be between integrin-dependent survival and tissue polarity and the clinical relevance of these findings.

We found that prior to malignant transformation the mammary gland exhibits a 'desmoplastic' response that is associated with an incremental and significant increase in global elastic modulus (stiffness) of the gland and elevated/altered expression of integrins and integrin adhesions (Krouskop et al., 1998; Paszek and Weaver, 2004; Paszek et al., 2005); (unpublished data; refer to previous progress report; data being prepared for manuscript submission). Consistent with results from other laboratories we determined that externally-applied mechanical force regulates the behavior and phenotype of multiple cell types including endothelial, fibroblasts, neurons, and MECs (Bershadsky et al., 2003; Geiger et al., 2001; Grinnell, 2003). Although the mammary gland is not traditionally viewed as a mechanically-regulated tissue, MECs within the ductal tree and alveolus experience passive (isometric) and active mechanical force throughout the lifetime of the mammary gland most notably during development, lactation and involution (Paszek and Weaver, 2004; Plewes et al., 2000; Samani et al., 2003). Similar to other solid tumors, the mammary gland also becomes appreciably stiffer in association with its malignant transformation and mammary epithelial cells within the tumorigenic mammary gland experience an array of additional compression and stress and interstitial associated forces (Kass et al., In progress). During the process of metastasis and once at the metastatic site breast tumor cells also



encounter an array of external mechanical forces that could conceivably influence their behavior and alter their response to treatment. For example, many of the common metastatic sites for breast cancer differ appreciably with respect to their stiffness and biochemical compositions than a normal mammary gland such as bone (very stiff, high vitronectin), in the vasculature (high pulsatile pressures, high fibronectin and fibrin), pleural cavity (very compliant with high fibrin composition but also adjacent fibrotic lung could be quite stiff with a high amount of elastin).

Because physical forces so profoundly influence cell proliferation, survival and differentiation of multiple cell types, we propose that we need to clarify whether and how mechanical cues regulate mammary tissue behavior and apoptosis responsiveness.

**Accordingly, we predict that the physical organization of the ECM (which contributes to its mechanical properties) constitutes an independent regulator of mammary epithelial behavior and apoptosis resistance.** Delineating the molecular basis for this phenotype will likely have important consequences for tumor therapy. To rigorously test this idea we are in the process of achieving the following specific aims:

**Specific Aim 1.** To engineer tractable 3D organo-typic model systems that recapitulate the biophysical properties of primary and metastatic breast tumor tissues, and then to use these models to identify and examine putative molecular mechanisms whereby mechanical force could regulate apoptosis resistance in culture and in vivo.

**Specific Aim 2.** To develop xenograft and transgenic mouse models to test whether ECM stiffness regulates apoptotic responsiveness of mammary epithelia in vivo.

**Specific Aim 3.** To build a computational model that can predict how changes in ECM compliance could influence integrin-dependent apoptosis responsiveness of mammary epithelia and query this model with clinical data.

**Specific Aim 4.** To develop non-invasive imaging tools that could be used to monitor changes in ECM stiffness or stiffness-induced changes in mammary tissue phenotype.

### **Summary of Achievements - Proposal Body:**

### **KEY RESEARCH ACCOMPLISHMENTS:**

**Task 1:** *Engineer tractable 3D organo-typic models that recapitulate the biophysical properties of primary and metastatic breast tumor tissues, and use these models to dissect candidate molecular mechanisms whereby ECM stiffness could regulate apoptosis resistance in culture and in vivo.*

### **PART A Development of natural 3D ECM models that recapitulate the biophysical properties of primary normal and malignant and metastatic breast tissues.**

- a. **Weaver laboratory** to conduct experimental measurements using compression analysis, indenter protocols and AFM to establish materials properties of normal and malignant mouse breast tissue and that of metastatic sites of breast cancer including the vascular and lymphatic systems, bone, brain, lung and liver (note: future experiments will be undertaken to measure human tissues, however until a new human protocol can be approved we will work with animal tissues which have been shown to have good correlation with human tissue). **Completed.**

- b. Weaver laboratory to manipulate natural ECM gel stiffness to recapitulate the range of stiffness/forces normal and malignant MECs would experience in vivo in both primary normal and malignant breast and in known metastatic tissues by keeping BM constant and increasing collagen concentration and obtain reliable rheological measurements of these gels using plane and cone rheometer (Shear modulus), compression analysis, AFM and an indenter method (Elastic modulus). **Completed**
- c. Weaver laboratory to manipulate natural ECM gel stiffness - keeping BM and collagen concentration constant through ECM cross linking induced through addition of metabolizable ribose and obtain reliable rheological measurements using compression, AFM and/or indenter methods. **Completed**
- d. Weaver laboratory to generate recombinant MECs and fibroblasts expressing recombinant lysyl oxidase for future experimental manipulations both in culture and in vivo. **Completed**
- e. Weaver laboratory to manipulate natural ECM gel stiffness - keeping BM and collagen concentration constant through ECM cross linking by addition of media from cells expressing recombinant lysyl oxidase and obtain reliable rheological measurements using compression, AFM and/or indenter methods. **Completed**
- f. Weaver laboratory to manipulate natural ECM gel stiffness - keeping BM and collagen concentration constant through ECM cross linking by addition of purified active transglutaminase and obtain reliable rheological measurements using compression, indenter and/or AFM. **Postponed - deemed redundant.**
- g. Weaver laboratory to design and engineer device to apply an exogenous force to reconstituted gels ex vivo. **Postponed (Purchased a force reactor and will be calibrating the machine and effects on cell spheroids in 3D years 2008-2009)**
- h. Weaver laboratory to manipulate natural ECM gel stiffness - keeping BM and collagen concentration constant through an increase in relative stiffness mediated by application of an exogenous force. The increase in stiffness will be deduced through calculations based upon the known magnitude of the force and the materials properties of the ECM gel. **Completed**
- i. Once we have assured ourselves that we can consistently manipulate ECM stiffness and have obtained reliable measurements the Weaver laboratory will analyze the morphogenesis behavior of normal and malignant MECs in BM gels of increasing stiffness - as mediated by: a) increasing collagen concentration b) cross linking collagen (via ribose, lysyl oxidase or transglutaminase) and c) by application of an exogenous stress force and compare the effectiveness of these different strategies so that we can choose two reliable methods for further study. **First half of these manipulations has been completed - force reactor manipulations postponed until reactor can be calibrated.**
- j. Weaver laboratory will analyze the growth behavior of normal and malignant MECs in collagen gels of increasing stiffness - as mediated by: a) increasing collagen concentration b) crosslinking collagen (via ribose, lysyl oxidase or transglutaminase) and c) by application of an exogenous stress force. **Completed except for the application of exogenous force - see above need to calibrate the force reactor**

- k. **Weaver laboratory** will analyze the survival behavior of normal and malignant MECs in BM gels of increasing stiffness - as mediated by: a) increasing collagen concentration b) crosslinking collagen (via ribose, lysyl oxidase or transglutaminase) and c) by application of an exogenous stress force. **Completed except for the application of exogenous force experiments which are deemed redundant.**
- i. **Weaver laboratory** will analyze the apoptosis sensitivity of normal and malignant MECs to three commonly used chemotherapeutic agents (taxol, doxorubicin, etoposide), and two immune receptor apoptotic agents (trails, TNFalpha) and gamma radiation grown within BM gels of increasing stiffness - as mediated by: a) increasing collagen concentration b) crosslinking collagen (via ribose, lysyl oxidase or transglutaminase) and c) by application of an exogenous stress force through viability and apoptosis assessment dose response curve generation. **Completed except for the application of exogenous force experiments which are deemed redundant.**

The work outlined in this aim has been almost all completed and results have been published thus far in two manuscripts (reported in Progress reports one and two). New results are currently being prepared for two additional manuscripts - one we anticipate submitting to Cell and the other is being prepared for a more specialized journal. The majority of these findings were reported in last year's progress report.

**PART B Development of synthetic 3D model systems that recapitulate the biophysical and biochemical properties of primary and metastatic breast tumor tissues. (NOTE: These studies are to be conducted in as a subcontract collaboration with Dr. Joyce Wong who is a Bioengineer and materials scientist at Boston University and as a new collaboration with Drs. Shuguang and Cam in the Biomedical Engineering Institute at MIT. Funds have been subcontracted to Dr. Wong at Boston University to cover materials costs and efforts of one graduate student to be able to achieve the goals set out in this S.O.W. including effective technology transfer to the Weaver laboratory).**

- a. **Wong laboratory** to conduct pilot studies to demonstrate the feasibility to consistently generate photo-activatable PVC gels that can be readily cross-linked to RGD. **Completed**
- b. **Cam and Shuguang laboratories** will train Weaver students to work with self-assembling peptide gels for work with human MECs. **Completed**
- c. **Weaver laboratory to test biocompatibility** of self-assembling peptides for 3D work with human nonmalignant and malignant MECs. **Completed**
- d. **Wong laboratory** to advise/teach Weaver laboratory personnel methodology for compliance measurements of self-assembling peptide gels. **Completed**
- e. **Weaver laboratory** with advice from **Cam and Shuguang laboratories** will set up methods to modulate compliance of self-assembling peptide gels and validation of measurements using indenter, rheology and compression analysis. **Completed**
- f. **Weaver laboratory** with advice from **Cam and Shuguang** and **Wong laboratories** will attempt to incorporate methods to cross-link laminin, RGD and collagenase sensitive collagen peptides into self-assembling peptide lattices for 3D studies. **Completed**

- g. Weaver laboratory will analyze the morphogenesis behavior of normal and malignant MECs in self-assembling peptide lattices for 3D studies with increasing stiffness with defined ECM (laminin) binding properties. **Completed**
- h. Weaver laboratory will analyze the growth behavior of normal and malignant MECs in self-assembling peptide lattices of increasing stiffness with defined ECM laminin binding properties. **Completed**
- i. Weaver laboratory will analyze the survival behavior of normal and malignant MECs in self-assembling peptide lattices of increasing stiffness with defined ECM laminin binding properties. **Completed**
- j. Weaver laboratory will analyze the apoptosis sensitivity of normal and malignant MECs to three commonly used chemotherapeutic agents (taxol, doxorubicin, etoposide), and two immune receptor apoptotic agents (trails, TNFalpha) and gamma radiation grown within self-assembling peptides lattices of increasing stiffness with defined ECM laminin binding properties. **Completed**
- k. Weaver laboratory to continue collaboration with Shuguang and Cam laboratories for technology transfer through continuous advising and consulting and transfer of new technology and information regarding self-assembling peptide gels for work with human MECs in 3D cultures. **Completed**
- l. Wong laboratory to expand methodology to incorporate cross-linking chemistry to laminin and collagen and collagenase sensitive collagen peptides with the PVD synthetic gels. **Completed**
- m. Wong laboratory to establish biocompatibility of synthetically generated photo-activatable PVD gels with generic cell type ie fibroblast. **Completed**
- n. Wong laboratory to send small shipment of PVD gel to Weaver laboratory where Weaver laboratory will establish the compatibility of synthetic PVD gels with immortalized human nonmalignant and malignant MECs. **Completed**
- o. Wong laboratory will establish protocols to generate PVD gels with controlled compliances matched to primary, pre-malignant, malignant and metastatic breast cancer sites. **In Progress - these studies are under way and we anticipate making good progress in this aim during the next year of the grant. NOTE: We have also begun to collaborate with Dr. Jason Burdick to apply cross linked "functionalized" hyluronic acid gels as an alternate strategy.**
- p. Wong laboratory will conduct compliance measurements using indenter and rheology devices to establish baseline measurements of newly synthesized PVD gels. **Completed**
- q. Wong laboratory will send PVD gels with different compliances to Weaver laboratory where Weaver laboratory staff will test the PVD gels for their biocompatibility in 2D and 3D with nonmalignant and malignant MECs. **Completed**
- r. Wong laboratory will send PVD gels with different compliances to Weaver laboratory where Weaver laboratory personnel will examine the PVD gels for compliance properties using compression analysis. **Completed**

- s. Weaver laboratory will analyze the morphogenesis behavior of normal and malignant MECs in PVD gels of increasing stiffness with defined ECM binding properties. **Delayed due to move to UCSF - see above - anticipate making good progress on this sub aim this coming year. Again here we also plan to use functionalized, cross linked HA gels with Jason Burdicks laboratory as an alternate strategy.**
- t. Weaver laboratory will analyze the growth behavior of normal and malignant MECs in PVD gels of increasing stiffness with defined ECM binding properties. **Delayed due to move to UCSF - see above - anticipate making good progress on this sub aim this coming year. See above use of HA gels.**
- u. Weaver laboratory will analyze the survival behavior of normal and malignant MECs in PVD gels of increasing stiffness with defined ECM binding properties. **Delayed due to move to UCSF - see above - anticipate making good progress on this sub aim this coming year. See above anticipated use of HA gels.**
- v. Weaver laboratory will analyze the apoptosis sensitivity of normal and malignant MECs to three commonly used chemotherapeutic agents (taxol, doxorubicin, etoposide), and two immune receptor apoptotic agents (trails, TNFalpha) and gamma radiation grown within PVD gels of increasing stiffness with defined ECM binding properties. **Delayed due to move to UCSF - see above anticipate making good progress on this sub aim this coming year. See above anticipated use of HA gels**
- w. Wong laboratory will conduct technology transfer starting first with compliance methods including indentor methodology and rheological measurement expertise to Weaver laboratory through student exchange and familiarity with method. **Completed**
- x. Wong laboratory will conduct technology transfer of compliance measurements with indentor and rheological method expertise to Weaver laboratory through aid in setting up methodology in Weaver laboratory. **Completed**
- y. Wong laboratory will complete technology transfer section of compliance measurements using indentor and rheological methodology through advisory capacity. **Completed**
- z. Wong laboratory will conduct technology transfer with PVD gel methodology through student exchange. **In Progress**
- aa. Wong laboratory will conduct technology transfer with PVD gel methodology through assistance of set up of chemistry and protocols in Weaver laboratory. **Delayed due to move to UCSF - see above - once we have conducted experimentation with the PVD gels then we will be working closely with the Wong laboratory to transfer technology. We have also begun to work with Dr. Jason Burdick from University of Pennsylvania on functionalized HA gels.**
- bb. Wong laboratory will complete technology transfer of PVD gel manufacture through continued advising and consulting of the Weaver laboratory until the termination of this grant. **Delayed due to move to UCSF - see above - anticipate making progress in this sub aim towards the end of this forthcoming year of funding. See above info on HA gels.**



Much of the work outlined in this aim was summarized in prior research reports - and portions were already published. Additional work - discussed and presented at conferences will be published in the next year. See below for more details.

**Task 2:** *Develop xenograft and transgenic mouse models to test whether ECM stiffness regulates apoptotic responsiveness of mammary epithelia in vivo.*

**PART A. Xenograft studies to test whether ECM stiffness could regulate apoptotic responsiveness of a mammary epithelium in vivo.** **NOTE:** These studies were to be conducted in collaboration with Dr. Bernhard from the Radiation Biology Department at the University of Pennsylvania. However Dr. Bernhard relocated to Oxford University at the beginning of the second year of funding of this proposal. Thereafter, Dr. Weaver began these studies with other colleagues at UPenn in the Radiation Biology Program. Thereafter, Dr. Weaver relocated to UCSF towards the end of the second year of funding of this proposal. After having relocating to UCSF, Dr. Weaver established collaborators in the area of radiation biology for breast cancer - she has recently begun to collaborate with Dr. Mary Helen Barcellos-Hoff at LBNL in Berkeley California. Dr. Barcellos-Hoff has more than 20 years of experience conducting radiation studies in culture and in vivo. While this delayed these experiments somewhat - we anticipate making good progress in this aim in the forthcoming year of funding.

- a. Weaver laboratory in collaboration with Bernhard laboratory will assess radiation sensitivity of single nonmalignant and tumorigenic MECs embedded within compliant rBM gels using short-term viability as end point. **Completed**
- b. Weaver laboratory in collaboration with Bernhard laboratory will assess radiation sensitivity of colonies of nonmalignant and tumorigenic MECs embedded within compliant rBM gels using short term viability as an end point. **Completed**
- c. Weaver laboratory in collaboration with Bernhard laboratory will assess radiation sensitivity of single nonmalignant and tumorigenic MECs embedded within compliant rBM gels ex vivo using long term re-growth assays as the end point. **Completed**
- d. Weaver laboratory in collaboration with the Bernhard laboratory will assess radiation sensitivity of colonies of nonmalignant and tumorigenic MECs embedded within compliant rBM gels ex vivo using long term re-growth assays as the end point. **Completed**
- e. Based upon doses of established short-term and long-term re-growth assays Weaver laboratory in collaboration with Bernhard laboratory will then conduct xenograft assays of radiation sensitivity of tumorigenic MECs in vivo following their injection and establishment of viable, palpable tumors sub-cutaneously in nude mice based upon short-term viability effects as the end point. **Postponed - to be conducted now with Dr. Barcellos-Hoff.**
- f. Based upon doses of established short term and long term re-growth assays Weaver laboratory in collaboration with Bernhard laboratory will conduct xenograft assays of radiation sensitivity of tumorigenic MECs in vivo following their injection and establishment of viable, palpable tumors sub-cutaneously in nude mice based upon long-term re-growth assays as an end point. **Postponed - see above.**
- g. Weaver laboratory will assess biocompatibility of self-assembling peptides injected sub-cutaneously into nude mice. **Postponed - see above**

- h. Weaver laboratory will assess biocompatibility of cross-linked collagen gel injected sub-cutaneously into nude mice. **Completed - see above**
- i. Weaver laboratory in collaboration with Bernhard laboratory will assess effect of radiation responsiveness of tumorigenic MECs embedded within soft versus stiff self-assembling peptides and/or cross-linked collagen gels in vivo, injected sub-cutaneously into nude mice and assessed for short term viability as the end point. **Postponed - see above**
- j. Weaver laboratory in collaboration with Bernhard laboratory will assess effect of radiation responsiveness of tumorigenic MECs embedded within soft versus stiff self-assembling peptides and/or cross-linked collagen gels in vivo, injected sub-cutaneously into nude mice, and assessed for long term re-growth as the end point. **Postponed - see above**
- k. Weaver laboratory in collaboration with Bernhard laboratory will assess effect of radiation responsiveness of tumorigenic MECs embedded within soft versus stiff self-assembling peptides and/or cross-linked collagen gels in vivo, injected sub-cutaneously into nude mice, and assessed for long term effects on tissue morphology as the end point. **Postponed - see above.**
- l. Weaver laboratory in collaboration with Bernhard laboratory will assess effect of radiation responsiveness of tumorigenic MECs embedded within soft versus stiff self-assembling peptides in vivo, injected sub-cutaneously into nude mice, and assessed for long term effects on gene expression as the end point. **Postponed - see above.**
- m. Weaver laboratory in collaboration with Bernhard laboratory will assess effect of radiation responsiveness of tumorigenic MECs embedded within soft versus stiff self-assembling peptides and/or cross-linked collagen gels in vivo, injected sub-cutaneously into nude mice, and assessed for long term effects on apoptosis resistance/stress response protein expression as the end point. **Postponed - see above.**

The first portion of these studies is now completed and the results which were summarized in last year's progress report are now being prepared for publication. We anticipate successful publication within the next several months time. In vivo studies are now beginning and we anticipate making good progress this next year.

**PART B. Transgenic animal studies designed to test whether ECM stiffness could influence apoptosis regulation in vivo. These studies are being conducted in collaboration with Dr. Gasser**

**NOTE: No detailed outline of tasks was submitted for this area of investigation - however over the past year we have been able to make considerable progress in this area particularly with respect to demonstrating the effect of modulating matrix stiffness on breast tumor progression. Details of experimental progress in this area are elaborated below. In addition, as outlined in an earlier progress report, we have also made good progress towards generating a novel transgenic mouse model that recapitulate altered ECM stiffness to elaborate effects on breast tumor progression and treatment responsiveness. To this end we have begun to collaborate with Dr. Zena Werb who is a world recognized expert in metallo proteinases in breast development and cancer and has access to several novel mouse models to study the effect of matrix stiffness on mammary epithelial behavior. In this regard we have allocated 5% salary support to Dr. Werb to support this research endeavor. This work is currently being prepared for publication. We intend to submit the article to Cell. The studies were the basis of the thesis of Kandice Johnson.**

**Task 3:** Build a computational model that can predict how changes in ECM compliance could influence integrin-dependent apoptosis responsiveness of mammary epithelia and query this model with clinical data.

**PART A.** To assemble and generate cell biology and published data required for basic computational model. These studies are to be conducted in collaboration with Dr. Tobias from the University of Pennsylvania Bioinformatics Center and Dr. Hammer from the Department of Bioengineering at the University of Pennsylvania. **NOTE: Although Dr. Weaver relocated her laboratory to the Departments of Surgery and Anatomy at UCSF in San Francisco she has maintained her interactions with Dr. Tobias and Dr. Hammer - she has furthermore extended her interactions with colleagues in Engineering and Systems biology. This is consistent with her new position as the Director for the Center for Bioengineering and Tissue Regeneration. Over the past year she and her collaborators and their groups have made encouraging progress towards building a tractable computational model of matrix force and breast cell behavior. This work has led to a novel discovery of a previously understudied area of breast cell behavior. Details on this model are elaborated below.**

- a. Analysis of integrin adhesions in natural and synthetic 3D gels of varying compliance. **Completed**
- b. Analysis of integrin signaling through ERK in natural and synthetic 3D gels of varying compliance. **Completed**
- c. Analysis of integrin signaling through JNK in natural and synthetic 3D gels of varying compliance. **Completed**
- d. Analysis of integrin signaling through PI3Kinase in natural and synthetic 3D gels of varying compliance. **Completed**
- f. Examination of correlation between matrix compliance, integrin-dependent signaling through ERK, JNK and PI3Kinase and apoptosis sensitivity to receptor-linked, chemo-therapy induced and radiation triggered apoptosis. **Completed**
- g. Pharmacological manipulation of ERK, JNK and PI3Kinase signaling to establish functional link between apoptosis sensitivity and matrix compliance. **Completed**
- h. Genetic manipulation of ERK, JNK and PI3Kinase signaling to establish function link between apoptosis sensitivity and matrix compliance. **Completed**
- i. Literature searches conducted to assembly published literature required for enzyme kinetics of signaling molecules, integrin adhesions and growth factor receptors to begin assembling the simple cell adhesion/growth factor receptor computational model. **Completed**

These studies have now been essentially completed and portions have already been published (see first progress report) or are currently being prepared for publication (see last progress report for experimental details. In this next year of funding we are continuing with these studies and anticipate elaborating more detailed molecular mechanisms for the effects of matrix stiffness on cell signaling and behavior.



**PART B. Generate a simple cell adhesion computational model based upon published values from the literature and data generated using culture models. These studies are to be conducted in collaboration with Dr. Hammer from the University of Pennsylvania Bioengineering Department.**

- a. Using published data and our experimental data initiate calculations and assumptions required for the basic cell adhesion model without incorporating force parameters. **Completed. See details below.**
- b. Pilot testing of basic computational model and comparison with experimental data obtained using cell culture model without incorporating force parameters. **In Progress - NOTE this aim was postponed due to the relocation of the Weaver laboratory to UCSF**
- c. Adjust basic cell adhesion model to incorporate experimental data. **In Progress - again this work has been delayed due to the relocation from UPenn to UCSF.**

**In preparation for this more elaborate model we generated a simple deterministic model of adhesion dependent growth factor receptor ERK activation and signaling. This article was published in early 2008. See attached article Yee, Weaver and Hammer, 2008.**

**PART C. Incorporate mechanical force values and assumptions into the basic adhesion model. These studies are to be conducted in collaboration with Dr. Hammer from the University of Pennsylvania Bioengineering Department.**

- a. Amend basic cell adhesion model to incorporate force parameters. **Completed**
- b. Test mechano-adhesion model and compare theoretical values with experimental data obtained using cell culture model. **In Progress - the work has been slightly delayed due to relocation of laboratory between UPenn and UCSF and freezing of funds**
- c. Adjust mechano-adhesion model to incorporate experimental data. **In Progress**

**We have made excellent progress in this area of investigation and attach a draft of a manuscript is in preparation that explores the role of matrix compliance in integrin clustering and activation which we intend to submit to the Biophysical Journal for publication by Paszek, Boettiger, Weaver and Hammer. This reportable will be submitted with the next annual report.**

**PART D. Initiate modeling studies using micro array data sets from the cell culture models. These studies are to be conducted in collaboration with Dr. Tobias in the Bioinformatics center and Dr. Hammer from the Department of Bioengineering.**

- a. Isolate RNA from MECs within a 3D matrix with varying matrix compliances. **Completed**
- b. Purify and prepare samples for micro array analysis. **Completed**
- c. Generate micro array data sets from samples of MECs in 3D matrices of varying compliances. **This work is now in progress.**
- d. Conduct statistical analysis of micro array data sets generated from MECs in 3D matrices of varying compliances. **Preliminary data has been obtained - and we are now in the process of increasing the number of data sets for an expanded analysis. Nevertheless the data**

**obtained has led to a novel discovery of an epigenetic mechanism regulating breast tumor therapy responsiveness. This in turn has yielded a patent application that is now pending. See attached patent application Weaver and Tsai.**

- e. Conduct bioinformatics analysis of micro array data sets generated from MECs in 3D matrices of varying compliances. **Initial studies have been completed - see patent being prepared by Tsai and Weaver.**
- f. Verify validity of micro array analysis by RT-PCR or real time PCR of 10 target genes. **Target validation for the initial studies has been completed. Once new data is generated we will also validate these targets. See preliminary article prepared by Tsai et al. appendix.**
- g. Initiate Monte Carlo analysis of micro array data sets to establish feasibility of generating both forward and reverse virtual analysis of gene expression profiles. **In Progress** (Months 36-48)
- h. Test predictability of new virtual model against micro array data sets using a bioinformatics approach. **In Progress** (Months 48-60)
- i. Test predictability of virtual model through either gene knock down or pharmacological blockage of identified loci of control followed by apoptosis sensitivity assay in the 3D culture models. **In Progress** (Months 36-60)
- j. Adjustment of virtual model based upon micro array analysis results and experimental data. **In Progress** (Months 48-60)

**We have exciting progress in this area of research over the past number of years and now have prepared a manuscript for publication which we anticipate submitting to Nature Medicine in the next few weeks time. See attached manuscript draft Tsai and Weaver. This article will be revised and submitted for review within the next few weeks.**

**PART E. Initiate pilot studies to analyze micro array data sets and clinical samples from neoadjuvant breast cancer clinical trial data using a simple model generated using gene data from culture systems. These studies are to be conducted in collaboration with Drs. DeMichele from the University of Pennsylvania and Esserman from UCSF and with Drs. Hammer from the Department of Bioengineering and Dr. Tobias from the Bioinformatics Center at the University of Pennsylvania. NOTE: These studies will now commence in this next upcoming year of support. To facilitate these studies we are in the process of preparing an IRB application which when approved we will send to the DOD.**

- a. Select clinical samples to be examined in collaboration with Drs. DeMichele and Esserman. **To be initiated once IRB application is approved.** (Months 36-40)
- b. Obtain micro array data sets from clinical samples. **To be initiated once IRB application is approved. In the meantime we were able to access publically available data bases and conducted an intensive data mining/analysis - results have been summarized in the attached manuscript by Tsai et al which will be submitted to Nature Medicine in the next few weeks.** (Months 40-42)
- c. Conduct statistical analysis of clinical micro array data sets. **See above** (Months 42-46)

- d. Conduct bioinformatics analysis of clinical micro array data sets. See above (*Months 42-48*)
- e. Test predictability of virtual model through comparison with micro array data set information. **See above** (*Months 48-60*)
- f. Secure clinical biopsy specimens for experimental validation. **In Progress - awaiting IRB approval before can begin analyzing clinical biopsies** (*Months 48-60*)
- g. Examine targets identified using virtual model analysis of micro array data sets using either immunohistochemistry or in situ analysis. **See above** (*Months 48-60*)

**Task 4:** *Develop non-invasive imaging tools that could be used to monitor changes in ECM stiffness or stiffness-induced changes in mammary tissue phenotype.*

**NOTE: This aim has changed in scope. We still aim to develop non-invasive imaging tools to monitor changes in ECM stiffness. However we have made progress in two separate areas. The first which we reported in our last progress report has been to begin collaborating with imaging colleagues to develop imaging sonoelastography and in the future MR elastography. Both of these approaches have been developed and are rapidly gaining application in the clinic. However neither approach has been explored together with molecular markers to use as a prognostic indicator or for monitoring therapy responsiveness. In addition, we recently began a fruitful collaboration with Dr. Paul Hansma from UC Santa Barbara who has developed a force indenter that could be quite useful as a tractable clinical tool. We will be working closely with Dr. Hansma this next year to determine the clinical versatility of this device. We have drafted an article together with Dr. Hansma which summarizes progress to date on this initiative. We intend to submit this manuscript for publication to Nature (see attached appendix for initial draft of this work).**

**PART A. Proof of principal studies for imaging sensitivity using 3D culture models.**

- a. Trial studies using quantum dots to image single well characterized abundant cell surface molecules in MEC colonies in 3D cultures. **Modified approach - see above explanation and last years progress report for more details** (*Months 24-30*)
- b. Trial studies using quantum dots to image two different well characterized abundant cell surface molecules in MECs in 3D cultures. **See above** (*Months 28-32*)
- c. Analysis of sensitivity of quantum dot technology against low abundance cell surface molecules in MECs in 3D cultures. **See above** (*Months 32-36*)
- d. Pilot study using quantum dots to image single well characterized abundant cell surface molecule in MECs in subcutaneous colony. **See above** (*Months 36-42*)
- e. Pilot study using quantum dots to image single well characterized abundant cell surface molecules in MECs in endogenously formed tumor. **See above** (*Months 40-48*)
- f. Trial studies using quantum dot technology to detect tension regulated molecules identified in Task 3 in MECs within soft versus stiff gels. **See above** (*Months 48-60*)

- g. Pilot in vivo studies to determine whether we can detect differences in tension regulated molecules identified in Task 3 in MECs embedded with a soft versus a stiff matrix subcutaneously in nude mice. [See above](#) (*Months 48-60*)
- h. Pilot in vivo studies using transgenically generated tumors in mice to determine whether we can detect any differences in candidate tension regulated molecules identified in Task 3 in cells surrounding developing malignant breast lesions previously shown to be stiffer than normal tissue. [See above](#) (*Months 48-60*)

**PART B. Set up and initial screening trials with peptide library for identification of novel stiffness markers in the ECM.**

- a. Procurement of phage display library for antibody production. [See above](#) (*Months 36-38*)
- b. Expansion of phage display library and titering. [See above](#) (*Months 36-40*)
- c. Testing and proof of principal of phage display library. [See above](#) (*Months 40-54*)
- d. Pilot study to identify novel conformational changes in collagen gels in which tension has been increased through an externally-applied force as compared to collagen gels in which tension is low. [See above](#) (*Months 50-60*)
- e. Expansion and maturation and screening of candidate phage molecules. [See above](#) (*Months 56-60+*)
- f. Testing and proof of principal demonstration in 3D matrix cultures that phage display antibodies can be identified that identify conformationally altered collagens that mark rigid collagen. [See above](#) (*Months 60+*)
- g. Pilot in vivo studies using quantum dot technology to determine whether we can detect matrix changes that mark an increase in stiffness in subcutaneously implant collagen gels with varying compliances. [See above](#) (*Months 60+*)
- h. Pilot in vivo studies using transgenic breast cancer models with previously determined compliance changes and alterations in the ECM surrounding the developing lesions to determine whether we can detect conformationally altered collagens that mark an increase in matrix stiffness. [See above](#) (*Months 60+*)

**Reportable Outcomes:**

**A. Manuscripts**

1. Friedland, J.C., Lakins, J.N., Kazanietz, M.G., Chernoff, J., Boettiger, D. and Weaver, V.M.  $\alpha 6 \beta 4$  integrin activates Rac-dependent p21-activated kinase 1 to drive NF $\kappa$ B-dependent apoptosis resistance in 3D mammary acini. J Cell Sci. 120: 3700-12, 2007. (NOTE: this was listed as accepted/In Press last report - see attached appendix)

2. Yee, K.L., Weaver, V.M., and Hammer, D. Integrin-mediated Signaling through the MAP-kinase Pathway. *IET Systems Biology*. 2:8-15, 2008. (NOTE: this was listed as accepted last report - the article has since been published - see attached appendix.)
3. Rizki, A., Weaver, V.M., Lee, S.Y. Rozenberg, G.I. Chin, K., Myers, C.A., Bascom, J.L., Mott, J.D., Semiks, J.R., Grate, L.R., Mian, I.S., Borowsky, A.D., Jensen, R.A., Idowu, M.O., Chen, F., Chen, D.J., Petersen, O.W., Gray, J.W., Bissell, M.J. A human breast cell model of preinvasive to invasive transition. *Cancer Res*. 68:1378-1387, 2008. (see attached appendix)
4. Kass, L, Erler, JT, Dembo, M, **Weaver, VM**, Mammary epithelial cell: Influence of extracellular matrix composition and organization during development and tumorigenesis. *Int J Biochem Cell Biol*. 39:1987-1994, 2007. (see attached appendix)
5. Hebner, C, **Weaver, VM**, and Debnath, J, Modeling Morphogenesis and Oncogenesis in Three dimensional Breast Epithelial Cultures. *Annu. Rev. Pathol*. 3: 313-319, 2007. (see attached appendix).
6. Erler, J., and Weaver V.M. Tissue Context and Tumor Metastasis, In a special issue of Clinical and Experimental Metastasis In Press, 2008. (see attached appendix)
7. Mouw, J., Desai, S., and Weaver V.M. Forcing transformation: biophysical regulation of mammary epithelial cell transformation, In The Pathomechanics of Tissue Injury and Disease, and the Mechanophysiology of Healing", In Press, 2008. (see attached appendix)

Articles In Preparation: Attached as part of the current progress report to illustrate experimental progress:

1. Tsai K.K.C. Chatterjee, C., Werner, M.E., Jonathan N. Lakins, Nuth, M., Tobias, J, Mian, S. and Weaver V.M. N-CoR2 and Epigenetic death resistance in the third dimension. To be Submitted. to Nature Medicine in the next few weeks.(draft article attached see appendix)
2. Hansma, P., Yu, H., Schultz, D., Rodriguez, A., Yurtsev, E., Peters, M.C., Miller, J., Wallace, J., Kang, I., Kohn, D., Buckley, J., Weaver, V.M., and Lotz, J. Tissue Diagnostic Instrument. To be Submitted to Nature in the next month. (draft article attached see appendix)

## **B. Abstracts**

1. Gilbert, P.M., Mouw, J.K., Gbegenon, M.K., Lakins, J.N., and Weaver, V.M. "The Breast Tumor Modulator HoxA9 Regulates BRCA1 and Integrin-Mediated Adhesion." ASCB 46th annual meeting, San Diego, CA, 2006.
2. Leight, J., Zahir, N., Lakins, J.N., Wong, J., and Weaver, V.M. "Force-dependent apoptosis resistance and breast tumorigenesis." ASCB 46th annual meeting, San Diego. 2006.
3. Nestor, K.M., Lakins, J.N., Imbalzano, A.N., Nickerson, J.A., and Weaver, V.M. "Loss of SWI/SNF Activity Alters Mammary Epithelial Cell Morphogenesis and Adhesion Dynamics." ASCB 46th annual meeting, San Diego, CA. 2006.

4. Tsai, K.C., Chatterjee, C., Lakins, J.N., and Weaver, V.M. "The SMRT Way to Resist Death." ASCB 46th annual meeting, San Diego, CA. 2006.
5. Leach JB, S Petrova, JN Lakins, K Johnson, J Leight, V Weaver. "Force-Dependent Mammary Morphogenesis and Malignancy in a Tunable 3D Model System." (Poster) American Society for Cell Biology Annual Meeting, San Diego, CA, Dec 2006 .
6. Zahir, N., Leight, J.L., Lakins, J.N., Alston-Mills, B., Tsai, K.C., and Weaver, V.M. "Force-dependent JNK activation promotes therapeutic responsiveness of a mammary epithelium." ASCB 46th annual meeting, San Diego, CA, 2006
7. Butcher, D.T., Friedland, J.C., Nuth, M., Dow, L.E., Bojadziewa, J., Humbert, P., and Weaver, V.M. "Force-dependent disruption of scribble/Dgl5-dependent tissue polarity." AACR Annual Meeting, Los Angeles, CA. 2007.
8. Nestor, K.M., Lakins, J.N., Imbalzano, A.N., Nickerson, J.A., and Weaver, V.M. "The Influence of Chromatin Remodeling on Mammary Epithelial Cell Behavior." University of California, San Francisco Graduate Students' Association Career & Research Days, San Francisco, CA. 2007.
9. Nestor, K.M., Lakins, J.N., Cohet, N., Ohkawa, Y., Nickerson, J.A., Imbalzano, A.N., and Weaver, V.M. "Flipping the SWI/SNF Switch: Chromatin Remodeling Alters the Adhesion-Dependent Phenotype of Mammary Epithelial Cells." AACR Annual Meeting, Los Angeles, CA. 2007.
10. Johnson, K.R., Kass, L., Zahir, N., Mrass, P., Erler, J.T., Weninger, W., Gasser, D., Wells, R.G., and Weaver, V.M. "Force dependent malignant transformation." Engineering Cell Bio II conference. 2007.
11. Kelvin K.C. Tsai, Chandrima Chatterjee, Jonathan N. Lakins, Manunya Nuth, Michael E. Werner, I. Saira Mian, Valerie M. Weaver, "Tissue Architecture Linked to Epigenetic Control of Therapeutic Response." Cambridge Healthtech Institute's Fourth Annual Stem Cell and 3D Models for Therapeutic Screening, Boston, MA, 2007
12. Kandice R. Levental, Laura Kass, Janine T. Erler, Paulus Mrass, Amato Giaccia, Wolfgang Weninger, David Gasser, Valerie M. Weaver, "Force-dependent malignant transformation", The 47th Annual Meeting of the American Society for Cell Biology, Washington, DC, 2007
13. I. Kang, J. Friedland, J. Lakins, W. Liu, J. Chernoff, M. Schwartz, C. Chen, D. Boettiger, V. Weaver, "Arf6 Restricts Rac Signaling to Promote Cell Survival in the 3<sup>rd</sup> Dimension", The 47th Annual Meeting of the American Society for Cell Biology, Washington, DC, 2007
14. Michael E. Werner, Nastaran Zahir, Kelvin Tsai, Chandrima Chatterjee, Johnathan N. Lakins and Valerie M. Weaver, "Matrix stiffness differentially regulates Jun Kinase and SMRT to modulate the apoptosis responsiveness of a 3D mammary epithelium", The 47th Annual Meeting of the American Society for Cell Biology, Washington, DC, 2007
15. Janna K. Mouw, Penney M. Gilbert, Mawuse K. Gbengono, Jonathan N. Lakins, and Valerie M. Weaver, "Biophysical Regulation of The Breast Tumor Modulator HoxA9 Through Integrin-

Mediated Adhesion” The 47th Annual Meeting of the American Society for Cell Biology, Washington, DC, 2007.

16. K. R. Johnson, S. J. Desai, J. N. Lakins, V. M. Weaver, “The Role of PTP-MEG1 in Mammary Epithelial Cell Morphogenesis” The 47th Annual Meeting of the American Society for Cell Biology, Washington, DC, 2007.
17. Kaiser, C., G Rozenberg, G., M Paszek, M., M Dembo, M., D Hammer, D. and Weaver, V.M. Force,  $\alpha 5 \beta 1$ -integrin and breast cancer metastasis., ASCB 47<sup>th</sup> Annual Meeting, Washington, D.C. 2007
18. Inkyung Kang, Kandice Levantal, Laura Kass, Hongmei Yu, David Gasser, Rebecca Wells and Valerie M. Weaver 1 “Remodeling of extracellular matrix in mammary tissues via lysyl oxidase drives tumorigenesis by enhancing PI3K signaling”, Keystone, Taos, NM. 2008.

### **C. Oral Meetings Presentations:**

1. Johnson, K.R., Kass, L., Zahir, N., Mrass, P., Weninger, W., Gasser, D., Margulies, S.S., Janmey, P.A., and Weaver, V.M. "Tissue Stiffness Promotes Mammary Tumorigenesis Through Enhanced PI3 Kinase Activation." Mini Symposium Speaker ASCB 46th annual meeting, San Diego, CA. 2006.
2. Manunya Nuth, M., Friedland, J.C., Lakins, J.N., Chernoff, J., Kennedy, A., and Weaver, V.M. Rac1, Matrix Force and Tissue Architecture: the Oxidative Effect. Mini Symposium Speaker ASCB 46<sup>th</sup> annual meeting, San Diego, CA, December 2006.
3. Weaver, V.M. Symposium speaker, "Tensional Stress". Special AACR Conference 'In the Forefront of Basic and Translational Cancer Research', Hilton Waikoloa Resort, Kona, Hawaii, 01/24/07
4. Weaver V.M. Symposium speaker, "Spatial-Mechanical Regulation of Malignant Transformation and Treatment Response", 4th International Conference on Tumor Microenvironment, Florence, Italy, 03/07/07
5. Weaver V.M. Symposium speaker, "Force, Dimensionality and Integrin – Dependent Survival", Fibronectin, Integrins and Related Molecules Gordon Conference, Lucca (Barga), Italy, 04/23/07
6. Weaver V.M. Symposium speaker "Force, Dimensionality and Tissue Morphogenesis and Malignancy", American Association of Anatomists, Plenary Symposium, FASEB, Washington, DC, 04/29/07
7. Tsai, K.C., Chatterjee, C., Lakins, J.N., Nuth, M., Werner, M.E., Mian, I.S., and Weaver, V.M. "Tissue Architecture Linked to Epigenetic Control of Therapeutic Response." Invited Symposium Speaker Fourth Annual Stem Cell and 3D Models for Therapeutic Screening conference. August 2007.
8. Weaver V.M. Symposium speaker, “Mechanics Meets Morphogenesis in Mammary Biology.” Engineering Cell Biology -- The Cell in Context, Massachusetts Institute of Technology- Cambridge, Massachusetts, 08/06/07

9. Weaver V.M. Symposium speaker, “Forcing form in the Third Dimension”, Mechanisms of Cell Signaling Gordon Conference, Oxford, United Kingdom, 09/16/07
10. Weaver V.M. Mini Symposium Speaker, Forcing form and function, Biomedical Sciences Graduate Student Retreat, Lake Tahoe, CA, October 13, 2007
11. Weaver V.M. Symposium speaker and Chair, “Spatial-Mechanical Cues from the Microenvironment Modulate Malignant Transformation and Treatment Efficacy.” AACR-NCI-EORTC International Conference on Molecular Targets and Cancer Therapeutics: Discovery, Biology, and Clinical Applications, San Francisco, California, 10/24/07
12. Weaver V.M. Symposium speaker, “Spatial-Mechanical Cues from the Microenvironment Modulate Malignant Transformation and Treatment Efficacy.” UC Davis BreastCancer Symposium, Sacramento, California, 10/25/07
13. Weaver V.M. Mini Symposium speaker "Forcing Transformation" UC Berkeley UCSF BioEngineering Graduate Retreat, Lake Tahoe, CA October 26, 2007
14. Weaver V.M. Major Symposium speaker, “Transformation: A Force To Resist” Force and Form in Cell Biology, ASCB 47th Annual Meeting, Washington, D.C. 12/02/07
15. Tsai, K.C., Chatterjee, C., Lakins, J.N., Nuth, M., Werner, M.E., Mian, I.S., and Weaver, V.M. Mini Symposium Speaker "Tissue Architecture Linked to Epigenetic Control of Therapeutic Response." ASCB 47th annual meeting. Washington, D.C. 2007.
16. Weaver V.M. Plenary presentation and chair, “Forcing Form and Function” AACR Special Interest Conference on Cytoskeleton Signaling in Cancer, San Diego, California. 02/04/08
17. Weaver V.M. Symposium Speaker, “Tension Contractility and the Microenvironment”, for Protrusion, Adhesion and Contractility session, in the Keystone Meeting on Cell Migration in Invasion and Inflammation (B7), Taos, New Mexico. 02/13/08
18. Kelvin K.C. Tsai, Chandrima Chatterjee, Michael E. Werner, I. Saira Mian, Manunya Nuth, Jonathan N. Lakins, John Tobias, Valerie M. Weaver  
Invited speaker, “Three Dimensional Dissection of Therapeutic Resistance in Breast Cancer.” The 6th Timberline Symposium: “3D Tissue Biology: Human Stem Cells, Cancer and the Microenvironment”, Mt. Hood, Oregon, USA (2008).

**D. Invited Institutional Presentations:**

1. Wong J.Y, Biomaterials for Early Detection and Treatment of Cardiovascular Disease, Invited Seminar Speaker, Dept of Chemistry, University of Calgary, December 2006, Calgary, CANADA.
2. Weaver V.M. Invited Lecture, "Form, Force and Mammary Morphogenesis: Implications for Stem Cell Function", NIH Mammary Gland Biology Group, Bethesda, Maryland, 05/01/07
3. Weaver V.M. Invited Speaker, "Force and Tumorigenesis", MRC, London, United Kingdom, 09/13/07



4. Weaver V.M. Seminar, "Forcing Tumorigenesis." Advances in Molecular and Cellular Pathology Seminar, Departments of Pathology and Genomics and Pathobiology, University of Alabama, Birmingham, Alabama, 09/27/07
5. Weaver V.M. Seminar, "Force, Dimensionality and Tissue Morphogenesis and Malignancy." Louisiana State University Health Science Center, New Orleans, Louisiana 11/08/07
6. Weaver V.M. Seminar, "Transformation: A Force to Resist" – Investigative Pathology Department, Seminar Series in Pathology, Vanderbilt University, Nashville, Tennessee, 02/24/08

**E. Patents**

1. Weaver, V.M., Tsai, K., Methods for predicting and treating drug-, immunotherapy- and/or radiation-resistant tumors. SF2008-034, 2007. Pending (see attached appendix)

**F. Graduate Students Matriculated**

1. Penney Gilbert Ph.D. Cell and Molecular Biology University of Pennsylvania 2006
2. Nas Zahir Ph.D. Bioengineering University of Pennsylvania 2006
3. Kate Nestor MSc Cell and Molecular Biology University of Pennsylvania 2006
4. Julie Friedland Ph.D. Pharmacology University of Pennsylvania 2006
5. Kelly Yee Ph.D. Bioengineering University of Pennsylvania 2007
6. Christina Kaiser MSc Bioengineering University of Pennsylvania 2007

**Progress Summary and Conclusions**

NOTE: Funding for this project was suspended for 9 1/1 months duration while my group relocated to the University of California San Francisco in San Francisco, California from the University of Pennsylvania in Philadelphia, Pennsylvania and we could transfer funding from the University of Pennsylvania to UCSF. The University of Pennsylvania administration was slow to complete the necessary paperwork and approve the closing out of the grant. Therefore, from the end of November 2006 until September 15, 2007 the experimental work supported by this grant was temporarily halted. Commencing mid September 2007 we reinitiated the experimental studies outlined in this proposal. Nevertheless I was able to use start up funds from UCSF to support personnel employed to conduct the studies outlined in the grants objectives and we spent our time reviewing data and writing articles and reviews. Therefore, while experimental work ceased we were able to make excellent progress on many other aspects of the ongoing work and have been able to complete several of the studies and summarize our findings for publication.

Now that funding has commenced I have hired new personnel to work on the project and my intention is to complete five major goals during this next funding year.

The first objective will be to summarize many of our findings and submit the work we have already completed for peer reviewed publication.

This includes:

1. Our studies aimed at exploring the role of matrix stiffness on apoptosis responsiveness in 3D synthetic and natural matrices (Zahir, Werner et al. to Journal of Cell Science or Molecular Biology of the Cell).
2. Our work identifying the epigenetic regulator NCoR2 as a key regulator of tissue architecture dependent apoptosis resistance and multi drug resistance in breast tumors. (Tsai et al., This should be submitted shortly to Nature Medicine)
3. Our deterministic studies describing the relationship between matrix compliance, integrin clustering and membrane biophysics. (Paszek et al., We have a workable draft of this article and anticipate submitting this to Biophysical Journal within the next few months).
4. Our examination of the effect of matrix stiffness and cross linking on breast tumor progression implicating PTEN and PI3 kinase regulation as key molecular mechanisms whereby matrix stiffness could influence the pathogenesis of breast cancer. (Johnson-Leventhal et al., This work has almost been completed and the figures are being prepared. We hope to submit this article by mid summer for publication in Cell).

The second objective will be to elaborate on our biomaterials development work using both durotaxis gradient gels and PEG gels with Dr. Wong and the HA gels we are developing with Dr. Burdick.

The third objective will be to conduct experimental proof of principal studies to follow up on our deterministic modeling of the mechano-ECM interface as a regulator of breast tumor progression/behavior.

The fourth objective will be to expand our effort towards elaborating clinical relevance of our work with Laura Essermans group. To this end we are in the process of submitting an IRB so that we can begin to examine the relevance of our NCoR2 gene signature to the pathogenesis of multi drug resistance human breast cancer. In this regard we have submitted a Patent on our work and hope that within the next year we will be granted these patent rights.

Our fifth objective is to continue working with Dr. Hansma on establishing the clinical relevance/feasibility of using his novel mechano probe to examine mechanical changes associated with human breast cancer progression.

**References:**

**Bershadsky, A. D., Balaban, N. Q. and Geiger, B.** (2003). Adhesion-dependent cell mechanosensitivity. *Annu Rev Cell Dev Biol* **19**, 677-95.

**Erler, J., and Weaver V.M.** (2008) Tissue Context and Tumor Metastasis, In a special issue of *Clinical and Experimental Metastasis* In Press.

**Geiger, B., Bershadsky, A., Pankov, R. and Yamada, K. M.** (2001). Transmembrane crosstalk between the extracellular matrix--cytoskeleton crosstalk. *Nat Rev Mol Cell Biol* **2**, 793-805.

**Grinnell, F.** (2003). Fibroblast biology in three-dimensional collagen matrices. *Trends Cell Biol* **13**, 264-9.

**Kass, L., Erler, J. T., Dembo, M. and Weaver, V. M.** (In progress). Matrix form and function regulate mammary tissue behavior. In Progress. *The International Journal of Biochemistry and Cell Biology/Cells in Focus*.

**Krouskop, T. A., Wheeler, T. M., Kallel, F., Garra, B. S. and Hall, T.** (1998). Elastic moduli of breast and prostate tissues under compression. *Ultrason Imaging* **20**, 260-74.

**Lewis, J. M., Truong, T. N. and Schwartz, M. A.** (2002). Integrins regulate the apoptotic response to DNA damage through modulation of p53. *Proc Natl Acad Sci U S A* **99**, 3627-32.

**Lo, C.M., H.B. Wang, M. Dembo, and Wang, Y.L.** (2000) Cell movement is guided by the rigidity of the substrate. *Biophys J* **79**, 144-52.

**Paszek, M. J. and Weaver, V. M.** (2004). The tension mounts: mechanics meets morphogenesis and malignancy. *J Mammary Gland Biol Neoplasia* **9**, 325-42.

**Paszek, M. J., Zahir, N., Johnson, K. R., Lakins, J. N., Rozenberg, G. I., Gefen, A., Reinhart-King, C. A., Margulies, S. S., Dembo, M., Boettiger, D. et al.** (2005). Tensional homeostasis and the malignant phenotype. *Cancer Cell* **8**, 241-54.

**Plewes, D. B., Bishop, J., Samani, A. and Sciarretta, J.** (2000). Visualization and quantification of breast cancer biomechanical properties with magnetic resonance elastography. *Phys Med Biol* **45**, 1591-610.

**Samani, A., Bishop, J., Luginbuhl, C. and Plewes, D. B.** (2003). Measuring the elastic modulus of ex vivo small tissue samples. *Phys Med Biol* **48**, 2183-98.

**Taylor, S. T., Hickman, J. A. and Dive, C.** (2000). Epigenetic determinants of resistance to etoposide regulation of Bcl-X(L) and Bax by tumor microenvironmental factors. *J Natl Cancer Inst* **92**, 18-23.

**Truong, T., Sun, G., Doorly, M., Wang, J. Y. and Schwartz, M. A.** (2003). Modulation of DNA damage-induced apoptosis by cell adhesion is independently mediated by p53 and c-Abl. *Proc Natl Acad Sci U S A* **100**, 10281-6.

**Unger, M. and Weaver, V. M.** (2003). The tissue microenvironment as an epigenetic tumor modifier. *Methods Mol Biol* **223**, 315-47.

**Weaver, V. M., Lelievre, S., Lakins, J. N., Chrenek, M. A., Jones, J. C., Giancotti, F., Werb, Z. and Bissell, M. J.** (2002). beta4 integrin-dependent formation of polarized three-dimensional architecture confers resistance to apoptosis in normal and malignant mammary epithelium. *Cancer Cell* **2**, 205-16.

**White, D.E., Kurpios, N.A., Zuo, D., J.A. Hassell, Blaess, S., Mueller, U., Muller, W.J.** (2004) Targeted disruption of beta-1-integrin in a transgenic mouse model of human breast cancer reveals an essential role in mammary tumor induction. **6**, 159-70.

**Wong, J.Y., Velasco, A., Rajagopalan, P., and Pham, Q.** (2003) Directed movement of vascular smooth muscle cells on gradient compliant hydrogels. *Langmuir*, **19**, 1908-13.

**Zaari, N., Rajagopalan, P., Kim, S.K., Engler, A., and Wong, J.Y.** (2004)

Photopolymerization in microfluidic gradient generators: Microscale control of substrate compliance to manipulate cell response. *Advanced Materials*, **16**, 2133-37.

**Zahir, N. and Weaver, V. M.** (2004). Death in the third dimension: apoptosis regulation and tissue architecture. *Curr Opin Genet Dev* **14**, 71-80.

Articles In Preparation: Attached as part of the current progress report to illustrate experimental progress:

1. Tsai K.K.C. Chatterjee, C., Werner, M.E., Jonathan N. Lakins, Nuth, M., Tobias, J, Mian, S. and Weaver V.M. N-CoR2 and Epigenetic death resistance in the third dimension. To be Submitted. to Nature Medicine in the next few weeks
2. Hansma, P., Yu, H., Schultz, D., Rodriguez, A., Yurtsev, E., Peters, M.C., Miller, J., Wallace, J., Kang, I., Kohn, D., Buckley, J., Weaver, V.M., and Lotz, J. Tissue Diagnostic Instrument. To be Submitted to Nature in the next month.

## **The Third Dimension Drives N-CoR2-dependent Death Resistance**

Kelvin K.C. Tsai<sup>1,5</sup>, Chandrima Chatterjee<sup>2,5</sup>, Michael E. Werner<sup>1</sup>, I. Saira Mian<sup>3</sup>, Manunya Nuth<sup>2</sup>, Jonathan N. Lakins<sup>1</sup>, John Tobias<sup>4</sup> & Valerie M. Weaver<sup>1</sup>

<sup>1</sup>Department of Surgery and Center for Bioengineering and Tissue Regeneration, University of California, San Francisco, 513 Parnassus Avenue, Medical Sciences, S1364, San Francisco, CA 94143, USA.

<sup>2</sup>Department of Pathology and Institute for Medicine and Engineering, University of Pennsylvania, 3340 Smith Walk, Philadelphia, PA 19104, USA.

<sup>3</sup>Life Sciences Division, Lawrence Berkeley National Laboratory, 1 Cyclotron Road, Berkeley, CA 94720, USA.

<sup>4</sup>Penn Bioinformatics Core, University of Pennsylvania, 423 Guardian Drive, Philadelphia, PA 19104, USA.

<sup>5</sup>These authors contributed equally to this work.

Correspondence should be addressed to:

Valerie M. Weaver, University of California, San Francisco  
513 Parnassus Avenue, Medical Sciences, S1364  
San Francisco, CA 94143  
Email: [WeaverV@surgery.ucsf.edu](mailto:WeaverV@surgery.ucsf.edu)  
Telephone: 415-476-3973  
Fax: 415-476-3985

## **Abstract**

Death resistance in tumors contributes to therapeutic failure. Using three-dimensional organoid cultures we determined that differentiated breast tissues resist death through elevated HDAC3-dependent nuclear corepressor2-(N-CoR2)-activity. Importantly, bioinformatics revealed that increased HDAC3 and N-CoR2 expression correlates significantly with percent relapse-free and overall reduced survival of breast cancer patients suggesting tumors could evade death by seconding this epigenetic survival mechanism. Consistently, gene manipulation and mutational studies demonstrated that enhanced N-CoR2/HDAC3 functional activity was necessary and sufficient for death resistance in breast tumors, regardless of tissue context. Expression profiling showed that the N-CoR2/HDAC3 repressor complex enhanced breast tumor survival by globally inhibiting pro-apoptotic and pro-inflammatory genes, specifically the treatment-effector TRAIL. Transcriptome analysis revealed that an N-CoR2/HDAC3 regulated transcript signature significantly predicts the pre-existence of treatment-refractory breast tumors with poor therapeutic outcome and clinical resistance following neoadjuvant chemotherapy. By exploiting a tractable three-dimensional assay we identified a death-resistance mechanism through which tumors resist treatment.

The development of drug resistance by tumor cells significantly limits the efficacy of antineoplastic agents and is the major contributing factor to therapeutic failure of human malignancies. Despite advances in understanding the genetic and molecular basis of drug resistance, significant discrepancies exist between drug resistance identified in experimental models and the multidrug resistance (MDR) phenotypes found in human cancers<sup>1</sup>. Such discrepancy may stem from the distinct multicellular and spatial-dimensional contexts under which tumor drug resistance develops *in vivo*. Consequently, the MDR phenotypes of cancers can only be recapitulated by culture models that incorporate elements mimicking *in vivo* tumor or tissue architectures instead of conventional monolayer cell cultures<sup>2</sup>. For instance, organization of tumor cells into three-dimensional (3D) multicellular spheroids endowed them resistance to cytotoxic agents and radiation, which was reversible by disaggregation of the structures<sup>3</sup>. When maintained *ex vivo* with preserved tissue architecture, malignant tumors displayed differential sensitivities to cytotoxic drugs similar to those observed *in vivo*<sup>4</sup>. The context-dependency of cell death sensitivity also holds true for non-neoplastic epithelial cells, as organization of mammary epithelial cells (MECs) into 3D acinar architectures in response to reconstituted basement membrane (rBM) endowed them a MDR phenotype<sup>5</sup>. Targeting MDR developed in these *in vivo*-like models shows particular promise to overcome drug resistance in human cancers, which however requires more complete understandings of its molecular basis.

Accumulating evidence suggests that phenotypic plasticity mediated by epigenetic mechanisms is an important source of tumor heterogeneity that serves to promote tumor progression<sup>6-9</sup>. Here we show a novel role of the epigenetic regulator nuclear receptor corepressor 2 (N-CoR2) in a MDR phenotype developed by MECs driven by tissue organization in three dimensions. N-CoR2 and its paralog N-CoR are transcriptional corepressors of nuclear receptors and non-receptor transcriptional factors and they mediate transcriptional repression by recruiting and activating histone deacetylases (HDACs)<sup>10,11</sup>. We find that, in both non-neoplastic and neoplastic MECs, N-CoR2 expresses in a context- and tissue organization-dependent manner and its expression levels parallel the degree of MDR. The N-CoR2-mediated death resistance was functionally-linked to chromatin remodeling-mediated altered gene expression through activation of HDAC3. When expressed in neoplastic MECs, N-CoR2 coordinately represses the induction of multiple apoptotic mediators in response to death stimuli. Transcriptome analysis on human breast cancers provides compelling evidence that N-CoR2 and its associated gene expression signature in primary tumors are among the strongest predictors of chemotherapy responsiveness and therapeutic outcome. The results suggest that N-CoR2/HDAC3-mediated death resistance in organized epithelial tissues can be usurped by chemo-refractory tumors and plays a key role in the treatment resistance of breast cancer.



## RESULTS

### Tissue organization in 3D coordinates N-CoR2 and epigenetic changes

Previously, it has been shown that tissue organization is accompanied with nuclear reorganization and chromatin remodeling<sup>12,13</sup>. When organized into mammary acinus-like architectures in rBM (**Fig. 1a**), non-neoplastic human breast epithelial S1 cells displayed histone hypoacetylation/hypermethylation (**Fig. 1b**) and underwent substantial transcriptional reprogramming (data not shown). Consistent with our previous findings<sup>5</sup>, organized S1 acini were considerably more resistant to death-receptor signaling or ionizing radiation (IR)-induced death than cells cultured as monolayers, which could be reversed by the histone deacetylase (HDAC) inhibitor trichostatin A (TSA) (**Fig. 1c**). These findings raised the possibility that tissue organization and death sensitivity are coordinated by epigenetic mechanisms. Comparing the transcriptomes of S1 monolayers and acini by gene expression profiling (data not shown), we found that the nuclear receptor corepressor 2 (N-CoR2) (*NCOR2*), or the silencing mediator for retinoid acid and thyroid hormone receptors (*SMRT*), was significantly upregulated in organized S1 acini at both the mRNA and protein levels (**Fig. 1d,e**). N-CoR2 exists in a large chromatin-binding complex that functions in repressing target gene transcription of unliganded nuclear receptors and transcriptional factors through histone hypoacetylation<sup>14,15</sup>. Interestingly, one of the components in the N-CoR2 protein complex, G protein pathway suppressor 2 (GPS2), was also upregulated in S1 acini compared with cell monolayers. In contrast, the expressions of the N-CoR2 paralog N-CoR1 (*NCOR1*) and HDAC3, a major deacetylase effector of the N-CoR2 protein complex<sup>14,15</sup>, did not change significantly in response to tissue organization. The upregulation of N-CoR2 was tissue organization dependent and reversible, as disruption of the organized acinal architectures by functional inhibition of E-cadherin (**Supplementary Fig. 1**) or culture in 3D collagen I gel and dissociation of S1 cells from 3D acini into monolayers significantly reduced N-CoR2 expressions in S1 cells (**Fig. 1f**).

### N-CoR2 is required for death resistance in organized epithelial tissues

To address whether N-CoR2 is necessary for the architecture-dependent death resistance, we downregulated N-CoR2 expression by retrovirus-mediated RNA interference (RNAi). Knockdown of N-CoR2 did not significantly alter the growth or acinar morphogenesis of S1 cells (**Supplementary Fig. 2a**) while rendered the acini more sensitive to multiple death inducers, including the death receptor ligand tumor necrosis factor-related apoptosis-inducing ligand (TRAIL), the cytotoxic drug Paclitaxel and IR, than the acini formed by control cells (**Fig. 1g**). Analogous to the structural organization of S1 cells into acini, reestablishment of tissue organization in neoplastic breast epithelial T4-2 cells also resulted in upregulation of N-CoR2 and acquisition of a death resistance phenotype (**Fig. 2a, b**). Knockdown of N-CoR2 re-sensitized the organized T4-2 architectures to exogenous death inductions (**Fig. 2b**),

suggesting that N-CoR2 may also mediate architecture-dependent death resistance in malignant cells under certain contexts.

### **N-CoR2 drives death resistance in a HDAC3-dependent manner**

The major biological function of N-CoR2 relies on its ability to stimulate the nuclear deacetylase activities of HDAC3<sup>14,15</sup>. Histone deacetylation and inappropriate transcriptional repression has been linked to tumor initiation and progression<sup>16</sup>. Although N-CoR was found to be transcriptionally or functionally down-regulated in non-Hodgkin lymphomas and colon cancers<sup>17,37</sup>, its mRNA expression is up-regulated in many other human malignant tumors (**Supplementary Table 1**). To recapitulate N-CoR2 upregulation in tumors and to investigate its role in the response of malignant cells to death stimuli, we stably overexpressed N-CoR2 in T4-2 cells and the metastatic breast cancer MDA-MB-231 cells (**Fig. 2c**). Overexpression of N-CoR2 in T4-2 cells resulted in a small (~20 %) but reproducible increase in their growth (**Supplementary Fig. 2b**) while rendering them markedly resistant to exogenous death inducers no matter when they were cultured as 3D multicellular aggregates, isolated cells or cell monolayers (**Fig. 2d, e**). These findings suggest that, once overexpressed in cells, N-CoR2 can override the cues originating from tissue architectures and regulate death sensitivity in a context-independent manner. To further ask whether the ability of N-CoR2 to regulate cell death is HDAC3-dependent, we knockdowned HDAC3 and found that HDAC3 deficiency restored the death sensitivity of N-CoR2-overexpressing cells (**Fig. 2f**). Moreover, stable overexpression of a mutant N-CoR2 (K449A) lacking the ability to activate the deacetylase activity of nuclear HDAC3<sup>14</sup> rendered T4-2 cells hypersensitive to death induction (**Fig. 2g** and **Supplementary Fig. 3**), reinforcing the idea that the deacetylase activity of HDAC3 is crucial to the N-CoR2-mediated death resistance.

### **N-CoR2 modulates expressions of apoptotic mediators upon death induction**

N-CoR2 is known to mediate repression of a wide array of nuclear receptor and nonreceptor transcriptional pathways<sup>18</sup>. Except nuclear histones, HDAC3 also deacetylates and regulates a variety of non-histone targets<sup>19</sup>. The pleiotropic functions of N-CoR2 and HDACs would therefore necessitate a systems approach to dissect the molecular processes responsible for N-CoR2-mediated death resistance. To this end, we treated N-CoR2-overexpressing T4-2 cells or the control cells cultured in rBM with the death ligand TRAIL and profiled the gene expressions (**Fig. 3a**). Using a relatively stringent selection criteria, we found a list of 304 genes (350 probe sets) whose expressions were significantly altered by N-CoR2 overexpression, designated thereafter as the “N-CoR2 signature genes” (**Fig. 3b**). Functional annotations of these genes suggested that, in the absence of death stimuli, N-CoR2 mainly regulated the transcription of genes involved in extracellular matrix assembly and remodeling (*e.g.*, *FNI*, *SDC2*, *TIMP3*, *MMP1*, *COL4A1*, *THBS1*, *TAGLN*, *TNC*,

*COL6A2*, *ITGA6*, *ITGB4*), inflammation (e.g., *IL6*, *TREM1*, *C3AR1*, *FOS*, *MAPK1*, *CXCL3*, *CXCL10*), growth and differentiation (e.g., *SFRP1*, *TGFA*, *CCNG2*, *CNAP1*, *EGFR*, *NOTCH2*, *NRG1*, *EREG*), and cytoskeleton and cell-cell adhesion (e.g., *TPX2*, *SPOCK1*, *ARHGAP1*, *PAK1*, *WASL*, *DSC2*, *DSG3*) (**Supplementary Fig. 4** and **Supplementary Table 2**). Notably, only 135 (~43%) of these genes were downregulated upon N-CoR2 overexpression while the remaining were upregulated (**Fig. 3c**), including two major components of the intercellular desmosome junctions, desmocollin 2 (*DSC2*) and desmoglein 3 (*DSG3*), which may relate to the tendency of these cells to form clusters in monolayer culture (**Supplementary Fig. 2c**). To explore the possibility that N-CoR2 might regulate different sets of genes upon death induction, we applied a *Differential Regulation Index (DRI)* to compare the transcriptomes of vehicle- and TRAIL-treated T4-2 cells in the presence or absence of N-CoR2 overexpression. A list of 1328 genes was identified and approximately 84% (1121 genes) of them were less TRAIL-inducible (i.e.,  $DRI \leq -1.0$ ) in N-CoR2-overexpressed cells (**Fig. 3c**). Venn diagram analysis revealed that only 166 (12.5 %) of the differentially TRAIL-responsive genes overlapped the 304 N-CoR2 signature genes (**Fig. 3b**), indicating an “induced” repressor function of N-CoR2 in response to death stimuli. Functional profiling of these gene sets according to Gene ontology (GO) biological process categories yielded results demonstrating the pleiotropic effect of N-CoR2 on diverse biological processes (**Fig. 3d** and **Supplementary Fig. 4**). Promoter analysis revealed that, upon death induction, N-CoR2 regulated an additional set of transcriptional pathways and genes (**Supplementary Table 3**), notably including many involved in apoptosis (**Fig. 3d (arrow), e**).

Neither overexpression nor knockdown of N-CoR2 significantly altered the expressions of genes previously known to be associated with MDR, including *p53*, *BCL2*, *MDR1* and *MRP* (data not shown). To understand mechanistically how N-CoR2 confers cells resistance to death stimuli, we focused on a list of 64 genes (**Fig. 3e**) that are related to programmed cell death (PCD) (GO:0012501) from the list of 1328 differentially responsive genes. The majority ( $n = 52$ ) of them were less TRAIL-inducible when N-CoR2 was overexpressed and most possess roles in the induction or regulation of apoptosis (**Supplementary Table 4**). Interestingly, the top-ranked gene in this list is *TNFSF10*, which encodes endogenous TRAIL. *TNFSF10* was transcriptional induced by exogenous TRAIL in the control cells while N-CoR2 overexpression rendered it repressed. Knockdown of TRAIL expression attenuated TRAIL-induced cell death in T4-2 cells (**Supplementary Fig. 5a**), suggesting that autocrine TRAIL was a feedforward circuit for TRAIL-induced cell death. The other highest-ranked gene displaying similar transcriptional responses was *STAT1* (signal transducer and activator of transcription-1), an important mediator of the interferon (INF) signaling<sup>20</sup> (**Supplementary Fig. 5b**). *STAT1*, along with its activator Janus kinase-1 (*JAK1*) and its

binding partner IRF9, lose their TRAIL inducibility upon N-CoR2 overexpression (**Fig. 3f**). In addition, the binding sites of INF regulatory factor 1 (*IRF1*) were found to be significantly enriched in the promoter segments of the 64 PCD genes (**Supplementary Table 2**). The STAT1/IRF1 signaling pathway acts in synergy with death ligands and mediate apoptosis in a caspase 1-, 7- and 8-dependent manner<sup>21-23</sup>, whose transcriptions were all rendered insensitive to TRAIL by N-CoR2 (**Fig. 3e, f**). Importantly, the transcriptional responses of these apoptotic mediators to death induction by TRAIL were restored when the mutant N-CoR2 (K449A) instead of the wild-type protein was overexpressed (**Fig. 3f**), reinforcing the idea that activation of the nuclear deacetylase activities of HDAC3 by N-CoR2 is required for suppression of pro-apoptotic pathways. Notably, although tumor necrosis factor (*TNF*) expression was relatively more inducible by TRAIL in N-CoR2-overexpressing cells than the control cells, its pro-apoptotic activity might be inhibited by the downregulations of caspase-8 (*CASP8*) and interleukin-1 $\alpha$  (*IL1A*) and the upregulation of *TRAF1*, which mediates anti-apoptotic signals from the TNF receptor<sup>24,25</sup>. Except *TRAF1*, several other genes whose expressions after TRAIL treatments were higher in N-CoR2-overexpressing cells also possess anti-apoptotic properties, such as *MYBL2*, *BIRC5* and *BCL2L1* (**Fig. 3e, f** and **Supplementary Table 4**). In aggregate, our results indicate that N-CoR2 may attenuate death induction by concordantly modulating the expressions of multiple apoptotic and anti-apoptotic mediators.

### **N-COR2 and HDAC3 are associated with clinical outcome of breast cancer patients who received adjuvant chemotherapy**

Previously, *in vitro* experiments have shown that N-CoR2 expression was higher in cancer cells resistant to methotrexate (**Supplementary Table 1**), in prostate cancer cells with reduced sensitivity to vitamin D3<sup>26</sup>, and in breast cancer cells resistant to anti-estrogen<sup>27</sup>. As the acetylation/deacetylation status of the target genes of HDACs has been associated with tumor cell sensitivities to cytotoxic agents<sup>28</sup>, we speculate that N-CoR2/HDAC3-mediated death resistance may be usurped by malignant cells to resist cytotoxic chemotherapy and contribute to therapeutic failure and poor outcome. To address this possibility, we analyzed the association between N-CoR2 and HDAC3 expressions and clinical outcome in a 295 breast cancer patients in the Netherlands Cancer Institute database<sup>29</sup>. The Kaplan-Meier curves shows that the patients with higher expression levels of N-CoR2 had significantly higher probability of post-therapeutic disease relapse than those with expression levels in the lower quartile (**Fig. 5**). In comparison, the expression levels of the N-CoR2 paralog N-CoR1 were not associated with clinical outcome (data not shown). Importantly, the associations of N-CoR2 with the probability of disease relapse and mortality were most prominent in patients with lymph node (LN) metastasis and those receiving adjuvant systemic chemotherapy (CT) (**Fig. 5 and supplementary Fig. 6**). In contrast, N-CoR2 expression was not associated with

clinical outcomes in the patients with LN-negative breast carcinomas or those who did not receive CT, implying that locally disseminated tumor cells with higher N-CoR2 expressions may be endowed with selective advantage during treatments.

Similar to N-CoR2, higher expression levels of HDAC3 were significantly associated with higher probability of post-therapeutic disease relapse and mortality in the patients with LN-positive disease and those who had received adjuvant CT (**Supplementary Fig. 7a**). Moreover, tumors that co-expressed high levels of N-CoR2 and HDAC3 had remarkably high probabilities of relapse and mortality and around two-thirds of the patients developed disease progression within 5 years, suggesting a synergistic effect of N-CoR2 and HDAC3 on poor therapeutic outcome of breast cancers (**Supplementary Fig. 7b**).

In the 295 patients with breast cancer, the expression levels of N-CoR2 were significantly associated with age ( $P < 0.05$ ) and the estrogen status ( $P < 0.01$ ) of the tumor, but not with other clinical characteristics or the molecular subtypes of breast cancers (**Supplementary Table 5**)<sup>30</sup>. In a multivariate Cox proportional-hazards analysis, N-CoR2 predicted death or disease relapse independent of the clinical characteristics of breast cancers (**Supplementary Table 6**). Further analysis showed that, in the 110 breast cancer patients who had received adjuvant systemic CT, both N-CoR2 and HDAC3 were independent predictive factors of the risk of mortality, while only N-CoR2 was independently associated with death and relapse ( $P < 0.001$ ). Compared with clinical characteristics and molecular classification of breast cancers, N-CoR2 was the strongest predictor of the likelihood of disease relapse and mortality with hazard ratios of 9.64 ( $P < 0.001$ ) and 5.45 ( $P < 0.001$ ), respectively (**Table 1**). In contrast, in the 185 breast cancer patients who did not received CT, neither N-CoR2 nor HDAC3 transcript expressions predicted disease relapse or death. Instead, the molecular subtype of breast cancers was the strongest prognosis predictor in this subgroup of the patients (**Supplementary Table 7**).

Interestingly, high N-CoR2 and/or HDAC3 expressions were also associated with unfavorable therapeutic outcome in malignant gliomas and ovarian cancers (**Supplementary Fig. 8**)<sup>31,32</sup>, suggesting that N-CoR2/HDAC3-mediated therapeutic resistance mechanisms may be shared by different types of human malignancies.

### **N-CoR2 and its gene expression signature predict chemotherapy-refractory breast cancers**

The finding that N-CoR2 expression was associated with higher rates of tumor relapse and death only in the patients who had received systemic CT raised the possibility that N-CoR2 contributes to poor prognosis of breast cancers by attenuating the sensitivity of breast tumors to CT-related death stimuli. To more directly investigate whether the transcription-regulatory activity of N-CoR2 has independent predictability of chemotherapy response, we analyzed the tumor transcriptome in a cohort of 130 breast cancer patients who

received pre-operative (neoadjuvant) systemic CT, including paclitaxel and fluorouracil-doxorubicin-cyclophosphamide, from the M.D. Anderson Cancer Center database wherein the treatment responses were pathologically defined<sup>33</sup>. Consistent with the role of N-CoR2 in death resistance, tumors with higher N-CoR2 expressions had a modest increase in the odds (2.2-fold) of unresponsiveness to pre-operative CT compared with those with lower expressions (**Table 2**). As N-CoR2 is subjected to complex post-transcriptional regulations and the mRNA expression level of N-CoR2 is not unambiguously linked to its activity<sup>34-37</sup>, we further adopted polygenic measures that might reflect more faithfully the transcription regulatory activity of N-CoR2. We used an unsupervised, hierarchical clustering algorithm to segregate the 130 tumors into two major subgroups based on patterns of expression of the 304 genes whose expressions were significantly altered by N-CoR2 in T4-2 cells (*i.e.*, N-CoR2 associated signature genes) (**Fig. 6a** and **Supplementary Fig. 9**). We next associated the pattern of expression of the N-CoR2 signature genes in T4-2 cells cultured in an *in vivo*-like 3D context (*i.e.*, 3D rBM culture) with clinical tumor transcriptome and developed a similarity algorithm that measured N-CoR2-associated transcriptional activities in breast tumors (**Fig. 6b**) and the 130 tumors were separated into two groups by their N-CoR2 similarity scores ( $S_{NCoR2}$ ). Interestingly, one of the subgroup (subgroup A) identified from hierarchical clustering transcriptomically resembled the tumors with higher  $S_{NCoR2}$  while the other (subgroup B) resembled those with lower scores (data not shown). Importantly, both approaches outperformed N-CoR2 expression level as treatment response predictors and tumors with higher  $S_{NCoR2}$  had a 5-fold odds ratio of unresponsiveness to chemotherapy compared with those with lower  $S_{NCoR2}$ . Moreover, when the expression level and the transcriptional regulatory activity (as represented by  $S_{NCoR2}$ ) of N-CoR2 were both higher, up to 82.9% of such tumors were refractory to neoadjuvant chemotherapy (**Table 2**).

To ask whether N-CoR2 and its associated gene expression signature are indeed independent predictors of chemotherapy responsiveness, the likelihood of unresponsiveness to neoadjuvant CT of the 130 breast cancer patients in the M.D. Anderson Cancer Center database was further analyzed using a logistic regression model including age, tumor size, nuclear grade, LN, ER and HER2 status as predictors. Of all the clinical characteristics, only ER status ( $P = 0.003$ ) and age ( $P = 0.037$ ) are significantly predictors. Patient stratification by hierarchical clustering analysis on the N-CoR2 signature genes was also an independent predictor of the likelihood of unresponsiveness to neoadjuvant CT with an odds ratio of 2.71 ( $P = 0.038$ ) (**Supplementary Table 8**). A similar logistic regression model including  $S_{NCoR2}$  and clinical characteristics shows that  $S_{NCoR2}$  also independently and strongly predicted CT resistance (Odds ratio 3.85;  $P = 0.005$ ) and its predictivity was only next to the ER status of the tumor (**Supplementary Table 9**). Notably, the approach using  $S_{NCoR2}$  predicts resistant tumors with a high specificity (75.6 %) and positive predictive value (84.6 %) and a relatively lower sensitivity (61.8 %) (**Supplementary Table 10**), implying the potential

involvement of other mechanisms that underlies chemotherapy resistance in breast cancers. Taken together, these findings reinforced the idea that N-CoR2 and its transcription-regulatory activity contribute to the drug resistance of breast cancers *in vivo* and demonstrated the usefulness of N-CoR2-associated polygenic determinants of chemotherapy response.

## DISCUSSION

We and others have observed previously that tissue-like organization of immortalized or neoplastic epithelial cells in three dimensions can dramatically alter their responses to death stimuli, which correlate excellently with the cytotoxic sensitivity of malignant tumors *in vivo*<sup>3-5</sup>. In non-neoplastic MECs grown in 3D rBM, this death resistance phenotype is independent of the growth status while requires tissue polarity, ligation of  $\beta$ 4-integrin and subsequent NF $\kappa$ B activation<sup>5</sup>. It should be noted that ECM-dependent tissue polarization is not absolutely indispensable for this death resistance phenotype as neoplastic epithelial cells grown as non-polarized multicellular spheroids are still rendered much less sensitive to cell death inducers compared with those cultured as 2D monolayers. Moreover, apoptotic stimuli such as TRAIL similarly activate NF $\kappa$ B signaling in non-neoplastic MECs no matter when they were cultured as 3D acini or 2D monolayers (data not shown). These findings suggest that the development of death resistance in 3D multicellular structures may involve other pathways that respond to the altered microenvironmental cues in 3D contexts. The substantial transcriptional alterations driven by the third dimension in cell culture implicate that this specific death resistance phenotype is polygenically related and regulated by a higher level of complexity than a single cellular pathway. The identification of N-CoR2 in the present study thus provides a novel and plausible mechanistic explanation for how death resistance developed in organized tissue architectures can be tied to death resistance of differentiated tissues or malignant tumors *in vivo*.

Originally identified as a transcriptional corepressor of unliganded nuclear receptors<sup>10</sup>, N-CoR2 also mediates repression of a wide variety of non-receptor transcriptional factors involved in differentiation, signal transduction and stress response<sup>18,38,39</sup>. The potential role of N-CoR2, but not N-CoR, in cell stress response was strengthened by the recent finding demonstrating that N-CoR2 contributes to cell recovery from IR-induced DNA damage due to its association with the DNA-dependent protein kinase complex in certain types of tumor cells<sup>40</sup>. Our findings also showed that N-CoR2 deficiency rendered MECs sensitive to IR-induced cell death while forced expression of N-CoR2 drove radioresistance. Nevertheless, the clinical relevance of these findings is unclear as there was no significant association between N-CoR2 expression and the risk of tumor recurrence in 248 LN-negative breast cancer patients who received adjuvant radiotherapy (data not shown)<sup>41</sup>. Our results indicate

that, in neoplastic MECs treated with the death ligand TRAIL (which represents a canonical apoptotic mechanism by which chemotherapeutic agents cause cancer cell death), N-CoR2 concordantly modulated the expressions of multiple apoptotic and anti-apoptotic mediators whereby the induction of cellular apoptotic program was attenuated. Although it remains to be established whether N-CoR2 can modulate the expression of different cell death mediators among different cell types or death stimuli, the prominent association between N-CoR2 and responsiveness to combination chemotherapy clearly indicates that N-CoR2 play an essential role in chemotherapy resistance in breast cancers.

Epigenetic changes are increasingly recognized as important sources of cancer-cell heterogeneity<sup>42</sup>. Our results add N-CoR2 to the growing list of epigenetic regulators that are associated with malignant progression in human cancers<sup>6-9</sup>. Notable examples included heterochromatin-associated protein 1 (*HPI*<sup>HS $\alpha$</sup> ), whose expression is inversely correlated with breast tumor cell invasion and metastasis<sup>6</sup>; the polycomb group protein EZH2, which promotes the proliferation and invasion of prostate and breast cancer cells through its interaction with HDAC2<sup>7</sup>; and the chromatin remodeling protein SATB1, which is necessary for breast cancer cells to become metastasis<sup>9</sup>. Importantly, both EZH2 and SATB1 correlate with poor prognosis of breast cancers, suggesting the clinical relevance of these findings. Conceivably, tumor cells can exploit the phenotypic plasticity elicited by epigenetic change-mediated large scale transcriptional alterations to evolve into more advanced malignant states that leads to tumor progression and drug resistance<sup>1</sup>. Previously, the focus in this new paradigm of drug resistance in malignant tumors has been placed on methylation-dependent silencing of individual genes involved in DNA repair and apoptosis, such as *APAF1* and *hMLH1*<sup>43,44</sup>. Our findings provide the first example in which MDR in normal or malignant epithelial tissues is driven by multigene alterations coordinated by an epigenetic mechanism. If epigenetic plasticity is a common strategy used by tumor cells, it is likely that there are other epigenetic regulators of MDR that have yet to be characterized.

Classically defined drug resistance mechanisms, such as the altered expression or functions of *TP53*, *BCL2* or *MDR1*, has only weak association with clinical drug resistance and the acquisition of the MDR phenotypes in malignant tumors *in vivo* is likely polygenically and multifactorially driven<sup>1</sup>. Consistent with this possibility, N-CoR2 does not alter the expressions of *TP53*, *BCL2* or *MDR1* while it attenuates cell death induction by simultaneously modulates the expression of multiple mediators in the apoptotic program.

The link between N-CoR2 expression and its associated gene expression signature in primary breast tumors and therapeutic outcome implies that the resistant phenotype is at least in part acquired at early stages of tumor development and is epigenetically pre-determined



prior to therapy. The gene expression signature associated with N-CoR2 reflects the patterns of dysregulation in the N-CoR2/HDAC3 pathway in breast tumor cells prior to chemotherapy, which conceivably can be used to predict the sensitivity to therapeutic agents that target this pathway. This multigene approach may show particular promise in the prediction of response to HDAC inhibitors or agents that target similar epigenetic pathways. Moreover, the finding that N-CoR2/HDAC3-mediated death resistance may be reversed by pharmacological or genetic means raises the possibility of targeting N-CoR2 and/or HDAC3 in the treatment of resistant breast cancers. Except intrinsic drug resistance, the strong MDR phenotype elicited by the N-CoR2/HDAC3 pathway also raises the possibility that tumors with higher N-CoR2 levels/activities may be endowed with selective advantage during treatments. It will be important to compare among recurrent breast tumors the expression and the activity of N-CoR2/HDAC3 in order to determine whether this epigenetic pathway also contributes to acquired resistance to chemotherapy.

## **METHODS**

### **Cell culture**

Human mammary HMT-3522 epithelial cells, including non-neoplastic S1 and neoplastic T4-2 cells, were propagated as monolayers on plastic surface in chemically defined medium and embedded in rBM (Matrigel, BD Biosciences) as described<sup>45, 46</sup>. Phenotypic reversion of T4-2 cells was performed using tyrphostin AG 1478 as described. The three-dimensional (3D) cultures were grown for 12 days before image or biochemical analysis. Monolayer cultures were performed on plastic surface coated with thin-layered rBM (1:100 Matrigel in PBS). To re-propagate S1 cells from rBM-embedded acini into monolayers (*i.e.*, 3D to 2D), the 3D cultures were dissociated with dispase (BD Biosciences) at 37°C for 2 h and the acini were recovered and trypsinized into single cells, which were then plated on Matrigel-coated plastic surface. MDA-MB-231 cells were grown as monolayers in DMEM supplemented with 10% fetal bovine serum and antibiotics.

For the culture of cells in 3D collagen (**Supplementary Fig. 1f**), S1 cells were embedded in type I collagen (2.0 mg/mL) (Inamed) and, after polymerization, the gel was released from the culture dish as described<sup>46</sup>. The culture was maintained for 12 days before biochemical analysis.

### **Induction and analysis of cell death**

Apoptotic cell death was initiated by treatment with recombinant, purified human TRAIL peptides or Paclitaxel as described<sup>5</sup>. DNA damage-induced cell death was initiated by IR using a Mark I Cesium 137 irradiator (JL Shepherd & Associates) located in Department of Radiation Oncology at University of Pennsylvania. Percent cell death induced by TRAIL or Paclitaxel was quantified using detection of active caspase 3 (Cell Signaling) by indirect

immunofluorescence. Percent cell death induced by IR was quantified using Live/Dead Viability/Cytotoxicity Assay (Molecular Probes). For both methods, cells were counterstained with 4',6-diamidino-2-phenylindole (DAPI) to label cell nuclei present at different focal planes in the 3D architectures. For the 3D clonogenic assay (**Supplementary Fig. 2e**), T4-2 cells were seeded as single cells on top of rBM for 3 hours and then treated with IR (9 Gy). The size of the resultant 3D colony was determined by measuring the maximal diameter of the structure under light microscopy at indicated time points following irradiation.

### Gene expression manipulations

Stable knockdown of N-CoR2 or HDAC3 was achieved by a retrovirus-mediated RNAi system using oligonucleotide sequences previously described (detailed methods are in **Supplementary Methods** online)<sup>47</sup>. The retroviral construct inducibly expressing HA- and EGFP-epitope tagged N-CoR2 was prepared by subcloning murine *NCOR2* cDNA (e isoform, NCBI RefSeq #NM\_011424) into pBluescriptII KS+ (Stratagene) and then recloned into pLZRS-MFG-*tet*-EGFP to generate the final expression construct pLZRS-MFG-*tet*-HA-EGFP-NCOR2. The mutant N-CoR2 (K449A) was constructed using the QuickChange Site-Directed Mutagenesis kit (Stratagene). Cells were spin infected with retrovirus carrying N-CoR2 constructs, followed by infection with a high titer MFG virus expressing the tetracycline-controlled transcriptional transactivator. The transduced cells were sorted for EGFP positive cells and the sorted cell were expanded in the presence of tetracycline until 2-3 days before the experiments. Cells expressing various shRNA constructs were generated by the same procedure without subsequent transduction with the tetracycline-controlled transactivator.

### Microarray experiments

To increase the yield of RNA for transcript profiling experiments, we grew  $2 \times 10^5$  cells T4-2 on top of rBM in a 60-mm tissue culture dish. Four replicate cultures were established for each of the 4 experiment groups, including those using T4-2 cells that stably expressed N-CoR2 (T4-2 N-CoR2 cells), T4-2 cells expressing the empty vector (T4-2 vector cells), TRAIL-treated T4-2 N-CoR2 cells, and TRAIL-treated T4-2 vector cells, designated as “V”, “N”, “VT” and “NT”, respectively. The cultures were maintained for 6 days and then treated with TRAIL (1  $\mu$ g/mL) (for groups VT and NT) or vehicles (for groups V and N) for 4 hours before the collection of RNA samples. To allow the study of gene expressions independent of cell death, the cells were pretreated with caspase inhibitors 2 hours before and throughout the TRAIL treatments to block apoptosis.

Gene expression analysis was performed on an Affymetrix Human Genome U133A 2.0 GeneChip platform containing 22,283 probes according to the manufacturer's protocol (Affymetrix) (**Supplementary Methods**). Affymetrix .cel files (probe intensity files) were

processed with ArrayAssist Lite (v3.4, Stratagene). The files were imported and processed with the GC-RMA algorithm to yield probe set intensities and additionally, Affymetrix Preset, Absent, Marginal flags were computed. These values were exported in .chp files, which were subsequently imported into the Partek Genomics Suite software (v6.2, Partek). The genes were filtered based on the Affymetrix P/A/M flags to retain only those genes that were present in at least 2 of the 16 samples. The gene expression data have been deposited in NCBI's Gene Expression Omnibus (GEO, <http://www.ncbi.nlm.nih.gov/geo/>) and are accessible through GEO Series accession number GSE8346.

### **Bioinformatical analysis**

To select genes that are differentially induced or repressed upon overexpression of N-CoR2 with or without death induction by TRAIL treatments, the GC-RMA expression values of all the 16 transcriptomes were log<sub>2</sub> transformed and a two way ANOVA was calculated, yielding 3 *P* values for each gene: the first for a gene's significant difference in response to the contents of the vector (*i.e.*, N-CoR2 versus vector), the second for a difference in response to treatment (*i.e.*, TRAIL versus vehicle) and the third for a gene's differential response to treatment depending on the contents of the vector. Additional pairwise contrasts were performed for each of the 4 pairs of conditions, yielding both *P* values and fold changes between the mean expression values of different conditions. The difference between TRAIL-induced changes in gene expression levels of T4-2 N-CoR2 cells and T4-2 vector cells was measured by using the equation " $\log_2(NT/N) - \log_2(VT/V)$ ", which was designated as a *differential regulation index (DRI)*. A filtering criterion ( $P < 0.05$  by two-way ANOVA,  $DRI \geq 1.0$  or  $\leq -1.0$ ) was used to select genes that were differentially responsive to TRAIL compared between T4-2 N-CoR2 and T4-2 vector cells.

We used oPOSSUM (<http://www.cisreg.ca/cgi-bin/oPOSSUM/opossum>) to search for enriched transcriptional factor binding sites in the promoter regions of different sets of genes identified from transcript profiling experiments<sup>48</sup>. Gene ontology (GO)-based functional classification of the identified genes was performed systematically by OntoExpress (<http://vortex.cs.wayne.edu/ontoexpress/>) (**Supplementary Methods**)<sup>49</sup>.

### **Data mining into the gene expression profiles of clinical cancer specimens**

Tumor transcriptome data sets used for therapeutic outcome and survival analysis were reported previously and obtained from respective sources (**Supplementary Methods**)<sup>29-33</sup>. The probability of remaining relapse-free or overall survival was computed using the method of Kaplan and Meier. The curves were plotted and compared using the log-rank test with the software packages SPSS 10.0 (SPSS) and GraphPad Prism 3.02 (GraphPad Software). The log-rank test was used to calculate the *P* values.

### **Hierarchical clustering analysis and construction of the SMRT-similarity score**

The 304 signature genes (represented by 350 Affymetrix probe sets) of N-CoR2 were identified from the microarray experiments described earlier based on their expression levels (on a  $\log_2$  base) significantly different (fold change  $\geq 2$  and a cutoff  $P$ -value  $< 0.05$  by Student's  $t$  test) between T4-2 vector cells and T4-2 N-CoR2 cells. We median-centered the genes and carried out average linkage clustering using the Cluster and TreeView software<sup>50</sup> and the tumors were segregated into two predominant classes based on the first bifurcation in the dendrogram (**Supplementary Fig. 8**).

The degree of resemblance between the average expression levels (on a  $\log_2$  scale) of the 304 N-CoR2 signature genes (350 probe sets) in T4-2 vector cells or T4-2 N-CoR2 cells and the levels of the corresponding genes in the tumor transcriptome data sets were measured using Spearman's rank correlation ( $\rho$ ). We determined the relative similarities of the expression profiles of the 350 probe sets in tumors with those in T4-2 N-CoR2 cells and T4-2 vectors cells, respectively, by comparing their Spearman's  $\rho$ , which was designated as a "N-CoR2 similarity score ( $S_{NCOR2}$ )",

$$S_{NCOR2} = \rho_{NCOR2}^2 \times \rho_{vector}^{-2}$$

where  $\rho_{NCOR2}$  represents the Spearman's correlation coefficient between the expression profile of the 350 probe sets in a given tumor sample and those in T4-2 N-CoR2 cells, and  $\rho_{vector}$  is the coefficient between those in the tumor and in T4-2 vector cells. For therapeutic response analysis the 130 breast tumors were separated into two groups according to the median value of  $S_{NCOR2}$  across all tumors. Tumors with higher  $S_{NCOR2}$  are considered to have higher N-CoR2 associated transcriptional activities.

## References

1. Glasspool, R.M., Teodoridis, J.M. & Brown, R. Epigenetics as a mechanism driving polygenic clinical drug resistance. *Br. J. Cancer* **94**, 1087-1092 (2006).
2. Kobayashi, H. *et al.* Acquired multicellular-mediated resistance to alkylating agents in cancer. *Proc. Natl. Acad. Sci. U.S.A.* **90**, 3294-3298 (1993).
3. Desoize, B. & Jardillier, J.C. Multicellular resistance: a paradigm for clinical resistance? *Crit. Rev. Oncol. Hematol.* **36**, 193-207 (2000).
4. Vescio, R.A. *et al.* *In vivo*-like drug responses of human tumors grown in three-dimensional gel-supported primary culture. *Proc. Natl. Acad. Sci. U.S.A.* **84**, 5029-5033 (1987).
5. Weaver, V.M. *et al.*  $\beta$ 4-integrin-dependent formation of polarized three-dimensional architectures confers resistance to apoptosis in normal and malignant mammary epithelium. *Cancer Cell* **2**, 205-216 (2002).
6. Kirschmann, D.A. *et al.* Down-regulation of HP1HS $\alpha$  expression is associate with the metastatic phenotype in breast cancer. *Cancer Res.* **60**, 3359-3363 (2000).
7. Varambally, S. *et al.* The polycomb group protein EZH2 is involved in progression of prostate cancer. *Nature* **419**, 624-629 (2002).
8. Glinsky G.V., Berezovska, O. & Glinskii, A.B. Microarray analysis identifies a death-from-cancer signature predicting therapy failure in patients with multiple types of cancer. *J. Clin. Invest.* **115**, 1503-1521 (2005).
9. Han, H.J., Russo, J, Kohwi, Y. & Kohwi-Shigematsu, T. SATB1 reprogrammes gene expression to promote breast tumour growth and metastasis. *Nature* **452**, 187-193 (2008).
10. Chen, J.D. & Evans, R.M. A transcriptional co-repressor that interacts with nuclear hormone receptors. *Nature* **377**, 454-457 (1995).
11. Privalsky, M.L. The role of corepressors in transcriptional regulation by nuclear hormone receptors. *Annu. Rev. Physiol.* **66**, 315-360 (2004).
12. Lelièvre, S.A. *et al.* Tissue phenotype depends on reciprocal interactions between the extracellular matrix and the structural organization of the nucleus. *Proc. Natl. Acad. Sci. U.S.A.* **95**, 14711-14716 (1998).
13. Plachot, C. & Lelièvre, S.A. DNA methylation control of tissue polarity and cellular differentiation in the mammary epithelium. *Exp. Cell Res.* **298**, 122-132 (2004).
14. Ishizuka, T. & Lazar, M.A. The N-CoR/histone deacetylase 3 complex is required for repression by thyroid hormone receptor. *Mol. Cell. Biol.* **23**, 5122-5131 (2003).
15. Codina, A. *et al.* Structural insights into the interaction and activation of histone deacetylase 3 by nuclear receptor corepressor. *Proc. Natl. Acad. Sci. U.S.A.* **102**, 6009-6014 (2005).
16. Johnstone, R.W. Histone-deacetylase inhibitors: novel drugs for the treatment of cancer. *Nat. Rev. Drug Discov.* **1**, 287-299 (2002).
17. Song, L. *et al.* Alteration of SMRT tumor suppressor function in transformed non-Hodgkin lymphomas. *Cancer Res.* **65**, 4554-4561 (2005).
18. Jepsen, K. & Rosenfeld, M.G. Biological roles and mechanistic actions of co-repressor complexes. *J. Cell Sci.* **115**, 689-698 (2002).
19. Karagianni, P. & Wong, J. HDAC3: taking the SMRT-N-CoRrect road to repression. *Oncogene* **26**, 5439-5449 (2007).
20. Aaronson, D.S. & Horvath, C.M. A road map for those who don't know JAK-STAT. *Science* **296**, 1653 (2002).
21. Sironi, J.J. & Ouchi, T. STAT1-induced apoptosis is mediated by caspases 2,3, and 7. *J. Biol. Chem.* **279**, 4066-4074 (2004).

22. Tamura, T. *et al.* An IRF-1-dependent pathway of DNA damage-induced apoptosis in mitogen-activated T lymphocytes. *Nature* **376**, 596-599 (2002).
23. Bouker, K.B. *et al.* Interferon regulatory factor-1 (IRF-1) exhibits tumor suppressor activities in breast cancer associated with caspase activation and induction of apoptosis. *Carcinogenesis* **26**, 1527-1535 (2005).
24. Janes, K.A. *et al.* A systems model of signaling identifies a molecular basis set for cytokine-induced apoptosis. *Science* **310**, 1646-1653 (2005).
25. Chen, G. & Goeddel, D.V. TNF-R1 signaling: a beautiful pathway. *Science* **296**, 1634-1635 (2002).
26. Khanim, F.L. *et al.* Altered SMRT levels disrupt vitamin D3 receptor signaling in prostate cancer cells. *Oncogene* **23**, 6712-6725 (2004).
27. Sarvilinna, N., Eronen, H., Miettinen, S., Vienonen, A. & Ylikomi, T. Steroid hormone receptors and coregulators in endocrine-resistant and estrogen-independent breast cancer cells. *Int. J. Cancer* **118**, 832-840 (2006).
28. Castro-Galache, M.D. *et al.* Susceptibility of multidrug resistance tumor cells to apoptosis induction by histone deacetylase inhibitors. *Int. J. Cancer* **104**, 579-586 (2003).
29. Van de Vijver, M.J. *et al.* A gene-expression signature as a predictor of survival in breast cancer. *N. Engl. J. Med.* **347**, 1999-2009 (2002).
30. Sørli, T. *et al.* Gene expression patterns of breast carcinomas distinguish tumor subclasses with clinical implications. *Proc. Natl. Acad. Sci. U.S.A.* **98**, 10869-10874 (2001).
31. Nutt, C.L. *et al.* Gene expression-based classification of malignant gliomas correlates better with survival than histological classification. *Cancer Res.* **63**, 1602-1607 (2003).
32. Spentzos, D. *et al.* Gene expression signature with independent prognostic significance in epithelial ovarian cancer. *J. Clin. Oncol.* **22**, 4700-4710 (2004).
33. Hess, K.R. *et al.* Pharmacogenomic predictor of sensitivity to preoperative chemotherapy with paclitaxel and fluorouracil, doxorubicin, and cyclophosphamide in breast cancer. *J. Clin. Oncol.* **24**, 4236-4244 (2006).
34. Zhang, J., Guenther, M.G., Carthew, R.W. & Lazar, M.A. Proteasomal regulation of nuclear receptor corepressor-mediated repression. *Gene Dev.* **12**, 1775-1780 (1998).
35. Hong, S.H. & Privalsky, M.L. The SMRT corepressor is regulated by a MEK-1 kinase pathway: inhibition of corepressor function is associated with SMRT phosphorylation and nuclear export. *Mol. Cell. Biol.* **20**, 6612-6625 (2000).
36. Hoberg, J.E., Yeung, F. & Mayo, M.W. SMRT derepression by the I $\kappa$ B kinase  $\alpha$ : a prerequisite to NF- $\kappa$ B transcription and survival. *Mol. Cell* **16**, 245-255 (2004).
37. Fernandez-Majada, V. *et al.* Nuclear IKK activity leads to dysregulated Notch-dependent gene expression in colorectal cancer. *Proc. Natl. Acad. Sci. U.S.A.* **104**, 276-281 (2007).
38. Lee, S.K., Kim, J.H., Lee, Y.C., Cheong, J. & Lee J.W. Silencing mediator of retinoic acid and thyroid hormone receptors, as a novel transcriptional corepressor molecule of activating protein-1, nuclear factor- $\kappa$ B, and serum response factor. *J. Biol. Chem.* **275**, 12470-12474 (2000).
39. Zhang, J., Kalkum, M., Chait, B.T. & Roeder, R.G. The N-CoR-HDAC3 nuclear receptor corepressor complex inhibits the JNK pathway through the integral subunit GPS2. *Cell* **9**, 611-623 (2002).
40. Yu, J., Palmer, C., Alenghat, T, Li, Y., Kao, G. & Lazar, M.A. The corepressor silencing mediator for retinoid acid and thyroid hormone receptor facilitates cellular recovery from DNA double-strand breaks. *Cancer Res.* **66**, 9316-9322 (2006).
41. Wang, Y. *et al.* Gene-expression profiles to predict distant metastasis of

- lymph-node-negative primary breast cancer. *Lancet* **365**, 671-679 (2005).
42. Feinberg, A.P., Ohlsson, R. & Henikoff, S. The epigenetic progenitor origin of human cancer. *Nat. Rev. Genet.* **7**, 21-33 (2006).
  43. Soengas, M.S. *et al.* Inactivation of the apoptotic effector *Apaf-1* in malignant melanoma. *Nature* **409**, 207-211 (2001).
  44. Gifford, G., Paul, J., Vasey, P.A., Kaye, S.B. & Brown, R. The Acquisition of hMLH1 Methylation in Plasma DNA after Chemotherapy Predicts Poor Survival for Ovarian Cancer Patients. *Clin. Cancer Res.* **10**, 4420-4426 (2004).
  45. Weaver, V.M. *et al.* Reversion of the malignant phenotype of human breast cells in three-dimensional culture and in vivo by integrin blocking antibodies. *J. Cell Biol.* **137**, 231-245 (1997).
  46. Johnson, K.R., Leight, J.L. & Weaver, V.M. Demystifying the effects of a three-dimensional microenvironment in tissue morphogenesis. *Method. Cell Biol.* **83**, 547-583 (2007).
  47. Ishizuka, T. & Lazar, M.A. The N-CoR/histone deacetylase 3 complex is required for repression by thyroid hormone receptor. *Mol. Cell. Biol.* **23**, 5122-5131 (2003).
  48. Ho Sui, S.J. *et al.* oPOSSUM: identification of over-represented transcription factor binding sites in co-expressed genes. *Nucleic Acids Res.* **33**, 3154-3164 (2005).
  49. Draghici, S., Khatri, P., Martins, R.P., Ostermeier, G.C. & Krawetz, S.A. Global functional profiling of gene expression. *Genomics* **81**, 98-104 (2003).
  50. Eisen, M.B., Spellman, P.T., Brown, P.O. & Botstein, D. Cluster analysis and display of genome-wide expression patterns. *Proc. Natl. Acad. Sci. U.S.A.* **95**, 14863-14868 (1998).

## Acknowledgments

We thank R. Bernards (Netherlands Cancer Institute) for providing us the clinical characteristics of the patients in the Netherlands Cancer Institute database, L. Pusztai (University of Texas M.D. Anderson Cancer Center) for the clinical data, M.J. Bissell (Lawrence Berkeley National Laboratory) and Z. Werb (University of California, San Francisco) for helpful advice and discussions. This research was supported by US Department of Defense (DOD) grant BCRP W81XWH-05-1-330 (to V.M.W.) and National Institute of Health (NIH) grant CA078731 (to V.M.W.).

## Legends

**Figure 1** Identification of N-CoR2 as a tissue-architecture-dependent death regulator. **(a)** Schematic representation of the 2D monolayer and 3D rBM culture models of S1 cells. **(b)** Western blot analysis of acetylated histones H4 and H3 and the methyl binding protein MeCP2 in S1 monolayers (2D) and acini (3D). **(c)** Death sensitivities of S1 monolayers or acini treated with TRAIL (upper panel) or IR (lower panel) with or without TSA pre-treatment. \* $P < 0.05$ , compared with 2D. **(d)** RT-PCR measurements of mRNA expression levels of the N-CoR2 protein complex components in S1 monolayers and acini. \* $P < 0.05$ , compared with 2D. **(e)** Protein abundancy of N-CoR2, GPS2 and E-cadherin (E-cad) in S1 monolayers and acini. **(f)** N-CoR2 protein abundancy of S1 cells expressing a dominant

negative E-cad mutant (dnEcad) (**Supplementary Fig. 1**) in 3D rBM culture and those expressing a control vector maintained as monolayers (2D), 3D polarized acini, monolayers re-propagated from 3D acini (3D to 2D) and 3D spheroids in collagen I gel (col). **(g)** Effect of N-CoR2 knockdown in S1 cells and their death sensitivities to TRAIL, Paclitaxel or IR when organized into 3D architectures. \* $P < 0.05$ , compared with control siRNA. Data are mean  $\pm$  SEM of triplicate experiments in (c), (d) and (g).

**Figure 2** N-CoR2-mediated death resistance can override architecture-dependency and is HDAC3-dependent in neoplastic epithelial cells. **(a)** Phase-contrast images and N-CoR2 protein expression of T4-2 cells cultured as 2D monolayers, 3D disorganized and reverted (rev) acinus-like architectures. *Bar*, 100  $\mu$ m. **(b)** Death sensitivities of T4-2 cells with N-CoR2 knockdown or the control cells to TRAIL (1.0  $\mu$ g/mL) or Paclitaxel (20  $\mu$ M) in different culture models as in (a).  $P < 0.05$ , compared with control RNAi in 2D\* or 3D<sup>†</sup>. **(c,d)** N-CoR2 protein abundancy (c) and the sensitivities of N-CoR2-overexpressing T4-2 cells or MDA-MB-231 cells to TRAIL-, Paclitaxel- or IR (12 Gy)-induced death (d) when cells were cultured as 3D multicellular aggregates, single cells or monolayers. Insets are schematic representations of different culture models. **(e)** Effect of IR on the size of the multicellular structures (colonies) formed by N-CoR2-overexpressing T4-2 cells or the control cells in 3D rBM cultures. **(f)** Effect of HDAC3 knockdown and the death sensitivities of N-CoR2-overexpressing T4-2 cells with HDAC3 knockdown to TRAIL. **(g)** Death sensitivities of T4-2 cells overexpressing N-CoR2, N-CoR2 (K449A) or the control vector to TRAIL. Data are mean  $\pm$  SEM of triplicate experiments; \* $P < 0.05$ , compared with vector in (d) to (g).

**Figure 3** Pleiotropic transcription regulatory effects of N-CoR2 identify the mechanisms of death resistance. **(a)** Schematic representation of the transcript profiling experiments, which permitted pairwise comparisons between the gene expressions of T4-2 N-CoR2 (N) and T4-2 vector (V) cells without or with TRAIL treatments (NT and VT). **(b)** Venn diagram showing the genes that were up- or down-regulated (N-CoR2 signature genes,  $n = 304$ ) or differentially responsive to TRAIL upon N-CoR2 overexpression (N-CoR2 & TRAIL,  $n = 1328$ ). **(c)** Distributions of differential gene expressions in gene sets shown in (B). **(d)** Functional gene classes identified from the list of genes that were differentially or less responsive to TRAIL upon N-CoR2 overexpression. The bar graphs represent the numbers of genes corresponding to each GO biological process category ( $P < 0.05$ ). **(e)** Expression patterns of the 64 PCD genes (76 probe sets) ranked according to *DRI*. The fold changes in the mean expression levels of each gene (on a  $\log_2$  scale) are plotted for visualization of their differential responses to TRAIL. **(f)** Fold changes in the mRNA expression levels of selected PCD genes comparing between TRAIL- and vehicle-treated T4-2 cells expressing N-CoR2,



N-CoR2 (K449A) or the empty vector as quantified by RT-PCR. \* $P < 0.05$ , TRAIL- versus vehicle-treated cells.

**Figure 4. #**

**Figure 5** Association between N-CoR2 transcript expression and clinical outcome of breast cancer. The probability of remaining relapse-free or survive as a function of time since diagnosis among 295 breast cancer patients, patients with LN-positive disease ( $n = 144$ ) or those who received adjuvant CT ( $n = 110$ ) in the Netherlands Cancer Institute database. The patients in each group were grouped into quartiles according to the expression levels of N-CoR2.  $P$  values were determined using the log-rank test.

**Figure 6** N-CoR2-associated gene signature divides breast cancer patients into prognostic groups. (a) Hierarchical clustering of the 130 breast tumors in the M.D. Anderson Cancer Center database using the 304 signature genes of N-CoR2. A dendrogram shown at the top segregated the tumors into subgroups A and B, with tumors from responders (R) or non-responders (NR) denoted. (b) A scatter plot showing the distribution of SNCOR2 of the 130 breast tumors, with the median value (red line) denoted.  $\rho$ , Spearman's rank correlation coefficient.

## Legends

**Figure 1** Identification of N-CoR2 as a tissue-organization-dependent death regulator. (a) Hierarchical clustering of genes differentially expressed between S1 cells cultured as monolayers (2D) and organized acini (3D) formed in rBM. Colorgram depicts high (red) and low (green) relative level of gene expression. (b) Western blot analysis of acetylated histones H4 and H3 and the methyl binding protein MeCP2 in S1 monolayers and acini. (c) Death sensitivities of S1 monolayers or acini treated with TRAIL or IR with or without TSA pre-treatment. \* $P < 0.05$ , compared with 2D. (d) RT-PCR measurements of mRNA expression levels of the N-CoR2 protein complex components in S1 monolayers and acini. \* $P < 0.05$ , compared with 2D. (e) Protein abundance of N-CoR2, GPS2 and E-cadherin (E-cad) in S1 monolayers and acini. \* $P < 0.05$ , compared with 2D. (f) Effect of N-CoR2 knockdown in S1 cells and their death sensitivities to TRAIL, Paclitaxel or IR when organized into 3D acini. \* $P < 0.05$ , compared with control siRNA. Data are mean  $\pm$  SEM of triplicate experiments in (c) to (f).

**Figure 2** Correlation of N-CoR2-mediated death resistance with tissue organization and clinical outcome of breast cancer. (a) N-CoR2 protein abundance of S1 cells expressing a dominant negative E-cad mutant (dnEcad) (**Supplementary Fig. 1**) in 3D rBM culture and those expressing a control vector maintained as 3D polarized acini, 2D monolayers and 3D spheroids in collagen I gel (col). (b) #Insert the result of death assay here#. (c) Association between N-CoR2 transcript expression and clinical outcome of breast cancer. The probability of remaining relapse-free (upper panel) or survive (lower panel) as a function of time since diagnosis among 110 breast cancer patients who received adjuvant CT ( $n = 110$ ). The patients were grouped into quartiles according to the expression levels of N-CoR2. (d) Phase-contrast images and N-CoR2 protein expression of T4-2 cells cultured as 2D monolayers, 3D disorganized and reverted (rev) acinus-like architectures. Bar, 100  $\mu\text{m}$ . (e) Death sensitivities of T4-2 cells with N-CoR2 knockdown (RNAi) or the control cells to TRAIL (1.0  $\mu\text{g/mL}$ ) or Paclitaxel (20  $\mu\text{M}$ ) in different culture models as in (d).  $P < 0.05$ , compared with control RNAi in 2D\* or 3D<sup>†</sup>. (f) N-CoR2 protein abundance and the sensitivities of N-CoR2-overexpressing T4-2 cells to TRAIL-, Paclitaxel- or IR (12 Gy)-induced death when cells were cultured as 3D multicellular aggregates (g) The sensitivities of N-CoR2-overexpressing T4-2 cells or MDA-MB-231 cells to TRAIL-induced death when cells were embedded as single cells in rBM or cultured as monolayers.

**Figure 3** N-CoR2-mediated death resistance is HDAC3 dependent. (a) Effect of HDAC3 knockdown and the death sensitivities of N-CoR2-overexpressing T4-2 cells

with HDAC3 knockdown to TRAIL. (b) HDAC activity of N-CoR2 and N-CoR2 (K449A) protein complexes immunoprecipitated from the nuclear extracts (Supplementary Fig. 3).  $P < 0.05$ , compared with vector\* or N-CoR2<sup>†</sup>. (c) Death sensitivities of T4-2 cells overexpressing N-CoR2, N-CoR2 (K449A) or the control vector to TRAIL. Data are mean  $\pm$  SEM of triplicate experiments; \* $P < 0.05$ , compared with vector.

**Figure 4** Pleiotropic transcription regulatory effects of N-CoR2 identify the mechanisms of death resistance. (a) Schematic representation of the transcript profiling experiments, which permitted pairwise comparisons between the gene expressions of T4-2 N-CoR2 and T4-2 vector cells without or with TRAIL treatments. (b) Venn diagram showing the genes differentially expressed between T4-2 N-CoR2 and vector control cells (N-CoR2 signature genes,  $n = 304$ ) or differentially responsive to TRAIL upon N-CoR2 overexpression (N-CoR2 & TRAIL,  $n = 1328$ ). (c) Distributions of differential gene expressions in gene sets shown in (b). (d) Functional gene classes identified from the list of genes that were differentially or less responsive to TRAIL upon N-CoR2 overexpression. The bar graphs represent the numbers of genes corresponding to each GO biological process category ( $P < 0.05$ ). (e) Expression patterns of the 64 PCD genes (76 probe sets) ranked according to *DRI*. The fold changes in the mean expression levels of each gene (on a  $\log_2$  scale) are plotted for visualization of their differential responses to TRAIL. (f) Fold changes in the mRNA expression levels of selected PCD genes comparing between TRAIL- and vehicle-treated T4-2 cells expressing N-CoR2, N-CoR2 (K449A) or the empty vector as quantified by RT-PCR. \* $P < 0.05$ , TRAIL- versus vehicle-treated cells.

**Figure 5** N-CoR2-associated transcript signature predicts responsiveness to neoadjuvant chemotherapy in breast cancer patients. (a) Hierarchical clustering of the 130 breast tumors in the M.D. Anderson Cancer Center database using the 304 signature genes of N-CoR2. A dendrogram shown at the left segregated the tumors into subgroups A and B, with tumors from responders (R) or non-responders (NR) denoted. (b) A scatter plot showing the distribution of *SNCOR2* of the 130 breast tumors, with the median value (red line) denoted.  $\rho$ , Spearman's rank correlation coefficient. (c) Odds ratios (OR) for unresponsiveness to adjuvant CT according to the expression levels of N-CoR2, the average linkage clustering (ALC),  $S_{NCoR2}$  or a combination of N-CoR2 and  $S_{NCoR2}$ . CI denotes 95% confidence interval.  $P$  values were calculated with use of Fisher's exact test.

Fig. 1

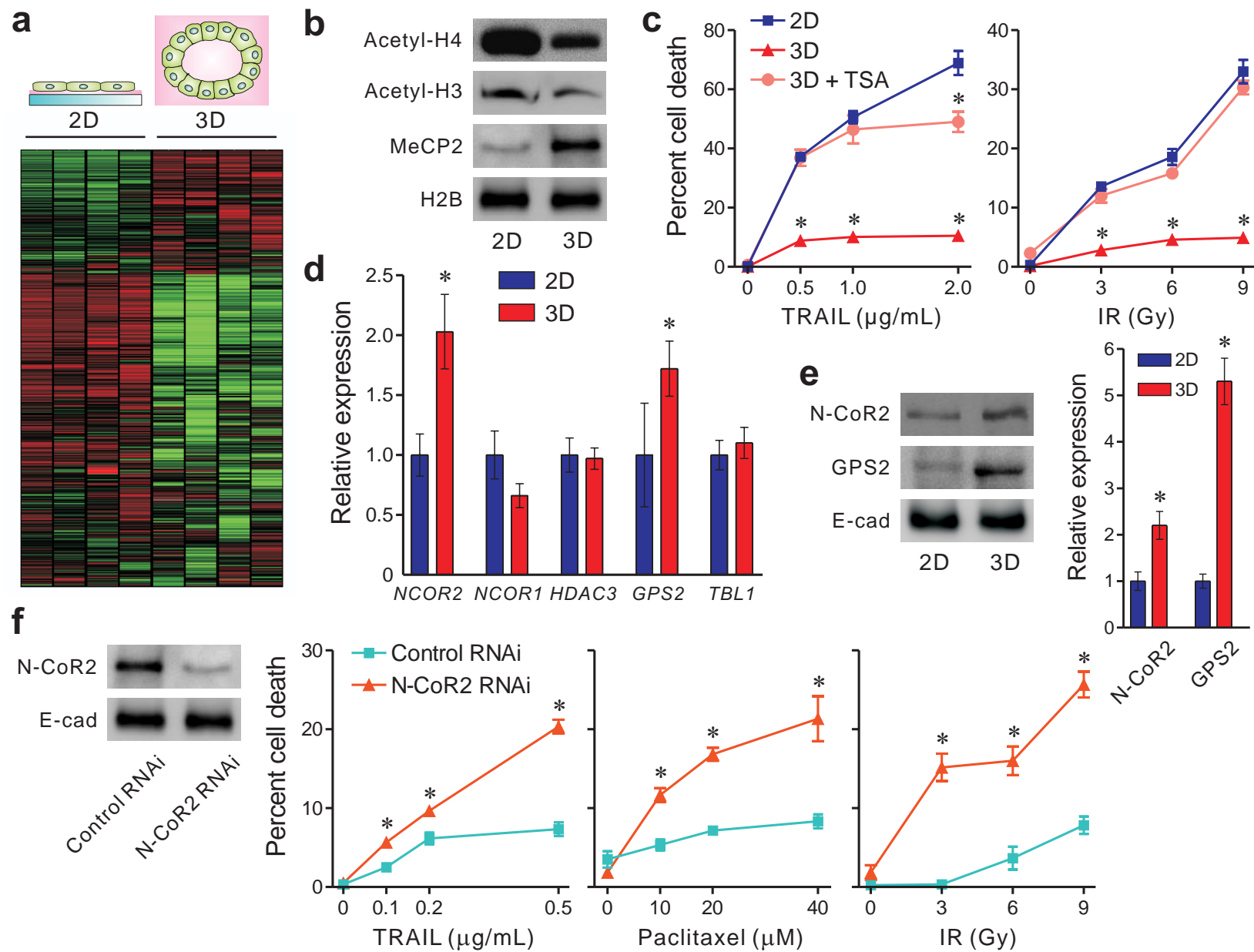


Fig. 2

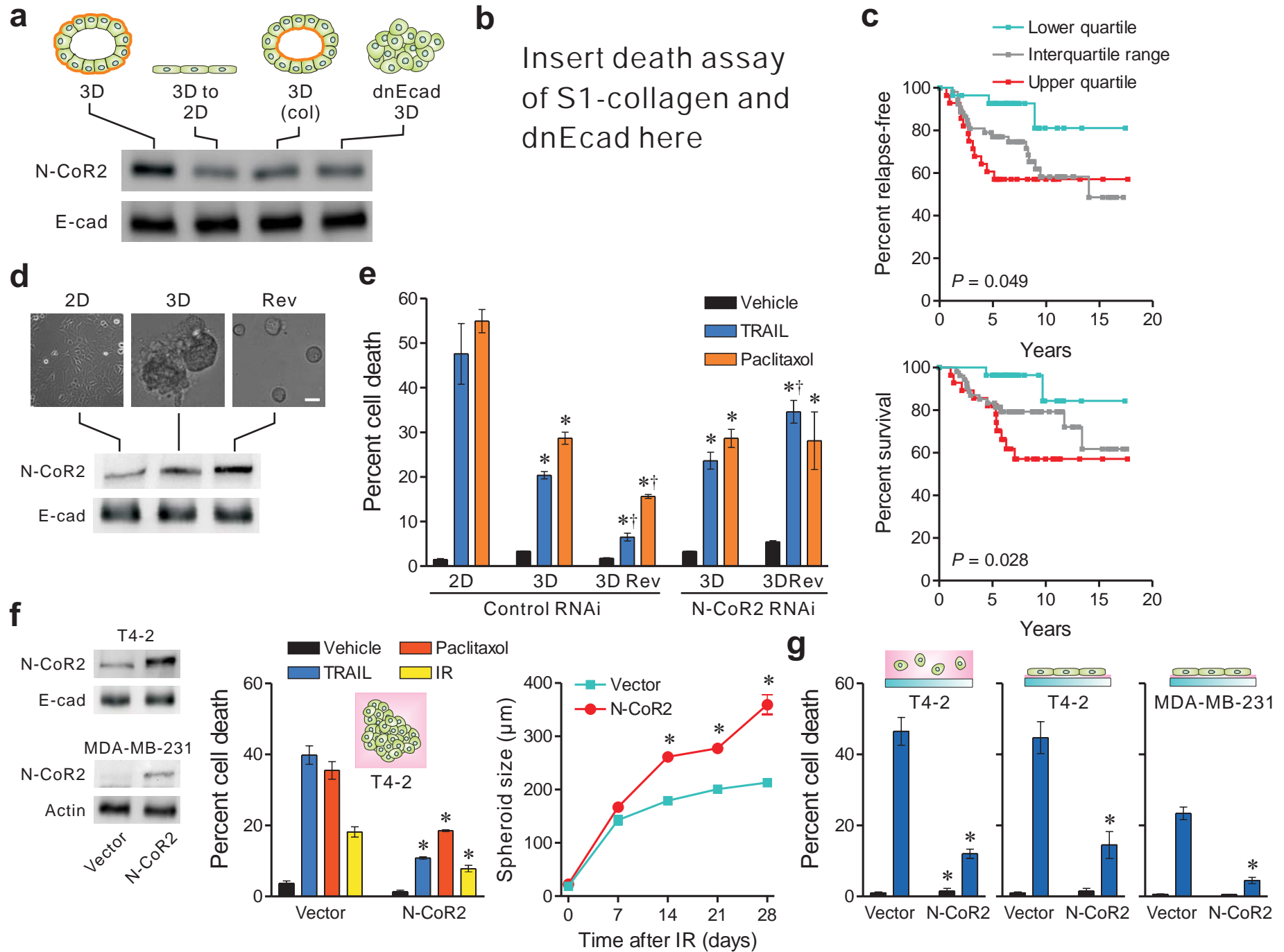


Fig. 3

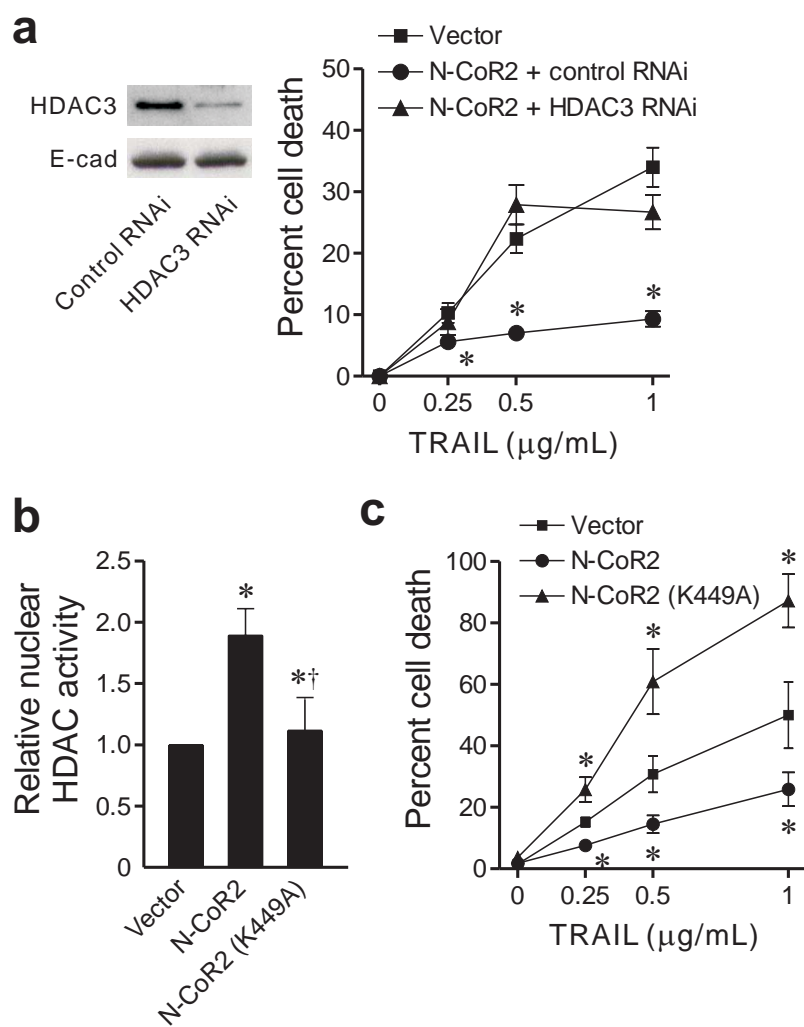


Fig. 4

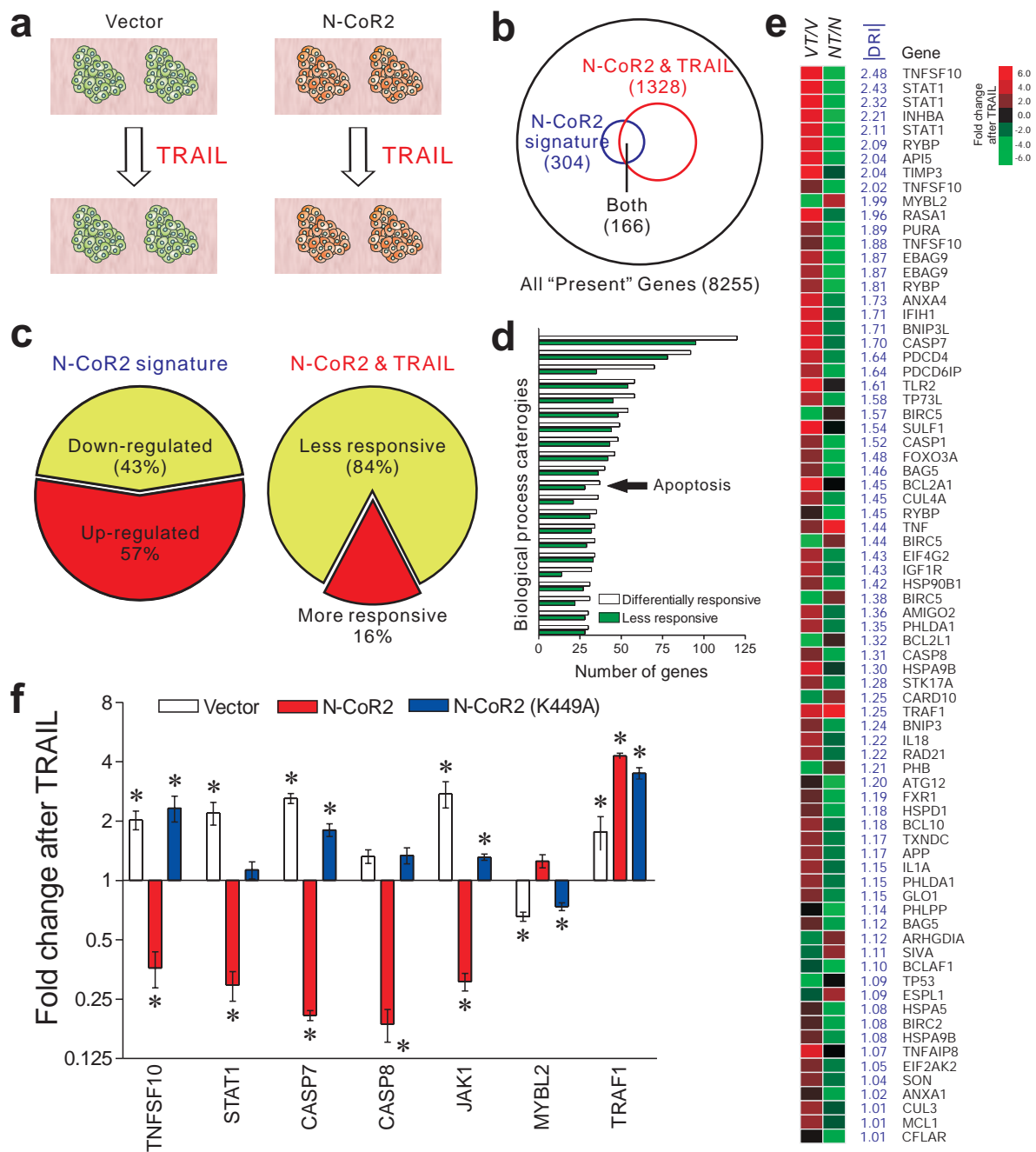
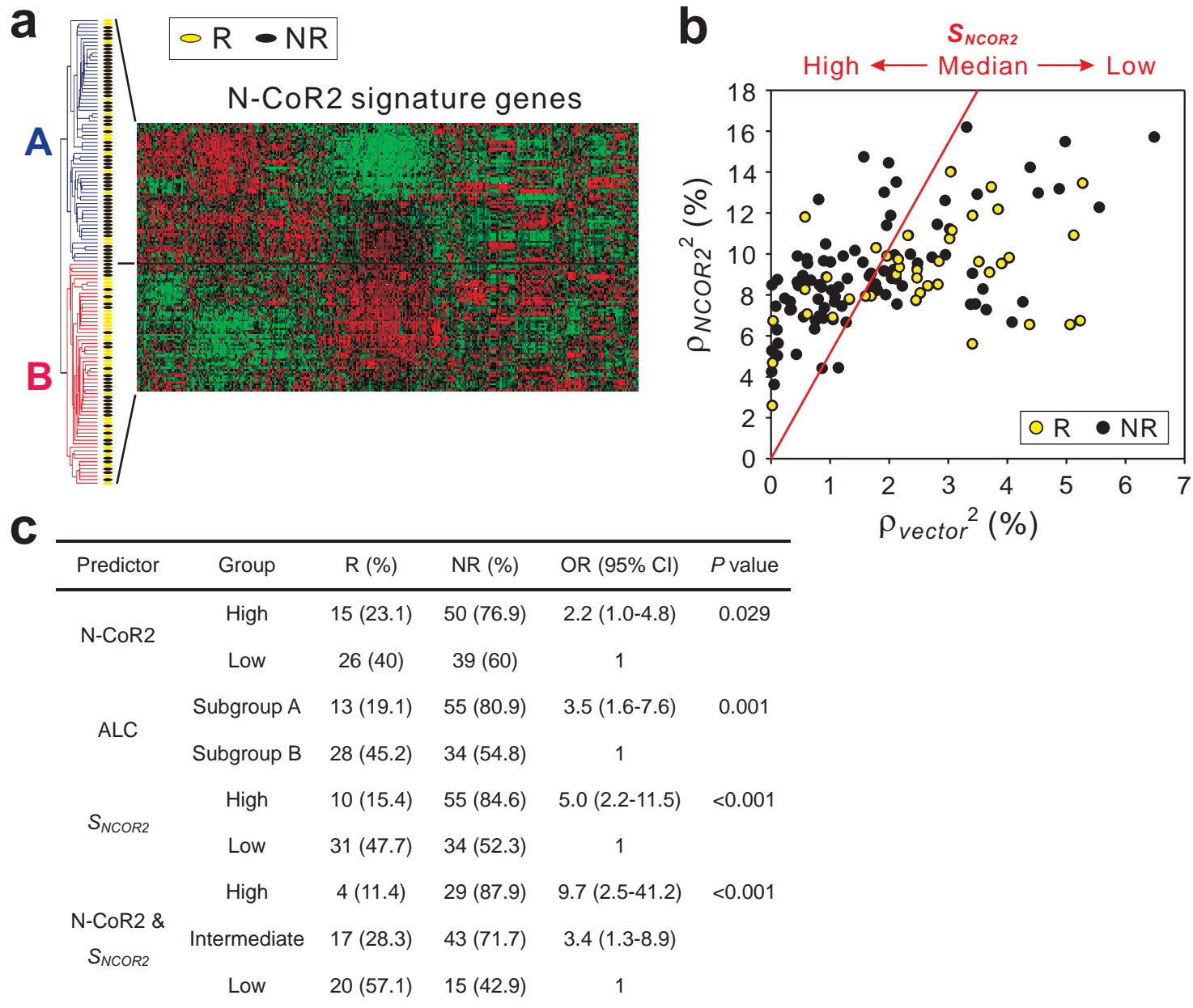


Fig. 5





**Table 1 Multivariate analysis for distant metastasis-free and overall survival according to N-CoR2 and HDAC3 transcript expression and clinical characteristics in breast cancer patients who received adjuvant CT**

Variable	Death		Relapse	
	Hazard Ratio (95% CI)	P Value	Hazard Ratio (95% CI)	P Value
N-CoR2	9.64 (3.27-28.43)	<0.001	5.45 (2.31-12.85)	<0.001
HDAC3	6.67 (1.67-26.65)	0.007	1.89 (0.5-7.11)	0.348
Age (per 10-yr increment)	0.57 (0.24-1.35)	0.199	0.69 (0.38-1.41)	0.305
Tumor size (per mm)	1.05 (1.0-1.1)	0.05	1.04 (1.0-1.08)	0.068
Tumor grade		0.12		0.18
Grade 2 vs. grade 1	1.82 (0.33-9.96)		1.2 (0.38-3.76)	
Grade 3 vs. grade 1	4.3 (0.84-22.11)		2.45 (0.79-7.58)	
Positive LN status vs. negative status	0.46 (0.09-2.28)	0.339	0.85 (0.19-3.87)	0.831
Positive ER status vs. negative status	0.09 (0.02-0.41)	0.002	0.23 (0.06-0.85)	0.027
Hormonal treatment vs. no treatment	0.24 (0.03-1.91)	0.176	0.53 (0.16-1.82)	0.315
Mastectomy vs. breast-conserving therapy	0.81 (0.32-2.04)	0.653	0.81 (0.38-1.75)	0.591
Molecular subtype		0.314		0.53
Normal-like & luminal B vs. luminal A	3.77 (0.63-22.64)		1.59 (0.51-4.95)	
Basal & ERBB2+ vs. luminal A	1.93 (0.3-12.41)		0.88 (0.22-3.58)	

The analysis included the 110 patients with breast cancers who had received adjuvant systemic CT in the Netherlands Cancer Institute database. N-CoR2, HDAC3 transcript expression, age and tumor size were modeled as continuous variables. CI denotes confidence interval.

### Legends for supplementary figures

**Supplementary Fig. 1** Functional inhibition of E-cadherin (E-cad) disrupted cell-cell adhesion and acinar organization of S1 cells. **(a)** Phase contrast micrographs of S1 cells that stably overexpress the dominant negative E-cad mutant H-2K<sup>d</sup>-E-cad or the control construct H-2K<sup>d</sup>-E-cad $\Delta$ C25 in monolayer or 3D rBM culture. *Bars*, 500  $\mu$ m (upper panels) or 100  $\mu$ m (lower panels). S1 cells expressing H-2K<sup>d</sup>-E-cad, compared with those expressing the control construct, displayed refractile borders and failed to form compact cell clusters when grown as 2D monolayers (upper panels). They grew into disorganized cellular aggregates in 3D rBM while the control cells were able to form organized acini that were indistinguishable from the wild-type S1 cells (lower panels). **(b)** Monolayer cultured S1 cells expressing H-2K<sup>d</sup>-E-cad or the control construct were immunostained with antibodies toward  $\beta$ -catenin ( $\beta$ -cat) (red). The nuclei were counterstained with DAPI (blue). Consistent with previous findings (**Error! Bookmark not defined.**), overexpression of the dominant negative E-cad mutant led to cytoplasmic and perinuclear localization of  $\beta$ -cat, which were instead concentrated at cell-cell borders in the control cells. *Bar*, 100  $\mu$ m. **(c)** The protein abundance of E-cad and  $\beta$ -cat in S1 cells expressing H-2K<sup>d</sup>-E-cad or the control construct. As described previously (**Error! Bookmark not defined.**), overexpression of the dominant negative E-cad mutant led to a reduction in the expression level of endogenous E-cad and a marked increase in the  $\beta$ -cat expression.

**Supplementary Fig. 2** Effect of N-CoR2 knockdown or overexpression on the growth rate and tissue organization of MECs. **(a)** Growth rates of S1 cells that stably express N-CoR2 shRNA or the control shRNA. Cells were seeded on culture plastics and the cell number was determined at indicated time points. Population doublings were calculated as  $\ln(\text{cell number at day } n / \text{cell number at day } 0) / \ln 2$ . Data are mean  $\pm$  SEM of triplicate experiments. **(b)** Phase-contrast micrographs of acinar structures formed by S1 cells that stably express N-CoR2 shRNA or the control shRNA in 3D rBM. The representative acini (*insets*) were immunostained with antibodies toward  $\beta$ 4-integrin (green) and  $\beta$ -catenin (red) to illustrate the basal surfaces and the intercellular junctions of the polarized structures. *Bar*, 500  $\mu$ m. **(c)** Growth rates of T4-2 cells that stably overexpress N-CoR2 or the control vector. Cells were seeded on collagen I-coated plastics and the population doubling numbers were determined as in (a). \* $P < 0.05$ , compared with the vector control cells. **(d)** Phase-contrast images of T4-2 cells that stably overexpressed N-CoR2 or the empty vector in monolayer cultures at day 3 following seeding as single cells on culture plastics. *Bar*, 500  $\mu$ m.

**Supplementary Fig. 3** The mutant N-CoR2 (K449A) protein compromised the

nuclear deacetylase activity of HDAC3. **(a)** Nuclear lysates from HEK 293 cells stably expressing myc-tagged N-CoR2, N-CoR2 (K449A) or empty vector were immunoprecipitated with the anti-myc antibody. The precipitates were analyzed by Western blot using anti-myc or anti-HDAC3 antibody. Lamin B1 was used as nuclear loading control. **(b)** Myc-immunoprecipitated N-CoR2, N-CoR2 (K449A) or empty vector complexes were analyzed for HDAC activity using a fluorimetric activity assay with or without 5  $\mu$ M of the HDAC inhibitor TSA. Results were repeated in quadruplicate.  $P < 0.05$ , compared with vector\* or N-CoR2<sup>†</sup>.

**Supplementary Fig. 4** Functional gene classes identified from the 304 genes that were differentially expressed (N-CoR2 signature genes) **(a)** or the 1328 genes that were differentially responsive to TRAIL **(b)** upon N-CoR2 overexpression in T4-2 cells. The bar graphs represent the numbers of genes ( $n \geq 5$  in (A);  $n \geq 25$  in (B)) corresponding to each GO biological process category with a Bonferroni-corrected significance of  $P < 0.05$ .

**Supplementary Fig. 5** **(a)** Stable knockdown of TRAIL by retrovirus-mediated RNAi in T4-2 vector cells significantly reduced TRAIL protein levels (*inset*) and compromised death induction by exogenous TRAIL (0.5  $\mu$ g/mL). **(b)** T4-2 cells expressing N-CoR2 or the control vector were treated with vehicle or TRAIL (1.0  $\mu$ g/mL) for 3 h and 6 h and cell lysates were analyzed for STAT1 and E-cad by Western blot. \* $P < 0.05$ , compared with control RNAi.

**Supplementary Fig. 6** Kaplan-Meier analysis of the probability that patient would remain relapse-free or survive after therapy in the 295 breast cancer patients in the Netherlands Cancer Institute database. The patients were stratified according to their LN status and whether or not they received adjuvant CT. In each group, the patients were grouped into quartiles according to the expression levels of N-CoR2. The log-rank test is used to calculate the  $P$  values.

**Supplementary Fig. 7** Kaplan-Meier analysis of the probability that patient would remain relapse-free or survive after therapy in the 295 breast cancer patients in the Netherlands Cancer Institute database. The patients were stratified according to their LN status and whether or not they received adjuvant CT. Patients in each group were stratified according to HDAC3 gene expression quartiles **(a)** or whether their N-CoR2 and HDAC3 gene expressions both fell into respective upper or lower quartiles **(b)**. The log-rank test is used to calculate the  $P$  values.

**Supplementary Fig. 8** Kaplan-Meier analysis of the probability that patient would remain survive after therapy among 50 malignant glioma patients (**a**) or 60 ovarian cancer patients (**b**)<sup>28,29</sup>. Patients were grouped into quartiles according to the expression levels of N-CoR2 or HDAC3 or both (N-CoR2/HDAC3). *P* values were determined using the log-rank test comparing the upper and the lower quartiles.

**Supplementary Fig. 9** Hierarchical clustering of 130 breast tumors in the M.D. Anderson Cancer Center database using the N-CoR2 gene signature. Each column represents expression levels of a probe set and each row represents the expression profile in a tumor. The expression levels (on a log<sub>2</sub> scale) were median-centered across all tumors and then normalized. The identities of each gene in the signature are denoted at the top. The dendrogram at the left provides a representation of the similarity of the gene expression patterns among the 130 tumors, which are segregated into two predominant subgroups (subgroup A and B), with tumors from responders to pre-operative chemotherapy (yellow circles) or non-responders (black circles) denoted. Colorgram depicts high (red) and low (green) relative level of gene expression.

### Legends for supplementary figures

**Supplementary Fig. 1** Functional inhibition of E-cadherin (E-cad) disrupted cell-cell adhesion and acinar organization of S1 cells. **(a)** Phase contrast micrographs of S1 cells that stably overexpress the dominant negative E-cad mutant H-2K<sup>d</sup>-E-cad or the control construct H-2K<sup>d</sup>-E-cad $\Delta$ C25 in monolayer or 3D rBM culture. *Bars*, 500  $\mu$ m (upper panels) or 100  $\mu$ m (lower panels). S1 cells expressing H-2K<sup>d</sup>-E-cad, compared with those expressing the control construct, displayed refractile borders and failed to form compact cell clusters when grown as 2D monolayers (upper panels). They grew into disorganized cellular aggregates in 3D rBM while the control cells were able to form organized acini that were indistinguishable from the wild-type S1 cells (lower panels). **(b)** Monolayer cultured S1 cells expressing H-2K<sup>d</sup>-E-cad or the control construct were immunostained with antibodies toward  $\beta$ -catenin ( $\beta$ -cat) (red). The nuclei were counterstained with DAPI (blue). Consistent with previous findings (**Error! Bookmark not defined.**), overexpression of the dominant negative E-cad mutant led to cytoplasmic and perinuclear localization of  $\beta$ -cat, which were instead concentrated at cell-cell borders in the control cells. *Bar*, 100  $\mu$ m. **(c)** The protein abundance of E-cad and  $\beta$ -cat in S1 cells expressing H-2K<sup>d</sup>-E-cad or the control construct. As described previously<sup>13</sup>, overexpression of the dominant negative E-cad mutant led to a reduction in the expression level of endogenous E-cad and a marked increase in the  $\beta$ -cat expression.

**Supplementary Fig. 2** Effect of N-CoR2 knockdown or overexpression on the growth rate and tissue organization of MECs. **(a)** Growth rates of S1 cells that stably express N-CoR2 shRNA or the control shRNA. Cells were seeded on culture plastics and the cell number was determined at indicated time points. Population doublings were calculated as  $\ln(\text{cell number at day } n / \text{cell number at day } 0) / \ln 2$ . Data are mean  $\pm$  SEM of triplicate experiments. **(b)** Phase-contrast micrographs of acinar structures formed by S1 cells that stably express N-CoR2 shRNA or the control shRNA in 3D rBM. The representative acini (*insets*) were immunostained with antibodies toward  $\beta$ 4-integrin (green) and  $\beta$ -catenin (red) to illustrate the basal surfaces and the intercellular junctions of the polarized structures. *Bar*, 500  $\mu$ m. **(c)** Growth rates of T4-2 cells that stably overexpress N-CoR2 or the control vector. Cells were seeded on collagen I-coated plastics and the population doubling numbers were determined as in (a). \* $P < 0.05$ , compared with the vector control cells. **(d)** Phase-contrast images of T4-2 cells that stably overexpressed N-CoR2 or the empty vector in monolayer cultures at day 3 following seeding as single cells on culture plastics. *Bar*, 500  $\mu$ m.

**Supplementary Fig. 3** The mutant N-CoR2 (K449A) protein compromised the

nuclear deacetylase activity of HDAC3. **(a)** Nuclear lysates from HEK 293 cells stably expressing myc-tagged N-CoR2, N-CoR2 (K449A) or empty vector were immunoprecipitated with the anti-myc antibody. The precipitates were analyzed by Western blot using anti-myc or anti-HDAC3 antibody. Lamin B1 was used as nuclear loading control. **(b)** Myc-immunoprecipitated N-CoR2, N-CoR2 (K449A) or empty vector complexes were analyzed for HDAC activity using a fluorimetric activity assay with or without 5  $\mu$ M of the HDAC inhibitor TSA. Results were repeated in quadruplicate.  $P < 0.05$ , compared with vector\* or N-CoR2<sup>†</sup>.

**Supplementary Fig. 4** Functional gene classes identified from the 304 genes that were differentially expressed (N-CoR2 signature genes) **(a)** or the 1328 genes that were differentially responsive to TRAIL **(b)** upon N-CoR2 overexpression in T4-2 cells. The bar graphs represent the numbers of genes ( $n \geq 5$  in (A);  $n \geq 25$  in (B)) corresponding to each GO biological process category with a Bonferroni-corrected significance of  $P < 0.05$ .

**Supplementary Fig. 5** **(a)** Stable knockdown of TRAIL by retrovirus-mediated RNAi in T4-2 vector cells significantly reduced TRAIL protein levels (*inset*) and compromised death induction by exogenous TRAIL (0.5  $\mu$ g/mL). **(b)** T4-2 cells expressing N-CoR2 or the control vector were treated with vehicle or TRAIL (1.0  $\mu$ g/mL) for 3 h and 6 h and cell lysates were analyzed for STAT1 and E-cad by Western blot. \* $P < 0.05$ , compared with control RNAi.

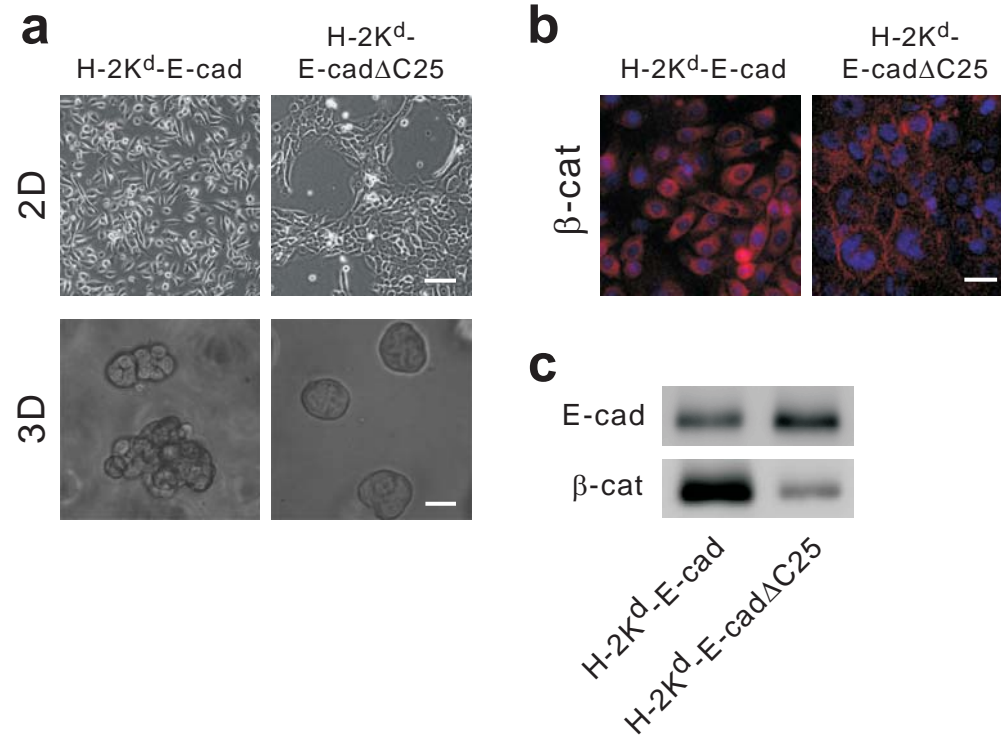
**Supplementary Fig. 6** Kaplan-Meier analysis of the probability that patient would remain relapse-free or survive after therapy in the 295 breast cancer patients in the Netherlands Cancer Institute database. The patients were stratified according to their LN status and whether or not they received adjuvant CT. In each group, the patients were grouped into quartiles according to the expression levels of N-CoR2. The log-rank test is used to calculate the  $P$  values.

**Supplementary Fig. 7** Kaplan-Meier analysis of the probability that patient would remain relapse-free or survive after therapy in the 295 breast cancer patients in the Netherlands Cancer Institute database. The patients were stratified according to their LN status and whether or not they received adjuvant CT. Patients in each group were stratified according to HDAC3 gene expression quartiles **(a)** or whether their N-CoR2 and HDAC3 gene expressions both fell into respective upper or lower quartiles **(b)**. The log-rank test is used to calculate the  $P$  values.

**Supplementary Fig. 8** Kaplan-Meier analysis of the probability that patient would remain survive after therapy among 50 malignant glioma patients (**a**) or 60 ovarian cancer patients (**b**)<sup>28,29</sup>. Patients were grouped into quartiles according to the expression levels of N-CoR2 or HDAC3 or both (N-CoR2/HDAC3). *P* values were determined using the log-rank test comparing the upper and the lower quartiles.

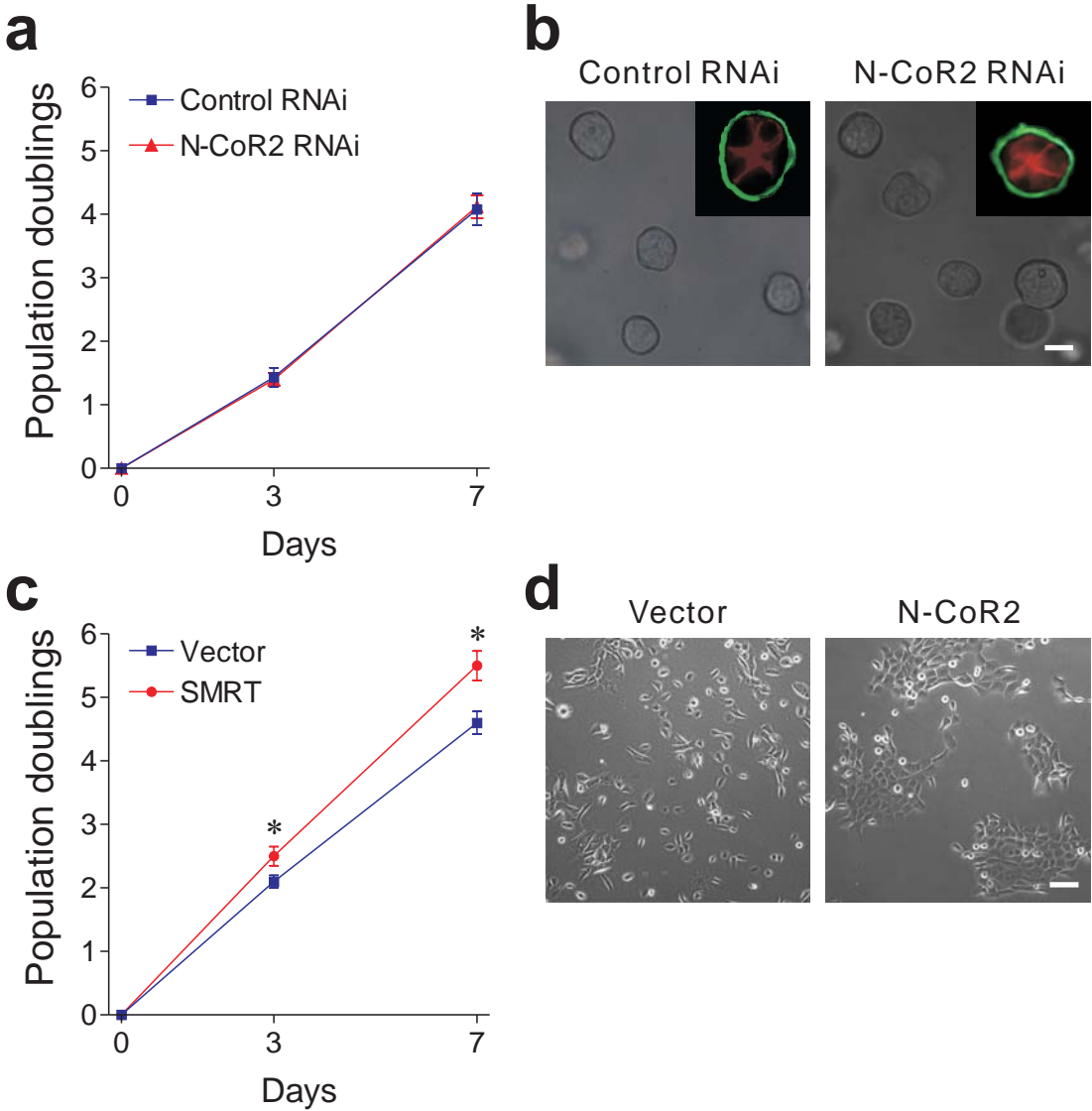
**Supplementary Fig. 9** Hierarchical clustering of 130 breast tumors in the M.D. Anderson Cancer Center database using the N-CoR2 gene signature. Each column represents expression levels of a probe set and each row represents the expression profile in a tumor. The expression levels (on a log<sub>2</sub> scale) were median-centered across all tumors and then normalized. The identities of each gene in the signature are denoted at the top. The dendrogram at the left provides a representation of the similarity of the gene expression patterns among the 130 tumors, which are segregated into two predominant subgroups (subgroup A and B), with tumors from responders to pre-operative chemotherapy (yellow circles) or non-responders (black circles) denoted. Colorgram depicts high (red) and low (green) relative level of gene expression.

## Supplementary Fig. 1



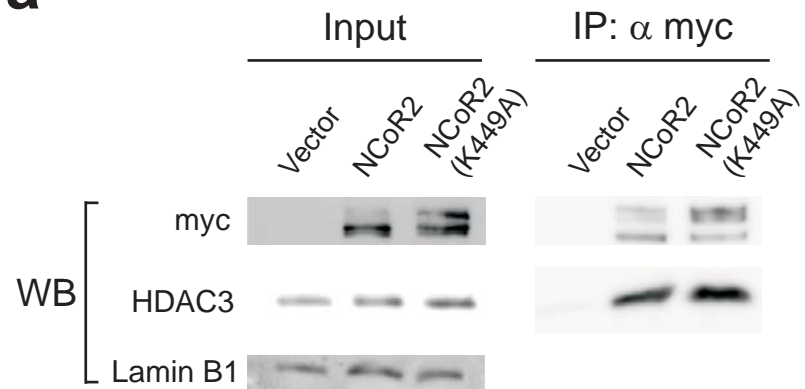


# Supplementary Fig 2

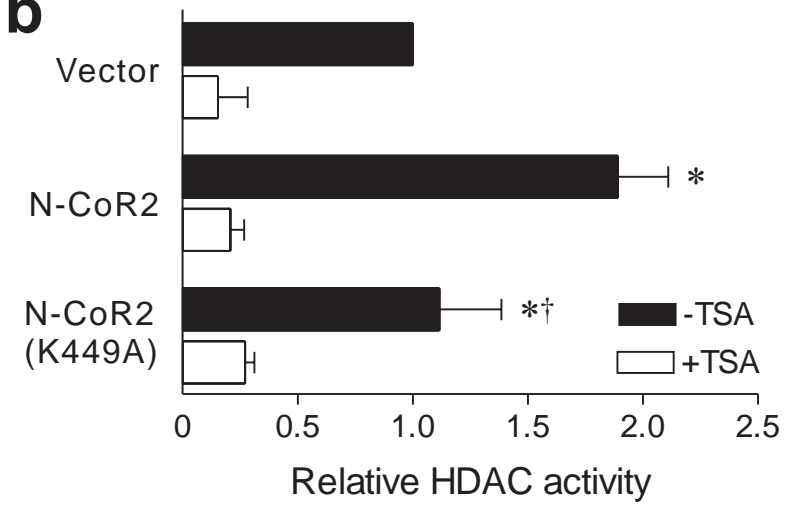


## Supplementary Fig 3

**a**

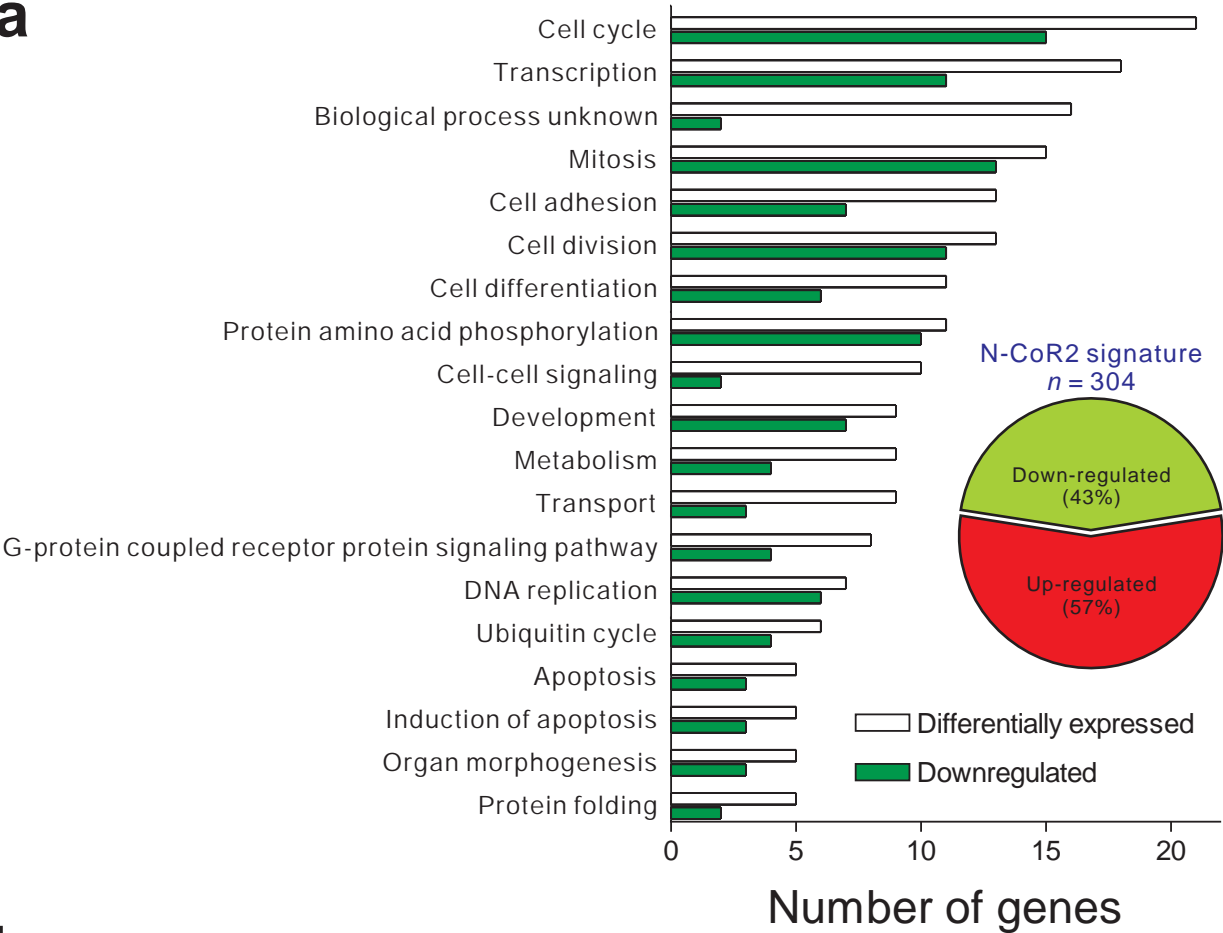


**b**

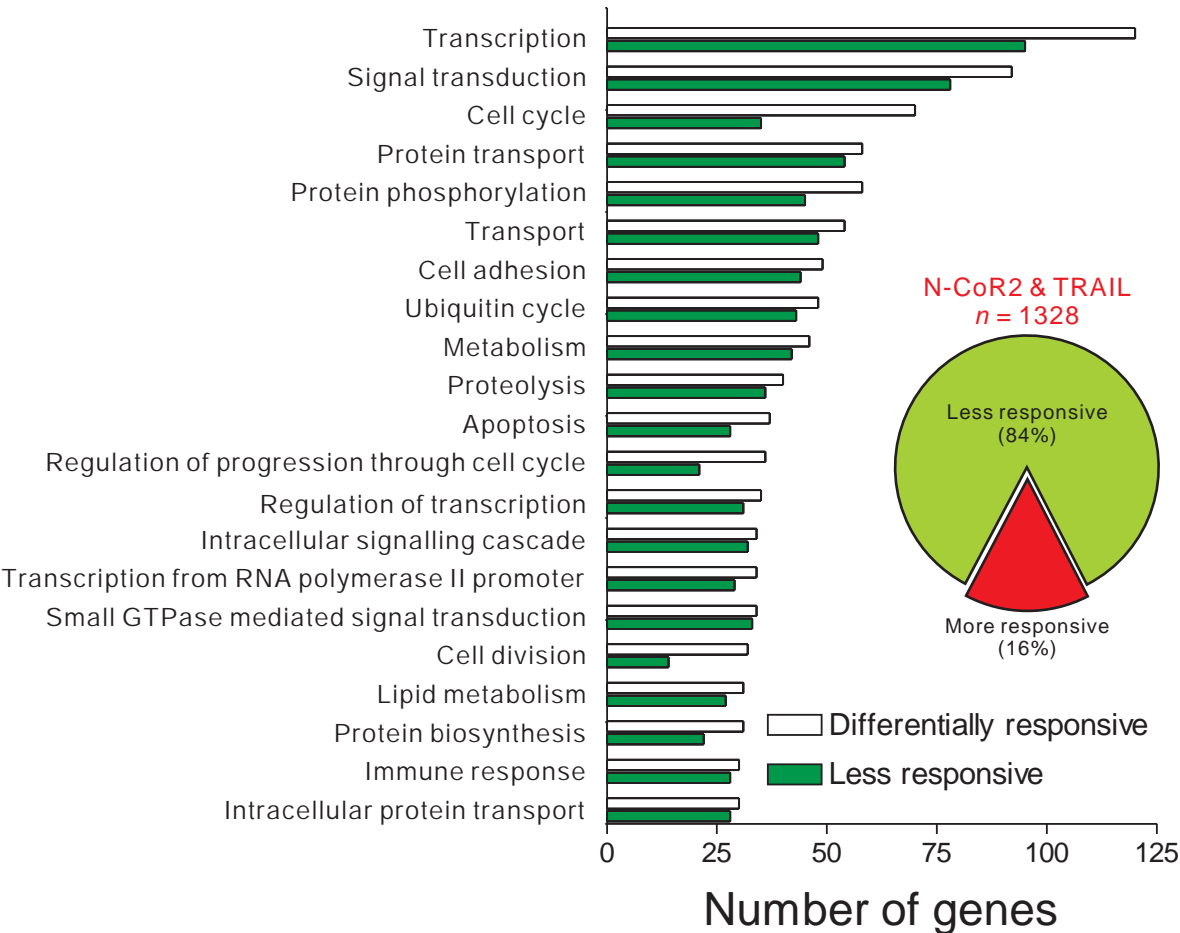


# Supplementary Fig 4

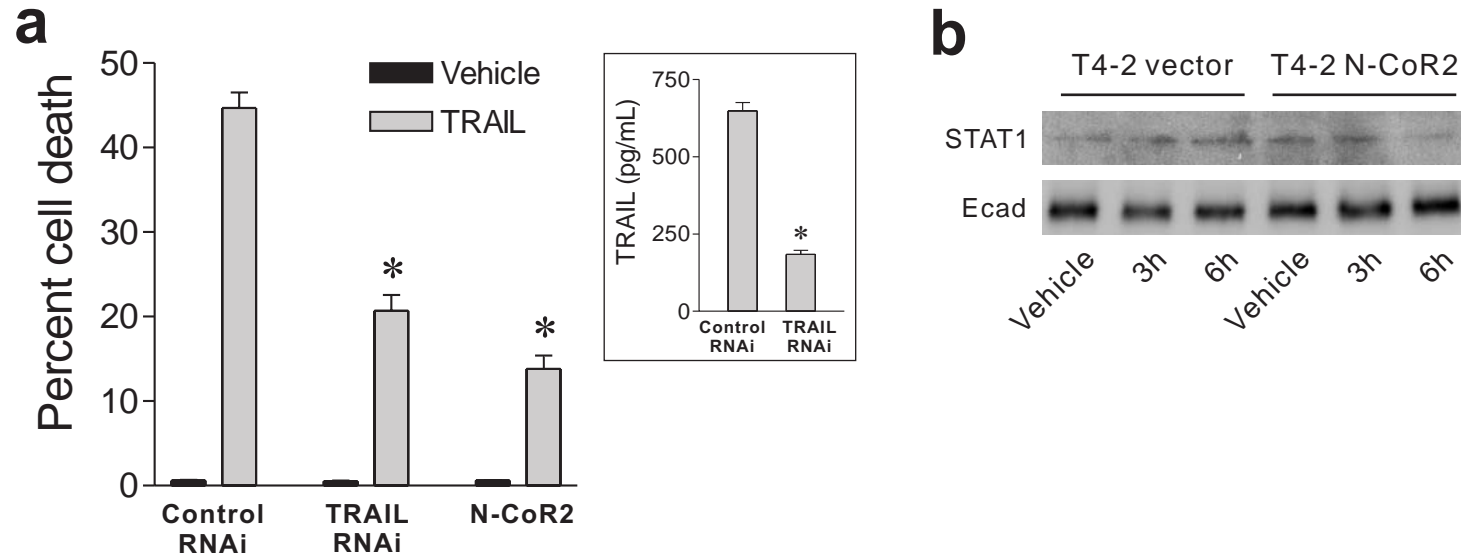
**a**



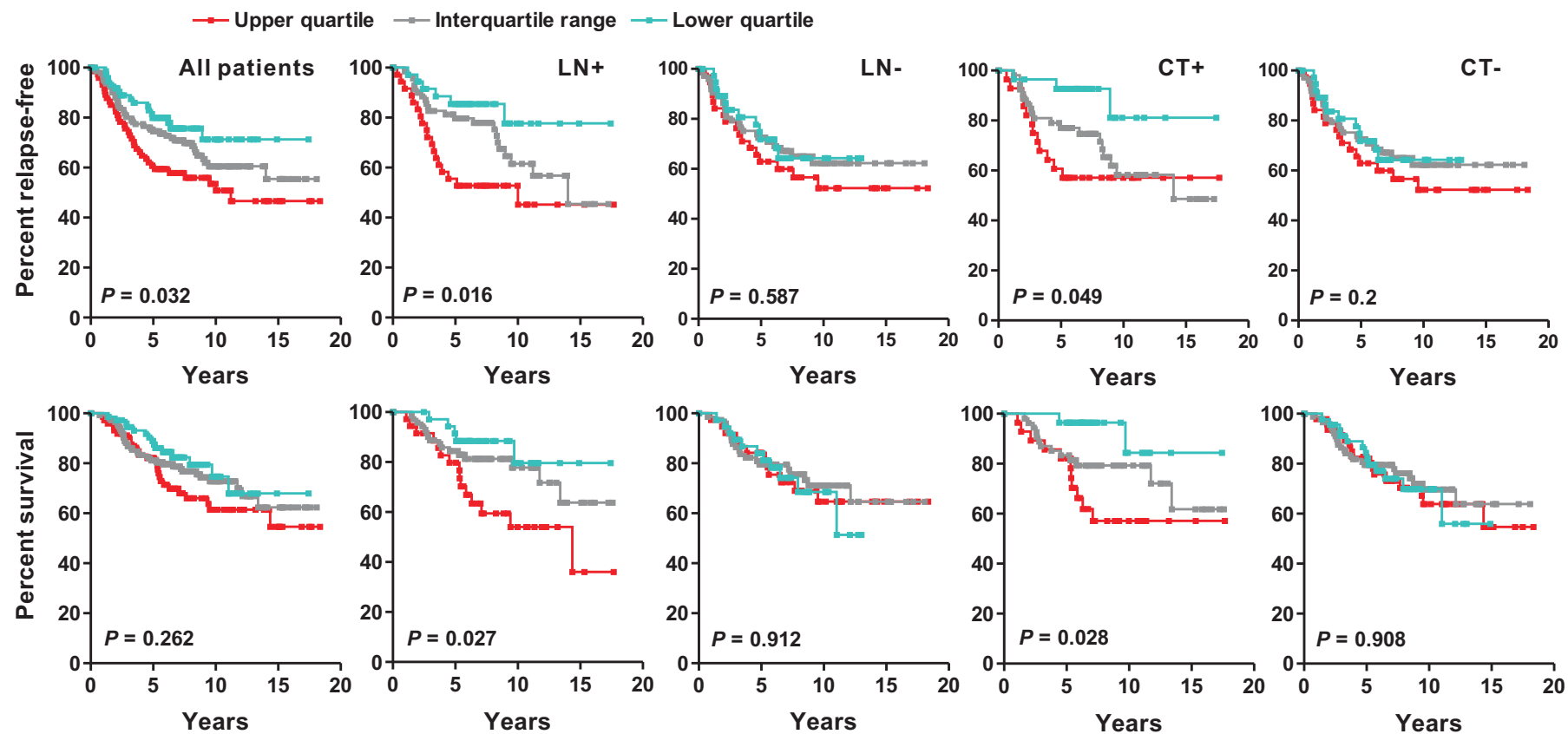
**b**



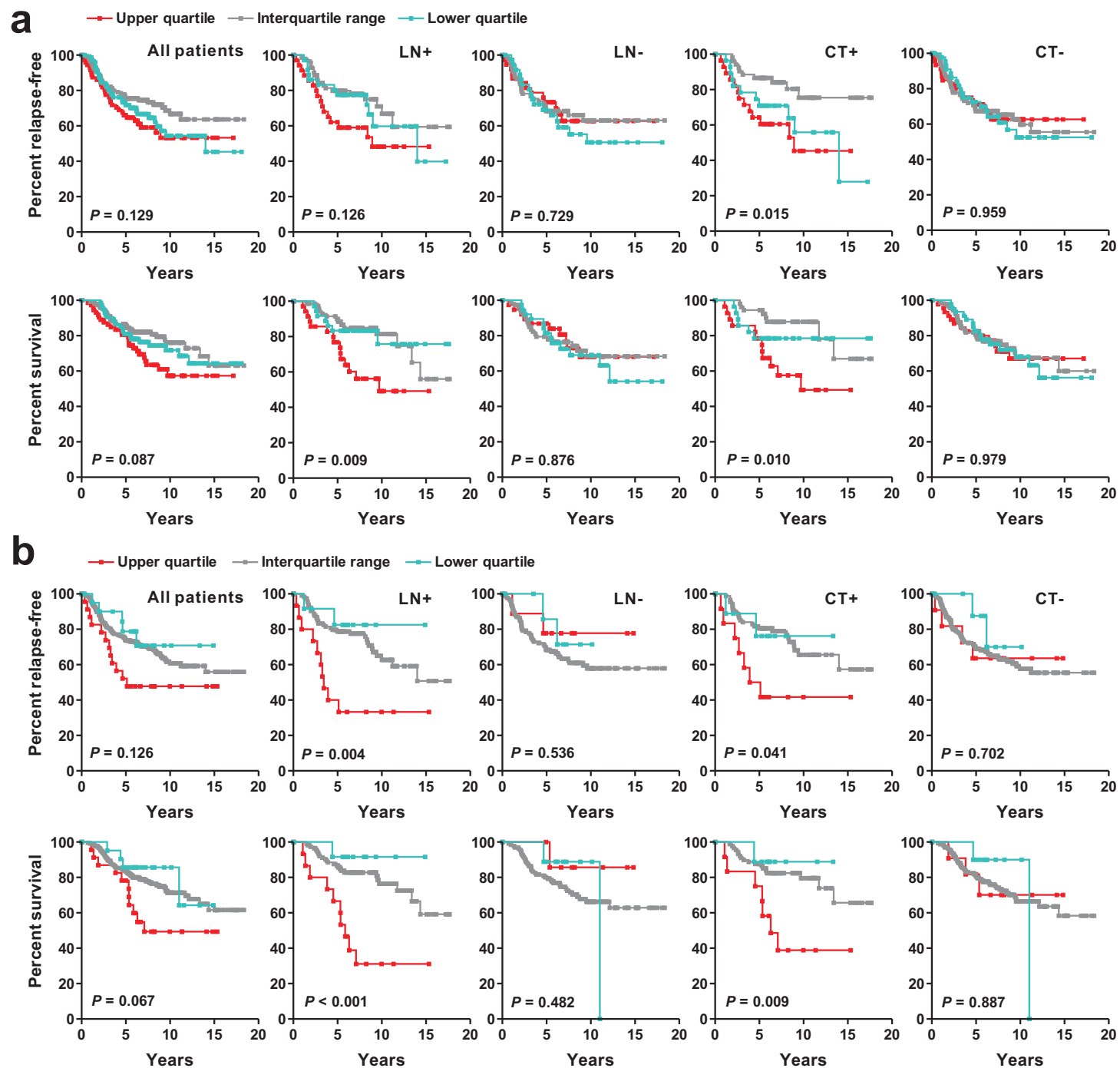
## Supplementary Fig 5



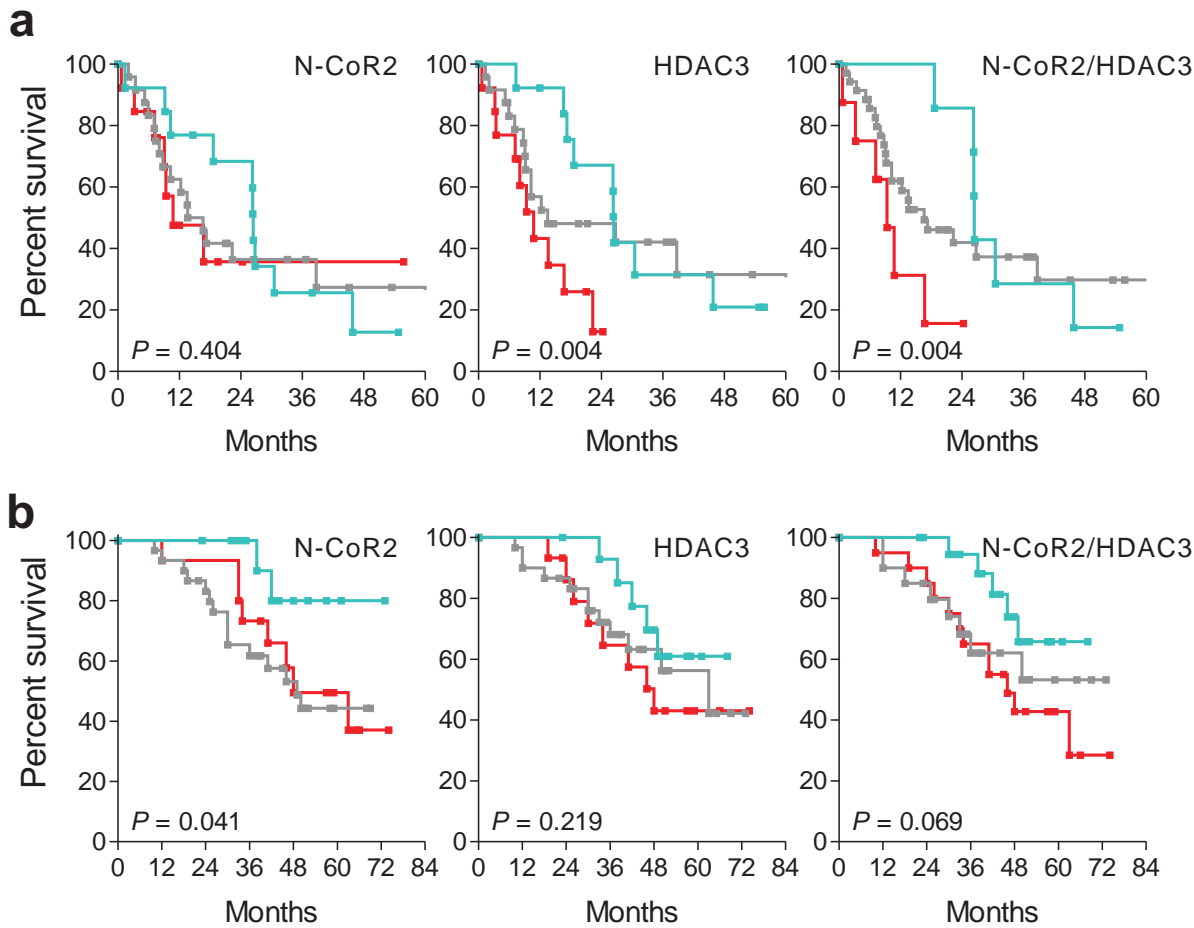
## Supplementary Fig. 6



# Supplementary Fig. 7



# Supplementary Fig. 8



Supplementary Fig. 9





**Supplementary Table 1 The expression levels of N-CoR2 and HDAC3 in human malignant tumors**

Tumor type ( <i>n</i> )	Median expression	Control ( <i>n</i> )	Median expression	<i>P</i> value	Source
Gene: <i>NCOR2</i>					
Hepatocellular carcinoma (104)	0.12567	Non-tumor liver tissue (76)	-0.16756	$5.2 \times 10^{-5}$	X. Chen <i>et al.</i> , <i>Mol. Cell. Biol.</i> <b>13</b> , 1929 (2002) <sup>1</sup>
Diffuse large B-cell lymphoma (274)	0.00812	Normal Blood CD19+ B-Cells (6), Normal Germinal Center B-Cells (4)	-0.34671, -0.50824	$1.1 \times 10^{-4}$	A. Rosenwald <i>et al.</i> , <i>N. Engl. J. Med.</i> <b>346</b> , 1937 (2002) <sup>1</sup>
Renal clear cell carcinoma (9)	2.01118	Normal kidney (9)	1.45521	$3.5 \times 10^{-8}$	M. E. Lenburg <i>et al.</i> , <i>BMC Cancer</i> <b>3</b> , 31 (2003) <sup>1</sup>
Oligodendroglioma (50)	1.8902	Normal brain (23)	1.71874	$7.3 \times 10^{-4}$	L. Sun <i>et al.</i> , <i>Cancer Cell</i> <b>9</b> , 287 (2006) <sup>1</sup>
Astrocytic tumor (5)	0.84852	Normal brain (4)	0.28266	$9.5 \times 10^{-4}$	M. Bredel <i>et al.</i> , <i>Cancer Res.</i> <b>65</b> , 8679 (2005) <sup>1</sup>
Adult Male Germ Cell Tumor (91)	-0.11491	Normal testis (6)	-0.19157	$7.6 \times 10^{-5}$	J. E. Korkola <i>et al.</i> , <i>Cancer Res.</i> <b>66</b> , 820 (2006) <sup>1</sup>
Seminoma (23)	-0.55357	Normal testis (14)	0.41112	$1.2 \times 10^{-5}$	J. M. Sperger <i>et al.</i> , <i>Proc. Natl. Acad. Sci. USA</i> <b>100</b> , 13350 (2003) <sup>1</sup>

Primary breast carcinoma (20)	1.01759	Normal breast (6)	0.89118	0.457	P. Novak <i>et al.</i> , <i>Cancer Res.</i> <b>66</b> , 10664 (2006) <sup>2</sup>
Metastatic breast carcinoma (7)	0.69075	Primary breast carcinoma (47)	-0.17034	$1.7 \times 10^{-7}$	L. Radvanyi <i>et al.</i> , <i>Proc. Natl. Acad. Sci. USA</i> <b>102</b> , 11005 (2005) <sup>1</sup>
Breast carcinoma with metastasis within 5 years (101)	0.1518	Breast carcinoma with disease-free > 5 years (194)	-0.18268	$9.9 \times 10^{-4}$	M. J. Van de Vijver <i>et al.</i> , <i>N. Eng. J. Med.</i> <b>347</b> , 1999 (2002) <sup>1</sup>
Breast carcinoma with metastasis within 5 years (93)	-1.39	Breast carcinoma with disease-free > 5 years (180)	-1.23084	$2.9 \times 10^{-5}$	Y. Wang <i>et al.</i> , <i>Lancet</i> <b>365</b> , 671 (2005) <sup>1</sup>
Cancer cell lines resistant to methotrexate (19)	1.26248	Cancer cell lines intermediately sensitive to methotrexate (6)	0.63474	$6.5 \times 10^{-4}$	B. Györfy <i>et al.</i> , <i>Int. J. Cancer</i> <b>118</b> , 1699 (2006) <sup>1</sup>
Multiple myeloma (12)	0.16634	Bone marrow (22)	-0.19155	$1.2 \times 10^{-4}$	F. Zhan <i>et al.</i> , <i>Blood</i> <b>109</b> , 1692 (2006) <sup>1</sup>
Head and neck squamous cell carcinoma (41)	1.21708	Oral mucosa (13)	0.94962	$1.1 \times 10^{-8}$	M. A. Ginos <i>et al.</i> , <i>Cancer Res.</i> <b>64</b> , 55 (2004) <sup>1</sup>
Head and neck squamous cell carcinoma with lymph node metastasis (59)	0.0333	Head and neck squamous cell carcinoma without lymph node metastasis (50)	-0.18346	$6.1 \times 10^{-4}$	P. Roepman <i>et al.</i> , <i>Nature Genet.</i> <b>37</b> , 182 (2005) <sup>1</sup>

Metastatic colon cancers (16)	-0.02307	Primary colon cancers (118)	-0.28668	$9.9 \times 10^{-4}$	M. Bittner, <i>International Genomics Consortium</i> (2006) <sup>1</sup>
Prostate carcinoma (44)	523.9	Normal prostate (13)	599.6	0.087	P. Liu <i>et al.</i> , <i>Cancer Res.</i> <b>66</b> , 4011 (2006) <sup>2</sup>
Prostate carcinoma (59)	-0.67042	Benign prostate hyperplasia (16), prostate gland (6)	-0.26949, 0.05348	$2.4 \times 10^{-4}$	S. M. Dhanasekaran <i>et al.</i> , <i>Nature</i> <b>412</b> , 822 (2001) <sup>1</sup>
Metastatic prostate carcinoma (6)	1.36203	Prostate carcinoma (7)	1.65267	$2.4 \times 10^{-4}$	S. Varambally <i>et al.</i> , <i>Cancer Cell</i> <b>8</b> , 393 (2005) <sup>1</sup>
Metastatic prostate carcinoma (9), prostate carcinoma (62)	0.60672, 0.11163	Normal prostate (41)	-0.08301	$1.1 \times 10^{-4}$	J. Lapointe <i>et al.</i> , <i>Proc. Natl. Acad. Sci. USA</i> <b>101</b> , 811 (2004) <sup>1</sup>
Tongue squamous cell carcinoma (31)	0.32207	Tongue (26)	0.48531	$2.4 \times 10^{-6}$	S. G. Talbot <i>et al.</i> , <i>Cancer Res.</i> <b>65</b> , 3063 (2005) <sup>1</sup>
Bladder carcinoma: grade 1 (17), grade 2 (21), grade 3 (55)	1153.2, 1350.1, 1582.4	Normal bladder (10)	1112.8	0.880, 0.310, 0.059	N. Stransky <i>et al.</i> , <i>Nature Genet.</i> <b>38</b> , 1386 (2006) <sup>2</sup>
Gene: <i>HDAC3</i>					
Glioblastoma multiform (77)	0.11955	Normal brain (23)	-0.02882	$2.2 \times 10^{-5}$	L. Sun <i>et al.</i> , <i>Cancer Cell</i> <b>9</b> , 287 (2006) <sup>1</sup>
Hepatocellular carcinoma (104)	-0.36107	Normal liver (76)	-0.66190	$8.7 \times 10^{-5}$	X. Chen <i>et al.</i> , <i>Mol. Biol. Cell</i> <b>13</b> , 1929 (2002) <sup>1</sup>

Clear renal cell carcinoma (26)	-0.19733	Normal kidney (3)	-0.59216	$4.1 \times 10^{-7}$	J. P. Higgins <i>et al.</i> , <i>Am. J. Pathol.</i> <b>162</b> , 925 (2003) <sup>1</sup>
Metastatic prostate carcinoma (25), prostate carcinoma (64)	-0.35344, -0.40056	Normal prostate (23)	-0.50996	$7.1 \times 10^{-6}$	Y. P. Yu <i>et al.</i> , <i>J. Clin. Oncol.</i> <b>22</b> , 2790 (2004) <sup>1</sup>
Tongue squamous cell carcinoma (31)	0.05968	Normal tongue (26)	-0.11841	$1.0 \times 10^{-4}$	S. G. Tablot <i>et al.</i> , <i>Cancer Res.</i> <b>65</b> , 3063 (2005) <sup>1</sup>
Breast carcinoma (20)	-0.1343	Normal breast (6)	0.1014	0.051	P. Novak <i>et al.</i> , <i>Cancer Res.</i> <b>66</b> , 10664 (2006) <sup>2</sup>
Colon cancer (10)	~2.8-fold higher protein expression	Paired normal colon tissue (10)		0.003	A. J. Wilson <i>et al.</i> , <i>J. Biol. Chem.</i> <b>281</b> , 13548 (2006)

<sup>1</sup>Data interrogated from the ONCOMINE tumor transcriptome database (<http://www.oncomine.org/>) with a *P*-value threshold of 0.001.

<sup>2</sup>Data interrogated from the ArrayExpress microarray data repository (<http://www.ebi.ac.uk/arrayexpress/>). Pairwise comparison was performed with use of Mann-Whitney's *U* test.

**Supplementary Table 2 Identities of the 304 genes (350 probe sets) differentially expressed in response to N-CoR2 overexpression in T4-2 cells.** The genes (probe sets) are ranked descendingly accordingly to the ratio between the mean hybridization intensity of each probe in T4-2 vector cells (V) and that in T4-2 N-CoR2 cells (N).

Affymetrix probe set ID	Gene symbol	RefSeq Transcript ID	Description	Mean intensity (V)	Mean intensity (N)	Ratio (V/N)
210119_at	<i>KCNJ15</i>	NM_002243 / NM_170736 / NM_170737	potassium inwardly-rectifying channel, subfamily J, member 15	136.33	11.06	12.33
211806_s_at	<i>KCNJ15</i>	NM_002243 / NM_170736 / NM_170737	potassium inwardly-rectifying channel, subfamily J, member 15	43.15	4.82	8.94
211719_x_at	<i>FNI</i>	NM_002026 / NM_054034 / NM_212474 / NM_212475 / NM_212476 / NM_212478 / NM_212482	fibronectin 1	7290.69	1237.54	5.89
216442_x_at	<i>FNI</i>	NM_002026 / NM_054034 / NM_212474 / NM_212475 / NM_212476 / NM_212478 / NM_212482	fibronectin 1	4490.64	781.95	5.74
214701_s_at	<i>FNI</i>	NM_002026 / NM_054034 / NM_212474 / NM_212475 / NM_212476 / NM_212478 / NM_212482	fibronectin 1	34.32	6.00	5.72

210495_x_at	<i>FNI</i>	NM_002026 / NM_054034 / NM_212474 / NM_212475 / NM_212476 / NM_212478 / NM_212482	fibronectin 1	4478.15	790.08	5.67
205207_at	<i>IL6</i>	NM_000600	interleukin 6 (interferon, beta 2)	421.76	79.36	5.31
212464_s_at	<i>FNI</i>	NM_002026 / NM_054034 / NM_212474 / NM_212475 / NM_212476 / NM_212478 / NM_212482	fibronectin 1	3877.24	730.91	5.30
214336_s_at	<i>COPA</i>	NM_004371	coatamer protein complex, subunit alpha	41.88	7.94	5.27
219434_at	<i>TREM1</i>	NM_018643	triggering receptor expressed on myeloid cells 1	275.64	54.65	5.04
212154_at	<i>SDC2</i>	NM_002998	syndecan 2 (heparan sulfate proteoglycan 1, cell surface-associated, fibroglycan)	517.35	117.88	4.39
211981_at	<i>COL4A1</i>	NM_001845	collagen, type IV, alpha 1	55.16	13.20	4.18
217859_s_at	<i>SLC39A9</i>	NM_018375	solute carrier family 39 (zinc transporter), member 9	80.47	21.36	3.77
201107_s_at	<i>THBS1</i>	NM_003246	thrombospondin 1	411.89	112.11	3.67
206184_at	<i>CRKL</i>	NM_005207	v-crk sarcoma virus CT10 oncogene homolog (avian)-like	26.61	7.52	3.54
212158_at	<i>SDC2</i>	NM_002998	syndecan 2 (heparan sulfate proteoglycan 1, cell surface-associated, fibroglycan)	88.69	25.07	3.54
209136_s_at	<i>USP10</i>	NM_005153	ubiquitin specific peptidase 10	111.34	32.25	3.45

205547_s_at	<i>TAGLN</i>	NM_001001522 / NM_003186	transgelin	187.92	54.58	3.44
203925_at	<i>GCLM</i>	NM_002061	glutamate-cysteine ligase, modifier subunit	469.78	136.88	3.43
200879_s_at	<i>EPAS1</i>	NM_001430	endothelial PAS domain protein 1	272.67	79.80	3.42
202037_s_at	<i>SFRP1</i>	NM_003012	secreted frizzled-related protein 1	81.81	24.36	3.36
201150_s_at	<i>TIMP3</i>	NM_000362	TIMP metalloproteinase inhibitor 3 (Sorsby fundus dystrophy, pseudoinflammatory)	64.52	19.75	3.27
212142_at	<i>MCM4</i>	NM_005914 / NM_182746	MCM4 minichromosome maintenance deficient 4 ( <i>S. cerevisiae</i> )	32.67	10.00	3.27
211559_s_at	<i>CCNG2</i>	NM_004354	cyclin G2	16.67	5.11	3.26
209456_s_at	<i>FBXW11</i>	NM_012300 / NM_033644 / NM_033645	F-box and WD-40 domain protein 11	66.57	20.42	3.26
210735_s_at	<i>CA12</i>	NM_001218 / NM_206925	carbonic anhydrase XII	190.16	58.46	3.25
210052_s_at	<i>TPX2</i>	NM_012112	TPX2, microtubule-associated, homolog ( <i>Xenopus laevis</i> )	691.71	216.33	3.20
204764_at	<i>FNTB</i>	NM_002028	farnesyltransferase, CAAX box, beta	95.95	30.47	3.15
209906_at	<i>C3AR1</i>	NM_004054	complement component 3a receptor 1	23.28	7.46	3.12
201774_s_at	<i>CNAP1</i>	NM_014865	chromosome condensation-related SMC-associated protein 1	467.66	149.85	3.12
211966_at	<i>COL4A2</i>	NM_001846	collagen, type IV, alpha 2	52.83	17.44	3.03
201147_s_at	<i>TIMP3</i>	NM_000362	TIMP metalloproteinase inhibitor 3	43.90	14.52	3.02
201830_s_at	<i>NET1</i>	NM_005863	neuroepithelial cell transforming gene 1	122.64	40.69	3.01
206363_at	<i>MAF</i>	NM_001031804 / NM_005360	v-maf musculoaponeurotic fibrosarcoma oncogene homolog (avian)	415.48	137.94	3.01

209401_s_at	<i>SLC12A4</i>	NM_005072	solute carrier family 12, member 4	53.10	17.66	3.01
204475_at	<i>MMP1</i>	NM_002421	matrix metalloproteinase 1	192.36	64.09	3.00
217445_s_at	<i>GART</i>	NM_000819 / NM_175085	phosphoribosylglycinamide formyltransferase, phosphoribosylglycinamide synthetase	224.08	75.91	2.95
208853_s_at	<i>CANX</i>	NM_001024649 / NM_001746	calnexin	237.89	81.66	2.91
211519_s_at	<i>KIF2C</i>	NM_006845	kinesin family member 2C	97.80	33.68	2.90
211964_at	<i>COL4A2</i>	NM_001846	collagen, type IV, alpha 2	486.47	167.64	2.90
219213_at	<i>JAM2</i>	NM_021219	junctional adhesion molecule 2	15.53	5.45	2.85
211607_x_at	<i>EGFR</i>	NM_005228 / NM_201282 / NM_201283 / NM_201284	epidermal growth factor receptor	463.55	163.46	2.84
210984_x_at	<i>EGFR</i>	NM_005228 / NM_201282 / NM_201283 / NM_201284	epidermal growth factor receptor	475.74	170.80	2.79
210756_s_at	<i>NOTCH2</i>	NM_024408	Notch homolog 2 (Drosophila)	328.26	118.38	2.77
203798_s_at	<i>VSNL1</i>	NM_003385	visinin-like 1	90.05	32.73	2.75
209189_at	<i>FOS</i>	NM_005252	v-fos FBJ murine osteosarcoma viral oncogene homolog	1156.59	420.66	2.75
210892_s_at	<i>GTF2I</i>	NM_001518 / NM_032999 / NM_033000 / NM_033001	general transcription factor II, i	95.29	34.75	2.74
205729_at	<i>OSMR</i>	NM_003999	oncostatin M receptor	89.57	32.83	2.73
203967_at	<i>CDC6</i>	NM_001254	CDC6 cell division cycle 6 homolog (S. cerevisiae)	14.73	5.41	2.72
202240_at	<i>PLK1</i>	NM_005030	polo-like kinase 1 (Drosophila)	367.26	134.92	2.72



221530_s_at	<i>BHLHB3</i>	NM_030762	basic helix-loop-helix domain containing, class B, 3	66.58	24.51	2.72
211249_at	<i>GPR68</i>	NM_003485	G protein-coupled receptor 68	16.79	6.20	2.71
202363_at	<i>SPOCK1</i>	NM_004598	sparc/osteonectin, cwcv and kazal-like domains proteoglycan (testican) 1	55.22	20.40	2.71
218115_at	<i>ASF1B</i>	NM_018154	ASF1 anti-silencing function 1 homolog B ( <i>S. cerevisiae</i> )	123.19	45.68	2.70
212022_s_at	<i>MKI67</i>	NM_002417	antigen identified by monoclonal antibody Ki-67	383.86	143.95	2.67
211980_at	<i>COL4A1</i>	NM_001845	collagen, type IV, alpha 1	550.91	206.88	2.66
212190_at	<i>SERPINE2</i>	NM_006216	serpin peptidase inhibitor, clade E (nexin, plasminogen activator inhibitor type 1), member 2	668.64	252.62	2.65
202444_s_at	<i>SPFH1</i>	NM_006459	SPFH domain family, member 1	102.12	38.60	2.65
208351_s_at	<i>MAPK1</i>	NM_002745 / NM_138957	mitogen-activated protein kinase 1	92.19	35.08	2.63
201755_at	<i>MCM5</i>	NM_006739	MCM5 minichromosome maintenance deficient 5, cell division cycle 46 ( <i>S. cerevisiae</i> )	93.87	36.11	2.60
221901_at	<i>KIAA1644</i>	XM_376018 / XM_936510	KIAA1644 protein	111.78	43.02	2.60
204318_s_at	<i>GTSE1</i>	NM_016426	G-2 and S-phase expressed 1	114.61	44.39	2.58
52837_at	<i>KIAA1644</i>	XM_376018 / XM_936510	KIAA1644 protein	69.64	27.20	2.56
209098_s_at	<i>JAG1</i>	NM_000214	jagged 1 (Alagille syndrome)	212.90	83.59	2.55
209347_s_at	<i>MAF</i>	NM_001031804 / NM_005360	v-maf musculoaponeurotic fibrosarcoma oncogene homolog (avian)	24.86	9.79	2.54

204879_at	<i>PDPN</i>	NM_001006624 / NM_001006625 / NM_006474 / NM_198389	podoplanin	329.72	129.96	2.54
207357_s_at	<i>GALNT10</i>	NM_017540 / NM_198321	UDP-N-acetyl-alpha-D-galactosamine:poly peptide N-acetylgalactosaminyltransferase 10 (GalNAc-T10)	212.98	84.03	2.53
208852_s_at	<i>CANX</i>	NM_001024649 / NM_001746	calnexin	333.80	131.78	2.53
40837_at	<i>TLE2</i>	NM_003260	transducin-like enhancer of split 2 (E(sp1) homolog, Drosophila)	107.13	42.69	2.51
221520_s_at	<i>CDCA8</i>	NM_018101	cell division cycle associated 8	200.88	80.78	2.49
205015_s_at	<i>TGFA</i>	NM_003236	transforming growth factor, alpha	34.75	14.02	2.48
210543_s_at	<i>PRKDC</i>	NM_006904	protein kinase, DNA-activated, catalytic polypeptide	157.63	63.61	2.48
219093_at	<i>FLJ20701</i>	NM_017933	hypothetical protein FLJ20701	403.42	162.82	2.48
209758_s_at	<i>MFAP5</i>	NM_003480	microfibrillar associated protein 5	44.75	18.23	2.45
204962_s_at	<i>CENPA</i>	NM_001809	centromere protein A, 17kDa	219.28	90.09	2.43
210082_at	<i>ABCA4</i>	NM_000350	ATP-binding cassette, sub-family A (ABC1), member 4	11.46	4.77	2.40
214686_at	<i>ZNF266</i>	NM_006631 / NM_198058	zinc finger protein 266	17.77	7.41	2.40
206429_at	<i>F2RL1</i>	NM_005242	coagulation factor II (thrombin) receptor-like 1	38.12	16.02	2.38
210105_s_at	<i>FYN</i>	NM_002037 / NM_153047 / NM_153048	FYN oncogene related to SRC, FGR, YES	35.10	14.78	2.37

218073_s_at	<i>TMEM48</i>	NM_018087	transmembrane protein 48	76.98	33.03	2.33
218365_s_at	<i>DARS2</i>	NM_018122	aspartyl-tRNA synthetase 2 (mitochondrial)	56.42	24.32	2.32
204147_s_at	<i>TFDP1</i>	NM_007111	transcription factor Dp-1	108.10	46.74	2.31
218717_s_at	<i>LEPREL1</i>	NM_018192	leprecan-like 1	196.30	85.17	2.30
212372_at	<i>MYH10</i>	NM_005964	myosin, heavy polypeptide 10, non-muscle	80.32	34.96	2.30
202954_at	<i>UBE2C</i>	NM_007019 / NM_181799 / NM_181800 / NM_181801 / NM_181802 / NM_181803	ubiquitin-conjugating enzyme E2C	3038.31	1325.26	2.29
221004_s_at	<i>ITM2C</i>	NM_001012514 / NM_001012516 / NM_030926	integral membrane protein 2C	96.07	42.05	2.28
217010_s_at	<i>CDC25C</i>	NM_001790 / NM_022809	cell division cycle 25C	15.92	6.98	2.28
209408_at	<i>KIF2C</i>	NM_006845	kinesin family member 2C	270.75	119.13	2.27
216033_s_at	<i>FYN</i>	NM_002037 / NM_153047 / NM_153048	FYN oncogene related to SRC, FGR, YES	11.66	5.15	2.27
202779_s_at	<i>UBE2S</i>	NM_014501 / XM_941060	ubiquitin-conjugating enzyme E2S	2736.53	1214.09	2.25
207850_at	<i>CXCL3</i>	NM_002090	chemokine (C-X-C motif) ligand 3	106.06	47.22	2.25
215253_s_at	<i>DSCR1</i>	NM_004414 / NM_203417 / NM_203418	Down syndrome critical region gene 1	25.11	11.19	2.24
201645_at	<i>TNC</i>	NM_002160	tenascin C (hexabrachion)	304.33	136.18	2.23
215942_s_at	<i>GTSE1</i>	NM_016426	G-2 and S-phase expressed 1	36.42	16.31	2.23
202479_s_at	<i>TRIB2</i>	NM_021643	tribbles homolog 2 (Drosophila)	77.65	34.81	2.23
204033_at	<i>TRIP13</i>	NM_004237	thyroid hormone receptor interactor 13	286.45	128.65	2.23

202870_s_at	<i>CDC20</i>	NM_001255	CDC20 cell division cycle 20 homolog (S. cerevisiae)	2583.94	1160.70	2.23
219928_s_at	<i>CABYR</i>	NM_012189 / NM_138643 / NM_138644 / NM_153768 / NM_153769 / NM_153770	calcium binding tyrosine-(Y)-phosphorylation regulated (fibrousheathin 2)	58.24	26.32	2.21
217080_s_at	<i>HOMER2</i>	NM_004839 / NM_199330 / NM_199331 / NM_199332	homer homolog 2 (Drosophila)	107.14	48.48	2.21
212016_s_at	<i>PTBP1</i>	NM_002819 / NM_031990 / NM_031991 / NM_175847	polypyrimidine tract binding protein 1	763.83	348.48	2.19
209156_s_at	<i>COL6A2</i>	NM_001849 / NM_058174 / NM_058175	collagen, type VI, alpha 2	12.80	5.88	2.18
211194_s_at	<i>TP73L</i>	NM_003722	tumor protein p73-like	65.03	29.89	2.18
200641_s_at	<i>YWHAZ</i>	NM_003406 / NM_145690	tyrosine 3-monooxygenase/tryptophan 5-monooxygenase activation protein, zeta polypeptide	1891.11	870.58	2.17
201529_s_at	<i>RPA1</i>	NM_002945	replication protein A1, 70kDa	112.68	51.92	2.17
217173_s_at	<i>LDLR</i>	NM_000527	low density lipoprotein receptor (familial hypercholesterolemia)	332.27	153.20	2.17
215177_s_at	<i>ITGA6</i>	NM_000210	integrin, alpha 6	806.65	372.47	2.17
204768_s_at	<i>FEN1</i>	NM_004111	flap structure-specific endonuclease 1	205.73	95.00	2.17
218755_at	<i>KIF20A</i>	NM_005733	kinesin family member 20A	341.77	158.10	2.16
203865_s_at	<i>ADARBI</i>	NM_001033049 / NM_001112 / NM_015833 / NM_015834	adenosine deaminase, RNA-specific, B1 (RED1 homolog rat)	177.68	82.32	2.16

209395_at	<i>CHI3L1</i>	NM_001276	chitinase 3-like 1 (cartilage glycoprotein-39)	145.15	67.32	2.16
212021_s_at	<i>MKI67</i>	NM_002417	antigen identified by monoclonal antibody Ki-67	181.65	84.26	2.16
203676_at	<i>GNS</i>	NM_002076	glucosamine (N-acetyl)-6-sulfatase (Sanfilippo disease IIID)	15.58	7.23	2.15
213562_s_at	<i>SQLE</i>	NM_003129	squalene epoxidase	492.91	229.04	2.15
209645_s_at	<i>ALDH1B1</i>	NM_000692	aldehyde dehydrogenase 1 family, member B1	116.91	54.64	2.14
216969_s_at	<i>KIF22</i>	NM_007317	kinesin family member 22	158.72	74.29	2.14
209278_s_at	<i>TFPI2</i>	NM_006528	tissue factor pathway inhibitor 2	50.76	23.81	2.13
214536_at	<i>SLURP1</i>	NM_020427	secreted LY6/PLAUR domain containing 1	38.09	17.87	2.13
202718_at	<i>IGFBP2</i>	NM_000597	insulin-like growth factor binding protein 2, 36kDa	201.29	94.69	2.13
221436_s_at	<i>CDCA3</i>	NM_031299	cell division cycle associated 3	195.39	91.95	2.12
209896_s_at	<i>PTPN11</i>	NM_002834	protein tyrosine phosphatase, non-receptor type 11 (Noonan syndrome 1)	17.55	8.26	2.12
208782_at	<i>FSTL1</i>	NM_007085	folliculin-like 1	210.15	98.97	2.12
215357_s_at	<i>POLDIP3</i>	NM_032311 / NM_178136	polymerase (DNA-directed), delta interacting protein 3	116.88	55.07	2.12
217202_s_at	<i>GLUL</i>	NM_001033044 / NM_001033056 / NM_002065	glutamate-ammonia ligase (glutamine synthetase)	79.13	37.34	2.12

200900_s_at	<i>M6PR</i>	NM_002355	mannose-6-phosphate receptor (cation dependent)	316.05	149.12	2.12
204589_at	<i>NUAK1</i>	NM_014840	NUAK family, SNF1-like kinase, 1	194.88	92.30	2.11
218009_s_at	<i>PRC1</i>	NM_003981 / NM_199413 / NM_199414	protein regulator of cytokinesis 1	337.52	159.87	2.11
201984_s_at	<i>EGFR</i>	NM_005228 / NM_201282 / NM_201283 / NM_201284	epidermal growth factor receptor (erythroblastic leukemia viral (v-erb-b) oncogene homolog, avian)	2124.37	1007.51	2.11
210935_s_at	<i>WDR1</i>	NM_005112 / NM_017491	WD repeat domain 1	559.44	265.33	2.11
211905_s_at	<i>ITGB4</i>	NM_000213 / NM_001005619 / NM_001005731	integrin, beta 4	1052.93	500.01	2.11
216689_x_at	<i>ARHGAP1</i>	NM_004308	Rho GTPase activating protein 1	222.84	106.03	2.10
201801_s_at	<i>SLC29A1</i>	NM_004955	solute carrier family 29 (nucleoside transporters), member 1	64.64	30.82	2.10
203145_at	<i>SPAG5</i>	NM_006461	sperm associated antigen 5	99.59	47.51	2.10
214710_s_at	<i>CCNB1</i>	NM_031966	cyclin B1	1404.09	670.35	2.09
209615_s_at	<i>PAK1</i>	NM_002576	p21/Cdc42/Rac1-activated kinase 1 (STE20 homolog, yeast)	78.62	37.63	2.09
218726_at	<i>DKFZp762E1312</i>	NM_018410	hypothetical protein DKFZp762E1312	60.36	28.91	2.09
211804_s_at	<i>CDK2</i>	NM_001798 / NM_052827	cyclin-dependent kinase 2	103.89	50.00	2.08
203976_s_at	<i>CHAF1A</i>	NM_005483	chromatin assembly factor 1, subunit A (p150)	38.07	18.35	2.07

211162_x_at	<i>SCD</i>	NM_005063	stearoyl-CoA desaturase (delta-9-desaturase)	1184.84	572.31	2.07
58916_at	<i>KCTD14</i>	NM_023930	potassium channel tetramerisation domain containing 14	28.95	14.00	2.07
218308_at	<i>TACC3</i>	NM_006342	transforming, acidic coiled-coil containing protein 3	202.69	98.40	2.06
200796_s_at	<i>MCL1</i>	NM_021960 / NM_182763	myeloid cell leukemia sequence 1 (BCL2-related)	34.79	16.94	2.05
209624_s_at	<i>MCCC2</i>	NM_022132	methylcrotonoyl-Coenzyme A carboxylase 2 (beta)	26.63	13.00	2.05
209396_s_at	<i>CHI3L1</i>	NM_001276	chitinase 3-like 1 (cartilage glycoprotein-39)	100.75	49.24	2.05
212614_at	<i>ARID5B</i>	NM_032199	AT rich interactive domain 5B (MRF1-like)	18.89	9.26	2.04
204140_at	<i>TPST1</i>	NM_003596	tyrosylprotein sulfotransferase 1	164.97	80.90	2.04
215739_s_at	<i>TUBGCP3</i>	NM_006322	tubulin, gamma complex associated protein 3	94.67	46.43	2.04
201555_at	<i>MCM3</i>	NM_002388	MCM3 minichromosome maintenance deficient 3 ( <i>S. cerevisiae</i> )	304.81	149.69	2.04
204508_s_at	<i>CA12</i>	NM_001218 / NM_206925	carbonic anhydrase XII	121.17	59.66	2.03
210301_at	<i>XDH</i>	NM_000379	xanthine dehydrogenase	245.51	120.99	2.03
207821_s_at	<i>PTK2</i>	NM_005607 / NM_153831	PTK2 protein tyrosine kinase 2	283.60	140.15	2.02
200644_at	<i>MARCKSL1</i>	NM_023009	MARCKS-like 1	166.24	82.36	2.02
212949_at	<i>BRRN1</i>	NM_015341	barren homolog 1 ( <i>Drosophila</i> )	28.66	14.21	2.02

202095_s_at	<i>BIRC5</i>	NM_001012270 / NM_001012271 / NM_001168	baculoviral IAP repeat-containing 5 (survivin)	473.20	235.27	2.01
202058_s_at	<i>KPNA1</i>	NM_002264	karyopherin alpha 1 (importin alpha 5)	187.66	93.38	2.01
221029_s_at	<i>WNT5B</i>	NM_030775 / NM_032642	wingless-type MMTV integration site family, member 5B	47.71	23.74	2.01
203963_at	<i>CA12</i>	NM_001218 / NM_206925	carbonic anhydrase XII	1086.47	540.99	2.01
208539_x_at	<i>SPRR2B</i>	NM_001017418	small proline-rich protein 2B	5343.04	2670.07	2.00
207655_s_at	<i>BLNK</i>	NM_013314	B-cell linker	122.03	244.59	0.50
209533_s_at	<i>PLAA</i>	NM_001031689 / NM_004253	phospholipase A2-activating protein	63.38	127.13	0.50
202219_at	<i>SLC6A8</i>	NM_005629	solute carrier family 6 (neurotransmitter transporter, creatine), member 8	356.75	718.43	0.50
213510_x_at	<i>LOC220594</i>	NM_145809	TL132 protein	12.83	25.89	0.50
221568_s_at	<i>LIN7C</i>	NM_018362	lin-7 homolog C (C. elegans)	21.41	43.29	0.49
213082_s_at	<i>SLC35D2</i>	NM_007001	solute carrier family 35, member D2	79.26	160.33	0.49
210580_x_at	<i>SULT1A3</i>	NM_001017387 / NM_001017389 / NM_001017390 / NM_001017391 / NM_003166 / NM_177552	sulfotransferase family, cytosolic, 1A, phenol-preferring, member 3	53.48	108.19	0.49
205660_at	<i>OASL</i>	NM_003733 / NM_198213	2'-5'-oligoadenylate synthetase-like	193.82	393.43	0.49
202357_s_at	<i>CFB</i>	NM_001710	complement factor B	94.01	191.29	0.49
212989_at	<i>TMEM23</i>	NM_147156	transmembrane protein 23	40.03	81.72	0.49



204686_at	<i>IRS1</i>	NM_005544	insulin receptor substrate 1	118.07	241.06	0.49
214329_x_at	<i>TNFSF10</i>	NM_003810	tumor necrosis factor (ligand) superfamily, member 10	44.20	90.28	0.49
209422_at	<i>PHF20</i>	NM_016436	PHD finger protein 20	77.62	158.60	0.49
202869_at	<i>OAS1</i>	NM_001032409 / NM_002534 / NM_016816	2',5'-oligoadenylate synthetase 1, 40/46kDa	126.11	258.43	0.49
218446_s_at	<i>FAM18B</i>	NM_016078	family with sequence similarity 18, member B	47.24	96.87	0.49
219424_at	<i>EBI3</i>	NM_005755	Epstein-Barr virus induced gene 3	19.66	40.35	0.49
208841_s_at	<i>G3BP2</i>	NM_012297 / NM_203504 / NM_203505	Ras-GTPase activating protein SH3 domain-binding protein 2	81.38	167.15	0.49
204454_at	<i>LDOC1</i>	NM_012317	leucine zipper, down-regulated in cancer 1	953.41	1959.60	0.49
203909_at	<i>SLC9A6</i>	NM_006359	solute carrier family 9 (sodium/hydrogen exchanger), member 6	35.79	73.82	0.48
222158_s_at	<i>Clorf121</i>	NM_016076	chromosome 1 open reading frame 121	14.79	30.54	0.48
208801_at	<i>SRP72</i>	NM_006947	signal recognition particle 72kDa	57.96	119.73	0.48
49452_at	<i>ACACB</i>	NM_001093	acetyl-Coenzyme A carboxylase beta	29.49	60.95	0.48
200994_at	<i>IPO7</i>	NM_006391	Importin 7	39.24	81.14	0.48
203247_s_at	<i>ZNF24</i>	NM_006965	zinc finger protein 24	12.43	25.73	0.48
203446_s_at	<i>OCRL</i>	NM_000276 / NM_001587	oculocerebrorenal syndrome of Lowe	51.08	105.81	0.48
201828_x_at	<i>CXX1</i>	NM_003928	CAAX box 1	1810.05	3750.20	0.48
219503_s_at	<i>TMEM40</i>	NM_018306	transmembrane protein 40	20.04	41.54	0.48
219628_at	<i>WIG1</i>	NM_022470 / NM_152240	p53 target zinc finger protein	26.58	55.17	0.48

218042_at	<i>COPS4</i>	NM_016129	COP9 constitutive photomorphogenic homolog subunit 4 (Arabidopsis)	19.22	39.94	0.48
202854_at	<i>HPRT1</i>	NM_000194	hypoxanthine phosphoribosyltransferase 1 (Lesch-Nyhan syndrome)	409.07	851.08	0.48
209565_at	<i>RNF113A</i>	NM_006978	ring finger protein 113A	158.91	330.99	0.48
201904_s_at	<i>CTDSPL</i>	NM_001008392 / NM_005808	CTD (carboxy-terminal domain, RNA polymerase II, polypeptide A) small phosphatase-like	167.47	349.18	0.48
205483_s_at	<i>ISG15</i>	NM_005101	ISG15 ubiquitin-like modifier	469.58	979.50	0.48
204897_at	<i>PTGER4</i>	NM_000958	prostaglandin E receptor 4 (subtype EP4)	15.27	31.87	0.48
204014_at	<i>DUSP4</i>	NM_001394 / NM_057158	dual specificity phosphatase 4	78.05	162.95	0.48
221514_at	<i>UTP14A</i>	NM_006649	UTP14, U3 small nucleolar ribonucleoprotein, homolog A (yeast)	156.08	326.84	0.48
203007_x_at	<i>LYPLA1</i>	NM_006330	lysophospholipase I	48.47	101.55	0.48
213883_s_at	<i>TM2D1</i>	NM_032027	TM2 domain containing 1	46.96	98.40	0.48
201921_at	<i>GNG10</i>	NM_001017998 / NM_004125 / XM_929619 / XM_940579	guanine nucleotide binding protein (G protein), gamma 10	368.56	775.54	0.48
207847_s_at	<i>MUC1</i>	NM_001018016 / NM_001018017 / NM_001018021 / NM_002456	mucin 1, cell surface associated	41.04	86.42	0.47
203108_at	<i>GPRC5A</i>	NM_003979	G protein-coupled receptor, family C, group 5, member A	208.08	438.12	0.47

213587_s_at	<i>ATP6V0E2L</i>	NM_145230	ATPase, H <sup>+</sup> transporting V0 subunit E2-like (rat)	25.27	53.41	0.47
218952_at	<i>PCSK1N</i>	NM_013271	proprotein convertase subtilisin/kexin type 1 inhibitor	169.94	359.28	0.47
221931_s_at	<i>SEH1L</i>	NM_001013437 / NM_031216	SEH1-like ( <i>S. cerevisiae</i> )	43.80	92.68	0.47
221989_at	<i>RPL10</i>	NM_006013 / XM_209178 / XM_209500 / XM_371781 / XM_497357 / XM_926723 / XM_929431 / XM_930080 / XM_931512 / XM_931519 / XM_931525 / XM_931532 / XM_931535 / XM_934704 / XM_934705 / XM_934706 / XM_937850 / XM_939745 / XM_941543 / XM_941661 / XM_942217 / XM_944311 / XM_944319 / XM_944324 / XM_945797 / XM_945798 / XM_945799 / XM_945800	ribosomal protein L10	4.90	10.38	0.47
205145_s_at	<i>MYL5</i>	NM_002477 / XM_938923	myosin, light polypeptide 5, regulatory	12.55	26.56	0.47
201238_s_at	<i>CAPZA2</i>	NM_006136	capping protein (actin filament) muscle Z-line, alpha 2	89.77	191.02	0.47

210645_s_at	<i>TTC3</i>	NM_001001894 / NM_003316	tetratricopeptide repeat domain 3	24.14	51.41	0.47
210136_at	<i>MBP</i>	NM_001025081 / NM_001025090 / NM_001025092 / NM_001025094 / NM_001025098 / NM_001025100 / NM_001025101 / NM_002385	myelin basic protein	8.49	18.08	0.47
201358_s_at	<i>COPB</i>	NM_016451	coatamer protein complex, subunit beta	142.12	304.25	0.47
210511_s_at	<i>INHBA</i>	NM_002192	inhibin, beta A (activin A, activin AB alpha polypeptide)	129.36	276.98	0.47
201888_s_at	<i>IL13RA1</i>	NM_001560	interleukin 13 receptor, alpha 1	23.61	50.66	0.47
209115_at	<i>UBE1C</i>	NM_003968 / NM_198195 / NM_198197	ubiquitin-activating enzyme E1C (UBA3 homolog, yeast)	27.53	59.10	0.47
217739_s_at	<i>PBEF1</i>	NM_005746 / NM_182790 / XM_929247	pre-B-cell colony enhancing factor 1	30.38	65.23	0.47
213361_at	<i>TDRD7</i>	NM_014290	tudor domain containing 7	8.68	18.65	0.47
210663_s_at	<i>KYNU</i>	NM_001032998 / NM_003937	kynureninase (L-kynurenine hydrolase)	104.25	224.59	0.46
204698_at	<i>ISG20</i>	NM_002201	interferon stimulated exonuclease gene 20kDa	383.20	826.64	0.46

204415_at	<i>IFI6</i>	NM_002038 / NM_022872 / NM_022873	interferon, alpha-inducible protein 6	34.19	73.79	0.46
218053_at	<i>PRPF40A</i>	XM_371575 / XM_931099 / XM_938514 / XM_943711	PRP40 pre-mRNA processing factor 40 homolog A (yeast)	61.31	132.43	0.46
207719_x_at	<i>CEP170</i>	NM_014812	centrosomal protein 170kDa	10.04	21.69	0.46
206295_at	<i>IL18</i>	NM_001562	interleukin 18 (interferon-gamma-inducing factor)	86.99	188.27	0.46
33304_at	<i>ISG20</i>	NM_002201	interferon stimulated exonuclease gene 20kDa	222.58	482.12	0.46
214112_s_at	<i>CXorf40A</i>	NM_001013845 / NM_178124	chromosome X open reading frame 40A	219.43	479.14	0.46
205315_s_at	<i>SNTB2</i>	NM_006750 / NM_130845	syntrophin, beta 2 (dystrophin-associated protein A1, 59kDa, basic component 2)	40.07	87.78	0.46
217948_at	---	---	---	322.08	706.40	0.46
214022_s_at	<i>IFITM1</i>	NM_003641	interferon induced transmembrane protein 1 (9-27)	1869.34	4135.74	0.45
211122_s_at	<i>CXCL11</i>	NM_005409	chemokine (C-X-C motif) ligand 11	5.81	12.87	0.45
212510_at	<i>GPDI1</i>	NM_015141	glycerol-3-phosphate dehydrogenase 1-like	10.17	22.53	0.45
205595_at	<i>DSG3</i>	NM_001944	desmoglein 3 (pemphigus vulgaris antigen)	80.07	177.64	0.45
202923_s_at	<i>GCLC</i>	NM_001498	glutamate-cysteine ligase, catalytic subunit	75.00	167.13	0.45
202169_s_at	<i>AASDHPPT</i>	NM_015423	aminoadipate-semialdehyde dehydrogenase-phosphopantetheinyl transferase	11.33	25.30	0.45

202351_at	<i>ITGAV</i>	NM_002210	integrin, alpha V (vitronectin receptor, alpha polypeptide, antigen CD51)	228.62	510.51	0.45
219356_s_at	<i>CHMP5</i>	NM_016410	chromatin modifying protein 5	108.75	242.88	0.45
201864_at	<i>GDI1</i>	NM_001493	GDP dissociation inhibitor 1	160.21	358.31	0.45
222266_at	<i>C19orf2</i>	NM_003796 / NM_134447	Chromosome 19 open reading frame 2	11.46	25.69	0.45
204020_at	<i>PURA</i>	NM_005859	purine-rich element binding protein A	89.35	200.32	0.45
218086_at	<i>NPDC1</i>	NM_015392	neural proliferation, differentiation and control, 1	147.25	330.55	0.45
209028_s_at	<i>ABI1</i>	NM_001012750 / NM_001012751 / NM_001012752 / NM_005470	abl-interactor 1	48.80	109.59	0.45
218237_s_at	<i>SLC38A1</i>	NM_030674	solute carrier family 38, member 1	269.77	608.07	0.44
202437_s_at	<i>CYP1B1</i>	NM_000104	cytochrome P450, family 1, subfamily B, polypeptide 1	27.81	62.70	0.44
213016_at	---	---	ARTC1 mRNA, complete sequence	15.13	34.12	0.44
201996_s_at	<i>SPEN</i>	NM_015001	spen homolog, transcriptional regulator (Drosophila)	32.11	72.47	0.44
217388_s_at	<i>KYNU</i>	NM_001032998 / NM_003937	kynureninase (L-kynurenine hydrolase)	280.28	634.02	0.44
212640_at	<i>PTPLB</i>	NM_198402	protein tyrosine phosphatase-like (proline instead of catalytic arginine), member b	202.85	459.88	0.44
219010_at	<i>C1orf106</i>	NM_018265	chromosome 1 open reading frame 106	257.64	585.64	0.44

219351_at	<i>TRAPPC2</i>	NM_001011658 / NM_014563	trafficking protein particle complex 2	31.50	71.62	0.44
213083_at	<i>SLC35D2</i>	NM_007001	solute carrier family 35, member D2	103.19	234.84	0.44
218163_at	<i>MCTS1</i>	NM_014060	malignant T cell amplified sequence 1	228.29	521.74	0.44
207941_s_at	<i>RNPC2</i>	NM_004902 / NM_184234 / NM_184237 / NM_184241 / NM_184244	RNA-binding region (RNP1, RRM) containing 2	34.40	78.71	0.44
214722_at	<i>NOTCH2NL</i>	NM_203458	Notch homolog 2 (Drosophila) N-terminal like	69.57	159.38	0.44
209726_at	<i>CA11</i>	NM_001217	carbonic anhydrase XI	45.82	105.08	0.44
203917_at	<i>CXADR</i>	NM_001338	coxsackie virus and adenovirus receptor	31.01	71.25	0.44
38043_at	<i>FAM3A</i>	NM_021806	family with sequence similarity 3, member A	29.77	68.61	0.43
218986_s_at	<i>FLJ20035</i>	NM_017631	hypothetical protein FLJ20035	12.73	29.34	0.43
222242_s_at	<i>KLK5</i>	NM_012427	kallikrein 5	11.35	26.38	0.43
53991_at	<i>DENND2A</i>	NM_015689	DENN/MADD domain containing 2A	8.82	20.60	0.43
209289_at	<i>NFIB</i>	NM_005596	nuclear factor I/B	27.75	64.90	0.43
201540_at	<i>FHL1</i>	NM_001449	four and a half LIM domains 1	451.06	1059.88	0.43
204097_s_at	<i>RBMX2</i>	NM_016024	RNA binding motif protein, X-linked 2	9.32	21.99	0.42
202602_s_at	<i>HTATSF1</i>	NM_014500	HIV-1 Tat specific factor 1	33.73	79.70	0.42
204981_at	<i>SLC22A18</i>	NM_002555 / NM_183233	solute carrier family 22 (organic cation transporter), member 18	86.64	205.14	0.42
200696_s_at	<i>GSN</i>	NM_000177 / NM_198252	gelsolin (amyloidosis, Finnish type)	385.91	914.82	0.42
221841_s_at	<i>KLF4</i>	NM_004235	Kruppel-like factor 4 (gut)	111.47	264.55	0.42

205709_s_at	<i>CDS1</i>	NM_001263	CDP-diacylglycerol synthase (phosphatidate cytidyltransferase) 1	18.03	42.93	0.42
216942_s_at	<i>CD58</i>	NM_001779	CD58 molecule	14.54	34.65	0.42
213294_at	---	---	Full-length cDNA clone CS0DK002YF13 of HeLa cells Cot 25-normalized of Homo sapiens (human)	7.66	18.29	0.42
212415_at	<i>SEPT6</i>	NM_015129 / NM_145799 / NM_145800 / NM_145802	septin 6	4.62	11.03	0.42
212616_at	<i>CHD9</i>	NM_025134	chromodomain helicase DNA binding protein 9	7.23	17.34	0.42
217947_at	<i>CMTM6</i>	NM_017801	CKLF-like MARVEL transmembrane domain containing 6	206.54	498.31	0.41
211612_s_at	<i>IL13RA1</i>	NM_001560	interleukin 13 receptor, alpha 1	43.45	104.96	0.41
212531_at	<i>LCN2</i>	NM_005564	lipocalin 2 (oncogene 24p3)	174.02	420.45	0.41
201661_s_at	<i>ACSL3</i>	NM_004457 / NM_203372	acyl-CoA synthetase long-chain family member 3	10.17	24.61	0.41
213729_at	<i>PRPF40A</i>	XM_371575 / XM_931099 / XM_938514 / XM_943711	PRP40 pre-mRNA processing factor 40 homolog A (yeast)	6.42	15.54	0.41
205220_at	<i>GPR109B</i>	NM_006018	G protein-coupled receptor 109B	266.95	645.95	0.41
203186_s_at	<i>S100A4</i>	NM_002961 / NM_019554	S100 calcium binding protein A4 (calcium protein, calvasculin, metastasin, murine placental homolog)	94.02	227.62	0.41
203821_at	<i>HBEGF</i>	NM_001945	heparin-binding EGF-like growth factor	403.66	977.38	0.41



221766_s_at	<i>FAM46A</i>	NM_017633	family with sequence similarity 46, member A	10.35	25.10	0.41
215813_s_at	<i>PTGSI</i>	NM_000962 / NM_080591	prostaglandin-endoperoxide synthase 1 (prostaglandin G/H synthase and cyclooxygenase)	31.23	76.88	0.41
202277_at	<i>SPTLC1</i>	NM_006415 / NM_178324	serine palmitoyltransferase, long chain base subunit 1	44.77	110.99	0.40
202829_s_at	<i>SYBL1</i>	NM_005638	synaptobrevin-like 1	15.37	38.13	0.40
201887_at	<i>IL13RA1</i>	NM_001560	interleukin 13 receptor, alpha 1	37.84	93.97	0.40
216095_x_at	<i>MTMR1</i>	NM_003828	myotubularin related protein 1	128.02	318.26	0.40
217813_s_at	<i>SPIN</i>	NM_006717	spindlin	23.85	59.32	0.40
205428_s_at	<i>CALB2</i>	NM_001740 / NM_007087 / NM_007088	calbindin 2, 29kDa (calretinin)	57.31	143.13	0.40
204343_at	<i>ABCA3</i>	NM_001089	ATP-binding cassette, sub-family A (ABC1), member 3	15.33	38.38	0.40
38037_at	<i>HBEGF</i>	NM_001945	heparin-binding EGF-like growth factor	144.05	361.24	0.40
209194_at	<i>CETN2</i>	NM_004344	centrin, EF-hand protein, 2	74.08	187.44	0.40
202371_at	<i>TCEAL4</i>	NM_001006935 / NM_001006936 / NM_001006937 / NM_024863	transcription elongation factor A (SII)-like 4	105.84	269.43	0.39
206645_s_at	<i>NR0B1</i>	NM_000475	nuclear receptor subfamily 0, group B, member 1	42.07	107.59	0.39
221829_s_at	<i>TNPO1</i>	NM_002270 / NM_153188	transportin 1	83.30	213.54	0.39

219045_at	<i>RHOF</i>	NM_019034	ras homolog gene family, member F (in filopodia)	210.67	540.25	0.39
211343_s_at	<i>COL13A1</i>	NM_005203 / NM_080798 / NM_080799 / NM_080800 / NM_080801 / NM_080802 / NM_080803 / NM_080804 / NM_080805 / NM_080806 / NM_080807 / NM_080808 / NM_080809 / NM_080810 / NM_080811 / NM_080812 / NM_080813 / NM_080814 / NM_080815	collagen, type XIII, alpha 1	34.51	88.75	0.39
205900_at	<i>KRT1</i>	NM_006121	keratin 1 (epidermolytic hyperkeratosis)	37.24	95.82	0.39
203156_at	<i>AKAP11</i>	NM_016248 / NM_144490	A kinase (PRKA) anchor protein 11	8.20	21.24	0.39
215245_x_at	<i>FMR1</i>	NM_002024	fragile X mental retardation 1	30.13	78.43	0.38
201215_at	<i>PLS3</i>	NM_005032	plastin 3 (T isoform)	155.28	411.68	0.38
221553_at	<i>RP11-217H1.1</i>	NM_032121 / XM_927839	implantation-associated protein	34.17	90.64	0.38
203042_at	<i>LAMP2</i>	NM_002294 / NM_013995	lysosomal-associated membrane protein 2	237.56	638.66	0.37
201132_at	<i>HNRPH2</i>	NM_001032393 / NM_019597	heterogeneous nuclear ribonucleoprotein H2 (H')	52.45	143.04	0.37
221581_s_at	<i>LAT2</i>	NM_014146 / NM_022040 / NM_032463	linker for activation of T cells family, member 2	59.56	163.24	0.36

201865_x_at	<i>NR3C1</i>	NM_000176 / NM_001018074 / NM_001018075 / NM_001018076 / NM_001018077 / NM_001020825 / NM_001024094	nuclear receptor subfamily 3, group C, member 1 (glucocorticoid receptor)	120.48	332.55	0.36
213593_s_at	<i>TRA2A</i>	NM_013293	Transformer-2 alpha	12.37	34.25	0.36
210367_s_at	<i>PTGES</i>	NM_004878	prostaglandin E synthase	88.52	246.35	0.36
212007_at	<i>UBXD2</i>	NM_014607	UBX domain containing 2	41.95	117.00	0.36
205767_at	<i>EREG</i>	NM_001432	epiregulin	65.08	183.71	0.35
200914_x_at	<i>KTN1</i>	NM_182926	kinectin 1 (kinesin receptor)	118.02	343.43	0.34
210387_at	<i>HIST1H2BG</i>	NM_003518	histone 1, H2bg	198.74	579.17	0.34
202378_s_at	<i>LEPROT</i>	NM_017526	leptin receptor overlapping transcript	78.41	228.55	0.34
203780_at	<i>EVA1</i>	NM_005797 / NM_144765	epithelial V-like antigen 1	45.59	133.29	0.34
202435_s_at	<i>CYP1B1</i>	NM_000104	cytochrome P450, family 1, subfamily B, polypeptide 1	15.25	44.59	0.34
221844_x_at	---	---	CDNA clone IMAGE:6208446	32.98	96.74	0.34
212622_at	<i>TMEM41B</i>	NM_015012	transmembrane protein 41B	8.86	26.02	0.34
201472_at	<i>VBPI</i>	NM_003372	von Hippel-Lindau binding protein 1	54.92	161.81	0.34
203303_at	<i>DYNLT3</i>	NM_006520	dynein, light chain, Tctex-type 3	15.03	44.35	0.34
204533_at	<i>CXCL10</i>	NM_001565	chemokine (C-X-C motif) ligand 10	8.07	24.04	0.34

212605_s_at	---	---	AF034176 Human mRNA (Tripodis and Ragoussis) Homo sapiens cDNA clone ntcon5 contig	13.86	41.36	0.34
214718_at	<i>GATAD1</i>	NM_021167	GATA zinc finger domain containing 1	11.00	33.09	0.33
209022_at	<i>STAG2</i>	NM_006603	stromal antigen 2	7.90	24.13	0.33
205623_at	<i>ALDH3A1</i>	NM_000691	aldehyde dehydrogenase 3 family, memberA1	24.99	77.90	0.32
219956_at	<i>GALNT6</i>	NM_007210	UDP-N-acetyl-alpha-D-galactosamine:poly peptide N-acetylgalactosaminyltransferase 6 (GalNAc-T6)	47.43	147.85	0.32
205128_x_at	<i>PTGS1</i>	NM_000962 / NM_080591	prostaglandin-endoperoxide synthase 1 (prostaglandin G/H synthase and cyclooxygenase)	39.76	125.00	0.32
202376_at	<i>SERPINA3</i>	NM_001085	serpin peptidase inhibitor, clade A (alpha-1 antiproteinase, antitrypsin), member 3	62.35	196.67	0.32
213229_at	<i>DICER1</i>	NM_030621 / NM_177438	Dicer1, Dcr-1 homolog (Drosophila)	146.36	464.53	0.32
212223_at	<i>IDS</i>	NM_000202 / NM_006123	iduronate 2-sulfatase (Hunter syndrome)	58.68	186.65	0.31
204584_at	<i>L1CAM</i>	NM_000425 / NM_024003	L1 cell adhesion molecule	102.94	327.45	0.31
219995_s_at	<i>FLJ13841</i>	NM_024702	hypothetical protein LOC79755	245.82	795.33	0.31
219001_s_at	<i>WDR32</i>	NM_024345	WD repeat domain 32	8.09	26.25	0.31

208241_at	<i>NRG1</i>	NM_004495 / NM_013956 / NM_013957 / NM_013958 / NM_013959 / NM_013960 / NM_013961 / NM_013962 / NM_013964	neuregulin 1	5.57	18.19	0.31
211671_s_at	<i>NR3C1</i>	NM_000176 / NM_001018074 / NM_001018075 / NM_001018076 / NM_001018077 / NM_001020825 / NM_001024094	nuclear receptor subfamily 3, group C, member 1 (glucocorticoid receptor)	78.44	263.10	0.30
204602_at	<i>DKK1</i>	NM_012242	dickkopf homolog 1 ( <i>Xenopus laevis</i> )	76.05	259.47	0.29
213135_at	<i>TIAM1</i>	NM_003253	T-cell lymphoma invasion and metastasis 1	7.06	24.42	0.29
204881_s_at	<i>UGCG</i>	NM_003358	UDP-glucose ceramide glucosyltransferase	34.89	120.86	0.29
206342_x_at	<i>IDS</i>	NM_000202 / NM_006123	iduronate 2-sulfatase (Hunter syndrome)	77.09	267.58	0.29
218085_at	<i>CHMP5</i>	NM_016410	chromatin modifying protein 5	23.89	84.03	0.28
212414_s_at	<i>SEPT6</i>	NM_015129 / NM_032569 / NM_145799 / NM_145800 / NM_145802	septin 6	19.17	68.28	0.28
215206_at	<i>EXT1</i>	NM_000127	Exostoses (multiple) 1	29.69	106.70	0.28
205097_at	<i>SLC26A2</i>	NM_000112	solute carrier family 26 (sulfate transporter), member 2	23.64	85.76	0.28

204976_s_at	<i>AMMECRI</i>	NM_001025580 / NM_015365	Alport syndrome, mental retardation, midface hypoplasia and elliptocytosis chromosomal region, gene 1	9.92	36.28	0.27
204351_at	<i>S100P</i>	NM_005980	S100 calcium binding protein P	48.68	180.28	0.27
217975_at	<i>WBP5</i>	NM_001006612 / NM_001006613 / NM_001006614 / NM_016303	WW domain binding protein 5	108.30	441.28	0.25
205363_at	<i>BBOX1</i>	NM_003986	butyrobetaine (gamma), 2-oxoglutarate dioxygenase (gamma-butyrobetaine hydroxylase) 1	29.13	120.76	0.24
209792_s_at	<i>KLK10</i>	NM_002776 / NM_145888	kallikrein 10	120.93	505.96	0.24
202439_s_at	<i>IDS</i>	NM_000202 / NM_006123	iduronate 2-sulfatase (Hunter syndrome)	64.34	270.52	0.24
212221_x_at	<i>IDS</i>	NM_000202 / NM_006123	iduronate 2-sulfatase (Hunter syndrome)	133.36	571.11	0.23
200821_at	<i>LAMP2</i>	NM_002294 / NM_013995	lysosomal-associated membrane protein 2	81.15	347.91	0.23
201917_s_at	<i>SLC25A36</i>	NM_018155	solute carrier family 25, member 36	6.22	28.72	0.22
205569_at	<i>LAMP3</i>	NM_014398	lysosomal-associated membrane protein 3	13.64	64.51	0.21
204750_s_at	<i>DSC2</i>	NM_004949 / NM_024422	desmocollin 2	33.27	159.80	0.21
218668_s_at	<i>RAP2C</i>	NM_021183	RAP2C, member of RAS oncogene family	11.22	54.25	0.21
205809_s_at	<i>WASL</i>	NM_003941	Wiskott-Aldrich syndrome-like	15.28	77.44	0.20
201007_at	<i>HADHB</i>	NM_000183	hydroxyacyl-Coenzyme A dehydrogenase	1389.06	7136.54	0.19
203453_at	<i>SCNN1A</i>	NM_001038	sodium channel, nonvoltage-gated 1 alpha	14.92	142.26	0.10
202411_at	<i>IFI27</i>	NM_005532	interferon, alpha-inducible protein 27	13.86	155.11	0.09

**Supplementary Table 3 Statistically over-represented transcription factor binding sites in gene lists identified from transcript profiling experiments<sup>1</sup>**

	Rank	Hits (%)	Z-score	Fisher <i>P</i> -value
A. Genes differentially expressed in response to N-CoR2 overexpression (N-CoR2 signature genes; 304 input; 203 analyzed):				
RREB-1	1	18 (8.87)	14.97	$7.99 \times 10^{-4}$
Pbx <sup>2</sup>	2	36 (17.73)	11.77	$1.86 \times 10^{-3}$
Pax-4	3	5 (2.46)	11.22	$3.38 \times 10^{-2}$
HLF	4	67 (33)	9.902	$2.68 \times 10^{-3}$
FREAC-2	5	41 (20.2)	9.449	$3.71 \times 10^{-2}$
c-FOS <sup>2</sup>	6	117 (57.64)	8.812	$1.24 \times 10^{-2}$
SOX-9	7	110 (54.19)	8.132	$6.89 \times 10^{-3}$
SOX-17	8	139 (68.47)	7.616	$2.83 \times 10^{-3}$
SRF <sup>2</sup>	9	14 (6.9)	7.367	$8.53 \times 10^{-3}$
cEBP	10	95 (46.8)	7.341	$4.34 \times 10^{-2}$
SRY	11	138 (67.98)	6.762	$6.45 \times 10^{-3}$
Nkx	12	161 (79.31)	6.413	$1.01 \times 10^{-3}$
FREAC-4	13	95 (46.8)	6.37	$1.35 \times 10^{-2}$
HFH-3	14	99 (48.77)	6.287	$3.47 \times 10^{-2}$
p65 <sup>2</sup>	15	62 (30.54)	6.129	$5.12 \times 10^{-3}$
Sox5	16	143 (70.44)	5.336	$3.83 \times 10^{-3}$
S8	17	146 (71.92)	4.744	$1.82 \times 10^{-2}$
ARNT	18	103 (50.74)	4.198	$3.59 \times 10^{-2}$
n-Myc	19	101 (49.75)	4.139	$3.99 \times 10^{-2}$
TEF-1	20	45 (22.17)	3.538	$8.19 \times 10^{-3}$
c-REL <sup>2</sup>	21	94 (46.31)	3.42	$1.12 \times 10^{-2}$
Max	22	76 (37.44)	3.031	$7.16 \times 10^{-3}$
USF	23	98 (48.28)	2.696	$2.66 \times 10^{-2}$
p50 <sup>2</sup>	24	35 (17.24)	2.417	$2.80 \times 10^{-2}$
c-MYB1	25	124 (61.08)	1.11	$9.87 \times 10^{-3}$
B. Genes differentially responsive to TRAIL upon N-CoR2 overexpression (1328 input; 919 analyzed):				
Sox-5	1	622 (67.68)	13.14	$4.36 \times 10^{-5}$
SRY	2	609 (66.27)	12.36	$1.28 \times 10^{-5}$
cEBP	3	426 (46.35)	11.01	$3.72 \times 10^{-4}$
HLF	4	279 (30.36)	10.8	$1.76 \times 10^{-5}$
Nkx	5	699 (76.06)	10.51	$7.47 \times 10^{-6}$
SAP-1	6	239 (26.01)	10.06	$1.72 \times 10^{-4}$

E4BP4	7	203 (22.09)	9.97	$1.30 \times 10^{-4}$
IRF-1	8	238 (25.9)	9.694	$2.18 \times 10^{-5}$
SOX-9	9	476 (51.8)	8.916	$7.48 \times 10^{-5}$
S8	10	653 (71.06)	7.132	$4.73 \times 10^{-5}$
CREB	11	245 (26.66)	7.085	$1.40 \times 10^{-2}$
NRF-2	12	264 (28.73)	6.692	$7.94 \times 10^{-4}$
FREAC-4	13	397 (43.2)	6.672	$5.45 \times 10^{-3}$
SRF <sup>2</sup>	14	41 (4.46)	5.535	$4.07 \times 10^{-2}$
SOX17	15	588 (63.98)	3.738	$9.41 \times 10^{-4}$
HFH-3	16	431 (46.9)	3.697	$2.91 \times 10^{-3}$
c-FOS <sup>2</sup>	17	492 (53.54)	2.989	$9.51 \times 10^{-3}$
Max	18	305 (33.19)	2.812	$5.83 \times 10^{-3}$
Elk-1	19	554 (60.28)	1.992	$2.64 \times 10^{-2}$
p65 <sup>2</sup>	20	232 (25.24)	1.612	$3.01 \times 10^{-2}$
c-MYB <sub>1</sub>	21	513 (55.82)	1.103	$3.35 \times 10^{-2}$
c-REL <sup>2</sup>	22	381 (41.46)	0.8524	$2.56 \times 10^{-2}$
ARNT	23	441 (47.99)	0.7265	$1.34 \times 10^{-2}$
n-MYC	24	430 (46.79)	0.2689	$2.33 \times 10^{-2}$
USF	25	412 (44.83)	0.1689	$1.90 \times 10^{-2}$
C. PCD genes from gene listed in B (64 input; 46 analyzed):				
IRF-1	1	16 (34.78)	10.11	$1.42 \times 10^{-2}$
SOX5	2	34 (73.91)	6.363	$4.95 \times 10^{-2}$
SOX17	3	33 (71.74)	3.002	$4.81 \times 10^{-2}$
cEBP	4	25 (54.34)	2.802	$4.12 \times 10^{-2}$

<sup>1</sup>Conserved human or mouse transcription factor binding sites detected by oPOSSUM (<http://www.cisreg.ca/cgi-bin/oPOSSUM/opossum>) and ranked by Z-scores with Fisher *P* value < 0.05.

<sup>2</sup>Transcriptional factors previously shown to be affected by N-CoR2.



**Supplementary Table 4. Identities of the 64 genes (76 probe sets) listed in Fig. 4e and their roles in PCD.** The genes are ranked descendingly accordingly to their respective value of *DRI*. Data in the last column indicate whether the expression of the gene is more TRAIL-inducible in T4-2 vector cells (*V*) or T4-2 N-CoR2 cells (*N*).

Affymetrix probe set ID	Gene symbol	RefSeq Transcript ID	Description	Role in PCD	<i>DRI</i> (absolute value)	More induced by TRAIL
214329_x_at	<i>TNFSF10</i>	NM_003810	tumor necrosis factor (ligand) superfamily, member 10	apoptosis	2.48	<i>V</i>
200887_s_at	<i>STAT1</i>	NM_007315 NM_139266	signal transducer and activator of transcription 1	apoptosis	2.43	<i>V</i>
97935_3_at	<i>STAT1</i>	NM_007315 NM_139266	signal transducer and activator of transcription 1	apoptosis	2.32	<i>V</i>
210511_s_at	<i>INHBA</i>	NM_002192	inhibin, beta A	apoptosis	2.21	<i>V</i>
209969_s_at	<i>STAT1</i>	NM_007315 NM_139266	signal transducer and activator of transcription 1	apoptosis	2.11	<i>V</i>
201845_s_at	<i>RYBP</i>	NM_012234	RING1 and YY1 binding protein	apoptosis	2.09	<i>V</i>
201687_s_at	<i>API5</i>	NM_006595	apoptosis inhibitor 5	anti-apoptosis	2.04	<i>V</i>
201150_s_at	<i>TIMP3</i>	NM_000362	TIMP metalloproteinase inhibitor 3	apoptosis	2.04	<i>V</i>
202688_at	<i>TNFSF10</i>	NM_003810	tumor necrosis factor (ligand) superfamily, member 10	apoptosis	2.02	<i>V</i>
201710_at	<i>MYBL2</i>	NM_002466	v-myb myeloblastosis viral oncogene homolog (avian)-like 2	anti-apoptosis	1.99	<i>N</i>
202677_at	<i>RASA1</i>	NM_002890 NM_022650	RAS p21 protein activator 1	regulation of apoptosis	1.96	<i>V</i>
204020_at	<i>PURA</i>	NM_005859	purine-rich element binding protein A	apoptosis	1.89	<i>V</i>

202687_s_at	<i>TNFSF10</i>	NM_003810	tumor necrosis factor (ligand) superfamily, member 10	apoptosis	1.88	V
204274_at	<i>EBAG9</i>	NM_004215 NM_198120	estrogen receptor binding site associated, antigen, 9	apoptosis	1.87	V
204278_s_at	<i>EBAG9</i>	NM_004215 NM_198120	estrogen receptor binding site associated, antigen, 9	apoptosis	1.87	V
201844_s_at	<i>RYBP</i>	NM_012234	RING1 and YY1 binding protein	apoptosis	1.81	V
201302_at	<i>ANXA4</i>	NM_001153	annexin A4	anti-apoptosis	1.73	V
219209_at	<i>IFIH1</i>	NM_022168	interferon induced with helicase C domain 1	regulation of apoptosis	1.71	V
221478_at	<i>BNIP3L</i>	NM_004331	BCL2/adenovirus E1B 19kDa interacting protein 3-like	apoptosis	1.71	V
207181_s_at	<i>CASP7</i>	NM_001227 NM_033338 NM_033339 NM_033340	caspase 7	apoptosis	1.7	V
212593_s_at	<i>PDCD4</i>	NM_014456 NM_145341	programmed cell death 4	apoptosis	1.64	V
217746_s_at	<i>PDCD6IP</i>	NM_013374	programmed cell death 6 interacting protein	apoptosis	1.64	V
204924_at	<i>TLR2</i>	NM_003264	toll-like receptor 2	apoptosis	1.61	V
209863_s_at	<i>TP73L</i>	NM_003722	tumor protein p73-like	apoptosis	1.58	V

202094_at	<i>BIRC5</i>	NM_001012270 NM_001012271 NM_001168	baculoviral IAP repeat-containing 5 (survivin)	anti-apoptosis	1.57	<i>N</i>
212354_at	<i>SULF1</i>	NM_015170	sulfatase 1	apoptosis	1.54	<i>V</i>
211368_s_at	<i>CASP1</i>	NM_001223 NM_033292 NM_033293 NM_033294 NM_033295	caspase 1, apoptosis-related cysteine peptidase (interleukin 1, beta, convertase)	apoptosis	1.52	<i>V</i>
204131_s_at	<i>FOXO3A</i>	NM_001455 NM_201559	forkhead box O3A	apoptosis	1.48	<i>V</i>
202985_s_at	<i>BAG5</i>	NM_001015048 NM_001015049 NM_004873	BCL2-associated athanogene 5	apoptosis	1.46	<i>V</i>
205681_at	<i>BCL2A1</i>	NM_004049	BCL2-related protein A1	anti-apoptosis /regulation of apoptosis	1.45	<i>V</i>
201424_s_at	<i>CUL4A</i>	NM_001008895 NM_003589	cullin 4A	apoptosis	1.45	<i>V</i>
201846_s_at	<i>RYBP</i>	NM_012234	RING1 and YY1 binding protein	apoptosis	1.45	<i>V</i>
207113_s_at	<i>TNF</i>	NM_000594	tumor necrosis factor	apoptosis/anti -apoptosis	1.44	<i>N</i>

210334_x_at	<i>BIRC5</i>	NM_001012270 NM_001012271 NM_001168	baculoviral IAP repeat-containing 5 (survivin)	anti-apoptosis	1.44	<i>N</i>
200004_at	<i>EIF4G2</i>	NM_001418	eukaryotic translation initiation factor 4 gamma, 2	cell death	1.43	<i>V</i>
203628_at	<i>IGF1R</i>	NM_000875	insulin-like growth factor 1 receptor	anti-apoptosis	1.43	<i>V</i>
200599_s_at	<i>HSP90B1</i>	NM_003299	heat shock protein 90kDa beta (Grp94), member 1	anti-apoptosis	1.42	<i>V</i>
202095_s_at	<i>BIRC5</i>	NM_001012270 NM_001012271 NM_001168	baculoviral IAP repeat-containing 5 (survivin)	anti-apoptosis	1.38	<i>N</i>
222108_at	<i>AMIGO2</i>	NM_181847	adhesion molecule with Ig-like domain 2	regulation of apoptosis	1.36	<i>V</i>
217999_s_at	<i>PHLDA1</i>	NM_007350	pleckstrin homology-like domain, family A, member 1	apoptosis	1.35	<i>V</i>
215037_s_at	<i>BCL2L1</i>	NM_001191 NM_138578	Bcl2-like 1 (Bcl-xL)	anti-apoptosis	1.32	<i>N</i>
213373_s_at	<i>CASP8</i>	NM_001228 NM_033355 NM_033356 NM_033358	caspase 8, apoptosis-related cysteine peptidase	apoptosis	1.31	<i>V</i>
200690_at	<i>HSPA9B</i>	NM_004134	heat shock 70kDa protein 9B (mortalin-2)	anti-apoptosis	1.3	<i>V</i>
202693_s_at	<i>STK17A</i>	NM_004760	serine/threonine kinase 17a	apoptosis	1.28	<i>V</i>

210025_s_at	<i>CARD10</i>	NM_014550	caspase recruitment domain family, member 10	regulation of apoptosis	1.25	<i>N</i>
205599_at	<i>TRAF1</i>	NM_005658	TNF receptor-associated factor 1	anti-apoptosis	1.25	<i>N</i>
201849_at	<i>BNIP3</i>	NM_004052	BCL2/adenovirus E1B 19kDa interacting protein 3	apoptosis	1.24	<i>V</i>
206295_at	<i>IL18</i>	NM_001562	interleukin 18	apoptosis	1.22	<i>V</i>
200608_s_at	<i>RAD21</i>	NM_006265	RAD21 homolog	apoptosis	1.22	<i>V</i>
200658_s_at	<i>PHB</i>	NM_002634	prohibitin	regulation of apoptosis	1.21	<i>N</i>
213026_at	<i>ATG12</i>	NM_004707	ATG12 autophagy related 12 homolog	autophagy	1.2	<i>V</i>
201637_s_at	<i>FXR1</i>	NM_001013438 NM_001013439 NM_005087	fragile X mental retardation, autosomal homolog 1	apoptosis	1.19	<i>V</i>
200807_s_at	<i>HSPD1</i>	NM_002156 NM_199440	heat shock 60kDa protein 1	regulation of apoptosis	1.18	<i>V</i>
205263_at	<i>BCL10</i>	NM_003921	B-cell CLL/lymphoma 10	apoptosis	1.18	<i>V</i>
209476_at	<i>TXNDC</i>	NM_030755	thioredoxin domain containing	anti-apoptosis	1.17	<i>V</i>
200602_at	<i>APP</i>	NM_000484 NM_201413 NM_201414	amyloid beta (A4) precursor protein	apoptosis	1.17	<i>V</i>
210118_s_at	<i>IL1A</i>	NM_000575	interleukin 1, alpha	apoptosis	1.15	<i>V</i>
217997_at	<i>PHLDA1</i>	NM_007350	pleckstrin homology-like domain, family A, member 1	apoptosis	1.15	<i>V</i>
200681_at	<i>GLO1</i>	NM_006708	glyoxalase I	anti-apoptosis	1.15	<i>V</i>

212719_at	<i>PHLPP</i>	NM_194449	PH domain and leucine rich repeat protein phosphatase	apoptosis	1.14	<i>V</i>
202984_s_at	<i>BAG5</i>	NM_001015048 NM_001015049 NM_004873	BCL2-associated athanogene 5	apoptosis	1.12	<i>V</i>
201167_x_at	<i>ARHGDIA</i>	NM_004309	Rho GDP dissociation inhibitor (GDI) alpha	anti-apoptosis	1.12	<i>N</i>
203489_at	<i>SIVA</i>	NM_006427 NM_021709	CD27-binding (Siva) protein	regulation of apoptosis	1.11	<i>N</i>
201084_s_at	<i>BCLAF1</i>	NM_014739	BCL2-associated transcription factor 1	apoptosis	1.1	<i>None</i>
211300_s_at	<i>TP53</i>	NM_000546	tumor protein p53	apoptosis	1.09	<i>None</i>
38158_at	<i>ESPL1</i>	NM_012291	extra spindle poles like 1	apoptosis	1.09	<i>N</i>
211936_at	<i>HSPA5</i>	NM_005347	heat shock 70kDa protein 5	anti-apoptosis	1.08	<i>V</i>
202076_at	<i>BIRC2</i>	NM_001166	baculoviral IAP repeat-containing 2	anti-apoptosis	1.08	<i>V</i>
200691_s_at	<i>HSPA9B</i>	NM_004134	heat shock 70kDa protein 9B	anti-apoptosis	1.08	<i>V</i>
210260_s_at	<i>TNFAIP8</i>	NM_014350	tumor necrosis factor, alpha-induced protein 8	regulation of apoptosis	1.07	<i>V</i>
204211_x_at	<i>EIF2AK2</i>	NM_002759	eukaryotic translation initiation factor 2-alpha kinase 2	apoptosis	1.05	<i>V</i>

214988_s_at	<i>SON</i>	NM_003103 NM_032195 NM_058183 NM_138925 NM_138926 NM_138927	SON DNA binding protein	anti-apoptosis	1.04	V
201012_at	<i>ANXA1</i>	NM_000700	annexin A1	anti-apoptosis	1.02	V
201371_s_at	<i>CUL3</i>	NM_003590	cullin 3	apoptosis	1.01	V
200797_s_at	<i>MCL1</i>	NM_021960 NM_182763	myeloid cell leukemia sequence 1	regulation of apoptosis	1.01	V
211316_x_at	<i>CFLAR</i>	NM_003879	CASP8 and FADD-like apoptosis regulator	regulation of apoptosis	1.01	V

**Supplementary Table 5 Association between clinical and pathological characteristics and N-CoR2 or HDAC3 transcript expression levels**

Characteristics	N-CoR2/HDAC3 expression levels			<i>P</i> value
	Lower quartile ( <i>n</i> = 74)	Interquartile ( <i>n</i> = 148)	Upper quartile ( <i>n</i> = 74)	
N-CoR2				
Age				0.031
<40 yr	12 (16.2%)	33 (22.4%)	18 (24.3%)	
40-44 yr	14 (18.9%)	44 (29.9%)	27 (36.5%)	
45-49 yr	36 (48.6%)	42 (28.6%)	20 (27.0%)	
≥50 yr	12 (16.2%)	28 (19.0%)	9 (12.2%)	
Tumor size				0.564
≤2 cm	41 (55.4%)	79 (53.7%)	35 (47.3%)	
>2 cm	33 (44.6%)	68 (46.3%)	39 (52.7%)	
No. of positive LNs				0.137
0	37 (50.0%)	79 (53.7%)	35 (47.3%)	
1-3	32 (43.2%)	44 (29.9%)	30 (40.5%)	
≥4	5 (6.8%)	24 (16.3%)	9 (12.2%)	
Tumor grade				0.125
I	18 (24.3%)	43 (29.3%)	14 (18.9%)	
II	19 (25.7%)	52 (35.4%)	30 (40.5%)	
III	37 (50.0%)	52 (35.4%)	30 (40.5%)	
ER statue				0.009
Negative	23 (31.1%)	38 (25.9%)	8 (10.8%)	
Positive	51 (68.9%)	109 (74.1%)	66 (89.2%)	
Molecular subtype				0.080
Basal	16 (21.6%)	24 (16.3%)	6 (8.1%)	
ERBB2+	11 (14.9%)	26 (17.7%)	12 (16.2%)	
Luminal A	17 (23.0%)	41 (27.9%)	30 (40.5%)	
Luminal B	26 (35.1%)	39 (26.5%)	16 (21.6%)	
Normal like	4 (5.4%)	17 (11.6%)	10 (13.5%)	
Surgery				0.023
Breast conserving therapy	50 (67.6%)	77 (52.4%)	34 (45.9%)	
Mastectomy	24 (32.4%)	70 (47.6%)	40 (54.1%)	
Adjuvant chemotherapy				0.896
No	46 (62.2%)	94 (63.9%)	45 (60.8%)	



Yes	28 (37.8%)	53 (36.1%)	29 (39.2%)	0.722
Hormonal therapy				
No	63 (85.1%)	126 (85.7%)	66 (89.2%)	
Yes	11 (14.9%)	21 (14.3%)	8 (10.8%)	
<b>HDAC3</b>				
Age				0.286
<40 yr	18 (24.3%)	27 (18.4%)	18 (24.3%)	
40-44 yr	20 (27.0%)	38 (25.9%)	27 (36.5%)	
45-49 yr	22 (29.7%)	54 (36.7%)	22 (29.7%)	
≥50 yr	14 (18.9%)	28 (19.0%)	7 (9.5%)	
Tumor size				0.645
≤2 cm	38 (51.4%)	81 (55.1%)	36 (48.6%)	
>2 cm	36 (48.6%)	66 (44.9%)	38 (51.4%)	
No. of positive LNs				0.688
0	35 (47.3%)	80 (54.4%)	36 (48.6%)	
1-3	31 (41.9%)	48 (32.7%)	27 (36.5%)	
≥4	8 (10.8%)	19 (12.9%)	11 (14.9%)	
Tumor grade				0.613
I	15 (20.3%)	42 (28.6%)	18 (24.3%)	
II	29 (39.2%)	49 (33.3%)	23 (31.1%)	
III	30 (40.5%)	56 (38.1%)	33 (44.6%)	
ER statue				0.038
Negative	25 (33.8%)	27 (18.4%)	17 (23.0%)	
Positive	49 (66.2%)	120 (81.6%)	57 (77.0%)	
Molecular subtype				0.545
Basal	15 (20.3%)	18 (12.2%)	13 (17.6%)	
ERBB2+	13 (17.6%)	26 (17.7%)	10 (13.5%)	
Luminal A	18 (24.3%)	51 (34.7%)	19 (25.7%)	
Luminal B	19 (25.7%)	37 (25.2%)	25 (33.8%)	
Normal like	9 (12.2%)	15 (10.2%)	7 (9.5%)	
Surgery				0.932
Breast conserving therapy	39 (52.7%)	81 (55.1%)	41 (55.4%)	
Mastectomy	35 (47.3%)	66 (44.9%)	33 (44.6%)	
Adjuvant chemotherapy				0.492
No	50 (67.6%)	92 (62.6%)	43 (58.1%)	
Yes	24 (32.4%)	55 (37.4%)	31 (41.9%)	

Hormonal therapy 0.469

No 61 (82.4%) 130 (88.4%) 64 (86.5%)

Yes 13 (17.6%) 17 (11.6%) 10 (13.5%)

---

The analysis included data for 295 patients with breast cancer in the Netherlands Cancer Institute database. Molecular subtypes of breast cancers are based on nearest centroid classification as used by Sorlie *et al.* and the data were downloaded from the website

([http://microarray-pubs.stanford.edu/wound\\_NKI/Clinical\\_Data\\_Supplement.xls](http://microarray-pubs.stanford.edu/wound_NKI/Clinical_Data_Supplement.xls)).

**Supplementary Table 6 Multivariate analysis for distant metastasis-free and overall survival according to N-CoR2 and HDAC3 transcript expressions and clinical characteristics**

Variable	Death		Relapse	
	Hazard Ratio (95% CI)	<i>P</i> Value	Hazard Ratio (95% CI)	<i>P</i> Value
N-CoR2	1.96 (1.2-3.18)	0.007	1.87 (1.21-2.9)	0.005
HDAC3	1.56 (0.76-3.19)	0.221	0.99 (0.5-1.95)	0.97
Age (per 10-yr increment)	0.7 (0.47-1.05)	0.087	0.6 (0.42-0.85)	0.005
Tumor size (per mm)	1.02 (1.0-1.05)	0.07	1.02 (1.00-1.05)	0.047
Tumor grade		0.011		0.017
Grade 2 vs. grade 1	3.94 (1.35-11.47)		2.24 (1.12-4.48)	
Grade 3 vs. grade 1	5.18 (1.77-15.14)		2.81 (1.38-5.7)	
Positive LN status vs. negative status	1.5 (0.75-2.97)	0.249	1.56 (0.86-2.85)	0.146
Positive ER status vs. negative status	0.66 (0.33-1.31)	0.232	0.97 (0.52-1.82)	0.927
Chemotherapy vs. no chemotherapy	0.59 (0.29-1.23)	0.16	0.54 (0.29-1.02)	0.056
Hormonal treatment vs. no treatment	0.83 (0.34-2.06)	0.693	0.7 (0.32-1.53)	0.372
Mastectomy vs. breast-conserving therapy	0.97 (0.6-1.57)	0.886	0.9 (0.59-1.38)	0.628
Molecular subtype		0.075		0.182
Normal-like & luminal B vs. luminal A	1.72 (0.81-3.66)		1.47 (0.82-2.62)	
Basal & ERBB2+ vs. luminal A	2.74 (1.15-6.53)		1.92 (0.96-3.85)	

The analysis included the 295 patients with breast cancers in the Netherlands Cancer Institute database. N-CoR2, HDAC3 transcript expression, age and tumor size were modeled as continuous variables. CI denotes confidence interval.

**Supplementary Table 7 Multivariate analysis for distant metastasis-free and overall survival according to N-CoR2 and HDAC3 transcript expressions and clinical characteristics in breast cancer patients who did not receive adjuvant CT**

Variable	Death		Relapse	
	Hazard Ratio (95% CI)	<i>P</i> Value	Hazard Ratio (95% CI)	<i>P</i> Value
N-CoR2	1.12 (0.54-2.31)	0.761	1.25 (0.69-2.28)	0.46
HDAC3	1.15 (0.46-2.88)	0.761	0.92 (0.39-2.15)	0.841
Age (per 10-yr increment)	0.71 (0.44-1.16)	0.177	0.58 (0.38-0.91)	0.018
Tumor size (per mm)	1.03 (0.99-1.06)	0.115	1.02 (0.99-1.05)	0.22
Tumor grade		0.057		0.047
Grade 2 vs. grade 1	5.28 (1.18-23.55)		2.81 (1.1-7.15)	
Grade 3 vs. grade 1	6.25 (1.4-28.0)		3.35 (1.27-8.83)	
Positive LN status vs. negative status	1.48 (0.69-3.15)	0.316	1.62 (0.84-3.12)	0.147
Positive ER status vs. negative status	1.48 (0.62-3.55)	0.375	1.87 (0.85-4.12)	0.123
Hormonal treatment vs. no treatment	1.16 (0.37-3.62)	0.8	0.75 (0.25-2.23)	0.604
Mastectomy vs. breast-conserving therapy	1.48 (0.81-2.71)	0.201	1.61 (0.93-2.78)	0.088
Molecular subtype		0.005		0.025
Normal-like & luminal B vs. luminal A	1.88 (0.76-4.64)		1.45 (0.71-2.95)	
Basal & ERBB2+ vs. luminal A	5.65 (1.93-16.52)		3.2 (1.35-7.55)	

The analysis included the 185 patients with breast cancers who did not receive adjuvant CT in the Netherlands Cancer Institute database. N-CoR2, HDAC3 transcript expression, age and tumor size were modeled as continuous variables. CI denotes confidence interval.

**Supplementary Table 8 Multivariate analysis for the likelihood of unresponsiveness to neoadjuvant CT according to clinical characteristics and the average linkage clustering (ALC) analysis based on the N-CoR2-associated gene expression signature**

Variable	Odds Ratio (95% CI)	<i>P</i> value
ALC (subgroup A vs. subgroup B)	2.71 (1.06-6.96)	0.038
Age (per 10-yr increment)	1.60 (1.00-1.01)	0.037
Tumor size ( $\geq 5$ cm vs. $< 5$ cm)	1.71 (0.64-4.54)	0.284
Tumor grade ( $\geq$ grade 3 vs. $<$ grade 3)	1.23 (0.42-3.63)	0.71
Positive LN status vs. negative status	0.37 (0.13-1.05)	0.061
Positive ER status vs. negative status	4.46 (1.66-12.01)	0.003
Positive HER2 vs. negative HER2	0.49 (0.18-1.33)	0.162

The analysis included the 130 patients with breast cancers who received neoadjuvant CT in the M.D. Anderson Cancer Center database. The tumors were segregated into subgroup A and B according to ALC or clinical characteristics. Age was modeled as a continuous variable. CI denotes 95% confidence interval.

**Supplementary Table 9 Multivariate analysis for the likelihood of unresponsiveness to neoadjuvant CT according to clinical characteristics and  $S_{NCOR2}$**

Variable	Odds Ratio (95% CI)	<i>P</i> value
High $S_{NCOR2}$ vs. low $S_{NCOR2}$	3.85 (1.5-9.89)	0.005
Age (per 10-yr increment)	1.60 (1.00-1.1)	0.047
Tumor size ( $\geq 5$ cm vs. $< 5$ cm)	1.86 (0.68-5.11)	0.227
Tumor grade ( $\geq$ grade 3 vs. $<$ grade 3)	1.19 (0.40-3.53)	0.754
Positive LN status vs. negative status	0.39 (0.14-1.13)	0.084
Positive ER status vs. negative status	4.68 (1.73-12.65)	0.002
Positive HER2 vs. negative HER2	0.45 (0.16-1.25)	0.127

The analysis included the 130 patients with breast cancers who received neoadjuvant CT in the M.D. Anderson Cancer Center database. The tumors were segregated into subgroups according to  $S_{NCOR2}$  or clinical characteristics. Age was modeled as a continuous variable. CI denotes 95% confidence interval.

**Supplementary Table 10 Performance metrics of the N-CoR2-related single- or multi-gene predictors for unresponsiveness to neoadjuvant CT**

	Predictor		
	N-CoR2 expression	ALC	$S_{NCOR2}$
Sensitivity	56.2 (49.8-61.9)	61.8 (55.4-67.2)	61.8 (55.5-66.7)
Specificity	63.4 (49.5-75.9)	68.3 (54.5-80.1)	75.6 (62.0-86.3)
PPV	76.9 (68.2-84.8)	80.9 (72.5-88.0)	84.6 (76.0-91.3)
NPV	40.0 (31.2-47.9)	45.2 (36.0-53.0)	47.7 (39.1-54.4)

The analysis included the 130 patients with breast cancers who received neoadjuvant CT in the M.D. Anderson Cancer Center database. The tumors were segregated into subgroups according to the expression levels of N-CoR2, ALC or  $S_{NCOR2}$ . PPV, Positive predictive value; NPV, Negative predictive value; ALC, average linkage clustering. Data in parenthesis are 95% confidence intervals.

## Tissue Diagnostic Instrument

Paul Hansma, Hongmei Yu, David Schultz, Azucena Rodriguez, Eugene Yurtsev, M. C. Peters, Jon Miller, Joseph Wallace, Inkyung Kang, David Kohn, Jenni Buckley, Valerie Weaver, Jeff Lotz

Changes in the mechanical properties of tissues are associated with the progression of diseases. Examples of such pathologies include intervertebral disc degeneration, cancer, atherosclerosis and tooth decay. Detection of changes in the mechanical properties has been used as a means of diagnosis for centuries as physicians palpate subsurface tissues. The general problem is that palpation is necessarily limited in spatial resolution and quantification. Here we introduce the Tissue Diagnostic Instrument (TDI), a device designed to probe the mechanical properties of tissues with high resolution. The TDI can measure mechanical properties of tissues having Elastic Moduli that vary over seven orders of magnitude. Here we report measurements on tissues with elastic moduli below 1 kPa (normal murine breasts) to over 10 GPa (human dentin). Having a positional resolution of order 1 mm. and force resolution of 10 mN, the TDI can distinguish the nucleus from the annulus fibrosis of the discs and normal from cancerous murine mammary glands. It can measure the elastic modulus and hardness of the dentin left in a cavity after excavation with various excavation tools and techniques. We anticipate that this first report will stimulate research on many tissue systems in living organisms, including plants. It could lead to new insights into the progression of pathologies and to improved diagnostics. This instrument may also be useful for materials research.

The TDI was redesigned from the Bone Diagnostic Instrument [Hansma et al RSI 200] to measure tissue mechanical properties in vivo (figure 1). It uses a probe assembly that can penetrate skin and soft tissue to measure subcutaneous mechanical properties. In our current design the disposable, sterilizable probe assembly consists of an outer reference probe made from a 23 gauge hypodermic needle and an inner test probe made from



stainless steel wire ranging in thickness from 175 to 300 microns in diameter. The test probe is held in a nickel tube that couples to a magnet which in turn is linked to a force generator. During operation the force generator applies a force, concurrently measured by a force transducer [Futek LSB200], to move the test probe in the tissue under test. The distance that the test probe moves relative to the reference probe is monitored by a distance transducer [Measurement Specialties 025 MHR]. We typically operate at a frequency of 4 Hz with a sinusoidal drive to the force generator because this is fast enough to allow hand holding but slow enough to allow easy decoupling of the elastic and viscous response of the tissue (see supplementary material for more details.)

To illustrate the type of data that can be obtained with the TDI, we begin with an application to measuring the mechanical properties of spinal discs. Spinal disc degeneration is now diagnosed with imaging. Though the result of disk degeneration is to cause mechanical problems and pain, there is no current diagnostic technique to measure the mechanical properties of intact discs in patients. Figure 2 shows that the TDI can measure the mechanical properties of intact discs from donors. Imaging can be used to guide the placement of the probe in the disc (figures 2(a) and (b)). The force vs. distance data from the TDI is plotted in real time and recorded digitally (figures 2(c) and (d)). The slope of the force vs. distance curve is a measure of the elasticity of the sample: in the case of a simple spring, the slope would be the spring constant. The slope is computed from the force vs. distance data by simply finding the least squares fit to slope. The energy dissipation in the force vs. distance curve is the area inside the curve and is a measure of the viscous forces. It vanishes for a simple spring and becomes large for a viscous material such as petroleum jelly, which has a slope near zero.

Note that the annulus is very different mechanically from the nucleus (figure 2). It has both higher slope and energy dissipation. This is consistent with the measurements of ???....An eventual goal would be to see if the measurement of mechanical properties of discs in patients could help in the diagnosis of disc degeneration and its possible role in causing back pain, which has proved elusive to diagnose with imaging alone. Perhaps it

could be used to decide between different treatment options such as spinal fusion or artificial disc technologies.

As an example of the softest tissue that can be probed with our current prototype, figure 3 shows a comparison of results on normal mammary glands and tumors in the same murine mammary glands (#2/3, #4 and #5). The normal mammary glands have Elastic Modulus, as measured with a conventional rheometer, of below 1 kPa, and can be clearly distinguished from the tumors by the TDI. This is consistent with calibration curves on polyacrylamide gels (see supplementary material) showing sensitivity of the TDI to below 1 kPa. Human breast tissue is stiffer (refs.) and is thus well within the range of the TDI. We have begun measurements of human breast tissue from cadavers and found easily detectable variations in mechanical properties, but correlations with structure and pathology are beyond the scope of this initial report. An eventual goal would be the use of the TDI (or a more compact and inexpensive future iteration of the TDI) in the diagnosis of breast cancer. One possibility would be locating margins of affected tissue and sites for biopsy. It could easily be combined with biopsy; the test probe could be withdrawn into the reference probe to collect a biopsy sample after mechanical testing.

As an example of the hardest tissue that can be probed with our current prototype, figure 4 shows an experiment on human dentin. One problem for practicing dentists is knowing when to stop drilling when removing degenerated dentin from a cavity since there are no currently available instruments to quantify the properties of the dentin remaining in the cavity. One proposed solution has been the development of a new experimental polymer bur (EPB) which is designed to remove soft dentin, but blunt on harder dentin and thus self limit the amount removed. Here we show the properties of the remaining dentin after a 1st excavation by such a bur and then after a 2nd excavation with a second polymer bur of the same type. Next was a 3rd excavation with a #4 round carbide bur and finally a cavity preparation into presumably sound dentin using a #330 carbide bur. Note that even after the cavity preparation the dentin did not have the full hardness of the healthy dentin. The ability of the TDI to measure Elastic Modulus and Hardness for irregularly shaped, fully-hydrated dentin cavities is, to our knowledge, a first. It could be used for

research projects without further modification. For individual clinical use, a smaller, less expensive version with a right angled probe would be desirable.

The interaction forces of antibody or other coated test probes with tissues should be detectable. Many papers have been written on measuring single molecule interaction forces with the Atomic Force Microscope (Gaub et al). Interaction forces in the range of 10 to 300 pN per molecular bond are typical. With these interaction forces, we can make order of magnitude estimates of forces we might find when trying to rotate or translate a test probe that had bound to a tissue with many molecular bonds in parallel. Assuming a molecular density of one molecule per  $10 \text{ nm}^2$ , an interaction force per molecule of 50 pN, a coated region of area  $4 \times 10^{-6} \text{ m}^2$  (the exposed area of the Type D probe) and a fractional binding of 1% we would get a force of  $50 \text{ pN/molecule} \times 4 \times 10^{-6} \text{ m}^2 \times 1 \text{ molecule}/10 \text{ nm}^2 \times .01 = 200 \text{ mN}$ . The current lower limits of sensitivity of the TDI for forces come from the friction between the test probe and the reference probe, of order 10 mN, and from the force noise in our force transducer, of order 5 mN in a 1 kHz bandwidth. Thus forces of the magnitude that could be expected from molecular interactions with coated tips should be measurable. The big problem would be non-specific interaction masking specific interactions. One approach to overcoming this masking effect would be to use a test probe coated on just one side that was exposed to the tissue under test through a window in the wall of a closed-end reference probe. The difference in the forces between the test probe and the tissue under test for the coated vs. uncoated side could be measured. This could naturally be extended with multiple coatings on multiple strips on the test probe, each exposed one by one through a slit in the wall of the closed-end reference probe.

It is important to note that though the present instrument is able to make basic measurements in a wide range of tissues (almost all tissues in the human body from very soft breast tissue to hard, mineralized tissues), it is in a very early stage of development. More versatile instruments with more measurement modalities, such as mentioned above, and more user convenience features, such as wireless operation, are possible. Specialized

instruments for specific measurements in specific tissues could be developed at a small fraction of the cost of the fully versatile instrument. For example, for soft tissue, the force generator and distance transducer could be replaced with a simple motor that moved the test probe up and down a fixed amount independent of the nature of the tissue as long as the tissue was soft compared to the rigidity of the motor drive system. Only the force would need to be measured since the displacements would be known. The magnitude of the oscillating force could be read with a simple meter or indicator lights as a measure of the stiffness of the tissue.

**Supplementary Information:** Detailed methods and a gel calibration figure are available in the online version.

**Acknowledgements:** We thank the NIH and DAMD W81XWH-05-1-330 for funding this research.

**Author contributions:** P.H. invented the TDI and participated in all the measurements reported here; D. S., A. R., J. B. and J. L. planned the spinal disc experiment, which was preformed by D. S. and A. R. on tissue obtained by J. B. and A. R.; H.Y. and V.W. planned the mouse breast experiment, which was preformed by H. Y.; the dentin experiments were planned by T. P.; J. W. in the laboratory of D. K. preformed preliminary dentin measurements on teeth prepared by T. P.; J. M. preformed the final set of measurements, which are presented here, on teeth prepared by T. P.; E. Y. wrote the computer program that operates the TDI.

**Author information:** Competing financial interests: P. H. is a member of Active Life Technologies Inc., which sells Bone Diagnostic and Tissue Diagnostic Instruments. He is a co-inventor on two US patent applications and inventor on a provisional patent application, which cover these instruments.

### **Figure Captions:**

**Figure 1 The Tissue Diagnostic Instrument, TDI.** a) The TDI can measure mechanical properties of tissues under test even if they are covered with skin and other soft tissues because it has a probe assembly that can be inserted into the tissue under test. b) It can be hand held and is connected to a computer for data generation, acquisition and processing. In this photo it is being used to measure differences in the mechanical properties of fruit and gel in a snack food. c) A probe assembly for the TDI consists of a test probe, which moves distances of order 200 microns relative to the reference probe, which also serves to shield the test probe from the influence of the skin and soft tissue that must be penetrated to reach the tissue under test. Type D probes are good for very soft tissue, such as the murine breast tissue of Figure 3. Type N probes are good for stiffer tissue, such as the spinal disc tissue of Figure 2. The novel sharpening of the reference probe for Type N probes decreases the problem of tissue being caught between the test probe and the reference probe during insertion and thus decreases the friction between the test probe and the reference probe.

**Figure 2: Demonstration of the ability of the TDI to distinguish between the annulus fibrosis and nucleus pulposus of a human intervertebral disc.** (a) X-ray image of transverse view of a cadaver lumbar motion segment L12 with test probe located in annulus fibrosus. (b) Similar view with probe centered in the nucleus pulposus. (c) Force vs. displacement curve measured by the TDI during a cyclic load cycle (4 Hz) in the annulus. (d) Force vs. displacement curve measured in the nucleus. Note that the annulus is much stiffer (higher slope) and dissipates more energy (higher area enclosed by the curve). (e) Histogram comparing the average least squares slope for 10 cycles in the annulus versus in the nucleus. (f) Histogram comparing the average energy dissipation in each of the 10 cycles for 10 cycles in the annulus versus in the nucleus. These results are representative of our measurements on 11 discs: the slope and energy dissipation are always greater in the annulus than the nucleus. The error bars indicate standard deviation for the 10 measurement in each of three different locations within the annulus and within the nucleus in the disc.

**Figure 3: Demonstration of the ability of the TDI to distinguish between normal mammary glands and tumors.** (a) Hematoxylin and eosin (H&E) staining of a normal mammary gland from this study (10x). (b) Hematoxylin and eosin (H&E) staining of a mammary gland tumor from this study (10x). (c) Histogram comparing TDI measurements of the average least squares slope for 10 cycles in three types of normal mammary glands and three types of mammary tumors. Note that the mammary tumors are much stiffer (higher slope). (d) Histogram comparing TDI measurements of the average energy dissipation in each of the 10 cycles for 10 cycles in three types of normal mammary glands and three types of mammary tumors. Note that the mammary tumors have higher energy dissipation. (e) Histogram comparing the Elastic Modulus, as measured by Rheology, for the normal mammary glands and tumors. (f) Histogram comparing the Loss Modulus, as measured by Rheology. The error bars indicate standard deviation for the measurements from two sections of the same tissues ...

Note that the results for elasticity and loss modulus for the two techniques reproduce the same general trends. Note also that the storage modulus, as measured by Rheology, is below 200 Pa (200 N/m<sup>2</sup>), showing that the TDI can make measurements on samples with Elastic Modulus below 200 Pa.

**Figure 4: Demonstration of the ability of the TDI to measure the Elastic Modulus and Hardness of human dentin to quantify the properties of the dentin left in a tooth cavity after each of multiple excavations and finally preparation.** (a) The probe assembly for these measurements was designed not to penetrate soft tissue, as above, but to indent the hard tissue. The reference probe was a hypodermic needle that rested on the surface under test. The test probe was sharpened into a 90 degree cone with a 30 micron radius at the end. (b) The teeth after the various excavations and finally preparation. At each successive stage of excavation and preparation more dentin was removed from the cavity, (c) The Elastic Modulus, as calculated from force vs. distance curves generated by the TDI and analyzed using a modified Oliver and Pharr method, (ref W. C. Oliver and G. M. Pharr, Journal of Materials Research **19**, 3 (2004).), for healthy dentin far from the cavity, and of the dentin in the cavity after the excavations and preparation. (d) The

Hardness, as calculated from force vs. distance curves generated by the TDI and analyzed using a modified Oliver and Pharr method, for healthy dentin far from the cavity, and of the dentin in the cavity after the excavations and preparation. Thus the TDI has the potential to quantify the properties of dentin left in a cavity and could be used to study the outcome of various strategies for how much dentin is left. The error bars indicate standard deviation of the 10 measurements that were taken on each of the 5 teeth (a total of 50 measurements). Note that the Elastic Modulus of the healthy dentin is over 10 GPa -- over 7 orders of magnitude greater than the normal mammary glands (Figure 3) -- demonstrating the range of the TDI.

Figure 1

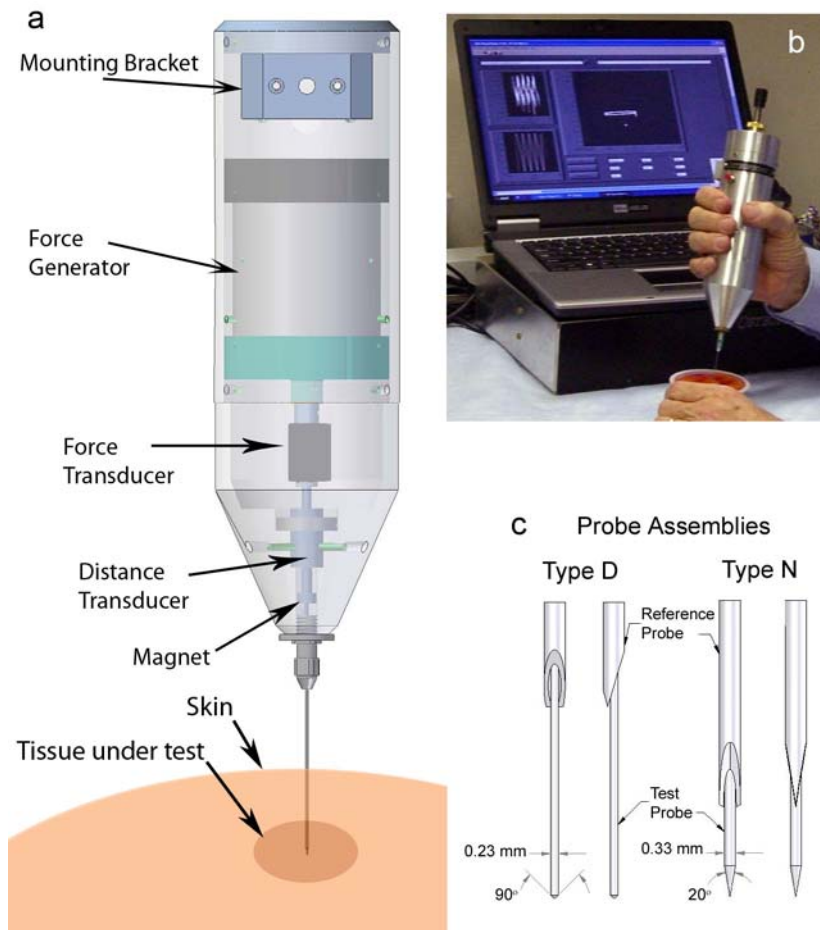


Figure 2



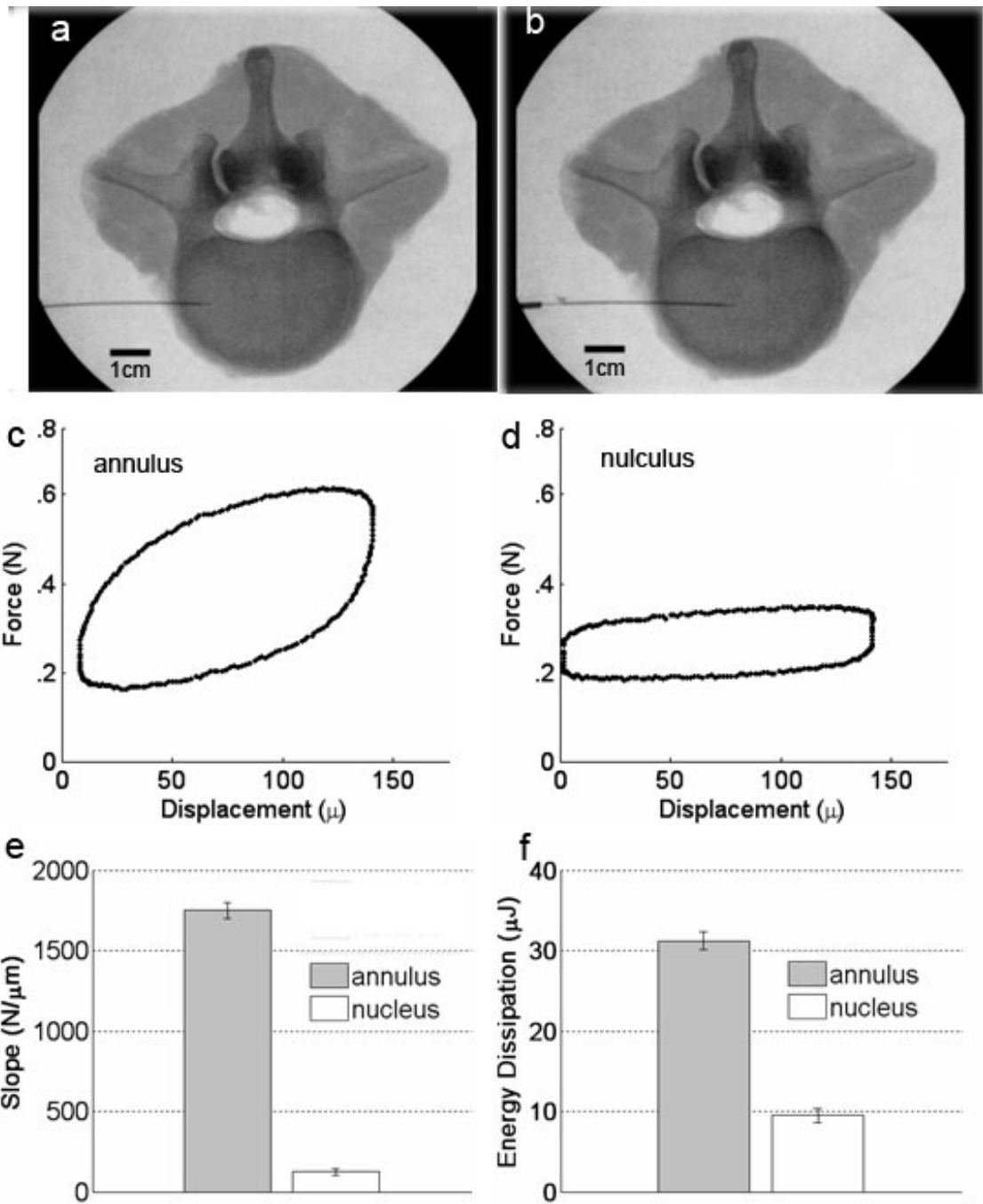
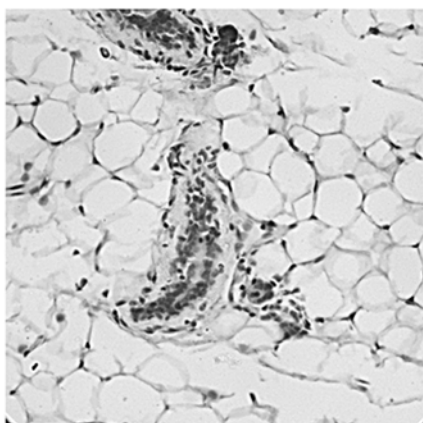


Figure 3

**a** Normal Mammary Glands #4



**b** Mammary Gland #4 Tumor

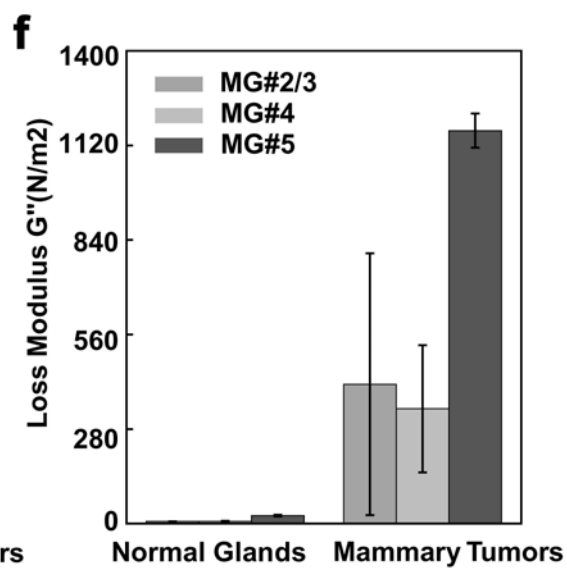
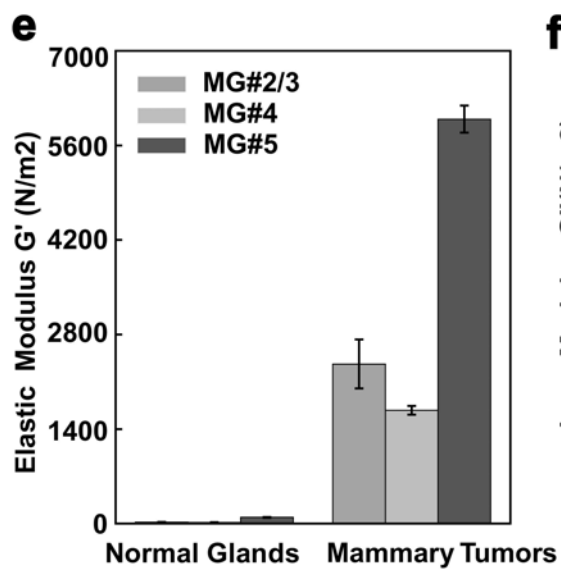
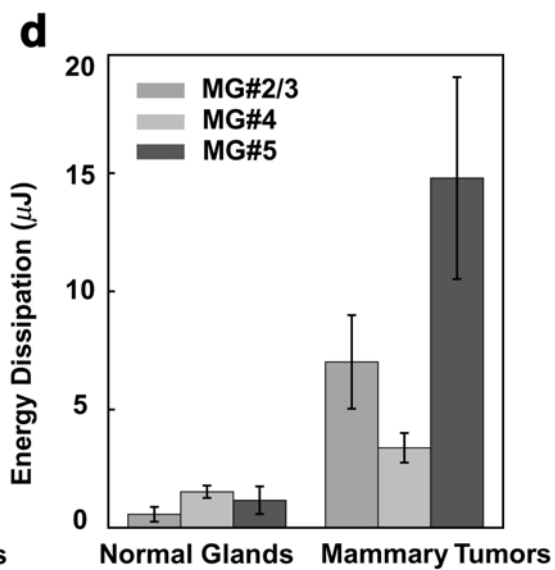
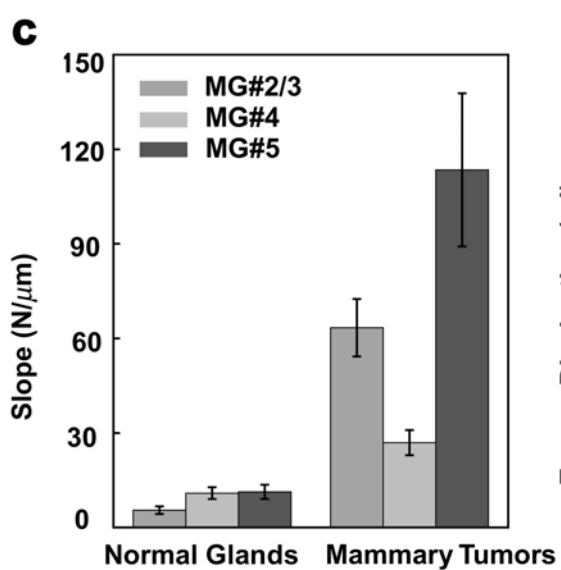
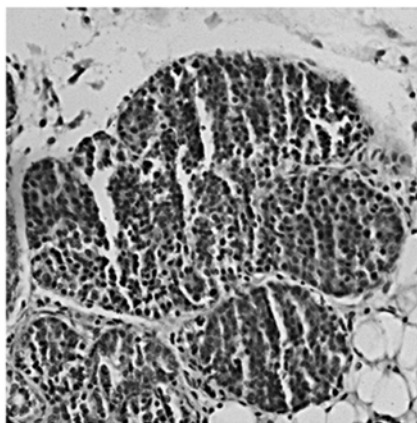
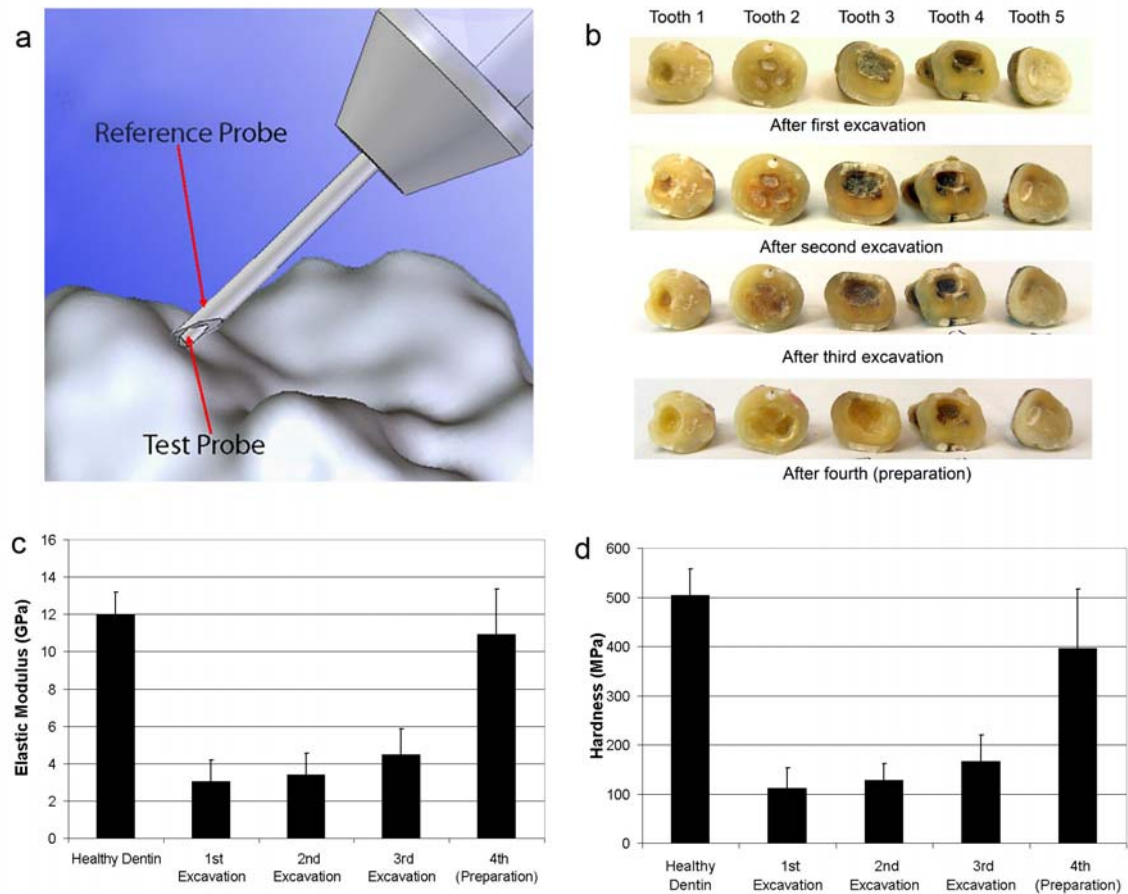


Figure 4



**Supplementary material for the online version:**

### The Measurement of Viscoelasticity with the Tissue Diagnostic Instrument

The measurement of viscoelasticity of biological tissues is an active area of current research with an extensive theoretical foundation. (see, for example, a recent book by Y. C. Fung [Fung, Biomechanics, springer-Verlag 1993]). Here we present a very simple theoretical model to help in the understanding of TDI data. Figure 5 shows the TDI driving (a) a simple spring and (b) a damper. In the simple spring the force measured by

the TDI will be proportional to the distance it is deflected,  $x$ , as shown in (c) and the Force vs Distance curve will be a straight line with a slope equal to the spring constant of the spring and no hysteresis (c). This is the elastic part of a viscoelastic response. For the damper, the Force vs Distance curve will have a net slope equal to zero but non zero hysteresis (d). It has zero slope because the damping does not depend on the position of the damping element within the damper, but only on its velocity. The force due to damping changes sign as the velocity changes sign. Thus the Force vs. Distance curve is symmetric upon reflection in either the Force or Distance axes. The area inside the Force vs. Distance curve will be the energy dissipated by the damper. This is the viscous part of the viscoelastic response. Thus the two parameters presented in this initial report, the Slope and the Energy Dissipation, are measures of the elastic and the viscous part of the viscoelastic response.

There are more sophisticated mechanical models of viscoelastic tissue [Fung, Biomechanics, Springer-Verlag 1993], which can, in the future, be used to more precisely model the tissue and its interactions with the TDI probe, but they all share the same basics: the slope of a Force vs. Distance curve is related to the elastic part of the viscoelastic response and the hysteresis is related to the viscous part of the viscoelastic response. These more sophisticated models become especially useful for describing frequency and time dependence of viscoelastic response. They can involve multiple springs and dampers in series and parallel combinations. Measurements at multiple frequencies and/or measurements of step responses can, in the future, be used to more fully specify the viscoelastic parameters of more sophisticated models.

It is important to note, however, that as Fung [Fung, Biomechanics, Springer-Verlag 1993] states: "The hysteresis curves of most biological soft tissues have a salient feature: the hysteresis loop is almost independent of the strain rate within several decades of rate variation. This insensitivity is incompatible with any viscoelastic model that consists of a finite number of springs and dashposts." This is in qualitative agreement with our preliminary observations of frequency independent hysteresis with the TDI and is also reflected in the nearly vertical ends of the hysteresis curves, especially in very soft tissue

like the breast tissue. That is, the dissipation depends on the sign of the velocity, but is relatively independent of the magnitude just as for simple models of friction.

Figure 5 (being prepared by David) goes here.

### **Disc Study Methods**

Human lumbar spine were harvested from donors and stored frozen at -20C. The lumbar segment featured in Figure 2 was evaluated on an MRI degeneration grading scale (Pfirrmann scale ranges from 1-5) and given a grade of 3 indicating mild degenerative characteristics typical of aged discs.

Prior to test the L12 motion segment was cut from the lumbar spine and thawed to room temperature. The medial-lateral axis of the disc was measured to be 55 mm. The reference probe from the TDI was then marked at insertion depths of 10% and 50% of that length corresponding to insertion depths for the annulus and nucleus respectively. At each of the two insertion depths 10 load cycles were recorded with the TDI. The friction was evaluated by taking one measurement in air before and after each insertion. The values from the air measurements were subtracted from the measurements in tissue. The transverse x-ray image was taken with a C-arm imaging system (Model Compact 7600, OEC Medical Systems, Salt Lake City, UT) (Figure 2).

### **Mammary Gland Methods**

The MMTV-PyMT mouse model (polyoma middle T antigen under the control of MMTV long terminal repeat promoter, Gay, 1993) was used in this work. MMTV-PyMT<sup>+/+</sup> and their WT littermates MMTV-PyMT<sup>-/-</sup> were housed and maintained in a barrier facility at UCSF until 13 week old when all the PyMT<sup>+/+</sup> females developed mammary tumors. Mice were euthanized with 15psi CO<sub>2</sub> followed by cervical dislocation. All protocols were approved by the Institutional Animal Care and Use Committee at UCSF.

After the mammary glands or associated tumors were located, the probe assembly was inserted through the skin and held inside the tissue for 10 measurements on each of three insertions. The friction was evaluated by taking one measurement in air before and after each insertion. The values from the air measurements were subtracted from the measurements in tissue.

The shear storage modulus ( $G'$ ) and loss modulus ( $G''$ ) of mammary gland tissues were obtained by using a AR2000ex rheometer (TA Instruments-Waters LLC., New Castle, DE). Briefly, 8mm-stainless steel plates were sanded to prevent the slippage between the samples and plates. The friction and inertia of instrument were then calibrated before and after the 8mm parallel plate geometry was attached (following the user-manual). Mouse mammary glands were isolated, punched into 8mm sections and placed between the plates. The tissues were tested at zero normal force, a controlled 2% strain and an angular frequency of 10 rads/s (at which the parameters under tests have minimal frequency dependency).

Hematoxylin and eosin (H&E) staining of the same tissue samples was performed for histological evaluation after the mechanical tests. Tissues were fixed in 4% paraformaldehyde overnight, dehydrated for paraffin embedding and then sectioned to 5mm thick sections. The sections were stained with hematoxylin (1 minutes) and eosin (2 minutes) and evaluated under brightfield microscope with a 10x objective (Nikon, IX80). Images were captured with a CCD camera (Spot scientific).

The TDI was hand held. The probe assembly was inserted through the skin and held inside the tissue for 10 measurements on each of three insertions. The friction was evaluated by taking one measurement in air before and after each insertion. The values from the air measurements were subtracted from the measurements in tissue.

## **Dentin methods**

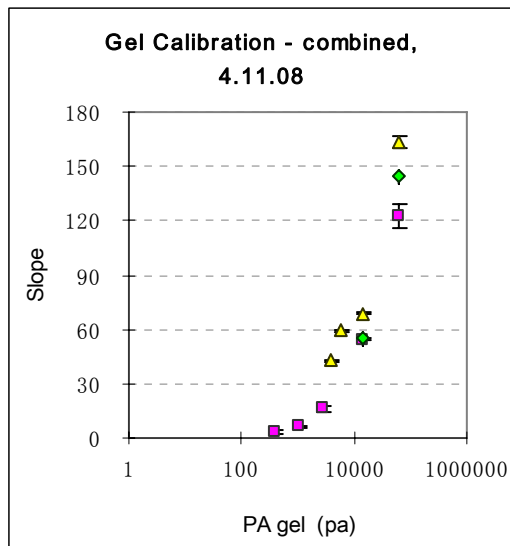
Extracted human teeth (N=8) with extensive carious lesions into inner third of dentin were excavated using standardized procedures for selective caries removal. Material properties of healthy and irregularly shaped, affected dentin at the cavity floor were determined using a novel handheld diagnostic instrument. The device, which measures the hardness and elastic modulus of dentin by indenting the surface on the order of 50-100  $\mu\text{m}$ , has a sharpened test probe which slides inside a hypodermic syringe that serves as a local reference. The instrument was hand held for convenience in positioning it over the interior surface of the cavity.

The automatic data collection protocol involves loading pre-cycles followed by 2 primary loading cycles that were trapezoidal waves. Each trapezoidal wave consists of 1/3 of a cycle of linear increase, followed by 1/3 of a cycle hold at maximum force, approximately 10 N, and then 1/3 of a cycle of linear decrease. The total cycle time was 500 msec. The purpose of the hold at maximum current is to monitor creep effects and to minimize the effect of the remaining creep during the linear decrease. This type of hold at the maximum is used in instrumented indentation analysis, pioneered by Oliver and Pharr {Oliver, 2004}, for getting valid retraction slopes for determining the elastic modulus. The purpose of the pre-cycles is to establish a good zero reference for indentation distance measurements. The pre-cycles are modified trapezoidal waves similar to the primary cycles mentioned above. Unlike the primary cycles, which are of constant amplitude, the pre-cycles have gradually increasing load amplitudes typically starting at 0.1 N and increasing on the order of 0.1 N after each cycle. The maximum force during the pre-cycles is monitored. When the maximum force reaches a preset threshold value, typically about 1 N, the reference position for indentation distance measurements is set at the distance where the preset threshold force was reached.

This reference position is used to compute E and H by the Oliver and Pharr method [Oliver and Pharr 2004] as if it were the contact point. Since the reference position is, however, inside the dentin this results in an overestimate of both E and H. This is corrected by measuring known standard, PMMA, with the same tip and protocol, then dividing the results on the dentin by the results on the standard, and finally multiplying these normalized results by the actual values of PMMA for the known standard:  $E = \text{normalized } E \times 4.483 \text{ GPa}$ .  $H = \text{normalized } H \times 292 \text{ MPa}$

## Gel Calibration

Polyacrylamide gels were prepared ...







---

## APPENDIX

### A. Manuscripts

1. Friedland, J.C., Lakins, J.N., Kazanietz, M.G., Chernoff, J., Boettiger, D. and Weaver, V.M.  $\alpha 6\beta 4$  integrin activates Rac-dependent p21-activated kinase 1 to drive NF $\kappa$ B-dependent apoptosis resistance in 3D mammary acini. *J Cell Sci.* 120: 3700-12, 2007. (NOTE: this was listed as accepted/In Press last report - see attached appendix)
2. Yee, K.L., Weaver, V.M., and Hammer, D. Integrin-mediated Signaling through the MAP-kinase Pathway. *IET Systems Biology.* 2:8-15, 2008. (NOTE: this was listed as accepted last report - the article has since been published)
3. Rizki, A., Weaver, V.M., Lee, S.Y. Rozenberg, G.I. Chin, K., Myers, C.A., Bascom, J.L., Mott, J.D., Semiks, J.R., Grate, L.R., Mian, I.S., Borowsky, A.D., Jensen, R.A., Idowu, M.O., Chen, F., Chen, D.J., Petersen, O.W., Gray, J.W., Bissell, M.J. A human breast cell model of preinvasive to invasive transition. *Cancer Res.* 68:1378-1387, 2008.
4. Kass, L, Erler, JT, Dembo, M, **Weaver, VM**, Mammary epithelial cell: Influence of extracellular matrix composition and organization during development and tumorigenesis. *Int J Biochem Cell Biol.* 39:1987-1994, 2007.
5. Hebner, C, **Weaver, VM**, and Debnath, J, Modeling Morphogenesis and Oncogenesis in Three dimensional Breast Epithelial Cultures. *Annu. Rev. Pathol.* 3: 313-319, 2007.
6. Erler, J., and Weaver V.M. Tissue Context and Tumor Metastasis, In a special issue of Clinical and Experimental Metastasis In Press, 2008.
7. Mouw, J., Desai, S., and Weaver V.M. Forcing transformation: biophysical regulation of mammary epithelial cell transformation, In The Pathomechanics of Tissue Injury and Disease, and the Mechanophysiology of Healing", In Press, 2008.

# $\alpha 6 \beta 4$ integrin activates Rac-dependent p21-activated kinase 1 to drive NF- $\kappa$ B-dependent resistance to apoptosis in 3D mammary acini

Julie C. Friedland<sup>1,2,3,\*</sup>, Johnathon N. Lakins<sup>2,3,4,5</sup>, Marcelo G. Kazanietz<sup>1</sup>, Jonathan Chernoff<sup>6</sup>, David Boettiger<sup>7</sup> and Valerie M. Weaver<sup>2,3,4,5,†</sup>

<sup>1</sup>Department of Pharmacology, University of Pennsylvania, Philadelphia, PA 19104, USA

<sup>2</sup>Department of Surgery, University of California San Francisco, San Francisco, CA 94143, USA

<sup>3</sup>Institute for Medicine and Engineering and <sup>4</sup>Department of Pathology, University of Pennsylvania, Philadelphia, PA 19104, USA

<sup>5</sup>Center for Bioengineering and Tissue Regeneration, University of California San Francisco, San Francisco, CA 94143, USA

<sup>6</sup>Fox Chase Cancer Center, Philadelphia, PA 19111, USA

<sup>7</sup>Department of Microbiology, University of Pennsylvania, Philadelphia, PA 19104, USA

\*Present address: Department of Microbiology, University of Pennsylvania, PA 19104, USA

†Author for correspondence (e-mail: weaverv@surgey.ucsf.edu)

Accepted 4 July 2007

*Journal of Cell Science* 120, 3700–3712 Published by The Company of Biologists 2007

doi:10.1242/jcs.03484

## Summary

Malignant transformation and multidrug resistance are linked to resistance to apoptosis, yet the molecular mechanisms that mediate tumor survival remain poorly understood. Because the stroma can influence tumor behavior by regulating the tissue phenotype, we explored the role of extracellular matrix signaling and tissue organization in epithelial survival. We report that elevated ( $\alpha 6 \beta 4$ ) integrin-dependent Rac-Pak1 signaling supports resistance to apoptosis in mammary acini by permitting stress-dependent activation of the p65 subunit of NF- $\kappa$ B through Pak1. We found that inhibiting Pak1 through expression of N17Rac or PID compromises NF- $\kappa$ B activation and renders mammary acini sensitive to death, but that resistance to apoptosis could be restored to these structures by overexpressing wild-type NF- $\kappa$ B p65. We also observed that acini expressing elevated levels of Pak1 can

activate p65 and survive death treatments, even in the absence of activated Rac, yet will die if activation of NF- $\kappa$ B is simultaneously inhibited through expression of I $\kappa$ B $\alpha$ M. Thus, mammary tissues can resist apoptotic stimuli by activating NF- $\kappa$ B through  $\alpha 6 \beta 4$  integrin-dependent Rac-Pak1 signaling. Our data emphasize the importance of the extracellular matrix stroma in tissue survival and suggest that  $\alpha 6 \beta 4$  integrin-dependent Rac stimulation of Pak1 could be an important mechanism mediating apoptosis-resistance in some breast tumors.

Supplementary material available online at  
<http://jcs.biologists.org/cgi/content/full/120/20/3700/DC1>

Key words:  $\alpha 6 \beta 4$  integrin, Rac, Pak1, NF- $\kappa$ B, Apoptosis resistance, Mammary epithelial cells

## Introduction

Apoptosis is essential for tissue development and homeostasis and is required for efficient tumor therapy (Fernandez et al., 2002; Igney and Krammer, 2002; Zakeri and Lockshin, 2002). Aberrant regulation of cell death contributes to the pathogenesis of various diseases in adult tissues, including cancer and neurodegeneration. Moreover, defects in the regulation of apoptosis and the execution of cell death have been implicated in the pathogenesis of treatment-resistant tumors (Fulda and Debatin, 2004; Sethi et al., 1999; Zahir and Weaver, 2004). While we know much about the molecular machinery and events driving the execution of apoptosis at the cellular level, by comparison we know little about how cell-death decisions are controlled in three-dimensional (3D) tissues.

In vivo, epithelial cells are incorporated into 3D tissues that are typically quite resistant to pro-apoptotic treatments such as gamma irradiation and chemotherapy (Barros et al., 1995; Bissell and Radisky, 2001; Unger and Weaver, 2003). Similar to tissues in vivo, mammary epithelial cells (MECs) embedded

within a reconstituted basement membrane (rBM) assemble 3D tissue-like structures (acini) that are highly resistant to diverse death stimuli. In contrast to tissues in vivo and differentiated 3D mammary acini, non-differentiated MECs grown as two dimensional (2D) monolayers are comparatively sensitive to induction of apoptosis (Weaver et al., 2002). The increased death resistance displayed by 3D multicellular structures in vivo and in culture (acini and spheroids) has been linked to the enhanced cell-cell associations and altered cell-ECM interactions found in these structures (Bates et al., 1994; Hermiston and Gordon, 1995; Kirshner et al., 2003; Santini et al., 2000; Zahir and Weaver, 2004). Cell adhesion can promote the viability of cells grown as non-differentiated monolayers by changing the activity or expression of Bcl2 family-member dimers, or by increasing Erk, phosphoinositide 3-kinase (PI 3-kinase) and Akt signaling to inhibit mitochondria-dependent death, modify cellular metabolism and sustain cell proliferation (Matter and Ruoslahti, 2001; Plas and Thompson, 2002; Vander Heiden et al., 2001). Cell-ECM interactions and integrin engagement can also protect cells grown as

monolayers from death stimuli by tempering death receptor signaling and altering cell-cycle dynamics (Dalton, 2003; Sethi et al., 1999). Interestingly, ECM-ligated epithelial cells incorporated into 3D tissue-like structures or spheroids are more resistant to death cues in comparison with epithelial cells interacting with the same ECM ligand in 2D where they grow as cellular monolayers (i.e. plated on top of the same ECM ligand) (Igney and Krammer, 2002). It is not clear whether the resistance phenotype of 3D spheroids is linked to previously characterized adhesion-dependent survival signaling or whether novel adhesion-regulated, death-resistance mechanisms become engaged in 3D spheroids.

Cells grown as 3D spheroids often exhibit reduced growth, altered cell-cycle regulation, hypoxia, compromised drug accessibility, increased matrix deposition and modified cell adhesion, and any one of these characteristics could account for the death-resistance phenotype of these structures (Kuh et al., 1999; Sminia et al., 2003; Tagliabue et al., 1998; Tannock et al., 2002). We found that  $\alpha 6\beta 4$  integrin and tissue polarity mediate resistance to apoptosis in 3D mammary acini in the absence of hypoxia, and irrespective of the growth status of the cells, by enhancing stress-dependent NF- $\kappa$ B activation (Weaver et al., 2002). The importance of  $\alpha 6\beta 4$  integrin-NF- $\kappa$ B signaling in resistance to apoptosis is underscored by the finding that aggressive and treatment-resistant solid tumors frequently show constitutive activation of NF- $\kappa$ B (Baldwin, 2001; Sovak et al., 1997), and NF- $\kappa$ B can protect epithelial cells in vivo from death induced through radiation treatment, stimulation of immune receptors and exposure to chemotherapies (Baeuerle and Baltimore, 1996; Baldwin, 2001). In addition, high-grade tumors with a poor clinical prognosis often express increased levels of  $\alpha 6\beta 4$  integrin and secrete abundant quantities of laminin-332 (Davis et al., 2001; Jones et al., 1997; Taylor-Papadimitriou et al., 1993), and elevated  $\alpha 6\beta 4$  integrin has been linked to tumor metastasis, which is a process that requires resistance to apoptosis (Lipscomb et al., 2005; Mercurio and Rabinovitz, 2001; Gupta and Massague, 2006). We showed that laminin-ligated  $\alpha 6\beta 4$  integrin can enhance anchorage-independent survival in 3D mammary spheroids by facilitating epidermal growth factor (EGF)-dependent activation of Rac and NF- $\kappa$ B (Zahir et al., 2003). Consistently, Rac levels and activity are often elevated in aggressive human epithelial tumors in vivo (Fritz et al., 1999), and Rac has been strongly implicated in tissue morphogenesis and polarity (O'Brien et al., 2001; Akhtar and Streuli, 2006). These findings implicate but do not prove that  $\alpha 6\beta 4$  integrin-Rac-NF- $\kappa$ B signaling mediates resistance to apoptosis in tissues. To explore this possibility, we asked whether  $\alpha 6\beta 4$  integrin-polarized 3D mammary acini resist diverse exogenous apoptosis stimuli through Rac-dependent NF- $\kappa$ B activation, and if so, how?

Using two non-malignant human MEC models and a reconstituted, laminin-rich rBM (Debnath et al., 2003; Johnson et al., 2007; Weaver et al., 1997), we grew MECs on top of rBM (2D) and compared their death-resistance behavior with that of mammary acini embedded within rBM (3D). We show that laminin-ligated  $\alpha 6\beta 4$  integrin confers resistance to apoptosis in 3D mammary acini by increasing the activity of Rac and p21-activated kinase 1 (Pak1 signaling) to enhance stress-induced NF- $\kappa$ B activation. Our findings emphasize the importance of matrix context in the regulation of cell death and

implicate  $\alpha 6\beta 4$  integrin-dependent Rac-Pak1-NF- $\kappa$ B signaling in the pathogenesis of treatment-resistant tumors.

## Results

### $\alpha 6\beta 4$ integrin regulates resistance to apoptosis and Rac activity

When compared with cells grown as 2D monolayers, epithelial cells assembled into 3D spheroids are more resistant to apoptosis to a degree that is similar to that exhibited by multidrug-, immune- and radiation-resistant tumors in vivo (Desoize and Jardillier, 2000). 3D spheroids are typically multilayered with a hypoxic core, and cells incorporated into these structures display growth patterns that appear to depend upon their location within the spheroid (reviewed in Zahir and Weaver, 2004; Santini et al., 2000). Accordingly, the increased survival behavior of 3D spheroids has been largely attributed to compromised drug penetration, altered cell-cycle dynamics or hypoxia (Kuh et al., 1999; Sminia et al., 2003; Tannock et al., 2002). By contrast, we found that rBM-generated 3D acini of S1 HMT-3522 and MCF10A non-malignant MECs, consisting of a single layer of non-hypoxic cells interacting directly with the rBM (Weaver et al., 2002) and proliferating at a rate similar to that of MECs ligated with rBM in 2D (monolayer; data not shown), are consistently more resistant to immune receptor stimuli such as Trail (Fig. 1A; top left and right), chemotherapy treatments including taxol (Fig. 1A; bottom left and right) and exposure to gamma irradiation (not shown).

We previously reported that the apoptosis-resistant phenotype of 3D mammary acini depends upon laminin-ligation of  $\alpha 6\beta 4$  integrin and NF- $\kappa$ B activation (data not shown) (Weaver et al., 2002). Laminin-ligated  $\alpha 6\beta 4$  integrin regulates Rac (Russell et al., 2003; Zahir et al., 2003), and Rac can promote anchorage-independent cell survival (Zahir et al., 2003; Jacquier et al., 2006). We found that the level of GTP-Rac is significantly elevated in BM-ligated 3D MEC acini in comparison with BM-ligated MECs grown as 2D monolayers, consistent with the idea that MECs incorporated into a 3D spheroid acquire death resistance through elevated adhesion-dependent survival signaling (Fig. 1B; quantified in 1C). We additionally observed that ectopic expression of a tail-less EGFP-tagged  $\beta 4$  integrin that competes with the endogenous wild-type  $\beta 4$  integrin to heterodimerize with  $\alpha 6$  integrin at the membrane and that mediates laminin-dependent adhesion, but does not permit hemidesmosome formation nor  $\alpha 6\beta 4$  integrin-dependent signaling (Zahir et al., 2003; Spinardi et al., 1995), significantly reduces Rac activity in rBM-ligated 2D (data not shown) (Zahir et al., 2003) and 3D cultures of MECs (Fig. 1D; quantified in 1E). Because we demonstrated that expression of the tail-less  $\beta 4$  integrin compromises tissue polarity and renders 3D MEC acini sensitive to exogenous death stimuli (immune receptor and chemotherapy), and Rac can regulate tissue polarity (Akhtar and Streuli, 2006; O'Brien et al., 2001) and cell survival (Zahir et al., 2003), these observations indicate that the elevated laminin- $\alpha 6\beta 4$ -integrin-dependent Rac activity displayed by 3D mammary acini could contribute to their apoptosis-resistance phenotype.

### Rac activity is necessary for apoptosis resistance

To examine the functional link between resistance to apoptosis and Rac in 3D mammary acini, we reduced GTP-Rac levels through stable retroviral expression of a dominant-negative

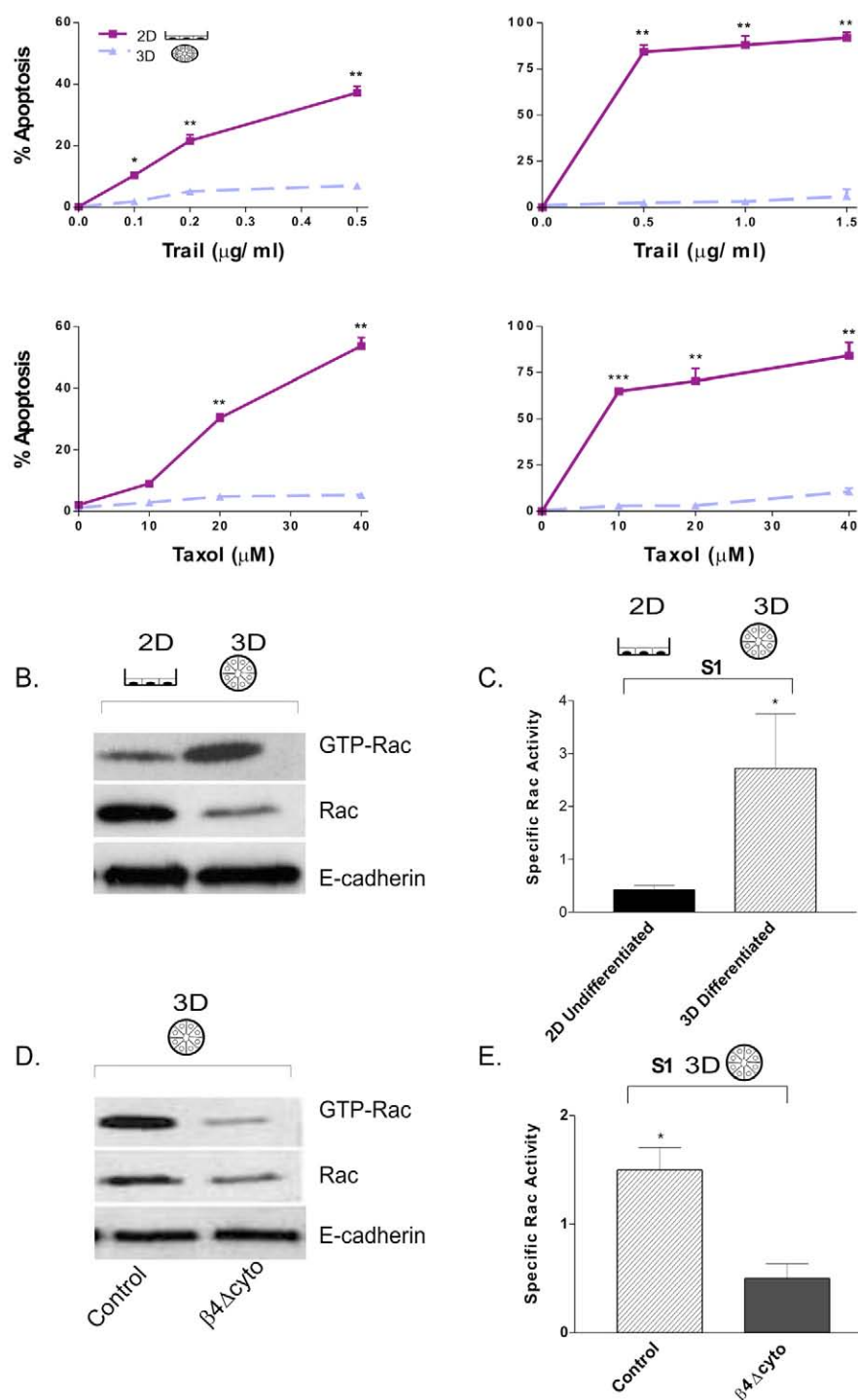


**Fig. 1.** Tissue differentiation is associated with an increase in  $(\alpha 6)\beta 4$  integrin-dependent Rac activity and enhanced resistance to apoptosis. (A) Dose-response curves showing that nonmalignant HMT-3522 S1 and MCF10A MECs acquire resistance to apoptosis induced by chemotherapeutics including taxol and immune receptor activators such as Trail following their rBM-induced differentiation into 3D polarized acini. The percentage apoptosis was calculated by scoring the number of activated caspase-3-positive cells 48 hours after treatment divided by the total cell number. MECs were either plated on top of a 1:100 diluted rBM for 48–96 hours (2D) or differentiated by embedment within rBM for 10–12 days (3D) followed by exposure to increasing doses of apoptotic stimuli. (B) Representative immunoblot of immunoprecipitated Pak-associated Rac (GTP-Rac), total Rac (Rac) and E-cadherin in MECs plated either on top (2D) as monolayers or within (3D) rBM to assemble acini. The data indicate that total Rac decreases noticeably following rBM-induced differentiation, whereas GTP-loaded Rac increases dramatically. (C) Average relative specific activity of Rac in 3D mammary acini calculated by densitometric analysis of immunoblots of GTP-Rac divided by total cellular Rac following E-cadherin normalization, as shown in B. (D) Representative immunoblot of GTP-Rac, total Rac (Rac) and E-cadherin in vector control and tail-less  $\beta 4$  integrin ( $\beta 4\Delta cyto$ ) 3D mammary acini grown within rBM (10–14 days). The data illustrate that Rac activity diminishes significantly in mammary acini that express the signaling-defective tail-less  $\beta 4$  integrin. (E) Average relative specific activity of Rac in control mammary acini versus mammary tissues expressing the tail-less  $\beta 4$  integrin calculated as above in C and shown in D. Results are the mean  $\pm$  s.e.m. of three to five separate experiments. \* $P \leq 0.05$ ; \*\* $P \leq 0.01$ ; \*\*\* $P \leq 0.001$ .

EGFP-tagged N17Rac (Fig. 2A). Consistent with the idea that elevated Rac activity contributes to apoptosis resistance, expression of N17Rac substantially reduced GTP-Rac levels (Fig. 2B; quantified in C) in MECs grown in monolayers and the activity of one of its effectors, Pak1, in 3D mammary acini (Fig. 2D; quantified in 2E). Reducing Rac and Pak activity also significantly sensitized the 3D mammary acini to apoptosis induced in response to immune-receptor ligation and chemo-reagent treatment (Trail and taxol-induced apoptosis; Fig. 2F).

Interestingly, although decreasing Rac activity sensitized the 3D mammary acini to death induction, N17 Rac expression did not appear to overtly compromise tissue integrity (Fig. 3A; compare top row left phase-contrast image with middle image). N17Rac expression also did not appear to compromise tissue polarity (Fig. 3A; compare first column of confocal images with second column), as illustrated by basally localized  $\beta 4$  integrin, basal deposition of laminin-332 and collagen IV, and maintenance of cellular adhesions, as indicated by cell-cell-localized scribble (Fig. 3A; left) and colocalized E cadherin

and  $\beta$ -catenin (data not shown). Because tissue polarity has been linked to resistance to apoptosis in mammary tissues (Weaver et al., 2002), and Rac has been strongly implicated in mammary morphogenesis (Akhtar and Streuli, 2006) and polarity (O'Brien et al., 2001), we further explored the effect of Rac on tissue polarity. First, we assessed the efficiency of exogenously expressed N17Rac in reducing GTP-Rac levels in MECs grown as 3D acini in comparison with MECs grown as 2D monolayers. N17Rac effectively reduced GTP-Rac by

greater than 80% in MECs grown as 2D rBM-ligated monolayers (Fig. 2B; quantified in 2C), whereas, somewhat surprisingly, despite similar expression of the transgene, N17Rac only reduced Rac activity in 3D MEC acini by 40% (Fig. 3B; quantified in 3C). Nevertheless, a 40% reduction in GTP-Rac substantially reduced Pak1 activity and was sufficient to sensitize 3D MEC acini to death stimuli including Trail and taxol (Fig. 2F), even in the absence of an effect on tissue polarity (Fig. 3A). These data imply that, while Rac

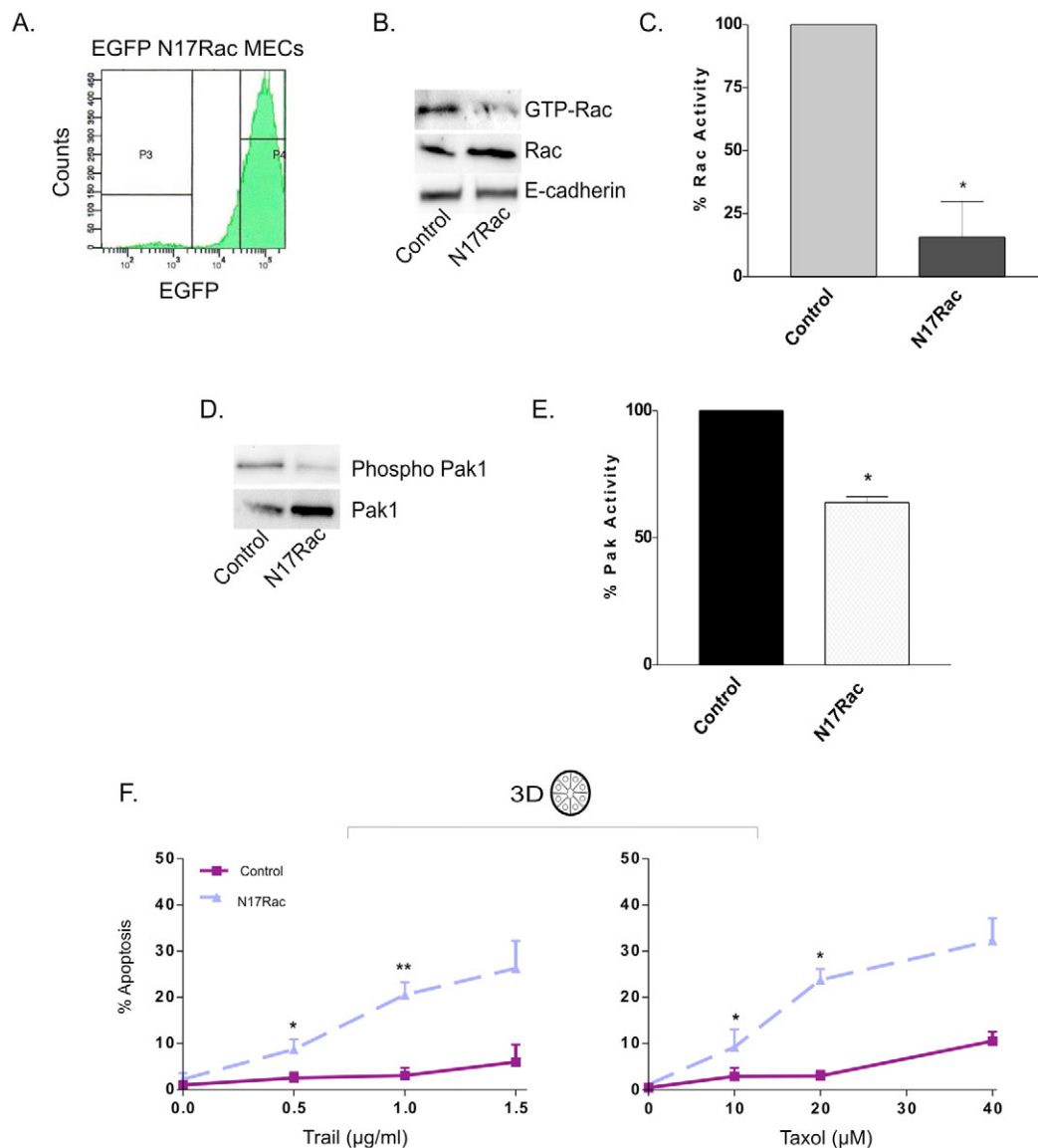


**Fig. 2.** Rac activity is necessary for resistance to apoptosis in 3D mammary acini. (A) FACS analysis showing increased EGFP expression in MECs expressing the EGFP-tagged N17 Rac (P4) in comparison with vector control MECs (P3). (B) Representative immunoblot of GTP-Rac, Rac and E-cadherin in vector control MECs grown as 2D monolayers in comparison with MECs expressing EGFP-tagged N17 Rac. The data illustrate that N17Rac significantly reduces GTP-Rac levels in MECs. (C) Average relative specific activity of Rac in MECs calculated by densitometric analysis of immunoblots of GTP-Rac divided by total cellular Rac following E-cadherin normalization of data illustrated in B. (D) Representative immunoblot of phospho-Pak1 and total Pak1 in 2D monolayer cultures of control MECs and MECs expressing EGFP-tagged N17Rac demonstrating how loss of Rac activity also reduces Pak1 activity. (E) Bar graph depicting the average degree of reduction of Pak1 activity in MECs expressing EGFP-N17Rac in comparison with control MECs. (F) Dose-response curves of the percentage apoptosis, as determined by calculating the number of activated caspase-3-positive cells divided by the total cell number, showing how 3D rBM polarized mammary acini with reduced Rac activity are now more sensitive to both chemotherapeutic (taxol) and receptor-mediated (Trail) apoptotic stimuli. Results are the mean  $\pm$  s.e.m. of three to five separate experiments. \* $P \leq 0.05$  (C,E,F); \*\* $P \leq 0.01$  (F).

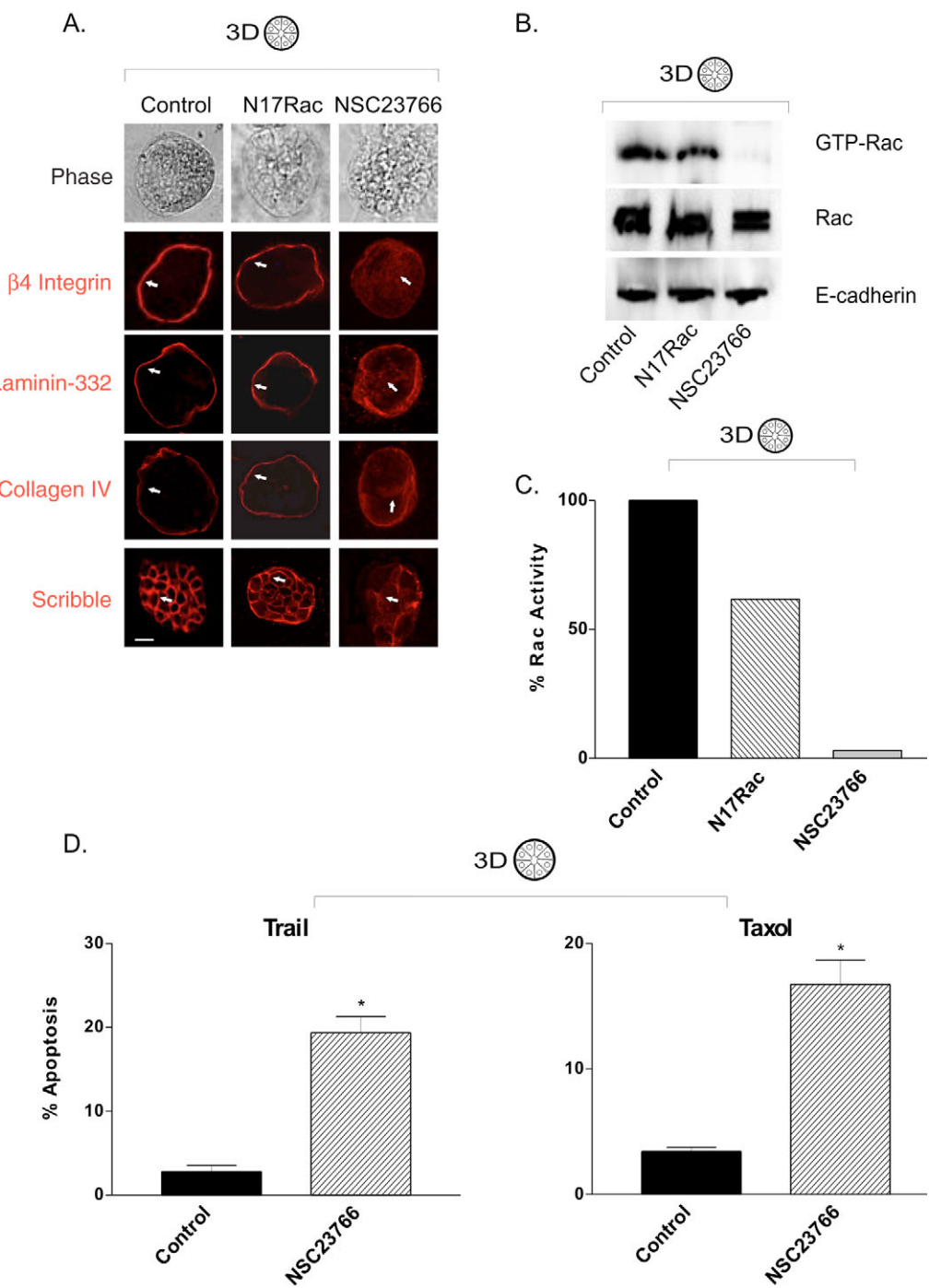


mediates resistance to apoptosis of 3D spheroids, it apparently does so through a mechanism independent from that controlling tissue polarity.

Rac elicits its cellular actions by activating a plethora of downstream effectors, each with different activation and

turnover dynamics. Accordingly, we reasoned that the Rac-effector pathways driving survival might be distinct from those that mediate tissue polarity. To test this possibility, we treated pre-formed death-resistant acini with pharmacologic inhibitors of RhoGTPase, including the general inhibitor toxin A and the

**Fig. 3.** Rac-mediates resistance to apoptosis and changes in tissue polarity through distinct mechanisms. (A) (top) Phase-contrast and confocal immunofluorescence images of colonies of control mammary acini (left panel; control), acini expressing EGFP-tagged N17Rac (middle panel; N17Rac) and acini treated with the Rac1 inhibitor NSC23766 (right panel; NSC23766) stained for  $\beta 4$  integrin, laminin-332, collagen IV and scribble (red). The data show that expression of N17Rac affects neither tissue integrity (compare regions highlighted by arrows in control phase-contrast images of acini with regions highlighted by arrows in images of N17Rac-expressing acini; top) nor tissue polarity (lower images; evidenced by similar basally localized  $\beta 4$  integrin; deposition of laminin-332 and collagen IV and intact cell-cell-localized scribble; compare images of control acini with images of acini expressing N17Rac). However, treatment of acini with the Rac inhibitor NSC23766 disrupted the integrity of acini (compare regions of image highlighted by arrows in phase-contrast images of control with images of NSC23766-treated acini) and severely perturbed tissue polarity, as evidenced by disturbed localization of  $\beta 4$  integrin, laminin-332, collagen IV and scribble (compare images of control with images of NSC23766-treated acini). Bar, 50  $\mu$ m. (B) Representative immunoblot of GTP-Rac, Rac and E-cadherin in vector control MECs grown as 3D acini in comparison to MECs expressing EGFP-tagged N17 Rac and control acini treated with the specific Rac inhibitor NSC23766. The data illustrate that while N17Rac partially reduces GTP-Rac levels in 3D mammary acini, treatment with the Rac inhibitor decreases Rac activity to barely detectable levels. (C) Average relative specific activity of Rac in MECs calculated by densitometric analysis of immunoblots of GTP-Rac divided by total cellular Rac following E-cadherin normalization of data illustrated in B. (D) Bar graphs illustrating increased percentage of apoptotic cells induced by treatment with Trail (1  $\mu$ g/ml) (left) or Taxol (40  $\mu$ M) right in 3D rBM differentiated MECs with significantly reduced Rac activity mediated by treatment with the specific Rac inhibitor NSC23766. The percentage apoptosis was calculated by scoring the number of activated caspase-3-positive MECs divided by the total number of MECs 24 hours following treatment with Trail or Taxol. Results are the mean  $\pm$  s.e.m. of three to five separate experiments. \* $P \leq 0.05$ ; \*\* $P \leq 0.01$ .



specific Rac inhibitor NSC23766. We found that directly inhibiting Rac activity with toxin A (see supplementary material Fig. S1) or with NSC23766 (Fig. 3B; quantified in 3C) substantially sensitized 3D mammary acini to induction of death induced through either immune receptor stimuli or chemotherapy treatment (Fig. 3D). More importantly, and consistent with previous data implicating Rac in polarity, reducing Rac activity to less than 10% was sufficient to disrupt mammary tissue integrity (Fig. 3A; compare phase-contrast images top left to far right showing control acini and NSC23766-treated structures) and to compromise tissue polarity, as illustrated by loss of basal  $\beta 4$  integrin localization, perturbed deposition of laminin-332 and collagen IV and aberrant distribution of scribble (Fig. 3A; compare confocal images in the first column with the images in the last column). While these results suggest that Rac does regulate tissue polarity, they also imply that the molecular mechanism(s) whereby Rac mediates

resistance to apoptosis and polarity in 3D tissues is most likely mediated through distinct effector pathways.

To further explore the functional link between Rac, tissue polarity and resistance to apoptosis in 3D mammary acini, we ectopically expressed the Rac-specific GAP  $\beta 2$ -chimerin, which accelerates the hydrolysis of GTP from Rac, without influencing Cdc42 or RhoA GTP activity (Caloca et al., 2003). Monolayers of non-differentiated MECs and rBM-differentiated 3D mammary acini infected with adenoviral  $\beta 2$ -chimerin showed uniform and sustained (8 days) expression of a hemagglutinin (HA)-tagged  $\beta 2$ -chimerin transgene (Fig. 4A,E middle images), which was associated with a significant reduction in Rac activity (Fig. 4B; quantified in 4C) and increased death sensitivity in the 3D mammary acini (Fig. 4D). Yet again, however, while  $\beta 2$ -chimerin expression substantially reduced Rac activity and reduced death resistance, acini integrity (Fig. 4E; compare phase-contrast

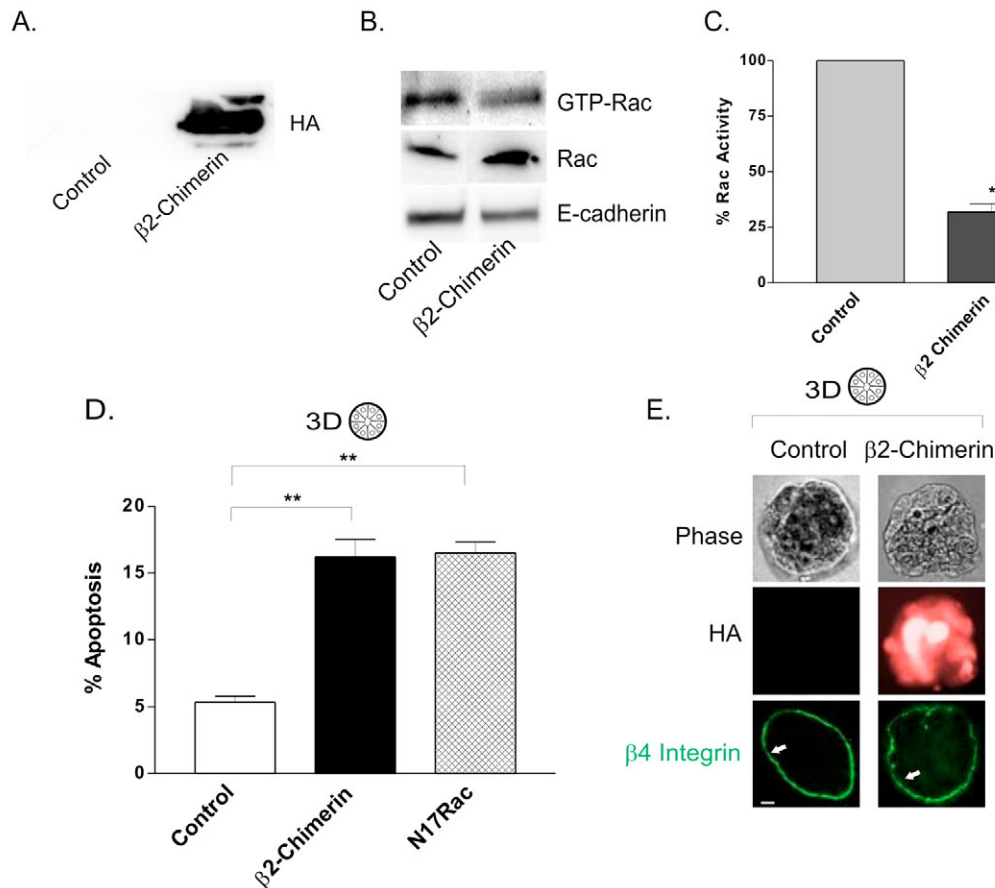


**Fig. 4.** GAP-dependent Rac inactivation sensitizes mammary acini to induction of death. (A) Representative immunoblot showing non-detectable amounts of hemagglutinin (HA) expressed in vector control MECs and high levels in MECs expressing an exogenous HA-tagged  $\beta 2$ -chimerin. (B) Representative immunoblot showing GTP-Rac, Rac and E-cadherin levels in vector control MECs in comparison with  $\beta 2$ -chimerin-expressing MECs. (C) Average relative specific-activity of GTP-loaded Rac illustrating reduced Rac activity in MEC-expressing exogenous  $\beta 2$ -chimerin in comparison with vector control MECs. (D) Bar graph illustrating increased percentage of apoptotic cells induced by treatment with Trail (1  $\mu$ g/ml) in 3D rBM differentiated MECs with reduced Rac activity mediated by expression of either the Rac GAP  $\beta 2$ -chimerin or dominant-negative N17Rac. The percentage apoptosis was calculated by scoring the number of activated caspase-3-positive MECs divided by the total number of MECs 24 hours following treatment with Trail. Similar results were obtained following treatment with chemotherapeutic agents (data not shown). (E) (top) Phase-contrast and (bottom) immunofluorescence images of 3D poly-HEMA rBM-generated vector control MEC colonies (left) and MEC colonies expressing HA-tagged  $\beta 2$ -chimerin (right; red) illustrating robust and uniform expression of the transgene 48 hours following adenoviral infection. Bar, 50  $\mu$ m. Arrows indicate the representative phenotype of acini morphology. Bar, 50  $\mu$ m. Results are the mean  $\pm$  s.e.m. of three separate experiments. \* $P \leq 0.05$ ; \*\* $P \leq 0.01$ .



images of control with  $\beta 2$ -chimerin-expressing acini; top row) and polarity (demonstrated by the maintenance of basally localized  $\beta 4$  integrin; Fig. 4E; compare confocal images of control with  $\beta 2$ -chimerin-expressing acini) remained essentially intact. Collectively, these data indicate that the elevated GTP-Rac observed in 3D mammary acini promotes resistance to apoptosis through a pathway that is independent from that directing polarity.

#### p21-activated kinase 1 activity is necessary and sufficient for Rac-mediated resistance to apoptosis in 3D mammary acini

The Rho GTPase Rac regulates cell behavior by stimulating the activity of multiple molecular effectors, including members of the Pak family (Boettner and Van Aelst, 1999; Schmitz et al., 2000; Van Aelst and D'Souza-Schorey, 1997). Pak proteins are important modulators of tissue development and homeostasis, they can repress anoikis (Menard et al., 2005) and they have been implicated in malignant transformation (Qu et al., 2001; Wang et al., 2006). Consistent with an important role for Pak proteins in mediating resistance to apoptosis in MEC acini, we found that total levels of Pak1 and activated Pak1 rise significantly following rBM-induced tissue differentiation (acini formation) in both MCF10A (Fig. 5A; quantified in B) and HMT-3522 S1 (data not shown) nonmalignant MECs. By contrast, we noted that the specific activity of Pak4 decreased (Fig. 5A) and Pak3 protein was nondetectable (Fig. 5A). Pak1 activity was also significantly reduced in 3D mammary acini expressing the tail-less  $\beta 4$  integrin (Fig. 5C; quantified in D), which we showed also abrogates Rac activity (Fig. 1D; quantified in E). Inhibiting GTP-Rac through ectopic expression of N17Rac, which sensitizes 3D mammary acini to apoptotic stimuli (Fig. 3D), concomitantly decreased Pak1 activity (data not shown). Consistently, a constitutively active adenoviral V12Rac could restore Pak activity and resistance to apoptosis to increasingly cytotoxic doses of Trail and taxol in N17Rac death-sensitized mammary acini (Fig. 5E). By contrast, infection with V12RacH40, which harbors a mutation that prevents the activated Rac from interacting with and stimulating Pak, could not (Fig. 5F). Indeed, direct inhibition of Pak activity through ectopic expression of the Pak inhibitor domain (PID) rendered 3D mammary acini sensitive to death stimulation by Trail (Fig. 5G) and taxol (data not shown). Finally, infection with a wild-type adenoviral Pak1 (Pak1 WT) restored resistance to apoptosis to the death-sensitive N17Rac-expressing acini, analogous to the resistance achieved through expression of the constitutively active V12Rac (Fig. 5H). These findings strongly implicate Rac-dependent Pak1 activity as being necessary and sufficient for mediating  $\alpha 6 \beta 4$  integrin-dependent resistance to apoptosis in 3D mammary acini.

#### Rac activates Pak1 and mediates resistance to apoptosis in 3D mammary acini by stimulating NF- $\kappa$ B

Having established a functional link between Rac, Pak and the increased survival phenotype of 3D mammary acini, we sought to delineate the molecular mechanism(s) whereby Rac activated Pak1 could promote resistance to apoptosis. Pak can regulate cell survival by inhibiting the activity of the pro-apoptotic Bcl2 family member Bad (Cotteret et al., 2003). However, whereas GTP-Rac and Pak activity were consistently and significantly elevated in the death-resistant 3D mammary acini, Bad levels

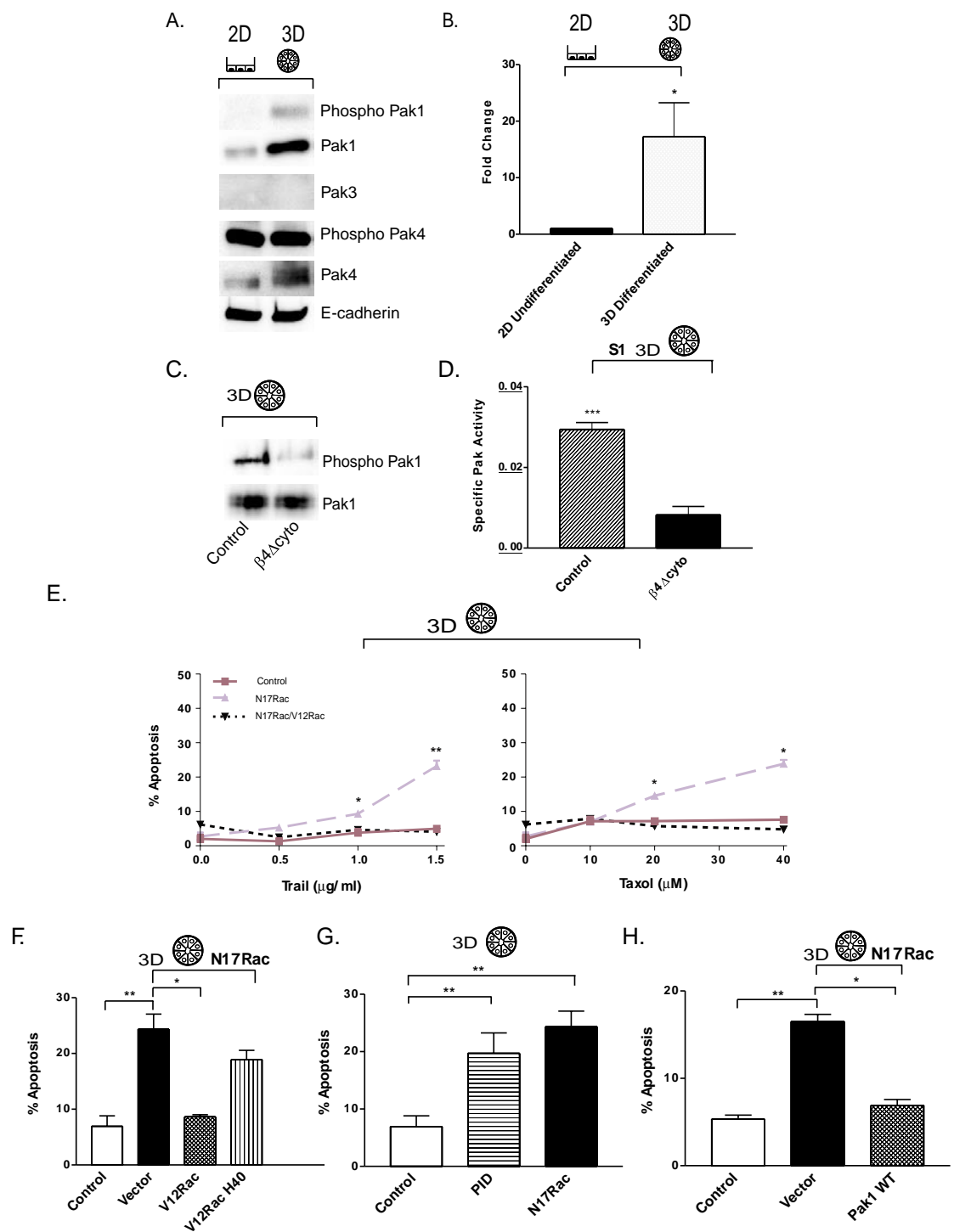
and activity remained unaltered in cultures of rBM-ligated MECs grown in 2D and 3D (data not shown). We therefore reasoned that Pak1 must be driving death resistance through an alternative mechanism. Pak proteins can activate NF- $\kappa$ B to mediate cell survival (Frost et al., 2000), and we showed that  $\alpha 6 \beta 4$  integrin-polarized 3D mammary acini resist apoptosis by activating NF- $\kappa$ B in response to an exogenous death-promoting stress (Weaver et al., 2002). Consistently, we could show that incubating 3D mammary acini with the membrane-soluble peptide SN50, which inhibits activation of NF- $\kappa$ B, but not with the nonfunctional peptide SN50M, prevented nuclear translocation of the p65 subunit of NF- $\kappa$ B (data not shown) (Zahir et al., 2003) and increased the sensitivity of the structures to death stimuli such as Trail (Fig. 6A). In addition, inhibiting nuclear translocation of p65 (and the subsequent activation of NF- $\kappa$ B), through treatment of the acini with SN50, also prevented exogenously expressed Pak1 from conferring resistance to apoptosis to N17Rac-expressing, death-sensitized mammary acini (Fig. 6B). Indeed, while control mammary acini survived and exhibited high levels of nuclear p65 following incubation with Trail, mammary structures with PID-reduced Pak activity had low to non-detectable nuclear p65 when exposed to Trail (Fig. 6C; quantified in 6D) and died 24 hours following treatment (Fig. 6E). Finally, we found that 3D mammary acini sensitized to apoptosis that constitutively expressed N17Rac showed lower levels of nuclear p65 following Trail exposure, but that nuclear p65 levels in these cells were restored following ectopic expression of a wild-type Pak1 adenoviral construct (Fig. 6C; quantified in 6D).

To implicate more directly Pak activation of NF- $\kappa$ B in the apoptosis-resistance phenotype of 3D mammary acini, we prepared populations of MECs stably expressing a retroviral wild-type p65, which promotes constitutive activation of NF- $\kappa$ B. MEC acini ectopically expressing p65 showed constitutive expression of nuclear p65 (supplementary material Fig. S2) that was not diminished by either reducing cellular GTP-Rac or decreasing Pak activity through coexpression of N17Rac or PID. More importantly, constitutive activation of NF- $\kappa$ B prevented the induction of apoptosis in 3D mammary acini treated with Trail even when they had reduced Rac or Pak activity (Fig. 6E). Furthermore, coexpression of the NF- $\kappa$ B signaling pathway super-repressor I $\kappa$ B $\alpha$ M, which prevents NF- $\kappa$ B activation by inhibiting nuclear translocation of p65, permitted death induction in 3D polarized mammary acini, even when these MECs expressed elevated levels of exogenous Pak1 (Fig. 6F). These data indicate that Rac-mediated activation of Pak1 supports resistance to apoptosis in 3D mammary acini by regulating NF- $\kappa$ B activation. However, because we determined that inhibiting Rac and Pak1 through expression of N17Rac reduced the levels of phospho-Bad, whereas increasing Pak levels increased the phosphorylation of Bad (see supplementary material), we cannot rule out the possibility that Rac-Pak-dependent modulation of Bad activity also increases the survival behavior of 3D mammary acini (Fig. 7). Nevertheless, we suggest that mammary acini primarily resist apoptotic stimuli through  $\alpha 6 \beta 4$  integrin-dependent Rac-Pak1-NF- $\kappa$ B signaling (Fig. 7).

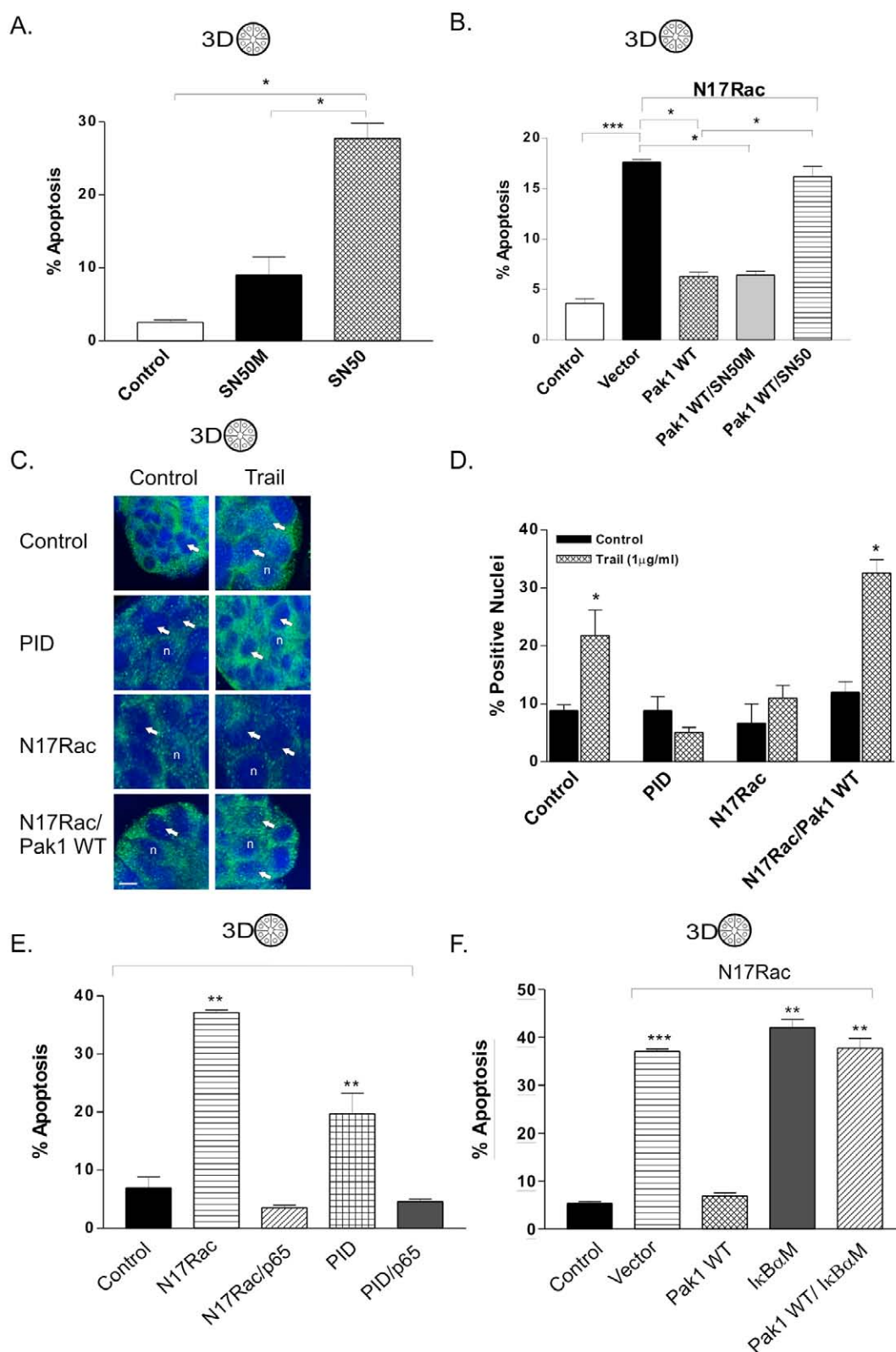
#### Discussion

Using a rBM assay and two non-malignant, immortalized MEC lines, HMT-3522 S-1 and MCF10A, we demonstrated that a

**Fig. 5.** Rac-dependent Pak1 activity is necessary and sufficient for the resistance to apoptosis of mammary acini. (A) Representative immunoblots of phospho-Pak1, total Pak1, Pak-3, phospho-Pak4, total Pak4 and E-cadherin in rBM-ligated MECs plated as 2D monolayers or 3D mammary acini. The data indicate that Pak1 activity is significantly higher, although the abundance of Pak4 is higher in 3D the specific activity of Pak4 is substantially lower and Pak3 is non-detectable in 3D mammary acini in comparison with 2D monolayers of MECs. (B) Quantification of averaged experimental data shown in A of Pak1 specific activity, calculated by densitometric analysis of immunoblots of phospho-Pak1 divided by total Pak1 after normalization to E-cadherin. Similar results were obtained for HMT-3522 S1 and MCF10A nonmalignant MECs. (C) Representative immunoblots of phospho-Pak1 and total Pak1 in 3D mammary acini expressing the tail-less  $\beta 4$  integrin ( $\beta 4\Delta$ cyto) in comparison with control acini. The data demonstrate that Pak1 activity, but not expression, is regulated by  $(\alpha 6)\beta 4$  integrin signaling. (D) Quantification of averaged experimental data shown in C of Pak1 specific activity calculated as described above in B. (E) Dose-response curves illustrating the percentage apoptosis induced in 3D mammary acini following 24 hours of treatment with increasing concentrations of Trail (left) and taxol (right), calculated by scoring the number of caspase-3-positive cells divided by the total number of cells. Mammary acini with reduced Rac activity were sensitized to Trail and taxol-induced apoptosis (N17Rac vector) but their death-resistance phenotype was restored following ectopic expression of V12Rac. (F) Bar graphs illustrating how expression of V12Rac restores resistance to apoptosis induced by Trail treatment in 3D mammary acini expressing N17Rac, whereas expression of V12Rac H40, which cannot activate Pak, does not restore resistance. The percentage apoptosis was calculated by scoring the number of activated caspase-3-positive cells divided by the total number of cells. (G) Bar graph demonstrating that inhibiting Pak activity, by expressing PID significantly sensitizes mammary acini to Trail-induced death, analogous to that mediated by N17Rac. (H) Bar graph showing how expression of wild-type Pak1 can restore resistance to Trail treatment to 3D mammary acini expressing N17Rac. Results are the mean  $\pm$  s.e.m. of three to five separate experiments. \* $P \leq 0.05$ ; \*\* $P \leq 0.01$ .



**Fig. 6.** Pak permits activation of NF- $\kappa$ B to mediate resistance to apoptosis in mammary acini. (A) Bar graph indicating how inhibiting activation of NF- $\kappa$ B by treating mammary acini with SN50 peptide permits Trail-induced apoptosis. MECs were grown in rBM for ten days and treated with SN50 or inactive, scrambled SN50M peptide. Polarized acini were treated with Trail (1  $\mu$ g/ml) and after 24 hours the acini were stained and quantified for activated caspase 3. (B) Bar graph illustrating how ectopically expressed wild-type Pak1 can restore resistance to apoptosis to N17Rac-expressing mammary acini treated with Trail (N17Rac), but the acini remain death sensitive if NF- $\kappa$ B activation is prevented by pre-incubation with SN50. 3D mammary acini were infected with adenovirus, pre-incubated for 24 hours with either SN50 to inhibit NF- $\kappa$ B activation or its non-active analogue SN50M, and treated with Trail (1  $\mu$ g/ml) for 24 hours. The percentage apoptosis for (A) and (B) was calculated by scoring the number of activated caspase-3-positive cells divided by the total cell number. (C) Confocal immunofluorescence microscopy images showing NF- $\kappa$ B p65 nuclear translocation in response to treatment with Trail (90 min) in 3D mammary acini expressing either vector (control), the Pak activity inhibitor (PID), N17Rac (N17Rac) or N17Rac and wild-type Pak1 (N17Rac/Pak1 WT). Note the presence of high nuclear levels of p65, as indicated by "n" and identified by arrow, in response to Trail stimulation in control and N17Rac/Pak1-WT-expressing mammary tissues and decreased levels in acini with reduced Rac or Pak activity. Bar, 10  $\mu$ m. n, nucleus. (D) Quantification of nuclear p65 in 50–100 representative images as shown in C. (E) Bar graph showing how expression of a wild-type p65 transgene restores Trail-induced death-resistance to apoptosis-sensitized N17Rac- and PID-expressing mammary acini. (F) Bar graph showing how inhibiting activation of NF- $\kappa$ B through expression of the I $\kappa$ B $\alpha$ M super-repressor permits Trail-dependent induction of death in 3D mammary acini despite elevated levels of Pak1. Results are the mean  $\pm$  s.e.m. of three separate experiments. \* $P$   $\leq$  0.05; \*\* $P$   $\leq$  0.01; \*\*\* $P$   $\leq$  0.001.



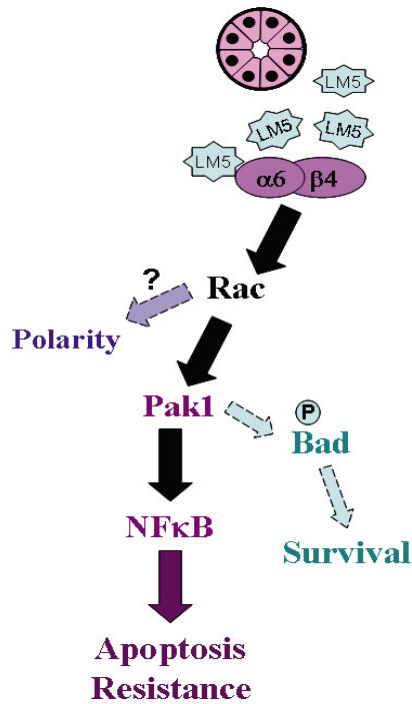


**Fig. 7.** Schematic illustrating proposed mechanism whereby  $\alpha 6 \beta 4$  integrin regulates Rac and Pak to mediate Bad- and NF- $\kappa$ B-dependent resistance to apoptosis in mammary acini. Nonmalignant MECs differentiate into polarized-tissue-like structures that assemble an endogenous laminin-332-containing basement membrane. Laminin-ligation of  $\alpha 6 \beta 4$  integrin stimulates Rac to drive tissue polarity and promote resistance to apoptosis in 3D mammary acini through Pak-dependent activation of NF- $\kappa$ B and phosphorylation of Bad. LM-332, laminin-5; P, phosphorylated.

polarized 3D mammary acinus resists diverse exogenous apoptotic stimuli including immune-receptor stimuli and chemotherapeutic agents by promoting Pak1-mediated activation of NF- $\kappa$ B. We determined that  $\alpha 6 \beta 4$  integrin signaling in 3D mammary acini is necessary to elevate the activity of Rac and Pak1 and that Pak1 enhances activation of NF- $\kappa$ B in response to an exogenous stress, leading to enhanced MEC survival. Although  $\alpha 6 \beta 4$  integrin can support epithelial survival through ERK and PI 3-kinase (Bachelder et al., 1999), and PI 3-kinase can activate Rac (Shaw et al., 1997), we found that the activity of ERK and PI 3-kinase was significantly diminished in 3D mammary acini, and that inhibiting the activity of these kinases failed to sensitize mammary acini to apoptotic stimuli (data not shown) (Zahir et al., 2003). Although we have no explanation for this finding, transgenic and 3D organoid experiments suggest that Akt might be more crucial for regulating cellular metabolism and tumor invasion in 3D tissues in vivo (Boxer et al., 2006; Hutchinson et al., 2004; Irie et al., 2005; Ju et al., 2007). Furthermore, studies that have linked  $\alpha 6 \beta 4$  integrin-dependent survival to ERK and PI 3-kinase signaling used transformed breast cells grown as 2D monolayers, whereas we used non-transformed mammary acini grown within a compliant 3D rBM to demonstrate that  $\alpha 6 \beta 4$  integrin-dependent survival depends upon elevated Rac and Pak1 and NF- $\kappa$ B. The compliance of hydrogels such as the rBM we used for our studies are similar in physical consistency

to the extracellular matrix stroma found in tissues in vivo, and both of these microenvironments are considerably softer than the rigid tissue-culture plastic or borosilicate glass surfaces used for traditional signal-transduction experimentation. Indeed, other investigators and ourselves have shown that matrix stiffness profoundly alters ERK and RhoGTPase activity and signaling (Engler et al., 2006; McBeath et al., 2004; Paszek et al., 2005). Whether matrix compliance could modify the molecular mechanisms whereby matrix adhesion regulates cell survival is being investigated.

Similar to metastatic tumors in vivo, tumor cells grown as 3D spheroids can rapidly acquire multidrug resistance in response to acute drug treatment (Durand and Olive, 2001; Kerbel, 1994; Sutherland and Durand, 1972). The treatment resistance behavior of 3D spheroids has been attributed to reduced drug penetration (Jain, 1987; Tong et al., 2004), hypoxia (Sminia et al., 2003) and altered growth or cell-cycle regulation (St Croix et al., 1996). However, we found that the viability of the drug-treated 3D polarized, apoptosis-resistant mammary acini was not modified by proliferation or cell-cycle status, that the structures were not hypoxic, and that the acini could resist even high doses of gamma irradiation, where drug penetration is not an issue (shown by increased resistance to apoptosis and high clonogenic survival; unpublished observations). Instead, our data indicate that the apoptosis-resistance phenotype of 3D acini is due to increased (integrin-dependent) adhesion signaling, similar to the enhanced-survival phenotype of myeloma, cervical, lung and lymphoid tumor cells exposed to pro-death stimuli (Dalton, 2003; Damiano et al., 1999; Sethi et al., 1999; Whitacre and Berger, 1997) and the higher drug-resistance of integrin-ligated monolayers of tumors and 3D spheroids (Damiano et al., 1999; Kerbel et al., 1996; Narita et al., 1998; Santini et al., 2000). To explain this adhesion-mediated resistance, we showed that laminin-mediated ligation of  $\alpha 6 \beta 4$  integrin promotes immune-receptor and multidrug resistance in mammary acini by permitting stress-induced activation of NF- $\kappa$ B (Weaver et al., 2002). We also reported that  $\alpha 6 \beta 4$  integrin permits epidermal growth factor-dependent activation of Rac that stimulates NF- $\kappa$ B and mediates anchorage-independent survival of MECs (Zahir et al., 2003). Our current findings extend our earlier observations by demonstrating that laminin-ligated  $\alpha 6 \beta 4$  integrin enhances Rac and Pak activity in 3D mammary acini resulting in stress-dependent NF- $\kappa$ B activation and increased survival through a mechanism that appears to be independent of tissue polarity. Although we do not know how  $\alpha 6 \beta 4$  integrin modulates tissue polarity, we did find that  $\alpha 6 \beta 4$  integrin regulates GTP-Rac and, in accordance with previous work, that Rac regulates tissue morphology and polarity (Akhtar and Streuli, 2006; O'Brien et al., 2001) (Fig. 3A). However, given that we could distinguish between Rac-dependent survival through Pak and Rac-mediated tissue polarity, we suggest that the Rac effectors directing tissue polarity differ from those that promote cell survival. Consistently, we determined that Rac regulates Pak activity to support resistance to apoptosis in mammary acini, but that modulating Pak had no detectable morphological effect on tissue organization or integrity. Clearly, additional experiments will be required to identify the Rac effectors directing tissue polarity and to determine whether these pathways are regulated by  $\alpha 6 \beta 4$  integrin.



It is not clear why  $\alpha 6 \beta 4$  integrin activation of Rac and Pak is dramatically enhanced in MECs grown as 3D rBM acini in comparison with 2D rBM monolayers. Plausible explanations for this observation include differences in matrix compliance, integrin adhesions and receptor dynamics or qualitative changes in RhoGTPase signaling linked to tissue organization. For example, other investigators and ourselves have reported that matrix stiffness increases the activity of Rho to promote assembly of focal adhesions (Bershadsky et al., 2006; Paszek et al., 2005) and that Rac activity is inhibited by matrix stiffness and increases significantly in MECs interacting with a compliant substrate (our unpublished observations). The targeting and functioning of RhoGTPase are also modified by tissue morphology such that the localization of activated Rac is restricted to tight junctions following epithelial polarization (Chen and Macara, 2005), and PTEN localizes activated cdc42 to stimulate  $\alpha$ PKC-dependent lumen formation in polarized kidney epithelial cysts (Martin-Belmonte et al., 2007).

Rac is often overexpressed in tumors of the breast (Fritz et al., 1999), it can support anchorage-independent growth of MECs (Bouzahzah et al., 2001; Zahir et al., 2003) and protects MDCK cells from anoikis (Coniglio et al., 2001). Depleting Rac in glioblastoma cells and breast cancer cells also strongly inhibits invasion (Chan et al., 2005). Rac elicits its pleiotropic effects on cell function by activating a plethora of cellular targets including the Pak family of signaling molecules. Pak proteins facilitate growth factor signaling and interact with multiple downstream effectors to alter cell growth, survival, migration and differentiation (Bokoch, 2003; Puto et al., 2003; Vadlamudi and Kumar, 2003; Wang et al., 2002), and Pak proteins can promote the tumorigenic behavior of cells (Menard et al., 2005; Schurmann et al., 2000; Tang et al., 1997). For example, Rac-dependent Pak activation drives cell migration and tumor invasion (Alahari, 2003; Alahari et al., 2004; Brown et al., 2005), and Pak proteins can enhance cell survival (Gnesutta et al., 2001; Johnson and D'Mello, 2005; Qu et al., 2001). Here, we show that the specific activity of Pak1 increases dramatically and significantly in apoptosis-resistant 3D mammary acini, and that Pak1 is essential for immune-receptor and drug-induced death because it permits stress-dependent NF- $\kappa$ B activation (Fig. 6C,D). Our results are consistent with experiments showing how Pak4 sustains anchorage-independent cell survival by stimulating NF- $\kappa$ B (Cammarano and Minden, 2001) and extend these observations to demonstrate that Pak1 can render cells resistant to diverse exogenous apoptotic stimuli by regulating NF- $\kappa$ B activity. Activated Pak can also prevent apoptosis by inducing phosphorylation of Bad on Ser112 to prevent mitochondria-mediated activation of executioner caspases (Cotteret et al., 2003; Deacon et al., 2003; Gnesutta et al., 2001; Schurmann et al., 2000), and we were able to establish a correlation between Bad phosphorylation, resistance to apoptosis and Pak activity (see supplementary material Fig. S3). However, we found that neither expression of Bad nor its phosphorylation increased in association with death resistance in 3D MEC acini, despite finding that Rac and Pak activity were significantly higher in these same structures. Thus, although we cannot rule out the possibility that decreased phosphorylation of Bad contributes to Rac-Pak-dependent resistance to apoptosis, we suggest that Pak-induced NF- $\kappa$ B activation is more likely the predominant anti-apoptotic mechanism operating in 3D mammary acini.

We established a functional link between laminin-mediated ligation of  $\alpha 6 \beta 4$  integrin and Rac-dependent activation of Pak1, and  $\beta 4$  integrin and laminins are frequently elevated in tumors (Davis et al., 2001), they cooperate to drive invasion and metastasis (Jones et al., 1997; Lipscomb and Mercurio, 2005; Lipscomb et al., 2005) and their coexpression is associated with a poor prognosis in breast cancer patients (Tagliabue et al., 1998). Our data offer an explanation for these findings and additionally explain why Pak proteins are often overexpressed in tumors (Vadlamudi and Kumar, 2003) and why hyper-activation of Pak1 efficiently drives mammary gland tumor formation (Wang et al., 2006). Indeed, expression of NF- $\kappa$ B increases during malignant transformation of the breast (Kim et al., 2000), and NF- $\kappa$ B is implicated in mammary tumor pathogenesis (Sovak et al., 1997), breast tumor metastasis (Nakshatri et al., 1997) and resistance to chemical, immune and radiation therapy (Baeuerle and Baltimore, 1996; Baldwin, 2001; Weaver et al., 2002). Moreover, Rac-Pak-dependent activation of NF- $\kappa$ B can drive Kaposi-sarcoma-associated malignant transformation (Dadke et al., 2003). Significantly, by linking matrix-dependent Rac-Pak activation to NF- $\kappa$ B-dependent resistance to apoptosis, our findings underscore the importance of identifying pharmacological Pak inhibitors that could be used as tractable anti-tumor therapies.

## Materials and Methods

### Antibodies and reagents

We used commercial EHS matrix (Matrigel<sup>TM</sup>; Collaborative Research) for the reconstituted basement membrane (rBM) assays. The sources of the primary antibodies used in these studies were as follows:  $\beta 4$  integrin, clone 3E1 (Chemicon); phospho-Bad (Ser136), Bad, cleaved caspase 3, phospho-Pak1 (Thr423)/Pak2 (Thr402), Pak1, Pak 3, Pak 4, phospho-Pak4 (Ser474)/Pak5 (Ser602)/Pak6 (Ser560), rabbit sera (all from Cell Signaling); E-cadherin, clone 36, and Rac1, clone 102 (BD Biosciences); HA.11, clone 16B12 (Covance); and NF- $\kappa$ B p65, rabbit sera (Santa Cruz Biotechnology). The secondary antibodies used were as follows: HRP-conjugated anti-rabbit and mouse (Amersham Laboratories); and Alexa-Fluor-488- and Alexa-Fluor-555-conjugated anti-mouse and rabbit IgGs (Molecular Probes). Reagents used in the studies were as follows: Rho GTPase inhibitor toxin A *Clostridium difficile* (10 mM in DMSO; Calbiochem); and Rac1 inhibitor NSC23766 (50 mM in H<sub>2</sub>O; Calbiochem); NF- $\kappa$ B SN50, active cell-permeable inhibitory peptide (50  $\mu$ M in H<sub>2</sub>O), NF- $\kappa$ B SN50M, inactive cell-permeable control peptide (50  $\mu$ M in H<sub>2</sub>O), Trail (approximately 0.5 mg/ml), and taxol (20 mM in DMSO; Biomol); etoposide (10–100  $\mu$ M in DMSO; TopoGen); live/dead viability cytotoxicity kit (Molecular Probes); and the in situ cell death detection kit (TUNEL; Roche).

### Cell culture

The HMT-3522 and MCF10A mammary epithelial cells (MECs) were grown and maintained exactly as previously described (Paszek et al., 2005).

### Flow cytometry

Live cells were isolated, re-suspended in Dulbecco's PBS with 0.5% Fetal Bovine Serum and immediately sorted for high EGFP expression on a FACScan (Becton Dickinson). All manipulations were conducted at 4°C.

### Immunofluorescence analysis

Cells were directly fixed using 100% methanol, and samples were incubated with primary antibody followed by either Alexa-Fluor-488 or Alexa-Fluor-555-conjugated secondary antibody. Nuclei were counterstained with diaminophenylindole (DAPI; Sigma-Aldrich). Cells were visualized using a Bio-Rad MRC 1024 laser-scanning confocal microscope attached to a Nikon Diaphot 200 microscope. Images were recorded at 60 $\times$  magnification.

### Apoptosis assay

Apoptosis was assayed by immuno-detection of activated caspase 3. The percentage apoptosis was quantified as the number of cells positive for activated caspase 3 divided by the total number of cells. The minimum number of cells scored was 200–300 per experimental condition. Results were confirmed using live/dead and TUNEL assays. Cells were visualized using a fluorescence microscope (Olympus model U-LH100HGAPO).

## Adenoviral and retroviral constructs and studies

EGFP-tagged N17Rac1 has been described previously (Russell et al., 2003). Stable MEC populations expressing EGFP-tagged N17Rac1 were antibiotic selected, FACS sorted and visually confirmed through immunofluorescence microscopy (Zahir et al., 2003). IkB $\alpha$ M and p65 cloned into PLZRS (provided by P. Khavari, Stanford Medical Center, CA) were used directly. Adenovirus Tet, V12Rac, V12Rac H40, PID, Pak1 WT, and HA-tagged  $\beta 2$ -chimerin have been described previously (Beeser et al., 2005; Tang et al., 1999; Yang et al., 2005), and were expanded and virus was purified by cesium chloride banding (He et al., 1998). 3D MEC tissue structures were generated using a polyHEMA-rBM suspension culture (Weaver et al., 2002), and polarized acini were then isolated in PBS supplemented with 10 mM EDTA, infected with adenovirus (15 minutes; 37°C), and transgene expression was confirmed by immunofluorescence microscopy and immunoblot and Rac GTPase activity assay. 24 hours following adenoviral infection, the acini were embedded within a 3D rBM and then assayed for resistance to apoptotic stimuli (Trail; 0.1–2.0  $\mu$ g/ml, 24 hours, 37°C), as described above.

## Immunoblot analysis

Cells were lysed in RIPA buffer containing protease and phosphatase inhibitors, and equal quantities of protein were separated on reducing SDS-PAGE gels, and immunoblotted for protein, as described previously (Zahir et al., 2003).

## Rac GTPase assay

Rac GTPase activity was assessed in cell extracts (G protein lysis buffer: 25 mM HEPES, pH 7.5, 150 mM NaCl, 1% Igepal CA-630, 10 mM MgCl<sub>2</sub>, 1 mM EDTA, 10% glycerol, 1 mM pefabloc SC, 1  $\mu$ g/ml leupeptin, 5  $\mu$ g/ml aprotinin, 1 mM sodium orthovanadate and 1 mM sodium fluoride) prepared from PBS-washed (4°C), equalized cell numbers plated as 2D monolayers on rBM-coated tissue-culture plastic (24 hours) or as 3D tissue-like acini structures within rBM (10–12 days). Cell lysates were centrifuged (5 minutes; 20,817 RCF; 4°C), and supernatants were mixed with GST-PBD and incubated with glutathione-sepharose beads (Amersham Biosciences; 60 minutes, 4°C). Cleared lysates were then washed (3 $\times$  lysis buffer), and bound protein was eluted with Laemmli buffer and separated on a 12% SDS-PAGE gel. Active Rac was detected by immunoblotting with antibody against Rac, and specific activity was calculated by normalizing densitometric values of Pak-associated Rac to total Rac and E-cadherin, as previously described (Zahir et al., 2003).

We thank G. Rozenberg for assistance with the confocal microscopy and J. Meinkoth and R. Assoian for helpful comments. This work was supported by grants from the National Cancer Institute CA078731 and Department of Defense DAMD17-01-100368, 1703-1-0496 and W81X WH-05-1-330 to V.M.W., NIH GM-57388 to D.B., National Cancer Institute CA 117884 to J.C., and DAMD17-01-1-0367 to J.N.L.

## References

- Akhtar, N. and Streuli, C. H. (2006). Rac1 links integrin-mediated adhesion to the control of lactational differentiation in mammary epithelia. *J. Cell Biol.* **173**, 781–793.
- Alahari, S. K. (2003). Nischarin inhibits Rac induced migration and invasion of epithelial cells by affecting signaling cascades involving PAK. *Exp. Cell Res.* **288**, 415–424.
- Alahari, S. K., Reddig, P. J. and Juliano, R. L. (2004). The integrin-binding protein Nischarin regulates cell migration by inhibiting PAK. *EMBO J.* **23**, 2777–2788.
- Bachelder, R. E., Ribick, M. J., Marchetti, A., Falcioni, R., Soddu, S., Davis, K. R. and Mercurio, A. M. (1999). p53 inhibits alpha 6 beta 4 integrin survival signaling by promoting the caspase 3-dependent cleavage of AKT/PKB. *J. Cell Biol.* **147**, 1063–1072.
- Baeuerle, P. A. and Baltimore, D. (1996). NF-kappa B: ten years after. *Cell* **87**, 13–20.
- Baldwin, A. S. (2001). Control of oncogenesis and cancer therapy resistance by the transcription factor NF-kappaB. *J. Clin. Invest.* **107**, 241–246.
- Barros, E. J., Santos, O. F., Matsumoto, K., Nakamura, T. and Nigam, S. K. (1995). Differential tubulogenic and branching morphogenetic activities of growth factors: implications for epithelial tissue development. *Proc. Natl. Acad. Sci. USA* **92**, 4412–4416.
- Bates, R. C., Buret, A., van Helden, D. F., Horton, M. A. and Burns, G. F. (1994). Apoptosis induced by inhibition of intercellular contact. *J. Cell Biol.* **125**, 403–415.
- Beeser, A., Jaffer, Z. M., Hofmann, C. and Chernoff, J. (2005). Role of group A p21-activated kinases in activation of extracellular-regulated kinase by growth factors. *J. Biol. Chem.* **280**, 36609–36615.
- Bershadsky, A. D., Ballestrem, C., Carramusa, L., Zilberman, Y., Gilquin, B., Khochbin, S., Alexandrova, A. Y., Verkhovskiy, A. B., Shemesh, T. and Kozlov, M. M. (2006). Assembly and mechanosensory function of focal adhesions: experiments and models. *Eur. J. Cell Biol.* **85**, 165–173.
- Bissell, M. J. and Radisky, D. (2001). Putting tumours in context. *Nat. Rev. Cancer* **1**, 46–54.
- Boettner, B. and Van Aelst, L. (1999). Rac and Cdc42 effectors. *Prog. Mol. Subcell. Biol.* **22**, 135–158.
- Bokoch, G. M. (2003). Biology of the p21-activated kinases. *Annu. Rev. Biochem.* **72**, 743–781.
- Bouzahzah, B., Albanese, C., Ahmed, F., Pixley, F., Lisanti, M. P., Segall, J. D., Condeelis, J., Joyce, D., Minden, A., Der, C. J. et al. (2001). Rho family GTPases regulate mammary epithelium cell growth and metastasis through distinguishable pathways. *Mol. Med.* **7**, 816–830.
- Boxer, R. B., Stairs, D. B., Dugan, K. D., Notarfrancesco, K. L., Portocarrero, C. P., Keister, B. A., Belka, G. K., Cho, H., Rathmell, J. C., Thompson, C. B. et al. (2006). Isoform-specific requirement for Akt1 in the developmental regulation of cellular metabolism during lactation. *Cell Metab.* **4**, 475–490.
- Brown, M. C., Cary, L. A., Jamieson, J. S., Cooper, J. A. and Turner, C. E. (2005). Src and FAK kinases cooperate to phosphorylate paxillin kinase linker, stimulate its focal adhesion localization, and regulate cell spreading and protrusiveness. *Mol. Biol. Cell* **16**, 4316–4328.
- Caloca, M. J., Wang, H. and Kazanietz, M. G. (2003). Characterization of the Rac-GAP (Rac-GTPase-activating protein) activity of beta2-chimaerin, a 'non-protein kinase C' phorbol ester receptor. *Biochem. J.* **375**, 313–321.
- Cammarano, M. S. and Minden, A. (2001). Dbp and the Rho GTPases activate NF kappaB by I kappaB kinase (IKK)-dependent and IKK-independent pathways. *J. Biol. Chem.* **276**, 25876–25882.
- Chan, A. Y., Coniglio, S. J., Chuang, Y. Y., Michaelson, D., Knaus, U. G., Philips, M. R. and Symons, M. (2005). Roles of the Rac1 and Rac3 GTPases in human tumor cell invasion. *Oncogene* **24**, 7821–7829.
- Chen, X. and Macara, I. G. (2005). Par-3 controls tight junction assembly through the Rac exchange factor Tiam1. *Nat. Cell Biol.* **7**, 262–269.
- Coniglio, S. J., Jou, T. S. and Symons, M. (2001). Rac1 protects epithelial cells against anoikis. *J. Biol. Chem.* **276**, 28113–28120.
- Cotteret, S., Jaffer, Z. M., Beeser, A. and Chernoff, J. (2003). p21-Activated kinase 5 (Pak5) localizes to mitochondria and inhibits apoptosis by phosphorylating BAD. *Mol. Cell Biol.* **23**, 5526–5539.
- Dadke, D., Fryer, B. H., Golemis, E. A. and Field, J. (2003). Activation of p21-activated kinase 1-nuclear factor kappaB signaling by Kaposi's sarcoma-associated herpes virus G protein-coupled receptor during cellular transformation. *Cancer Res.* **63**, 8837–8847.
- Dalton, W. S. (2003). The tumor microenvironment: focus on myeloma. *Cancer Treat. Rev.* **29** Suppl. 1, 11–19.
- Damiano, J. S., Cress, A. E., Hazlehurst, L. A., Shtil, A. A. and Dalton, W. S. (1999). Cell adhesion mediated drug resistance (CAM-DR): role of integrins and resistance to apoptosis in human myeloma cell lines. *Blood* **93**, 1658–1667.
- Davis, T. L., Cress, A. E., Dalkin, B. L. and Nagle, R. B. (2001). Unique expression pattern of the alpha6beta4 integrin and laminin-5 in human prostate carcinoma. *Prostate* **46**, 240–248.
- Deacon, K., Mistry, P., Chernoff, J., Blank, J. L. and Patel, R. (2003). p38 Mitogen-activated protein kinase mediates cell death and p21-activated kinase mediates cell survival during chemotherapeutic drug-induced mitotic arrest. *Mol. Biol. Cell* **14**, 2071–2087.
- Debnath, J., Muthuswamy, S. K. and Brugge, J. S. (2003). Morphogenesis and oncogenesis of MCF-10A mammary epithelial acini grown in three-dimensional basement membrane cultures. *Methods* **30**, 256–268.
- Desoize, B. and Jardillier, J. (2000). Multicellular resistance: a paradigm for clinical resistance? *Crit. Rev. Oncol. Hematol.* **36**, 193–207.
- Durand, R. E. and Olive, P. L. (2001). Resistance of tumor cells to chemo- and radiotherapy modulated by the three-dimensional architecture of solid tumors and spheroids. *Methods Cell Biol.* **64**, 211–233.
- Engler, A. J., Sen, S., Sweeney, H. L. and Discher, D. E. (2006). Matrix elasticity directs stem cell lineage specification. *Cell* **126**, 677–689.
- Fernandez, Y., Gu, B., Martinez, A., Torregrosa, A. and Sierra, A. (2002). Inhibition of apoptosis in human breast cancer cells: role in tumor progression to the metastatic state. *Int. J. Cancer* **101**, 317–326.
- Fritz, G., Just, I. and Kaina, B. (1999). Rho GTPases are over-expressed in human tumors. *Int. J. Cancer* **81**, 682–687.
- Frost, J. A., Swantek, J. L., Stippec, S., Yin, M. J., Gaynor, R. and Cobb, M. H. (2000). Stimulation of NFkappaB activity by multiple signaling pathways requires PAK1. *J. Biol. Chem.* **275**, 19693–19699.
- Fulda, S. and Debatin, K. M. (2004). Apoptosis signaling in tumor therapy. *Ann. N. Y. Acad. Sci.* **1028**, 150–156.
- Gnesutta, N., Qu, J. and Minden, A. (2001). The serine/threonine kinase PAK4 prevents caspase activation and protects cells from apoptosis. *J. Biol. Chem.* **276**, 14414–14419.
- Gupta, G. P. and Massague, J. (2006). Cancer metastasis: building a framework. *Cell* **127**, 679–695.
- He, T. C., Zhou, S., da Costa, L. T., Yu, J., Kinzler, K. W. and Vogelstein, B. (1998). A simplified system for generating recombinant adenoviruses. *Proc. Natl. Acad. Sci. USA* **95**, 2509–2514.
- Hermiston, M. L. and Gordon, J. I. (1995). In vivo analysis of cadherin function in the mouse intestinal epithelium: essential roles in adhesion, maintenance of differentiation, and regulation of programmed cell death. *J. Cell Biol.* **129**, 489–506.
- Hutchinson, J. N., Jin, J., Cardiff, R. D., Woodgett, J. R. and Muller, W. J. (2004). Activation of Akt-1 (PKB-alpha) can accelerate ErbB-2-mediated mammary tumorigenesis but suppresses tumor invasion. *Cancer Res.* **64**, 3171–3178.
- Igney, F. H. and Krammer, P. H. (2002). Death and anti-death: tumour resistance to apoptosis. *Nat. Rev. Cancer* **2**, 277–288.
- Irie, H. Y., Pearline, R. V., Grueneberg, D., Hsia, M., Ravichandran, P., Kothari, N., Natesan, S. and Brugge, J. S. (2005). Distinct roles of Akt1 and Akt2 in regulating cell migration and epithelial-mesenchymal transition. *J. Cell Biol.* **171**, 1023–1034.
- Jacquier, A., Buhler, E., Schafer, M. K., Bohl, D., Blanchard, S., Beclin, C. and Haese,

- G. (2006). Alsin/Rac1 signaling controls survival and growth of spinal motoneurons. *Ann. Neurol.* **60**, 105-117.
- Jain, R. K. (1987). Transport of molecules across tumor vasculature. *Cancer Metastasis Rev.* **6**, 559-593.
- Johnson, K. and D'Mello, S. R. (2005). p21-Activated kinase-1 is necessary for depolarization-mediated neuronal survival. *J. Neurosci. Res.* **79**, 809-815.
- Johnson, K. R., Leight, J. L. and Weaver, V. M. (2007). Demystifying the effects of a three-dimensional microenvironment in tissue morphogenesis. *Methods Cell Biol.* **83**, 547-583.
- Jones, J. L., Royall, J. E., Critchley, D. R. and Walker, R. A. (1997). Modulation of myoepithelial-associated alpha6beta4 integrin in a breast cancer cell line alters invasive potential. *Exp. Cell Res.* **235**, 325-333.
- Ju, X., Katiyar, S., Wang, C., Liu, M., Jiao, X., Li, S., Zhou, J., Turner, J., Lisanti, M. P., Russell, R. G. et al. (2007). Akt1 governs breast cancer progression in vivo. *Proc. Natl. Acad. Sci. USA* **104**, 7438-7443.
- Kerbel, R. S. (1994). Impact of multicellular resistance on the survival of solid tumors, including micrometastases. *Invasion Metastasis* **14**, 50-60.
- Kerbel, R. S., St Croix, B., Florenes, V. A. and Rak, J. (1996). Induction and reversal of cell adhesion-dependent multicellular drug resistance in solid breast tumors. *Hum. Cell* **9**, 257-264.
- Kim, D. W., Sovak, M. A., Zanieski, G., Nonet, G., Romieu-Mourez, R., Lau, A. W., Hafer, L. J., Yaswen, P., Stampfer, M., Rogers, A. E. et al. (2000). Activation of NF-kappaB/Rel occurs early during neoplastic transformation of mammary cells. *Carcinogenesis* **21**, 871-879.
- Kirshner, J., Chen, C. J., Liu, P., Huang, J. and Shively, J. E. (2003). CEACAM1-4S, a cell-cell adhesion molecule, mediates apoptosis and reverts mammary carcinoma cells to a normal morphogenic phenotype in a 3D culture. *Proc. Natl. Acad. Sci. USA* **100**, 521-526.
- Kuh, H. J., Jang, S. H., Wientjes, M. G., Weaver, J. R. and Au, J. L. (1999). Determinants of paclitaxel penetration and accumulation in human solid tumor. *J. Pharmacol. Exp. Ther.* **290**, 871-880.
- Lipscomb, E. A. and Mercurio, A. M. (2005). Mobilization and activation of a signaling competent alpha6beta4 integrin underlies its contribution to carcinoma progression. *Cancer Metastasis Rev.* **24**, 413-423.
- Lipscomb, E. A., Simpson, K. J., Lyle, S. R., Ring, J. E., Dugan, A. S. and Mercurio, A. M. (2005). The alpha6beta4 integrin maintains the survival of human breast carcinoma cells in vivo. *Cancer Res.* **65**, 10970-10976.
- Martin-Belmonte, F., Gassama, A., Datta, A., Yu, W., Rescher, U., Gerke, V. and Mostov, K. (2007). PTEN-mediated apical segregation of phosphoinositides controls epithelial morphogenesis through Cdc42. *Cell* **128**, 383-397.
- Matter, M. L. and Ruoslahti, E. (2001). A signaling pathway from the alpha5beta1 and alpha(v)beta3 integrins that elevates bcl-2 transcription. *J. Biol. Chem.* **276**, 27757-27763.
- McBeath, R., Pirone, D. M., Nelson, C. M., Bhadriraju, K. and Chen, C. S. (2004). Cell shape, cytoskeletal tension, and RhoA regulate stem cell lineage commitment. *Dev. Cell* **6**, 483-495.
- Menard, R. E., Jovanovski, A. P. and Mattingly, R. R. (2005). Active p21-activated kinase 1 rescues MCF10A breast epithelial cells from undergoing anoikis. *Neoplasia* **7**, 638-645.
- Mercurio, A. M. and Rabinovitz, I. (2001). Towards a mechanistic understanding of tumor invasion – lessons from the alpha6beta 4 integrin. *Semin. Cancer Biol.* **11**, 129-141.
- Nakshatri, H., Bhat-Nakshatri, P., Martin, D. A., Goulet, R. J., Jr and Sledge, G. W., Jr (1997). Constitutive activation of NF-kappaB during progression of breast cancer to hormone-independent growth. *Mol. Cell. Biol.* **17**, 3629-3639.
- Narita, T., Kimura, N., Sato, M., Matsuura, N. and Kannagi, R. (1998). Altered expression of integrins in adriamycin-resistant human breast cancer cells. *Anticancer Res.* **18**, 257-262.
- O'Brien, L. E., Jou, T. S., Pollack, A. L., Zhang, Q., Hansen, S. H., Yurchenco, P. and Mostov, K. E. (2001). Rac1 orientates epithelial apical polarity through effects on basolateral laminin assembly. *Nat. Cell Biol.* **3**, 831-838.
- Paszek, M. J., Zahir, N., Johnson, K. R., Lakins, J. N., Rozenberg, G. I., Gefen, A., Reinhart-King, C. A., Margulies, S. S., Dembo, M., Boettiger, D. et al. (2005). Tensional homeostasis and the malignant phenotype. *Cancer Cell* **8**, 241-254.
- Plas, D. R. and Thompson, C. B. (2002). Cell metabolism in the regulation of programmed cell death. *Trends Endocrinol. Metab.* **13**, 75-78.
- Puto, L. A., Pestonjamas, K., King, C. C. and Bokoch, G. M. (2003). p21-activated kinase 1 (PAK1) interacts with the Grb2 adapter protein to couple to growth factor signaling. *J. Biol. Chem.* **278**, 9388-9393.
- Qu, J., Cammarano, M. S., Shi, Q., Ha, K. C., de Lanerolle, P. and Minden, A. (2001). Activated PAK4 regulates cell adhesion and anchorage-independent growth. *Mol. Cell. Biol.* **21**, 3523-3533.
- Russell, A. J., Fincher, E. F., Millman, L., Smith, R., Vela, V., Waterman, E. A., Dey, C. N., Guide, S., Weaver, V. M. and Marinkovich, M. P. (2003). Alpha 6 beta 4 integrin regulates keratinocyte chemotaxis through differential GTPase activation and antagonism of alpha 3 beta 1 integrin. *J. Cell Sci.* **116**, 3543-3556.
- Santini, M. T., Rainaldi, G. and Indovina, P. L. (2000). Apoptosis, cell adhesion and the extracellular matrix in the three-dimensional growth of multicellular tumor spheroids. *Crit. Rev. Oncol. Hematol.* **36**, 75-87.
- Schmitz, A. A., Govek, E. E., Bottner, B. and Van Aelst, L. (2000). Rho GTPases: signaling, migration, and invasion. *Exp. Cell Res.* **261**, 1-12.
- Schurmann, A., Mooney, A. F., Sanders, L. C., Sells, M. A., Wang, H. G., Reed, J. C. and Bokoch, G. M. (2000). p21-activated kinase 1 phosphorylates the death agonist bad and protects cells from apoptosis. *Mol. Cell. Biol.* **20**, 453-461.
- Sethi, T., Rintoul, R. C., Moore, S. M., MacKinnon, A. C., Salter, D., Choo, C., Chilvers, E. R., Dransfield, I., Donnelly, S. C., Strieter, R. et al. (1999). Extracellular matrix proteins protect small cell lung cancer cells against apoptosis: a mechanism for small cell lung cancer growth and drug resistance in vivo. *Nat. Med.* **5**, 662-668.
- Shaw, L. M., Rabinovitz, I., Wang, H. H., Toker, A. and Mercurio, A. M. (1997). Activation of phosphoinositide 3-OH kinase by the alpha6beta4 integrin promotes carcinoma invasion. *Cell* **91**, 949-960.
- Sminia, P., Acker, H., Eikesdal, H. P., Kaaijk, P., Enger, P., Slotman, B. and Bjerkvig, R. (2003). Oxygenation and response to irradiation of organotypic multicellular spheroids of human glioma. *Anticancer Res.* **23**, 1461-1466.
- Sovak, M. A., Bellas, R. E., Kim, D. W., Zanieski, G. J., Rogers, A. E., Traish, A. M. and Sonenshein, G. E. (1997). Aberrant nuclear factor-kappaB/Rel expression and the pathogenesis of breast cancer. *J. Clin. Invest.* **100**, 2952-2960.
- Spinardi, L., Einheber, S., Cullen, T., Milner, T. A. and Giancotti, F. G. (1995). A recombinant tail-less integrin beta 4 subunit disrupts hemidesmosomes, but does not suppress alpha 6 beta 4-mediated cell adhesion to laminins. *J. Cell Biol.* **129**, 473-487.
- St Croix, B., Florenes, V. A., Rak, J. W., Flanagan, M., Bhattacharya, N., Slingerland, J. M. and Kerbel, R. S. (1996). Impact of the cyclin-dependent kinase inhibitor p27Kip1 on resistance of tumor cells to anticancer agents. *Nat. Med.* **2**, 1204-1210.
- Sutherland, R. M. and Durand, R. E. (1972). Radiosensitization by nifuroxime of the hypoxic cells in an in vitro tumour model. *Int. J. Radiat. Biol. Relat. Stud. Phys. Chem. Med.* **22**, 613-618.
- Tagliabue, E., Ghirelli, C., Squicciarini, P., Aiello, P., Colnaghi, M. I. and Menard, S. (1998). Prognostic value of alpha 6 beta 4 integrin expression in breast carcinomas is affected by laminin production from tumor cells. *Clin. Cancer Res.* **4**, 407-410.
- Tang, Y., Chen, Z., Ambrose, D., Liu, J., Gibbs, J. B., Chernoff, J. and Field, J. (1997). Kinase-deficient Pak1 mutants inhibit Ras transformation of Rat-1 fibroblasts. *Mol. Cell. Biol.* **17**, 4454-4464.
- Tang, Y., Yu, J. and Field, J. (1999). Signals from the Ras, Rac, and Rho GTPases converge on the Pak protein kinase in Rat-1 fibroblasts. *Mol. Cell. Biol.* **19**, 1881-1891.
- Tannock, I. F., Lee, C. M., Tunggal, J. K., Cowan, D. S. and Egorin, M. J. (2002). Limited penetration of anticancer drugs through tumor tissue: a potential cause of resistance of solid tumors to chemotherapy. *Clin. Cancer Res.* **8**, 878-884.
- Taylor-Papadimitriou, J., D'Souza, B., Berdichevsky, F., Shearer, M., Martignone, S. and Alford, D. (1993). Human models for studying malignant progression in breast cancer. *Eur. J. Cancer Prev.* **2** Suppl. 3, 77-83.
- Tong, R. T., Boucher, Y., Kozin, S. V., Winkler, F., Hicklin, D. J. and Jain, R. K. (2004). Vascular normalization by vascular endothelial growth factor receptor 2 blockade induces a pressure gradient across the vasculature and improves drug penetration in tumors. *Cancer Res.* **64**, 3731-3736.
- Unger, M. and Weaver, V. M. (2003). The tissue microenvironment as an epigenetic tumor modifier. *Methods Mol. Biol.* **223**, 315-347.
- Vadlamudi, R. K. and Kumar, R. (2003). P21-activated kinases in human cancer. *Cancer Metastasis Rev.* **22**, 385-393.
- Van Aelst, L. and D'Souza-Schorey, C. (1997). Rho GTPases and signaling networks. *Genes Dev.* **11**, 2295-2322.
- Vander Heiden, M. G., Plas, D. R., Rathmell, J. C., Fox, C. J., Harris, M. H. and Thompson, C. B. (2001). Growth factors can influence cell growth and survival through effects on glucose metabolism. *Mol. Cell. Biol.* **21**, 5899-5912.
- Wang, R. A., Zhang, H., Balasenthil, S., Medina, D. and Kumar, R. (2006). PAK1 hyperactivation is sufficient for mammary gland tumor formation. *Oncogene* **25**, 2931-2936.
- Wang, W., Wyckoff, J. B., Frohlich, V. C., Oleynikov, Y., Huttelmaier, S., Zavadil, J., Cermak, L., Bottinger, E. P., Singer, R. H., White, J. G. et al. (2002). Single cell behavior in metastatic primary mammary tumors correlated with gene expression patterns revealed by molecular profiling. *Cancer Res.* **62**, 6278-6288.
- Weaver, V. M., Petersen, O. W., Wang, F., Larabell, C. A., Briand, P., Damsky, C. and Bissell, M. J. (1997). Reversion of the malignant phenotype of human breast cells in three-dimensional culture and in vivo by integrin blocking antibodies. *J. Cell Biol.* **137**, 231-245.
- Weaver, V. M., Lelievre, S., Lakins, J. N., Chrenek, M. A., Jones, J. C., Giancotti, F., Werb, Z. and Bissell, M. J. (2002). beta4 integrin-dependent formation of polarized three-dimensional architecture confers resistance to apoptosis in normal and malignant mammary epithelium. *Cancer Cell* **2**, 205-216.
- Whitacre, C. M. and Berger, N. A. (1997). Factors affecting topotecan-induced programmed cell death: adhesion protects cells from apoptosis and impairs cleavage of poly(ADP-ribose)polymerase. *Cancer Res.* **57**, 2157-2163.
- Yang, C., Liu, Y., Leskow, F. C., Weaver, V. M. and Kazanietz, M. G. (2005). Rac-GAP-dependent inhibition of breast cancer cell proliferation by {beta}2-chimerin. *J. Biol. Chem.* **280**, 24363-24370.
- Zahir, N. and Weaver, V. M. (2004). Death in the third dimension: apoptosis regulation and tissue architecture. *Curr. Opin. Genet. Dev.* **14**, 71-80.
- Zahir, N., Lakins, J. N., Russell, A., Ming, W., Chatterjee, C., Rozenberg, G. I., Marinkovich, M. P. and Weaver, V. M. (2003). Autocrine laminin-5 ligates alpha6beta4 integrin and activates RAC and NFkappaB to mediate anchorage-independent survival of mammary tumors. *J. Cell Biol.* **163**, 1397-1407.
- Zakeri, Z. and Lockshin, R. A. (2002). Cell death during development. *J. Immunol. Methods* **265**, 3-20.



# Integrin-mediated Signaling through the MAP-kinase Pathway

Ka Lai Yee, Valerie M. Weaver, and Daniel A. Hammer

## Correspondence Address:

Daniel A. Hammer  
120 Hayden Hall  
3320 Smith Walk  
Dept of Bioengineering  
University of Pennsylvania  
Philadelphia, PA 19104

Email: [hammer@seas.upenn.edu](mailto:hammer@seas.upenn.edu)



## Abstract

The MAP kinase cascade, leading to ERK activation, is a key regulator of cell growth and proliferation. The effects of ERK are mediated by differences in ERK signaling dynamics, including magnitude and duration. In vivo, ERK signaling, is stimulated by both growth factors and adhesion signals. Here, a model for adhesion-mediated ERK activation is presented. Outputs of the model such as ERK and FAK activation, as well as responses to different ligand densities, are matched to published experimental data. The model then serves as a basis for understanding how adhesion may contribute to ERK signaling through changes in the dynamics of FAK activation. The main parameters influencing ERK are determined through screening analyses and parameter variation. With these parameters, key points in the pathway that give rise to changes in downstream signaling dynamics are identified. In particular, we propose that oncogenic Raf and Ras promote cell growth by increasing the magnitude and duration, respectively, of ERK activity.

## 1 Introduction

The MAP kinase cascade is an important signaling pathway associated with tumorigenic behavior. In cancerous cells, the pathways that regulate proliferation are disrupted so that cells experience unchecked growth. A major factor in proliferation is the increased activity of the MAPK cascade, which can be caused by increased external stimuli or mutations along the pathway that promote pathway activation [1]. The MAPK involved in growth regulation is extracellular-regulated kinase (ERK). Upon double phosphorylation by MEK, ERKPP translocates to the nucleus and induces gene transcription by phosphorylation of transcription factors [2]. One of ERK's targets is fos, a member of the AP-1 transcription factor heterodimer [3]. AP-1 family transcription factors induce the transcription of cyclin D1, which promotes cell cycle entry [4, 5]. Modeling this pathway to gain an understanding of how specific elements give rise to different ERK signaling dynamics is an important step towards regulating signal transduction, and ultimately cell behavior, *in vivo*.

The signaling pathway that culminates in ERK activation is initiated by extracellular stimuli such as adhesion to the extracellular matrix or growth factors. Cell adhesion activates ERK by binding of  $\alpha 5\beta 1$  integrins at the cell surface to extracellular matrix proteins such as fibronectin [6, 7]. Integrins activate ERK via a pathway involving Shc, Grb2, Sos, the GTPase Ras, and focal adhesion kinase (FAK) [5, 6, 8]. Epidermal growth factor (EGF) binding to its receptor is also known to activate ERK through the same Shc-Grb2-Sos-Ras pathway as integrins [9-11]. Though integrins may activate ERK in the absence of growth factors, cells *in vivo* are exposed to both adhesion signals and growth factor signals. In addition, there is cross talk between growth factor and integrin activated pathways to ERK activation at different levels of the pathway [12-14]. This cross-talk likely gives rise to distinctive ERK activation signals that

can regulate different behaviors [12]. For example, ERK activity stimulated by growth factors and adhesion independently is transient, whereas ERK activity in adherent, growth factor stimulated cells is sustained. Moreover, the cell cycle protein cyclin D1 is only induced by sustained ERK signals [5, 15].

The MAPK cascade and activation by EGF have been previously explored with deterministic, computational models. A basic model of the Shc-Grb2-Sos-Ras pathway activated by EGF was described by Kholodenko [16]. A more comprehensive model of ERK activation in response to EGF stimulation has also been examined [17]. In that model, EGF receptor-ligand binding and dimerization initiates the traditional Shc-Grb2-Sos-Ras pathway that leads into the MAPK cascade. More recently, Chapman and Asthagiri undertook an exploration of MAPK cascade dynamics [18]. Their work demonstrated that adjusting rate constants and protein or phosphatase concentrations controls ERK activation dynamics. Similarly, Hornberg and colleagues [19] applied control analysis to the model developed by Schoeberl, identifying specific proteins that are important in EGF-mediated ERK signaling.

As a first step towards developing a model of ERK activation by both EGF and integrins, a computational model for integrin activation of ERK is presented in this paper. In this model, the ERK signaling pathway is initiated by  $\alpha 5 \beta 1$  integrin binding to its extracellular ligand fibronectin. The model successfully simulates experimental FAK and ERK activation time courses. Semi-quantitative data on FAK and ERK activation after adhesion [20] are used to verify the results of the model. After matching simulated signals to experimental results, the pathways were explored to gain insight into specific characteristics that contribute to ERK activation dynamics. To systematically explore the set of parameters used in the model, a screening method developed by Morris [21] was used to identify the key parameters that affect

different characteristics of the output signal, such as overall dynamics, maximum value, and time to reach maximum.

## **2 Methodology**

### **2.1 Biological Considerations**

The signaling events culminating in ERK activation are modeled as a set of differential equations. The protein-protein interactions included in the pathway were chosen based on published pathways and experimental data and are illustrated in Figure 1a. The full pathway and a list of reactions and rate constants are provided in the Supplementary Materials Spreadsheet.

The Integrin/FAK activation portion of the model deals with receptor-ligand binding as a cell spreads on fibronectin. The cell-surface contact area begins at zero and increases according to an experimentally determined profile [22] (see Supplementary Materials). The increase in contact area regulates the transport of receptors and ligands into the contact area where binding occurs. Integrin-fibronectin binding is modeled according to the Bell model for receptor-ligand binding [23]. Because integrin clustering is a complex process involving the many cytoskeletal proteins and the transduction for force, clustering is modeled as dimerization of receptor-ligand pairs (see Supplementary Materials). We assume only dimerized receptor-ligand pairs are able to recruit FAK, which becomes autophosphorylated at tyrosine 397 (FAKP)[24].

Src activation occurs after cell adhesion, though it is unclear how adhesion signals regulate the Src activation machinery [25]. Activation begins with the dephosphorylation of cytoplasmic Src at tyrosine 527. The protein then undergoes a conformational change and translocates to the membrane [26]. To be fully active, Src undergoes an intermolecular autophosphorylation at Y416. However, fully active Src can be re-phosphorylated and dephosphorylated, thereby cycling it from active to inactive conformations [27-29]. This module

is linked to the rest of the pathway by the ability of Src to phosphorylate its substrate FAK at Y925 [30]. Src and FAK are both capable of phosphorylating Shc [9, 11, 31]. This interaction leads into the same sequence of signaling events activated by the EGF receptor, ultimately resulting in activation of the MAPK cascade [32, 33].

Evidence suggests that integrins may also activate ERK through a FAK independent pathway [9]. Such a pathway likely involves Fyn, a member of the Src kinase family, and the alpha integrin subunit [34]. Because of limited experimental data on this pathway, this model focuses on the FAK dependent pathways to ERK activation.

## 2.2 Model Parameters

Rate constants and protein concentrations were either found in literature or estimated based on known constants for similar reactions. For protein interactions without published binding constants,  $K_d$ 's,  $k_f$ 's, and  $k_r$ 's were estimated from available peptide binding data. For example, binding constants for Src and FAKP in the Src activation module were estimated with rate constants for Src SH2 domain binding to the pYEEI peptide, which is similar to the autophosphorylation site for FAK [35, 36]. Most binding events in this pathway involve SH2-phosphotyrosine and SH3-PXXP binding [37, 38].

During integrin activation of FAK,  $k_I$  is the rate of dimerization of receptor-ligand pairs while  $k_p$  and  $k_m$  are the forward and backward rate constants for FAK binding to receptor-ligand dimers and subsequent autophosphorylation.  $k_I$  is a phenomenological rate constant assigned a value of  $0.01s^{-1}$ , which corresponds to maximum levels of FAK activation. Decreasing  $k_I$  will decrease the final magnitude of FAK activation without significantly changing the kinetics. Values for  $k_p$  and  $k_m$  were estimated to obtain a variety of time scales for FAK autophosphorylation, which are discussed in the Results section. The Src activation module also

contains the phenomenological rate constant  $k_t$ , which represents the rate of Src transport from the cytoplasm to the membrane by the cytoskeleton [39]. Because these steps are not easily modeled, they are lumped into the transport rate  $k_t$ ;  $k_t$  is set at  $0.1 \text{ s}^{-1}$ , at which the rate of cytoskeletal transport is maximal. Rate constants for the phosphatase and kinase reactions in Src activation were obtained from literature [40-42]. Subsequent analyses of FAK and downstream signaling focus on the relative effects of different parameter values on kinetics and magnitude, so that the conclusions drawn are valid regardless of the specific phenomenological constants used.

Initial protein concentrations were obtained from Schoeberl [17] and were varied over several orders of magnitude to explore their effects on signal dynamics. The constant concentrations of phosphatases were also estimated based on these initial values. The initial conditions specify protein concentrations for FAK, Src, Shc, Grb2, Sos, MEK, and ERK. All other protein species present in the system at any given time are derived from these proteins and have an initial concentration of zero.

The resulting set of equations with initial conditions was solved in MATLAB 6.5 using the ODE15s solver.

### **3 Results**

#### **3.1 Kinetics of FAK and ERK Activation**

Asthaagiri [20] has shown that activation of ERK by adhesion occurs before maximal FAK activation. Simulations of ERK and FAK activation showed similar behavior (Figure 2). Over a range of FAK recruitment rates ( $k_p$ ), the ERK activation peak consistently occurs ahead of full FAK activation. Since FAK is the only means by which ERK is activated in this model, early and therefore relatively low levels of FAK activation are sufficient for stimulating the MAP kinase cascade. For FAK to achieve sufficient levels of activation to stimulate the MAPK

cascade at early times, it was found that the total level of FAK must be higher than that of downstream effectors such as Sos, the activator of the MAPK cascade. For example, a peak magnitude of 1.4nM ERKPP at  $t=2800s$  requires the amount of total FAK to be nearly 22 times the amount of Sos. As a result, it is assumed that the amount of FAK is in excess of other signaling proteins in the system. Lastly, sustained FAK activation does not necessarily result in sustained ERK activation, implying that FAK serves as an initial stimulus for ERK activation, but the duration of ERK activation is also regulated by downstream factors that will be discussed.

### **3.2 FAK and ERK Activation in Response to Ligand Density**

Fibronectin density is one of the most readily controllable experimental parameters in the system and has been shown to affect both the magnitude and kinetics of ERK activation [20]. As ligand density increases, the magnitude of the ERKPP peak also increases while the peak occurs faster. The effects of ligand density were successfully replicated *in silico* for similar fibronectin densities, assuming a high receptor density of  $7.89 \times 10^{10}$  molecules/cm<sup>2</sup> ( $\sim 1.5 \times 10^6$ /cell) (Figure 3a). Not surprisingly, changes in ligand density had substantial effects on ERKPP dynamics only when ligand density is non-saturating ( $R_t > L_t$ ), thus requiring a high assumed receptor density. Furthermore, the linear correlation between the ligand density and initial rates of FAK and ERK activation observed by Asthagiri [20] was also seen in simulations (Figure 3b). At saturating ligand densities, the linear correlation fails.

### **3.3 Exploration of Signaling Dynamics**

#### **3.3.1 The relationship between FAK and ERK Activation**

The effects of ligand density on ERK raise the question of how the signal is transduced downstream. Since FAK is a major mediator between adhesion-based signals and downstream signaling, it is reasonable to examine the effects of ligand density on FAK activation to

understand how such changes can affect ERK. Because FAK is in excess of ligand and receptor binding sites, the magnitude of FAKP is directly proportional to ligand density while the time required to reach maximal FAKP is unchanged. As shown in Figure 3a, increases in ligand density correspond to increases in ERKPP magnitude and decreases in the time to reach maximum. To determine whether such effects are specific to changes in the magnitude of FAKP, we considered the effects of changes in the time to reach maximal FAKP by changing the total amount of FAK. Increased levels of FAK drive the rate of its activation, resulting in increased kinetics without changing the magnitude of FAKP. Figure 4a shows that equivalent increases in ligand density and FAK decrease the time of the ERKPP peak similarly. Figure 4a also illustrates that ligand density has a more pronounced affect on ERKPP magnitude than does FAK. In order to better compare the effects of magnitude and kinetics directly, FAK activation dynamics are expressed as an initial rate of activation (Figure 4b). If the effects of FAKP magnitude and kinetics are equivalent, each initial rate calculated from either ligand density or total FAK changes should correspond to a unique change in ERK activation dynamics. However, the curves for ERKPP dynamics differ depending on ligand density or total FAK changes, indicating that the effects are parameter-specific. In fact, ligand density, via changes in the magnitude of FAKP, appears to be a stronger regulator of ERKPP dynamics than total FAK, which changes the kinetics of FAKP. Furthermore, the differing curves in response to ligand density and FAK imply that the initial rate of FAKP is not the sole determinant of ERKPP dynamics and that other factors affected by these two parameters are also playing a role. Moreover, FAK-independent pathways are not likely the source of these factors since their contributions to ERK activation are only on the order of  $10^{-19}$ - $10^{-18}$  M. Regardless of these factors, the relationship between ERKPP



and initial rate is non-linear and plateaus as the initial rate increases. Thus, the effects of Fn density and FAK will attenuate as these two factors reach saturation.

### **3.3.2 Ras and Raf as Regulators of ERK Activity**

To better understand the behavior of the system, parameters that play a key role in regulating the dynamics of the ERK signal were identified by parameter variations. The duration of ERK activation is found to be particularly sensitive to the concentrations of Ras and Raf. Testing Raf concentrations over an order of magnitude from 10 nM to 100 nM produced ERKPP signals with a range of durations (Figure 5a). At or above a [Raf] of 100 nM, the ERKPP signal is a sharp peak at approximately 5 minutes, which falls off quickly by 30 minutes. As [Raf] is decreased, the ERKPP signal duration increases until a sustained signal is obtained at 10 nM. Between 20 nM and 60 nM, very small changes in Raf concentration can give rise to significant changes in signal duration. For example, a 25% concentration decrease from 40 nM to 30 nM results in a signal duration increase of nearly 45%. For high [Raf], the ERKPP signal is very similar to that obtained by Asthagiri [20]. Similarly, the duration of the ERKPP signal increases with increasing levels of Ras (Figure 5b). While the changes in ERKPP are not as sensitive to small changes in [Ras], large increases in [Ras] do yield significant prolongation of ERK activation.

The sensitivity of ERKPP to Raf and Ras originates at the locus of intersection between the RasGTP/GDP cycle and the MAPK cascade (Figure 1b), where RasGTP binds and activates Raf, forming Raf\*. The fast drop off in signaling that forms the peak in ERKPP signals results from the depletion of RasGTP available for interaction with Raf. When RasGTP is depleted, no more Raf can be activated causing the Raf\* and subsequently ERKPP signals to fall off, resulting in the formation of a peak. Therefore, as [Raf] increases, the velocity of the Raf-RasGTP binding

reaction also increases, thereby increasing the rate at which RasGTP is depleted. Similarly, Sydor [43] has shown that the Raf-Ras complex has an extremely short lifetime, after which Raf is released for downstream signaling. The resulting Ras species, denoted RasGTP\*, is no longer capable of activating Raf and will undergo GTP hydrolysis catalyzed by GAPs, which are recruited to focal adhesions after integrin-ligand binding [44, 45]. In the case of high [Raf], Ras accumulates as RasGTP\*, suggesting that the Raf-RasGTP reaction is much faster than the action of GAPs in recycling Ras. Thus, nearly 80% of Ras accumulates in the GTP\* form and is not recycled fast enough to the RasGTP form to prevent depletion. As [Raf] is reduced, the rate of RasGTP conversion to RasGTP\* is more comparable to the rate of recycling to RasGTP. Depletion of RasGTP is delayed and an increasingly sustained ERKPP signal is obtained. An increase in [Ras], conversely, increases the amount of RasGTP available, prolonging the ERKPP signal.

### **3.4 Sensitivity Analysis**

#### **3.4.1 Morris Screening**

To systematically identify key parameters involved in ERK signaling, the Morris screening method [21] was applied to the model. The Morris method allows for the effects of a particular parameter variation to be seen in the context of different values for every other parameter, as opposed to fixing all other parameters. The result of the model is a measure of the effect each parameter has on the output signal. For the dynamics of ERK activation, the effect of each parameter on the overall ERK time course as measured by the norm of the change in output, time to reach maximum, peak magnitude, and 3 specific time points were calculated. These values were normalized by the relative change in input values. However, because parameters were sampled over a log uniform distribution, the fractional change remains constant between

parameters. Morris runs were performed until at least the top 20% of parameters converged (n = 160).

The main parameters involved in regulating ERK activation are rate constants associated with the MAPK cascade. However, of the factors that could be readily manipulated experimentally, Ras and Raf fall within the top 15% of key parameters for several measures of ERK dynamics, confirming the effects on ERKPP signal duration described above (Table 1). Out of 106 parameters, Ras ranked second in importance for the time of the ERKPP peak, 16<sup>th</sup> based on overall time course and 29<sup>th</sup> based on a late time point that indicates signal duration. Similarly, Raf ranks 4<sup>th</sup> in determining the time of the ERKPP peak and 7<sup>th</sup> in early activation. Both Ras and Raf also fall within the top 20% of parameters affecting the magnitude of ERK activation, ranking 18<sup>th</sup> and 19<sup>th</sup> respectively. Interestingly, RasGAP ranks first out of all parameters for the time of the ERK activation peak, again highlighting the importance of the RasGDP/GTP cycle in regulating ERK activation dynamics. Receptor density also falls within the top 15% of key parameters affecting the ERKPP signal. Moreover, integrin density and contact area, which determines the total amount of fibronectin available, are ranked 7<sup>th</sup> and 5<sup>th</sup> respectively as regulators of the kinetics of ERK activation. FAK is also identified as a key parameter in ERK activation kinetics, supporting the idea that initial FAK signaling contributes significantly to the activation of ERK. Integrin density, and not fibronectin density, was likely identified in the Morris screening because of the relative values the two parameters used. Depending on the values of receptor and ligand density, the rate limiting density will be identified as the more important parameter. As a result, the importance of integrin density also points to the importance of fibronectin density in modulating the magnitude and kinetics of ERKPP.

### **3.4.2 One-at-a-time Parameter Variation**

In order to gauge the robustness of the model to changes in parameters, one-at-a-time parameter variations were performed while holding every other parameter fixed at their assumed values. Parameters were varied over 3 orders of magnitude above and below their assumed values and the range over which the conclusions drawn in the results section held qualitatively was determined (Figure 6). The model is found to be robust and tolerant of significant changes in many parameters. Parameters 24 to 64 and 85 to 105 refer to reactions involved in Src activation, Shc phosphorylation, and recruitment of both Grb2 and Sos. Even many of the MAP kinase cascade reaction rates, including some that were identified as key regulators by Morris screening (ex. 81, 79, 74, 83, 82, etc), do not limit the qualitative conclusions drawn from the model.

#### **4 Discussion**

This model for the integrin activation of ERK successfully replicated experimentally observed behavior for FAK and ERK activation, as well as changes in ERK activation in response to fibronectin density. Application of the Morris method to the model allowed the identification of key parameters contributing to ERKPP dynamics. Thus, the model serves as a tool for understanding and identifying characteristics of the pathway that contribute to different ERKPP behavior. The insights gained by such models are important steps to ultimately controlling signaling pathways in vivo.

The ability of the model to replicate experimentally measured time courses for FAK and ERK in response to adhesion on fibronectin is an important foundation for understanding the adhesion specific parameters that might contribute to ERK activation. The appearance of an early peak for ERKPP is not surprising as long as there is an excess of FAK, which serves as an early stimulus for ERKPP. Factors affecting FAKP magnitude, such as fibronectin density, are found to be stronger regulators of ERKPP dynamics than those affecting only FAKP kinetics. However,

the effects of ligand density are not solely dependent on the initial rate of FAK activation, but are likely transduced downstream by additional pathways. While additional western blot time courses have been published, we chose a semi-quantitative time course for the purposes of comparing to simulated results. Deviations between the experimental data used here and other available data may be due to a myriad of differences including cell type and experimental procedure.

The simplified integrin clustering model used is shown to be sufficient for predicting the effects of ligand density on ERK activation. The model based on dimerization predicts that increases in ligand density will increase the magnitude of FAK activation, which has been shown by Garcia and Boettiger [46]. Changes in the magnitude of FAK activation are then translated into changes in the kinetics and magnitude of ERK activation. While  $k_p$  and  $k_m$  may alter the time at which FAK activation reaches its maximum, the ultimate magnitude, as specified by ligand density will not be affected. Changes in  $k_l$  may also affect the magnitude of FAK activation, but the relative changes that result from ligand density variations will remain the same. More generally, the magnitude of FAK activation increases with ligand density regardless of the assumed value of  $k_l$  or  $k_p$  and  $k_m$ . As a result, changes in downstream signaling that originate with ligand density will also remain the same qualitatively. Future work should include a more detailed model of the integrin clustering process so that the roles of additional parameters involved in clustering can be tested.

Raf and Ras were identified as key regulators of ERK signaling magnitude and duration, in agreement with the control analysis performed by Hornberg [19]. Furthermore, the behavior of proteins involved in RasGDP/GTP cycling reveal that Raf and Ras may function as a key checkpoint in the MAPK cascade because of the relative kinetics of RasGDP/GTP cycling and

Ras-Raf binding, which allow for the formation of transient and sustained ERKPP signals. However, the main effects of the Raf oncogene may not be mediated by this particular characteristic of the signaling pathway, as was suggested by Hornberg. Increases in [Raf] result in increasing magnitudes of ERK activation, but increasingly transient activation signals. For cell cycle progression and uncontrolled growth, one would expect that increasingly the levels of oncogenic Raf would instead lead to sustained signaling. On the other hand, this model shows that increases in the level of the oncogene Ras result in more sustained ERK signals, though larger changes in the Ras concentration are required. This is consistent with the role of Ras as an oncogene that promotes tumorigenic behavior. Moreover, the behavior of the Raf/Ras checkpoint suggests that mutations in Ras that affect the GDP/GTP cycling, such as its affinity for GAPs or GTPases may be a mechanisms for modulating cell behavior. Therefore, the oncogenic effects of Raf may be mediated mainly by changes in the magnitude of ERK activation, whereas the effects of Ras are more likely to involve changes in signal duration.

This is consistent with Roovers' and Assoian's [5] suggestion that cell cycle progression requires a large transient ERK activation that will induce p21cip expression in the early G1 phase followed by a sustained mid-level activation that promotes cyclin D1 expression and stops the induction of p21cip by late G1 phase. It has also been shown that p21cip is induced by high levels of Raf [47, 48]. Our results would suggest that an ideal combination of Raf and Ras levels could create cell growth promoting ERK activities. To determine these levels, Raf and Ras concentrations were varied and their effects on the magnitude and duration of ERK activation were observed (Figure 7). While the concentrations plotted are model-specific, the trends hold regardless of parameter values. Increasing Ras concentration promotes transition of ERK activity from transient to sustained behavior. Here, transient and sustained behavior refer to initial ERK

activation that falls to less than a  $1/3$  and between  $1/3$  and  $2/3$  of initial activation respectively. At low [Raf], a plateau in ERK activation may form in addition to transient and sustained behavior for certain [Ras]. Also, the magnitude of ERK activity is found to significantly decrease with [Raf] so that cell cycle progression might be inhibited regardless of the signal duration. When both Raf and Ras concentrations are high, ERK activation exhibited a large magnitude initial peak that fell off to sustained mid-level activation. This behavior is consistent with cell cycle progression. This may correspond to cells in which both Raf and Ras oncogenes are over-expressed or contain activating mutations. Thus, both Raf and Ras may act together to promote cell growth. Raf contributes to the magnitude of the signal, bringing the initial transient activation of ERK to levels that allow for induction of p21cip, while Ras primarily extends the duration of ERK, sustaining mid-level activation for long times. .

It has been suggested that the peak in ERK activation arises from negative feedback, which turns off the ERK activation signal [49-51]. Feedback, either positive or negative, has not been included in this system. While negative feedback may occur, we have shown that the Raf/Ras checkpoint can also play a role in regulating signal duration, particularly in controlling the fall off of the ERK activation signal. In fact, for certain Raf and Ras concentrations, the transient activity of ERK decreases rapidly, but does not approach zero, instead remaining at some lower level of ERK activation. In such cases, a negative feedback might be an important mechanism for shutting down the remaining ERK activity.

Src and Shc represent parallel pathways by which the MAPK cascade can be activated by FAK. As the model is run now, the Shc pathway dominates signaling to ERK. While it is possible for Src to be the main contributor to ERK activation, that assumption is not explored in detail in this paper. However, the overall effects seen in this paper were confirmed in a pathway

in which the levels of Shc are significantly reduced so as to allow the Src pathway to dominate [data not shown].

Though our model is robust and sufficient for predicting ERK activation by adhesion, a complete model of ERK activation should take into account the contributions of both growth factors and adhesion. Crosstalk between growth factor and adhesion signaling are vital for producing high magnitude, sustained ERK activation. In this paper, a model for adhesion-based activation is presented. Future work will involve the addition of the growth-factor mediated pathway. Coupled with the detailed model of clustering described above, the model not only complements experimental systems in which signaling in adhesive, growth factor stimulated cells is measured, but is also a means for exploring the cross-talk between growth factors and receptors.



1. Hanahan D and Weinberg RA. The hallmarks of cancer. *Cell* 2000; 100(1):57-70.
2. Aplin AE and Juliano RL. Regulation of nucleocytoplasmic trafficking by cell adhesion receptors and the cytoskeleton. *J Cell Biol* 2001; 155(2):187-91. Epub 2001 Oct 15.
3. Shaulian E and Karin M. AP-1 in cell proliferation and survival. *Oncogene* 2001; 20(19):2390-400.
4. Marshall C. How do small GTPase signal transduction pathways regulate cell cycle entry? *Current Opinion in Cell Biology* 1999; 11(6):732-736.
5. Roovers K and Assoian RK. Integrating the MAP kinase signal into the G1 phase cell cycle machinery. *Bioessays* 2000; 22(9):818-26.
6. Danen EH and Yamada KM. Fibronectin, integrins, and growth control. *J Cell Physiol* 2001; 189(1):1-13.
7. Renshaw MW, Ren XD, Schwartz MA. Growth factor activation of MAP kinase requires cell adhesion. *Embo J* 1997; 16(18):5592-9.
8. Giancotti FG and Ruoslahti E. Integrin signaling. *Science* 1999; 285(5430):1028-32.
9. Barberis L, Wary KK, Fiucci G, Liu F, Hirsch E, Brancaccio M, et al. Distinct roles of the adaptor protein Shc and focal adhesion kinase in integrin signaling to ERK. *Journal of Biological Chemistry* 2000; 275(47):36532-36540.
10. Schlaepfer DD and Hunter T. Integrin signalling and tyrosine phosphorylation: just the FAKs? *Trends Cell Biol* 1998; 8(4):151-7.
11. Wary KK, Mainiero F, Isakoff SJ, Marcantonio EE, Giancotti FG. The adaptor protein Shc couples a class of integrins to the control of cell cycle progression. *Cell* 1996; 87(4):733-43.

12. Assoian RK and Schwartz MA. Coordinate signaling by integrins and receptor tyrosine kinases in the regulation of G1 phase cell-cycle progression. *Current Opinion in Genetics & Development* 2001; 11(1):48-53.
13. Giancotti FG. Integrin signaling: specificity and control of cell survival and cell cycle progression. *Current Opinion in Cell Biology* 1997; 9(5):691-700.
14. Schwartz MA and Ginsberg MH. Networks and crosstalk: integrin signalling spreads. *Nature Cell Biology* 2002; 4(4).
15. Roovers K, Davey G, Zhu X, Bottazzi ME, Assoian RK. Alpha5beta1 integrin controls cyclin D1 expression by sustaining mitogen-activated protein kinase activity in growth factor-treated cells. *Mol Biol Cell* 1999; 10(10):3197-204.
16. Kholodenko BN, Demin OV, Moehren G, Hoek JB. Quantification of short term signaling by the epidermal growth factor receptor. *J Biol Chem* 1999; 274(42):30169-81.
17. Schoeberl B, Eichler-Jonsson C, Gilles ED, Muller G. Computational modeling of the dynamics of the MAP kinase cascade activated by surface and internalized EGF receptors. *Nat Biotechnol* 2002; 20(4):370-5.
18. Chapman S and Asthagiri AR. Resistance to signal activation governs design features of the MAP kinase signaling module. *Biotechnol Bioeng* 2004; 85(3):311-22.
19. Hornberg JJ, Binder B, Bruggeman FJ, Schoeberl B, Heinrich R, Westerhoff HV. Control of MAPK signalling: from complexity to what really matters. *Oncogene* 2005; 24(36):5533-5542.
20. Asthagiri AR, Nelson CM, Horwitz AF, Lauffenburger DA. Quantitative relationship among integrin-ligand binding, adhesion, and signaling via focal adhesion kinase and extracellular signal-regulated kinase 2. *Journal of Biological Chemistry* 1999; 274(38):27119-27.

21. Morris MD. Factorial Sampling Plans For Preliminary Computational Experiments. *Technometrics* 1991; 33(2):161-174.
22. Giannone G, Dubin-Thaler BJ, Dobereiner HG, Kieffer N, Bresnick AR, Sheetz MP. Periodic lamellipodial contractions correlate with rearward actin waves. *Cell* 2004; 116(3):431-43.
23. Bell GI. Models for the specific adhesion of cells to cells. *Science* 1978; 200(4342):618-27.
24. Parsons JT. Focal adhesion kinase: the first ten years. *J Cell Sci* 2003; 116(8):1409-1416.
25. Aplin AE, Howe A, Alahari SK, Juliano RL. Signal transduction and signal modulation by cell adhesion receptors: the role of integrins, cadherins, immunoglobulin-cell adhesion molecules, and selectins. *Pharmacol Rev* 1998; 50(2):197-263.
26. Kaplan KB, Bibbins KB, Swedlow JR, Arnaud M, Morgan DO, Varmus HE. Association of the Amino-Terminal Half of C-Src with Focal Adhesions Alters Their Properties and Is Regulated by Phosphorylation of Tyrosine-527. *Embo Journal* 1994; 13(20):4745-4756.
27. Bjorge JD, Jakymiw A, Fujita DJ. Selected glimpses into the activation and function of Src kinase. *Oncogene* 2000; 19(49):5620-35.
28. Boerner RJ, Kassel DB, Barker SC, Ellis B, DeLacy P, Knight WB. Correlation of the phosphorylation states of pp60c-src with tyrosine kinase activity: the intramolecular pY530-SH2 complex retains significant activity if Y419 is phosphorylated. *Biochemistry* 1996; 35(29):9519-25.
29. Cole P, Burn P, Takacs B, Walsh C. Evaluation of the catalytic mechanism of recombinant human Csk (C- terminal Src kinase) using nucleotide analogs and viscosity effects. *J. Biol. Chem.* 1994; 269(49):30880-30887.

30. Schlaepfer DD and Hunter T. Focal adhesion kinase overexpression enhances ras-dependent integrin signaling to ERK2/mitogen-activated protein kinase through interactions with and activation of c-Src. *J Biol Chem* 1997; 272(20):13189-95.
31. Schlaepfer DD, Jones KC, Hunter T. Multiple Grb2-mediated integrin-stimulated signaling pathways to ERK2/mitogen-activated protein kinase: summation of both c-Src- and focal adhesion kinase-initiated tyrosine phosphorylation events. *Mol Cell Biol* 1998; 18(5):2571-85.
32. Downward J. The GRB2/Sem-5 adaptor protein. *FEBS Lett* 1994; 338(2):113-7.
33. Howe AK and Juliano RL. Distinct mechanisms mediate the initial and sustained phases of integrin-mediated activation of the Raf/MEK/mitogen-activated protein kinase cascade. *J Biol Chem* 1998; 273(42):27268-74.
34. Wary KK, Mariotti A, Zurzolo C, Giancotti FG. A requirement for caveolin-1 and associated kinase Fyn in integrin signaling and anchorage-dependent cell growth. *Cell* 1998; 94(5):625-34.
35. Ladbury JE, Lemmon MA, Zhou M, Green J, Botfield MC, Schlessinger J. Measurement of the binding of tyrosyl phosphopeptides to SH2 domains: a reappraisal. *Proc Natl Acad Sci U S A* 1995; 92(8):3199-203.
36. Payne G, Shoelson SE, Gish GD, Pawson T, Walsh CT. Kinetics of p56lck and p60src Src homology 2 domain binding to tyrosine-phosphorylated peptides determined by a competition assay or surface plasmon resonance. *Proc Natl Acad Sci U S A* 1993; 90(11):4902-6.
37. Kaneko T, Kumasaka T, Ganbe T, Sato T, Miyazawa K, Kitamura N, et al. Structural insight into modest binding of a non-PXXP ligand to the signal transducing adaptor molecule-2 Src homology 3 domain. *J Biol Chem* 2003; 278(48):48162-8. Epub 2003 Sep 16.

38. Matsuda M, Ota S, Tanimura R, Nakamura H, Matuoka K, Takenawa T, et al. Interaction between the Amino-terminal SH3 Domain of CRK and Its Natural Target Proteins. *J. Biol. Chem.* 1996; 271(24):14468-14472.
39. Fincham VJ, Unlu M, Brunton VG, Pitts JD, Wyke JA, Frame MC. Translocation of Src kinase to the cell periphery is mediated by the actin cytoskeleton under the control of the Rho family of small G proteins. *Journal of Cell Biology* 1996; 135(6 Pt 1):1551-64.
40. Wang D, Esselman WJ, Cole PA. Substrate Conformational Restriction and CD45-catalyzed Dephosphorylation of Tail Tyrosine-phosphorylated Src Protein. *J. Biol. Chem.* 2002; 277(43):40428-40433.
41. Wang J and Walsh CT. Mechanistic studies on full length and the catalytic domain of the tandem SH2 domain-containing protein tyrosine phosphatase: analysis of phosphoenzyme levels and Vmax stimulatory effects of glycerol and of a phosphotyrosyl peptide ligand. *Biochemistry* 1997; 36(10):2993-9.
42. Zhang Z. Kinetic and mechanistic characterization of a mammalian protein- tyrosine phosphatase, PTP1. *J. Biol. Chem.* 1995; 270(19):11199-11204.
43. Sydor JR, Engelhard M, Wittinghofer A, Goody RS, Herrmann C. Transient Kinetic Studies on the Interaction of Ras and the Ras-Binding Domain of c-Raf-1 Reveal Rapid Equilibration of the Complex. *Biochemistry* 1998; 37(40):14292-14299.
44. Hecker TP, Ding Q, Rege TA, Hanks SK, Gladson CL. Overexpression of FAK promotes Ras activity through the formation of a FAK/p120RasGAP complex in malignant astrocytoma cells. *Oncogene* 2004; 23(22):3962-3971.

45. Sharma SV. Rapid recruitment of p120RasGAP and its associated protein, p190RhoGAP, to the cytoskeleton during integrin mediated cell-substrate interaction. *Oncogene* 1998; 17(3):271-281.
46. Garcia AJ and Boettiger D. Integrin-fibronectin interactions at the cell-material interface: initial integrin binding and signaling. *Biomaterials* 1999; 20(23-24):2427-2433.
47. Sewing A, Wiseman B, Lloyd AC, Land H. High-intensity Raf signal causes cell cycle arrest mediated by p21Cip1. *Mol. Cell. Biol.* 1997; 17(9):5588-5597.
48. Woods D, Parry D, Cherwinski H, Bosch E, Lees E, McMahon M. Raf-induced proliferation or cell cycle arrest is determined by the level of Raf activity with arrest mediated by p21Cip1. *Mol. Cell. Biol.* 1997; 17(9):5598-5611.
49. Dougherty MK, Muller J, Ritt DA, Zhou M, Zhou XZ, Copeland TD, et al. Regulation of raf-1 by direct feedback phosphorylation. *Molecular Cell* 2005; 17(2):215-224.
50. Sundberg-Smith LJ, Doherty JT, Mack CP, Taylor JM. Adhesion stimulates direct PAK1/ERK2 association and leads to ERK-dependent PAK1 Thr(212) phosphorylation. *Journal Of Biological Chemistry* 2005; 280(3):2055-2064.
51. Brummer T, Naegele H, Reth M, Misawa Y. Identification of novel ERK-mediated feedback phosphorylation sites at the C-terminus of B-Raf. *Oncogene* 2003; 22(55):8823-8834.

<Separate Section>

## **Supplementary Materials**

### **General rate equations**

A differential equation for the rate of concentration change of each protein species present in the system was written using rates of species formation and reaction. The full list of equations and rate constants in the model is contained in the Supplemental Materials.

### **Cell-Surface Contact Area during Spreading**

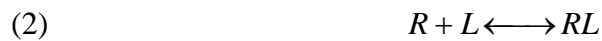
The increase in contact area over time during cell spreading was modeled based on experimental data from Giannone (1). The experimental data was fit using an equation for area as a function of time:

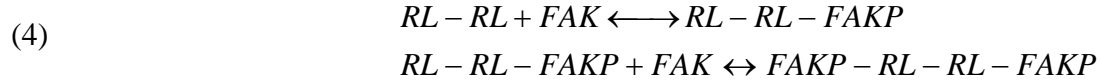
$$(1) \quad A(t) = A_{\max} e^{-t/85} \left[ -1 + e^{t/85} - \frac{t}{85} - \frac{t^2}{14450} - \frac{t^3}{3684750} \right],$$

where  $A_{\max}$ , the maximum cell-surface contact area is equal to  $1.9 \times 10^{-5} \text{ cm}^2$ .

### **Integrin-Fibronectin Binding**

For integrin-fibronectin binding, the Bell model (2) that describes binding between ligand and receptors diffusing in the plane of the membrane was used. In this model, however, the ligand was assumed to be immobile because surface adsorbed fibronectin is not free to diffuse. After integrin-fibronectin binding, the model for integrin clustering assumes that receptor ligand pairs (RL) dimerize and subsequently recruit FAK to the RL dimer. Because there is little quantitative data on FAK's response after integrin-ligand binding, FAK recruitment and phosphorylation are modeled with one reaction governed by forward and reverse rates that are fit to experimental time courses of FAK activation. This process was modeled with the following set of equations,





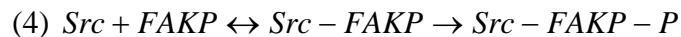
where Eq 2 has forward and reverse rate constants of  $k_f$  and  $k_r$ , Eq 3 has a forward rate constant of  $k_l$ , and Eq 4 has forward and reverse rate constants  $k_p$  and  $k_m$ . The receptor-ligand binding rate constants  $k_f$  and  $k_r$  were obtained from Takagi (3) and converted from three- dimensional to two dimensional rate constants for the case of immobilized ligand and membrane-diffusive receptors. The method for this conversion is described by English and Hammer (4). Fibronectin was assumed to have a negligible diffusion constant compared to integrins. The diffusion constant for membrane-bound integrins was assumed to be  $10^{-10} \text{ cm}^2/\text{s}$ . The diffusion constant for integrins in solution was estimated from the Stokes-Einstein equation, assuming a radius of 5nm and cytoplasmic viscosity. The encounter distance was assumed to be .75 nm.

### Modeling Src Activation

The steps that bridge extracellular stimulation with the initial de-phosphorylation of Src at tyrosine 527 have not yet been elucidated, but involve some signaling mechanism that activates a phosphatase, in this model SHP, and causes it to de-phosphorylate it. Because these steps are still largely unknown, SHP activation was assumed to be proportional to FAK activation. The proportionality constant was set so that SHP concentration was 3.5 times the magnitude of FAK activation in order to make the maximum SHP concentration comparable to that for the other phosphatases and kinases involved in the Src activation reactions.

### Decomposition of Src-FAKP Binding

To estimate the kinetics of the Src-FAKP binding, the enzymatic reaction was broken down into binding and catalytic steps:





$k_1$  and  $k_2$  are the forward and reverse binding constants respectively and  $k_{cat}$  is the catalytic rate constant.  $k_1$  was calculated from published Michaelis-Menten data (5) using the equation

$$(4) \quad K_m = \frac{k_2 + k_{cat}}{k_1}$$

assuming that  $k_2$  is  $1 \times 10^{-2} \text{ s}^{-1}$ .

1. Giannone G, Dubin-Thaler BJ, Dobereiner HG, Kieffer N, Bresnick AR, Sheetz MP. Periodic lamellipodial contractions correlate with rearward actin waves. Cell 2004;116(3):431-43.
2. Bell GI. Models for the specific adhesion of cells to cells. Science 1978;200(4342):618-27.
3. Takagi J, Strokovich K, Springer TA, Walz T. Structure of integrin  $\alpha 5 \beta 1$  in complex with fibronectin. Embo J 2003;22(18):4607-15.
4. English TJ, Hammer DA. Brownian adhesive dynamics (BRAD) for simulating the receptor-mediated binding of viruses. Biophys J 2004;86(6):3359-72.
5. Boerner RJ, Kassel DB, Barker SC, Ellis B, DeLacy P, Knight WB. Correlation of the phosphorylation states of pp60c-src with tyrosine kinase activity: the intramolecular pY530-SH2 complex retains significant activity if Y419 is phosphorylated. Biochemistry 1996;35(29):9519-25.

### Supplementary Material Spreadsheet

**Table 1** List of differential equations for model.

**Table 2** Model parameters.

## Figure Legends

**Figure 1** (a) Signaling pathways for ERK Activation by Adhesion. (b) Ras cycle of GDP/GTP Binding.

**Figure 2** FAK and ERK activation over a range of  $k_p$ , assuming that  $K_d=k_m/k_p=1066$  is constant. Experimentally observed time courses (Asthagiri) are also plotted.

**Figure 3** (a) ERK Activation in response to changes in fibronectin density. (b) Initial rates of FAK and ERK activation with ligand density. Initial rates were calculated from 470-480s, which falls within the linear phase of activation. The onset of the linear phase is subject to a time lag due to the clustering process.

**Figure 4** (a) Fold changes in ERK activation dynamics as a function of fold changes in ligand density and total FAK. All fold changes are normalized to the starting values ( $53/\mu\text{m}^2$  and  $2 \times 10^6$  respectively). (b) Fold changes in ERK activation dynamics as function of the initial rate of FAK activation. Initial rates in response to changes in ligand density and total FAK were calculated based on the dynamics of FAK activation from  $t=470-480\text{s}$ , where the signal is linear.

**Figure 5** (a) ERK activation in response to [Raf]. [Ras] is assumed to be  $1.072 \times 10^{-5}$  M. (b). ERK activation in response to [Ras]. Raf is assumed to be  $3.76 \times 10^{-7}$  M.

**Figure 6** Parameter ranges over which qualitative results hold. Parameters were varied one at a time over 6 orders of magnitude while holding all other fixed. Changes in parameter are

expressed as  $\log_{10}$  of the fold change. The parameters that correspond to each parameter number along the x-axis are listed in the Supplementary Materials.

**Figure 7** Effects of Raf and Ras concentrations on ERK activity. Concentrations of Ras and Raf are expressed as multiples of the minimum plotted values ( $5 \times 10^{-7}$  M and  $1 \times 10^{-8}$  M respectively). The magnitude of ERK, expressed as a percentage of the maximal ERK activation, is also plotted for different values of Raf (■). The shaded regions represent an initial transient activation followed by sustained mid level signaling at 33-66% of maximum (red “sustained”), sustained high level signaling at 66-100% of maximum (green “plateau”), a decrease to less than 33% of maximal signal within 6 hours (blue “transient”), or a decrease to less than 33% of maximum between 6 and 12 hours (yellow “transition”).

**Table 1.** Experimentally controllable parameters identified by Morris screening within the top 85<sup>th</sup> percentile of parameters important for ERK activation. Each parameter’s rank out of the total 106 parameters is included in parentheses. PP1, PP2, and PP3 refer to phosphatases for Raf, MEK, and ERK respectively. CA denotes contact area.

Figure 1

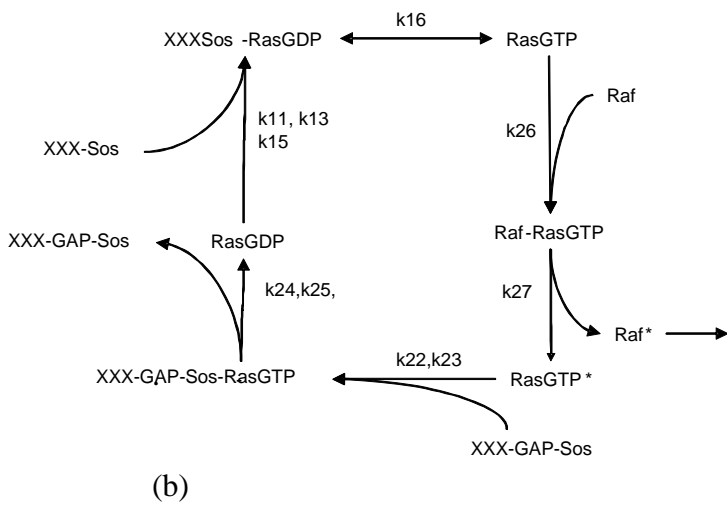
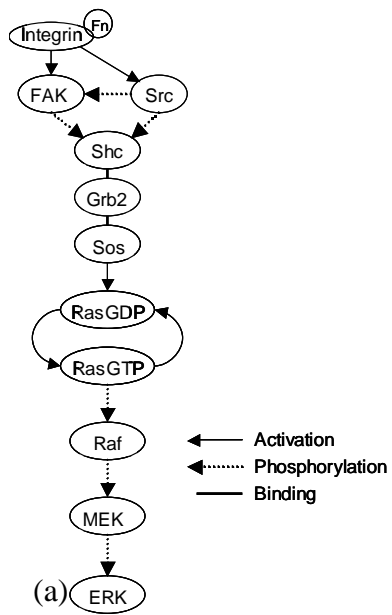


Figure 2

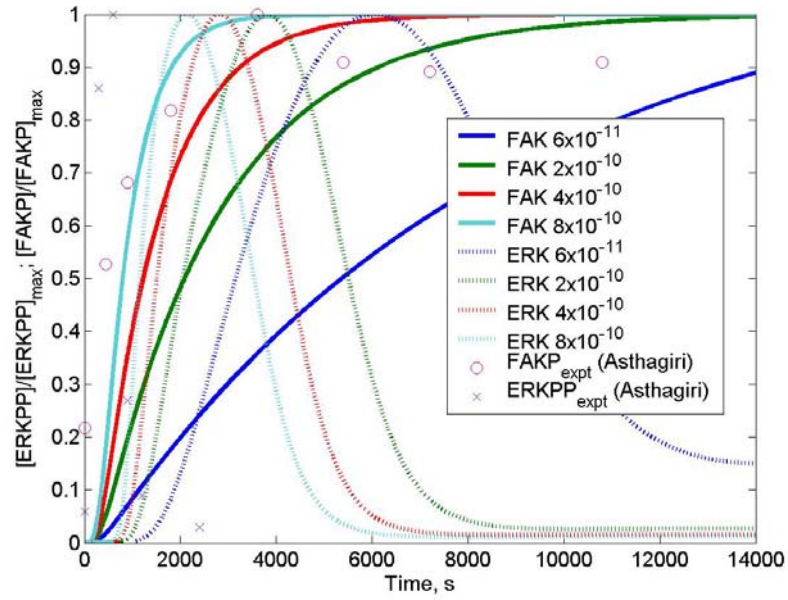
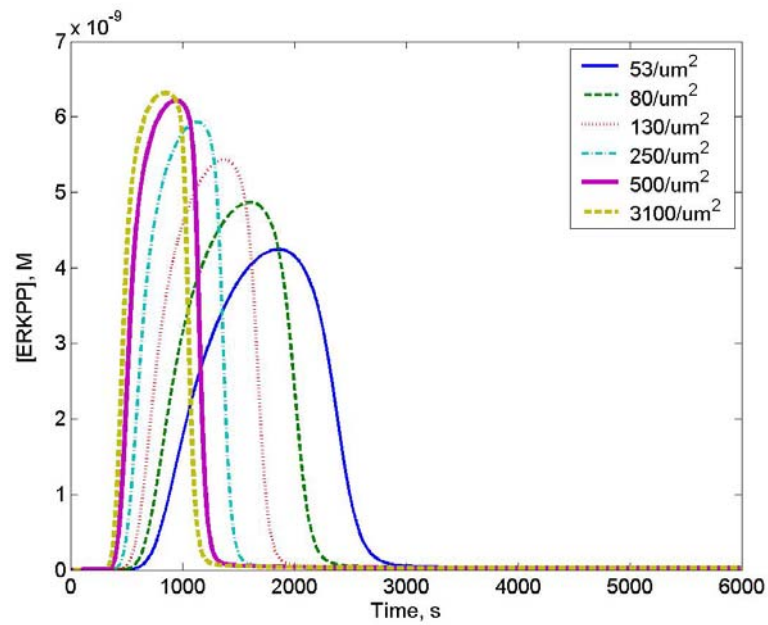
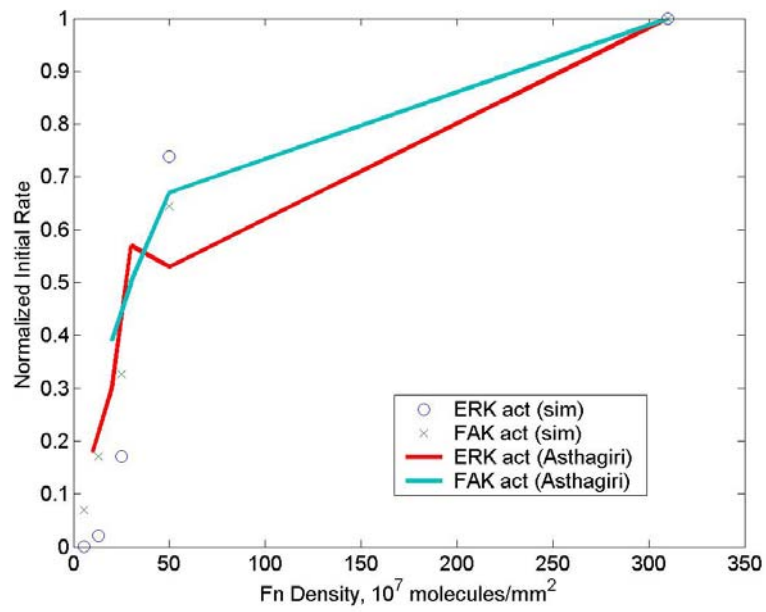


Figure 3

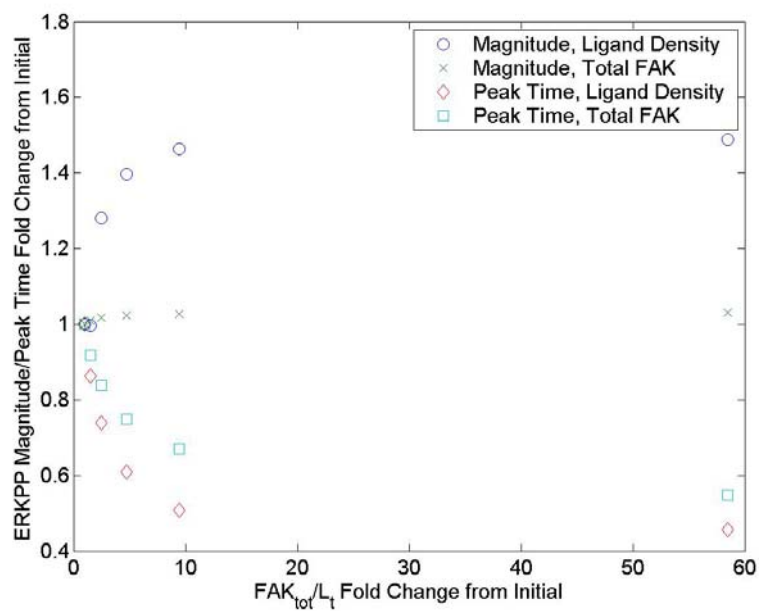


(a)

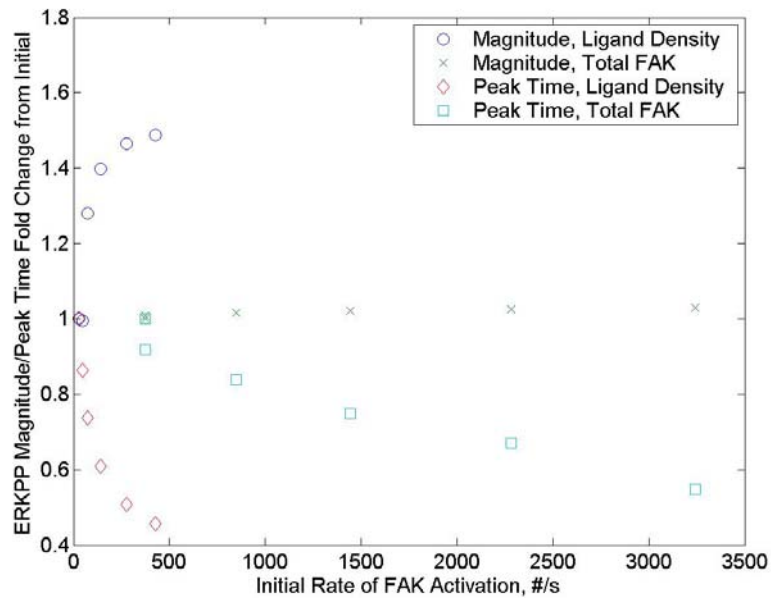


(b)

Figure 4

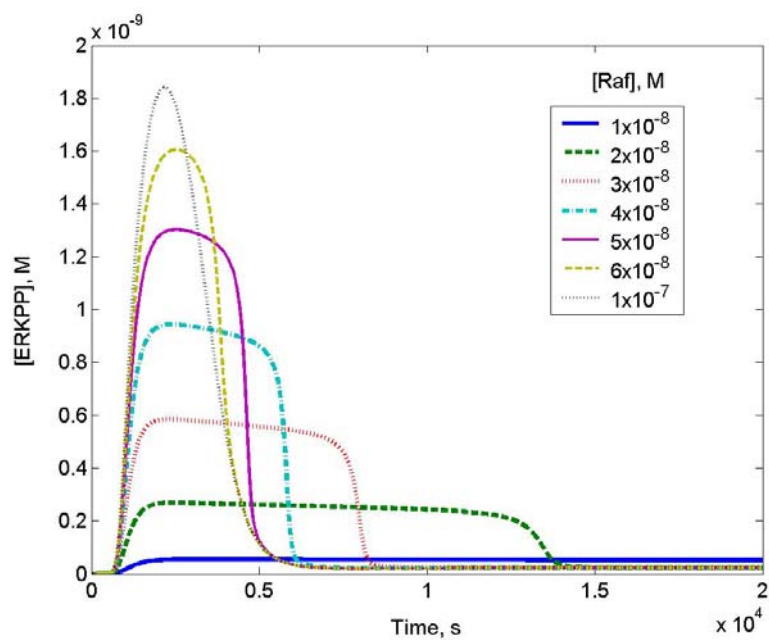


(a)

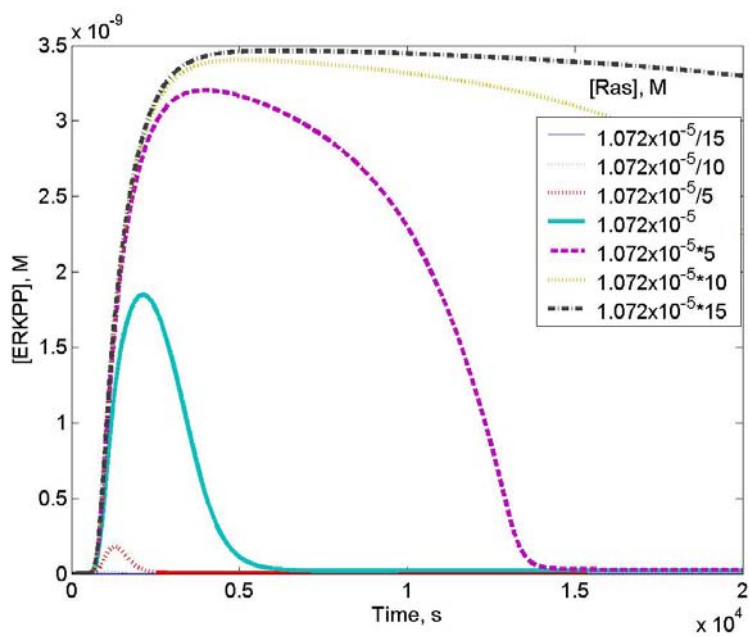


(b)

Figure 5



(a)



(b)



Figure 6

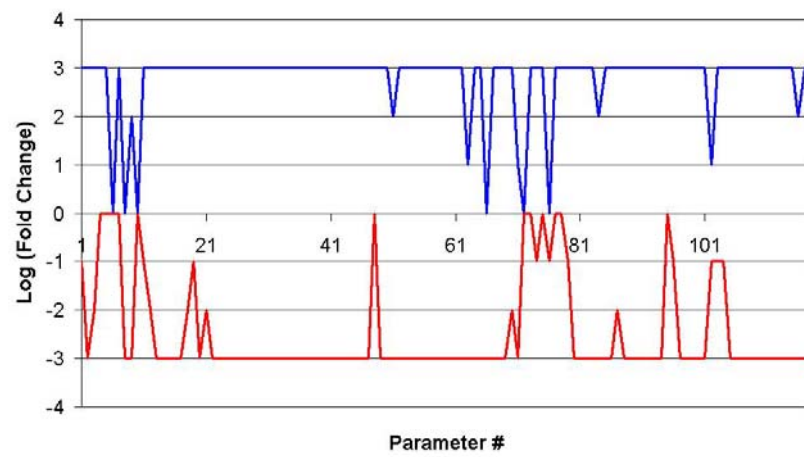


Figure 7

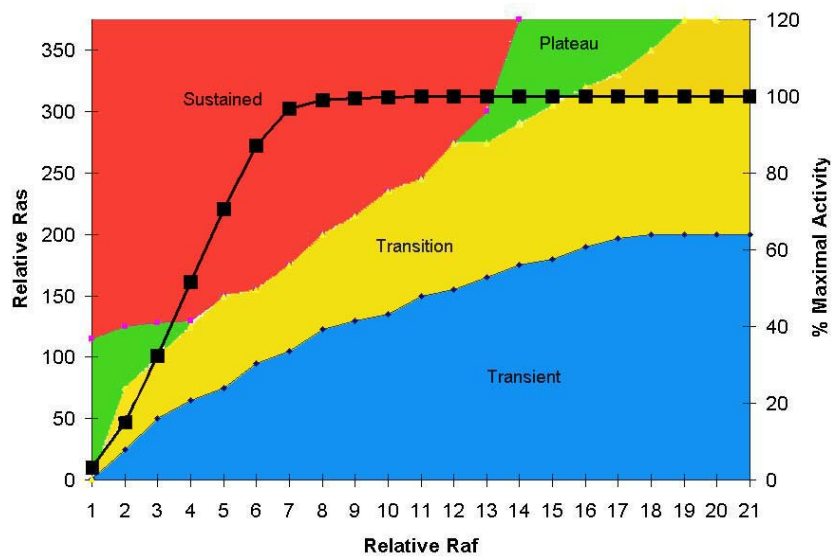


Table 1

<b>ERKPP Behavior</b>	<b>Experimentally Controllable Parameters within 85th Percentile</b>
Overall Time Course	PP3 (2), ERK (3), PP2 (7), MEK (8), PP1 (9), Raf (12), Rt (15), Ras (16)
Time to max	RasGAP (1), Ras (2), MEK (3), Raf (4), CA (5), PP2 (6), Rt (7), FAK (11), Grb2 (16)
t1=1500s	PP3 (2), ERK (3), PP2 (5), Raf (7), PP1 (9), Grb2 (11), MEK (14)
t2=4000s	PP3 (2), ERK (3), PP2 (5), MEK (8), Ras (10), Rt (11), PP1 (13)
t3=15000s	ERK (2), PP3 (4), MEK(6), PP2 (7), PP1 (10)
Maximum Value	PP3(2), ERK (3), PP2 (6), PP1 (8), Grb2 (10), MEK (11), Rt (12)

**Supplementary Materials, Table 1: A list of all protein species in the model, including their initial concentrations and differential equations.**

Protein Species	Eqn #	IC (M)	Differential Equations
FAK	1	2e6 (#)	$\frac{d[FAK]}{dt} = -2kp[(RL)_2][FAK] - kp[(RL)_2-FAKP][FAK] + km^*(((RL)_2-FAKP)/((RL)_2-FAKP)+((RL)_2-FAKP2)))^*[FAK] + 2^*km^*(((RL)_2-FAKP2)/((RL)_2-FAKP)+((RL)_2-FAKP2)))^*[FAK]$
FAKP	2	0	$\frac{d[FAKP]}{dt} = 2kp[(RL)_2][FAK] + kp[(RL)_2-FAKP][FAK] - km^*(((RL)_2-FAKP)/((RL)_2-FAKP)+((RL)_2-FAKP2)))^*[FAK] - 2^*km^*(((RL)_2-FAKP2)/((RL)_2-FAKP)+((RL)_2-FAKP2)))^*[FAK] - Vmax4[Shc]/(Km4+[Shc]) + k6[FAKP-ShcP317] - k6b[ShcP317][FAKP] + k20[FAKP-ShcP317-Grb2-Sos] - k20b[FAKP][ShcP317-Grb2-Sos] - k50[FAKP][Src^***] + k50b[Src^***-FAKP] - k51[Src^**][FAKP] + k51b[Src^*-FAKP] - k52[Src^*][FAKP] + k52b[Src^*-FAKP] + k8[FAKP-ShcP317Grb2] - k8b[FAKP][ShcP317Grb2] - k3[FAKP][RasGAP] + k3b[FAKP-RasGAP] - k3[FAKP-ShcP317-Grb2-Sos][RasGAP] + k3b[FAKP-RasGAP-ShcP317-Grb2-Sos]$
p120RasGAP	3	1.00E-08	$\frac{d[RasGAP]}{dt} = -k3[FAKP][RasGAP] + k3b[FAKP-RasGAP] - k3[FAKPP-Grb2][RasGAP] + k3b[FAKPP-RasGAP-Grb2] - k3[FAKP-ShcP317][RasGAP] + k3b[FAKP-RasGAP-ShcP317] - k3[FAKP-ShcP317-Grb2][RasGAP] + k3b[FAKP-RasGAP-ShcP317-Grb2] - k3[FAKP-ShcP317-Grb2-Sos][RasGAP] + k3b[FAKP-RasGAP-ShcP317-Grb2-Sos] - k3[FAKPP-Grb2-Sos][RasGAP] + k3b[FAKPP-RasGAP-Grb2-Sos]$
FAKP-RasGAP	4		$\frac{d[FAKP-RasGAP]}{dt} = k3[FAKP][RasGAP] - k3b[FAKP-RasGAP] - Vmax5[Shc]/(Km5+[Shc]) + k6[FAKP-RasGAP-ShcP317] - k6b[ShcP317][FAKP-RasGAP] + k20[FAKP-RasGAP-ShcP317-Grb2-Sos] - k20b[FAKP-RasGAP][ShcP317-Grb2-Sos] + k8[FAKP-RasGAP-ShcP317Grb2] - k8b[FAKP-RasGAP][ShcP317Grb2] - k50[FAKP-RasGAP][Src^***] + k50b[Src^***-FAKP-RasGAP] - k51[Src^**][FAKP-RasGAP] + k51b[Src^*-FAKP-RasGAP] - k52[Src^*][FAKP-RasGAP] + k52b[Src^*-FAKP-RasGAP] - k53[FAKP-RasGAP][RasGTP^*] + k53b[FAKP-RasGAP-RasGTP] + k55[FAKP-RasGAP-RasGTP] - k55b[FAKP-RasGAP][RasGDP]$
Shc	5	9.4949E-07	$\frac{d[Shc]}{dt} = -Vmax4[Shc]/(Km4+[Shc]) - Vmax5[Shc]/(Km5+[Shc]) + Vmax10[ShcP317]/(Km10+[ShcP317]) + Vmax10[ShcP239]/(Km10+[ShcP239]) - VmaxSrc[Shc]/(KmSrc+[Shc]) - VmaxSrc2[Shc]/(KmSrc2+[Shc]) - VmaxSrc3[Shc]/(KmSrc3+[Shc])$
ShcP317	6	0	$\frac{d[ShcP317]}{dt} = k6([FAKP-ShcP317]+[FAKP-RasGAP-ShcP317]) - k6b[ShcP317]([FAKP]+[FAKP-RasGAP]) - k9[ShcP317][Grb2] + k9b[Grb2-ShcP317] - Vmax10[ShcP317]/(Km10+[ShcP317]) + k19[ShcP317-Grb2-Sos] - k19b[ShcP317][Grb2-Sos]$
ShcP239	7	0	$\frac{d[ShcP239]}{dt} = VmaxSrc[Shc]/(KmSrc+[Shc]) + VmaxSrc2[Shc]/(KmSrc2+[Shc]) - VmaxSrc3[Shc]/(KmSrc3+[Shc]) + k46[ShcP239-Grb2-Sos] - k46b[ShcP239][Grb2-Sos] + k47[ShcP239-Grb2] - k47b[ShcP239][Grb2] - Vmax10[ShcP239]/(Km10+[ShcP239])$
Grb2	8	4.7944E-08	$\frac{d[Grb2]}{dt} = -k2([FAKPP]+[FAKPP-RasGAP])[Grb2] + k2b([FAKPP-Grb2]+[FAKPP-RasGAP-Grb2]) - k7([FAKP-ShcP317]+[FAKP-RasGAP-ShcP317])[Grb2] + k7b([FAKP-ShcP317-Grb2]+[FAKP-RasGAP-ShcP317-Grb2]) - k9[ShcP317][Grb2] + k9b[Grb2-ShcP317] - k47b[ShcP239][Grb2] + k47[ShcP239-Grb2] + k21[Grb2-Sos] - k21b[Grb2][Sos]$
Sos	9	6.2328E-08	$\frac{d[Sos]}{dt} = -k49[ShcP239-Grb2][Sos] + k49b[ShcP239-Grb2-Sos] - k12([FAKPP-Grb2]+[FAKPP-RasGAP-Grb2])[Sos] + k12b([FAKPP-Grb2-Sos]+[FAKPP-RasGAP-Grb2-Sos]) - k14([FAKP-ShcP317-Grb2]+[FAKP-RasGAP-ShcP317-Grb2])[Sos] + k14b([FAKP-ShcP317-Grb2-Sos]+[FAKP-RasGAP-ShcP317-Grb2-Sos]) + k21[Grb2][Sos] - k21b[Grb2][Sos]$
Grb2-Sos	10	0	$\frac{d[Grb2-Sos]}{dt} = k17([FAKPP-Grb2-Sos]+[FAKPP-RasGAP-Grb2-Sos]) - k17b([FAKPP]+[FAKPP-RasGAP])[Grb2-Sos] + k19[ShcP317-Grb2-Sos] - k19b[ShcP317][Grb2-Sos] + k46[ShcP239-Grb2-Sos] - k46b[ShcP239][Grb2-Sos] - k21[Grb2-Sos] + k21b[Grb2][Sos] + k18([FAKPShcP317Grb2Sos]+[FAKPRasGAPShcP317Grb2Sos]) - k18b([FAKPShcP317]+[FAKPRasGAP-ShcP317])[Grb2Sos]$
ShcP317-Grb2	11	0	$\frac{d[ShcP317-Grb2]}{dt} = k9[ShcP317][Grb2] - k9b[ShcP317-Grb2] - k48[ShcP317-Grb2][Sos] + k48b[ShcP317-Grb2-Sos] + k8([FAKPShcP317Grb2]+[FAKPRasGAPShcP317Grb2]) - k8b([FAKP]+[FAKP-RasGAP])[ShcP317Grb2]$
ShcP239-Grb2	12	0	$\frac{d[ShcP239-Grb2]}{dt} = -k47[ShcP239-Grb2] + k47b[ShcP239][Grb2] - k49[ShcP239-Grb2][Sos] + k49b[ShcP239-Grb2-Sos]$
ShcP239-Grb2-Sos	13	0	$\frac{d[ShcP239-Grb2-Sos]}{dt} = k49[ShcP239-Grb2][Sos] - k49b[ShcP239-Grb2-Sos] - k11[ShcP239-Grb2-Sos][RasGDP] + k11b[ShcP239-Grb2-Sos-RasGDP] - k46[ShcP239-Grb2-Sos] + k46b[ShcP239][Grb2-Sos] + k16[ShcP239Grb2SosRasGDP] - k16b[ShcP239Grb2Sos][RasGTP]$
ShcP317-Grb2-Sos	14	0	$\frac{d[ShcP317-Grb2-Sos]}{dt} = -k19[ShcP317-Grb2-Sos] + k19b[ShcP317][Grb2-Sos] + k20([FAKP-ShcP317-Grb2-Sos]+[FAKP-RasGAP-ShcP317-Grb2-Sos]) - k20b([FAKP]+[FAKP-RasGAP])[ShcP317-Grb2-Sos] + k48[ShcP317-Grb2][Sos] - k48b[ShcP317-Grb2-Sos]$
ShcP239-Grb2-Sos-RasGDP	15	0	$\frac{d[ShcP239-Grb2-Sos-RasGDP]}{dt} = k11[ShcP239-Grb2-Sos][RasGDP] - k11b[ShcP239-Grb2-Sos-RasGDP] - k16[ShcP239-Grb2-Sos-RasGDP] + k16[ShcP239-Grb2-Sos][RasGTP]$
FAKP-ShcP317	16	0	$\frac{d[FAKP-ShcP317]}{dt} = Vmax4[Shc]/(Km4+[Shc]) - k6[FAKP-ShcP317] + k6b[FAKP][ShcP317] - k7[FAKP-ShcP317][Grb2] + k7b[FAKP-ShcP317-Grb2] + k18[FAKP-ShcP317-Grb2-Sos] - k18b[FAKP-ShcP317][Grb2-Sos] - k3[FAKP-ShcP317][RasGAP] + k3b[FAKP-RasGAP-ShcP317]$
FAKP-ShcP317-Grb2	17	0	$\frac{d[FAKP-ShcP317-Grb2]}{dt} = k7[FAKP-ShcP317][Grb2] - k7b[FAKP-ShcP317-Grb2] - k8[FAKP-ShcP317-Grb2] + k8b[FAKP][Grb2-ShcP317] - k14[FAKP-ShcP317-Grb2][Sos] + k14b[FAKP-ShcP317-Grb2-Sos] - k3[FAKP-ShcP317-Grb2][RasGAP] + k3b[FAKP-RasGAP-ShcP317-Grb2]$
FAKP-ShcP317-Grb2-Sos	18	0	$\frac{d[FAKP-ShcP317-Grb2-Sos]}{dt} = k14[FAKP-ShcP317-Grb2][Sos] - k14b[FAKP-ShcP317-Grb2-Sos] - k15[FAKP-ShcP317-Grb2-Sos][RasGDP] + k15b[FAKP-ShcP317-Grb2-Sos-RasGDP] - k18[FAKP-ShcP317-Grb2-Sos] + k18b[FAKP-ShcP317][Grb2-Sos] - k20[FAKP-ShcP317-Grb2-Sos] + k20b[FAKP][ShcP317-Grb2-Sos] - k23[FAKP-ShcP317-Grb2-Sos][RasGTP^*] + k23b[FAKP-ShcP317-Grb2-Sos-RasGTP] + k25[FAKP-ShcP317-Grb2-Sos-RasGTP] - k25b[FAKP-ShcP317-Grb2-Sos][RasGDP] + k16[FAKP-ShcP317Grb2SosRasGDP] - k16b[FAKP-ShcP317Grb2Sos][RasGTP] - k3[FAKP-ShcP317-Grb2-Sos][RasGAP] + k3b[FAKP-RasGAP-ShcP317-Grb2-Sos]$
FAKP-ShcP317-Grb2-Sos-RasGDP	19	0	$\frac{d[FAKP-ShcP317-Grb2-Sos-RasGDP]}{dt} = k15[FAKP-ShcP317-Grb2-Sos][RasGDP] - k15b[FAKP-ShcP317-Grb2-Sos-RasGDP] - k16[FAKP-ShcP317-Grb2-Sos-RasGDP] + k16b[FAKP-ShcP317-Grb2-Sos][RasGTP]$
FAKP-RasGAP-ShcP317	20	0	$\frac{d[FAKP-RasGAP-ShcP317]}{dt} = Vmax5[Shc]/(Km5+[Shc]) - k6[FAKP-RasGAP-ShcP317] + k6b[FAKP-RasGAP][ShcP317] - k7[FAKP-RasGAP-ShcP317][Grb2] + k7b[FAKP-RasGAP-ShcP317-Grb2] + k18[FAKP-RasGAP-ShcP317-Grb2-Sos] - k18b[FAKP-RasGAP-ShcP317][RasGAP] - k3b[FAKP-RasGAP-ShcP317-Grb2-Sos] - k53[FAKP-RasGAP-ShcP317][RasGTP^*] + k53b[FAKP-RasGAP-ShcP317-RasGTP] + k55[FAKP-RasGAP-ShcP317-RasGTP] - k55b[FAKP-RasGAP-ShcP317][RasGDP]$
FAKP-RasGAP-ShcP317-Grb2	21	0	$\frac{d[FAKP-RasGAP-ShcP317-Grb2]}{dt} = k7[FAKP-RasGAP-ShcP317][Grb2] - k7b[FAKP-RasGAP-ShcP317-Grb2] - k8[FAKP-RasGAP-ShcP317-Grb2] + k8b[FAKP-RasGAP][Grb2-ShcP317] - k14[FAKP-RasGAP-ShcP317-Grb2][Sos] + k14b[FAKP-RasGAP-ShcP317-Grb2-Sos] + k3[FAKP-ShcP317-Grb2][RasGAP] - k3b[FAKP-RasGAP-ShcP317-Grb2] - k53[FAKP-RasGAP-ShcP317-Grb2][RasGTP^*] + k53b[FAKP-RasGAP-ShcP317-Grb2-RasGTP] + k55[FAKP-RasGAP-ShcP317-Grb2-RasGTP] - k55b[FAKP-RasGAP-ShcP317-Grb2][RasGDP]$

Table 1, Continued			
Protein Species	Eqn #	IC (M)	Differential Equations
FAKP-RasGAP-ShcP317-Grb2-Sos	22	0	$\frac{d[\text{FAKP-RasGAP-ShcP317-Grb2-Sos}]}{dt} = k_{14}[\text{FAKP-RasGAP-ShcP317-Grb2}][\text{Sos}] - k_{14b}[\text{FAKP-RasGAP-ShcP317-Grb2-Sos}] - k_{15}[\text{FAKP-RasGAP-ShcP317-Grb2-Sos}][\text{RasGDP}] + k_{15b}[\text{FAKP-RasGAP-ShcP317-Grb2-Sos-RasGDP}] - k_{18}[\text{FAKP-RasGAP-ShcP317-Grb2-Sos}] + k_{18b}[\text{FAKP-RasGAP-ShcP317}][\text{Grb2-Sos}] - k_{20}[\text{FAKP-RasGAP-ShcP317-Grb2-Sos}] + k_{20b}[\text{FAKP-RasGAP}][\text{ShcP317-Grb2-Sos}] - k_{23}[\text{FAKP-RasGAP-ShcP317-Grb2-Sos}][\text{RasGTP}^*] + k_{23b}[\text{FAKP-RasGAP-ShcP317-Grb2-Sos-RasGTP}] + k_{25}[\text{FAKP-RasGAP-ShcP317-Grb2-Sos-RasGTP}] - k_{25b}[\text{FAKP-RasGAP-ShcP317-Grb2-Sos}][\text{RasGDP}] + k_{16}[\text{FAKP-RasGAP-ShcP317Grb2SosRasGDP}] - k_{16b}[\text{FAKP-RasGAP-ShcP317Grb2Sos}][\text{RasGTP}] + k_{3}[\text{FAKP-ShcP317-Grb2-Sos}][\text{RasGAP}] - k_{3b}[\text{FAKP-RasGAP-ShcP317-Grb2-Sos}]$
FAKP-RasGAP-ShcP317-Grb2-Sos-RasGDP	23	0	$\frac{d[\text{FAKP-RasGAP-ShcP317-Grb2-Sos-RasGDP}]}{dt} = k_{15}[\text{FAKP-RasGAP-ShcP317-Grb2-Sos}][\text{RasGDP}] - k_{15b}[\text{FAKP-RasGAP-ShcP317-Grb2-Sos-RasGDP}] - k_{16}[\text{FAKP-RasGAP-ShcP317-Grb2-Sos-RasGDP}] + k_{16b}[\text{FAKP-RasGAP-ShcP317-Grb2-Sos}][\text{RasGTP}]$
FAKP-RasGAP-ShcP317-Grb2-Sos-RasGTP	24	0	$\frac{d[\text{FAKP-RasGAP-ShcP317-Grb2-Sos-RasGTP}]}{dt} = k_{23}[\text{FAKP-RasGAP-ShcP317-Grb2-Sos}][\text{RasGTP}^*] - k_{23b}[\text{FAKP-RasGAP-ShcP317-Grb2-Sos-RasGTP}] - k_{25}[\text{FAKP-RasGAP-ShcP317-Grb2-Sos-RasGTP}] + k_{25b}[\text{FAKP-RasGAP-ShcP317-Grb2-Sos}][\text{RasGDP}]$
FAKPP	25	0	$\frac{d[\text{FAKPP}]}{dt} = k_{cat50}[\text{Src}^{***}\text{-FAKP}] + k_{cat51}[\text{Src}^{**}\text{-FAKP}] + k_{cat52}[\text{Src}^*\text{-FAKP}] - k_2[\text{FAKPP}][\text{Grb2}] + k_{2b}[\text{FAKPP-Grb2}] + k_{17}[\text{FAKPP-Grb2-Sos}] - k_{17b}[\text{FAKPP}][\text{Grb2-Sos}] - k_3[\text{FAKPP}][\text{RasGAP}] + k_{3b}[\text{FAKPP-RasGAP}]$
FAKPP-Grb2	26	0	$\frac{d[\text{FAKPP-Grb2}]}{dt} = k_2[\text{FAKPP}][\text{Grb2}] - k_{2b}[\text{FAKPP-Grb2}] - k_{12}[\text{FAKPP-Grb2}][\text{Sos}] + k_{12b}[\text{FAKPP-Grb2-Sos}] - k_3[\text{FAKPP-Grb2}][\text{RasGAP}] + k_{3b}[\text{FAKPP-RasGAP-Grb2}]$
FAKPP-Grb2-Sos	27	0	$\frac{d[\text{FAKPP-Grb2-Sos}]}{dt} = k_{12}[\text{FAKPP-Grb2}][\text{Sos}] - k_{12b}[\text{FAKPP-Grb2-Sos}] - k_{13}[\text{FAKPP-Grb2-Sos}][\text{RasGDP}] + k_{13b}[\text{FAKPP-Grb2-Sos-RasGDP}] - k_{17}[\text{FAKPP-Grb2-Sos}] + k_{17b}[\text{FAKPP}][\text{Grb2-Sos}] - k_{22}[\text{FAKPP-Grb2-Sos}][\text{RasGTP}^*] + k_{22b}[\text{FAKPP-Grb2-Sos-RasGTP}] + k_{24}[\text{FAKPP-Grb2-Sos-RasGTP}] - k_{24b}[\text{FAKPP-Grb2-Sos}][\text{RasGDP}] + k_{16}[\text{FAKPPGrb2SosRasGDP}] - k_{16b}[\text{FAKPPGrb2Sos}][\text{RasGTP}] - k_3[\text{FAKPP-Grb2-Sos}][\text{RasGAP}] + k_{3b}[\text{FAKPP-RasGAP-Grb2-Sos}]$
FAKPP-Grb2-Sos-RasGDP	28	0	$\frac{d[\text{FAKPP-Grb2-Sos-RasGDP}]}{dt} = k_{13}[\text{FAKPP-Grb2-Sos}][\text{RasGDP}] - k_{13b}[\text{FAKPP-Grb2-Sos-RasGDP}] - k_{16}[\text{FAKPP-Grb2-Sos-RasGDP}] + k_{16b}[\text{FAKPP-Grb2-Sos}][\text{RasGTP}]$
FAKPP-RasGAP	29	0	$\frac{d[\text{FAKPP-RasGAP}]}{dt} = k_{cat50}[\text{Src}^{***}\text{-FAKP-RasGAP}] + k_{cat51}[\text{Src}^{**}\text{-FAKP-RasGAP}] + k_{cat52}[\text{Src}^*\text{-FAKP-RasGAP}] - k_2[\text{FAKPP-RasGAP}][\text{Grb2}] + k_{2b}[\text{FAKPP-RasGAP-Grb2}] + k_{17}[\text{FAKPP-RasGAP-Grb2-Sos}] - k_{17b}[\text{FAKPP-RasGAP}][\text{Grb2-Sos}] + k_3[\text{FAKPP}][\text{RasGAP}] - k_{3b}[\text{FAKPP-RasGAP}] - k_{53}[\text{FAKPP-RasGAP}][\text{RasGTP}^*] + k_{53b}[\text{FAKPP-RasGAP-RasGTP}] + k_{54}[\text{FAKPP-RasGAP-RasGTP}] - k_{54b}[\text{FAKPP-RasGAP}][\text{RasGDP}]$
FAKPP-RasGAP-Grb2	30	0	$\frac{d[\text{FAKPP-RasGAP-Grb2}]}{dt} = k_2[\text{FAKPP-RasGAP}][\text{Grb2}] - k_{2b}[\text{FAKPP-RasGAP-Grb2}] - k_{12}[\text{FAKPP-RasGAP-Grb2}][\text{Sos}] + k_{12b}[\text{FAKPP-RasGAP-Grb2-Sos}] + k_3[\text{FAKPP-Grb2}][\text{RasGAP}] - k_{3b}[\text{FAKPP-RasGAP-Grb2}] - k_{53}[\text{FAKPP-RasGAP-Grb2}][\text{RasGTP}^*] + k_{53b}[\text{FAKPP-RasGAP-Grb2-RasGTP}] + k_{54}[\text{FAKPP-RasGAP-Grb2-RasGTP}] - k_{54b}[\text{FAKPP-RasGAP-Grb2}][\text{RasGDP}]$
FAKPP-RasGAP-Grb2-Sos	31	0	$\frac{d[\text{FAKPP-RasGAP-Grb2-Sos}]}{dt} = k_{12}[\text{FAKPP-RasGAP-Grb2}][\text{Sos}] - k_{12b}[\text{FAKPP-RasGAP-Grb2-Sos}] - k_{13}[\text{FAKPP-RasGAP-Grb2-Sos}][\text{RasGDP}] + k_{13b}[\text{FAKPP-RasGAP-Grb2-Sos-RasGDP}] - k_{17}[\text{FAKPP-RasGAP-Grb2-Sos}] + k_{17b}[\text{FAKPP-RasGAP}][\text{Grb2-Sos}] - k_{22}[\text{FAKPP-RasGAP-Grb2-Sos}][\text{RasGTP}^*] + k_{22b}[\text{FAKPP-RasGAP-Grb2-Sos-RasGTP}] + k_{24}[\text{FAKPP-RasGAP-Grb2-Sos-RasGTP}] - k_{24b}[\text{FAKPP-RasGAP-Grb2-Sos}][\text{RasGDP}] + k_{16}[\text{FAKPP-RasGAPGrb2SosRasGDP}] - k_{16b}[\text{FAKPP-RasGAPGrb2Sos}][\text{RasGTP}] + k_3[\text{FAKPP-Grb2-Sos}][\text{RasGAP}] - k_{3b}[\text{FAKPP-RasGAP-Grb2-Sos}]$
FAKPP-RasGAP-Grb2-Sos-RasGDP	32	0	$\frac{d[\text{FAKPP-RasGAP-Grb2-Sos-RasGDP}]}{dt} = k_{13}[\text{FAKPP-RasGAP-Grb2-Sos}][\text{RasGDP}] - k_{13b}[\text{FAKPP-RasGAP-Grb2-Sos-RasGDP}] - k_{16}[\text{FAKPP-RasGAP-Grb2-Sos-RasGDP}] + k_{16b}[\text{FAKPP-RasGAP-Grb2-Sos}][\text{RasGTP}]$
FAKPP-RasGAP-Grb2-Sos-RasGTP	33	0	$\frac{d[\text{FAKPP-RasGAP-Grb2-Sos-RasGTP}]}{dt} = k_{22}[\text{FAKPP-RasGAP-Grb2-Sos}][\text{RasGTP}^*] - k_{22b}[\text{FAKPP-RasGAP-Grb2-Sos-RasGTP}] - k_{24}[\text{FAKPP-RasGAP-Grb2-Sos-RasGTP}] + k_{24b}[\text{FAKPP-RasGAP-Grb2-Sos}][\text{RasGDP}]$
RasGDP	34	1.0717E-05	$\frac{d[\text{RasGDP}]}{dt} = -k_{11}[\text{ShcP239-Grb2-Sos}][\text{RasGDP}] + k_{11b}[\text{ShcP239-Grb2-Sos-RasGDP}] - k_{13}([\text{FAKPP-Grb2-Sos}] + [\text{FAKPP-RasGAP-Grb2-Sos}][\text{RasGDP}] + k_{13b}([\text{FAKPP-Grb2-Sos-RasGDP}] + [\text{FAKPP-RasGAP-Grb2-Sos-RasGDP}]) - k_{15}([\text{FAKP-ShcP317-Grb2-Sos}] + [\text{FAKP-RasGAP-ShcP317-Grb2-Sos}][\text{RasGDP}] + k_{15b}([\text{FAKP-ShcP317-Grb2-Sos-RasGDP}] + [\text{FAKP-RasGAP-ShcP317-Grb2-Sos-RasGDP}]) + k_{24}[\text{FAKPP-RasGAP-Grb2-Sos-RasGTP}] - k_{24b}[\text{FAKPP-RasGAP-Grb2-Sos}][\text{RasGDP}] + k_{25}[\text{FAKP-RasGAP-ShcP317-Grb2-Sos-RasGTP}] - k_{25b}[\text{FAKP-RasGAP-ShcP317-Grb2-S$

Table 1, Continued			
Protein Species	Eqn #	IC (M)	Differential Equations
ERKPP-PP3	52	0	$d[ERKPP-PP3]/dt = k42[ERKPP][PP3] - k42b[ERKPP-PP3] - k43[ERKPP-PP3]$
ERKP-PP3	53	0	$d[ERKP-PP3]/dt = k44[ERKP][PP3] - k44b[ERKP-PP3] - k45[ERKP-PP3]$
ERKPP	54	0	$d[ERKPP]/dt = -k42[ERKPP][PP3] + k42b[ERKPP-PP3] + k41[ERKP-MEKPP]$
RL	55		$d[RL] = kf[R][L] - kr[RL] - k1[RL]^2$
R	56		$d[R] = -kf[R][L] + kr[RL] + (dA/dt)*Rt$
L	57		$d[R] = -kf[R][L] + kr[RL] + (dA/dt)*Lt$
(RL) <sup>2</sup>	58		$d[(RL)^2] = k1[RL]^2 - kp[(RL)^2][FAK] + km*(((RL)^2-FAK)/((RL)^2-FAK)+((RL)^2-FAK_2))*[FAK]$
Srcp527closed	59	9.00E-08	$d[Srcp527closed]/dt = -kopen[Srcp527closed] + kclose[Srcp527open] - VmaxSHP2[Srcp527closed]/(KmSHP2+[Srcp527closed])$
Srcp527open	60	0	$d[Srcp527open]/dt = kopen[Srcp527closed] - kclose[Srcp527open] - VmaxSHP[Srcp527open]/(KmSHP+[Srcp527open]) + VmaxCsk[Srcp]/(KmCsk+[Srcp])$
Srcp	61	0	$d[Srcp]/dt = VmaxSHP[Srcp527open]/(KmSHP+[Srcp527open]) + VmaxSHP2[Srcp527closed]/(KmSHP2+[Srcp527closed]) - VmaxCsk[Srcp]/(KmCsk+[Srcp]) - kt[Srcp]$
Srcp	62	0	$d[Srcp]/dt = kt[Srcp] - Vmaxauto[Srcp]/(Kmauto+[Srcp]) + VmaxPTP1B[Srcp]/(KmPTP1B+[Srcp]) + VmaxPTPa2[Srcp527]/(KmPTPa2+[Srcp527]) + VmaxPTPa[Srcp527]/(KmPTPa+[Srcp527])$
Src*** (pY416)	63	0	$d[Srcp]/dt = Vmaxauto[Srcp]/(Kmauto+[Srcp]) - VmaxCsk[Srcp]/(KmCsk+[Srcp]) - k50[Srcp][FAK] + k50b[Srcp-FAK] + kcat50[Srcp-FAK] - VmaxPTP1B[Srcp]/(KmPTP1B+[Srcp])$
Src** (pY416+pY527open)	64	0	$d[Srcp]/dt = VmaxCsk[Srcp]/(KmCsk+[Srcp]) - VmaxPTP1B[Srcp]/(KmPTP1B+[Srcp]) - k51[Srcp][FAK] + k51b[Srcp-FAK] + kcat51[Srcp-FAK] - kclose2[Srcp] + kopen2[Srcp]$
Srcp527	65	0	$d[Srcp527]/dt = VmaxPTP1B[Srcp]/(KmPTP1B+[Srcp]) - VmaxPTPa[Srcp527]/(KmPTPa+[Srcp527]) - kclose[Srcp527] + kopen[Srcp527]$
Srcp527	66	0	$d[Srcp527]/dt = -VmaxPTPa2[Srcp527]/(KmPTPa2+[Srcp527]) + kclose[Srcp527] - kopen[Srcp527] + VmaxPTP1B2[Srcp]/(KmPTP1B2+[Srcp])$
Src***-FAK	67	0	$d[Srcp-FAK]/dt = k50[FAK][Srcp] - k50b[Srcp-FAK] - kcat50[Srcp-FAK]$
Src***-FAK (pY416+pY527open)	68	0	$d[Srcp-FAK]/dt = k51[FAK][Srcp] - k51b[Srcp-FAK] - kcat51[Srcp-FAK]$
SHP (phosphatase)	69	0	$d[SHP]/dt = 2*kp[(RL)^2][FAK] + kp*[(RL)^2-FAK][FAK] - km[FAK]$ (proportional to FAK)
Src* (pY416+pY527closed)	70	0	$d[Srcp]/dt = kclose2[Srcp] - kopen2[Srcp] - VmaxPTP1B2[Srcp]/(KmPTP1B2+[Srcp]) - k52[Srcp][FAK] + k52b[Srcp-FAK] + kcat52[Srcp-FAK]$
Src*-FAK (pY416+pY527closed)	71	0	$d[Srcp-FAK]/dt = k52[FAK][Srcp] - k52b[Srcp-FAK] - kcat52[Srcp-FAK]$
Src***-FAK-RasGAP	72	0	$d[Srcp-FAK-RasGAP]/dt = k50[FAK-RasGAP][Srcp] - k50b[Srcp-FAK-RasGAP] - kcat50[Srcp-FAK-RasGAP]$
Src**-FAK-RasGAP (pY416+pY527open)	73	0	$d[Srcp-FAK-RasGAP]/dt = k51[FAK-RasGAP][Srcp] - k51b[Srcp-FAK-RasGAP] - kcat51[Srcp-FAK-RasGAP]$
Src*-FAK-RasGAP (pY416+pY527closed)	74	0	$d[Srcp-FAK-RasGAP]/dt = k52[FAK-RasGAP][Srcp] - k52b[Srcp-FAK-RasGAP] - kcat52[Srcp-FAK-RasGAP]$
FAK-RasGAP-RasGTP	75		$d[FAK-RasGAP-RasGTP]/dt = k53[FAK-RasGAP][RasGTP] - k53b[FAK-RasGAP-RasGTP] - k55[FAK-RasGAP-RasGTP] + k55b[FAK-RasGAP][RasGDP]$
FAK-RasGAP-ShcP317-RasGTP	76	0	$d[FAK-RasGAP-ShcP317-RasGTP]/dt = k53[FAK-RasGAP-ShcP317][RasGTP] - k53b[FAK-RasGAP-ShcP317-RasGTP] - k55[FAK-RasGAP-ShcP317-RasGTP] + k55b[FAK-RasGAP-ShcP317-RasGAP][RasGDP]$
FAK-RasGAP-ShcP317-Grb2-RasGTP	77	0	$d[FAK-RasGAP-ShcP317-Grb2-RasGTP]/dt = k53[FAK-RasGAP-ShcP317-Grb2][RasGTP] - k53b[FAK-RasGAP-ShcP317-Grb2-RasGTP] - k55[FAK-RasGAP-ShcP317-Grb2-RasGTP] + k55b[FAK-RasGAP-ShcP317-Grb2][RasGDP]$
FAKPP-RasGAP-RasGTP	78	0	$d[FAKPP-RasGAP-RasGTP]/dt = k53[FAKPP-RasGAP][RasGTP] - k53b[FAKPP-RasGAP-RasGTP] - k54[FAKPP-RasGAP-RasGTP] + k54b[FAKPP-RasGAP][RasGDP]$
FAKPP-RasGAP-Grb2-RasGTP	79	0	$d[FAKPP-RasGAP-Grb2-RasGTP]/dt = k53[FAKPP-RasGAP-Grb2][RasGTP] - k53b[FAKPP-RasGAP-Grb2-RasGTP] - k54[FAKPP-RasGAP-Grb2-RasGTP] + k54b[FAKPP-RasGAP-Grb2][RasGDP]$
(RL) <sub>2</sub> -FAK	80	0	$d[(RL)^2-FAK]/dt = 2kp[(RL)^2][FAK] - km*(((RL)^2-FAK)/((RL)^2-FAK)+((RL)^2-FAK_2))*[FAK] + 2*km*(((RL)^2-FAK_2)/((RL)^2-FAK)+((RL)^2-FAK_2))*[FAK]$
(RL) <sub>2</sub> -FAK <sub>2</sub>	81	0	$d[(RL)^2-FAK_2]/dt = kp[(RL)^2-FAK][FAK] - 2*km*(((RL)^2-FAK_2)/((RL)^2-FAK)+((RL)^2-FAK_2))*[FAK]$
PP1		3.7603E-08	constant
PP2		3.7603E-08	constant
PP3		9.4008E-06	constant

Supplementary Materials, Table 2: Reactions included in the model with rate constants, assigned parameter numbers used for sensitivity analysis, and references						
Reaction	kf	Units	kr	Units	SA Parameter #	Reference
<b>Integrin initiation</b>						
FN + b1int $\leftrightarrow$ b1int-FN	kf=6.12e-10;	cm <sup>2</sup> # <sup>-1</sup> s <sup>-1</sup>	kr=1.6e-4;	s <sup>-1</sup>	20	(15)
b1int-Fn + b1int-Fn $\leftrightarrow$ (b1int-Fn) <sub>2</sub>	k1=.01;	s			21	Estimate - phenomenological rate constant
(b1int-Fn) <sub>2</sub> + FAK $\leftrightarrow$ (b1int-Fn) <sub>2</sub> -FAKP	kp=2e-10;	# s	km=1065.54/kp		22; 23	Based on Kd=1nM for bimolecular rxn
(b1int-Fn) <sub>2</sub> -FAKP + FAK $\leftrightarrow$ (b1int-Fn) <sub>2</sub> -FAKP <sub>2</sub>	kp=2e-10;	# s	km=1065.54/kp		22; 23	
<b>FAK, Src, and Shc Interactions</b>						
FAKP(-ShcP317-Grb2-Sos)/FAKPP(-Grb2-Sos) + RasGAP $\leftrightarrow$ FAKP(-ShcP317-Grb2-Sos)/FAKPP(-Grb2-Sos)-RasGAP	k3=1e6	M <sup>-1</sup> s <sup>-1</sup>	k3b=1e-3	s <sup>-1</sup>	24	Estimate from (14)
FAKPP + Grb2 $\leftrightarrow$ FAKPP-Grb2	k2=2.69e5;	M <sup>-1</sup> s <sup>-1</sup>	k2b=.03;	s <sup>-1</sup>	25	Estimate from (1) and (7)
FAKP + Shc $\rightarrow$ FAKP-ShcP317	kcat4=13	s <sup>-1</sup>	Km4=400e-6	M	26; 27	(16)
FAKP-RasGAP + Shc $\rightarrow$ FAKP-RasGAP-ShcP317	kcat5=13	s <sup>-1</sup>	Km5=400e-6	M	26; 27	
FAKP(-RasGAP)-ShcP317 $\rightarrow$ ShcP317 + FAKP(-RasGAP)	k6=.1	s <sup>-1</sup>	k6b=1e5	M <sup>-1</sup> s <sup>-1</sup>	28	Estimate - bimolecular binding
FAKP(-RasGAP)-ShcP317 + Grb2 $\leftrightarrow$ FAKP(-RasGAP)-FAKP(-RasGAP)-ShcP317-Grb2 $\leftrightarrow$ FAKP(-RasGAP) + ShcP317 + Grb2 $\leftrightarrow$ Grb2-ShcP317	k7=4.2e6;	M <sup>-1</sup> s <sup>-1</sup>	k7b=.1;	s <sup>-1</sup>	29	Estimate from (1) & (7)
	k8=.05;	s <sup>-1</sup>	k8b=1.657e6;	M <sup>-1</sup> s <sup>-1</sup>	30	Estimate based on (14) & (7)
	k9=1e7;	M <sup>-1</sup> s <sup>-1</sup>	k9b=.24;	s <sup>-1</sup>	31	Estimate from (1) & (4)
Shc (+pY416Src) $\rightarrow$ ShcP239	kcatSrc=8.33	s <sup>-1</sup>	KmSrc=134e-6	M	32; 33	(2)
Shc (+ pY416+pY527openSrc) $\rightarrow$ ShcP239	kcatSrc=1.67	s <sup>-1</sup>	KmSrc=89e-6	M	34; 35	(2)
Shc (+ pY416+pY527closedSrc) $\rightarrow$ ShcP239	kcatSrc=1.67	s <sup>-1</sup>	KmSrc=89e-6	M	36; 37	(2)
pY416Src + FAKP $\leftrightarrow$ pY416Src-FAKP	k50=6.23e4;	M <sup>-1</sup> s <sup>-1</sup>	k50b=.012;	s <sup>-1</sup>	38	Estimate - see Model Section
pY416+pY527oSrc* + FAKP $\leftrightarrow$ pY416+pY527oSrc- FAKP	k51=1.98e4;	M <sup>-1</sup> s <sup>-1</sup>	k51b=.012;	s <sup>-1</sup>	39	Estimate - see Model Section
pY416+pY527cSrc* + FAKP $\leftrightarrow$ pY416+pY527cSrc- FAKP	k52=1.98e4;	M <sup>-1</sup> s <sup>-1</sup>	k52b=.012;	s <sup>-1</sup>	40	Estimate - see Model Section
pY416Src-FAKP $\leftrightarrow$ pY416Src-FAKPP	kcat50=8.33;	s <sup>-1</sup>			41	(2)
pY416+pY527oSrc*-FAKP $\leftrightarrow$ pY416+pY527oSrc- FAKPP	kcat51=1.67;	s <sup>-1</sup>			42	(2)
pY416+pY527cSrc*-FAKP $\leftrightarrow$ pY416+pY527cSrc-FAKPP	kcat52=1.67;	s <sup>-1</sup>			43	(2)
ShcP239-Grb2 $\leftrightarrow$ ShcP239 + Grb2	k47=5e-2;	s <sup>-1</sup>	k47b=5e6;	M <sup>-1</sup> s <sup>-1</sup>	44	Estimate based on (4) & (5)
ShcP317 $\rightarrow$ Shc	Vmax10=1.7	s <sup>-1</sup>	Km10 = 340e-9	M	45; 46	(14)
<b>Grb2, Sos, Ras Portion</b>						
ShcP239-Grb2-Sos + RasGDP $\leftrightarrow$ -ShcP239-Grb2-Sos-RasGDP	k11=1.5e7;	M <sup>-1</sup> s <sup>-1</sup>	k11b=1.3;	s <sup>-1</sup>	47	Estimate based on (14)
FAKPP(-RasGAP)-Grb2 + Sos $\leftrightarrow$ FAKPP(-RasGAP)-Grb2-Sos	k12=3e5;	M <sup>-1</sup> s <sup>-1</sup>	k12b=3e-2;	s <sup>-1</sup>	48	Estimate based on (10) & (13)
FAKPP(-RasGAP)-Grb2-Sos + RasGDP $\leftrightarrow$ FAKPP(-RasGAP)-Grb2-Sos-RasGDP	k13=k11;	s <sup>-1</sup>	k13b=1.3;	s <sup>-1</sup>	49	Estimate based on (14)
FAKP(-RasGAP)-ShcP317-Grb2 + Sos $\leftrightarrow$ FAKP(-RasGAP)-ShcP317-Grb2-Sos	k14=9.59e6;	M <sup>-1</sup> s <sup>-1</sup>	k14b=2.1e-2;	s <sup>-1</sup>	50	Estimate based on (7)
FAKP(-RasGAP)-ShcP317-Grb2-Sos + RasGDP $\leftrightarrow$ FAKP(-RasGAP)-ShcP317-Grb2-Sos-RasGDP	k15=k11;	s <sup>-1</sup>	k15b=1.3;	s <sup>-1</sup>	51	Estimate based on (14)
FAKPP(-RasGAP)-Grb2-Sos/FAKP(-RasGAP)-ShcP317-Grb2-Sos-RasGDP $\leftrightarrow$ FAKPP(-RasGAP)-Grb2-Sos/FAKP(-RasGAP)-ShcP317-Grb2-Sos + RasGTP	k16=.5;	s <sup>-1</sup>	k16b=1e5;	M <sup>-1</sup> s <sup>-1</sup>	52	Estimate based on (14)
FAKPP(-RasGAP)-Grb2-Sos $\leftrightarrow$ FAKPP(-RasGAP) + Grb2-Sos	k17=.055;	s <sup>-1</sup>	k17b=3.29e6;	M <sup>-1</sup> s <sup>-1</sup>	53	Chook et al.
FAKP(-RasGAP)-ShcP317-Grb2-Sos $\leftrightarrow$ Grb2-Sos + FAKP(-RasGAP)-ShcP317	k18=4.76e-2;	s <sup>-1</sup>	k18b=1.39e7;	M <sup>-1</sup> s <sup>-1</sup>	54	Estimate based on (7)
ShcP239-Grb2-Sos $\leftrightarrow$ ShcP239 + Grb2-Sos	k46=.31;	s <sup>-1</sup>	k46b=1e7;	M <sup>-1</sup> s <sup>-1</sup>	55	Estimate based on (14)
ShcP317-Grb2-Sos $\leftrightarrow$ ShcP317 + Grb2-Sos	k19=.1;	s <sup>-1</sup>	k19b=2.9e7;	M <sup>-1</sup> s <sup>-1</sup>	56	(4)
FAKP(-RasGAP)-ShcP317-Grb2-Sos $\leftrightarrow$ FAKP(-RasGAP) + ShcP317-Grb2-Sos	k20=.1;	s <sup>-1</sup>	k20b=4.24e6;	M <sup>-1</sup> s <sup>-1</sup>	57	Estimate based on (14)
Grb2-Sos $\leftrightarrow$ Grb2 + Sos	k21=1.5e-3;	s <sup>-1</sup>	k21b=1e5;	M <sup>-1</sup> s <sup>-1</sup>	58	Estimate based on (13) & (7)
ShcP317-Grb2 + Sos $\leftrightarrow$ ShcP317-Grb2-Sos	k48=3e7;	M <sup>-1</sup> s <sup>-1</sup>	k48b=6.4e-2;	s <sup>-1</sup>	59	(14)
ShcP239-Grb2 + Sos $\leftrightarrow$ ShcP239-Grb2-Sos	k49=3e7;	M <sup>-1</sup> s <sup>-1</sup>	k49b=6.4e-2;	s <sup>-1</sup>	60	(14)
FAKPP-RasGAP-Grb2-Sos + RasGTP* $\leftrightarrow$ FAKPP-RasGAP-Grb2-Sos-RasGTP	k22=2.1e6;	M <sup>-1</sup> s <sup>-1</sup>	k22b=.4;	s <sup>-1</sup>	61	(14)
FAKP-RasGAP-ShcP317-Grb2-Sos + RasGTP* $\leftrightarrow$ FAKP-RasGAP-ShcP317-Grb2-Sos-RasGTP	k23=k22;	M <sup>-1</sup> s <sup>-1</sup>	k23b=.4;	s <sup>-1</sup>	62	(14)
FAKPP-RasGAP-Grb2-Sos-RasGTP $\leftrightarrow$ FAKPP-RasGAP-Grb2-Sos + RasGDP	k24=2.3e-2;	s <sup>-1</sup>	k24b=2.2e6;	M <sup>-1</sup> s <sup>-1</sup>	63	(14)
FAKP-RasGAP-ShcP317-Grb2-Sos-RasGTP $\leftrightarrow$ FAKP-RasGAP-ShcP317-Grb2-Sos + RasGDP	k25=2.3e-2;	s <sup>-1</sup>	k25b=k24b;	M <sup>-1</sup> s <sup>-1</sup>		(14)
FAKPP-RasGAP(-Grb2)/FAKP-RasGAP(-ShcP317)(-Grb2) + RasGTP* $\leftrightarrow$ FAKPP-RasGAP(-Grb2)-RasGTP/FAKP-RasGAP(-ShcP317)(-Grb2)-RasGTP	k53=2.1e6;	M <sup>-1</sup> s <sup>-1</sup>	k53b=.4;	s <sup>-1</sup>	64	
FAKPP-RasGAP(-Grb2)-RasGTP $\leftrightarrow$ FAKPP-RasGAP(-Grb2) + RasGDP	k54=k24;	s <sup>-1</sup>	k54b=k24b;	M <sup>-1</sup> s <sup>-1</sup>		
FAKP-RasGAP(-ShcP317)(-Grb2)-RasGTP $\leftrightarrow$ FAKP-RasGAP(-ShcP317)(-Grb2) + RasGDP	k55=k25;	s <sup>-1</sup>	k55b=k25b;	M <sup>-1</sup> s <sup>-1</sup>		
<b>Raf, MEK, ERK Pathway</b>						
Raf + RasGTP $\leftrightarrow$ Raf-RasGTP	k26=1e6;	M <sup>-1</sup> s <sup>-1</sup>	k26b=.0054;	s <sup>-1</sup>	65	(14)
Raf-RasGTP $\leftrightarrow$ Raf* + RasGTP*	k27=1;	s <sup>-1</sup>	k27b=7e5;	M <sup>-1</sup> s <sup>-1</sup>	66	(14)
Raf* + Phosphatase1 sphatase1 $\leftrightarrow$ Raf*-Phosphatase1	k28=7.17e7;	M <sup>-1</sup> s <sup>-1</sup>	k28b=.2;	s <sup>-1</sup>	67	(14)
Raf*-Phosphatase1 $\rightarrow$ Raf + Phosphatase1	k29=1;	s <sup>-1</sup>			68	(14)
MEK + Raf* $\leftrightarrow$ MEK-Raf*	k30=1.11e7;	M <sup>-1</sup> s <sup>-1</sup>	k30b=.01833;	s <sup>-1</sup>	69	(14)
MEK-Raf* $\rightarrow$ MEK-P + Raf*	k31=3.5;	s <sup>-1</sup>			70	(14)
MEK-P + Raf* $\leftrightarrow$ MEK-P-Raf*	k32=1.11e7;	M <sup>-1</sup> s <sup>-1</sup>	k32b=.01833;	s <sup>-1</sup>	71	(14)
MEK-P-Raf* $\rightarrow$ MEK-PP + Raf*	k33=2.9;	s <sup>-1</sup>			72	(14)
MEK-PP + Phosphatase2 $\leftrightarrow$ MEK-PP-Phosphatase2	k34=1.43e7;	M <sup>-1</sup> s <sup>-1</sup>	k34b=.8;	s <sup>-1</sup>	73	(14)
MEK-PP-Phosphatase2 $\rightarrow$ MEK-P + Phosphatase2	k35=.058;	s <sup>-1</sup>			74	(14)
MEK-P + Phosphatase2 $\leftrightarrow$ MEK-P-Phosphatase2	k36=2.5e5;	M <sup>-1</sup> s <sup>-1</sup>	k36b=.5;	s <sup>-1</sup>	75	(14)
MEK-P-Phosphatase2 $\rightarrow$ MEK + Phosphatase2	k37=.053;	s <sup>-1</sup>			76	(14)
ERK + MEK-PP + MEK-PP $\leftrightarrow$ ERK-MEK-PP	k38=1.1e5;	M <sup>-1</sup> s <sup>-1</sup>	k38b=.033;	s <sup>-1</sup>	77	(14)
ERK-MEK-PP $\rightarrow$ ERK-P + MEK-PP	k39=16;	s <sup>-1</sup>			78	(14)

Table 2, continued						
Reaction	kf	Units	kr	Units	SA Parameter #	Reference
ERK-P + MEK-PP ↔ ERK-P-MEK-PP	k40=1.1e5;	M <sup>-1</sup> s <sup>-1</sup>	k40b=.033;	s <sup>-1</sup>	79	(14)
ERK-P-MEK-PP → ERK-PP + MEK-PP	k41=5.7;	s <sup>-1</sup>			80	(14)
ERK-PP + Phosphatase3 ↔ ERK-PP-Phosphatase3	k42=1.45e7;	M <sup>-1</sup> s <sup>-1</sup>	k42b=.6;	s <sup>-1</sup>	81	(14)
ERK-PP-Phosphatase3 → ERK-P + Phosphatase3	k43=.27;	s <sup>-1</sup>			82	(14)
ERK-P + Phosphatase3 ↔ ERK-P-Phosphatase3	k44=5e6;	M <sup>-1</sup> s <sup>-1</sup>	k44=5e6;	M <sup>-1</sup> s <sup>-1</sup>	83	(14)
ERK-P-Phosphatase3 → ERK + Phosphatase3	k45=.3;	s <sup>-1</sup>			84	(14)
<b>Src Activation</b>						
pY527cSrc ↔ pY527oSrc	kopen=.1;	s <sup>-1</sup>	kclose=kopen/(.7e-6);	M <sup>-1</sup> s <sup>-1</sup>	85; 86	(17)
pY527cSrc (+SHP2) → Src	kcatSHP2=.28;		KmSHP2=12e-6*10;	M	87; 88	
pY527oSrc (+SHP) → Src	kcatSHP=.28;	s <sup>-1</sup>	KmSHP=12e-6;	M	89; 90	(18)
Src (+Csk) → pY527oSrc	kcatCsk=53.8;	min <sup>-1</sup>	KmCsk=5.7e-6;	M	91; 92	(9)
Src → Src <sub>membrane</sub>	kt=.1	s <sup>-1</sup>			93	Estimate - phenomenological rate constant
Src <sub>m</sub> → pY416Src <sub>m</sub>	kcatauto=500;	min <sup>-1</sup>	Kmauto=134e-6;		94; 95	(2)
pY416Src <sub>m</sub> (+Csk) → pY416+pY527oSrc <sub>m</sub>	kcatCsk=53.8;	s <sup>-1</sup>	KmCsk=5.7e-6;	M		(9)
pY416+pY527oSrc <sub>m</sub> ↔ pY416+pY527cSrc <sub>m</sub>	kopen2=.1;	s <sup>-1</sup>	kclose2=kopen2/Kd2;	s <sup>-1</sup>	96; 97	Kd2=.6; Estimate
pY416+pY527oSrc <sub>m</sub> (+PTP1B) → pY527oSrc <sub>m</sub>	kcatPTP1B=20;	s <sup>-1</sup>	KmPTP1B=9e-6;	M	98; 99	(19)
pY416+pY527cSrc <sub>m</sub> (+PTP1B) → pY527cSrc <sub>m</sub>	kcatPTP1B2=11;	s <sup>-1</sup>	KmPTP1B2=4.5e-3;	M	100; 101	Estimate based on (12) & (19)
pY527cSrc <sub>m</sub> ↔ pY527Src <sub>m</sub>	kopen=.1;	s <sup>-1</sup>	kclose=kopen/(.7e-6);	M <sup>-1</sup> s <sup>-1</sup>		(17)
pY527cSrc <sub>m</sub> ↔ Src <sub>m</sub>	kcatPTPa2=10;	s <sup>-1</sup>	KmPTPa2=KmPTPa*10	M	102; 103	Estimate based on (12)
pY527oSrc <sub>m</sub> (+PTPa) → Src <sub>m</sub>	kcatPTPa=10;	s <sup>-1</sup>	KmPTPa=50e-4;	M	104; 105	(12)
c = closed (intramolecular)						
o = open						
m = membrane localized						
<b>Protein Concentrations</b>			<b>Source</b>			
Phosphatase 1 (MAPK cascade)	3.76E-08	M	(14)		13	
Phosphatase 2	3.76E-08	M	(14)		14	
Phosphatase 3	9.40E-06	M	(14)		15	
Csk	3.00E-08	M	Estimate		16	
PTP1B	5.00E-08	M	Estimate		17	
PTPa	5.00E-08	M	Estimate		18	
SHP factor ([FAKact]*factor)	3.50E+00				19	
FAK	2.00E+06	#			1	
RasGAP	3.00E-08	M			2	
Src	9.00E-08	M			3	
Shc	9.49E-07	M			4	
Grb2	4.79E-08	M			5	
Sos	6.23E-08	M			6	
Ras	1.07E-05	M			7	
Raf	1.76E-07	M			8	
MEK	2.07E-05	M			9	
ERK	1.97E-05	M			10	
Rt	3.33E+10	#/cm2			11	
Lt	3.10E+11	#/cm2			12	
<b>Other constants</b>						
Cell volume	1.77E-12	L	(14)			
Maximum Cell-Surface Contact Area	1.90E-05	cm <sup>2</sup>	(6)		106	
<b>References</b>						
1. Batzer, A.G., Rotin, D., Urena, J.M., Skolnik, E.Y. & Schlessinger, J. Hierarchy of binding sites for Grb2 and Shc on the epidermal growth factor receptor. Mol. Cell. Biol. 14, 5192-5201 (1994).						
2. Boerner RJ, Kassel DB, Barker SC, Ellis B, DeLacy P, Knight, WB. 1996. Correlation of the phosphorylation states of pp60c-src with tyrosine kinase activity: the intramolecular pY530-SH2 complex retains significant activity if Y419 is phosphorylated. Biochemistry 35(25):9519-9525						
3. Bradshaw JM and Waksman G. 1998 Calorimetric investigation of proton linkage by monitoring both the enthalpy and association constant of binding: application to the interaction of the Src SH2 domain with a high-affinity tyrosyl phosphopeptide. Biochemistry 37(44):15400-15407						
4. Chook YM, Gish GD, Kay CM, Pai EF, Pawson T. 1996. The Grb2-mSos1 complex binds phosphopeptides with higher affinity than Grb2. J Biol Chem 271(48):30472-8						
5. Felder S, Zhou M, Hu P, Urena J, Ullrich A, Chaudhuri M, White M, Shoelson SE, Schlessinger J. 1993 SH2 domains exhibit high-affinity binding to tyrosine-phosphorylated peptides yet also exhibit rapid dissociation and exchange. Mol Cell Biol 13(3):1449-1455						
6. Giannone G, Dubin-Thaler BJ, Dobereiner HG, Kieffer N, Bresnick AR, Sheetz MP. 2004 Periodic lamellipodal contractions correlate with rearward actin waves. Cell 116(3):431-443						
7. Kholodenko BN, Demin OV, Moehren G, Hoek JB. 1999 Quantification of short term signaling by the epidermal growth factor receptor. J Biol Chem 274(42):30169-30181						
8. Ladbury JE, Lemmon MA, Zhou M, Green J, Botfield MC, Schlessinger J. 1995. Measurement of the binding of tyrosyl phosphopeptides to SH2 domains: a reappraisal. Proc Natl Acad Sci USA 92(8):3199-3203						
9. Lee S, Lin X, Nam NH, Parang K, Sun G. 2003. Determination of the substrate-docking site of protein tyrosine kinase C-terminal Src kinase Proc Natl Acad Sci, 100(25):14707-14712						
10. Matsuda M, Ota S, Tanimura R, Nakamura H, Matuoka K, Takenawa T, Nagashima K, Kurata T. 1996 Interaction between the amino-terminal SH3 domain of CRK and its natural target proteins. J Biol Chem. 271(24):14468-14472						
11. Payne G, Shoelson SE, Gish GD, Pawson, T Walsh CT. 1993 Kinetics of p56lck and p60src Src homology 2 domain binding to tyrosine-phosphorylated peptides determined by a competition assay or surface plasmon resonance. Proc Natl Acad Sci USA 90(11):4902-4906						
12. Peters GH						



# A Human Breast Cell Model of Preinvasive to Invasive Transition

Aylin Rizki,<sup>1</sup> Valerie M. Weaver,<sup>2</sup> Sun-Young Lee,<sup>1</sup> Gabriela I. Rozenberg,<sup>2</sup> Koei Chin,<sup>3</sup> Connie A. Myers,<sup>1</sup> Jamie L. Bascom,<sup>1</sup> Joni D. Mott,<sup>1</sup> Jeremy R. Semeiks,<sup>1</sup> Leslie R. Grate,<sup>1</sup> I. Saira Mian,<sup>1</sup> Alexander D. Borowsky,<sup>4</sup> Roy A. Jensen,<sup>5</sup> Michael O. Idowu,<sup>6</sup> Fanqing Chen,<sup>1</sup> David J. Chen,<sup>1,7</sup> Ole W. Petersen,<sup>8</sup> Joe W. Gray,<sup>1,4</sup> and Mina J. Bissell<sup>1</sup>

<sup>1</sup>Life Sciences Division, Ernest Orlando Lawrence Berkeley National Laboratory, Berkeley, California; <sup>2</sup>Department of Pathology and Institute for Medicine and Engineering, University of Pennsylvania, Philadelphia, Pennsylvania; <sup>3</sup>Department of Laboratory Medicine and Comprehensive Cancer Center, University of California, San Francisco, California; <sup>4</sup>Department of Pathology and Laboratory Medicine and Center for Comparative Medicine, University of California, Davis, California; <sup>5</sup>Kansas Masonic Cancer Research Institute, Kansas City, Kansas; <sup>6</sup>Department of Pathology, Virginia Commonwealth University, Richmond, Virginia; <sup>7</sup>Department of Radiation Oncology, UT Southwestern Medical Center at Dallas, Dallas, Texas; and <sup>8</sup>Department of Cellular and Molecular Medicine, Faculty of Health Sciences, University of Copenhagen, Copenhagen, Denmark

## Abstract

A crucial step in human breast cancer progression is the acquisition of invasiveness. There is a distinct lack of human cell culture models to study the transition from preinvasive to invasive phenotype as it may occur “spontaneously” *in vivo*. To delineate molecular alterations important for this transition, we isolated human breast epithelial cell lines that showed partial loss of tissue polarity in three-dimensional reconstituted basement membrane cultures. These cells remained noninvasive; however, unlike their nonmalignant counterparts, they exhibited a high propensity to acquire invasiveness through basement membrane in culture. The genomic aberrations and gene expression profiles of the cells in this model showed a high degree of similarity to primary breast tumor profiles. The xenograft tumors formed by the cell lines in three different microenvironments in nude mice displayed metaplastic phenotypes, including squamous and basal characteristics, with invasive cells exhibiting features of higher-grade tumors. To find functionally significant changes in transition from preinvasive to invasive phenotype, we performed attribute profile clustering analysis on the list of genes differentially expressed between preinvasive and invasive cells. We found integral membrane proteins, transcription factors, kinases, transport molecules, and chemokines to be highly represented. In addition, expression of matrix metalloproteinases MMP9, MMP13, MMP15, and MMP17 was up-regulated in the invasive cells. Using small interfering RNA-based approaches, we found these MMPs to be required for the invasive phenotype. This model provides a new tool for dissection of mechanisms by which preinvasive breast cells could acquire invasiveness in a metaplastic context. [Cancer Res 2008;68(5):1378–87]

## Introduction

Breast carcinomas are phenotypically and behaviorally heterogeneous (1). Subtypes of breast cancer with distinct behavioral characteristics have been recognized morphologically as well as by molecular analyses. For all breast cancers, conversion to the invasive phenotype is distinct from metastasis but is an obligate prerequisite for metastasis, thus representing a crucial step in cancer progression. Molecular profiling studies have begun to determine markers that are associated with progression in different breast cancer subtypes (2–17). Relevant models that recapitulate the morphologic and molecular aspects of progression within subtypes are needed to determine which of these molecular changes function in acquisition of the invasive phenotype.

Culture models of human breast cells could provide such an opportunity if relevance to cancer progression *in vivo* were established. Pathways associated with transition to malignancy have traditionally been studied using either transgenic mouse models or primary human cells engineered to express genes with oncogenic properties. To deal with the heterogeneity of human breast tumors, cell lines originating from a large number of malignant breast carcinomas have been used (18). It would also be useful to have models of “spontaneous” transition to malignancy, as opposed to transgenic, which could include intermediate noninvasive and preinvasive stages of carcinogenesis, as opposed to modeling only the invasive carcinoma stage. Such models could facilitate the discovery of steps in progression to the invasive phenotype in a context that recapitulates more the complexity of carcinogenesis.

The HMT-3522 human breast epithelial cell line series (S1, S2, and T4-2) were derived from a reduction mammoplasty specimen of a patient with fibrocystic breast disease more than 20 years ago. The epithelial component of the tissue was grown in defined medium to give rise to S1 cells that became immortalized spontaneously; these cells are epidermal growth factor (EGF) dependent for growth and are nontumorigenic (19). Continuous culturing in the absence of EGF gave rise to a cell population referred to as S2, a cell line that is heterogeneous and essentially still nonmalignant (20). Inoculation of S2 cells into mice produced a rare tumor that was cultured and passaged again through mice (20). The cell line derived from this tumor is referred to as T4-2 (20). Previously, we designed a three-dimensional laminin-rich basement membrane (3DlrbM) assay to model both the normal breast and breast cancers (ref. 21; Fig. 1A). In 3DlrbM, S1 cells produce growth-arrested acini that express differentiation markers mimicking *in vivo* polar patterns of localization of a number of

**Note:** Supplementary data for this article are available at Cancer Research Online (<http://cancerres.aacrjournals.org/>).

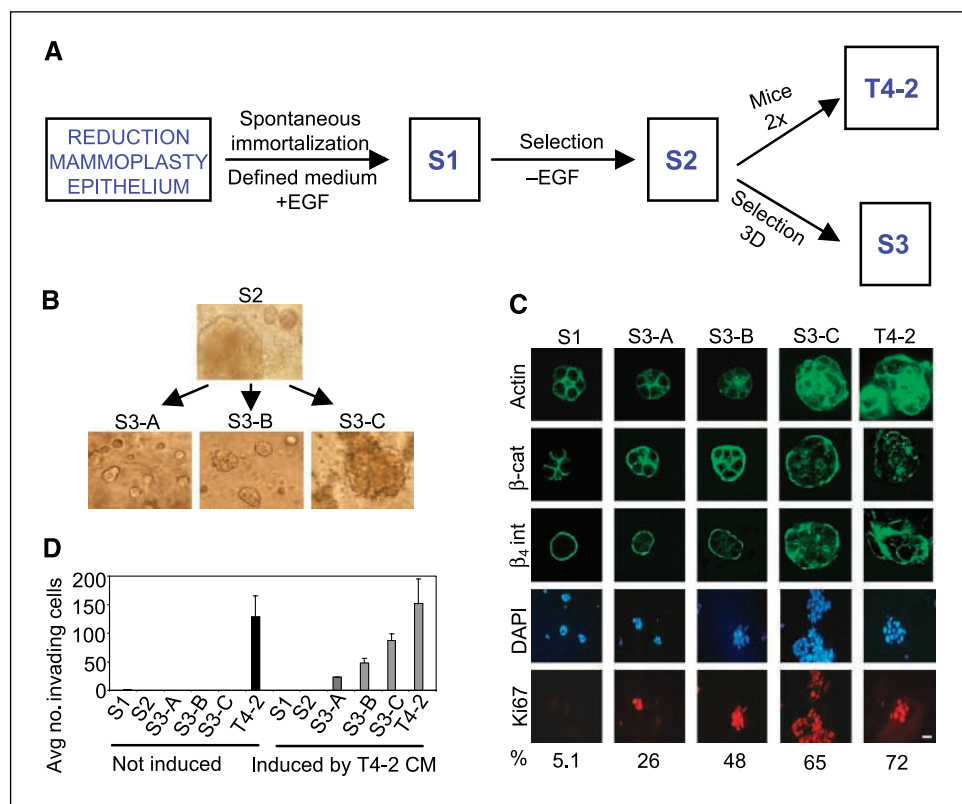
Current address for A. Rizki: Department of Radiation Oncology, Virginia Commonwealth University, Richmond, VA 23298; Current address for C.A. Myers: Department of Pathology and Immunology, Washington University, St. Louis, MO 63110; Current address for L.R. Grate: Molecular, Cell, and Developmental Biology Department, University of California at Santa Cruz, Santa Cruz, CA 95064.

**Requests for reprints:** Mina J. Bissell or Aylin Rizki, Life Sciences Division, Ernest Orlando Lawrence Berkeley National Laboratory, One Cyclotron Road, Mailstop 977R225A, Berkeley, CA 94720. Phone: 510-486-4365; Fax: 510-486-5586; E-mail: MJBissell@lbl.gov or ARizki@vcu.edu.

©2008 American Association for Cancer Research.

doi:10.1158/0008-5472.CAN-07-2225

**Figure 1.** Partial loss of tissue polarity and preinvasive phenotypes of S3 cells. **A**, steps involved in the isolation of the HMT-3522 series of cell lines. **B**, 3DlBrM cultures of HMT-3522-S2 cells and small (S3-A), medium (S3-B), and large (S3-C) colonies isolated from the parent culture of S2 on day 10. **C**, confocal images of immunostained colonies in 3DlBrM, day 10. **D**, invasion assays: two experiments, triplicate samples. *Black columns*, untreated cells; *gray columns*, cells treated with T4-2 conditioned medium (CM).



markers (21): S2 colonies are heterogeneous (this study) and T4-2 cells form large and disorganized colonies (22).

Here, we isolated three essentially homogeneous cell populations from S2 cells, which we refer to as S3-A, S3-B, and S3-C, using colony size in 3DlBrM as a screening tool (Fig. 1A). These cells were noninvasive but had a higher potential for acquiring invasiveness than the parent S2. We found a substantial number of similarities between the model of S3 versus T4-2 and preinvasive to invasive transition in breast carcinogenesis based on progressive loss of tissue polarity, ability to form tumors with squamous and basal metaplastic histology, 76% similarity to recurrent comparative genomic hybridization (CGH) abnormalities found in breast tumors, and gene expression changes in classes of genes previously identified as being important for malignancy and invasion. These observations establish the S3 cell lines as the preinvasive counterpart of a model of breast cancer progression within a metaplastic context. Using matrix metalloproteinases (MMP), we show the utility of this model in identifying functionally significant changes in transition from the preinvasive to the invasive phenotype in metaplastic breast cancer. The usefulness of the model is further shown in another report (23), which describes the discovery of a novel pathway involved in invasion using this progression series.

## Materials and Methods

### Cell Culture

S1 and T4-2 cells were grown in tissue culture monolayers two-dimensionally using Falcon tissue culture plastic or three-dimensionally in laminin-rich basement membrane (Matrigel) in defined medium as previously described (21, 22); S2 and S3 cells were grown under the same conditions as T4-2.

### Indirect Immunofluorescence Analysis and Image Acquisition in 3DlBrM

Cells in 3DlBrM were perfused in sucrose and frozen on dry ice in Tissue-Tek optimum cutting temperature (Miles Laboratories), sectioned, and immunostained as previously described (22).

### Comparative Genomic Hybridization

Chromosomal CGH and BAC array CGH were done essentially as previously described (24). Hierarchical clustering analysis was done with GeneSpring software (Silicon Genetics), using standard correlation with a minimum distance metric of 0.001 to determine relatedness of cell lines. This was done using both the chromosomal and the BAC array data, with only significant amplification/deletion data points, as well as with the complete data sets, producing comparable results.

### Analysis of Tumor Formation *In vivo*

We injected the cells into female BALB/c athymic nude mice (Simonsen Laboratories), measured tumors weekly with a caliper, and graphed the tumor frequency and volumes of tumors taken out after 9 to 10 weeks of tumor growth, at which time the animals were sacrificed. Statistical analysis of the mean tumor volumes was done by pairwise comparison using one-tailed homoscedastic *t* test analysis. We injected 10 million cells s.c. into the rear flanks, 5 million cells in 50% Matrigel s.c. into the front flanks, or 2 million cells into the left and right fourth inguinal mammary glands. Tumors from all injections and surrounding tissues were fixed in 4% formaldehyde, paraffin embedded, sectioned into 5-μm slices, and stained with H&E (HRL Laboratories). Three hundred fifty H&E sections were independently examined by two expert breast pathologists (A.D.B. and R.A.J.).

### Global mRNA Expression Analysis by cDNA Microarrays

cDNA microarrays with ~8,000 known gene spots on poly-L-lysine-coated chips (custom arrayed at LBNL using Research Genetics 8k human clones) were used. mRNA samples were directly compared with each other by cohybridization to the same slide using dendrimer technology to label with red-Cy5 or green-Cy3 (Genisphere). Total RNA

(1  $\mu$ g) isolated with Qiagen RNeasy reagents was used for each sample hybridized. Cells in 3Dlrbm were extracted with 5 mmol/L EDTA in cold PBS to dissolve the Matrigel. For each comparison, three independent sets of cultures were processed, and cells were examined at day 10 of culture. For each comparison, four slides were hybridized. This corresponded to three sets of RNAs from independent cultures plus a dye-swap experiment in which the red and green labels were switched for the two samples in question. Data were analyzed as described in Supplementary File 8.

### Reverse Transcription-PCR

**Quantitative.** The RNA prepared for microarrays was used to prepare cDNA after DNase I (Invitrogen) treatment, using Superscript First-Strand Synthesis System for reverse transcription-PCR (RT-PCR; Invitrogen). Quantitative real-time PCR was done using LightCycler (Roche) and FastStart SYBR Green (Roche). Primer sequences were as follows (5'-3'): MMP13 forward, aagatgcatccagggtctct; MMP13 reverse, gtcagggttcatcatcatca; glyceraldehyde-3-phosphate dehydrogenase (GAPDH) forward, ccctggccaaggtcatcatcatgac; and GAPDH reverse, caccagggaatgagcttgacaag. LightCycler reaction cycles were as recommended by Roche with the following modifications: for MMP13, 57°C for annealing, 27 seconds of extension, and signal acquisition at 84°C; for GAPDH, 56°C for annealing and 25 seconds for extension.

**Semiquantitative.** For MMP9, MMP13, MMP15, and MMP17, semiquantitative RT-PCR was done using the following primer sets (5'-3'): MMP9, atcgctggagagtcgaatc (forward) and tacacgcgagtgaggtgag (reverse); MMP13, aagatgcatccagggtctct (forward) and gtcagggttcatcatcatca (reverse); MMP15, ccatatgtccaccatgcgtt (forward) and atgatggcattgggtgtgct (reverse); and MMP17, acgcaaggagagctgtctaa (forward) and acatggcttaaccatggc (reverse). The conditions used (after having determined linear range) were, for MMP9, MMP15, and MMP17, 96°C 3 minutes, 34  $\times$  (96°C 30 seconds, 55°C 1 minutes, 72°C 1 minutes), 72°C 5 minutes; for MMP13, 96°C 3 minutes, 29  $\times$  (96°C 30 seconds, 55°C 30 seconds, 72°C 1 minutes), 72°C 5 minutes.

### Expression Analysis of Cell-Surface Proteins by Fluorescence-Activated Cell Sorting

Live cells were immunostained in suspension before fixing with 2% paraformaldehyde. Primary antibodies were used at 1:10 dilution, and FITC-conjugated secondary antibodies were used at 1:100 dilution. Primary antibodies were MMP15, clone 162-22G5 (Oncogene); MMP17, rabbit polyclonal 475934 (Calbiochem). Fluorescence-activated cell sorting (FACS) analysis was done using EPICS XL-MCL data acquisition and display software on XL flow cytometry analyzers (University of California Berkeley, Flow Cytometry Facility). Gating of forward light scatter versus light scatter (90-degree scatter) allowed us to obtain data relevant to intact cells only; FITC fluorescence peak was evaluated for its median value and was corrected using samples that had not been treated with primary antibody.

### Gelatin Zymography

Conditioned medium (for 48 hours) from 10-day cultures of S1, S2, S3, and T4-2 were used. Samples were analyzed by SDS-PAGE zymography (25) to determine the molecular weights and the relative abundance of the gelatinases present.

### Invasion Assay

The ability to invade through laminin-rich basement membrane (Matrigel) was measured in Boyden chamber assays, essentially as described (26). The number of invading T4-2 or S3-C cells (of  $1 \times 10^5$  seeded) was determined after 48 hours of incubation in regular growth medium, in medium containing T4-2 conditioned medium, in medium with DMSO with different concentrations of the MMP inhibitor GM6001 (AMS Scientific) or its inactive analogue (C1004), or in conditioned medium that had previously been treated with DMSO, GM6001, or C1004. For small interfering RNA (siRNA)-treated T4-2 cells, transfection of 30 to 150 nmol/L oligo with 4  $\mu$ L of siPORT NeoFX (Ambion) per milliliter of media was done 1 day after plating cells at regular density. siRNAs were allowed to down-regulate

protein levels for 2 days. Cells were then trypsinized and  $1 \times 10^5$  cells were seeded for Boyden chamber assays. siRNAs against MMP9 (oligo 1, Ambion ID143941; oligo 2, Ambion ID 113182; oligo 3, Ambion ID 113183), MMP13 (oligo 1, Ambion ID 143556; oligo 2, Ambion ID 212725; oligo 3, Ambion ID 112915), MMP15 (oligo 1, Ambion ID 112917; oligo 2, Ambion ID 143557; oligo 3, Ambion ID 112916), MMP17 (oligo 1, Ambion ID 105396; oligo 2, Ambion ID 113514; oligo 3, Ambion ID 24016), or scrambled control siRNA (Ambion, Silencer-Cy3 labeled) were used.

### Immunohistochemistry

**Ki67.** Formalin-fixed mouse xenograft tissue was paraffin embedded and sectioned into 5- $\mu$ m-thick tissue sections (HRL Laboratories). The paraffin was removed by serial incubation in xylene, 100% ethanol, 95% ethanol, 70% ethanol, and water. Tissues were blocked with 3% hydrogen peroxide in PBS for 5 minutes. Antigen retrieval was done by incubating in 0.01% prewarmed trypsin in PBS for 15 minutes, followed by 10 minutes of microwaving in 10 mmol/L sodium citrate buffer. Tissues were blocked in 1.5% normal horse serum in PBS for 30 minutes and incubated with primary Ki67 antibody, which specifically recognizes human, but not mouse, Ki67 protein [Calbiochem, anti-Ki67 human (mouse), NA59] at 5  $\mu$ g/mL overnight at 4°C. Slides were washed with PBS and incubated with biotinylated antirabbit antibody [1:200 dilution; Vector Laboratories, biotinylated antimouse IgG/antirabbit IgG (H + L), BA-1400] for 30 minutes at room temperature, followed by streptavidin-horseradish peroxidase (Vector Laboratories, Vectastain ABC kit, Elite PK-6100) for 30 minutes and complete 3,3'-diaminobenzidine tetrahydrochloride (Sigma) medium for 5 minutes. Slides were washed and counterstained with hematoxylin, followed by dehydration in 70% ethanol, 95% ethanol, 100% ethanol, and xylene; coverslips were mounted using Permount (Fisher Scientific, SP15). Strong nuclear staining was scored as positive and %Ki67 positive nuclei was determined for at least three tumor areas for each cell type injection, counting a minimum of 100 cells per area.

**p63.** Immunohistochemistry was done essentially as described for Ki67, except for omitting the trypsin step in antigen retrieval and increasing hydrogen peroxide blocking to 15 minutes. Primary antibody (Lab Vision, p63 Ab-1, clone 4A4) was used at 2  $\mu$ g/mL.

**CK5/6, estrogen receptor, and progesterone receptor.** Immunohistochemistry was done as described in ref. 27, using CK5/6 primary antibodies from Zymed (1:100), estrogen receptor from DAKO (1:25), and progesterone receptor from DAKO (1:200); for *HER2-neu*, the Herceptest kit from DAKO was used.

## Results

**S3 cells display partial loss of tissue polarity in 3Dlrbm, a preinvasive phenotype.** Using colony size in 3Dlrbm as an initial screen, we isolated multiple small-, medium-, and large-sized colonies; expanded and propagated these clones for at least six generations; and examined their morphology in the three-dimensional assay (Fig. 1B). We chose three isolates that essentially bred true for the size of colony formed. We refer to these as S3-A, S3-B, and S3-C cell lines where colony size is  $A < B < C$ . S3-A cultures contain  $\sim 10\%$  very large colonies (not shown); otherwise the colony size, especially for S3-Cs, is essentially homogeneous. S3 cells displayed intermediate phenotypes compared with S1 and T4-2 colonies in 3Dlrbm, as determined by markers that have been extensively used to describe tissue (acinar) polarity (22, 28-31), such as basolateral expression of  $\beta$ -catenin, basal  $\beta_4$  integrin, cortical actin, and Ki67 labeling (Fig. 1C). In Boyden chamber assays, S1, S2, and S3 cell lines did not invade laminin-rich basement membrane, but T4-2 cells were invasive (Fig. 1D). When conditioned medium from T4-2 cells was added to the chambers, S1 and S2 cells did not invade, whereas S3-A, S3-B, and S3-C became invasive, with the S3-C cells displaying the highest propensity to invade:  $T4-2 > C > B > A$ .

**S3 cells display an intermediate potential to form tumors.** We determined tumorigenicity of the cells when injected into nude mice under three different microenvironments: in the flank with cells alone or cells plus Matrigel, and into mammary fat pads with cells alone (Fig. 2). In none of the injections did S1 cells or media control produce any measurable growth but T4-2 cells formed palpable tumors at high frequency, as shown also previously (refs. 20, 22, 32, 33; Fig. 2A–C, *top*). When injected s.c., S2 cells and the S3 series formed very small tumors at low frequencies. S.c. injection in the presence of Matrigel (Fig. 2A–C, *middle*) resulted in tumor formation in 50% of S2, 75% of S3-A, 73% of S3-B, 56% of S3-C (see following section on tumor histology), and 100% of T4-2 cell injection sites. Importantly, mammary fat pad injections (Fig. 2A–C, *bottom*) resulted in progressively increasing tumor frequency going from S2, S3-A, S3-B, S3-C, to T4-2, mirroring the rate of invasion observed in Boyden chambers (Fig. 1D). Comparing the *P* values for tumor volume (Fig. 2C) showed that the mammary fat pad most clearly distinguished the nontumorigenic S1, the preinvasive S3, and the malignant T4-2.

**Tumor histology reveals similarities to cancer progression within a metaplastic context.** In s.c. injections (Supplementary File 1B), the T4-2 tumors had viable, dividing cells with squamous metaplastic morphology. The S2 and S3 tumors had nondividing cells, suggesting they did not maintain growth, but they contained keratin clusters and inflammatory cells, which are characteristics of well-differentiated squamous carcinomas of the breast. An average increase of 27-fold in tumor volume was observed when half the number of cells was injected in the presence of Matrigel. In the Matrigel injections (Fig. 2A–D, *middle*; Supplementary File 1A and C), 5 of 18 of the S1 injection sites showed a phenotype similar to low-grade adenosquamous carcinomas despite the lack of a palpable tumor at the time of sacrifice (Fig. 2J). Whereas 100% of the S2 and S3 tumors displayed the more benign mixed tumor histology, only 25% of the T4-2 tumors were mixed, with the remainder being pure squamous. In addition, T4-2 tumors had features of higher-grade squamous carcinoma than did the S2 and S3 tumors: 83% of the S2 and S3 tumors were well differentiated, compared with only 11% of the T4-2 tumors. Soft tissue involvement, indicating either invasion or proliferative expansion into neighboring tissues, was observed only in T4-2 tumors (Fig. 2J). Similarly, calcifications, which are an indication of necrosis usually observed in high-grade tumors, were found in almost all T4-2 tumors but only in a few of S2 or S3s. The fat pad tumor histology also showed similarities to squamous metaplasias of the breast (Fig. 2J; Supplementary File 1D), with T4-2 tumors being of higher “grade” in general based on the degree of differentiation, soft tissue involvement, and calcification phenotypes.

**S3 cells display genomic aberrations that are distinct from those found in S1 and T4-2, but are relevant to some human breast cancers.** We determined the genomically amplified or deleted regions by CGH (Supplementary File 2). The number of aberrations increased progressively when S1, S2-S3, and T4-2 cells were compared (Fig. 3A and B). Hierarchical clustering analysis (Fig. 3C) showed that the S2-S3 and T4-2 cell lines were more closely related to each other than they were to the S1 cells, and that the malignant T4-2 chromosomal aberration profiles were distinct from those of the S2-S3 cells. S2, S3, and T4-2 cell lines contained 76% (22 of 29) of the chromosomal gains or losses that are reported to be commonly found in

primary breast tumors (Fig. 3D; Supplementary File 2). Of the aberrations recurrently found in carcinoma *in situ* (preinvasive), 6 of 10 were present in S3-A, S3-B, and S3-C cells, but all 10 were found in T4-2. The aberrations that were present in T4-2, but not in S3, were those found in high-grade *in situ* or invasive carcinomas.

**Transition from S3-C to T4-2 phenotype is associated with altered expression of gene classes previously implicated in human breast cancer progression.** We determined differences in global gene expression between S3-C and T4-2 when cells were grown in either two-dimensional (monolayers) or 3DlRBM cultures (Supplementary File 3). To discover groups of genes with shared attributes in an unbiased manner, we analyzed these two sets of differentially expressed genes by model-based clustering according to their Gene Ontology (GO) terms and other annotations by developing and using a method called Attribute Profile Clustering (ref. 34; Supplementary File 8). The 141 genes altered between S3-C and T4-2 in two dimensions were divided into four groups summarized as integral membrane proteins, transcription factors, kinases, and transport molecules (Supplementary Files 4, 6, and 8). The groups for the 502 genes with different expression levels between S3-C and T4-2, when grown in three-dimensional cultures were integral membrane proteins, transcription factors, kinases, and chemokines (Supplementary Files 5, 7, and 8). The best-defined group in the comparison of S3-C and T4-2 in three dimensions, but not in two dimensions, revealed a class with 100% of the genes sharing the GO term “Chemokine Activity.” Chemokines have been shown previously to play a significant role in metastasis (35) and were shown to increase dramatically during human breast cancer progression (36).

**MMP9, MMP13, MMP15, and MMP17 are functionally significant in the acquisition of invasiveness.** In addition to the genes that were relevant to human breast cancer progression by attribute clustering analysis, the microarray data contained another class of genes, the MMPs, which showed differential expression when S3-C and T4-2 were compared only in 3DlRBM. Microarray analysis showed that MMP13 (collagenase-3), MMP15 (MT-2 MMP), and MMP17 (MT-4 MMP) had ~30% higher expression in T4-2 versus S3-C in three-dimensional cultures (Supplementary File 3). For MMP13, we confirmed these results by quantitative RT-PCR (Fig. 4A) and Western blots of conditioned medium (not shown). For the membrane-bound MMP15 and MMP17, FACS analysis showed that cell-surface expression was higher in T4-2 than in S3-C cells (Fig. 4B and C). MMP15 has been shown to activate proMMP2 by cleavage (37). Therefore, we determined overall gelatinolytic activity, including MMP2 and MMP9 activity, present in S1, S2, S3, and T4-2 cell lines using zymograms. S1 cells expressed proMMP2 but not MMP9; S2, S3-A, and S3-B had no detectable expression of MMP2 or MMP9; S3-C had a small amount of proMMP9 expression; and T4-2 showed high levels of proMMP9 but no MMP2 expression (Fig. 4D).

In this model, we could directly assess the significance of MMP expression changes for the invasive phenotype. A broad-spectrum MMP inhibitor, GM6001 (38), abrogated T4-2 invasiveness whereas treatment of cells with C1004, an inactive analogue of GM6001, had no detectable effect (Fig. 5B). To confirm the inhibitor data specifically, we used siRNAs to transiently and individually knock down the levels of MMP9, MMP13, MMP15, and MMP17 (Fig. 5A) and found that siRNAs that successfully



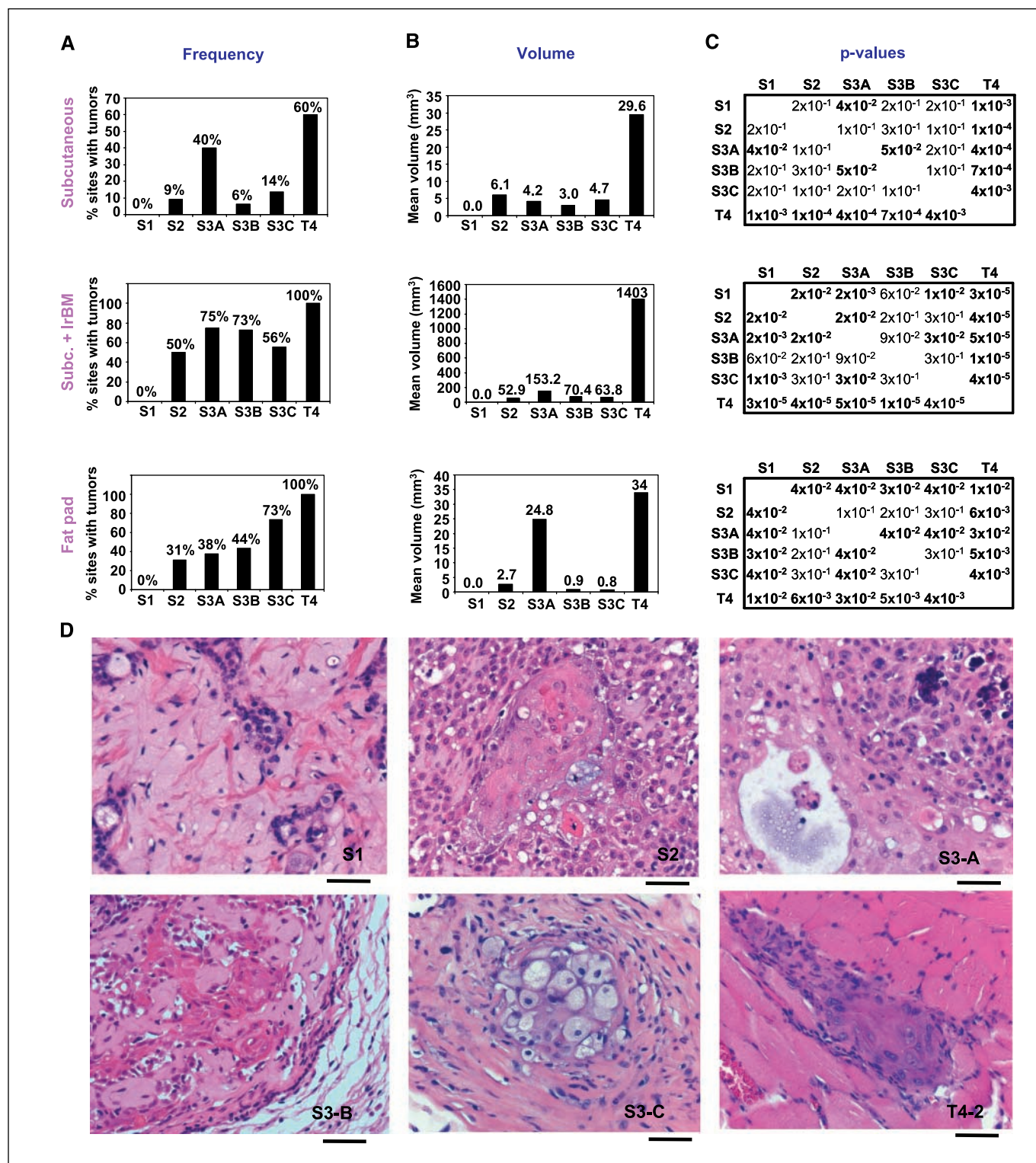


**Figure 2.** S3 cells display low tumorigenicity and squamous metaplastic phenotype in nude mice. *A*, percent injection sites that produced tumors sustained for the duration of the experiment. *Top*, s.c. injections (three experiments); 14 S1, 22 S2, 20 S3-A, 16 S3-B, 22 S3-C, 30 T4-2, and 3 media controls. *Middle*, s.c. + Matrigel (laminin-rich basement membrane, *IrBM*) injections (two experiments); 18 S1, 18 S2, 20 S3-A, 22 S3-B, 18 S3-C, and 18 T4-2 injections. *Bottom*, mammary fat pad injections; 15 S1, 16 S2, 16 S3-A, 16 S3-B, 15 S3-C, 24 T4-2, and 4 media controls. *B*, mean tumor volume (in mm<sup>3</sup>) excised from sacrificed animals. *C*, *P* values for the volume comparisons indicated; *P* < 0.05 in bold. *Top*, s.c. injections; *middle*, s.c. + Matrigel injections; *bottom*, mammary fat pad injections. *D*, H&E images of S1, S2, and S3-B s.c. + Matrigel tumors and of S3-A, S3-C, and T4-2 fat pad tumors. *Bar*, 50  $\mu$ m. S1, low-grade adenosquamous carcinoma-like phenotype at the injection site; S2, squamous differentiation with whorls and bridges, transition from cuboidal cells to larger squamous cells in the center; S3-A, well-differentiated area with a small cyst, less well differentiated area with calcification; S3-B, cords of cells surrounding areas of extracellular matrix showing solid tumor areas with proliferation and squamous differentiation and displaying pleomorphic adenoma phenotype; S3-C, squamous differentiation, foamy squamous carcinoma cells, abundant stromal reaction; T4-2, squamous carcinoma invading the skeletal muscle.

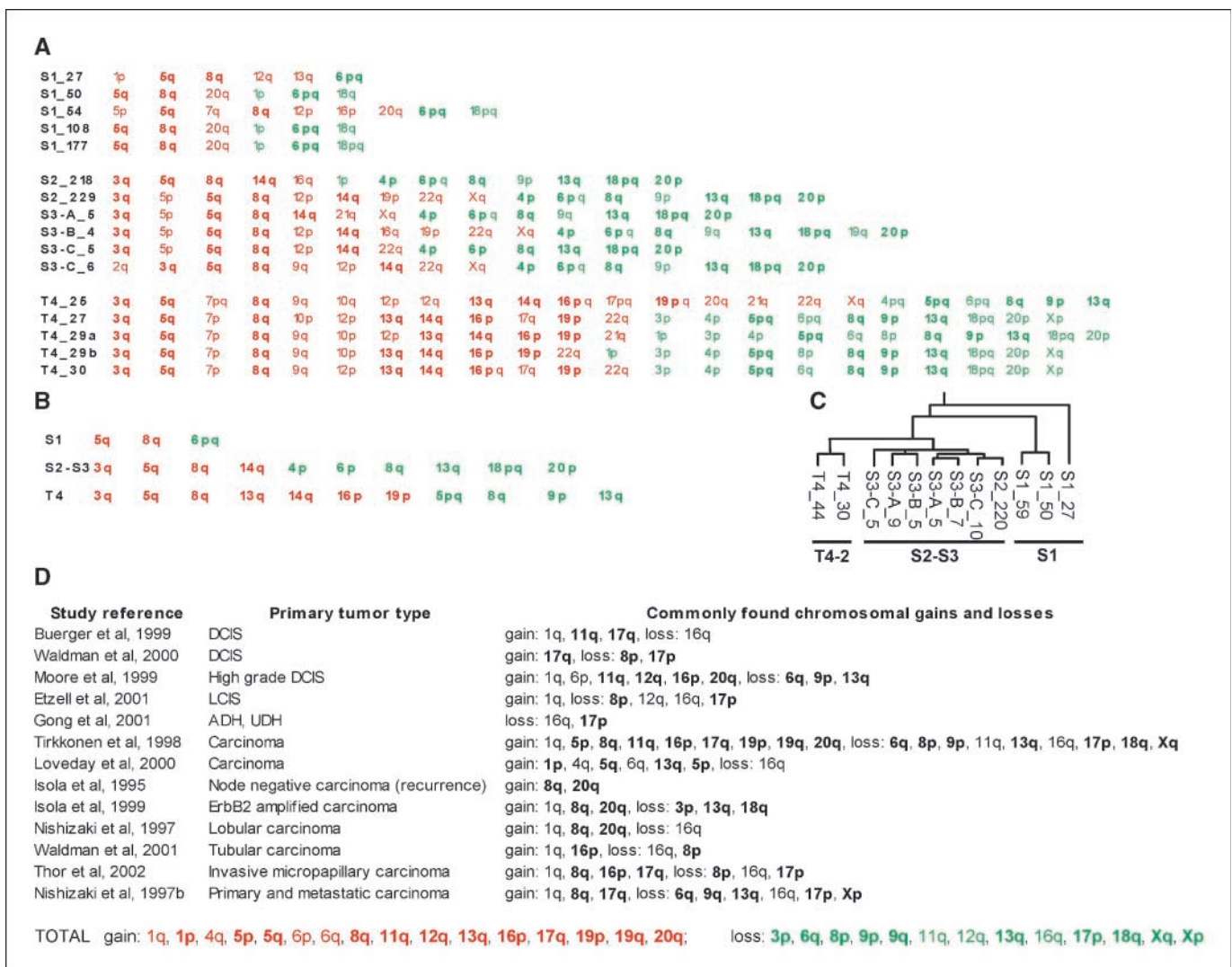


**Figure 3.** CGH profile of S3 cells compared with other HMT-3522 cells and with primary tumors (for details of CGH data, see Supplementary File 2). *A*, chromosomal amplifications (red) and deletions (green) for each cell type examined at the indicated passage number (e.g., S1\_27: S1 cells at passage 27). *B*, chromosomal aberrations common to all cell lines shown on the left (e.g., "S1" means common to all S1 lineages shown in *A*). *C*, hierarchical clustering of 119 significantly amplified or deleted regions for the indicated cell lines. *D*, chromosomal aberrations commonly found in primary tumors, as described in each study cited; shown in bold if shared with HMT-3522 cell lines; complete list of aberrations shared between the cell lines and primary tumors listed at the bottom (*TOTAL*).

knocked down these MMPs decreased the amount of invasiveness of T4-2 cells compared with the scrambled control siRNA (Fig. 5C). MMPs were important for acquisition of invasiveness in S3-C cells as well: addition of GM6001, and not the control

C1004, to either the S3-C or T4-2 media (the conditioned medium was taken from the latter) inhibited the ability of the T4-2 conditioned medium to induce invasiveness in S3-C (Fig. 5D).

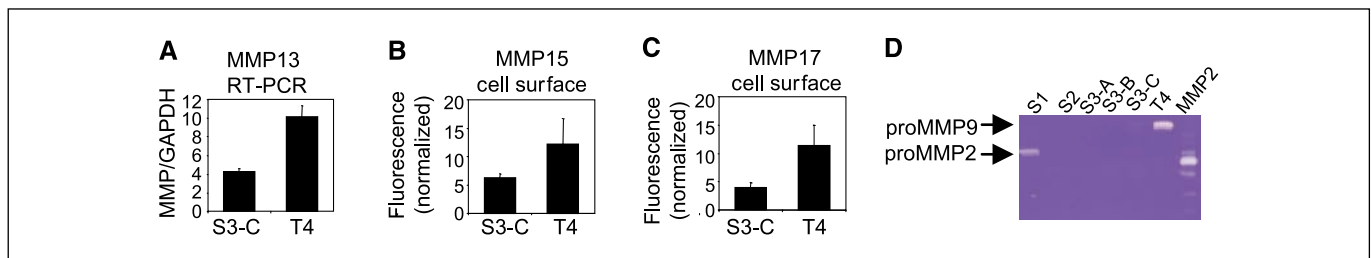


**Figure 4.** Candidate MMPs from microarrays are differentially expressed between S3-C and T4-2 cells. *A*, quantitative RT-PCR for MMP13, normalized to GAPDH internal control, for S3-C and T4-2 in 3DlBM ( $P < 0.05$ ). *B* and *C*, cell-surface expression of MMP15 and MMP17; four independent experiments ( $P < 0.05$ ). *D*, zymogram detecting gelatinolytic activity in cell lines, compared with *p*-aminophenylmercuric acetate-activated recombinant MMP2 control.

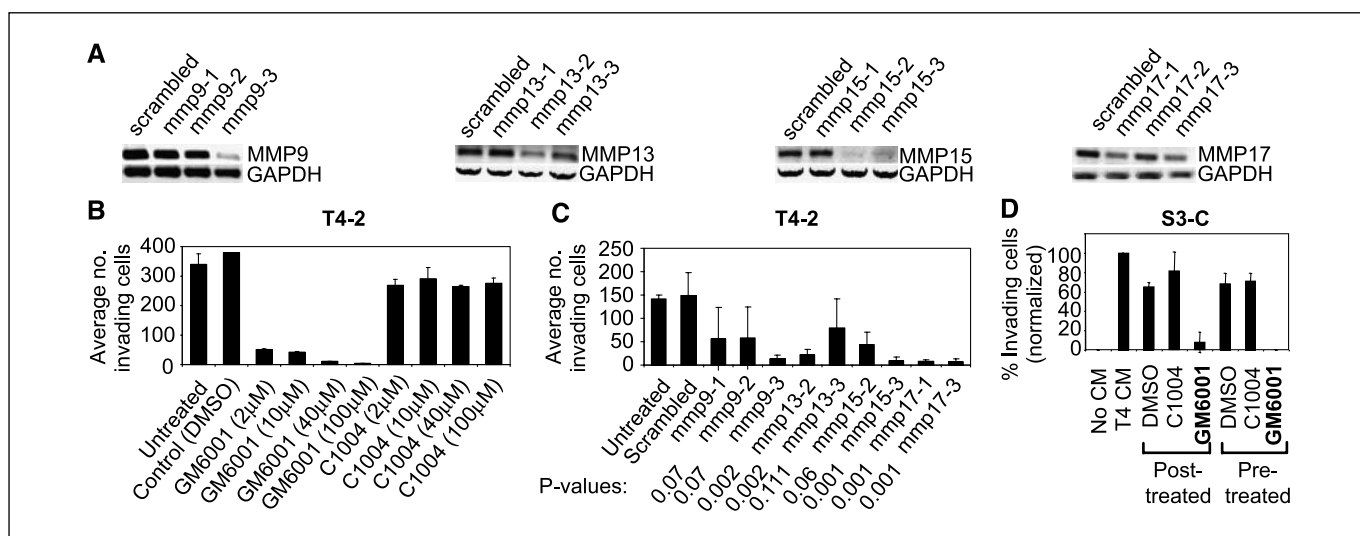


**Figure 5.** Candidate MMPs function in invasion through laminin-rich basement membrane. *A*, RT-PCR for MMP9, MMP13, MMP15, and MMP17 in cells transfected with siRNAs to the respective MMPs or a scrambled control. *B*, invasion assays for T4-2 cells treated with the indicated MMP inhibitor or control; two experiments, duplicate samples. *C*, invasion assays for T4-2 cells transfected with MMP9, MMP13, MMP15, or MMP17 siRNAs versus scrambled control; *P* values compared with scrambled control. *D*, invasion assays for S3-C cells; number of invading cells normalized to S3-C cells treated with T4-2 conditioned medium. *Posttreated*, conditioned medium was added to the S3-C medium after the indicated MMP inhibitor or control (40 μmol/L); *Pretreated*, conditioned medium was pretreated with the MMP inhibitor or control (40 μmol/L) for 48 h before being added to the S3-C medium in the invasion assays; three experiments.

## Discussion

Modeling human breast cancer in culture traditionally has relied on carcinoma-derived cell lines or addition of potent oncogenic stimuli to nonmalignant cells. What we have lacked thus far are models with which we can recapitulate intermediate stages of cancer progression to simulate the complexity of different types of breast cancers (39). Here we describe one such human cell culture model. Neither the process of immortalization nor the process of selection of the preinvasive S3 or malignant T4-2 cells entailed introduction of oncogenic transgenes. The T4-2 population was generated by removal of EGF but provides a transgene-free opportunity to study the involvement of different and possibly unrelated pathways in malignant transition (Table 1; Supplementary File 8). The cell lines produced tumors with various metaplastic features, such as rare low-grade adenosquamous carcinoma, mixed benign tumors, and aggressive squamous metaplasia, suggesting progression within a metaplastic context (Supplementary File 1).

Pure squamous carcinomas of the breast are rare, although mixed adenocarcinomas are diagnosed at a higher frequency (40). Some studies describe squamous metaplastic breast cancers as being extremely aggressive and they have been characterized to be at least as aggressive as grade 3 hormone receptor-negative adenocarcinomas (40–43). Five-year survival for patients with pure squamous carcinomas of the breast seems to be only marginally worse than what is reported for all breast cancers, although these comparisons suffer from lack of a sufficient number of squamous carcinomas with follow up data (41). Squamous metaplasias of the breast share similarities with the aggressive basal-like subtype of carcinomas in clinical behavior as well as in the expression of a panel of markers (40, 44). HMT-3522 cells resemble the basal-like subtype of breast cancers at the molecular level by gene expression profiling (45). In addition, the HMT-3522 xenograft tumors are p63 and CK5/6 positive as well as estrogen receptor, progesterone receptor, and HER2 negative (Supplementary File 1F and G), similar to squamous metaplastic

carcinomas (46). In addition to the rare pure squamous carcinomas of the breast, 39% of breast cancers in premenopausal African Americans and the majority of tumors in BRCA1 mutation carriers are estrogen receptor and progesterone receptor negative and have basal characteristics (47, 48). Understanding whether such similarities in marker expression translate to overlap in the mechanism of transition to invasiveness would require developing models that recapitulate these subtypes, as described for at least one subtype developed here.

The HMT-3522 cells display xenograft tumor histology consistent with the breast cancer type represented by their molecular makeup. This is a rare situation. Most human breast cancer cell line xenografts display an undifferentiated phenotype (observations of A.D.B.). To our knowledge, in addition to the cell line model described here, the MCF10A series of Ha-Ras transformed cell lines compose the only other model that recapitulates the histologic characteristics of human carcinomas (ductal carcinoma *in situ* and infiltrating ductal carcinoma) as xenograft tumors (49). To capture a more complete picture of the malignant progression *in vivo*, more complex microenvironments need to be created in three-dimensional cultures, and a number of laboratories including ours are engaged in this endeavor.

Comparison of the phenotypes of S3 cells in culture to their ability to form tumors in three different microenvironments *in vivo* show that these cells are particularly sensitive to their host microenvironment, producing complex phenotypes *in vivo*. For example, the S3-A cell line throws off ~10% large colonies in the 3DlrbM, but these do not invade through laminin-rich basement membrane in Boyden chambers, possibly because the duration of the assay is too short (2 days). However, S3-A tumor frequency is higher than the other S3s in the skin injections, but interestingly not in the skin + Matrigel or fat pad injections, and the S3-A tumor volumes in the skin + Matrigel and fat pad injections are higher than the other S3s (Fig. 2). The other S3 cell lines also seem to be very sensitive to their particular host microenvironment, resulting in the breakdown of a one-to-one correlation between the



**Table 1.** Attribute profile clustering of differentially expressed genes between S3-C and T4-2

GenBank no.	Gene	Avg	P	GenBank no.	Gene	Avg	P	GenBank no.	Gene	Avg	P
2D integral membrane (20/30)				3D integral membrane (62/62)							
NM_005050	<i>ABCD4</i>	1.17	0.0295	NM_000927	<i>ABCB1</i>	0.82	0.0398	AA450336	<i>NRXN3</i>	0.74	0.0210
NM_014567	<i>BCAR1</i>	0.74	0.0222	NM_012089	<i>ABCB10</i>	0.61	0.0165	AA598582	<i>OXAIL</i>	0.62	0.0054
NM_004054	<i>C3AR1</i>	1.20	0.0350	NM_005689	<i>ABCB6</i>	1.22	0.0029	NM_002561	<i>P2RX5</i>	0.74	0.0467
NM_000722	<i>CACNA2D1</i>	0.62	0.0450	NM_019624	<i>ABCB9</i>	1.33	0.0175	NM_005446	<i>P2RX1</i>	0.68	0.0446
NM_013230	<i>CD24</i>	1.29	0.0093	NM_000683	<i>ADRA2C</i>	1.24	0.0321	NM_000919	<i>PAM</i>	1.24	0.0170
NM_000760	<i>CSF3R</i>	1.17	0.0488	NM_001671	<i>ASGR1</i>	1.50	0.0384	AA663440	<i>PLXNC1</i>	0.83	0.0460
NM_001381	<i>DOK1</i>	0.80	0.0062	NM_001681	<i>ATP2A2</i>	1.43	0.0335	NM_000952	<i>PTAFR</i>	1.22	0.0019
NM_000118	<i>ENG</i>	0.64	0.0315	NM_004335	<i>BST2</i>	1.42	0.0106	NM_002838	<i>PTPRC</i>	0.72	0.0020
NM_014211	<i>GABRP</i>	0.68	0.0164	NM_006137	<i>CD7</i>	1.31	0.0421	NM_002855	<i>PVRL1</i>	1.09	0.0137
NM_004482	<i>GALNT3</i>	0.88	0.0219	NM_001782	<i>CD72</i>	1.24	0.0439	NM_001037	<i>SCN1B</i>	0.69	0.0030
H07878	<i>GPR19</i>	1.23	0.0295	NM_004356	<i>CD81</i>	0.80	0.0182	NM_005072	<i>SLC12A4</i>	0.54	0.0230
NM_000856	<i>GUCY1A3</i>	1.16	0.0171	NM_004233	<i>CD83</i>	0.75	0.0092	NM_015865	<i>SLC14A1</i>	0.77	0.0417
H11482	<i>IFNGR1</i>	0.74	0.0029	NM_005745	<i>DXS1357E</i>	0.84	0.0156	NM_004207	<i>SLC16A3</i>	0.79	0.0054
NM_000612	<i>IGF2</i>	1.13	0.0280	NM_001400	<i>EDG1</i>	1.69	0.0181	NM_004694	<i>SLC16A6</i>	1.23	0.0273
NM_000598	<i>IGFBP3</i>	0.62	0.0092	NM_000604	<i>FGFR1</i>	1.25	0.0311	NM_005495	<i>SLC17A4</i>	1.17	0.0471
NM_002195	<i>INSL4</i>	1.14	0.0360	NM_006338	<i>GAC1</i>	0.89	0.0454	NM_007256	<i>SLC21A9</i>	0.56	0.0133
NM_012282	<i>KCNE1L</i>	1.15	0.0007	NM_000160	<i>GCGR</i>	0.72	0.0317	NM_000441	<i>SLC26A4</i>	0.77	0.0389
NM_002333	<i>LRP3</i>	1.19	0.0085	NM_000832	<i>GRIN1</i>	1.50	0.0285	NM_001860	<i>SLC31A2</i>	0.83	0.0102
AA496022	<i>MFAP4</i>	0.60	0.0469	NM_000840	<i>GRM3</i>	0.60	0.0367	NM_014437	<i>SLC39A1</i>	1.31	0.0039
AA598582	<i>OXAIL</i>	0.52	0.0009	NM_005477	<i>HCN4</i>	0.75	0.0172	NM_002394	<i>SLC3A2</i>	1.30	0.0077
NM_002571	<i>PAEP</i>	1.15	0.0092	AA464246	<i>HLA-C</i>	0.79	0.0248	AA487543	<i>SORL1</i>	0.83	0.0397
NM_024411	<i>PDYN</i>	1.37	0.0492	NM_033554	<i>HLA-DPA1</i>	1.31	0.0498	NM_000544	<i>TAP2</i>	1.46	0.0217
NM_004705	<i>PRKRIR</i>	0.80	0.0021	H11482	<i>IFNGR1</i>	0.59	0.0003	NM_006335	<i>TIMM17A</i>	1.28	0.0042
NM_000452	<i>SLC10A1</i>	1.06	0.0296	NM_000877	<i>IL1R1</i>	0.80	0.0169	NM_005834	<i>TIMM17B</i>	0.79	0.0361
NM_006749	<i>SLC20A2</i>	0.85	0.0041	NM_004633	<i>IL1R2</i>	0.63	0.0217	NM_003265	<i>TLR3</i>	0.71	0.0272
NM_003127	<i>SPTAN1</i>	1.17	0.0450	NM_012276	<i>IL7</i>	1.28	0.0260	NM_006827	<i>TMP21</i>	1.17	0.0109
NM_003235	<i>TG</i>	1.19	0.0297	NM_002223	<i>ITPR2</i>	0.75	0.0100	NM_001192	<i>TNFRSF17</i>	1.28	0.0190
NM_003243	<i>TGFBR3</i>	1.41	0.0218	NM_002233	<i>KCNA4</i>	0.73	0.0097	NM_003810	<i>TNFSF10</i>	1.15	0.0373
NM_012471	<i>TRPC5</i>	0.61	0.0346	NM_002286	<i>LAG3</i>	0.73	0.0064	NM_006564	<i>TYMSTR</i>	0.45	0.0322
NM_000371	<i>TTR</i>	0.87	0.0485	NM_015364	<i>MD-2</i>	0.68	0.0027	NM_004738	<i>VAPB</i>	1.35	0.0212
				NM_000908	<i>NPR3</i>	1.17	0.0156	NM_021083	<i>XK</i>	1.23	0.0150
2D transcription (23/26)				3D transcription (51/51)							
NM_004301	<i>BAF53A</i>	1.19	0.0280	NM_005180	<i>BM11</i>	0.78	0.0355	NM_006186	<i>NR4A2</i>	1.18	0.0166
NM_006317	<i>BASP1</i>	0.92	0.0007	NM_000092	<i>COL4A4</i>	0.68	0.0387	NM_003884	<i>PCAF</i>	0.62	0.0031
NM_012116	<i>CBLC</i>	0.67	0.0249	H54686	<i>DAB2</i>	0.64	0.0163	NM_021128	<i>POLR2L</i>	0.88	0.0464
NM_003651	<i>CSDA</i>	0.86	0.0318	NM_000399	<i>EGR2</i>	1.37	0.0486	NM_007244	<i>PROL4</i>	1.43	0.0057
NM_004111	<i>FEN1</i>	0.82	0.0081	NM_006874	<i>ELF2</i>	0.74	0.0044	NM_002892	<i>RBBP1</i>	0.63	0.0012
NM_001465	<i>FYB</i>	0.96	0.0002	AA010400	<i>ETV4</i>	1.36	0.0371	NM_002919	<i>RFX3</i>	1.22	0.0469
NM_001515	<i>GTF2H2</i>	0.86	0.0261	NM_001987	<i>ETV6</i>	1.28	0.0386	NM_002938	<i>RNF4</i>	1.22	0.0414
NM_005324	<i>H3F3B</i>	1.10	0.0482	AA181023	<i>EV11</i>	1.31	0.0024	NM_002955	<i>RREB1</i>	1.36	0.0482
NM_005336	<i>HDLBP</i>	0.50	0.0200	AI346582	<i>EVX1</i>	0.69	0.0477	NM_003071	<i>SMARCA3</i>	1.30	0.0208
NM_014213	<i>HOXD9</i>	0.81	0.0059	NM_003862	<i>FGF18</i>	0.55	0.0374	NM_007017	<i>SOX30</i>	0.82	0.0371
NM_016270	<i>KLF2</i>	1.32	0.0361	NM_000801	<i>FKBP1A</i>	0.87	0.0237	NM_004509	<i>SP110</i>	0.66	0.0173
NM_002485	<i>NBS1</i>	1.22	0.0159	NM_005087	<i>FXR1</i>	0.74	0.0038	NM_012446	<i>SSBP2</i>	1.35	0.0139
NM_004555	<i>NEATC3</i>	1.13	0.0302	NM_002095	<i>GTF2E2</i>	1.32	0.0018	NM_005636	<i>SSX4</i>	0.85	0.0450
NM_002582	<i>PARN</i>	0.78	0.0034	NM_003483	<i>HMG2A</i>	1.05	0.4378	NM_007375	<i>TARDBP</i>	1.36	0.0089
NM_002779	<i>PSD</i>	0.59	0.0062	NM_014213	<i>HOXD9</i>	0.58	0.0021	NM_007108	<i>TCEB2</i>	1.19	0.0476
NM_002938	<i>RNF4</i>	1.17	0.0420	NM_002200	<i>IRF5</i>	1.22	0.0153	NM_003201	<i>TFAM</i>	1.15	0.0263
NM_007252	<i>RPF-1</i>	0.60	0.0308	NM_005853	<i>IRX5</i>	0.59	0.0014	NM_005077	<i>TLE1</i>	1.18	0.0242
NM_003079	<i>SMARCE1</i>	1.14	0.0106	NM_002228	<i>JUN</i>	1.30	0.0038	NM_005120	<i>TNRC11</i>	0.61	0.0064
NM_003084	<i>SNAPC3</i>	0.91	0.0081	NM_014368	<i>LHX6</i>	0.74	0.0210	NM_001068	<i>TOP2B</i>	1.24	0.0498
NM_005839	<i>SRRM1</i>	1.05	0.0047	NM_012321	<i>LSM4</i>	0.78	0.0046	NM_016936	<i>UBN1</i>	1.27	0.0347
NM_003152	<i>STAT5A</i>	1.14	0.0462	NM_002397	<i>MEF2C</i>	0.84	0.0118	AI925821	<i>USP22</i>	0.76	0.0034
NM_006284	<i>TAF10</i>	1.17	0.0133	NM_005933	<i>MLL</i>	0.58	0.0164	NM_000378	<i>WT1</i>	0.67	0.0150
NM_005644	<i>TAF12</i>	1.24	0.0035	NM_004641	<i>MLLT10</i>	1.24	0.0292	NM_003443	<i>ZNF151</i>	0.62	0.0241
NM_005481	<i>TRAP95</i>	0.59	0.0271	NM_002479	<i>MYOG</i>	0.73	0.0299	NM_016423	<i>ZNF219</i>	1.27	0.0198

(Continued on the following page)



**Table 1.** Attribute profile clustering of differentially expressed genes between S3-C and T4-2 (Cont'd)

GenBank no.	Gene	Avg	<i>P</i>	GenBank no.	Gene	Avg	<i>P</i>	GenBank no.	Gene	Avg	<i>P</i>
NM_004236	<i>TRIP15</i>	0.65	0.0394	NM_016170	<i>NCX</i>	1.36	0.0116	NM_005741	<i>ZNF263</i>	1.49	0.0055
NM_005082	<i>ZNF147</i>	0.63	0.0243	AA703115	<i>NEAT5</i>	1.22	0.0183				
2D kinases (4/4)				3D kinases (23/23)							
NM_001105	<i>ACVR1</i>	1.24	0.0206	NM_000020	<i>ACVRL1</i>	0.64	0.0383	NM_014002	<i>IKKE</i>	0.81	0.0493
NM_001259	<i>CDK6</i>	0.79	0.0258	NM_004327	<i>BCR</i>	1.26	0.0102	NM_003010	<i>MAP2K4</i>	1.23	0.0109
NM_004783	<i>TAO1</i>	1.24	0.0053	NM_004333	<i>BRAF</i>	1.28	0.0071	NM_005923	<i>MAP3K5</i>	0.79	0.0114
NM_003565	<i>ULK1</i>	0.80	0.0293	NM_016508	<i>CDKL3</i>	1.17	0.0413	NM_002378	<i>MATK</i>	0.73	0.0410
2D intracellular transport (4/4)				NM_001274	<i>CHEK1</i>	0.74	0.0073	AA496964	<i>NEK1</i>	0.76	0.0475
				NM_001278	<i>CHUK</i>	0.71	0.0341	NM_005030	<i>PLK</i>	0.81	0.0046
				NM_001328	<i>CTBP1</i>	1.34	0.0251	NM_005406	<i>ROCK1</i>	0.80	0.0333
NM_016451	<i>COPB</i>	0.67	0.0461	NM_004734	<i>DCAMK1</i>	1.32	0.0095	NM_003161	<i>RPS6KB1</i>	1.36	0.0272
NM_007357	<i>COG2</i>	0.82	0.0162	NM_001982	<i>ERBB3</i>	1.21	0.0281	NM_005627	<i>SGK</i>	0.77	0.0403
NM_006323	<i>SEC24B</i>	0.91	0.0056	NM_001465	<i>FYB</i>	0.63	0.0039	NM_004783	<i>TAO1</i>	1.31	0.0137
NM_004766	<i>COPB2</i>	1.31	0.0074	NM_005734	<i>HIPK3</i>	1.31	0.0080	NM_003331	<i>TYK2</i>	0.77	0.0382
				NM_000875	<i>IGF1R</i>	1.30	0.0233				
				3D chemokines (4/4)							
				NM_006419	<i>SCYB13</i>	1.38	0.0039	NM_000609	<i>SDF1</i>	1.37	0.0246
				NM_001735	<i>C5</i>	1.23	0.0203	NM_000584	<i>IL8</i>	1.45	0.0157

NOTE: The titles (e.g., transport, kinase, etc.) describe the most common gene function in each class; the ratio of genes in the class that fit this functional definition is shown in parentheses. For each gene, the row of information contains the GenBank number (e.g., NM\_005050), gene name (e.g., *ABCD4*), the mean value of the ratio of T4-2/S3-C expression over four microarray experiments (e.g., 0.15), and *t*-test penalized *P* value (*P* < 0.05).

Abbreviations: 2D, two-dimensional; 3D, three-dimensional; Avg, average.

progressive phenotypes observed in culture for S3-A, S3-B, S3-C, and the more complex phenotypes found in the xenografts. It is conceivable that, given the length of the 9- to 10-week time period, the host microenvironment within which the injected cells are in dynamic and reciprocal interactions with the stromal and humoral factors could allow for selection of the aggressive subpopulations, resulting in gain or loss of necessary functions to become malignant. In addition, results confirm that the cells poised to become malignant have not yet inactivated all pathways or gained all the new functions needed for a stable malignant phenotype.

What was found to be consistent across all assays done (invasion, three-dimensional polarity, CGH profile, tumorigenicity) is that all of the S3 cells displayed a phenotype distinct from both S1 and T4-2 cells *in vivo* as well as in the 3DlrBM assay. For tumorigenicity, this was supported by statistical analysis of tumor volume, as well as by histologic analysis showing that S3 tumors manifested more benign characteristics than the T4-2 tumors. In addition, S3 cells displayed more homogeneous phenotypes and a higher propensity to become invasive than the parent S2 cells when induced with T4-2 conditioned medium. Therefore, by these criteria, S3 cells have indeed progressed further than their parent S2 cells toward malignancy and are intermediate between the nontumorigenic S1 and malignant T4-2s.

Here we have described this model as one of transition from preinvasive to invasive phenotype to mimic the multistep carcinogenesis hypothesis of breast cancer (50, 51). However, the emerging cancer stem/progenitor cell hypothesis also needs to be considered. Sontag and Axelrod (1) have proposed four separate models to describe how atypical hyperplasia, ductal carcinoma *in situ*, invasive ductal carcinoma, and metastasis may relate to each other. These are the linear, nonlinear, branched, and parallel pathways. Unlike the other three hypotheses, the parallel pathway does not assume that *in situ* carcinoma develops into invasive carcinoma, but rather that

*in situ* and invasive carcinomas can arise from the same progenitor. In our cell lines, S2 gave rise to both the preinvasive S3-C and the invasive T4-2 cells via different steps of manipulation in culture and in mice, respectively (Fig. 1A). Therefore, it is tempting to speculate that the model described here could be placed as supporting the parallel progression hypothesis. Regardless of which mathematical model we consider, what we have developed are human breast epithelial cells with preinvasive and invasive characteristics, which recapitulate some aspects of preinvasive and invasive carcinomas with basal and squamous histologic and molecular phenotypes.

Analysis of this malignant transition in three-dimensional cultures allowed us to identify candidate genes as potential therapeutic targets. For example, of the MMPs we identified as having a function in invasion, MMP9, MMP13, and, recently, MMP17 have been shown to be associated with, and increased in, breast cancer progression (52–54). Although broad-spectrum inhibitors of MMPs have failed in clinical trials, targeting specific genes for certain subtypes of cancers may eliminate nonspecific effects, thereby producing more desirable clinical outcomes (55). In addition to the list of genes differentially expressed between S3-C and T4-2 (Table 1; Supplementary File 8), this model system is conducive to functional siRNA screens probing either gain of invasion function in S3-C or loss of invasion of T4-2 to find new genes involved in invasion. Using the same model, we recently discovered a new pathway of invasion regulated by polo-like kinase I (23). In general, the results described here provide a proof-of-principle for the development of spontaneous transition models for additional subtypes of breast cancers, with potential utility in discovering other mechanisms of invasion and other potential targets for therapy.

## Acknowledgments

Received 6/14/2007; revised 11/19/2007; accepted 1/8/2008.

**Grant support:** U.S. Department of Energy, Office of Biological and Environmental Research grant DEAC0376SF00098 (M.J. Bissell); NIH grant CA64786 (M.J. Bissell and O.W. Petersen); Department of Defense (DOD) Breast Cancer Research Program (BCRP) Innovator Award DAMD170210438 (M.J. Bissell); California Breast Cancer Research Program (CBCRP) Postdoctoral Fellowship Award 8FB0184 (A. Rizki); DOD BCRP Innovative, Developmental, and Exploratory Award DAMD170110368, NIH grant CA78731, and American Cancer Society New Investigator Internal Award IRG7800223 (V.M. Weaver); DOD BCRP Predoctoral Fellowship Award DAMD170310421 (G.I. Rozenberg); NIH grant CA88858 (J.D. Mott); NIH grants CA80067 and CA098131 (R.A. Jensen); CBCRP grant 8PB0171 and NIH grants P01 AG017242 and U01 ES011044 (I.S.

Mian); DOD BCRP Predoctoral Fellowship Award BC021231 (J.L. Bascom); and NIH grant CA58207 (K. Chin and J.W. Gray). NIH grant CA50519 and DOD BCRP grant DAMD170210439 (D.J. Chen). M.J. Bissell is a recipient of a distinguished fellowship from the U.S. Department of Energy, Office of Biological and Environmental Research.

The costs of publication of this article were defrayed in part by the payment of page charges. This article must therefore be hereby marked *advertisement* in accordance with 18 U.S.C. Section 1734 solely to indicate this fact.

We thank Eva Lee, Hui Zhang, Genec Lee, and Shraddha Ravani (Lawrence Berkeley National Laboratory) and Travis Mullan (Virginia Commonwealth University) for technical assistance and/or advice.

## References

- Sontag L, Axelrod DE. Evaluation of pathways for progression of heterogeneous breast tumors. *J Theor Biol* 2005;232:179–89.
- Buerger H, Otterbach F, Simon R, et al. Comparative genomic hybridization of ductal carcinoma *in situ* of the breast-evidence of multiple genetic pathways. *J Pathol* 1999;187:396–402.
- Etzell JE, Devries S, Chew K, et al. Loss of chromosome 16q in lobular carcinoma *in situ*. *Hum Pathol* 2001;32:292–6.
- Gong G, DeVries S, Chew KL, Cha I, Ljung BM, Waldman FM. Genetic changes in paired atypical and usual ductal hyperplasia of the breast by comparative genomic hybridization. *Clin Cancer Res* 2001;7:2410–4.
- Isola J, Chu L, DeVries S, et al. Genetic alterations in ERBB2-amplified breast carcinomas. *Clin Cancer Res* 1999;5:4140–5.
- Isola JJ, Kallioniemi OP, Chu LW, et al. Genetic aberrations detected by comparative genomic hybridization predict outcome in node-negative breast cancer. *Am J Pathol* 1995;147:905–11.
- Loveday RL, Greenman J, Simcox DL, et al. Genetic changes in breast cancer detected by comparative genomic hybridization. *Int J Cancer* 2000;86:494–500.
- Ma XJ, Salunga R, Tuggle JT, et al. Gene expression profiles of human breast cancer progression. *Proc Natl Acad Sci U S A* 2003;100:5974–9.
- Nishizaki T, DeVries S, Chew K, et al. Genetic alterations in primary breast cancers and their metastases: direct comparison using modified comparative genomic hybridization. *Genes Chromosomes Cancer* 1997;19:267–72.
- Nishizaki T, Chew K, Chu L, et al. Genetic alterations in lobular breast cancer by comparative genomic hybridization. *Int J Cancer* 1997;74:513–7.
- Polyak K. Molecular alterations in ductal carcinoma *in situ* of the breast. *Curr Opin Oncol* 2002;14:92–6.
- Porter DA, Krop IE, Nasser S, et al. A SAGE (serial analysis of gene expression) view of breast tumor progression. *Cancer Res* 2001;61:5697–702.
- Sgroi DC, Teng S, Robinson G, LeVangie R, Hudson JR, Jr., Elkahoul AG. *In vivo* gene expression profile analysis of human breast cancer progression. *Cancer Res* 1999;59:5656–61.
- Thor AD, Eng C, Devries S, et al. Invasive micropapillary carcinoma of the breast is associated with chromosome 8 abnormalities detected by comparative genomic hybridization. *Hum Pathol* 2002;33:628–31.
- Tirkkonen M, Tanner M, Karhu R, Kallioniemi A, Isola J, Kallioniemi OP. Molecular cytogenetics of primary breast cancer by CGH. *Genes Chromosomes Cancer* 1998;21:177–84.
- Waldman FM, DeVries S, Chew KL, Moore DH II, Kerlikowske K, Ljung BM. Chromosomal alterations in ductal carcinomas *in situ* and their *in situ* recurrences. *J Natl Cancer Inst* 2000;92:313–20.
- Waldman FM, Hwang ES, Etzell J, et al. Genomic alterations in tubular breast carcinomas. *Hum Pathol* 2001;32:222–6.
- Neve RM, Chin K, Fridlyand J, et al. A collection of breast cancer cell lines for the study of functionally distinct cancer subtypes. *Cancer Cell* 2006;10:515–27.
- Briand P, Petersen OW, Van Deurs B. A new diploid nontumorigenic human breast epithelial cell line isolated and propagated in chemically defined medium. *In Vitro Cell Dev Biol* 1987;23:181–8.
- Briand P, Nielsen KV, Madsen MW, Petersen OW. Trisomy 7p and malignant transformation of human breast epithelial cells following epidermal growth factor withdrawal. *Cancer Res* 1996;56:2039–44.
- Petersen OW, Ronnov-Jessen L, Howlett AR, Bissell MJ. Interaction with basement membrane serves to rapidly distinguish growth and differentiation pattern of normal and malignant human breast epithelial cells. *Proc Natl Acad Sci U S A* 1992;89:9064–8.
- Weaver VM, Petersen OW, Wang F, et al. Reversion of the malignant phenotype of human breast cells in three-dimensional culture and *in vivo* by integrin blocking antibodies. *J Cell Biol* 1997;137:231–45.
- Rizki A, Mott JD, Bissell MJ. Polo-like kinase I is involved in invasion through extracellular matrix. *Cancer Res* 2007;67:11106–10.
- Pinkel D, Segrevas R, Sudar D, et al. High resolution analysis of DNA copy number variation using comparative genomic hybridization to microarrays. *Nat Genet* 1998;20:207–11.
- Herron GS, Werb Z, Dwyer K, Banda MJ. Secretion of metalloproteinases by stimulated capillary endothelial cells. I. Production of procollagenase and prostromelysin exceeds expression of proteolytic activity. *J Biol Chem* 1986;261:2810–3.
- Lochter A, Srebrow A, Sympon CJ, Terracio N, Werb Z, Bissell MJ. Misregulation of stromelysin-1 expression in mouse mammary tumor cells accompanies acquisition of stromelysin-1-dependent invasive properties. *J Biol Chem* 1997;272:5007–15.
- Taylor MA, Cote RJ. Immunomicroscopy: a diagnostic tool for the surgical pathologist. Philadelphia: W.B. Saunders; 1994. p. 300–78.
- Liu H, Radisky DC, Wang F, Bissell MJ. Polarity and proliferation are controlled by distinct signaling pathways downstream of PI3-kinase in breast epithelial tumor cells. *J Cell Biol* 2004;164:603–12.
- Muthuswamy SK, Li D, Lelievre S, Bissell MJ, Brugge JS, ErbB2, but not ErbB1, reinitiates proliferation and induces luminal repopulation in epithelial acini. *Nat Cell Biol* 2001;3:785–92.
- Weaver VM, Lelievre S, Lakins JN, et al.  $\beta_1$  integrin-dependent formation of polarized three-dimensional architecture confers resistance to apoptosis in normal and malignant mammary epithelium. *Cancer Cell* 2002;2:205–16.
- Lelievre SA, Weaver VM, Nickerson JA, et al. Tissue phenotype depends on reciprocal interactions between the extracellular matrix and the structural organization of the nucleus. *Proc Natl Acad Sci U S A* 1998;95:14711–6.
- Muschler J, Levy D, Boudreau R, Henry M, Campbell K, Bissell MJ. A role for dystroglycan in epithelial polarization: loss of function in breast tumor cells. *Cancer Res* 2002;62:7102–9.
- Wang F, Weaver VM, Petersen OW, et al. Reciprocal interactions between  $\beta_1$ -integrin and epidermal growth factor receptor in three-dimensional basement membrane breast cultures: a different perspective in epithelial biology. *Proc Natl Acad Sci U S A* 1998;95:14821–6.
- Semeiks JR, Rizki A, Bissell MJ, Mian IS. Ensemble attribute profile clustering: discovering and characterizing groups of genes with similar patterns of biological features. *BMC Bioinformatics* 2006;7:147.
- Muller A, Homey B, Soto H, et al. Involvement of chemokine receptors in breast cancer metastasis. *Nature* 2001;410:50–6.
- Allinen M, Beroukhim R, Cai L, et al. Molecular characterization of the tumor microenvironment in breast cancer. *Cancer Cell* 2004;6:17–32.
- d'Ortho MP, Will H, Atkinson S, et al. Membrane-type matrix metalloproteinases 1 and 2 exhibit broad-spectrum proteolytic capacities comparable to many matrix metalloproteinases. *Eur J Biochem* 1997;250:751–7.
- Grobely D, Poncz L, Galaray RE. Inhibition of human skin fibroblast collagenase, thermolysin, and *Pseudomonas aeruginosa* elastase by peptide hydroxamic acids. *Biochemistry* 1992;31:7152–4.
- Leaf C. Why we're losing the war on cancer (and how to win it). *Fortune* 2004;149:76–82, 4–6, 8 passim.
- Hennessey BT, Krishnamurthy S, Giordano S, et al. Squamous cell carcinoma of the breast. *J Clin Oncol* 2005;23:7827–35.
- Aparicio I, Martinez A, Hernandez G, Hardisson D, De Santiago J. Squamous cell carcinoma of the breast. *Eur J Obstet Gynecol Reprod Biol* 2007; online ahead of print (dx.doi.org/10.1016/j.ejogrb.2007.03.021).
- Tse GM, Tan PH, Putti TC, Lui PC, Chaiwun B, Law BK. Metaplastic carcinoma of the breast: a clinico-pathological review. *J Clin Pathol* 2006;59:1079–83.
- Behranwala KA, Nasiri N, Abdullah N, Trott PA, Gui GP. Squamous cell carcinoma of the breast: clinico-pathologic implications and outcome. *Eur J Surg Oncol* 2003;29:386–9.
- Reis-Filho JS, Milanezi F, Steele D, et al. Metaplastic breast carcinomas are basal-like tumours. *Histopathology* 2006;49:10–21.
- Kenny PA, Lee GY, Myers CA, et al. The morphologies of breast cancer cell lines in three-dimensional assays correlate with their profiles of gene expression. *Mol Oncol* 2007;1:84–96.
- Tse GM, Tan PH, Chaiwun B, et al. p63 is useful in the diagnosis of mammary metaplastic carcinomas. *Pathology* 2006;38:16–20.
- Carey LA, Perou CM, Livasy CA, et al. Race, breast cancer subtypes, and survival in the Carolina Breast Cancer Study. *JAMA* 2006;295:2492–502.
- Honrado E, Benitez J, Palacios J. Histopathology of BRCA1- and BRCA2-associated breast cancer. *Crit Rev Oncol Hematol* 2006;59:27–39.
- Santner SJ, Dawson PJ, Tait L, et al. Malignant MCF10CA1 cell lines derived from premalignant human breast epithelial MCF10AT cells. *Breast Cancer Res Treat* 2001;65:101–10.
- Allred DC, Mohsin SK. Biological features of premalignant disease in the human breast. *J Mammary Gland Biol Neoplasia* 2000;5:351–64.
- Burstein HJ, Polyak K, Wong JS, Lester SC, Kaelin CM. Ductal carcinoma *in situ* of the breast. *N Engl J Med* 2004;350:1430–41.
- Nielsen BS, Rank F, Lopez JM, et al. Collagenase-3 expression in breast myofibroblasts as a molecular marker of transition of ductal carcinoma *in situ* lesions to invasive ductal carcinomas. *Cancer Res* 2001;61:7091–100.
- Rha SY, Yang WI, Kim JH, et al. Different expression patterns of MMP-2 and MMP-9 in breast cancer. *Oncol Rep* 1998;5:875–9.
- Chabottaux V, Sounni NE, Pennington CJ, et al. Membrane-type 4 matrix metalloproteinase promotes breast cancer growth and metastases. *Cancer Res* 2006;66:5165–72.
- Fingleton B. Matrix metalloproteinases: roles in cancer and metastasis. *Front Biosci* 2006;11:479–91.

Cells in focus

# Mammary epithelial cell: Influence of extracellular matrix composition and organization during development and tumorigenesis

Laura Kass<sup>a</sup>, Janine T. Erler<sup>b</sup>, Micah Dembo<sup>c</sup>, Valerie M. Weaver<sup>a,d,e,\*</sup>

<sup>a</sup> Department of Surgery, University of California, San Francisco, San Francisco, CA 94143, USA

<sup>b</sup> Department of Radiation Oncology, Stanford University School of Medicine, Stanford, CA 94305, USA

<sup>c</sup> Department of Biomedical Engineering, Boston University, Boston, MA 02215, USA

<sup>d</sup> Center for Bioengineering and Tissue Regeneration, Department of Surgery, University of California, San Francisco, San Francisco, CA 94143, USA

<sup>e</sup> Department of Anatomy, University of California, San Francisco, San Francisco, CA 94143, USA

Received 22 March 2007; received in revised form 25 June 2007; accepted 27 June 2007

Available online 19 July 2007

## Abstract

Stromal–epithelial interactions regulate mammary gland development and are critical for the maintenance of tissue homeostasis. The extracellular matrix, which is a proteinaceous component of the stroma, regulates mammary epithelial growth, survival, migration and differentiation through a repertoire of transmembrane receptors, of which integrins are the best characterized. Integrins modulate cell fate by reciprocally transducing biochemical and biophysical cues between the cell and the extracellular matrix, facilitating processes such as embryonic branching morphogenesis and lactation in the mammary gland. During breast development and cancer progression, the extracellular matrix is dynamically altered such that its composition, turnover, processing and orientation change dramatically. These modifications influence mammary epithelial cell shape, and modulate growth factor and hormonal responses to regulate processes including branching morphogenesis and alveolar differentiation. Malignant transformation

## Cell facts

- Stromal–epithelial interactions regulate mammary epithelial cell growth and differentiation during embryonic and postnatal development.
- The spatial organization and composition of the extracellular matrix influence mammary epithelial cell behavior.
- Alterations in extracellular matrix receptor expression can enable malignant transformation of the mammary epithelial cells.
- Differences in the biophysical properties of the extracellular matrix due to an increase in deposit and/or cross-linking can induce the malignant transformation of mammary epithelial cells.

**Abbreviations:** ECM, extracellular matrix; MMP(s), metalloproteinase(s); EGFR, epidermal growth factor receptor; ER $\alpha$ , estrogen receptor alpha; PRL, prolactin; BM, basement membrane; MEC, mammary epithelial cell; 2D or 3D, two or three dimensions; TIMPs, tissue inhibitors of metalloproteinase(s); Stat5, signal transducers and activators of transcription protein 5; LOX, lysyl oxidase.

\* Corresponding author at: Department of Surgery, University of California, San Francisco, 513 Parnassus Avenue, Room S1364C, Box 0456, San Francisco, CA 94143, USA. Tel.: +1 415 476 3826; fax: +1 415 476 3985.

E-mail address: [WeaverV@surgery.ucsf.edu](mailto:WeaverV@surgery.ucsf.edu) (V.M. Weaver).

of the breast is also associated with significant matrix remodeling and a progressive stiffening of the stroma that can enhance mammary epithelial cell growth, perturb breast tissue organization, and promote cell invasion and survival. In this review, we discuss the role of stromal–epithelial interactions in normal and malignant mammary epithelial cell behavior. We specifically focus on how dynamic modulation of the biochemical and biophysical properties of the extracellular matrix elicit a dialogue with the mammary epithelium through transmembrane integrin receptors to influence tissue morphogenesis, homeostasis and malignant transformation.

© 2007 Elsevier Ltd. All rights reserved.

**Keywords:** Mammary epithelial cells; Extracellular matrix; Matrix stiffness; Integrins

---

## 1. Introduction

The mammary gland is a dynamic tissue derived from the epidermis that achieves full maturity in the adult. The development of the mammary ductal tree depends on stromal–epithelial interactions, and these interactions are important in embryonic and postnatal development. The stroma not only modulates the normal development of the mammary gland but also actively participates in malignant transformation of the tissue. Mammary ducts consist of luminal cells associated with myoepithelial cells surrounded by the basement membrane (BM) that separates the epithelium from the stroma. The stromal compartment is composed of mesenchymal cells (fibroblasts, blood cells and leukocytes) and extracellular matrix (ECM) (laminin, fibronectin, collagen, proteoglycans, etc.), which influence mammary development. In this short review, we focus on how the ECM modulates mammary epithelial growth and differentiation in embryonic development, postnatal ductal growth, branching morphogenesis, and carcinogenesis. Of the myriad of ECM–mammary epithelial cell interactions, integrin signaling will be discussed in more detail. The biochemical and biophysical cues from the extracellular stroma that guide mammary epithelial morphogenesis, homeostasis and malignant transformation will also be described.

## 2. Cell origin and plasticity

The mammary gland is a modified sweat gland derived from the ectoderm. Mammary gland development begins with ectodermal cell migration induced by the mesenchyme, followed by the formation of five pairs of disk-shaped placodes (emerging epithelial formations) and invasion of the cells into the dermis (Veltmaat, Mailleux, Thiery & Bellusci, 2003). The mesenchyme is instructive and provides critical information to drive mammary differentiation. For example, mammary mesenchyme can induce embryonic epidermis from dorsal or

midventral sites to form mammary buds that will undergo functional differentiation and milk synthesis (Cunha et al., 1995), whereas recombination of embryonic mammary epithelial cells with salivary mesenchyme produces epithelial salivary structures (Sakakura, Nishizuka, & Dawe, 1976).

The stroma is not a static compartment; the cellular and ECM compositions evolve over time adapting to changes in the development of the gland. Two different mesenchymal tissues are involved in mammary gland development during embryogenesis: the fibroblastic cells surrounding the epithelial rudiment (the fibroblastic mesenchyme), and the fat pad cells (the fat pad mesenchyme). These two mesenchymes have different developmental properties demonstrated through tissue recombination studies. The fibroblastic mammary mesenchyme induces embryonic or adult mammary epithelial cells to form atypical ductal branching with hyperplastic ducts, while the fat pad induces epithelial cell elongation and branching (Sakakura, Sakagami, & Nishizuka, 1982). These changes in mammary development can be explained, in part, by differences in ECM composition between the fibroblastic mesenchyme and the fat pad. For example, expression of laminin and protoheparan sulphate induced by the fat pad occurs simultaneously with epithelial rudiment elongation and branching (Kimata, Sakakura, Inaguma, Kato, & Nishizuka, 1985). Similar changes in ECM composition have been found in the growing ductal structure during puberty. The BM at the tip of the duct (the invasive front) is rich in hyaluronic acid, whereas the BM surrounding the duct is composed of collagen type IV, laminin, and proteoglycans (Fata, Werb, & Bissell, 2004). These data suggest that the abundance and composition of the ECM can regulate epithelial cell behavior.

Remodeling of the ECM is a tightly regulated process where the action of metalloproteinases (MMPs), the principal matrix-degrading enzymes, is regulated by tissue inhibitors of metalloproteinase (TIMPs). Inappropriate expression of MMPs or TIMPs can drive



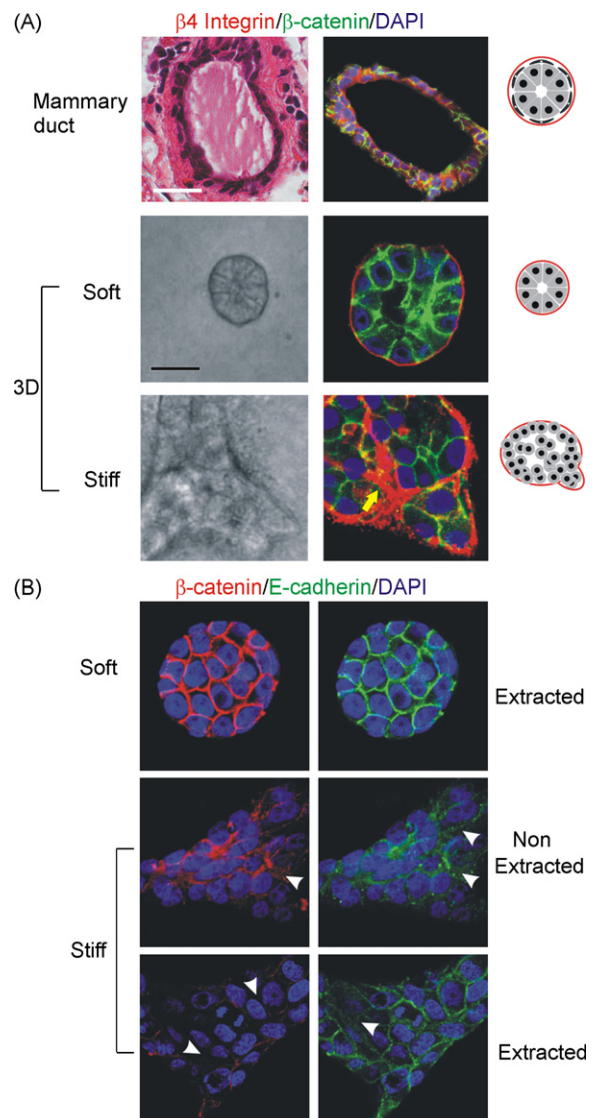
aberrant mammary gland phenotypes (Fata et al., 2004). For example, MMP2-null mammary glands have an excessive lateral branching with reduced ductal length, MMP3-deficient glands can elongate the ducts but with reduced secondary branching, and TIMP1-overexpressing glands demonstrate reduced ductal length (Fata et al., 2004).

The epithelial cells sense modifications in ECM composition through transmembrane receptors. These receptors, which include integrins (collagen, laminin, and fibronectin receptors), dystroglycan (laminin-1 receptor), discoidin domain receptor 1 tyrosine kinase (collagen receptor), and syndecans (co-receptors for heparan sulfate proteoglycans and fibronectin, laminin, collagen and growth factors), can modulate branching morphogenesis (Fata et al., 2004). For example, gene knockout models showed that while  $\alpha 2$  integrin is necessary for branching morphogenesis,  $\alpha 3$ ,  $\alpha 6$  or  $\alpha 4$  subunits are dispensable (Chen, Diacovo, Grenache, Santoro, & Zutter, 2002; Klinowska et al., 2001). Similarly, mice deficient in discoidin domain receptor 1 tyrosine kinase display excessive collagen deposition, delayed ductal development, and incomplete lactational differentiation (Vogel, Aszodi, Alves, & Pawson, 2001).

Increased collagen deposition can also alter the biophysical properties of the ECM augmenting extracellular tension. This elevation in tension has been shown to perturb mammary epithelial cell differentiation. For example, the functional and morphological differentiation of primary mammary epithelial cells (MECs) in response to lactogenic hormones can proceed only when

mixed mammary cell populations isolated from pre-lactating mice are plated on floating collagen gels with reduced tensional forces. Indeed, mechanically loaded collagen gels fail to support acinar morphogenesis and functional differentiation ( $\beta$ -casein expression), because these rigid gels (similar to two-dimensional rigid plastic) drive focal adhesion assembly to promote cell spreading, increase MMP activity, and thereby interfere with endogenous BM maturation (reviewed in Paszek & Weaver, 2004). Our laboratory has been investigating how the biophysical properties of the ECM can regulate cell shape and BM-dependent MECs morphogenesis (acini formation). Using two- and three-dimensional (2D, 3D) natural and synthetic laminin-rich matrices of precisely calibrated stiffness, we have demonstrated

Fig. 1. Mammary epithelial growth and morphogenesis is regulated by matrix stiffness. (A) 3D cultures of normal mammary epithelial cells within collagen gels of different concentration. Stiffening the ECM through an incremental increase in collagen concentration (soft gels: 1 mg/ml Collagen I, 140 Pa; stiff gels 3.6 mg/ml Collagen I, 1200 Pa) results in the progressive perturbation of morphogenesis, and the increased growth and modulated survival of MECs. Altered mammary acini morphology is illustrated by the destabilization of cell–cell adherens junctions and disruption of basal tissue polarity indicated by the gradual loss of cell–cell localized  $\beta$ -catenin (green) and disorganized  $\beta 4$  integrin (red) visualized through immunofluorescence and confocal imaging. On the right side of the panel is an illustration of a mammary ductal structure (luminal and myoepithelial cells surrounded by BM), and depicting MEC morphogenesis in soft and stiff gels. Scale bars represent 25  $\mu$ m. (B) Confocal immunofluorescence images of MEC colonies on soft and stiff gels (140 vs. >5000 Pa) stained for  $\beta$ -catenin (red) and E-cadherin (green), and counterstained with DAPI (blue) after triton X-100 extraction.  $\beta$ -catenin could be extracted from the sites of cell–cell interaction in MEC colonies formed on a stiff but not on a soft gel, indicating that adherens junctions are less stable in MEC structures formed on stiff gels. White arrowheads indicate diffuse staining patterns of  $\beta$ -catenin and E-cadherin. Modified from Paszek et al. (2005).



that substrate compliance regulates cell shape (rounding), mammary tissue morphogenesis, and endogenous BM assembly (Paszek et al., 2005) (Fig. 1). Recently, matrix compliance has also been implicated in modulating functional differentiation of MECs, as determined by  $\beta$ -casein expression (Alcaraz et al., personal communication).

### 3. Functions

During pregnancy, epithelial cells within the alveoli proliferate and differentiate in response to lactogenic hormones and growth factors, achieving full milk production capacity during lactation. The pregnancy-induced alveolar morphogenesis of the mammary gland is dependent upon ECM cues that are interpreted by the mammary epithelial cells through  $\beta$ 1 integrin signaling. The association of  $\beta$ 1 integrins with their heterodimeric  $\alpha$  integrin subunit partners anchor the cell to the BM (through laminin and collagen IV binding) and to the surrounding stroma (such as through binding to collagen I or fibronectin). In the mammary gland, both  $\alpha$ 5 $\beta$ 1 (fibronectin receptor) and  $\alpha$ 2 $\beta$ 1 (collagen and laminin receptor) integrin expression levels are regulated by ovarian hormones and, as such, have been implicated as key transducers of hormonal cues that drive growth and differentiation of the gland during pregnancy (Woodward, Mienaltowski, Modi, Bennett, & Haslam, 2001).

Conditional deletion of  $\beta$ 1 integrin in luminal mammary cells demonstrated an essential role for  $\beta$ 1 integrin in alveolar development and differentiation during pregnancy and lactation (Naylor et al., 2005). The ablation of  $\beta$ 1 integrin not only resulted in malformed alveoli, but also in failure of prolactin (PRL)-induced mammary epithelial cell differentiation and milk synthesis (Naylor et al., 2005).

How does  $\beta$ 1 integrin regulate mammary epithelial cell differentiation? In response to ECM cues such as changes in matrix composition, integrins assemble into intracellular signaling complexes that are connected to the actin cytoskeleton and that activate growth and survival pathways, thereby transmitting cues from the matrix to influence cell morphology and fate. For example, cell anchorage to laminin-1 through  $\beta$ 1 integrin permits PRL-dependent activation of Janus Kinase-2 and signal transducer and activator of transcription-5 (Stat5) signaling pathways, and the transcription of PRL- and Stat5-regulated milk proteins (Naylor et al., 2005). The small Rho GTPase Rac1 has been shown to be a critical downstream effector of  $\beta$ 1 integrin signaling for the activation of PRL/Stat5 signaling cascade (Akhtar & Streuli,

2006). However, the precise cross-talk between integrin and PRL signaling has not been fully elucidated.

### 4. Associated pathologies

Modifying ECM-integrin interactions can profoundly influence expression of the malignant phenotype in culture and *in vivo* (Park et al., 2006). However, the molecular mechanisms whereby altered stromal–epithelial interactions regulate tumorigenesis are not well defined. The cellular component of the stroma has been implicated in promoting breast cancer development. Infiltrating leukocytes, which are recruited to the tumor as a result of tumor cell expression of chemotactic cytokines, provide cytokines, proteases and growth factors to stimulate tumor growth and promote neo-angiogenesis (Pollard, 2004). Moreover, the overexpression of transforming growth factor- $\beta$  or hepatocyte growth factor by tumor associated-fibroblasts has also been implicated in the initiation of breast cancer (Kuperwasser et al., 2004). Besides secreting growth factors, activated fibroblasts are a vast source for ECM proteins. Changes in ECM composition can induce changes in epithelial cell integrin expression. For example, altered expression of  $\beta$ 1-,  $\beta$ 4-,  $\alpha$ 2-,  $\alpha$ 3- and  $\alpha$ 6-integrins has been observed in mammary cancer cells (Taddei et al., 2004).

Integrin-mediated adhesion to the ECM is essential for cell growth and survival through activation of focal adhesion kinase (FAK) signaling cascades that promote cell viability (White et al., 2004). Moreover, reciprocal interactions between epidermal growth factor receptor (EGFR) and integrin signaling pathways control proliferation and survival of MECs, such that inhibiting either  $\beta$ 4 integrin,  $\beta$ 1 integrin or EGFR represses the malignant phenotype of tumor MECs growing in 3D BM matrix (Weaver et al., 1997). The functional integrity of  $\beta$ 1 integrin signaling is also essential for the induction of mammary tumors, as the ablation of  $\beta$ 1 integrin expression in tumor cells *in vivo* inhibits proliferation and expansion of the tumors cells (White et al., 2004). Recently, it was shown that  $\beta$ 4 integrin promotes tumor progression through amplified ErbB2 signaling, and that the loss of  $\beta$ 4 integrin signaling suppresses mammary tumor onset and invasive growth *in vivo* (Guo et al., 2006). These data demonstrate a key role for integrins in malignant progression.

The development of breast cancer is characterized by the loss of tissue organization (Fig. 2A). Although breast tumor cells originate from epithelial cells, the stroma is an active participant of the epithelial malignant transformation. In the past decade, the stroma surrounding

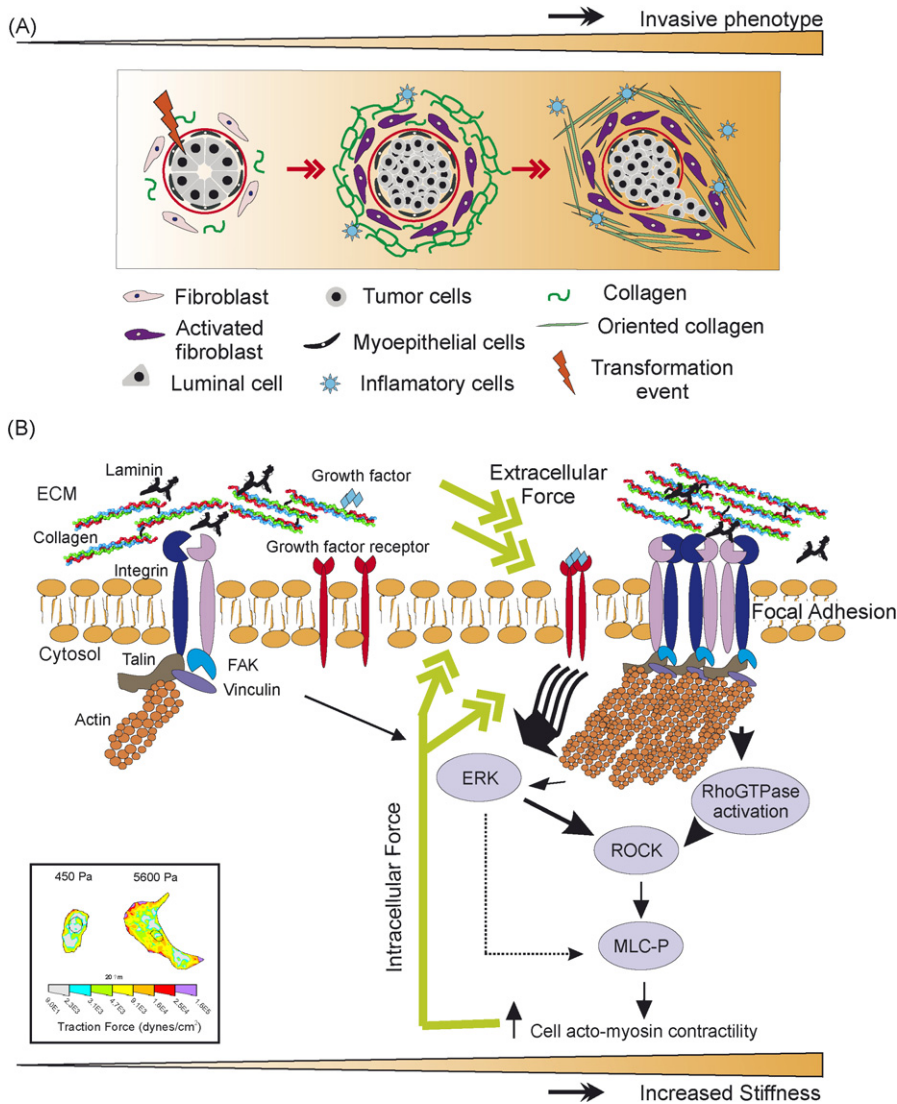


Fig. 2. Malignant transformation of mammary epithelial cells is regulated by matrix stiffness. Breast transformation ensues through progressive acquisition of genetic alterations in the luminal epithelial cells residing within the mammary ducts. The tissue stroma responds to these epithelial alterations by initiating a desmoplastic response that is characterized by activation and transdifferentiation of fibroblasts, infiltration of immune cells, increased secretion of growth factors and cytokines, and elevated matrix synthesis and remodeling that manifests as matrix stiffening. (A) Cartoon depicting the stages of breast tumorigenesis (from left to right; normal ducts, ductal carcinoma *in situ* and invasive phenotype), highlighting key desmoplastic changes within the tissue stroma. (B) Force-dependent focal adhesion maturation mediated by elevated tumor matrix stiffness. Integrins are bidirectional mechanosensors that integrate biochemical and biophysical cues from the matrix and the actin cytoskeleton and transduce cell-generated force to the surrounding microenvironment. Activated integrins bind to ECM proteins via cooperative interactions between their alpha and beta extracellular domains and form nascent highly dynamic adhesion signaling complexes. In response to external mechanical force or elevated cell-generated contractility integrin clustering is enhanced and the recruitment of multiple integrin adhesion plaque proteins including talin and vinculin is favored. These, in turn, associate with the actin cytoskeleton and multiple signaling proteins including focal adhesion kinase (FAK), Src family kinases, and integrin-linked kinase, to promote cell growth, survival, migration and differentiation. Matrix stiffening, which reflects elevated matrix deposition, linearization and cross-linking, can co-operate with oncogenic signaling to enhance cell-generated contractility to foster integrin associations and focal adhesion maturation. Maturation of focal adhesions promotes cell generated forces by enhancing Rho GTPase and ERK-mediated acto-myosin contractility—which feed forward to further promote integrin clustering and focal adhesion assembly and transmit acto-myosin-generated cellular forces to the ECM, as outlined in Paszek et al. (2005). Inset: representative traction maps showing the typical force distribution in fibroblasts on soft (450 Pa) and on stiff fibronectin gels (5600 Pa). These maps allow the measurement of the forces generated by the cell, which are dependent on the stiffness of the substrate. Modified from Paszek et al. (2005).

developing lesions has increasingly been appreciated as a critical regulator of malignant transformation and as a vital modifier of tumor behavior including metastasis and treatment responsiveness. The stromal desmoplastic response is characterized by the activation of fibroblasts, increased deposition, cross-linking and remodeling of the ECM, angiogenesis, and invasion of leukocytes. Up-regulated ECM gene expression and elevated MMP activities are not only found in tumors but can also correlate with poor patient prognosis (Jinga et al., 2006). For example, expression levels of the ECM protein lysyl oxidase (LOX), which is responsible for collagen cross-linking, is elevated in cancer patients and associated with metastasis and reduced patient survival (Erler et al., 2006). Furthermore, the increased ratios of MMP2:TIMP2 and MMP9:TIMP1 found in malignant breast tissues have been suggested to play a role in the aggressiveness of invasive breast carcinomas (Jinga et al., 2006).

Metastasis of breast cancer cells is associated with the majority of the disease fatalities, such that restricting disease progression and preventing metastasis represents the primary objective of many cancer prevention programs. In order for a tumor cell to metastasize, it must first degrade the BM and migrate into the surrounding stroma. Cleavage of laminin-5 by MMPs (2 and 14) exposes cryptic sites of the proteins that induce epithelial migration (Giannelli, Falk-Marzillier, Schiraldi, Stetler-Stevenson, & Quaranta, 1997). Another consequence of MMP activity is the release of growth factors trapped in the ECM that in turn can stimulate further epithelial cell invasion. During invasion, cells extend pseudopodia at the leading edge that attach to collagen fibers in the ECM at the migration front, allowing the cells to “crawl” linearly along the fibers toward the blood vessels (Condeelis & Segall, 2003).

Cell migration is also tightly regulated by cell adhesion, cell-generated contractility and cell haptotaxis to maximize their ligand binding and even durotaxis towards a stiffer matrix to increase cell tension (Sheetz, Felsenfeld, & Galbraith, 1998; Wong, Velasco, Rajagopalan, & Pham, 2003). This suggests that elevated matrix deposition and tension likely couple with degradation to modulate tumor invasion and metastasis. In this respect, small Rho GTPases are functionally linked to cell migration and MMP-mediated invasion. Rac and Rho expression and activity are elevated in tumors and RhoC is implicated in the metastatic, aggressive phenotype of inflammatory breast tumors (Fritz, Just, & Kaina, 1999; Kleer et al., 2004). Consistently, inhibition of LOX involved in collagen cross-linking and fiber formation dramatically reduces invasion and metastasis

in a mouse model of breast cancer (Erler et al., 2006).

Given that the ECM profoundly modulates tissue morphogenesis and that the stroma changes dramatically during breast tumorigenesis, it is logical to ask if modifications in matrix organization and stiffness could drive tumor invasion and contribute to metastasis. Consistently, we have shown that the mammary gland progressively stiffens during tumor progression and that is associated with increased collagen deposition, cross-linking and reorientation (Paszek et al., 2005). In concordance with these results, matrix stiffness, in association with growth factors, enhances ERK activation and increases cell contractility (Fig. 2B) (Paszek et al., 2005). Interestingly, force-generated activation of ERK may also influence cell proliferation, alter tissue behavior and drive anti-estrogen resistance during breast cancer treatment, through phosphorylation of ER $\alpha$ , recruitment of ER $\alpha$  co-activators or enhanced transcriptional activity, in a ligand-independent manner (Likhite, Stossi, Kim, Katzenellenbogen, & Katzenellenbogen, 2006). Indeed, tamoxifen, the anti-estrogen used in the treatment of breast cancer, has been shown to reduce breast density and therefore the risk of recurrences (Atkinson, Warren, Bingham, & Day, 1999).

We showed that matrix stiffness and/or exogenous force independently induce cell-generated contractility to promote focal adhesion maturation and enhance integrin-dependent signaling thus compromising multi-cellular tissue morphogenesis and promoting a tumor-like behavior in mammary cells (Paszek et al., 2005). This suggests that matrix stiffness likely promotes breast tumorigenesis through altering integrins and their adhesion interactions. Conversely, we found that blocking integrin-dependent cell contractility reverted the malignant phenotype in culture (Paszek et al., 2005; Weaver et al., 1997). Consistent with these findings, ectopic expression of  $\beta 1$  integrin mutants with increased transmembrane molecular associations (V737N and G744N), elevated cellular contractility and forced focal adhesion maturation increase integrin/growth factor-dependent signaling, again to compromise multi-cellular tissue morphogenesis and promote tumorigenic behavior in culture and *in vivo* (Paszek et al., 2005).

Investigating ECM composition and stiffness as a risk factor is critical given the profound changes in the mammary stroma associated with breast cancer and the diversity of diseases associated with changes in collagen deposition, orientation and cross-linking. Indeed, inhibition of matrix modifying ECM proteins can dramatically reduce tumor progression through effects on invasion and metastasis. It is plausible that as a consequence of



matrix rigidity, altered mechanotransduction constitutes a key mechanism in regulating malignant transformation of epithelial cells. Moreover, there is evidence to suggest that changes in mammary ECM modify treatment responsiveness to anti-estrogens promoting the progression of breast carcinoma and thereby decreasing patient survival. Understanding the molecular mechanisms behind this process could lead to the design of a unique, targeted strategy to diagnose and treat this disease.

## Acknowledgments

We apologize to the many authors whose work is not cited due to space limitations. This work was supported by NIH grants CA078731 to VMW, R01 GM072002-04 to MD, and DOD grants DAMD1701-1-0368, 1703-1-0496, and W81XWH-05-1-330 to VMW.

## References

- Akhtar, N., & Streuli, C. H. (2006). Rac1 links integrin-mediated adhesion to the control of lactational differentiation in mammary epithelia. *Journal of Cell Biology*, 173, 781–793.
- Atkinson, C., Warren, R., Bingham, S. A., & Day, N. E. (1999). Mam-mographic patterns as a predictive biomarker of breast cancer risk: Effect of tamoxifen. *Cancer Epidemiology Biomarkers & Prevention*, 8, 863–866.
- Chen, J., Diacovo, T. G., Grenache, D. G., Santoro, S. A., & Zutter, M. M. (2002). The alpha(2) integrin subunit-deficient mouse: A multifaceted phenotype including defects of branching morphogenesis and hemostasis. *American Journal of Pathology*, 161, 337–344.
- Condeelis, J., & Segall, J. E. (2003). Intravital imaging of cell movement in tumours. *Nature Reviews Cancer*, 3, 921–930.
- Cunha, G. R., Young, P., Christov, K., Guzman, R., Nandi, S., Talamantes, F., et al. (1995). Mammary phenotypic expression induced in epidermal cells by embryonic mammary mesenchyme. *Acta Anatomica (Basel)*, 152, 195–204.
- Erler, J. T., Bennewith, K. L., Nicolau, M., Dornhöfer, N., Kong, C., Le, Q. T., et al. (2006). Lysyl oxidase is essential for hypoxia-induced metastasis. *Nature*, 440, 1222–1226.
- Fata, J. E., Werb, Z., & Bissell, M. J. (2004). Regulation of mammary gland branching morphogenesis by the extracellular matrix and its remodeling enzymes. *Breast Cancer Research*, 6, 1–11.
- Fritz, G., Just, I., & Kaina, B. (1999). Rho GTPases are over-expressed in human tumors. *International Journal of Cancer*, 81, 682–687.
- Giannelli, G., Falk-Marzillier, J., Schiraldi, O., Stetler-Stevenson, W. G., & Quaranta, V. (1997). Induction of cell migration by matrix metalloproteinase-2 cleavage of laminin-5. *Science*, 277, 225–228.
- Guo, W., Pylayeva, Y., Pepe, A., Yoshioka, T., Muller, W. J., Inghirami, G., et al. (2006). Beta 4 integrin amplifies ErbB2 signaling to promote mammary tumorigenesis. *Cell*, 126, 489–502.
- Jinga, D. C., Blidaru, A., Condrea, I., Ardeleanu, C., Dragomir, C., Szegli, G., et al. (2006). MMP-9 and MMP-2 gelatinases and TIMP-1 and TIMP-2 inhibitors in breast cancer: Correlations with prognostic factors. *Journal of Cellular and Molecular Medicine*, 10, 499–510.
- Kimata, K., Sakakura, T., Inaguma, Y., Kato, M., & Nishizuka, Y. (1985). Participation of two different mesenchymes in the developing mouse mammary gland: Synthesis of basement membrane components by fat pad precursor cells. *Journal of Embryology and Experimental Morphology*, 89, 243–257.
- Kleer, C. G., Zhang, Y., Pan, Q., Gallagher, G., Wu, M., Wu, Z. F., et al. (2004). WISP3 and RhoC guanosine triphosphatase cooperate in the development of inflammatory breast cancer. *Breast Cancer Research*, 6, R110–R115.
- Klinowska, T. C., Alexander, C. M., Georges-Labouesse, E., Van der Neut, R., Kreidberg, J. A., Jones, C. J., et al. (2001). Epithelial development and differentiation in the mammary gland is not dependent on alpha 3 or alpha 6 integrin subunits. *Developmental Biology*, 233, 449–467.
- Kuperwasser, C., Chavarria, T., Wu, M., Magrane, G., Gray, J. W., Carey, L., et al. (2004). Reconstruction of functionally normal and malignant human breast tissues in mice. *Proceedings of the National Academy of Science, USA*, 101, 4966–4971.
- Likhite, V. S., Stossi, F., Kim, K., Katzenellenbogen, B. S., & Katzenellenbogen, J. A. (2006). Kinase-specific phosphorylation of the estrogen receptor changes receptor interactions with ligand, deoxyribonucleic acid, and coregulators associated with alterations in estrogen and tamoxifen activity. *Molecular Endocrinology*, 20, 3120–3132.
- Naylor, M. J., Li, N., Cheung, J., Lowe, E. T., Lambert, E., Marlow, R., et al. (2005). Ablation of beta1 integrin in mammary epithelium reveals a key role for integrin in glandular morphogenesis and differentiation. *Journal of Cell Biology*, 171, 717–728.
- Park, C. C., Zhang, H., Pallavicini, M., Gray, J. W., Baehner, F., Park, C. J., et al. (2006). Beta1 integrin inhibitory antibody induces apoptosis of breast cancer cells, inhibits growth, and distinguishes malignant from normal phenotype in three dimensional cultures and in vivo. *Cancer Research*, 66, 1526–1535.
- Paszek, M. J., & Weaver, V. M. (2004). The tension mounts: Mechanics meets morphogenesis and malignancy. *Journal of Mammary Gland Biology & Neoplasia*, 9, 325–342.
- Paszek, M. J., Zahir, N., Johnson, K. R., Lakins, J. N., Rozenberg, G. I., Gefen, A., et al. (2005). Tensional homeostasis and the malignant phenotype. *Cancer Cell*, 8, 241–254.
- Pollard, J. W. (2004). Tumour-educated macrophages promote tumour progression and metastasis. *Nature Reviews Cancer*, 4, 71–78.
- Sakakura, T., Nishizuka, Y., & Dawe, C. J. (1976). Mesenchyme-dependent morphogenesis and epithelium-specific cytodifferentiation in mouse mammary gland. *Science*, 194, 1439–1441.
- Sakakura, T., Sakagami, Y., & Nishizuka, Y. (1982). Dual origin of mesenchymal tissues participating in mouse mammary gland embryogenesis. *Developmental Biology*, 91, 202–207.
- Sheetz, M. P., Felsenfeld, D. P., & Galbraith, C. G. (1998). Cell migration: Regulation of force on extracellular-matrix-integrin complexes. *Trends in Cell Biology*, 8, 51–54.
- Taddei, I., Faraldo, M. M., Teulière, J., Deugnier, M. A., Thiery, J. P., & Glukhova, M. A. (2004). Integrins in mammary gland development and differentiation of mammary epithelium. *Journal of the Mammary Gland Biology and Neoplasia*, 8, 383–394.
- Veltmaat, J. M., Mailleux, A. A., Thiery, J. P., & Bellusci, S. (2003). Mouse embryonic mammaryogenesis as a model for the molecular regulation of pattern formation. *Differentiation*, 71, 1–17.
- Vogel, W. F., Aszódi, A., Alves, F., & Pawson, T. (2001). Discoidin domain receptor 1 tyrosine kinase has an essential role in mammary gland development. *Molecular Cell Biology*, 21, 2906–2917.
- Weaver, V. M., Petersen, O. W., Wang, F., Larabell, C. A., Briand, P., Damsky, C., et al. (1997). Reversion of the malignant phe-

- notype of human breast cells in three-dimensional culture and in vivo by integrin blocking antibodies. *Journal of Cell Biology*, 137, 231–245.
- White, D. E., Kurpios, N. A., Zuo, D., Hassell, J. A., Blaess, S., Mueller, U., et al. (2004). Targeted disruption of beta1-integrin in a transgenic mouse model of human breast cancer reveals an essential role in mammary tumor induction. *Cancer Cell*, 6, 159–170.
- Wong, J. Y., Velasco, A., Rajagopalan, A., & Pham, Q. (2003). Directed movement of vascular smooth muscle cells on gradient-compliant hydrogels. *Langmuir*, 19, 1908–1913.
- Woodward, T. L., Mienaltowski, A. S., Modi, R. R., Bennett, J. M., & Haslam, S. Z. (2001). Fibronectin and the alpha(5)beta(1) integrin are under developmental and ovarian steroid regulation in the normal mouse mammary gland. *Endocrinology*, 142, 3214–3222.

# Modeling Morphogenesis and Oncogenesis in Three-Dimensional Breast Epithelial Cultures

Christy Hebner,<sup>1</sup> Valerie M. Weaver,<sup>1</sup>  
and Jayanta Debnath<sup>2</sup>

Department of Surgery and Center for Bioengineering and Tissue Regeneration,<sup>1</sup>  
Department of Pathology,<sup>2</sup> University of California, San Francisco, California;  
email: jayanta.debnath@ucsf.edu, WeaverV@surgery.ucsf.edu,  
Christy.Hebner@gilead.com

Annu. Rev. Pathol. Mech. Dis. 2008. 3:313–39

First published online as a Review in Advance on  
September 20, 2007

The *Annual Review of Pathology: Mechanisms of Disease* is online at pathmechdis.annualreviews.org

This article's doi:  
10.1146/annurev.pathmechdis.3.121806.151526

Copyright © 2008 by Annual Reviews.  
All rights reserved

1553-4006/08/0228-0313\$20.00

## Key Words

ECM, lumen formation, apicobasal polarity, force

## Abstract

Three-dimensional (3D) epithelial culture systems recreate the cardinal features of glandular epithelium in vivo and represent a valuable tool for modeling breast cancer initiation and progression in a structurally appropriate context. 3D models have emerged as a powerful method to interrogate the biological activities of cancer genes and oncogenic pathways, and recent studies have poignantly illustrated their utility in dissecting the emerging role of tensional force in regulating epithelial tissue homeostasis. We review how 3D models are being used to investigate fundamental cellular and biophysical mechanisms associated with breast cancer progression that have not been readily amenable to traditional genetic or biochemical analysis.

**DCIS:** ductal carcinoma in situ

**EGFR/ErbB:** members of the epidermal growth factor receptor tyrosine kinase family

**Apicobasal polarity:** asymmetric organization of epithelial cells within glands where the apical pole borders the lumen, while the basal surface adheres to the extracellular matrix

## INTRODUCTION

Breast carcinoma is the most common female cancer in the Western world (1). For the practicing pathologist, epithelial cancers arising in the breast are remarkable for both their clinical significance as well as their diverse histopathological architecture. Breast carcinomas also represent a growing diagnostic challenge for pathologists because preinvasive lesions, such as atypical ductal hyperplasias and ductal carcinomas in situ (DCIS), are being diagnosed with increasing frequency (2, 3). The ability to effectively diagnose these early lesions, where the tumor does not invade the basement membrane or myoepithelial layer, and confidently predict future outcome for these patients has assumed great significance in breast cancer diagnosis and treatment (4).

For decades, pathologists have recognized that certain histological patterns harbor valuable prognostic information. For example, in the breast, tubular carcinomas, mucinous (colloid) carcinomas, and invasive lobular carcinomas are associated with better clinical outcome compared with the most commonly diagnosed pattern, invasive ductal carcinoma (5, 6). Furthermore, clear relationships between a specific genomic abnormality and histological phenotype have been defined. First, the comedo subtype of DCIS possesses amplifications in the *HER2/NEU* oncogene, which encodes the epidermal growth factor receptor (EGFR) tyrosine kinase ErbB2 (7). Second, basal-like breast cancers, an aggressive subtype of invasive ductal carcinoma remarkable for significant aneuploidy and a lack of hormone receptor expression, are strongly associated with mutations in the tumor suppressor gene *BRCA1* or with abnormalities in X chromosome inactivation (8). Third, invasive lobular carcinoma is commonly associated with genomic losses in *CDH1*, which codes for E-cadherin, an important epithelial cell-cell adhesion molecule (9). Moreover, high-throughput analytical approaches have provided a wealth of information about ep-

ithelial cancers and have raised new questions about how cancer genes and pathways influence both clinical prognosis and histological architecture (10–12). Despite these advances, much remains to be learned about the precise molecular and biophysical mechanisms that elicit the actual phenotypic changes observed under the microscope. A better understanding of the mechanisms and pathways involved in the disruption of normal tissue architecture will undoubtedly provide biological insight into breast carcinoma progression and aid in the discovery of new diagnostic markers and therapeutic strategies.

Over the past decade, three-dimensional (3D) organotypic culture systems have been increasingly utilized as powerful cell-based models to investigate the functions of cancer genes and pathways in a biologically relevant context and high-throughput manner (13, 14). These culture systems have provided unique insights into how basic cell biological and biophysical processes impact higher-order tissue architecture. In recent years, 3D models have significantly enhanced our understanding of carcinoma biology in the following four areas: (a) the formation and maintenance of a hollow glandular lumen and its disruption by cancer genes, (b) the regulation of apicobasal polarity in normal and cancerous epithelium, (c) the discovery that cell-cell and cell-matrix adhesion pathways can dominantly interfere with the phenotypic expression of the tumorigenic state, and (d) the emerging importance for tensional force in driving 3D tissue architecture and homeostasis. In this review, we focus on these four major areas of discovery and their potential implications for breast cancer pathogenesis. Importantly, we do not encyclopedically review findings in several important research areas—such as branching morphogenesis, invasion, epithelial-mesenchymal transition, and the role of the stroma in tumorigenesis—because these topics have been covered in recent reviews (13, 14). Finally, although most of the experiments discussed here employ normal and cancerous breast epithelial cells, we also

delineate salient experiments that use non-breast 3D culture systems, most notably cysts derived from Madin Darby Canine Kidney cells (MDCKs), because they provide valuable insight into the basic processes driving normal glandular architecture and its disruption in carcinomas.

## MAMMARY GLAND MORPHOGENESIS IN VIVO

Cells in the human body organize into dynamic tissue complexes, orchestrated by numerous factors including cell-cell and cell-extracellular matrix (ECM) interactions, soluble ligands, and physical force. In epithelial tissues, these elements create an intricate architecture notable for tightly controlled cell growth, proliferation, differentiation, polarity, and survival. This phenotypic control is mediated not only by intracellular signaling pathways, but also by signals from the surrounding microenvironment. For instance, in the developing mouse, death signals initiated by the endoderm induce cells in the ectoderm to undergo apoptosis (15). In the developing kidney, tubule formation is mediated by soluble factors including hepatocyte growth factor and transforming growth factor- $\alpha$ , as well as by chemical and physical cues initiated by the adjacent mesenchyme (16, 17). Furthermore, intracellular signaling pathways and physical signals initiating from force and adhesion are elaborately linked; disruption of these interrelationships plays a major role in epithelial carcinogenesis (18). Indeed, this is beautifully illustrated in the human breast.

### Mammary Gland Development

The breast is one of the few organs that develops and matures after birth, making it ideal for studying tissue development. The mammary gland forms via branching morphogenesis in which a two-dimensional (2D) layer forms a fluid-filled lumen via budding through a 3D mesenchymal mass (19). The mature breast is a complex organ consisting of a central lu-

men encapsulated by luminal epithelial cells, and further delimited by myoepithelial cells and the ECM. Hence, a unique microenvironment influences mammary tissue homeostasis through hormones, soluble factors, stroma, and physical stress and strain (20).

The mammary gland comprises an extensive network of branched ductal structures with epithelial-cell-lined hollow luminal spaces (19, 21). Two bilateral ridges of epidermal tissue known as milk lines form during the first trimester (22). Pairs of disk-shaped mammary placodes, which mark the site of each nipple, separate along these lines and form a bulb-shaped bud by proliferating into the adjacent mesenchyme. This structure forms the primary rudimentary mammary gland known as an anlage. Upon penetration of the mesenchyme, the epithelial bud branches into the mammary fat pad and forms several ductal trees. However, upon cessation of hormonal influences in the newborn, the mammary gland enters a quiescent state until puberty.

Upon reaching puberty, hormone-dependent development of the breast initiates with expansion, beginning at the ends of the ducts known as terminal end buds (TEBs) (**Figure 1**) (23). Two different cell types are contained within the TEBs: cap cells and body cells. The cap cells are ceded as a single layer at the edge of the TEBs in contact with the basal lamina, whereas the majority of the TEBs are composed of body cells structured in multicellular layers. The TEBs undergo ductal arborization via sprouting through the mammary fat pad. Although the resting gland is relatively static, during pregnancy the breast undergoes dynamic changes in which lobules form on the ends of the branched structures and secrete milk during lactation. With pregnancy, differentiation of the ducts occurs, resulting in the formation of luminal structures required for lactation. Lumen formation is intrinsic to milk production, and transport and is controlled by cell death as body cells bordering the TEBs exhibit high rates of apoptosis (24). Interestingly, in premalignant breast cancer lesions, either

---

#### Extracellular matrix (ECM):

noncellular tissue components produced by cells such as collagen and basement membrane proteins

#### Apoptosis:

programmed cell death marked by caspase activation, nuclear fragmentation, and subsequent phagocytic elimination of cellular remnants

**TEB:** terminal end bud

---

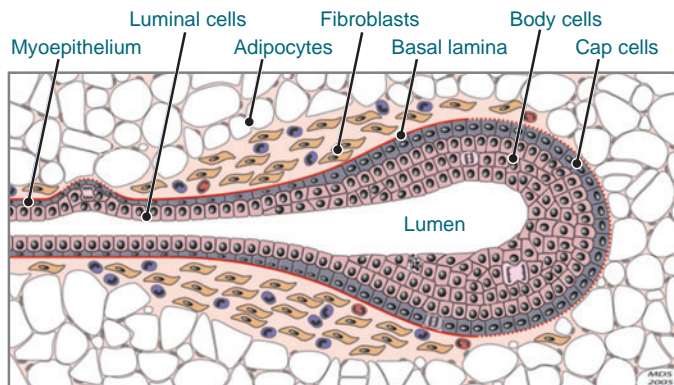


**Figure 1**

Terminal end bud morphology. Diagram depicting the terminal end bud, including the highly prevalent body cells found adjacent to the lumen as well as the surrounding single layer of cap cells. Large numbers of stromal fibroblasts are found around the collar of the duct. The dotted red line represents the thinning basal lamina that occurs at the edge of the invading ducts, although no evidence exists that ductal cells cross the basement membrane. Figure adapted with permission from References 19 and 21.

complete or partial filling of the lumen is observed, suggesting that normal apoptotic pathways may be altered in the early phases of mammary carcinogenesis.

## MODELING GLANDULAR EPITHELIUM USING THREE-DIMENSIONAL CULTURES

Cell culture systems are well suited for dissecting the biochemical and cell signaling pathways necessary for studying oncogenic transformation. Although significant information has been gleaned from studies of 2D monolayer cells, these systems do not lend themselves to the 3D architecture characteristic of epithelial cells *in vivo*. To address the limitations imposed by monolayer cell culture, 3D methods were developed to model the *in vivo* environment of epithelial cells. In contrast to mouse models or human tissue studies, 3D systems can be exploited to rapidly identify genes and deconstruct signaling pathways that regulate mammary morphogenesis and epithelial cancer development. In this review, we focus on the use of 3D models as a

means to uncover the basic cellular mechanisms that contribute to normal breast morphogenesis and malignancy.

The terminal ductal lobular unit, which is composed of mammary epithelial cells (MECs), is the smallest functional unit of the breast (25). When MECs are placed in traditional 2D cultures, they grow as monolayers and fail to differentiate, even in the presence of prolactogenic hormones (26). However, upon culture within basement membrane proteins, these cells organize into spherical acini in which the lumen becomes hollow and milk is secreted. A breakdown in this formation is seen in the early stages of breast cancer, where loss of polarized organization, increased cellular proliferation, and filling of the luminal space are observed (1, 14). Therefore, understanding the basic mechanisms that regulate acini formation and luminal clearance provides key insights into the early events in carcinoma formation.

If one uses 3D culture conditions, epithelial cells initially proliferate to eventually form growth-arrested spherical acini characterized by polarized cells surrounding a hollow lumen (12, 27, 28). Two different methods are typically used to induce acini formation (**Figure 2a**). The first involves completely embedding epithelial cells within a gelled ECM, which is grown in the presence of culture media that contain growth factors and hormones (28). The second method utilizes a thin gel bed (approximately 1 mm thick) of ECM molecules upon which epithelial cells are seeded as single cells and overlaid with culture media that contain diluted ECM (12). Both methods are highly advantageous compared with traditional 2D cultures because cells proliferate and develop into polarized growth-arrested structures that resemble normal glands *in vivo* (**Figure 2b**).

## Matrices for Three-Dimensional Culture

A salient feature of 3D organotypic methods is the utilization of an ECM to provide

**MEC:** mammary epithelial cell

**Acini:** although anatomically imprecise, a widely used operational term for epithelial cyst-like spheroids grown in 3D culture



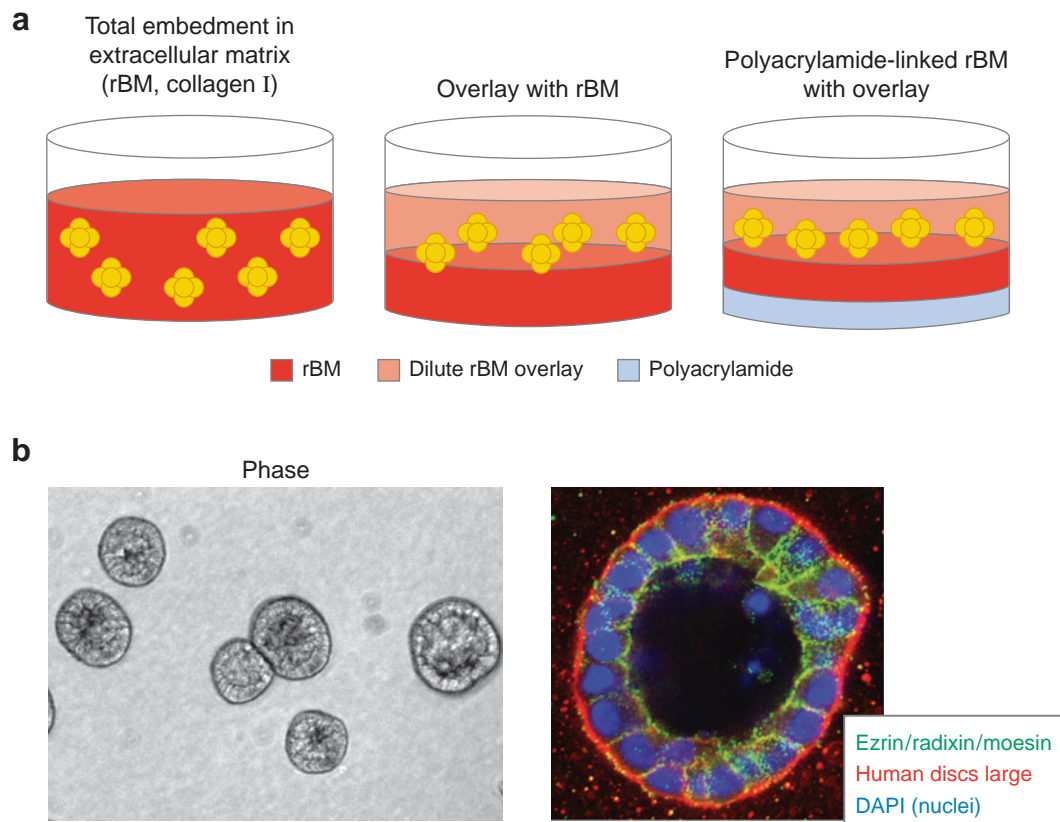


**Figure 2**

3D culture methods. (*a*) Schematic of commonly used techniques. (*Left*) Complete embedding of mammary epithelial cells (MECs) in reconstituted basement membrane (rBM). (*Center*) MECs seeded upon a thin layer of solidified rBM are overlaid with a dilute solution of rBM in culture media. (*Right*) Polyacrylamide gel of a given elastic modulus is cast upon a glass coverslip and rBM is allowed to cross-link to the polyacrylamide. MECs are seeded upon the rBM/polyacrylamide matrix and overlaid with dilute rBM in culture media. (*b*) Phase micrographs of day 18 MCF-10A acini grown in overlay culture. Equatorial confocal cross sections of a single acinus stained with ezrin/radixin/moesin (green), human discs large (red), and the nuclear dye 4', 6-diamidino-2-phenylindole (DAPI, blue).

the necessary structural and biochemical cues for proper glandular differentiation and homeostasis. A wide variety of materials have been utilized, each with their own pros and cons (**Table 1**). Reconstituted basement membranes (rBMs) from Engelbreth-Holm-Swarm tumor-derived basement membrane matrix (EHS) mouse sarcomas have been routinely employed to study mammary morphogenesis as well as cellular transformation and carcinogenesis (12, 28). EHS is composed primarily of the basement membrane compo-

nents laminin-1, collagen 4, and entactin (29). Recent studies have shown that the exogenously provided laminin in the EHS-derived matrix drives the morphogenetic process when MECs are cultured three-dimensionally (30). Various nontransformed MEC lines can be induced to undergo acinar morphogenesis, including S1 cells (from the HMT-3522 progression series) and MCF-10A cells, which are human in origin, as well as mouse MEC lines, such as Scp2 and Eph4 (28, 31–35). In addition, primary mouse and human MECs also

**Reconstituted basement membrane (rBM):** preparations of basement membrane-derived ECM proteins, most notably laminin, which can drive 3D epithelial acini morphogenesis

**Table 1** Advantages and disadvantages of various matrices for 3D culture studies

Component	Advantages	Disadvantages
Reconstituted basement membrane	Successfully applied to many 3D systems	Poorly defined content; lot-to-lot variability
Fibrin	Successfully applied to many 3D systems	Easily proteolyzed by cellular proteases
Collagen I	More biologically defined; easy to manipulate	Lot-to-lot variability; limited range of elastic moduli
Polyacrylamide gels	Easy to manipulate; nonreactive; large range of elastic moduli	Acrylamide toxicity; not a true 3D system

form polarized structures with a hollow lumen when cultured three-dimensionally (30, 36).

However, because EHS is isolated from a mouse tumor xenograft, it has a complex and ill-defined composition, which is subject to inherent lot-to-lot variability. In contrast, employing an ECM scaffold in which the stoichiometry of critical components can be easily manipulated and controlled provides certain experimental advantages. Accordingly, collagen I has been utilized as a 3D matrix. Certain epithelial cells, most notably MDCK epithelial cells, develop into polarized cysts with a hollow lumen when embedded within matrices composed of collagen I (37). Collagen I is biologically better defined than EHS and can be easily manipulated through changes in concentration, orientation, and biochemical modification (30, 38–41). Unfortunately, numerous epithelial cell types fail to form polarized acini when cultured in collagen I gels, whereas in laminin-rich rBM they do polarize. Growing evidence indicates that the mechanical properties of the 3D matrix are also critical for the development of polarized, differentiated acinar structures. This was revealed originally in a series of studies involving normal breast epithelium grown on top of floating or attached collagen gels; mammary architecture, metabolic function, and differentiation could be maintained only in the malleable,

floating collagen gel (42, 43). Nonetheless, the range in elastic modulus achieved through the use of collagen I remains limited owing to biochemical constraints. This becomes especially problematic with the increasing prominence of studies deciphering the effects of mechanotransduction in tissues. Finally, like rBM, collagen I is a biologically derived material and thus can present with experimental variability between preparations. Thus, newer techniques incorporating synthetic materials are now being utilized in 3D organotypic culture systems.

One system currently in use involves the deployment of polyacrylamide gels functionally cross-linked to ECM components upon which cells can be seeded (44). Polyacrylamide is a nonreactive material that can be easily manipulated through altering the concentrations of acrylamide and bisacrylamide cross-linker, thereby allowing for precisely controlled biochemical and mechanical properties. However, because acrylamide is cytotoxic in monomeric form, cells cannot be embedded directly in this material for 3D studies. To preclude this limitation, cells seeded upon polyacrylamide gels are overlaid with a blanket of rBM, resulting in a pseudo-3D system (**Figure 2a**) (45). As this system is neither 2D nor 3D, cell behavior can be different than that observed in more traditional 3D culture systems, which can lead to difficulty in interpreting results. Alternatively, conjugated self-assembling peptide polymer gels and protein-conjugated methylcellulose and peptide-immobilized polyethylene glycol gels that are biocompatible for 3D and in vivo studies are now available for study, yet await rigorous experimental validation (46, 47).

Overall, a variety of matrix substrates and scaffolds can be utilized for 3D organotypic culture systems. As a result, interpretations of data from such experiments need to be weighed against limitations of the particular system in use. Below, we highlight some of the applications of these techniques and recent findings regarding mammary development and carcinogenesis.

**EHS:** Engelbreth-Holm-Swarm tumor-derived basement membrane matrix



## APOPTOSIS AND LUMEN FORMATION

The 3D culture of MEC lines has been commonly used as an *in vitro* model of epithelial development. When cultured in rBM, MECs form growth-arrested acini in an ordered sequence of events (**Figure 3**). In the early stages of culture, cells form clusters surrounded by the ECM. As cultures progress, two distinct cell populations emerge within each acinus: polarized cells around the outer layer in contact with the ECM that secrete basement membrane proteins, and nonpolarized cells comprising the inner region. With further culturing, these inner cells undergo

cell death and clearance, leading to lumen formation.

### Luminal Apoptosis

Lumen formation appears to be due in part to apoptosis. Inhibition of apoptosis with caspase inhibitors in 3D cultures of primary mouse MECs results in delayed lumen formation (36). This is consistent with *in vivo* data in which mice overexpressing the antiapoptotic protein Bcl-2 in a mammary-specific fashion exhibit a delay in mammary lumen development (24). Furthermore, studies utilizing the cultured nonmalignant mammary cell

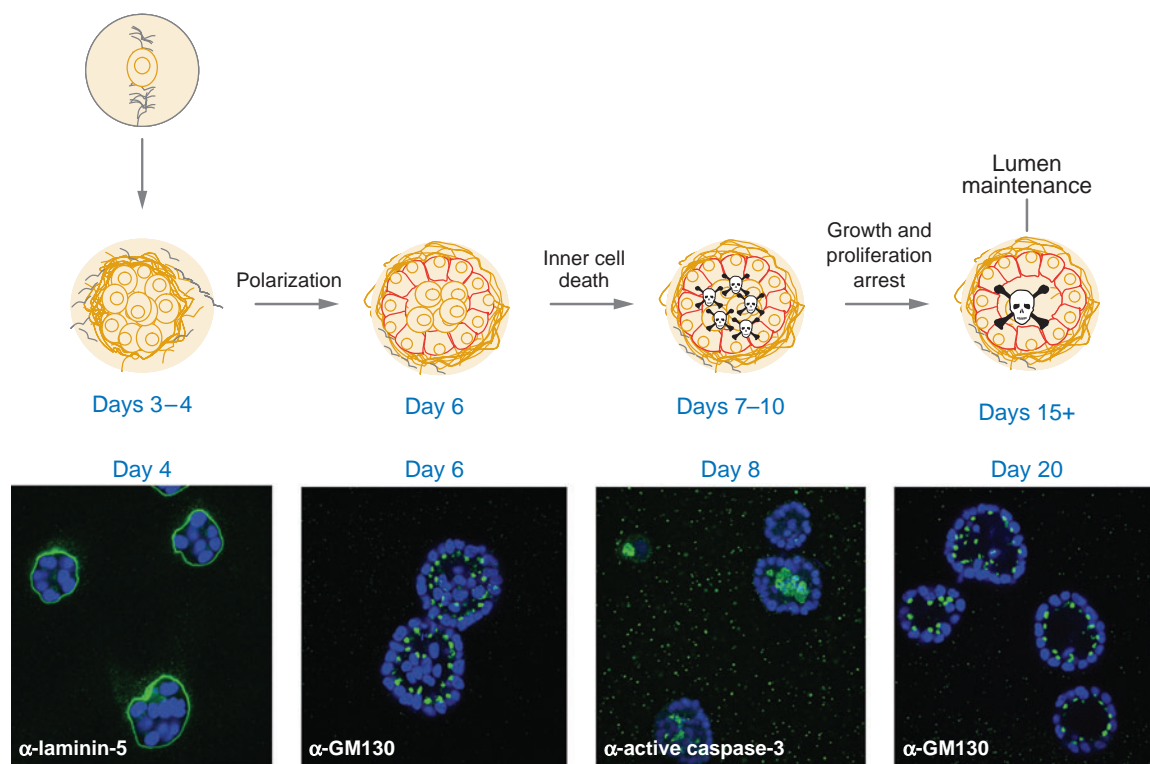


**Figure 3**

Lumen formation in MCF-10A acini. MCF-10A cells undergo an ordered series of morphogenetic events when grown in 3D culture. In early stages, developing cell clusters exhibit apicobasal polarization; thereafter, two distinct cell populations become discernable within each acinus: a well-polarized outer layer of cells in direct contact with extracellular matrix, and an inner subset of cells that is poorly polarized and lacking contact with the matrix. These inner cells undergo apoptosis, characterized by the expression of processed caspase-3, resulting in a hollow lumen. The hollow acinar structure remains stable thereafter. Figure adapted with permission from Reference 48.

line MCF-10A have shown similar effects. MCF-10A cells undergo polarized formation of acini and lumen formation in 3D culture (**Figure 3**). In experiments in which Bcl-2 or Bcl-xL was overexpressed, luminal clearance was delayed in acini, again implicating apoptosis in lumen development (48).

Epithelial cells depend critically upon integrin-mediated cell adhesion to ECM for proper growth and survival; *anoikis*, a form of apoptosis that epithelial cells undergo upon detachment from ECM, may contribute to lumen formation (49–51). Protection from *anoikis* may constitute a fundamental mechanism for tumor cell survival in vivo and may be responsible for luminal filling in glandular structures in vitro and in vivo (52, 53). As centrally located cells do not contact ECM, these cells may undergo death through *anoikis*. Consistent with this hypothesis, both MCF-10A *anoikis* and 3D lumen formation coincide with increased levels of the BH3-only proapoptotic protein Bim; RNA-interference-mediated Bim depletion prevents both MCF-10A *anoikis* as well as luminal apoptosis in 3D culture (53, 54). Moreover, disrupting Bim in the mouse mammary gland prevents apoptosis and luminal clearance in TEBs during puberty (55). Overall, these studies highlight Bim as an important regulator of apoptosis resulting from the matrix detachment of cells occupying the 3D lumen.

In addition to cell-matrix interactions, cell-cell interactions may also regulate cell death, affecting lumen formation as well. The molecule CEACAM1 (carcinoembryonic antigen-related cell adhesion molecule 1) is a cell-cell adhesion molecule that has been identified as a regulator of lumen development. In MCF-10A cells, inhibition of CEACAM1 function results in the inhibition of lumen formation (56). Conversely, expression of CEACAM1 in MCF-7 cells, a mammary carcinoma cell line that does not normally express CEACAM1 or form a lumen in 3D culture, results in luminal development, showing that extracellular cues contribute to lumen formation as well (57).

## Luminal Filling Induced by Cancer Genes

Although apoptosis plays an important role in the formation of the mammary lumen, inhibition of apoptotic pathways delays, but does not completely inhibit, luminal clearing. The tight control of proliferation also plays a role because overexpression of cyclin D1 or inhibition of the retinoblastoma proteins through expression of the HPVE7 results in a similar delay in lumen clearance (48). However, as is true of apoptosis inhibition, lumen formation is postponed, not ablated, with enhanced cellular proliferation. Filling of the lumen results from a combination of both apoptotic inhibition and enhanced proliferation, as activation of ErbB2—the gene product of *HER2/NEU*, which can induce both proliferation and inhibit apoptosis—results in luminal filling (34, 48). Notably, in some early human breast precancerous lesions, such as atypical ductal hyperplasias, a hollow architecture is maintained in the context of hyperproliferation, whereas advanced lesions such as DCIS exhibit varying degrees of luminal filling. Hence, one may speculate that in early breast lesions, architectural changes induced by proliferative signals are limited owing to compensatory increases in apoptosis. In contrast, more advanced phenotypes may express antiapoptotic signals that allow survival of these excess proliferating cells.

ErbB2 is a receptor tyrosine kinase from a group of four kinases (ErbB1–4) that bind growth factors from the EGF family. Binding of the ErbB receptors to EGF ligands can occur via homo- or heterodimerization, thereby leading to a complex array of signaling (58–60). ErbB2 is often overexpressed or amplified in breast tumors and correlates with a poor clinical prognosis (61, 62). Activation of the ErbB2 receptor during MCF-10A morphogenesis elicits a complex multi-acinar phenotype. Similar hyperplastic lesions, notable for the presence of multi-acinar clusters, have been observed in vivo in tumors upon transgenic expression of activated *Neu*

(NeuT) in the mouse mammary gland, as well as when primary tumor cells isolated from these mice are cultured on EHS (63–65). These altered structures exhibit the cardinal features of early-stage cancers, including high levels of proliferation, filling of the lumen, and the disruption of cell polarity. However, activation of ErbB2 in MCF-10A cells does not cause anchorage-independent growth or an invasive phenotype in 3D culture. These results suggest that ErbB2 can play a role in the initial stages of transformation, but ErbB2 alone is not sufficient for progression to invasive breast cancer (34).

Hence, other factors may synergize with ErbB2 to promote invasion and metastasis. Recent work utilizing a mutant version of  $\beta 4$  integrin, in which the signaling capacity but not the ability for adhesion was ablated, demonstrates that  $\beta 4$  integrin can amplify the signaling capability of ErbB2, thereby contributing to mammary tumor progression.  $\beta 4$  integrin can form a complex with ErbB2, thus enabling it to activate c-Jun and STAT3 and induce two hallmarks of oncogenesis, proliferation, and loss of cell adhesion. This study suggests that  $\beta 4$  integrin can function as an essential component of ErbB2-induced oncogenesis and serve as a potential therapeutic target (66).

Following the groundbreaking studies of ErbB2 in 3D culture, the activation of numerous other growth factor receptors and oncogenes have subsequently been interrogated in the MCF-10A acini model; some examples include colony-stimulating factor 1 receptor (67), insulin growth factor receptor (68), Akt/PKB (69), and phosphatidylinositol 3-kinase (70). As predicted, activation of these pathways elicits varying degrees of luminal filling, which results from increased proliferation combined with protection from apoptosis in the 3D lumen. Nonetheless, each of these molecules mediates additional distinctive biological activities in 3D culture, which ultimately influences the morphogenetic phenotype in unexpected ways. These phenotypes, in addition to the corresponding *in vivo* histo-

logical correlates, have already been the subject of a recent review (14).

## Autophagy

Although much work has been done analyzing the effects of the classical pathways of cell death in lumen formation, recent work suggests that another process, autophagy, may play a role in lumen clearance. Autophagy is an evolutionarily conserved lysosomal degradation process in which a cell degrades its own cytoplasmic contents (i.e., eats itself). In eukaryotic cells, autophagy is a key mechanism for long-lived protein degradation and organelle turnover and serves as a critical pro-survival mechanism during nutrient deprivation or stress (71, 72). It has been proposed that when excessive autophagy occurs within a cell, a distinct form of programmed cell death ensues (termed type 2 death) (73). Remarkably, in experiments investigating the ultrastructure of cells during postlactational involution of the mouse mammary gland, autophagic vacuoles were seen in the early stages of involution (74). Similarly, 3D culture studies suggest the involvement of autophagy in lumen formation (48). Furthermore, TRAIL (tumor necrosis factor–related apoptosis-inducing ligand) may be involved in this process, as treatment with exogenous TRAIL induces autophagy in MCF-10A cells and expression of a dominant negative TRAIL receptor cooperates with Bcl-2 overexpression to increase luminal filling (75). Although these results implicate the potential for TRAIL-induced autophagy during luminal clearance, they are nonetheless correlative and ignore that the outer cells of developing acini exhibit direct ECM contact on their basal surface, whereas the central cells do not (48). Thus, one can alternatively predict that autophagy is actually induced during *anoikis* as a protective mechanism to mitigate the stresses of ECM detachment. Loss-of-function studies of autophagy genes (known as *ATGs*) are required to precisely validate the role of autophagy in cell survival versus

---

**Autophagy:** tightly regulated lysosomal process where a cell self-digests cytoplasmic contents; proposed to mediate nonapoptotic (type 2) programmed cell death

---

type 2 death during 3D lumen formation (73).

## MAMMARY EPITHELIAL POLARITY

In addition to luminal filling, mammary carcinoma can also be characterized by a loss in epithelial polarity. Glandular epithelial tissues consist of cells exhibiting a characteristic polarity in which the apical poles face inward toward the central lumen, the lateral face mediates cell-cell contacts, and the basal face contacts the ECM (**Figure 4**). This polarity is often disrupted in early carcinomas, which is generally considered a poor prognostic sign. 3D culture models are beginning to address if intrinsic polarity regulators di-

rectly regulate cancer-promoting functions. The best-characterized 3D model to study epithelial polarization utilizes MDCK cells grown in a collagen I matrix. MDCK cells undergo cystogenesis in 3D culture characterized by polarized cells surrounding a cleared central lumen; moreover, the cells comprising these cysts form tight junctions, making this model advantageous for the study of mechanisms that govern epithelial polarity.

## Cell-Intrinsic Regulators of Polarity

Invertebrate models have provided a wealth of genetic information about the regulation of polarity in epithelial tissues (76, 77). Cell polarity is believed to be controlled by the interplay of three major complexes, broadly

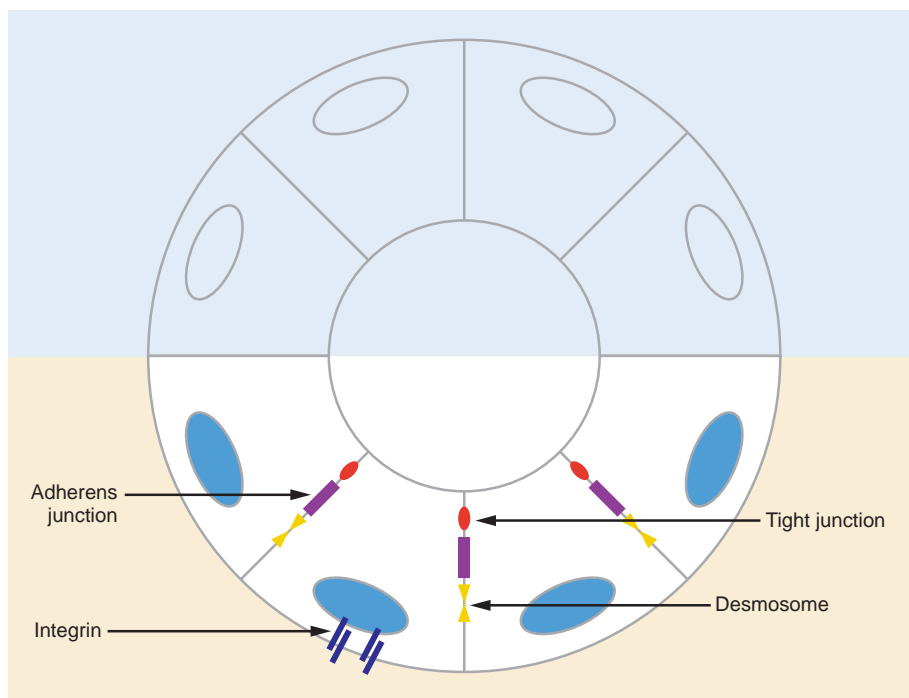


**Figure 4**

Cross section of a polarized gland architecture. Each individual epithelial cell within an intact gland has a microvilli-rich apical membrane facing the lumen, a lateral membrane contacting adjacent cells, and a basal surface contacting the basement membrane (extracellular matrix). The extracellular matrix attachment is mediated through integrin receptors, and cell-cell junctions consist of tight junctions, adherens junctions, and desmosomes. Tight junctions demarcate the boundary between apical and basolateral surfaces.

defined as the Par complex, the Scribble complex, and the Crumbs complex (78, 79). The concurrent activities of these three complexes combine to formulate apical and basal polarity in epithelial cells (80–82). Nonetheless, much remains to be learned about these fundamental regulators during cancer initiation and progression.

Recent studies of MDCK cyst formation have illustrated that specific proteins in these polarity regulator complexes are critical for the development of polarity and lumen formation. The mammalian orthologs of three genes involved in epithelial polarity in *Drosophila*—CRB3, PALS1, and PATJ—exist in a macromolecular complex that localizes to the tight junction in MDCK cells (83, 84). The ablation of PALS1 by RNA interference elicits a concomitant loss of PATJ in MDCK cells and completely disrupts apicobasal polarity when these cells are grown in 3D culture. The resulting structures do not form a central lumen; instead, they contain multiple small and incomplete lumens, or completely lack a lumen. In addition, well-established markers of apical polarity in MDCK cells, such as GP135, are completely mislocalized in these structures (85). Notably, the formation of multiple small lumens in these MDCK structures highly resembles the cribriform patterns observed in breast DCIS and in certain prostate hyperplasias (14).

Two key recent reports have focused specifically on the convergence of signaling pathways upon the apical protein complex Par-3/Par6/atypical PKC (aPKC), resulting in the establishment of epithelial polarity. The first analyzes a molecular mechanism connecting phosphatase and tensin homolog on chromosome 10 (PTEN), which signals to form the apical surface and lumen. siRNA-mediated PTEN depletion in MDCK cells grown in rBM results in the formation of multiple small lumens upon cystogenesis versus the single central lumen seen in controls, suggesting that PTEN signaling regulates epithelial polarity and central lumen formation (86). Furthermore, markers segregating with

the PTEN phospholipid product PI(4,5)P<sub>2</sub>, which is normally confined to the apical border, and PI(3,4,5)P<sub>3</sub>, its basolateral precursor, show altered localization. Furthermore, addition of exogenous PI(4,5)P<sub>2</sub> basolaterally to cysts resulted in the relocation of the apical marker gp135 and of the tight junction component zona occludins 1 to basolateral membranes, thus highlighting a role for this PTEN-regulated lipid product in establishing polarity. Moreover, PI(4,5)P<sub>2</sub> exogenously applied to the basolateral membrane of MDCK cysts also targets activated Cdc42 to the basolateral membrane. Finally, both PTEN and Cdc42 regulate the apical location of Par6/aPKC because depletion of either molecule results in the aberrant intracellular localization of aPKC. Importantly, aPKC inhibition disrupts central lumen formation in cysts. Overall, these results elegantly delineate interconnections between PTEN, Par6/aPKC, Cdc42, and the establishment of epithelial polarity and central lumen formation.

A second report establishes a link between Par6/aPKC and the effects of the oncogene ErbB2 on polarity (87). In this report, ErbB2 activation disrupts apicobasal polarity as characterized by changes in zona occludins 1, a tight junction protein, and gp135 localization in 2D cultures of MDCK cells. This coincides with loss of Par6 localization at the apical-lateral border. Interestingly, activation of ErbB2 leads to a decrease in the association of Par3 with Par6 and aPKC, as seen in contact-naïve cells, thereby suggesting that ErbB2 inhibits appropriate cell-cell junction assembly through inhibition of Par3/Par6/aPKC complex formation. Furthermore, ErbB2 associates directly with Par6 and aPKC, suggesting that the formation of this trimeric complex inhibits Par3 association. In addition, this interaction requires ErbB2 dimerization, thereby suggesting a mechanism by which ErbB2 leads to a breakdown in cell-cell contacts in *HER2/NEU*-positive cancers. Similar results are observed in ErbB2-expressing MCF-10A cells. Also,



in 3D MCF-10A culture, multi-acinar structures are observed in cells expressing wild-type Par6, but not in cells expressing an aPKC binding-deficient mutant of Par6, suggesting that the ErbB2/Par6/aPKC complex is responsible for the multi-acinar phenotype induced by ErbB2. Interestingly, cellular proliferation is similar in wild-type and mutant Par6 cells, demonstrating that the signaling pathways through which ErbB2 induces proliferation are completely distinct from those that alter cell polarity.

### Extracellular Matrix and Polarity

In addition to the cell-intrinsic regulators and pathways, the ECM itself plays a critical instructive role in the generation of apicobasal polarity. Classical 3D studies investigating polarity reversal in MDCK cysts and thyroid follicles point to the importance of ECM as a polarity cue (37, 88). When grown in liquid suspension culture, these cells form structures in which the free apical surface points away from the central axis of the sphere and toward the surrounding culture medium on the outside; these structures still generate a basal surface but it is in the interior of the structure, created by depositing basement membrane into an internal cavity. When the inverted MDCK cysts are embedded in collagen I, thus providing a strong ECM cue on the outside of these structures, extensive cellular remodeling occurs, resulting in cysts with a central hollow lumen (37). The plasticity of cyst organization in response to varying external cues indicates that epithelial cells possess hard-wired mechanisms for generating polarity within the context of a 3D tissue structure and, furthermore, that ECM plays a fundamental instructive role in directing these mechanisms.

Interestingly, intracellular signaling pathways regulate the polarity of a glandular structure by actively modifying the surrounding basement membrane. In MDCK cysts, the orientation of apical poles requires the small GTPase Rac1, which mediates the proper assembly of laminin at the cyst-ECM inter-

face. Expression of a dominant negative Rac1 (N17Rac) in MDCK cysts inverts the apical pole toward the cyst periphery; remarkably, this polarity reversion is observed only in 3D, but not 2D, cultures. By providing an exogenous source of laminin to the cyst periphery, one can rescue the phenotypic effects of Rac inhibition on MDCK cyst formation (89). Once again, these results illustrate how cell-intrinsic pathways can influence tissue morphogenesis.

Overall, several questions on the relationship between ECM and the generation of apicobasal polarity remain unanswered, all of which are fundamental for understanding the role of polarity in early carcinoma pathogenesis. First, what are the signaling pathways downstream of ECM, tensional force, and adhesion (integrin) receptors responsible for generating the proper apicobasal axis in normally formed glands? Second, what is the cross talk between cell-matrix adhesion pathways and the intrinsic polarity-regulating complexes? Finally, do specific components exist in any of the aforementioned pathways that can be used as biomarkers for early detection or targeted for therapeutic intervention in premalignant breast lesions? 3D culture models may prove useful for answering these important questions.

### HMT-3522 SERIES: A REVERSIBLE MODEL OF TUMOR PROGRESSION

Early studies revealed that human breast tumor cell lines do not form acini when grown in 3D culture; rather, they develop into nonpolarized clusters with limited differentiation (28). These landmark experiments demonstrated the stark contrast between the behavior of normal and tumor cells in 3D culture, even though only subtle phenotypic differences were evident when the same cells were grown as 2D monolayers. They also broached a fundamental biological and clinically relevant question regarding cancerous epithelium: Could the disorganized, nonpolarized

phenotype of tumorigenic cells be reorganized into a well-ordered normal architecture? Subsequently, numerous studies in the HMT-3522 model of human breast cancer progression demonstrated that modulating aberrantly expressed cell adhesion proteins in tumor cells can dominantly interfere with the phenotypic expression of the transformed state, even in the context of multiple oncogenic mutations (90).

### Phenotypic Reversion in Three-Dimensional Culture

The HMT-3522 progression series is a model of human breast cancer that progressively spans the continuum of morphological phenotype from normal cells to tumorigenesis (**Figure 5**). In the series, a nonmalignant S1 cell population forms growth-arrested normal acinar structures in 3D culture; premalignant S2 cells form noninvasive proliferating non-polarized colonies; and malignant T4-2 cells exhibit a highly disorganized, rapidly proliferating invasive structure in culture (31, 91, 92; A. Rizki & V.M. Weaver, unpublished results).

In investigating the differences in these cell lines at the molecular level, T4-2 cells were found to display dramatically higher levels of  $\beta 1$  integrin and EGFR as compared with nonmalignant S1 cells. The T4-2 phenotype could be reversed by blocking  $\beta 1$  integrin signaling via a function-blocking antibody, leading to the formation of growth-arrested acini similar to those observed in S1 cells (31). Moreover, this phenotypic reversion was functionally linked to the downregulation of both  $\beta 1$  integrin and the EGFR and their associated signaling networks, highlighting the intricate connection between  $\beta 1$  integrin and the EGFR signaling pathways. Conversely, neutralizing EGFR signaling results in normalized levels of  $\beta 1$  integrin signaling. Provocatively, these observed effects on tumor behavior depend completely upon a 3D context because such reciprocal cross talk between  $\beta 1$  integrin and EGFR is not observed in 2D monolayer cultures (93). Overall, these studies highlight the interplay of cell adhesion and growth factor receptor signaling pathways essential for maintaining the complex phenotypes during breast cancer progression.

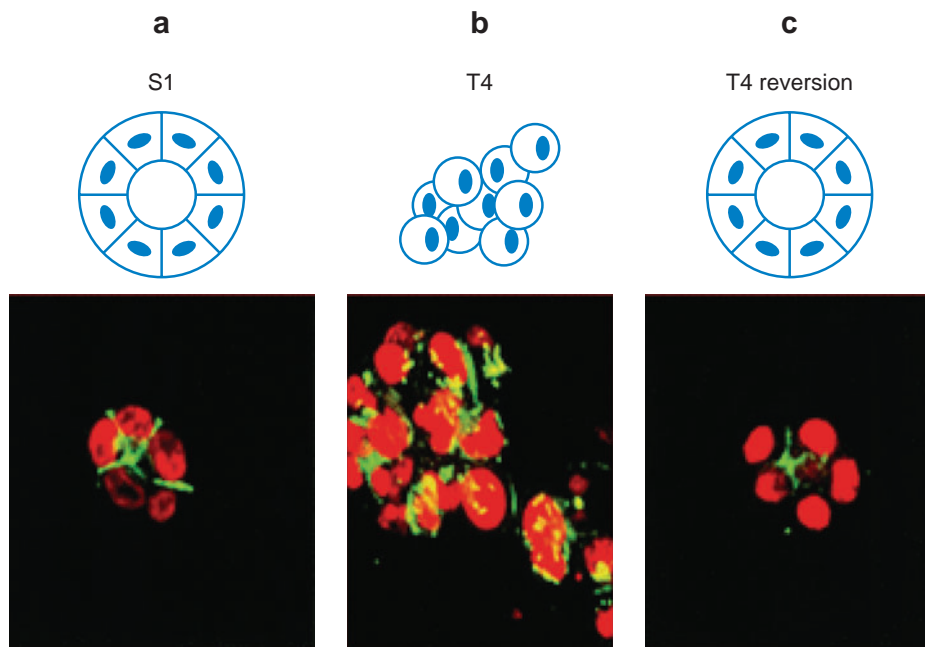


**Figure 5**

(a) HMT-3522 progression series. S1 cells form normal polarized acini in 3D culture. (b) T4 cells show a disruption in ductal morphology and uncontrolled cellular proliferation. (c) Following treatment with an antibody that blocks  $\beta 1$  integrin function, T4 cells undergo a morphogenetic reversion and form normal-appearing acini similar to the phenotype observed in S1 cells. Figure adapted with permission from Reference 31.

The HMT-3522 series has also facilitated the identification of novel molecules with potential tumor suppressor function. T4-2 cells possess reduced levels of  $\alpha$ -dystroglycan ( $\alpha$ -DG), a basement membrane receptor. Upon restoration of DG in T4-2 cells, polarized structures that are growth arrested form in 3D cultures; these cells also exhibit reduced tumorigenicity when engrafted into nude mice (94). Finally, analysis of multiple carcinoma cell lines indicates that higher levels of  $\alpha$ -DG correlated with the increased ability of these cells to form polarized structures in 3D culture, and examination of human breast and prostate cancers revealed losses in DG expression (94, 95). Although the exact role of DG in breast cancer remains unclear, these initial results obtained from 3D culture assays strongly suggest that it functions as a tumor suppressor and serves as a critical mediator of polarization effects induced by the basement membrane (96).

Studies in other models have further substantiated the importance of cell adhesion proteins in modulating the tumor phenotype.  $\alpha$ 2 integrin is expressed in normal differentiated MECs and frequently lost in undifferentiated carcinomas. Re-expression of  $\alpha$ 2 in the Mm5MT mouse adenocarcinoma cell line causes a dramatic reversion from disorganized clusters of spindle-shaped cells to organized gland-like structures in 3D culture (97). In addition, re-expression of the cell adhesion molecule CEACAM1 in the MCF-7 human breast cancer cell line and the restoration of gap junctions in MDA-435 breast tumor cells have both been shown to promote the formation of organized spheroid structures (57, 98).

### Polarity and Cell Survival

The importance of polarity in tumor cell survival has also been demonstrated through 3D culture studies of the HMT-3522 progression series and MCF-10A cells. The formation of polarized 3D structures confers protection from apoptosis to a variety of chemotherapeutic insults in both normal and malignant

MECs from the HMT-3522 progression series and MCF-10A cells (99; J. Friedland & V. Weaver, manuscript submitted). In contrast, nonpolarized cells are uniformly sensitive to apoptosis (99). Accordingly, disrupting the activation of the laminin receptor,  $\alpha$ 6 $\beta$ 4 integrin, perturbs hemidesmosome organization, disrupts polarity, and promotes apoptosis (99). Interestingly, resistance to apoptosis can be acquired in nonpolar cells by the autocrine secretion of laminin-5, which results in the ligation of  $\alpha$ 6 $\beta$ 4 integrin, as well as the activation of Rac and NF $\kappa$ B, a known positive modulator of cell survival (100). The excess secretion of laminin-5 in a nonpolarized manner upon hyperactivation of growth factor receptors, such as ErbB2, has also been observed during MCF-10A morphogenesis and may contribute to the ability of cells to survive in the lumen (34). Overall, these results indicate that the prosurvival effects associated with the polarized state in 3D culture can be co-opted by the activation of specific survival signals provided by nonpolarized laminin-5 secretion.

### Predicting Patient Outcome Using Three-Dimensional Models

More recently, a microarray analysis was conducted in S1 cells to search for transcripts that changed upon transition to an organized, growth-arrested state in 3D culture. These expression profiles were compared against a breast cancer-specific gene expression signature derived from patients of known outcomes to identify potential prognostic markers (101). In comparing transcripts that were downregulated in growth-arrested acini to previously published human breast cancer microarray data, a group of 19 genes was selected to test as markers for cancer prognosis. Of these 19 genes, 14 correlated significantly with disease-free survival. In addition, by using a second less-restrictive strategy, 287 genes that were downregulated with the formation of growth-arrested 3D acini were tested for their ability to predict cancer prognosis and showed



significant correlation with poor prognosis patient outcomes. This study thus represents an innovative method for identifying genome-wide prognostic markers in breast cancer (101).

## FORCE AS A REGULATOR OF ADHESION FORMATION AND SIGNALING

In addition to intracellular signaling pathways mediating effects on tissue morphogenesis, the impact of force upon cells is quickly emerging as a mediator of cell growth, differentiation, and 3D tissue architecture. Within a given tissue, individual cells are subject to dynamic macroforces mediated by the tissue as a whole, as well as microphysical forces resulting from local cell-cell and cell-ECM adhesion (see What is Force?). These forces dictate tissue architecture and have been demonstrated to be critical for normal embryogenesis. Venous embryo explants require mechanical stress and strain for normal development and tissue differentiation (102). In *Drosophila*, formation of the dorsal-ventral axis in the fly embryo via the Armadillo-Twist signaling pathway requires cell compression, which occurs through normal movement during morphogenesis; remarkably, this compression can be simulated by externally applying force with a micropipette (103). In addition, cells transduce force onto their surrounding milieu, which is required for development. For example, *Xenopus* gastrulation requires the specific patterning of the small GTP-binding proteins Rho and Rac, main mediators of cell adhesion and contractility, for orientation of the trunk and head mesoderm (104, 105).

### Focal Adhesions and Force

A variety of distinct adhesions form between cells and the ECM, each with their own size, shape, and molecular composition (106, 107). These include focal adhesions (FAs), focal complexes, fibrillar adhesions, and 3D ma-

## WHAT IS FORCE?

Cells within tissues are exposed to a variety of mechanical stresses that differ in magnitude and duration. These stresses are defined as force per unit area in Newtons per meters squared. They can be macroforces, occurring at the level of the tissue, or microforces, owing to the interaction of the cell with other cells or with the ECM. The intrinsic resistance of a given tissue to a stress is measured by the elastic modulus of that tissue,  $E$ , which is defined in Pascals and can be obtained by applying a force to a section of tissue and measuring the relative change in length or strain. Generally, cells sense mechanical stress as either a parallel applied force, also known as shear stress, or a perpendicularly applied force that includes both compressive stresses and tensile stresses.

trix adhesions; the best characterized of these is the FA (108–110). FAs are relatively stable complexes that form through the coordinated interactions of various signaling, adaptor, and structural molecules, thereby linking the ECM and integrin receptors to the cytoskeleton (111). Binding of the ECM by adherent cells occurs via integrins, making them a central component of microenvironmental sensing. Interestingly, force appears to play a role in the development of FAs, as maturation of this complex has been shown to require mechanical tension (112, 113). Within minutes of placement of cells upon an ECM-coated surface, cells form focal complexes, small precursor adhesions to the larger FAs (114). By utilizing flexible substrates that deform upon cellular contraction, investigators have found that FA assembly and individual FA size correlate positively with the local distribution of force at adhesions (113, 115, 116). Similarly, in experiments in which external forces are applied directly to adhesions, the strength of the FA increases with the amount of force applied (117–119). These results suggest that external stress and strain promote the formation and strength of adhesion complexes.

Many signaling proteins are located at cell-ECM contacts, including focal adhesion kinase (FAK) and Src family kinases (120–122).

---

**Focal adhesions (FAs):** dynamic complexes of signaling, adaptor, and structural proteins that transmit extracellular matrix/integrin-based biochemical and mechanical signals to the cytoskeleton

---

As these proteins function in growth-factor-mediated signaling cascades, their presence strongly suggests that signaling through adhesions coordinates integrin and growth factor signaling; moreover, they may translate ECM-associated mechanical stimuli to elicit changes in cellular morphology and function (123). FAK is an essential regulator of mechanotransduction; increased mechanical stress at FAs through increased intracellular tension or externally applied forces results in signaling changes at FAs through FAK activation of downstream signaling effectors (**Figure 6**) (124, 125). When mechanical stretch is applied to cells, FAK is activated,

resulting in both increased magnitude and duration of activation of the mitogen-activated protein kinase ERK, and increased cellular proliferation (126, 127). FAK activation is required for ERK activation and subsequent progression of cells through G1 (**Figure 6**) (128). Interestingly, use of a kinase-dead mutant of FAK results in the abrogation of ERK activation and leads to a block in mechanically induced cellular proliferation (129, 130). Conversely, expression of a constitutively activated FAK leads to cellular transformation and adherence-independent growth (131). Taken together, these results suggest that FAK serves as a major mediator of

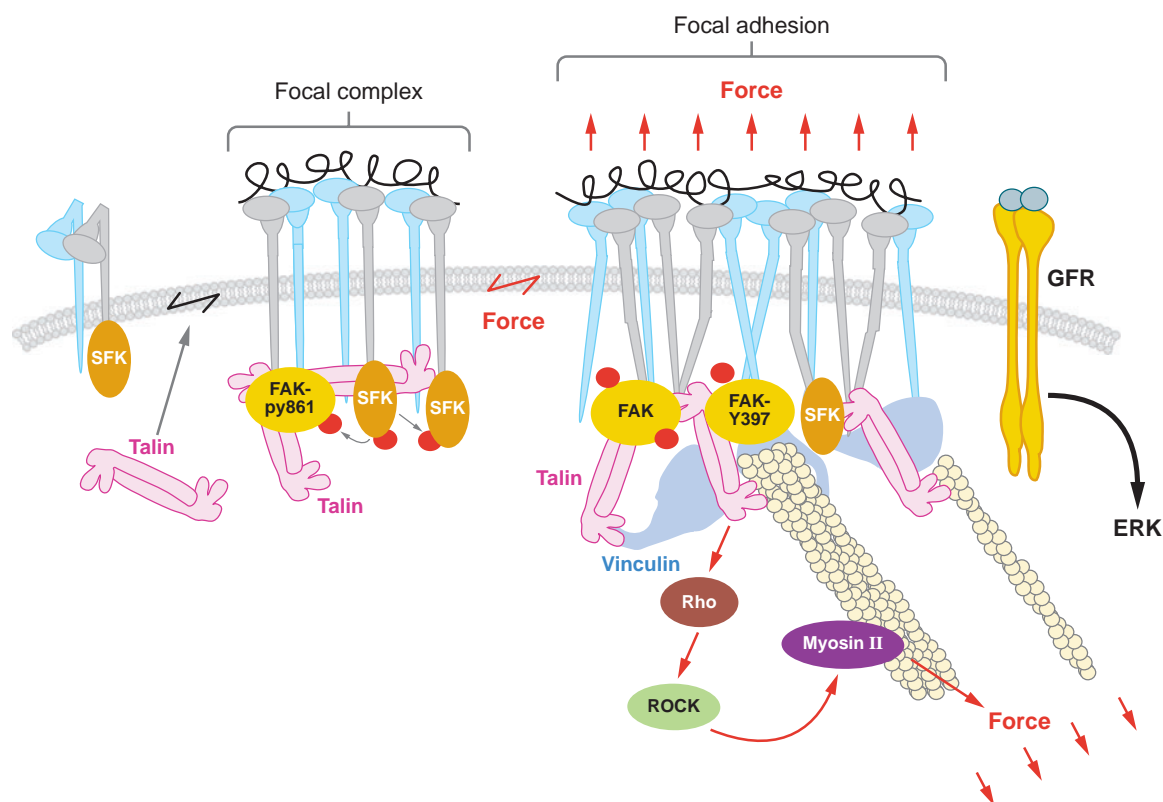


**Figure 6**

Force-dependent focal adhesion assembly. Application of force implemented by the presence of a stiff matrix results in activation-specific phosphorylation of focal adhesion kinase (FAK) at tyrosine 397 and tethering of the mature adhesion complex, including Src family kinases (SFK), to the cytoskeleton. Integrin clustering and subsequent focal adhesion maturation is accompanied by subsequent growth factor receptor (GFR)-induced activation of ERK signaling and potential activation of cell growth. Figure adapted with permission from Reference 45.

mechanotransduction and acts to translate extracellular forces sensed by integrins into proliferative cellular cues.

## Force and Mammary Tissue Homeostasis

During mammary morphogenesis, physical force, including clefting force and surface tension resulting from the interplay between the epithelial and mesenchymal tissues, tremendously impacts the shaping of the ductal branches (132). In similarly branched tissues, such as the lung and kidney, the activity of the small protein GTPase Rho, a major signaling molecule in intracellular tension generation, plays a regulatory role in branching morphogenesis (133, 134), suggesting a similar role for Rho in the developing mammary gland. Indeed, rigid 3D collagen gels influence branching behavior of malignant transformed MECs in culture by regulating RhoA GTPase activity (135). Furthermore, the mechanical properties of the basement membrane are crucial for normal 3D mammary differentiation in vitro because expression of milk proteins, such as  $\beta$  casein expression, occurs only on a highly compliant basement membrane or on floating collagen gels (26, 42). Conversely, the morphogenesis and functional differentiation of mammary epithelial acini cannot occur when MECs are placed on rigid collagen gels because collagen I does not facilitate proper cell rounding and, thus, hinders the assembly of an endogenous basement membrane at the basal cell surface. Therefore, the mechanical environment in which MECs exist can dictate their behavior.

Breast malignancy is characterized by a dramatic increase in mammary gland tension due to increased compression force and tensile stress resulting from altered vasculature and tumor growth as well as stiffening of the ECM due to fibrosis (18, 136). Such increased rigidity has been postulated to both impede treatment effectiveness and enhance metastasis (137, 138). Because force is required for FA maturation and FAK-induced signaling,

one can hypothesize that increased tensional force in the mammary gland contributes to tumorigenesis via activation of integrin-linked proliferative signaling pathways in individual MECs. Moreover, because cells grown as 3D cultures behave differently with regard to cell morphology, integrin signaling, and actin cytoskeletal structures (108, 139), it is important to analyze the contribution of force to mammary malignancy within a 3D context.

Recently, matrix stiffness was linked to malignancy in the context of 3D architecture (**Figure 7**) (45). When 3D tissue culture methods utilizing basement membrane/collagen I gels of increasing stiffness were employed, MCF-10A cells and S1 cells from the HMT-3522 series were grown and allowed to form acini. Interestingly, acinar morphology was increasingly perturbed with increases in matrix stiffness, resulting in non-spherical structures devoid of a central lumen and increased cell spreading, suggesting that the architectural tension surrounding MECs can alter normal 3D morphogenesis (**Figure 3**). Furthermore, increased FAK activation was observed in cells grown in a stiff environment, implying that integrin adhesions may be altered in cells grown on a stiff matrix and that maturation of focal complexes into FAs may take place more readily in a stiff environment. Interestingly, expression of mutant integrin subunits that promote integrin self-association and clustering led to a stiff-matrix cell phenotype with altered acini formation and increased cell spreading in a soft-matrix environment. In addition, repressing ERK activity elicited phenotypic reversion in these cells, implicating ERK signaling as a critical mediator of integrin-associated sensing of ECM compliance. Finally, matrix rigidity increased Rho activity, and a constitutively active Rho mutant increased the number and size of FAs as well as promoted cell spreading in a soft environment (45). Overall, these 3D studies broached the concept that changes in mechanical properties may regulate cell behavior relevant for malignant transformation.

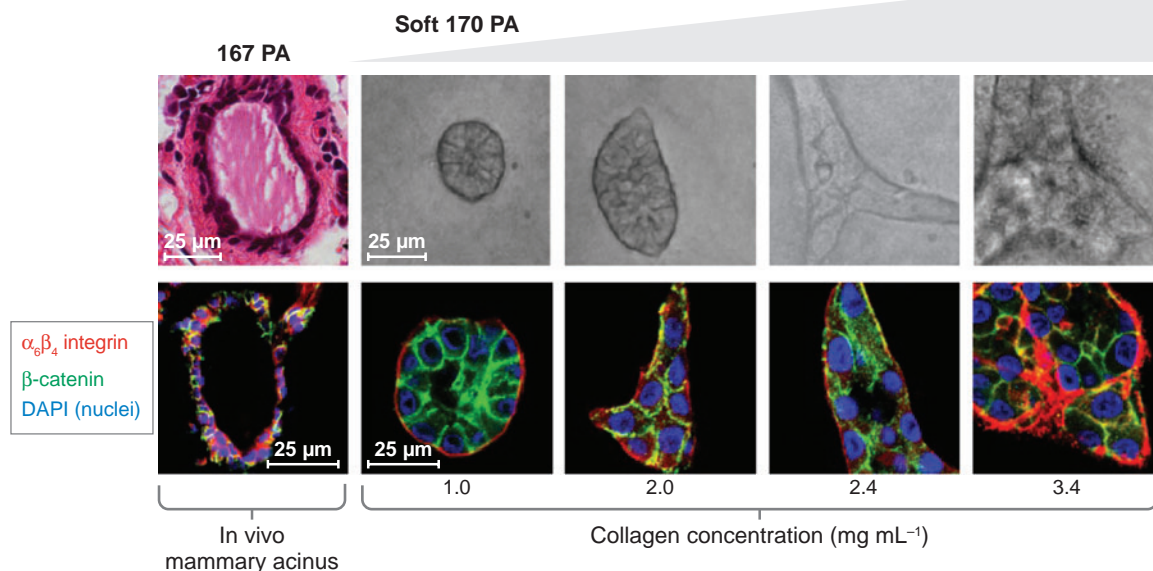


**Figure 7**

Altered 3D growth and morphogenesis of mammary epithelial cells with increased matrix rigidity. (*Top*) Phase contrast images and images of H&E-stained tissue comparing the morphogenesis of a mammary gland duct in a normal compliant environment (167 Pa) to mammary epithelial cells grown in reconstituted basement membrane/collagen I gels of increasing stiffness (170–1200 Pa). (*Bottom*) Confocal microscopic cross sections of a normal mammary duct versus mammary epithelial cell colonies cultured in increasingly stiff environments. Figure adapted with permission from Reference 45.

## CONCLUSION

The studies overviewed here illustrate the power of 3D epithelial culture models as a tractable *in vitro* approach to model the early events in breast carcinoma formation. In recent years, these models have greatly illuminated our understanding of the fundamental biological processes that direct the histological abnormalities observed microscopically during the earliest stages of breast cancer. They also have provided a unique platform to discover previously unappreciated

mechanical influences on glandular epithelial architecture and homeostasis. Nevertheless, current 3D culture models do have inherent limitations in modeling *in vivo* tissue behavior. The further improvement of 3D culture systems, particularly the development of innovative heterotypic coculture strategies and tunable biomaterial scaffolds, will be invaluable in modeling cancer progression and testing novel therapeutic strategies in a biologically relevant context.

## SUMMARY POINTS

1. Epithelial cells grown in 3D recreate several cardinal features of glandular epithelium *in vivo*, including the formation of cyst-like acini with a hollow lumen, the apicobasal polarization of cells surrounding this luminal space, and the tight regulation of cell growth and proliferation. Cancer genes produce diverse morphogenetic phenotypes

in 3D cultures that resemble important histopathological features observed in carcinomas in vivo.

2. Cells occupying the hollow lumen of acini normally undergo apoptosis owing to the lack of ECM attachment (*anoikis*). However, numerous oncogenes and pathways aberrantly promote cell survival in the luminal space of 3D structures; the resultant phenotypes recapitulate the luminal filling observed in premalignant breast lesions.
3. Apicobasal polarity is a fundamental characteristic of glandular epithelium in vivo and in vitro. Recent studies using 3D culture systems are beginning to delineate how cell polarity regulates normal gland architecture and how the disruption of this polarity may contribute to carcinoma formation.
4. Studies of epithelial tumor cells in 3D culture demonstrate that modulating cell adhesion and growth factor receptor pathways can repress the phenotypic expression of their transformed state, even in the context of multiple oncogenic mutations.
5. Breast cancers are characterized by a dramatic increase in tissue stiffness due in part to bulk tumor growth, altered vasculature, and the expansion of a rigid (desmoplastic) stroma. Recent studies reveal that increasing matrix stiffness disrupts normal 3D morphogenesis and promotes several architectural features associated with malignancy.

## FUTURE ISSUES

1. Immortalized human MEC lines commonly utilized for 3D culture assays express markers of both luminal and myoepithelial cell lineages. The hybrid nature of such lines limits 3D culture models in terms of their ability to simulate events in breast carcinoma progression in vivo. Improving cell culture conditions to propagate primary human mammary cells is critical in developing faithful 3D models for studying breast cancer initiation and progression.
2. A large fraction of human breast cancers are hormonally regulated; indeed, estrogen receptor and progesterone receptor status are a major prognostic determinant in breast tumors. However, owing to the lack of availability of human MECs (both primary cells and cell lines) responsive to these principal mammary hormones, the impact of hormone receptor activation on 3D breast morphogenesis remains completely unknown. 3D culture systems incorporating the intricate hormonal signaling unique to the mammary gland should be developed.
3. The studies discussed here utilize monotypic culture systems, in which epithelial cells are grown in isolation within a 3D scaffold. Because both normal epithelial tissues and tumors represent a community of heterotypic cell types, the use of such monotypic 3D cultures has inherent limitations. Hence, both current and future research efforts demand heterotypic culture systems that recreate the histological complexity of epithelial tissue in vivo.

## DISCLOSURE STATEMENT

The authors are not aware of any biases that might be perceived as affecting the objectivity of this review.

## ACKNOWLEDGMENTS

V.M.W. is supported by the National Institutes of Health (RO1CA078731) and the Department of Defense (DAMD1701-1-0368, 1703-1-0496, and W81XWH-05-1-330). J.D. is supported by the National Institutes of Health (K08CA098419), a Culpeper Medical Scholarship (Partnership for Cures), a Howard Hughes Medical Institute Early Career Award, and the University of California, San Francisco, Sandler Program in Basic Sciences.

## LITERATURE CITED

1. Harris J, Lippman M, Morrow M, Osborne C. 1999. *Diseases of the Breast*. Philadelphia, PA: Lippincott, Williams & Wilkins
2. Ernster VL, Barclay J, Kerlikowske K, Grady D, Henderson C. 1996. Incidence of and treatment for ductal carcinoma in situ of the breast. *JAMA* 275:913-18
3. Page DL, Dupont WD, Rogers LW, Rados MS. 1985. Atypical hyperplastic lesions of the female breast. A long-term follow-up study. *Cancer* 55:2698-708
4. Burstein HJ, Polyak K, Wong JS, Lester SC, Kaelin CM. 2004. Ductal carcinoma in situ of the breast. *N. Engl. J. Med.* 350:1430-41
5. Toikkanen S, Pylkkanen L, Joensuu H. 1997. Invasive lobular carcinoma of the breast has better short- and long-term survival than invasive ductal carcinoma. *Br. J. Cancer* 76:1234-40
6. Simpson JF, Page DL. 2001. Pathology of preinvasive and excellent prognosis breast cancer. *Curr. Opin. Oncol.* 13:426-30
7. van de Vijver MJ, Peterse JL, Mooi WJ, Wisman P, Lomans J, et al. 1988. Neu-protein overexpression in breast cancer. Association with comedo-type ductal carcinoma in situ and limited prognostic value in stage II breast cancer. *N. Engl. J. Med.* 319:1239-45
8. Ganesan S, Richardson AL, Wang ZC, Iglehart JD, Miron A, et al. 2005. Abnormalities of the inactive X chromosome are a common feature of BRCA1 mutant and sporadic basal-like breast cancer. *Cold Spring Harbor Symp. Quant. Biol.* 70:93-97
9. Berr G, Cleton-Jansen AM, Strumane K, de Leeuw WJ, Nollet F, et al. 1996. E-cadherin is inactivated in a majority of invasive human lobular breast cancers by truncation mutations throughout its extracellular domain. *Oncogene* 13:1919-25
10. Perou CM, Sorlie T, Eisen MB, van de Rijn M, Jeffrey SS, et al. 2000. Molecular portraits of human breast tumours. *Nature* 406:747-52
11. Ramaswamy S, Tamayo P, Rifkin R, Mukherjee S, Yeang CH, et al. 2001. Multiclass cancer diagnosis using tumor gene expression signatures. *Proc. Natl. Acad. Sci. USA* 98:15149-54
12. Debnath J, Muthuswamy SK, Brugge JS. 2003. Morphogenesis and oncogenesis of MCF-10A mammary epithelial acini grown in three-dimensional basement membrane cultures. *Methods* 30:256-68
13. Schmeichel KL, Bissell MJ. 2003. Modeling tissue-specific signaling and organ function in three dimensions. *J. Cell Sci.* 116:2377-88
14. Debnath J, Brugge JS. 2005. Modelling glandular epithelial cancers in three-dimensional cultures. *Nat. Rev. Cancer* 5:675-88
15. Coucouvanis E, Martin GR. 1995. Signals for death and survival: a two-step mechanism for cavitation in the vertebrate embryo. *Cell* 83:279-87
16. Dressler GR. 2006. The cellular basis of kidney development. *Annu. Rev. Cell Dev. Biol.* 22:509-29
17. Barros EJ, Santos OF, Matsumoto K, Nakamura T, Nigam SK. 1995. Differential tubulogenic and branching morphogenetic activities of growth factors: implications for epithelial tissue development. *Proc. Natl. Acad. Sci. USA* 92:4412-16



18. Paszek MJ, Weaver VM. 2004. The tension mounts: mechanics meets morphogenesis and malignancy. *J. Mammary Gland Biol. Neoplasia* 9:325–42
19. Sternlicht MD. 2006. Key stages in mammary gland development: the cues that regulate ductal branching morphogenesis. *Breast Cancer Res.* 8:201
20. Fata JE, Werb Z, Bissell MJ. 2004. Regulation of mammary gland branching morphogenesis by the extracellular matrix and its remodeling enzymes. *Breast Cancer Res.* 6:1–11
21. Sternlicht MD, Kouros-Mehr H, Lu P, Werb Z. 2006. Hormonal and local control of mammary branching morphogenesis. *Differentiation* 74:365–81
22. Howard BA, Gusterson BA. 2000. Human breast development. *J. Mammary Gland Biol. Neoplasia* 5:119–37
23. Hennighausen L, Robinson GW. 2005. Information networks in the mammary gland. *Nat. Rev. Mol. Cell Biol.* 6:715–25
24. Humphreys RC, Krajewska M, Krnacik S, Jaeger R, Weiher H, et al. 1996. Apoptosis in the terminal endbud of the murine mammary gland: a mechanism of ductal morphogenesis. *Development* 122:4013–22
25. Bissell MJ, Barcellos-Hoff MH. 1987. The influence of extracellular matrix on gene expression: Is structure the message? *J. Cell Sci. Suppl.* 8:327–43
26. Barcellos-Hoff MH, Aggeler J, Ram TG, Bissell MJ. 1989. Functional differentiation and alveolar morphogenesis of primary mammary cultures on reconstituted basement membrane. *Development* 105:223–35
27. Streuli CH, Bissell MJ. 1990. Expression of extracellular matrix components is regulated by substratum. *J. Cell Biol.* 110:1405–15
28. Petersen OW, Ronnov-Jessen L, Howlett AR, Bissell MJ. 1992. Interaction with basement membrane serves to rapidly distinguish growth and differentiation pattern of normal and malignant human breast epithelial cells. *Proc. Natl. Acad. Sci. USA* 89:9064–68. Erratum 1993. *Proc. Natl. Acad. Sci. USA* 90:2556
29. Grant DS, Kleinman HK, Leblond CP, Inoue S, Chung AE, et al. 1985. The basement-membrane-like matrix of the mouse EHS tumor: II. Immunohistochemical quantitation of six of its components. *Am. J. Anat.* 174:387–98
30. Gudjonsson T, Ronnov-Jessen L, Villadsen R, Rank F, Bissell MJ, Peterson OW. 2002. Normal and tumor-derived myoepithelial cells differ in their ability to interact with luminal breast epithelial cells for polarity and basement membrane deposition. *J. Cell Sci.* 115:39–50
31. Weaver VM, Petersen OW, Wang F, Larabell CA, Briand P, et al. 1997. Reversion of the malignant phenotype of human breast cells in three-dimensional culture and in vivo by integrin blocking antibodies. *J. Cell Biol.* 137:231–45
32. Niemann C, Brinkmann V, Spitzer E, Hartmann G, Sachs M, et al. 1998. Reconstitution of mammary gland development in vitro: requirement of c-met and c-erbB2 signaling for branching and alveolar morphogenesis. *J. Cell Biol.* 143:533–45
33. Roskelley CD, Desprez PY, Bissell MJ. 1994. Extracellular matrix-dependent tissue-specific gene expression in mammary epithelial cells requires both physical and biochemical signal transduction. *Proc. Natl. Acad. Sci. USA* 91:12378–82
34. Muthuswamy SK, Li D, Lelievre S, Bissell MJ, Brugge JS. 2001. ErbB2, but not ErbB1, reinitiates proliferation and induces luminal repopulation in epithelial acini. *Nat. Cell Biol.* 3:785–92
35. Dimri G, Band H, Band V. 2005. Mammary epithelial cell transformation: insights from cell culture and mouse models. *Breast Cancer Res.* 7:171–79

---

**28. Demonstrates stark phenotypic contrasts between normal cells and tumor cells when they are grown in 3D but not 2D cultures.**

---



---

**31. The tissue phenotype of genotypically abnormal cells can be regulated in 3D by altering specific cell adhesion pathways.**

---



---

**34. The inducible dimerization of two closely related receptor tyrosine kinases of the EGFR family, ErbB1 and ErbB2, elicits distinct and unexpected effects on 3D epithelial architecture.**

---

---

**45. Increasing matrix stiffness disrupts normal 3D morphogenesis, demonstrating that mechanotransduction may directly regulate malignant transformation.**

---



---

**48. Demonstrates that filling of the 3D lumen commonly found in early breast cancers requires increased proliferation combined with increased survival of the excess proliferating cells in the lumen.**

---

36. Blatchford DR, Quarrie LH, Tonner E, McCarthy C, Flint DJ, et al. 1999. Influence of microenvironment on mammary epithelial cell survival in primary culture. *J. Cell Physiol.* 181:304–11
37. Wang AZ, Ojakian GK, Nelson WJ. 1990. Steps in the morphogenesis of a polarized epithelium. II. Disassembly and assembly of plasma membrane domains during reversal of epithelial cell polarity in multicellular epithelial (MDCK) cysts. *J. Cell Sci.* 95(Pt. 1):153–65
38. Roeder BA, Kokini K, Sturgis JE, Robinson JP, Voytik-Harbin SL. 2002. Tensile mechanical properties of three-dimensional type I collagen extracellular matrices with varied microstructure. *J. Biomech. Eng.* 124:214–22
39. Christner PJ, Gentiletti J, Peters J, Ball ST, Yamauchi M, et al. 2006. Collagen dysregulation in the dermis of the *Sagg*<sup>+/+</sup> mouse: a loose skin model. *J. Invest. Dermatol.* 126:595–602
40. Girton TS, Oegema TR, Tranquillo RT. 1999. Exploiting glycation to stiffen and strengthen tissue equivalents for tissue engineering. *J. Biomed. Mater. Res.* 46:87–92
41. Martin RB, Lau ST, Mathews PV, Gibson VA, Stover SM. 1996. Collagen fiber organization is related to mechanical properties and remodeling in equine bone. A comparison of two methods. *J. Biomech.* 29:1515–21
42. Emerman JT, Pitelka D. 1977. Maintenance and induction of morphological differentiation in dissociated mammary epithelium on floating collagen membranes. *In Vitro* 13:316–28
43. Emerman JT, Bartley JC, Bissell MJ. 1980. Interrelationship of glycogen metabolism and lactose synthesis in mammary epithelial cells of mice. *Biochem. J.* 192:695–702
44. Pelham RJ Jr, Wang Y. 1997. Cell locomotion and focal adhesions are regulated by substrate flexibility. *Proc. Natl. Acad. Sci. USA* 94:13661–65
45. Paszek MJ, Zahir N, Johnson KR, Lakins JN, Rozenberg GI, et al. 2005. Tensional homeostasis and the malignant phenotype. *Cancer Cell* 8:241–54
46. Raeber GP, Lutolf MP, Hubbell JA. 2005. Molecularly engineered PEG hydrogels: a novel model system for proteolytically mediated cell migration. *Biophys. J.* 89:1374–88
47. Vinatier C, Magne D, Weiss P, Trojani C, Rochet N, et al. 2005. A silanized hydroxypropyl methylcellulose hydrogel for the three-dimensional culture of chondrocytes. *Biomaterials* 26:6643–51
48. Debnath J, Mills KR, Collins NL, Reginato MJ, Muthuswamy SK, Brugge JS. 2002. The role of apoptosis in creating and maintaining luminal space within normal and oncogene-expressing mammary acini. *Cell* 111:29–40
49. Meredith JE Jr, Fazeli B, Schwartz MA. 1993. The extracellular matrix as a cell survival factor. *Mol. Biol. Cell* 4:953–61
50. Frisch SM, Francis H. 1994. Disruption of epithelial cell-matrix interactions induces apoptosis. *J. Cell Biol.* 124:619–26
51. Boudreau N, Sympson CJ, Werb Z, Bissell MJ. 1995. Suppression of ICE and apoptosis in mammary epithelial cells by extracellular matrix. *Science* 267:891–93
52. Gilmore AP. 2005. Anoikis. *Cell Death Differ.* 12(Suppl. 2):1473–77
53. Reginato MJ, Mills KR, Becker EB, Lynch DK, Bonni A, et al. 2005. Bim regulation of lumen formation in cultured mammary epithelial acini is targeted by oncogenes. *Mol. Cell Biol.* 25:4591–601
54. Reginato MJ, Mills KR, Paulus JK, Lynch DK, Sgroi DC, et al. 2003. Integrins and EGFR coordinately regulate the proapoptotic protein Bim to prevent anoikis. *Nat. Cell Biol.* 5:733–40



55. Mailleux AA, Overholtzer M, Schmelzle T, Bouillet P, Strasser A, et al. 2007. BIM regulates apoptosis during mammary ductal morphogenesis, and its absence reveals alternative cell death mechanisms. *Dev. Cell* 12:221–34
56. Huang J, Hardy JD, Sun Y, Shively JE. 1999. Essential role of biliary glycoprotein (CD66a) in morphogenesis of the human mammary epithelial cell line MCF10F. *J. Cell Sci.* 112:4193–205
57. Kirshner J, Chen CJ, Liu P, Huang J, Shively JE. 2003. CEACAM1–4S, a cell-cell adhesion molecule, mediates apoptosis and reverts mammary carcinoma cells to a normal morphogenic phenotype in a 3D culture. *Proc. Natl. Acad. Sci. USA* 100:521–26
58. Alroy I, Yarden Y. 1997. The ErbB signaling network in embryogenesis and oncogenesis: signal diversification through combinatorial ligand-receptor interactions. *FEBS Lett.* 410:83–86
59. Riese D, Stern D. 1998. Specificity within the EGF family/ErbB receptor family signaling network. *BioEssays* 20:41–48
60. Olayioye M, Neve R, Lane H, Hynes N. 2000. The ErbB signaling network: receptor heterodimerization in development and cancer. *EMBO J.* 19:3159–67
61. Hynes N, Stern D. 1994. The biology of erbB-2/neu/HER-2 and its role in cancer. *Biochim. Biophys. Acta* 1198:165–84
62. Harari D, Yarden Y. 2000. Molecular mechanisms underlying ErbB2/HER2 action in breast cancer. *Oncogene* 19:6102–14
63. Moody SE, Sarkisian CJ, Hahn KT, Gunther EJ, Pickup S, et al. 2002. Conditional activation of Neu in the mammary epithelium of transgenic mice results in reversible pulmonary metastasis. *Cancer Cell* 2:451–61
64. Muraoka RS, Koh Y, Roebuck LR, Sanders ME, Brantley-Sieders D, et al. 2003. Increased malignancy of Neu-induced mammary tumors overexpressing active transforming growth factor  $\beta$ 1. *Mol. Cell Biol.* 23:8691–703
65. Wulf G, Garg P, Liou YC, Iglehart D, Lu KP. 2004. Modeling breast cancer in vivo and ex vivo reveals an essential role of Pin1 in tumorigenesis. *EMBO J.* 23:3397–407
66. Wenjun G, Pylayeva Y, Pepe A, Yoshioka T, Muller W, et al. 2006.  $\beta$  four integrin amplifies ErbB2 signaling to promote mammary tumorigenesis. *Cell* 126:489–502
67. Wrobel CN, Debnath J, Lin E, Beausoleil S, Roussel MF, et al. 2004. Autocrine CSF-1R activation promotes Src-dependent disruption of mammary epithelial architecture. *J. Cell Biol.* 165:263–73
68. Irie HY, Pearline RV, Grueneberg D, Hsia M, Ravichandran P, et al. 2005. Distinct roles of Akt1 and Akt2 in regulating cell migration and epithelial-mesenchymal transition. *J. Cell Biol.* 171:1023–34
69. Debnath J, Walker SJ, Brugge JS. 2003. Akt activation disrupts mammary acinar architecture and enhances proliferation in an mTOR-dependent manner. *J. Cell Biol.* 163:315–26
70. Isakoff SJ, Engelman JA, Irie HY, Luo J, Brachmann SM, et al. 2005. Breast cancer-associated PIK3CA mutations are oncogenic in mammary epithelial cells. *Cancer Res.* 65:10992–1000
71. Klionsky DJ, Emr SD. 2000. Autophagy as a regulated pathway of cellular degradation. *Science* 290:1717–21
72. Levine B, Klionsky DJ. 2004. Development by self-digestion: molecular mechanisms and biological functions of autophagy. *Dev. Cell* 6:463–77
73. Debnath J, Baehrecke EH, Kroemer G. 2005. Does autophagy contribute to cell death? *Autophagy* 1:66–74
74. Helminen H, Ericsson J. 1968. Studies on mammary gland involution II. Ultrastructural evidence for auto- and heterophagocytosis. *J. Ultrastruct. Res.* 25:214–27

75. Mills K, Reginato M, Debnath J, Queenan B, Brugge J. 2004. Tumor necrosis factor-related apoptosis-inducing ligand (TRAIL) is required for induction of autophagy during lumen formation in vitro. *Proc. Natl. Acad. Sci. USA* 101:3438–43
76. Humbert P, Russell S, Richardson H. 2003. Dlg, Scribble and Lgl in cell polarity, cell proliferation and cancer. *BioEssays* 25:542–53
77. Knust E, Bossinger O. 2002. Composition and formation of intercellular junctions in epithelial cells. *Science* 298:1955–59
78. Nelson WJ. 2003. Adaptation of core mechanisms to generate cell polarity. *Nature* 422:766–74
79. Bilder D. 2004. Epithelial polarity and proliferation control: links from the *Drosophila* neoplastic tumor suppressors. *Genes Dev.* 18:1909–25
80. Médina E, Lemmers C, Lane-Guermonprez L, Le Bivic A. 2002. Role of the Crumbs complex in the regulation of junction formation in *Drosophila* and mammalian epithelial cells. *Biol. Cell* 94:305–13
81. Suzuki A, Ohno S. 2006. The PAR-aPKC system: lessons in polarity. *J. Cell Sci.* 119:979–87
82. Humbert PO, Dow LE, Russell SM. 2006. The Scribble and Par complexes in polarity and migration: friends or foes? *Trends Cell Biol.* 16:622–30
83. Roh MH, Makarova O, Liu CJ, Shin K, Lee S, et al. 2002. The Maguk protein, Pals1, functions as an adapter, linking mammalian homologues of Crumbs and Discs Lost. *J. Cell Biol.* 157:161–72
84. Makarova O, Roh MH, Liu CJ, Laurinec S, Margolis B. 2003. Mammalian Crumbs3 is a small transmembrane protein linked to protein associated with Lin-7 (Pals1). *Gene* 302:21–29
85. Straight SW, Shin K, Fogg VC, Fan S, Liu CJ, et al. 2004. Loss of PALS1 expression leads to tight junction and polarity defects. *Mol. Biol. Cell* 15:1981–90
86. Martin-Belmonte F, Gassama A, Datta A, Yu W, Rescher U, et al. 2007. PTEN-mediated apical segregation of phosphoinositides controls epithelial morphogenesis through Cdc42. *Cell* 128:383–97
87. Aranda V, Haire T, Nolan ME, Calarco JP, Rosenberg AZ, et al. 2006. Par6-aPKC uncouples ErbB2 induced disruption of polarized epithelial organization from proliferation control. *Nat. Cell Biol.* 8:1235–45
88. Chambard M, Verrier B, Gabrion J, Mauchamp J. 1984. Polarity reversal of inside-out thyroid follicles cultured within collagen gel: reexpression of specific functions. *Biol. Cell* 51:315–25
89. O'Brien LE, Jou TS, Pollack AL, Zhang Q, Hansen SH, et al. 2001. Rac1 orientates epithelial apical polarity through effects on basolateral laminin assembly. *Nat. Cell Biol.* 3:831–38
90. Kenny PA, Bissell MJ. 2003. Tumor reversion: correction of malignant behavior by microenvironmental cues. *Int. J. Cancer* 107:688–95
91. Briand P, Petersen OW, Van Deurs B. 1987. A new diploid nontumorigenic human breast epithelial cell line isolated and propagated in chemically defined medium. *In Vitro Cell Dev. Biol.* 23:181–88
92. Nielsen KV, Madsen MW, Briand P. 1994. In vitro karyotype evolution and cytogenetic instability in the nontumorigenic human breast epithelial cell line HMT-3522. *Cancer Genet. Cytogenet.* 78:189–99
93. Wang F, Weaver VM, Petersen OW, Larabell CA, Dedhar S, et al. 1998. Reciprocal interactions between  $\beta$ 1-integrin and epidermal growth factor receptor in three-dimensional

- basement membrane breast cultures: a different perspective in epithelial biology. *Proc. Natl. Acad. Sci. USA* 95:14821–26
94. Muschler J, Levy D, Boudreau R, Henry M, Campbell K, et al. 2002. A role for dystroglycan in epithelial polarization: loss of function in breast tumor cells. *Cancer Res.* 62:7102–9
95. Henry MD, Cohen MB, Campbell KP. 2001. Reduced expression of dystroglycan in breast and prostate cancer. *Hum. Pathol.* 32:791–95
96. Weir ML, Muschler J. 2003. Dystroglycan: emerging roles in mammary gland function. *J. Mammary Gland Biol. Neoplasia* 8:409–19
97. Zutter MM, Santoro SA, Staatz WD, Tsung YL. 1995. Re-expression of the  $\alpha 2 \beta 1$  integrin abrogates the malignant phenotype of breast carcinoma cells. *Proc. Natl. Acad. Sci. USA* 92:7411–15
98. Hirschi KK, Xu CE, Tsukamoto T, Sager R. 1996. Gap junction genes Cx26 and Cx43 individually suppress the cancer phenotype of human mammary carcinoma cells and restore differentiation potential. *Cell Growth Differ.* 7:861–70
99. Weaver VM, Lelièvre S, Lakins JN, Chrenek MA, Jones JC, et al. 2002.  $\beta 4$  integrin-dependent formation of polarized three-dimensional architecture confers resistance to apoptosis in normal and malignant mammary epithelium. *Cancer Cell* 2: 205–16
100. Zahir N, Lakins JN, Russell A, Ming W, Chatterjee C, et al. 2003. Autocrine laminin-5 ligates  $\alpha 6 \beta 4$  integrin and activates RAC and NF $\kappa$ B to mediate anchorage-independent survival of mammary tumors. *J. Cell Biol.* 163:1397–407
101. Fournier MV, Martin KJ, Kenny PA, Xhaja K, Bosch I, et al. 2006. Gene expression signature in organized and growth-arrested mammary acini predicts good outcome in breast cancer. *Cancer Res.* 66:7095–102
102. Beloussov L, Lakirev A, Naumidi I. 1988. The role of external tensions in differentiation of *Xenopus laevis* embryonic tissues. *Cell Differ. Dev.* 25:165–76
103. Farge E. 2003. Mechanical induction of Twist in the *Drosophila* foregut/stomodaeal primordium. *Curr. Biol.* 13:1365–77
104. Tahinci E, Symes K. 2003. Distinct functions of Rho and Rac are required for convergent extension during *Xenopus* gastrulation. *Dev. Biol.* 259:318–35
105. Ren R, Nagel M, Tahinci E, Winklbauer R, Symes K. 2006. Migrating anterior mesoderm cells and intercalating trunk mesoderm cells have distinct responses to Rho and Rac during *Xenopus* gastrulation. *Dev. Dyn.* 235:1090–99
106. Zamir E, Geiger B. 2001. Molecular complexity and dynamics of cell-matrix adhesions. *J. Cell Sci.* 114:3583–90
107. Zimerman B, Volberg T, Geiger B. 2004. Early molecular events in the assembly of the focal adhesion-stress fiber complex during fibroblast spreading. *Cell Motil. Cytoskelet.* 58:143–59
108. Cukierman E, Pankov R, Stevens D, Yakamada K. 2001. Taking cell-matrix adhesions to the third dimension. *Science* 294:1708–12
109. Burridge K, Fath K, Kelly T, Nuckolls G, Turner C. 1988. Focal adhesions: transmembrane junctions between the extracellular matrix and the cytoskeleton. *Annu. Rev. Cell Biol.* 4:487–525
110. Zamir E, Katz M, Posen Y, Erez N, Yamada K, et al. 2000. Dynamics and segregation of cell-matrix adhesions in cultured fibroblasts. *Nat. Cell Biol.* 2:191–96
111. Webb D, Parsons J, Horwitz A. 2002. Adhesion assembly, disassembly and turnover in migrating cells—over and over and over again. *Nat. Cell Biol.* 4:E97–100
112. Ridley A, Hall A. 1992. The small GTP-binding protein rho regulates the assembly of focal adhesions and actin stress fibers in response to growth factors. *Cell* 70:389–99

113. Balaban N, Schwarz U, Reveline D, Goichberg P, Tzur G, et al. 2001. Force and focal adhesion assembly: a close relationship studied using elastic micropatterned substrates. *Nat. Cell Biol.* 3:466–72
114. Nobes C, Hall A. 1995. Rho, rac, and cdc42 GTPases regulate the assembly of multi-molecular focal complexes associated with actin stress fibers, lamellipodia, and filopodia. *Cell* 81:53–62
115. Beningo K, Wang Y. 2002. Flexible substrata for the detection of cellular traction forces. *Trends Cell Biol.* 12:79–84
116. Tân J, Tien J, Pirone D, Gray D, Bhadriraju K, et al. 2003. Cells lying on a bed of microneedles: an approach to isolate mechanical force. *Proc. Natl. Acad. Sci. USA* 100:1484–89
117. Riveline D, Zamir E, Balaban N, Schwarz U, Ishizaki T, et al. 2001. Focal contacts as mechanosensors: Externally applied local mechanical force induces growth of focal contacts by an mDia1-dependent and ROCK-independent mechanism. *J. Cell Biol.* 153:1175–86
118. Galbraith CG, Yamada KM, Sheetz MP. 2002. The relationship between force and focal complex development. *J. Cell Biol.* 159:695–705
119. Choquet D, Felsenfeld DP, Sheetz MP. 1997. Extracellular matrix rigidity causes strengthening of integrin-cytoskeleton linkages. *Cell* 88:39–48
120. Wang HB, Dembo M, Hanks SK, Wang Y. 2001. Focal adhesion kinase is involved in mechanosensing during fibroblast migration. *Proc. Natl. Acad. Sci. USA* 98:11295–300
121. Volberg T, Romer L, Zamir E, Geiger B. 2001. pp60 (c-src) and related tyrosine kinases: a role in the assembly and reorganization of matrix adhesions. *J. Cell Sci.* 114:2279–89
122. Felsenfeld DP, Schwartzberg PL, Venegas A, Tse R, Sheetz MP. 1999. Selective regulation of integrin-cytoskeleton interactions by the tyrosine kinase Src. *Nat. Cell Biol.* 1:200–6
123. Lee J, Juliano R. 2004. Mitogenic signal transduction by integrin- and growth factor receptor-mediated pathways. *Mol. Cells* 17:188–202
124. Sawada Y, Sheetz MP. 2002. Force transduction by Triton cytoskeletons. *J. Cell Biol.* 156:609–15
125. Leopoldt D, Yee HJ, Roszengurt E. 2001. Calculin-A induces focal adhesion assembly and tyrosine phosphorylation of p125 Fak, p130 Cas, and paxillin in Swiss 3T3 cells. *J. Cell Physiol.* 188:106–19
126. Torsoni A, Constancio S, Nadruz WJ, Hanks S, Franchini K. 2003. Focal adhesion kinase is activated and mediates the early hypertrophic response to stretch in cardiac myocytes. *Circ. Res.* 93:140–47
127. Numaguchi K, Eguchi S, Yamakawa T, Motley E, Inagami T. 1999. Mechanotransduction of rat aortic vascular smooth muscle cells requires RhoA and intact actin filaments. *Circ. Res.* 85:5–11
128. Renshaw MW, Price LS, Schwartz MA. 1999. Focal adhesion kinase mediates the integrin signaling requirement for growth factor activation of MAP kinase. *J. Cell Biol.* 147:611–18
129. Li S, Kim M, Hu YL, Jalali S, Schlaepfer DD, et al. 1997. Fluid shear stress activation of focal adhesion kinase. Linking to mitogen-activated protein kinases. *J. Biol. Chem.* 272:30455–62
130. Li W, Duzgun A, Sumpio BE, Basson MD. 2001. Integrin and FAK-mediated MAPK activation is required for cyclic strain mitogenic effects in Caco-2 cells. *Am. J. Physiol. Gastrointest. Liver Physiol.* 280:G75–87
131. Frisch SM, Vuori K, Ruoslahti E, Chan-Hui PY. 1996. Control of adhesion-dependent cell survival by focal adhesion kinase. *J. Cell Biol.* 134:793–99

132. Fleury V, Watanabe T. 2002. Morphogenesis of fingers and branched organs: how collagen and fibroblasts break the symmetry of growing biological tissue. *C. R. Biol.* 325:571–83
133. Miao H, Nickel CH, Cantley LG, Bruggeman LA, Bennardo LN, Wang B. 2003. EphA kinase activation regulates HGF-induced epithelial branching morphogenesis. *J. Cell Biol.* 162:1281–92
134. Moore KA, Huang S, Kong Y, Sunday ME, Ingber DE. 2002. Control of embryonic lung branching morphogenesis by the Rho activator, cytotoxic necrotizing factor1. *J. Surg. Res.* 104:95–100
135. Wozniak MA, Desai R, Solski PA, Der CJ, Keely PJ. 2003. ROCK-generated contractility regulates breast epithelial cell differentiation in response to the physical properties of a three-dimensional collagen matrix. *J. Cell Biol.* 163:583–95
136. Padera TP, Stoll BR, Tooredman JB, Capen D, di Tomaso E, Jain RK. 2004. Pathology: cancer cells compress intratumour vessels. *Nature* 427:695
137. Netti PA, Berk DA, Swartz MA, Grodzinsky AJ, Jain RK. 2000. Role of extracellular matrix assembly in interstitial transport in solid tumors. *Cancer Res.* 60:2497–503
138. Akiri G, Sabo E, Dafni H, Vadasz Z, Kartvelishvily Y, et al. 2003. Lysyl oxidase-related protein-1 promotes tumor fibrosis and tumor progression in vivo. *Cancer Res.* 63:1657–66
139. Beningo KA, Dembo M, Wang YL. 2004. Responses of fibroblasts to anchorage of dorsal extracellular matrix receptors. *Proc. Natl. Acad. Sci. USA* 101:18024–29



# Contents

The Relevance of Research on Red Cell Membranes to the Understanding of Complex Human Disease: A Personal Perspective <i>Vincent T. Marchesi</i> .....	1
Molecular Mechanisms of Prion Pathogenesis <i>Adriano Aguzzi, Christina Sigurdson, and Mathias Heikenwalder</i> .....	11
The Aging Brain <i>Bruce A. Yankner, Tao Lu, and Patrick Loerch</i> .....	41
Gene Expression Profiling of Breast Cancer <i>Maggie C.U. Cheang, Matt van de Rijn, and Torsten O. Nielsen</i> .....	67
The Inflammatory Response to Cell Death <i>Kenneth L. Rock and Hajime Kono</i> .....	99
Molecular Biology and Pathogenesis of Viral Myocarditis <i>Mitra Esfandiarei and Bruce M. McManus</i> .....	127
Pancreatic Cancer <i>Anirban Maitra and Ralph H. Hruban</i> .....	157
Kidney Transplantation: Mechanisms of Rejection and Acceptance <i>Lynn D. Cornell, R. Neal Smith, and Robert B. Colvin</i> .....	189
Metastatic Cancer Cell <i>Marina Bacac and Ivan Stamenkovic</i> .....	221
Pathogenesis of Thrombotic Microangiopathies <i>X. Long Zheng and J. Evan Sadler</i> .....	249
Anti-Inflammatory and Proresolving Lipid Mediators <i>Charles N. Serhan, Stephanie Yacoubian, and Rong Yang</i> .....	279
Modeling Morphogenesis and Oncogenesis in Three-Dimensional Breast Epithelial Cultures <i>Christy Hebner, Valerie M. Weaver, and Jayanta Debnath</i> .....	313

The Origins of Medulloblastoma Subtypes <i>Richard J. Gilbertson and David W. Ellison</i> .....	341
Molecular Biology and Pathology of Lymphangiogenesis <i>Terhi Karpanen and Kari Alitalo</i> .....	367
Endoplasmic Reticulum Stress in Disease Pathogenesis <i>Jonathan H. Lin, Peter Walter, and T.S. Benedict Yen</i> .....	399
Autophagy: Basic Principles and Relevance to Disease <i>Mondira Kundu and Craig B. Thompson</i> .....	427
The Osteoclast: Friend or Foe? <i>Deborah V. Novack and Steven L. Teitelbaum</i> .....	457
Applications of Proteomics to Lab Diagnosis <i>Raghothama Chaerkady and Akhilesh Pandey</i> .....	485
The Pathology of Influenza Virus Infections <i>Jeffrey K. Taubenberger and David M. Morens</i> .....	499
Airway Smooth Muscle in Asthma <i>Marc B. Hershenov, Melanie Brown, Blanca Camoretti-Mercado, and Julian Solway</i> .....	523
Molecular Pathobiology of Gastrointestinal Stromal Sarcomas <i>Christopher L. Corless and Michael C. Heinrich</i> .....	557
Notch Signaling in Leukemia <i>Jon C. Aster, Warren S. Pear, and Stephen C. Blacklow</i> .....	587
The Role of Hypoxia in Vascular Injury and Repair <i>Tony E. Walshe and Patricia A. D'Amore</i> .....	615

## Indexes

Cumulative Index of Contributing Authors, Volumes 1–3 .....	645
Cumulative Index of Chapter Titles, Volumes 1–3 .....	647

## Errata

An online log of corrections to *Annual Review of Pathology: Mechanisms of Disease* articles may be found at <http://pathol.annualreviews.org>



# Three-Dimensional Context Regulation of Metastasis

Janine T. Erler<sup>1\*</sup> and Valerie M. Weaver<sup>2\*</sup>

1. Section of Cell & Molecular Biology, Institute of Cancer Research, 237 Fulham Road, London SW3 6JB, UK.

2. Department of Surgery, University of California San Francisco, 513 Parnassus Avenue, San Francisco, CA 94143-0456, USA.

\* corresponding addresses: Janine.erler@icr.ac.uk; [WeaverV@surgery.ucsf.edu](mailto:WeaverV@surgery.ucsf.edu).

**ABSTRACT:** Dynamic interactions between tumor cells and their microenvironment create a context that promotes tumor progression. The tumor microenvironment consists of cellular and non-cellular components. Although cellular constituents of the microenvironment undoubtedly contribute to cancer pathogenesis, non-cellular components including the extracellular matrix and hypoxia are also key players. In particular, extracellular matrix remodeling and collagen cross-linking stiffen the tissue stroma to promote tumor growth, migration and invasion and enhance cancer cell survival. Tumor hypoxia, which is functionally linked to altered stromal-epithelial interactions, additionally induces the expression of pro migratory, survival and invasion genes that enhance tumor progression and metastasis. Symbiotic interactions between matrix remodeling and tumor hypoxia influence common mechanisms that maximize tumor progression and cooperate to drive metastasis. Thus, clarifying the molecular pathways by which extracellular matrix remodeling and tumor hypoxia intersect to promote tumor progression should reveal novel therapeutic targets.



**KEYWORDS:** collagen cross-linking; hypoxia; matrix remodeling; matrix stiffness; metastasis; tumor progression.

**ABBREVIATIONS:** 2- and 3- dimensional (2D, 3D, respectively); Pascals (Pa); extracellular matrix (ECM); matrix metalloproteinase (MMP); lysyl oxidase (LOX); hypoxia-inducible factor (HIF); tumor-associated macrophage (TAM); tissue growth factor (TGF); bone marrow-derived cell (BMDC); mammary epithelial cell (MEC).

## Introduction

Tissue context profoundly influences malignant transformation and tumor progression [1]. This concept was vividly demonstrated experimentally by Mintz and colleagues who showed that the normal mouse embryonic tissue microenvironment could repress expression of the tetra carcinoma tumor phenotype [2, 3], and thereafter was shown by Bissell and colleagues who demonstrated that the normal chicken embryonic microenvironment could suppress transformation mediated by the Rous Sarcoma tumor oncogene and that wounding promoted tumor progression [3]. Experimental data presented by multiple laboratories has since confirmed these seminal observations and showed that the tissue stroma can either promote or restrict tumor progression [4-7]. More recently the individual or combined activities of various cellular components of the stroma such as activated endothelial and lymphatic cells, altered fibroblasts, infiltrating immune cells, modified adipocytes and even stimulated mesenchymal stem cells have been shown to modulate various stages of tumor progression [8-10]. Non-cellular aspects of the tumor microenvironment, such as hypoxia and an altered extracellular matrix, have also been shown to contribute to tumor progression either by directly destabilizing tissue integrity and promoting tumor cell motility, invasion and survival, or indirectly by inducing tumor angiogenesis and enhancing tumor cell survival and selection [4, 11, 12]. Here, we focus on the mammary gland and discuss the critical role of non-cellular microenvironmental factors in normal tissue homeostasis and tumor evolution and metastasis. We outline how a symbiotic interaction between extracellular matrix remodeling and hypoxia, two non-cellular components of the tissue microenvironment, can cooperatively drive tumor metastasis by influencing common molecular targets that may therefore constitute tractable drug targets.

## **The importance of non-cellular components of the tissue microenvironment on tissue homeostasis**

The stroma consists of multiple cell types including fibroblasts, endothelial cells, adipocytes and infiltrating immune cells as well as non-cellular components including soluble factors such as growth factors and cytokines and an insoluble protein network to which these soluble factors can bind called the extracellular matrix (ECM). There are two major categories of ECM. The first type is the basement membrane which interacts directly with the epithelium and endothelium and consists primarily of collagen IV, laminins, entactin/nidogen and heparan sulfate proteoglycans [13-15]. The second type is the interstitial matrix which makes up the bulk of the ECM in the body. The interstitial matrix consists of collagens I and III, which together with fibronectin contribute to the mechanical strength of the tissue, as well as tenascin, and proteoglycans that provide tissue hydration, growth factor and cytokine binding functions, and cross-link the matrix to enhance its integrity. Although originally thought of as merely a support system for the cells within the tissue, the ECM is now recognized as a central regulator of cell and tissue behavior. Indeed, while the basic characteristics and composition of the basement membrane and interstitial matrix are constant across tissues, variations in isomer expression and post-translational modifications ensure tissue specificity and contribute to differences in ECM organization and topology and likely direct tissue-specific differentiation.

The ECM can regulate cell and tissue behavior by initiating biochemical signaling cascades in cells through interactions with a number of specialized transmembrane ECM receptors including integrins, DDRs and syndecans. Integrins are perhaps the best characterized ECM receptors particularly with respect to their molecular behavior, crystal structure and signaling functions and therefore are an excellent model with which to understand how an altered ECM could promote tumor progression. Integrins consist of 24 distinct transmembrane heterodimers that relay cues

from the surrounding ECM to regulate cell growth, survival, motility/invasion and differentiation [16]. By virtue of their ability to interact with the ECM externally and cytoplasmic adhesion plaque proteins and the cytoskeleton intracellularly, integrins are able to transmit dynamic cues from the tissue microenvironment to influence cell fate. Thus, integrin-ECM interactions regulate cell fate by activating multiple biochemical signaling circuits and altering cell and nuclear shape, either through direct interactions with actin linker proteins or by activating cytoskeletal remodeling enzymes such as RhoGTPases to modulate cytoskeletal organization [17-19]. ECM topology which reflects the organization, orientation and post translational modifications of the matrix per se, and which regulates its mechanical properties, also modulates cell and tissue phenotype by influencing cytoskeletal remodeling and receptor signaling to influence cell behavior [13, 20]. Although it is not clear how ECM topology and its mechanical properties regulate cell fate, it is fast becoming clear that these matrix parameters are likely as important as its biochemical composition and can profoundly affect cell behaviors to regulate processes as disparate as stem cell differentiation and tumor phenotype [21-28].

The architecture of the tissue ECM is influenced by its biochemical composition, matrix concentration and post-translational modifications such as glycosylation and cross-linking, which significantly affect its mechanical properties, herein defined as its visco-elasticity or stiffness (measured in Pascals; Pa) and its three dimensional organization and orientation termed its topology [29-32]. Both the stiffness and topology of the ECM regulate the growth/remodeling, differentiation, migration and phenotype of a wide variety of cell and tissue types [12, 28]. Consistently, mechanical force mediated at the cellular and tissue level specifies tissue organization and cell migration during early embryogenesis and modulates tissue function and homeostasis in the adult organism, and much of the force mediating these behaviors is functionally linked to ECM architecture and cell-generated actomyosin-dependent contractility [29, 30].

The importance of ECM topology and its mechanical properties in tissue-specific differentiation is exemplified by the fact that cells grown as monolayers (two dimensional; 2D) on top of either a plastic substrate or a glass cover slip, either with or without ECM ligand (plastic has a stiffness approaching the GPa range; which is infinitely stiff), fail to assemble tissue-like structures (three dimensional; 3D) and do not express differentiated proteins, even if stimulated with the appropriate exogenously added factors [12, 20]. These phenotypic disparities can be explained in part by the fact that the consistency of living tissues is dramatically softer than conventional 2D substrata such as tissue culture plastic (poly styrene) or borosilicate glass (soft tissues such as the breast; liver and lung range between 150 and 3,000 Pascals, whereas borosilicate glass is by comparison to 1-2 GPa) [12, 20]. The post-translational state and topology (architecture) of the interstitial tissue matrix in vivo also differs substantially from that found typically in tissue culture plastic experiments and this too can have dramatic effects on cell behavior [33]. For instance epithelial cells in a tissue either interact with "other" cells and basally contact a basement matrix (which itself has a complex 3D topology), whereas tissue fibroblasts are surrounded by interstitial collagen fibrils that can be heavily glycosylated and cross linked and that have diameters that range from 0.1 microns upwards to 10 microns. Furthermore, the orientation of these collagen fibers can also critically regulate cell and tissue behavior [24, 30]. Consistently, if epithelial cells and melanocytes are grown in the context of a 3D compliant ECM microenvironment (150-400 Pa) they assemble into tissue-like structures and express differentiated proteins when given the correct soluble stimuli (reviewed in [8, 34, 35]).

ECM remodeling and changes in matrix stiffness play a crucial role in branching morphogenesis observed during both embryonic development and mammary gland maturation and lactational differentiation. Hypoxia another important non-cellular component of the physiological tissue microenvironment is also a key regulator of branching morphogenesis [36]. Hypoxia-mediated

gene expression and signaling is critical for embryonic development, bone marrow cell differentiation, and wound healing responses [37]. Hypoxic conditions stimulate blood cell proliferation and blood vessel formation, and modulate expression of ECM components and remodeling enzymes thereby maintaining tissue homeostasis. Hypoxia-driven changes in gene expression are mediated primarily by hypoxia-inducible factor (HIF)-1 [38]. For instance, HIF-1 deficient trophoblast stem cells exhibit reduced adhesion and migration toward vitronectin compared with wild-type cells [39], and the defective trophoblast invasion in the absence of HIF-1 was associated with decreased cell surface expression of integrin  $\alpha v\beta 3$  and significantly reduced assembly of  $\alpha v\beta 3$  expression focal adhesions. Thus, hypoxia stimulates cell adhesion and migration, as well as angiogenesis and ECM remodeling.

### **The importance of non-cellular components of the tissue microenvironment on tumor evolution**

Cancer has been defined as a wound that fails to heal [1, 40]. Tumor evolution and the wound-response are characterized by ECM remodeling, hypoxia, angiogenesis, and the recruitment of a repertoire of non-transformed host cells. What is now clear is that non-cellular components of the tumor microenvironment critically drive tumor evolution, primarily through increased matrix deposition, cross-linking and remodeling that create a microenvironmental context that enhances tumor cell survival, migration and growth and increases tumor angiogenesis and lymph angiogenesis. Indeed, hypoxia and matrix remodeling that leads to a progressive stiffening of the ECM are associated with tumor progression, and many ECM components and remodelling enzymes including MMPs and matrix cross linkers are elevated in cancer patients.

Hypoxia increases collagen biosynthesis, collagen orientation and collagen processing [41]. For example, hypoxia up-regulates the P4H  $\alpha 1$  subunit of collagen prolyl 4-hydroxylase (P4H) which is the rate-limiting subunit for the hydroxylation of proline residues of procollagens [42]. The formation of hydroxyproline is an essential post-transcriptional process for stabilization of the helical trimer of procollagen polypeptides. Prolonged hypoxic incubation of fetal rat lung fibroblasts enhanced this post-transcriptional step of collagen synthesis and accelerated the deposition of collagen molecules and fibrils [43]. In addition, cytoplasmic P4Hs play a critical role in the regulation of the HIF $\alpha$  [44].

Micro-array analysis revealed that expression of an ECM protein, lysyl oxidase (LOX), was consistently over-expressed by hypoxic human tumor cells [45]. LOX expression is induced by hypoxia-inducible factor (HIF)-1 and is associated with experimental hypoxia in vitro and in vivo, and clinically in breast and head and neck cancer patients [11]. LOX initiates the covalent cross-linking of collagens and elastins, thereby increasing insoluble matrix deposition and tensile strength [46]. LOX is synthesized in fibrogenic cells as a pre-pro-enzyme that is cleaved and glycosylated prior to its secretion [46]. After secretion, the LOX pro-enzyme is proteolytically processed by procollagen C-proteinase (bone morphogenic protein-1) which releases the 32-kDa biologically active mature form of the protein. Procollagen C-proteinase (bone morphogenic protein-1) is also hypoxia-induced [45], and cleaves pro-collagens thereby permitting processing and collagen fibril assembly, in addition to activating LOX.

Matrix stiffness is indicated by increased collagen deposition and ECM cross-linking, and is one of the major consequences of LOX activity. Increased matrix stiffness can drive malignant transformation through disruption of normal structures. For example, human mammary epithelial cells grown on a stiffer matrix develop malignant morphology that is characterized by destabilized E-cadherin adherens junctions, loss of tissue polarity and acquisition of invasive

behavior (Figure 1). Increased matrix stiffness has been observed in fibrotic lungs, in scar tissue, in tissue exposed to high doses of radiation, in aged skin and in women with dense breasts, all conditions that predispose these individuals and tissues to a higher cancer risk. Consistently, tumors are characteristically stiffer than their normal adjacent tissue and while increased cell mass undoubtedly contributes to the increase in tissue force in tumors, altered stiffness is often detected as a global increase in the physical properties of the transformed tissue [47, 48]. Indeed, over the years imaging methods such as ultra sound sono elastography and MR imaging elastography have been exploited to monitor tissues for evidence of transformation based upon differential stiffness profiles of not only the tumor itself but also of the surrounding non-transformed tissue [48]. This suggests that the stiffening associated with tumor progression is likely linked to changes in the ECM stroma that track with the tumor phenotype, such as elevated levels of collagen, linearization of the collagen fibrils, enhanced expression of proteoglycans implicated in matrix cross-linking including lumican and biglycan, and higher amounts of matrix cross-linking enzymes such as LOX [49]. Tumor stiffness has also been attributed to the elevated interstitial pressure due to leaky blood vessels and lymphatics [50]. Although the density and cross-linking of the matrix, which modulates the stiffness of the tissue can regulate the therapeutic efficacy of tumors by modulating drug penetration into the tissue, the relevance of tissue stiffness to malignant progression including tumor metastasis has yet to be studied at the molecular level and its relevance to prognosis and therapy remain unknown.

The importance of collagen remodeling, cross-linking and stiffening to tumor progression was emphasized by our recent work in which we primed the mammary stroma of nude mice with fibroblasts expressing a constitutively active LOX. In these studies, LOX-dependent collagen cross-linking of the mammary fat pad promoted the linearization of the interstitial collagens, stiffened the gland and induced the neoplastic progression of Ha-Ras pre-malignant human mammary epithelial cells (MECs). Consistently, we found that the elastic modulus (indenter) and



the storage modulus (shear) (i.e. stiffness) of the mammary tissue in MMTV-Her2/neu transgenic mice increased incrementally, coincident with and prior to the establishment of large, invasive tumors. Although the tissue stiffening could be attributed in part to an increase in cell mass, we noted that both the tumor and the surrounding stroma were significantly stiffer than normal tissue [12]. Moreover, second generation harmonics imaging as well as polarized light scanning of picrosirius-stained tissues revealed that tissue stiffening correlated with collagen linearization. Importantly, we found that collagen linearization was associated with elevated levels of the collagen cross-linker LOX, which we could detect in the stroma prior to tumor formation. Matrix stiffening and cross-linking were also associated with enhanced mechanoresponsiveness of the epithelium, as evidenced by elevated activated focal adhesion kinase, and p130 Cas. Intriguingly, inhibiting LOX-dependent collagen cross-linking in Her2/neu mice, tempered collagen linearization, reduced gland stiffening and enhanced the latency and decreased the incidence of breast transformation. These data imply that altering the cell's mechano homeostasis could promote the malignant behavior of an epithelium in culture and promote transformation in vivo, and that inhibiting matrix stiffening could temper reducing matrix stiffness can diminish breast transformation in vivo.

## **Metastasis**

The organization and composition of the ECM changes dramatically during tumor progression and these modifications alter tumor behavior and likely contribute to tumor metastasis. For instance, the mammary gland matrix stiffens progressively during tumor progression and this mechanical alteration is associated with increased collagen, fibronectin, and tenascin deposition and elevated collagen cross linking and linearization [12]. Matrix stiffness, in association with growth factors, enhances cell survival and increases cell contractility [12]. Matrix stiffness and/or

exogenous force independently induce cell-generated contractility to promote focal adhesion maturation and enhance integrin-dependent signaling thus compromising multi-cellular tissue morphogenesis and promoting a tumor-like behavior in mammary cells [12]. This suggests that matrix stiffness likely promotes breast tumorigenesis through altering integrins and their adhesion interactions. Conversely, blocking integrin-dependent cell contractility reverted the malignant phenotype in culture [40]. Consistent with these findings, ectopic expression of  $\beta 1$  integrin mutants with increased transmembrane molecular associations (V737N, G744N), elevated cellular contractility and forced focal adhesion maturation increase integrin/growth factor-dependent signaling, again to compromise multi-cellular tissue morphogenesis and promote tumorigenic behavior in culture and in vivo [12].

The acquisition of the metastatic phenotype is not simply the result of dysregulated signal transduction pathways, but instead is achieved through a stepwise selection process driven by microenvironmental pressures including ECM remodeling and hypoxia. Hypoxia, for instance, can disrupt tissue integrity and enhance cell motility and invasion directly by repressing E-cadherin and enhancing N-cadherin expression and hepatocyte growth factor (HGF)-MET receptor signaling, or indirectly by promoting cell-ECM interactions through enhancement of  $\alpha v \beta 3$  integrin membrane localization, or by fostering ECM remodeling through up-regulation of uPAR and uPAR-dependent MMP activation and by inducing ECM stiffening through elevated expression of LOX and LOX-dependent collagen cross linking. Hypoxia also indirectly enhances tumor dissemination by directly regulating the expression and activity of hypoxia-induced vascular endothelial growth factor (VEGF) to promote angiogenesis and lymphangiogenesis and increase vascular permeability to promote intravasation at the primary tumor site and extravasation at the distant metastatic site.

LOX expression is not only associated with hypoxia but is also associated with metastasis and decreased survival in human cancer patients [11]. Inhibition of LOX expression or activity was found to prevent in vitro invasion and in vivo metastasis [11]. LOX activity outside of the cell resulted in matrix remodeling and activation of focal adhesion kinase (FAK) enabling cell motility. LOX inhibition resulted in decreased cell-matrix adhesion interactions critical for invasive migration and metastatic dissemination. A dependence on LOX expression for metastatic growth was also observed and may be explained by LOX's role in the formation and maintenance of the metastatic niche (see below). While LOX-induced matrix cross-linking can activate MMPs, MMP-2 is reported to cleave pro-LOX releasing the mature enzyme [51].

Under physiological non-hypoxic conditions, angiogenesis can be driven by mechanical forces. For example, capillary endothelial cells subjected to mechanical stretch demonstrate in elevated MMP-2 and HIF-1 $\alpha$  expression, and MMP-2 activity [52]. These findings additionally suggest that ECM remodeling can increase hypoxic responses, a phenomenon supported by the presence of hypoxia as a result of increased ECM remodeling and fibrosis during wound-healing. Hypoxia in turn increases the expression and activity of genes involved in fibrosis and ECM remodeling, resulting in a feed-forward mechanism that increases matrix stiffness and drives tumor progression (Figure 2).

### **The importance of cellular components of the tissue microenvironment on tumor evolution**

The non-tumor cellular component of the microenvironment consists of activated and/or recruited host cells such as fibroblasts and immune cells. It is the reciprocal interactions between these host cells, the tumor cells and the ECM that drive tumor progression including

metastatic dissemination. Innate immune cells are strong mediators of disease progression through their release of potent soluble factors that enable growth, motility and angiogenesis. In particular, tumor-associated macrophages (TAMs) are associated with metastasis and poor patient outcome [53]. TAMs have been shown to direct tumor cell migration towards blood vessels and to enable intravasation [54]. Of note, TAMs accumulate in regions of hypoxia [53, 55].

Recent in vivo data has suggested there is formation of a pre-metastatic niche that is essential for the growth of extravasating metastatic tumor cells [56]. Factors secreted by primary tumor cells stimulate mobilization of bone marrow-derived cells that enter circulation and reside in sites of future metastasis. These bone marrow-derived cells express VEGFR-1, c-kit, CD133, CD34 and integrin VLA-4, and increase angiogenesis at the pre-metastatic sites. Targeted inhibition of VEGFR-1 prevented niche formation and subsequent metastatic progression. This pre-conditioning may thus represent a key step that could be targeted therapeutically, although studies with anti-VEGF therapy fail to show significant benefit in preventing metastatic growth for long periods of time.

Elevated fibronectin expression in fibroblasts and fibroblast-like cells resident at pre-metastatic sites appears to be a critical factor in the development of the pre-metastatic niche. The key tumor-secreted factors that determine metastatic sites and mediate pre-metastatic niche formation have yet to be identified, although TNF- $\alpha$ , TGF- $\beta$  and VEGF-a pathways have been implicated [57]. MMPs may also play an important role in this process. For example, VEGF-R1 signaling has been shown to be required for pre-metastatic induction of MMP-9 expression in endothelial cells and macrophages of the lungs by distant primary tumors [58]. This is thought to make the lung microenvironment more compliant for invasion of metastasizing cells. In addition, pericyte recruitment and angiogenesis is not observed in tumor-bearing mice with MMP-9

knock-out bone marrow cells [59]. Furthermore, stromal-derived MMP-2 and MMP-9 have also been shown to contribute to establishment and growth of metastases [60].

In recent studies performed by Giaccia et al, we found that LOX secreted by hypoxic tumor cells played a critical role in the formation of the pre-metastatic niche in vivo [Erler, Bennewith and Giaccia, unpublished]. We could show that bone marrow-derived cells (BMDCs) were recruited to pre-metastatic sites through LOX-mediated matrix remodeling and MMP activation. BMDC recruitment enabled pre-metastatic niche formation that was able to support metastatic growth. This process could be disrupted by administering LOX-targeting therapies. These studies stress the importance tumor-stromal interplay and ECM remodeling, and demonstrate the therapeutic potential of targeting these processes to prevent tumor progression.

### **Future Directions**

ECM remodeling proteins such as MMPs and matrix cross-linkers such as lysyl oxidase, by virtue of their ability to modulate ECM phenotype and induce hypoxia, can drive tumor angiogenesis to promote coordinated tissue responses such as tumor metastasis. Yet, ECM synthesis and deposition and the expression and function of ECM receptors and ECM remodeling enzymes are themselves regulated by hypoxia. Thus, there is a critical reciprocal and functional link between multiple non-cellular microenvironmental components that control tumor evolution that we are only just beginning to clarify. Indeed, emerging evidence indicate that changes at the primary tumor, including those driven by stiffness and hypoxia, could profoundly influence distant metastatic sites. Preliminary studies suggest that a complex interplay between matrix remodeling and tumor hypoxia likely "primes" the metastatic niche. Nevertheless, clearly, to develop effective anti-metastatic therapies it will be critical to

understand and identify the key molecular mechanisms whereby tissue context, as exemplified by mechanical force and hypoxia, regulate tumor metastasis.

## **ACKNOWLEDGEMENTS**

We apologize to those authors whose excellent work could not be cited due to space limitations.

## REFERENCES

1. Bissell MJ, Radisky D, Putting tumours in context. *Nat Rev Cancer* 2001; 1: 46-54.
2. Mintz B, Illmensee K, Normal genetically mosaic mice produced from malignant teratocarcinoma cells. *Proc Natl Acad Sci U S A* 1975; 72: 3585-9.
3. Dolberg DS, Bissell MJ, Inability of Rous sarcoma virus to cause sarcomas in the avian embryo. *Nature* 1984; 309: 552-6.
4. Weaver VM, Petersen OW, Wang F, Larabell CA, Briand P, Damsky C, Bissell MJ, Reversion of the malignant phenotype of human breast cells in three-dimensional culture and in vivo by integrin blocking antibodies. *J Cell Biol* 1997; 137: 231-45.
5. Barcellos-Hoff MH, Ravani SA, Irradiated mammary gland stroma promotes the expression of tumorigenic potential by unirradiated epithelial cells. *Cancer Res* 2000; 60: 1254-60.
6. Wiseman BS, Werb Z, Stromal effects on mammary gland development and breast cancer. *Science* 2002; 296: 1046-9.
7. Burdelya LG, Komarova EA, Hill JE, Browder T, Tararova ND, Mavrikakis L, DiCorleto PE, Folkman J, Gudkov AV, Inhibition of p53 response in tumor stroma improves efficacy of anticancer treatment by increasing antiangiogenic effects of chemotherapy and radiotherapy in mice. *Cancer Res* 2006; 66: 9356-61.
8. Haass NK, Smalley KS, Herlyn M, The role of altered cell-cell communication in melanoma progression. *J Mol Histol* 2004; 35: 309-18.
9. Karnoub AE, Dash AB, Vo AP, Sullivan A, Brooks MW, Bell GW, Richardson AL, Polyak K, Tubo R, Weinberg RA, Mesenchymal stem cells within tumour stroma promote breast cancer metastasis. *Nature* 2007; 449: 557-63.
10. Coussens LM, Raymond WW, Bergers G, Laig-Webster M, Behrendtsen O, Werb Z, Caughey GH, Hanahan D, Inflammatory mast cells up-regulate angiogenesis during squamous epithelial carcinogenesis. *Genes Dev* 1999; 13: 1382-97.

11. Erler JT, Bennewith KL, Nicolau M, Dornhofer N, Kong C, Le QT, Chi JT, Jeffrey SS, Giaccia AJ, Lysyl oxidase is essential for hypoxia-induced metastasis. *Nature* 2006; 440: 1222-6.
12. Paszek MJ, Zahir N, Johnson KR, Lakins JN, Rozenberg GI, Gefen A, Reinhart-King CA, Margulies SS, Dembo M, Boettiger D, Hammer DA, Weaver VM, Tensional homeostasis and the malignant phenotype. *Cancer Cell* 2005; 8: 241-54.
13. Kass L, Erler JT, Dembo M, Weaver VM, Mammary epithelial cell: influence of extracellular matrix composition and organization during development and tumorigenesis. *Int J Biochem Cell Biol* 2007; 39: 1987-94.
14. Sinkus R, Lorenzen J, Schrader D, Lorenzen M, Dargatz M, Holz D, High-resolution tensor MR elastography for breast tumour detection. *Phys Med Biol* 2000; 45: 1649-64.
15. Myllyharju J, Kivirikko KI, Collagens, modifying enzymes and their mutations in humans, flies and worms. *Trends Genet* 2004; 20: 33-43.
16. Hynes RO, Integrins: bidirectional, allosteric signaling machines. *Cell* 2002; 110: 673-87.
17. Miranti CK, Brugge JS, Sensing the environment: a historical perspective on integrin signal transduction. *Nat Cell Biol* 2002; 4: E83-90.
18. Clark EA, Brugge JS, Integrins and signal transduction pathways: the road taken. *Science* 1995; 268: 233-9.
19. Caswell PT, Norman JC, Integrin trafficking and the control of cell migration. *Traffic* 2006; 7: 14-21.
20. Paszek MJ, Weaver VM, The tension mounts: mechanics meets morphogenesis and malignancy. *J Mammary Gland Biol Neoplasia* 2004; 9: 325-42.
21. Zahir N, Lakins JN, Russell A, Ming W, Chatterjee C, Rozenberg GI, Marinkovich MP, Weaver VM, Autocrine laminin-5 ligates alpha6beta4 integrin and activates RAC and NFkappaB to mediate anchorage-independent survival of mammary tumors. *J Cell Biol* 2003; 163: 1397-407.



22. Weaver VM, Lelievre S, Lakins JN, Chrenek MA, Jones JC, Giancotti F, Werb Z, Bissell MJ, beta4 integrin-dependent formation of polarized three-dimensional architecture confers resistance to apoptosis in normal and malignant mammary epithelium. *Cancer Cell* 2002; 2: 205-16.
23. Hotary KB, Allen ED, Brooks PC, Datta NS, Long MW, Weiss SJ, Membrane type I matrix metalloproteinase usurps tumor growth control imposed by the three-dimensional extracellular matrix. *Cell* 2003; 114: 33-45.
24. O'Brien LE, Jou TS, Pollack AL, Zhang Q, Hansen SH, Yurchenco P, Mostov KE, Rac1 orientates epithelial apical polarity through effects on basolateral laminin assembly. *Nat Cell Biol* 2001; 3: 831-8.
25. Cukierman E, Pankov R, Stevens DR, Yamada KM, Taking cell-matrix adhesions to the third dimension. *Science* 2001; 294: 1708-12.
26. Yamada KM, Pankov R, Cukierman E, Dimensions and dynamics in integrin function. *Braz J Med Biol Res* 2003; 36: 959-66.
27. Beacham DA, Cukierman E, Stromagenesis: the changing face of fibroblastic microenvironments during tumor progression. *Semin Cancer Biol* 2005; 15: 329-41.
28. Engler AJ, Sen S, Sweeney HL, Discher DE, Matrix elasticity directs stem cell lineage specification. *Cell* 2006; 126: 677-89.
29. Discher DE, Janmey P, Wang YL, Tissue cells feel and respond to the stiffness of their substrate. *Science* 2005; 310: 1139-43.
30. Pedersen JA, Swartz MA, Mechanobiology in the third dimension. *Ann Biomed Eng* 2005; 33: 1469-90.
31. Georges PC, Janmey PA, Cell type-specific response to growth on soft materials. *J Appl Physiol* 2005; 98: 1547-53.
32. Janmey PA, Weitz DA, Dealing with mechanics: mechanisms of force transduction in cells. *Trends Biochem Sci* 2004; 29: 364-70.

33. Yamada KM, Cukierman E, Modeling tissue morphogenesis and cancer in 3D. *Cell* 2007; 130: 601-10.
34. Bogenrieder T, Herlyn M, Cell-surface proteolysis, growth factor activation and intercellular communication in the progression of melanoma. *Crit Rev Oncol Hematol* 2002; 44: 1-15.
35. Haass NK, Smalley KS, Li L, Herlyn M, Adhesion, migration and communication in melanocytes and melanoma. *Pigment Cell Res* 2005; 18: 150-9.
36. van Tuyl M, Liu J, Wang J, Kuliszewski M, Tibboel D, Post M, Role of oxygen and vascular development in epithelial branching morphogenesis of the developing mouse lung. *Am J Physiol Lung Cell Mol Physiol* 2005; 288: L167-78.
37. Hockel M, Vaupel P, Tumor hypoxia: definitions and current clinical, biologic, and molecular aspects. *J Natl Cancer Inst* 2001; 93: 266-76.
38. Semenza GL, Targeting HIF-1 for cancer therapy. *Nat Rev Cancer* 2003; 3: 721-32.
39. Cowden Dahl KD, Robertson SE, Weaver VM, Simon MC, Hypoxia-inducible factor regulates alphavbeta3 integrin cell surface expression. *Mol Biol Cell* 2005; 16: 1901-12.
40. Unger M, Weaver VM, The tissue microenvironment as an epigenetic tumor modifier. *Methods Mol Biol* 2003; 223: 315-47.
41. Phillips PG, Birnby LM, Narendran A, Hypoxia induces capillary network formation in cultured bovine pulmonary microvessel endothelial cells. *Am J Physiol* 1995; 268: L789-800.
42. Takahashi Y, Takahashi S, Shiga Y, Yoshimi T, Miura T, Hypoxic induction of prolyl 4-hydroxylase alpha (I) in cultured cells. *J Biol Chem* 2000; 275: 14139-46.
43. Horino Y, Takahashi S, Miura T, Takahashi Y, Prolonged hypoxia accelerates the posttranscriptional process of collagen synthesis in cultured fibroblasts. *Life Sci* 2002; 71: 3031-45.

44. Myllyharju J, Prolyl 4-hydroxylases, the key enzymes of collagen biosynthesis. *Matrix Biol* 2003; 22: 15-24.
45. Denko NC, Fontana LA, Hudson KM, Sutphin PD, Raychaudhuri S, Altman R, Giaccia AJ, Investigating hypoxic tumor physiology through gene expression patterns. *Oncogene* 2003; 22: 5907-14.
46. Kagan HM, Li W, Lysyl oxidase: properties, specificity, and biological roles inside and outside of the cell. *J Cell Biochem* 2003; 88: 660-72.
47. Krouskop TA, Wheeler TM, Kallel F, Garra BS, Hall T, Elastic moduli of breast and prostate tissues under compression. *Ultrason Imaging* 1998; 20: 260-74.
48. Khaled W, Reichling S, Bruhns OT, Boese H, Baumann M, Monkman G, Egersdoerfer S, Klein D, Tunayar A, Freimuth H, Lorenz A, Pessavento A, Ermert H, Palpation imaging using a haptic system for virtual reality applications in medicine. *Stud Health Technol Inform* 2004; 98: 147-53.
49. Decitre M, Gleyzal C, Raccurt M, Peyrol S, Aubert-Foucher E, Csiszar K, Sommer P, Lysyl oxidase-like protein localizes to sites of de novo fibrinogenesis in fibrosis and in the early stromal reaction of ductal breast carcinomas. *Lab Invest* 1998; 78: 143-51.
50. Padera TP, Stoll BR, Tooredman JB, Capen D, di Tomaso E, Jain RK, Pathology: cancer cells compress intratumour vessels. *Nature* 2004; 427: 695.
51. Panchenko MV, Stetler-Stevenson WG, Trubetskoy OV, Gacheru SN, Kagan HM, Metalloproteinase activity secreted by fibrogenic cells in the processing of prolyllysyl oxidase. Potential role of procollagen C-proteinase. *J Biol Chem* 1996; 271: 7113-9.
52. Milkiewicz M, Haas TL, Effect of mechanical stretch on HIF-1 $\alpha$  and MMP-2 expression in capillaries isolated from overloaded skeletal muscles: laser capture microdissection study. *Am J Physiol Heart Circ Physiol* 2005; 289: H1315-20.
53. Lewis CE, Pollard JW, Distinct role of macrophages in different tumor microenvironments. *Cancer Res* 2006; 66: 605-12.

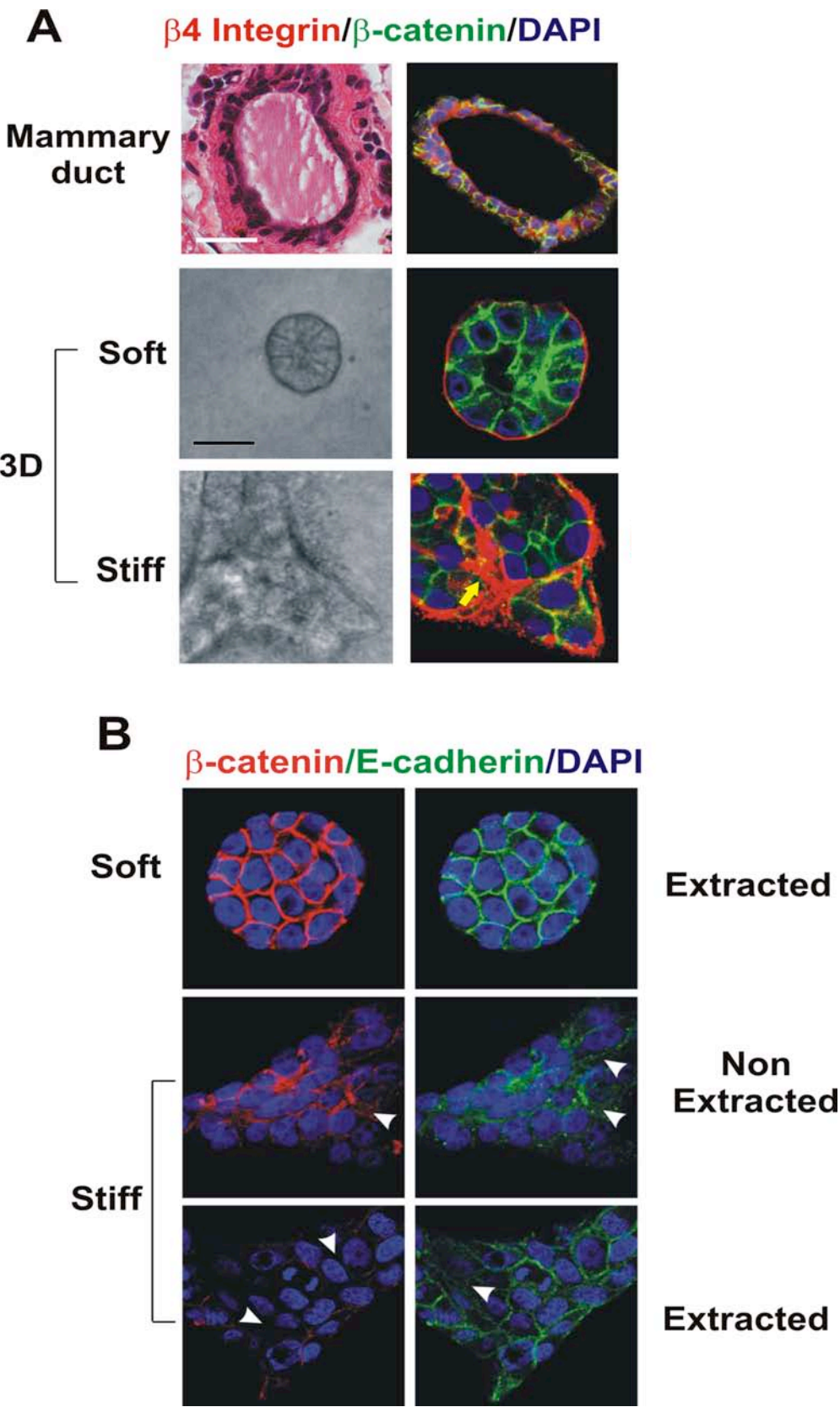
54. Condeelis J, Pollard JW, Macrophages: obligate partners for tumor cell migration, invasion, and metastasis. *Cell* 2006; 124: 263-6.
55. Knowles HJ, Harris AL, Macrophages and the hypoxic tumour microenvironment. *Front Biosci* 2007; 12: 4298-314.
56. Kaplan RN, Riba RD, Zacharoulis S, Bramley AH, Vincent L, Costa C, MacDonald DD, Jin DK, Shido K, Kerns SA, Zhu Z, Hicklin D, Wu Y, Port JL, Altorki N, Port ER, Ruggero D, Shmelkov SV, Jensen KK, Rafii S, Lyden D, VEGFR1-positive haematopoietic bone marrow progenitors initiate the pre-metastatic niche. *Nature* 2005; 438: 820-7.
57. Hiratsuka S, Watanabe A, Aburatani H, Maru Y, Tumour-mediated upregulation of chemoattractants and recruitment of myeloid cells predetermines lung metastasis. *Nat Cell Biol* 2006; 8: 1369-75.
58. Hiratsuka S, Nakamura K, Iwai S, Murakami M, Itoh T, Kijima H, Shipley JM, Senior RM, Shibuya M, MMP9 induction by vascular endothelial growth factor receptor-1 is involved in lung-specific metastasis. *Cancer Cell* 2002; 2: 289-300.
59. Chantrain CF, Shimada H, Jodele S, Groshen S, Ye W, Shalinsky DR, Werb Z, Coussens LM, DeClerck YA, Stromal matrix metalloproteinase-9 regulates the vascular architecture in neuroblastoma by promoting pericyte recruitment. *Cancer Res* 2004; 64: 1675-86.
60. Masson V, de la Ballina LR, Munaut C, Wielockx B, Jost M, Maillard C, Blacher S, Bajou K, Itoh T, Itohara S, Werb Z, Libert C, Foidart JM, Noel A, Contribution of host MMP-2 and MMP-9 to promote tumor vascularization and invasion of malignant keratinocytes. *Faseb J* 2005; 19: 234-6.

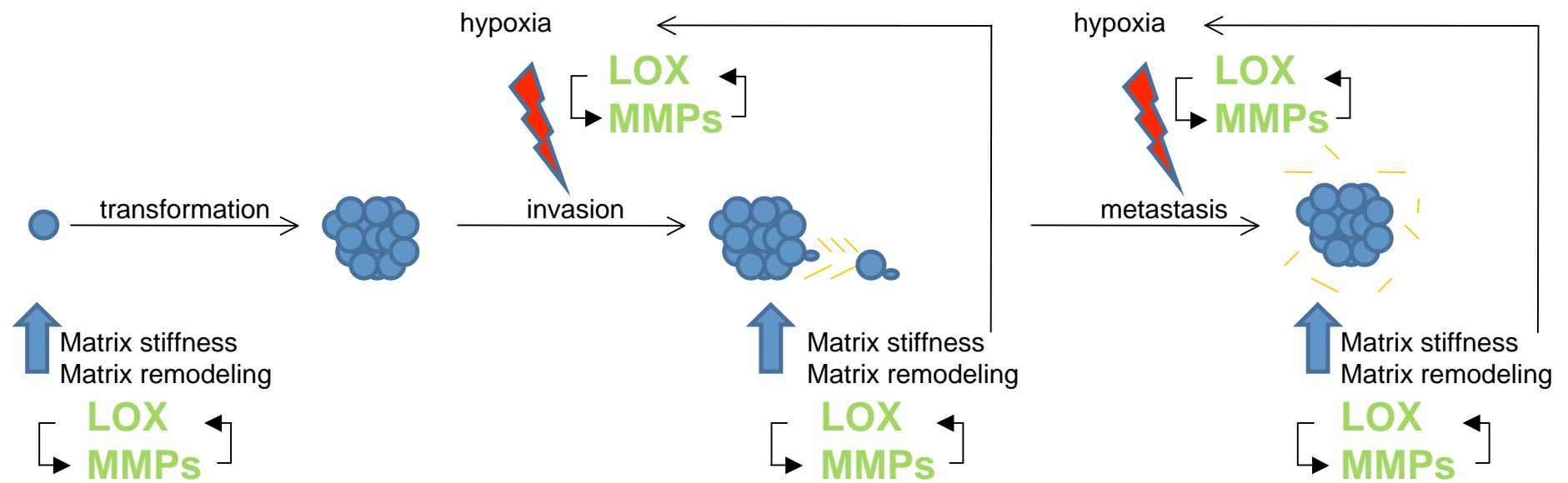
## FIGURE LEGENDS

**Figure 1.** Mammary epithelial growth and morphogenesis is regulated by matrix stiffness. A) 3D cultures of normal mammary epithelial cells (MECs) within collagen gels of different concentration. Stiffening the ECM through an incremental increase in collagen concentration (soft gels: 1mg/ml Collagen I, 140Pa; stiff gels 3.6mg/ml Collagen I, 1200Pa) results in the progressive perturbation of morphogenesis, and the increased growth and modulated survival of MECs. Altered mammary acini morphology is illustrated by the destabilization of cell-cell adherens junctions and disruption of basal tissue polarity indicated by the gradual loss of cell-cell localized  $\beta$ -catenin (green) and disorganized  $\beta$ 4 integrin (red) visualized through immunofluorescence and confocal imaging. B) Confocal immunofluorescence images of MEC colonies on soft and stiff gels (140 versus >5000 Pa) stained for  $\beta$ -catenin (red) and E-cadherin (green), and counterstained with DAPI (blue) after triton X-100 extraction.  $\beta$ -catenin could be extracted from the sites of cell-cell interaction in MEC colonies formed on a stiff but not on a soft gel, indicating that adherens junctions are less stable in MEC structures formed on stiff gels. White arrows indicate diffuse staining patterns of  $\beta$ -catenin and E-cadherin. [Modified from Paszek et al., 2005].

**Figure 2.** Schematic to demonstrate the interplay between hypoxia and matrix remodeling, using lysyl oxidase (LOX) as an example. LOX expression is increased in pre-malignant tissue, where it cross-links collagens in the ECM increasing matrix stiffness and enabling ECM remodeling. This allows for malignant transformation and primary tumor growth. As the tumor grows larger, regions become subjected to hypoxic conditions. In response to hypoxia, tumor cells increase expression of proteins involved in collagen biosynthesis and processing, including LOX. This

results in increased matrix deposition, collagen cross-linking, matrix remodeling and matrix stiffness, which in turn encourage a hypoxic environment. LOX secreted by hypoxic tumor cells is also involved in the formation of a pre-metastatic niche at distant sites of future metastasis. Increased collagen cross-linking and matrix remodeling attract bone marrow-derived cells to the site which create a niche permissive for metastatic tumor cell attachment and growth. Again, subsequent matrix remodeling and increased stiffness at these metastatic sites enhance hypoxia which in turn elevates expression of proteins involved in collagen biosynthesis and processing further increasing matrix remodeling and matrix stiffness. This feed-forward mechanism is further enhanced by matrix metalloproteinase (MMP) activity. MMP expression and activity is elevated by both increased matrix stiffness and by hypoxia, and is reported to increase abundance of LOX through pro-LOX processing. Thus, the symbiotic interaction between ECM remodeling and hypoxia, two non-cellular components of the tissue microenvironment, can cooperatively drive tumor metastasis by influencing common targets.







Research Signpost  
37/661 (2), Fort P.O., Trivandrum-695 023, Kerala, India



Recent Res. Devel. Immunology, 3(2001): 145-159 ISBN: 81-7736-073-6

---

## **Forcing transformation: Biophysical regulation of mammary epithelial cell transformation**

---

**Janna K. Mouw, Sonal J. Desai and Valerie M. Weaver\***

Department of Surgery, Center for Bioengineering and Tissue  
Regeneration, University of California, San Francisco, San Francisco  
CA 94143 USA

## Abstract

*The mechanical microenvironment plays an important role in modulating mammary gland development, maintenance, and remodeling, and regulates the behavior of the epithelium and cellular stroma. The cellular and extracellular components which comprise the three-dimensional stroma regulate the growth, survival, migration and differentiation of the mammary epithelium. Disruption of microenvironmental cues and the loss of tissue architecture are associated with and may drive malignant progression. Malignant progression of the breast is associated with regional increases in compressive stresses and/or high tensional resistance forces, and a global stiffening of the extracellular matrix. These mechanical forces can modulate growth factor and cytokine activation and signaling within the cellular components of the tissue to alter mammary epithelial morphology and growth and promote survival and invasion. Because mammary gland development and tumorigenesis are linked to altered biomechanics, and both differentiating and transformed cells experience altered mechano-responsiveness, defining the role of biomechanics in mammary gland development and tumorigenesis is important. In this chapter, we discuss the participation of stromal-epithelial interactions in normal and malignant epithelial cell behavior, specifically focusing on how the biochemical and biomechanical properties of the extracellular matrix dramatically influence mammary gland development and homeostasis, as well as tumor progression and the malignant phenotype. We also provide a brief overview of tools and methods available for studying the extracellular matrix and biomechanics in breast carcinogenesis.*

---

Correspondence/Reprint request: Dr. Valerie M. Weaver, Department of Surgery, UCSF, 513 Parnassus Ave. Room S-1364, San Francisco, CA 94122-0456. E-mail: weaverv@surgery.ucsf.edu

## INTRODUCTION

Breast cancer is the most common cancer in Western women, with a cancer mortality rate second only to lung cancer [1]. Due to the mechanical changes associated with mammary carcinoma, including increased extracellular matrix (ECM) deposition and interstitial pressure, breast palpation is often an initial measure used to detect breast carcinoma. Despite the connection between altered ECM biophysical properties and breast cancer, cancer research has historically focused on biochemical changes [2]. Nevertheless, a novel paradigm has emerged over the past few decades, bringing a three-dimensional (3D) tissue perspective to breast cancer and breast cancer research that encompasses a dynamic feedback

loop between epithelial morphogenesis and transformation and the biochemical and biophysical properties of the breast stroma [3-5].

Biomechanical cues influence development, regulate cell fate and contribute to disease [6-9]. At the cellular level there exist a number of molecular mechanisms through which cells sense and transduce mechanical cues that are localized within the membrane, the cytoskeleton and at specific cell-matrix complexes [10-12]. In particular, branched epithelial structures, such as the mammary gland, present multiple opportunities for force sensing. The mammary ductal tree is embedded within an architecturally complex extracellular microenvironment that broadly encompasses both cellular (myofibroblasts, fibroblasts, adipocytes, endothelial cells and immune cells) and non-cellular (structural extracellular and soluble factors such as cytokines and growth factors) components. In the context of a 3D tissue, such as the breast, mechanical loading can physically alter the conformation of extracellular receptor complexes present in fibroblasts and in mammary epithelial cells (MECs). Domains within these complexes can be stretched or compressed, either directly or indirectly altering the structure and function of the ECM receptor complexes influencing their signaling. Force can also directly or indirectly modify the activity and function of other membrane complexes such as growth factor receptors, cytokine receptors, ion channels, and cell-cell junctional complexes [13].

The mammary gland is a dynamic tissue, with the cellular and ECM compositions evolving over time, guiding and responding to changes in the development of the gland by a process termed dynamic reciprocity [14]. By incorporating the interplay between soluble factors, cell-cell and cell-ECM interactions and the mechanical microenvironment in the regulation of mammary morphogenesis and differentiation and tissue homeostasis the concept can be broadened as mechano-reciprocity [15]. Perturbations in dynamic reciprocity and mechano-reciprocity have been implicated in breast tumor progression. Specifically, interactions between the ECM and adhesion receptor complexes, such as integrin focal adhesions, influence both branching morphogenesis and mammary gland involution through directed cycles of ECM remodeling of the stromal-epithelial interface [16, 17]. Alterations in the ECM ligand or receptor expression and/or activity and aberrant matrix remodeling and matrix stiffening can drive mammary tumorigenesis and metastasis [18, 19]. Consistently, inhibiting aberrant ECM remodeling, reducing stromal stiffness and normalizing integrin receptor function can revert the malignant phenotype or restrict tumor progression [19]. Interestingly, dysregulated expression and activity of growth factors that participate in embryonic and adult mammary tissue development, including members of

the transforming growth factor (TGF), epidermal growth factor (EGF), hepatocyte growth factor (HGF) and fibroblast growth factor (FGF) families, not only drive breast tumorigenesis and metastasis by increasing cell growth and survival but also alter integrin and ECM ligand expression and induce cell-generated force to modify cell-ECM interactions [20-25].

Breast cancer is characterized by a persistent increase in mammary gland stiffness and the transformed behavior of MECs [25, 26]. Transformed MECs exhibit increased mechano-sensitivity [27, 28]. In this chapter, we summarize experimental evidence that the ECM content and structure dramatically influence mammary gland development and homeostasis, as well as tumor progression and the malignant phenotype. Of the various perspectives contributing to mammary epithelial cell behavior, the roles of biomechanics in guiding mammary epithelial morphogenesis, homeostasis and transformation are discussed. Several approaches used to study the participation of mechanical forces on cell behavior are described. Methods used to elucidate the biochemical pathways associated with cell-generated forces are also provided. This chapter highlights how the critical interplay of cell and tissue mechanics within the mammary microenvironment could influence development and carcinogenesis, and reviews strategies useful for experimentally exploring this phenomenon.

## **MAMMARY GLAND DEVELOPMENT AND MAINTENANCE**

The mammary gland is a functional secretory unit and a modified sweat gland. Normal breast development begins *in utero* and continues after birth. The mammary gland is the only branching organ that becomes fully mature during adulthood. The general structure of the mature mammary gland is a network of highly organized and branched ducts made up of epithelial cells. These ducts are surrounded by myoepithelial cells and basement membrane (BM), the entirety of which is embedded in a complex stroma consisting of extracellular matrix (ECM), mesenchymal cells, connective tissue and adipose tissue. Control of mammary development is a carefully orchestrated exchange of biochemical and biophysical cues between the cells of the developing mammary gland and the surrounding microenvironment. A great deal of effort has been invested in identifying biochemical regulatory mechanisms involved in all stages of breast development and a plethora of information about the key signals and molecules involved is readily available; however, an exhaustive discussion of all such regulatory mechanisms is beyond the scope of this review. There have been excellent reviews about biochemical cues, such

as hormonal regulation and signaling mechanisms, that regulate mammary gland development and we direct the reader to those comprehensive and elegant publications for more detail [29-35]. In this section, we will first focus on the development of the mammary gland and then discuss how ECM-cell interactions and mechanical force could modulate this process.

#### THE DEVELOPMENT PROCESS

The mammary gland develops in four stage of a female's life: embryogenesis, puberty, pregnancy and lactation, and menopause. During embryogenesis, the mammary gland arises from cells of the ectoderm which migrate in response to signals from the mesenchyme [36]. These epithelial cells initially proliferate to form two mammary ridges, or milk lines, that then regress back to become two solid epithelial masses, called the mammary buds, which subsequently give rise to the nipples [33]. Approximately 10-15 ducts arise from the nipple. The tips of the ducts, bulbous terminal end buds, invade into the mammary fat pad as the ducts elongate and branch to form the rudimentary ductal tree [37]. The ducts terminate in clusters of alveoli called terminal ductal lobular units. The luminal epithelial layer differentiates into secretory cells while the basal epithelial layer becomes the myoepithelium. The breast remains in this state until puberty.

At the onset of puberty, the mammary gland changes in response to hormonal cues and undergoes branching morphogenesis [35]. The breast is stimulated to develop in response to estrogen signaling in mesenchymal cells and increases in size due to adipose tissue expansion during puberty. The epithelial cells proliferate and the BM is remodeled, as the rudimentary ductal tree further elongates and branches into the expanding stroma [38]. By the end of puberty, the lumens of the secretory alveoli have been established at the ends of the smaller ducts of the branched structure. At this point, the mammary gland is considered mature but inactive, and remains in this state until pregnancy. It is interesting to note that there are small cyclical changes during the menstrual cycle, such as changes in epithelial cell shape, proliferation and apoptosis, BM remodeling, luminal size and stromal density, underscoring the theory that the adult breast, although considered "inactive" outside of pregnancy, is by no means static.

In response to estrogens and progesterone, the epithelium of the mammary gland undergoes extensive and rapid proliferation during pregnancy. The terminal ductal lobular units branch further and elongate and the terminal end buds differentiate into alveoli [39]. As the glandular structure enlarges, the stromal components thin. The myoepithelial cells extend contractile processes in a network around the alveolus. In the final stages of pregnancy, the luminal epithelial cells become cuboidal as the

alveoli mature and distend. After childbirth, there is a drop in estrogen and progesterone levels, and the structure of the gland is maintained by prolactin signaling. Suckling stimulates milk production by the secretory cells, causing the alveoli to dilate until they comprise most of the mammary gland [40]. The stroma is reduced to a fibrous capsule surrounding the lobules. Suckling also stimulates the release of oxytocin which induces myoepithelial cell contraction, facilitating expulsion of the alveolar contents and milk delivery to the young. At the end of the lactation period, the ECM undergoes extensive matrix metalloproteinase (MMP)-dependent remodeling, the extraneous epithelial cells undergo apoptosis, and the remaining epithelial cells become smaller and inactive [41]. The ducts and alveoli degenerate back to a resting state while the stroma is reconstructed [42, 43], though the glandular structure and the stromal composition of the post-lactation breast is not identical to their counterparts before pregnancy. The breast remains in this state, with the ability to become fully functional again during subsequent pregnancies, until menopause. After menopause, stromal density increases, adipose density decreases and the glandular structure regresses.

#### BIOCHEMICAL REGULATION

Mammary gland development is a dynamic process mediated through reciprocal interactions between the epithelium and the stroma that continue throughout the life span of the female. A myriad of continuously evolving biochemical and biophysical cues are required to direct the proper formation and function of the breast. The stroma is an instructive compartment of the mammary gland which changes in composition and architecture during mammary gland development and with age. The composition of the stroma includes the non-cellular ECM which is made up primarily of laminins (1, 5 and 10), collagens (I, III and IV), proteoglycans (including lumican and decorin), entactin, tenascin and fibronectin, and the cellular constituents which include fibroblasts, endothelial cells, adipocytes and infiltrating leukocytes (e.g. macrophages and lymphocytes). The BM constitutes the part of the ECM that is directly associated with the ductal epithelium, which is embedded within the interstitial ECM. The interstitial ECM, composed primarily of type I collagen, fibronectin and proteoglycans, is particularly important since it provides structure and support for the ductal tissue and stromal cells. In addition, it is also a repository for various growth factors and chemokines. ECM-cell interactions transmit physical cues from outside of the cell, modifying cell behavior by inducing cytoskeletal remodeling and inducing biochemical signaling cascades [44].

During embryogenesis, signals from fat pad adipocytes and interstitial fibroblasts direct mammary gland development. These two cell types express distinct ECM receptors and secrete different types of ECM ligands that reciprocally regulate their differentiated function and direct the development of the gland. For instance, the cells of the fat pad express laminin receptors and secrete laminin 5 and perlecan sulfate to promote the elongation of the ductal tree, whereas fibroblasts express high levels of  $\alpha 5\beta 1$  and  $\alpha 2\beta 1$  integrins, and deposit fibronectin and collagen to facilitate duct maturation and branching [45, 46]. During the branching morphogenesis associated with the onset of puberty, the composition of the BM changes. The BM surrounding the ducts consists primarily of laminins 1, 5 and 10, collagen IV, entactin and various heparin sulfate proteoglycans, except at the invasive front of the ductal tree which is enriched in hyaluronic acid [38]. However, the BM is not static and is continuously being remodeled during development by multiple MMPs. For instance, MMP2 activity is important for ductal elongation, while MMP3 and MMP14 activities are important for branching [38, 47, 48]. MMP activity is tempered by tissue inhibitors of metalloproteinases (TIMPs) to tightly regulate spatial and temporal remodeling of the ECM during development [38, 49, 50].

Transmembrane receptors within the epithelium interact with the ECM to physically anchor the cell within the tissue and to relay biochemical and mechanical information into the cell. Multiple families of ECM receptors exist including the syndecans, the discoidin receptors (DDR1 and DDR2), dystroglycan, and integrins. Loss of DDR1 results in excessive collagen deposition, impeded ductal formation and incomplete lactational differentiation [51]. Integrins are the best characterized and most abundant of the ECM receptors. Integrins are composed of  $\alpha$  and  $\beta$  subunits which heterodimerize to form an array of 24 different receptors that can bind to specific collagens, laminins, tenascin and fibronectin. Integrins can also associate with other ECM receptors such as syndecans, growth factor receptors and members of the tetraspanin transmembrane protein family, to cooperatively modulate cell fate and tissue processes such as branching morphogenesis, injury and fibrosis [38, 52]. For instance,  $\alpha 2$  integrin but not  $\alpha 3$ ,  $\alpha 4$  or  $\alpha 6$  is required for branching morphogenesis during pregnancy in gene knockout mouse models [53, 54]. During pregnancy, alveolar maturation is primarily mediated through  $\beta 1$  signaling; loss of  $\beta 1$  results in improper alveoli formation and lack of prolactin-induced epithelial cell differentiation and milk synthesis [55, 56].

## MECHANICAL REGULATION

The mammary gland is not generally thought of as a mechanically active tissue. However, given that physical force regulates embryogenesis and tissue-specific differentiation, it is highly likely that the mammary gland is also subject to a range of forces that shape its development and homeostasis [57, 58]. For instance, MECs migrate and invade the mammary fat pad early during embryogenesis and the coordinated movement of these cells appears to be largely governed by an exchange between exerted force and the mechanical properties of the tissue, including the ECM. During development, MECs also experience variations in intracellular tension that modulate their shape and behavior and dictate the architecture of the tissue. This cellular tension arises from two sources including actomyosin contractility linked to actin cytoskeletal dynamics and an “opposing” reaction force resisting the cytoskeletal contraction (physical adhesions to another cell or the ECM) (Figure 1). Physical movement of the cells occurs early in embryogenesis when the MECs migrate and invade the mammary fat pad, and continues through adolescent- and pregnancy-associated branching morphogenesis. The coordinated movement of cells is largely determined by an exchange between exerted forces and the mechanical properties of the reactive tissue, primarily the ECM. Migration appears to be mediated by remodeling of the ECM, which is driven by tension fields and a combination of durotaxis (migration along a stiffness gradient) and chemotaxis (migration along a chemical gradient), similar to the migration of fibroblast along ECM fibers [59-61]. Interestingly, tensional force can activate  $\beta$ -catenin, an effector of Wnt signaling which directs embryonic mammary gland development, and FGF and HGF, which also participate in breast development and activate actomyosin contractility in MECs [20, 61-67]. While these observations suggest that ECM-directed tensional stress is important in embryogenesis and mammary development, neither definitive evidence nor molecular mechanisms have been described.

ECM remodeling influences terminal end bud invasion, modulating branching morphogenesis by activating biochemical signaling cascades within the epithelium and by releasing soluble factors that regulate epithelial cell behavior. Physical parameters exerted by fluid flow or contractility within cells in the stroma and epithelium or via cellular interactions also influence epithelial morphogenesis [38]. For instance, cleaving forces and surface tension between the epithelium and the stroma have been proposed to affect the shape of the branched mammary ductal structure, using computational fluid dynamics modeling [68, 69]. External forces can alter epithelial invasion directly or cooperatively with cytokine and growth factor receptors by stimulating ERK and RhoGTPases to



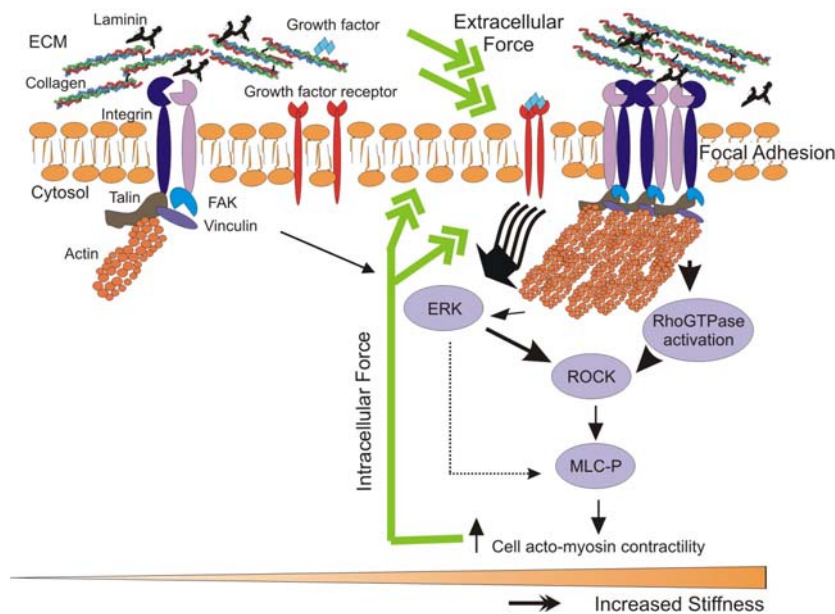


**Figure 1:** Force-dependent focal adhesion maturation mediated by extracellular force. Integrins are bi-directional mechanosensors that integrate biochemical and biophysical cues from the matrix and the actin cytoskeleton and transduce cell-generated force to the surrounding microenvironment. Activated integrins bind to ECM proteins via cooperative interactions between their alpha and beta extracellular domains and form nascent highly dynamic adhesion signaling complexes. In response to external mechanical force or elevated cell-generated contractility, integrin clustering is enhanced and the recruitment of multiple integrin adhesion plaque proteins including talin and vinculin is favored. These, in turn, associate with the actin cytoskeleton and multiple signaling proteins including FAK, Src family kinases, and integrin-linked kinase, to promote cell growth, survival, migration and differentiation. Matrix stiffening, which reflects elevated matrix deposition, linearization and cross-linking, can cooperate with oncogenic signaling to enhance cell-generated contractility to foster integrin associations and focal adhesion maturation. Maturation of focal adhesions promotes cell generated forces by enhancing Rho GTPase and ERK-mediated actomyosin contractility - which feed forward to further promote integrin clustering and focal adhesion assembly and transmit actomyosin-generated cellular forces to the ECM, as outlined in Paszek et al., 2005. Modified from Paszek et al., 2005. (reprinted from *Int J Biochem Cell Biol*, 39, Kass L, Erler JT, Dembo M, Weaver VM, "Mammary epithelial cell: influence of extracellular matrix composition and organization during development and tumorigenesis", 1987-1984, 2007, with permission from Elsevier.)

induce actomyosin contractility and cytoskeletal remodeling [70] (Figure 1). In the lung and kidney, inhibiting Rho activity restricts branching morphogenesis whereas activating Rho promotes abnormal branching [71, 72]. In the breast, elevated collagen levels, elevated crosslinking of the ECM or reduced MMP-dependent remodeling modifies matrix stiffness to

reduce terminal end bud invasion (unpublished observations) and disrupt acinar morphogenesis by possibly altering RhoGTPase activity. Consistently, mammary tumor cells exert significantly more force on their surrounding microenvironment than normal mammary cells and have elevated ERK and RhoGTPase activity. Reducing actomyosin or RhoGTPase activity can revert the malignant phenotype [28].

Functional differentiation of the mammary gland following pregnancy proceeds within the context of a highly compliant interstitial matrix and a mechanically-relaxed BM. Consistent with the observation that elevated matrix stiffness compromises mammary epithelial morphogenesis, culture studies have shown that mechanically loading collagen gels inhibits the functional differentiation ( $\beta$ -casein expression) of MECs [73]. For instance, early studies showed that functional acinar formation occurs only when a mixed cell population isolated from pre-lactating mice are plated on floating collagen gels (conditions in which the fibrillar tension is significantly reduced as compared to gels left attached to the tissue culture plate) and are able to assemble their own endogenous BM [73, 74]. This observation is supported by recent studies demonstrating that elevated matrix stiffness compromises  $\beta$ -casein expression by immortalized murine MECs (personal communication with M. Bissell). Although the molecular mechanisms underlying these phenotypes remain poorly understood, data suggest that matrix stiffness promotes focal adhesion assembly, destabilizes tissue architecture and enhances integrin and growth factor-dependent signaling [75, 76]. Furthermore, data suggest that elevated substrate stiffness might also interfere with tissue differentiation by stimulating the activity of MMPs to compromise BM assembly and stability and destabilize cell-cell E cadherin junctions [77]. Our own laboratory has been able to precisely calibrate ECM stiffness using both natural and synthetic laminin-containing matrices and we have shown that BM matrix compliance regulates cell shape, tissue morphogenesis and endogenous BM assembly in part by regulating focal adhesion maturation and signaling [25].

The most profound mechanical activity in the breast occurs during breastfeeding. Oxytocin is released in response to suckling and stimulates the myoepithelial cells to contract and secrete milk from the ducts. Build up of the secreted milk within the gland produces an increase in the intra-gland pressure, causing the alveoli to distend due to elevated tensional “hoop” stress, similar to the increase in air volume when blowing up a balloon. This force is countered by a reaction force generated by the surrounding tissue and by the tensile stress of the contracting myoepithelium [78]. These counteracting forces are essential for efficient milk delivery and functional strength of the lactating gland. Once lactation

ceases, the breast undergoes involution during which hormonal changes signal the remodeling of the mammary gland [41]. The specific mechanical forces that regulate involution have yet to be fully elucidated; however compression forces have been implicated in this process [79].

## **MAMMARY GLAND TRANSFORMATION**

### **THE DESMOPLASTIC RESPONSE AND TUMOR PROGRESSION**

The tissue desmoplasia that accompanies breast cancer was first described by pathologists several decades ago; however its significance to tumorigenesis was only recently appreciated. The desmoplastic response is distinguished by changes in the stromal mechanical environment arising with the inappropriate activation or induction of resident fibroblasts and myofibroblasts, as well as infiltrating immune cells [80] (Figure 2). For instance, macrophages recruited to the tumor site by chemokines secrete cytokines, growth factors and proteases that stimulate remodeling of the tissue stroma and promote angiogenesis [81]. Similarly, tumor-associated fibroblasts upregulate or stimulate the activity of various growth factors to promote cancer progression, including TGF- $\beta$ , insulin-like growth factor (IGF) and HGF [82, 83]. Characteristics of the tumor stroma include an increase in matrix proteins such as collagens I, III and IV, fibronectin, elastin and tenascin [4, 84-86]. There is also elevated crosslinking of these matrix proteins by lysyl oxidase (LOX) family members, transglutaminase and the proteoglycans lumican and decorin [4, 87-89]. An abnormal MMP-9/TIMP-1 balance has been shown to participate in tumor growth and overall invasiveness, while an abnormal MMP-2/TIMP-2 balance could be associated with lymph node invasion [90].

The desmoplastic response is characterized by dramatic changes in the composition of the ECM and the mechanical properties of the mammary tissue. Thus, invasive ductal breast tumors with pronounced desmoplasia are characteristically stiffer than normal tissue and this feature has permitted the detection of breast tumors by physical palpation. More recently, ultrasound imaging modalities including sonoelastography and magnetic resonance elastography have been developed to visualize the mechanical changes in the tissue surrounding the primary lesion and have been proposed as alternative detection strategies [91]. Direct measurement of the stiffnesses (as represented by the Young's moduli) of fibrocystic tissue, as well as benign and pre-malignant lesions, showed these lesions to be 3-6-fold stiffer than normal tissue, and high-grade invasive ductal carcinoma to be 13-fold stiffer, suggesting that changes in the material properties of the tissue temporally parallel and may even contribute to the malignant behavior of the tissue [26].

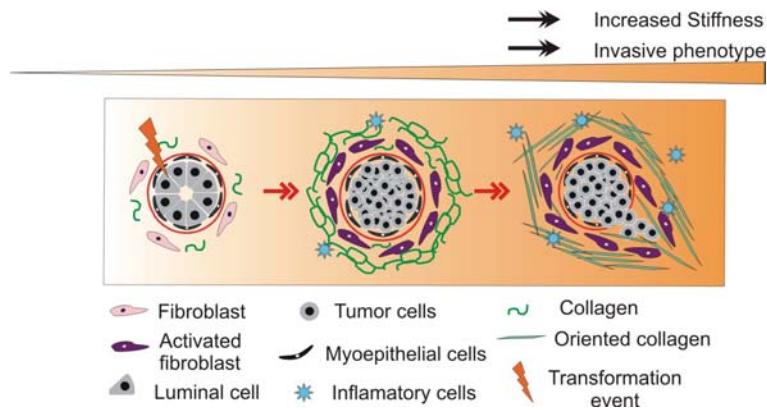


**Figure 2:** Malignant transformation of MECs is regulated by matrix stiffness. Breast transformation ensues through progressive acquisition of genetic alterations in the luminal epithelial cells residing within the mammary ducts. The tissue stroma responds to these epithelial alterations by initiating a desmoplastic response that is characterized by activation and trans-differentiation of fibroblasts, infiltration of immune cells, increased secretion of growth factors and cytokines, and elevated matrix synthesis and remodeling that manifests as matrix stiffening. Cartoon depicts the stages of breast tumorigenesis, (from left to right; normal ducts, ductal carcinoma in situ and invasive phenotype) highlighting key desmoplastic changes within the tissue stroma. (reprinted from *Int J Biochem Cell Biol*, 39, Kass L, Erler JT, Dembo M, Weaver VM, “Mammary epithelial cell: influence of extracellular matrix composition and organization during development and tumorigenesis”, 1987-1984, 2007, with permission from Elsevier.)

The enhanced deposition, elevated crosslinking and abnormal MMP-dependent remodeling contribute to an overall increase in stromal stiffness. Specific changes in the mechanics of the breast include zones of both increased intraductal compression and elevated intracellular and extracellular tension, as well as an overall progressive increase in ECM stiffening. When the extracellular microenvironment becomes perturbed, the mammary tissue and all of its inclusive cell types respond with alterations in their intracellular tension. Specifically, MECs within a transformed breast experience areas of increased resistance force in their stromal environment linked to elevated matrix stiffness [25, 26].

Changes in the form and function of the breast ECM can influence mammary tissue behavior not only on a mechanical level, but also biochemically through the release and activation of soluble growth factors, cytokines, matrix degrading enzymes and bioactive peptides [92]. Altered mammary mechanics, such as a dramatic increase in ECM stiffness, may promote the malignant transformation of MECs by altering growth factor responsiveness [27], increasing adhesion receptor expression and activation [93], or by enhancing motility and migration [94, 95]. Additionally,

transformed cells influenced by oncogenes such as Ras and ErbB/HER experience increased stiffness [96, 97]. Ras and ErbB/HER can also activate Rho and ERK, which drive alterations in actomyosin assembly, also altering intracellular tension.

Cell-ECM interactions actively participate in epithelial cell transformation and can modify tumor behavior and treatment responsiveness [98]. Aberrant expression of ECM receptors such as  $\beta 1$ -,  $\beta 4$ -,  $\alpha 2$ -,  $\alpha 3$ - and  $\alpha 6$ -integrins have been documented in transformed MECs; *in vitro* and *in vivo* work has functionally implicated these ECM receptor alterations in breast tumor progression. Elevated levels of  $\beta 4$ -integrin via direct interactions with either the ErbB2 or MET receptors perturb matrix adhesion and promote tumor invasion, and reducing  $\beta 4$  signaling or decreasing  $\beta 1$  integrin levels or function inhibit mammary tumor progression and revert expression of the malignant phenotype in culture and *in vivo* [19, 99-103].

Metastasis of transformed MECs is associated with a high percentage of disease fatalities and, thus, restricting metastasis is a primary objective of many cancer prevention programs. During invasion, cells extend pseudopodia at the leading edge that attach to collagen fibers in the ECM, allowing cells to migrate along the fibers towards blood vessels [104]. To promote metastasis of tumor cells, the basement membrane must be compromised and transformed MECs must migrate into the surrounding stroma. MMP-2 and -14 have been shown to cleave laminin-5, exposing a cryptic site of this protein involved in epithelial migration [105]. Additionally, increased MMP activity release and activate growth factors trapped in the stroma which, in turn, leads to increased growth factor signaling, thereby stimulating further invasion. Migration is regulated by cellular adhesion, cell-generated contractility and cell haptotaxis to maximize ligand binding [106]. Durotaxis linked to enhanced cytoskeletal remodeling and increased intracellular tension might also contribute to tumor metastasis [59, 107]. Importantly, elevated matrix deposition and tension may couple with ECM degradation, modulating tumor invasion and metastasis. For instance, it has been shown that the family of Rho GTPases is linked to cell migration and MMP-mediated invasion. Consistent with this paradigm, Rho and Rac expression and activity are increased in tumors and, specifically, over-expression of RhoC and loss of the tumor growth suppressor WISP3, have been implicated in aggressive, metastatic forms of inflammatory breast cancers [108, 109]. Interestingly, inhibiting the collagen cross-linking LOX dramatically reduced metastasis in a xenograft model of breast cancer [110].

Taken together, the cellular response to both altered biochemical signaling, as well as a stiffer microenvironment, may create a

synergistically negative, tumorigenic feedback loop. These overall changes in the cell-generated forces alter the activity and function of signaling cascades that ultimately determine their growth, survival, motility and invasion. Such changes might also modulate the response of the transformed MECs to chemo- and radiation therapies.

#### MAMMOGRAPHIC DENSITY

Mammographic density is defined by the percentage of the breast rich in stroma and epithelium, as opposed to adipose tissue. Clinical studies suggest that mammographic density is a strong risk factor for breast cancer [111, 112]. Data indicate that risk increases 4-fold in women whose breast tissue is greater than 75% mammographically dense. In fact, some studies showed that approximately one-third of patients with breast cancer had mammographic densities that scored equal to or greater than 50% [113]. Moreover, DCIS predominantly occurs in mammographically dense areas of the breast, and may be preceded by increased density [114]. One explanation for the associated risk between mammographic density and breast cancer risk is that increased breast density masks the tumor, making clinical detection difficult. Yet, mammographic density is a heterogeneous condition that is not always associated with elevated breast tumor risk. Histologically, mammographic density is associated with epithelial and stromal cell proliferation, and increased deposition of collagen [111]. While some studies suggest elevated collagen could actively promote tumor progression by promoting local invasion of tumor cells [115-117], contributing factors such as collagen remodeling and post-translational modifications complicate the paradigm. In this regard, increased levels of small leucine-rich proteoglycans, such as lumican and decorin, have also been implicated in dense breasts [89]. Additionally, elevated expression of LOXL2, a member of the LOX family of collagen crosslinking proteins, correlates with increased tumor fibrosis and progression in vivo [87]; and increased LOX and LOXL2 expressions correlate with invasive potential in many highly invasive/metastatic breast cancer cell lines [118]. Mammographically dense breasts have also been linked to increased IGF-1 and metalloproteinase-3 (TIMP-3) expression [119]. These findings suggest the mechanical changes in breast tissue associated with increased mammographic density drive tumorigenesis, most likely due to perturbations in mechanical homeostasis. Increased breast stiffness is a critical readout of altered tissue homeostasis during the early events of tumor progression.

## TISSUE COMPRESSIVE FORCES

Compressive forces are generated by the resistance of the mammary tissue adjacent to the pool of transformed MECs actively proliferating within the ductal tree, as well as the invasive tumorigenic MECs confined within the expanding fibrotic tumor mass [120]. Additionally, dysfunctional vascular and lymphatic transport can lead to increases in interstitial fluid and pressure of the transformed tissue. These increases in intraductal compression and interstitial pressure can lead to an overall decrease in blood flow through the tumor vasculature, resulting in hypoxic areas. Hypoxia has been linked to increased tumor aggressiveness, as well as resistance to radiation and chemotherapy [121, 122].

At the molecular level, normal and transformed MEC behavior can be altered by compression through the activation and function of various soluble cytokines and growth factors, as well as through alterations in gene and protein expression. Compression-induced changes in microtubule dynamics can alter cell motility and morphology [123]. Compressive mechanical loading has been shown to upregulate inflammatory cytokines such as IL-8 [124] and receptor activator nuclear factor kappa-B ligand [125], stimulate cell growth through FGF-dependent activation of ERK [126], facilitate invasion through elevations in MMP-9 and MMP-28 release and activation [127, 128], and drive cell differentiation through upregulated TGF- $\beta$  signaling [129]. Increases in TGF- $\beta$  signaling in response to increase hydrostatic and dynamic compression can trigger a pro-fibrotic response of the stromal fibroblast population of the breast tumor, resulting in an increase in tumor growth and viability, an induction of angiogenesis and promotion of an epithelial-mesenchymal transition (EMT) [130, 131].

Compressive forces could regulate tumor behavior indirectly through non-molecular and more “physical” mechanisms. A decrease in interstitial space around ductal structures within a compliant environment such as the mammary gland has been shown to slow the transport of secreted ligand away from the cell surface, triggering an autocrine ligand-receptor signaling response. Tschumperlin et al. have shown that compressive stress elicits ERK phosphorylation through autocrine ligand-receptor signaling involving heparin-binding EGF (HB-EGF), leading to subsequent binding and activation of the EGFR [132]. This suggests that proliferating DCIS lesions could experience an increase in EGFR activation in response to increased compressive pressure, enhancing tumor growth without ErbB receptor amplification.

## INTRACELLULAR TENSION & MATRIX RIGIDITY

The tissue adjacent to an expanding tumor mass responds to the tumor-generated compressive force by exerting a reaction force on the expanding tumor mass itself. These tumor-initiated resistance forces may translate to transformed cells as tensional forces. By regulating the activity of various biochemical signaling cascades, cytoskeletal-mediated tensional forces alter tumor behavior. Tensional forces can be transmitted from tumor cell to tumor cell through adhesion plaques, and within the tumor cells via the cytoskeleton to cell-ECM adhesions [133]. The expanding tumor mass and actively migrating tumor cells can each independently deliver direct forces to cell-ECM and cell-cell adhesion plaques, impacting tumor cell behavior by physically distorting the ECM. Tensional forces can incur conformational changes of proteins at the integrin adhesion plaque, such as vinculin, to activate integrin adhesion signaling either directly, by influencing receptor clustering or indirectly, inducing changes in lipid packing and thus affecting ion channel gating [134]. Tensile mechanical loading has also been shown to modulate intracellular signaling. For instance, mechanical strain increased the ligand-binding and activation of  $\alpha V\beta 3$  integrin leading to the upregulation of JNK signaling through PI3 kinase [135] and promoted angiogenesis through increased vascular endothelial growth factor (VEGF) expression [136]. Cell survival is also mediated by mechanical stress through the activation of PI3 kinase, AKT, p38 SAPK2 and JNK, independent of ErbB2 and angiotensin receptor type I activation [137, 138]. Tensional forces may not only exert oriented alterations in the cytoskeleton, but could also induce changes in overall dynamic remodeling of the cytoskeleton. Therefore, a tissue-derived tensional force could additionally influence cell-cell adhesion dependent signaling to alter cell behavior.

Our laboratory has found that even a small increase in matrix rigidity will perturb normal MEC architecture, disrupting polarity and cell-cell junctions, and ultimately enhancing MEC growth through an increase in Rho-generated cytoskeletal tension, promotion of focal adhesions, and upregulation of growth factor-dependent ERK activation (Figure 3). Increasing ECM stiffness increased the recruitment of actin-binding proteins, such as vinculin, to  $\beta 1$  integrins, thereby promoting large focal adhesion assembly and increased cell-generated traction forces. Similarly, by inhibiting Rho-generated cytoskeletal tension or ERK activity, highly contractile, EGFR-transformed MECs could be phenotypically reverted to form differentiated acini lacking focal adhesions and with reduced EGFR activity and ERK signaling [25]. These findings suggest that breast tumors react to stromal stiffening via tensional homeostasis, with maximum intracellular forces exerted at the focal adhesion through assembly by



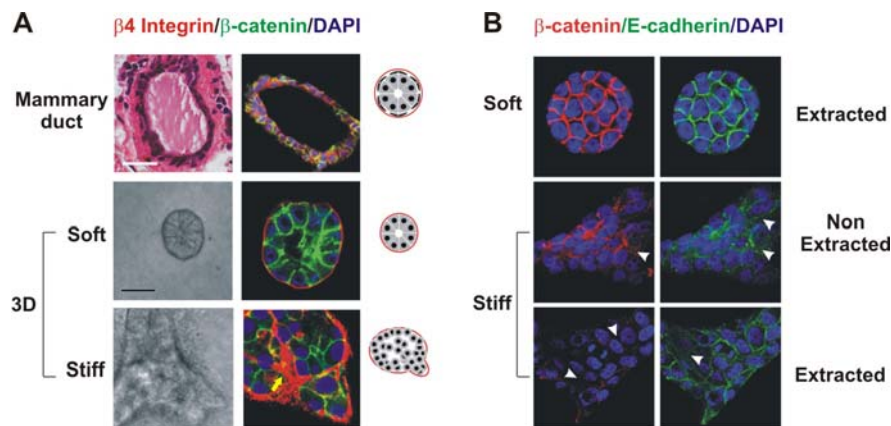


**Figure 3:** MEC growth and morphogenesis is regulated by matrix stiffness. **A)** 3D cultures of normal MECs within collagen gels of different concentration. Stiffening the ECM through an incremental increase in collagen concentration (soft gels: 1mg/ml Collagen I, 140Pa; stiff gels 3.6mg/ml Collagen I, 1200Pa) results in the progressive perturbation of morphogenesis, and the increased growth and modulated survival of MECs. Altered mammary acini morphology is illustrated by the destabilization of cell-cell adherens junctions and disruption of basal tissue polarity, indicated by the gradual loss of cell-cell localized  $\beta$ -catenin (green) and disorganized  $\beta 4$  integrin (red)(visualized through immunofluorescence and confocal imaging). Column 2 illustrates mammary ductal structure (luminal and myoepithelial cells surrounded by BM), and depicts MEC morphogenesis in soft and stiff gels. Scale bars represent 25 $\mu$ m. **B)** Confocal immunofluorescence images of MEC colonies on soft and stiff gels (140 versus >5000 Pa) stained for  $\beta$ -catenin (red) and E-cadherin (green), and counterstained with DAPI (blue) after triton X-100 extraction.  $\beta$ -catenin could be extracted from the sites of cell-cell interaction in MEC colonies formed on a stiff but not on a soft gel, indicating that adherens junctions are less stable in MEC structures formed on stiff gels. White arrows indicate diffuse staining patterns of  $\beta$ -catenin and E-cadherin. Modified from Paszek et al., 2005. (reprinted from *Int J Biochem Cell Biol*, 39, Kass L, Erler JT, Dembo M, Weaver VM, "Mammary epithelial cell: influence of extracellular matrix composition and organization during development and tumorigenesis", 1987-1984, 2007, with permission from Elsevier.)

actomyosin cytoskeletal networks. According to this model, the resulting effect of the mechanical environment amplifies oncogene-driven ERK activation, facilitating malignant transformation through cytoskeletal contractility via the small GTPase, Rho.

In summary, tensional homeostasis may be critical for normal tissue growth and differentiation. Thus, increasing matrix rigidity through changes in ECM composition, organization and crosslinking, or by elevated Rho signaling, could induce cytoskeletal contractility to enhance integrin-dependent growth and destabilize tissue architecture [139]. Increased cell contractility through Rho could facilitate malignant transformation in conditions accompanied by the induction of tissue

fibrosis and/or the amplification of ERK signaling through oncogenic activity. In this regard, tumors that have undergone EMT have vastly reorganized cytoskeletons and altered adhesions, and, as such, respond differently to the physical forces present in the tumor microenvironment [140, 141]. Part of a potentially negative feedback loop, induction of a tumor EMT could alter how tensional force is sensed and transduced within a transformed cell, leading to further progression of the EMT phenomena.

#### UNDERSTANDING MAMMARY GLAND MECHANOTRANSDUCTION

While the overall importance of mechanical force to tissue behavior is generally acknowledged, much remains to be discovered about cell and tissue mechanotransduction, and how such mechanosensory signals might guide cellular behavior. Investigators are just beginning to elucidate how mechanical stimulation induces structural, compositional and functional changes at the cellular level, and how these cues could alter the structural integrity and function of differentiated tissues. What is clear is that cells must have elements that can detect and integrate different combinations of forces and magnitudes, in a multitude of contexts. Once stimulated, these “mechanosensor” elements must be able to propagate these cues by signaling a cascade of downstream events that alter cell behavior through effector mechanisms such as cytoskeletal reorganization, conformational changes in transmembrane proteins (ion channels, etc.) and alterations in gene and protein expression. As reviewed in this chapter, cellular growth, differentiation and migration have all been linked to mechanotransduction mechanisms [142].

Multiple mechano-sensitive players have emerged: the cytoskeleton, integrins, receptor tyrosine kinases, mitogen-activated protein kinases, G proteins, and stretch-activated ion channels, to name a few [143]. Currently, the best studied mechanotransduction pathway is the ECM-integrin-cytoskeletal interface [142, 144, 145]. Because the expression and activity of integrins and adhesion-plaque associated proteins differ so dramatically in breast cancer cells, mechanotransduction is likely altered in transformed MECs. This raises the intriguing possibility that mammary gland transformation may be functionally linked to perturbed mechanical-homeostasis. Future research in the area of cell mechanobiology will require novel experimental and theoretical methodologies to determine the type and magnitude of the forces experienced at the cellular and sub-cellular levels, and to identify the force sensors/receptors that initiate the cascade of cellular and molecular events.

## MODELS OF MAMMARY MORPHOGENESIS AND TRANSFORMATION

To investigate mammary epithelial morphogenesis and malignant transformation, 3D culture systems have been developed to model the *in vivo* environment of MECs. The original 3D models were designed to completely embed MECs within a polymerized ECM to closely recapitulate the structure and composition of the mammary gland *in vitro*. These models have been modified to study how mechanical properties affect morphogenesis and biochemical processes [146]. In this review, we present an overview of these 3D models and the modifications used to study mechanotransduction. Additionally, engineering approaches to modulating the physical forces applied to cells are discussed.

### 3D CULTURE SYSTEMS

As discussed in this chapter, ECM composition and architecture are frequently altered in breast transformation and can influence MEC growth, differentiation and migration. Methods to study these biological processes traditionally involve culturing isolated cells on a 2D surface. However, cells *in vivo* exist in a complex 3D environment. To more accurately study MEC morphogenesis *in vitro*, models have been developed to recapitulate the *in vivo* 3D environment. The simplest 3D model involves embedding a single type of cell in a biocompatible scaffold. These biocompatible scaffolds provide cells with a prefabricated ECM, which is often modifiable by the embedded cells. Scaffolding materials commonly used for complete embedment of MECs include recombinant basement membranes (rBMs) produced and isolated from Engelbreth-Holm-Swarm (EHS) mouse tumor matrices, collagen I, and fibrin. Laminin 1, collagen IV, entactin and heparin sulfate proteoglycans are the major components of the EHS rBM. rBM has been utilized extensively to study morphogenesis and transformation in normal, non-transformed MECs, such as MCF-10A cells and S1 cells (from the HMT-3522 progression series) [19, 147-149]. Indeed, when various non-transformed MECs (primary and cell lines) are mixed with rBM they form polarized structures, with hollow lumens, within the polymerized rBM [150][151]. A modified version of this method is to apply a layer of rBM to the tissue culture surface, plate cells on to the rBM and then add another layer of rBM, resulting in a pseudo 3D system [146, 149]. Although the cells are not mixed directly with the rBM, they are nevertheless surrounded by rBM and are able to form acinar structures, presumably by remodeling the rBM. Drawbacks of using rBM matrices are that it is not fully characterized and therefore has an ill-defined content and lot to lot variability. Another commonly used total embedment

scaffold, collagen I, is biologically better defined than rBM derived from EHS cells. While certain epithelial cells types polarize in collagen I, such as MDCK epithelial cells, many other epithelial cell types fail to undergo acinar morphogenesis, or form structures with reverse polarity [152]. One advantage collagen I has over rBM is that the mechanical properties can be adjusted by titrating the collagen concentration and the extent of crosslinking. However, since collagen is biologically derived, there is variability between lots, species and processing techniques (for instances, intact- versus telepeptide free- collagen).

Synthetic materials are now being utilized to more precisely control the substrate stiffness of the matrix presented to the cell. Polyacrylamide gels, traditionally used to separate biomolecules, have been manipulated in the 3D culture system [153]. By varying the concentration of polyacrylamide to bisacrylamide crosslinker, a range of quantifiable stiffnesses can be achieved. The limitation of this system is that polyacrylamide can be cytotoxic to the cells and therefore total embedment can not be utilized. Applying the cells to the top of the polyacrylamide gel may limit the cytotoxic effect, but is not a 3D environment. To circumvent these issues, the gels are modified by crosslinkers that facilitate the binding of rBM or ECM components to the gels [154]. Cells are then applied to these gels and overlaid with more rBM or ECM component to construct a pseudo-3D environment. These gels have a precisely calibrated modulus range (200 – 10,000 Pascals) and have been used successfully to study matrix stiffness and mechanotransduction in normal and malignant mammary development [25].

#### ENGINEERED BIOREACTORS

Knowledge of the types, magnitude and duration of forces throughout the cell are essential in understanding the molecular mechanisms involved in mechanotransduction. The cellular response to mechanical stimulation is dependent on the type of force applied, with tensile and compressive forces being applied perpendicular to the surface of the cell or 3D construct and shear forces being applied parallel to the cell or 3D construct surface. The cellular response is also dependent on the magnitude, frequency and duration of the applied stimuli. To delineate the roles of physical forces in cell behavior and tissue homeostasis, researchers apply physiologically-relevant mechanical stimuli at the cellular and tissue levels using specially engineered devices which have been designed to control temporal, spatial and intensity parameters.

There are two general approaches to studying cellular mechanotransduction. The first approach uses multiple cells, mechanically stimulating a group of cells, and mimicking forces inherent in various

physiological environments. This first set of techniques include the simple application of hydrostatic pressure, compression, tension and shear stress to cell monolayers, or in the context of a tissue (*ex vivo* explant culture or cells embedded in a tissue engineering scaffold). Flow chambers apply shear stress to monolayers of cells, either through pressure-driven systems applying a parabolic laminar flow profile or cone-and-plate flow chambers which apply a uniform shear stress with a linear flow profile [155]. The role of hydrostatic pressure in cell and tissue growth and differentiation can be investigated in 2D by applying a transmembrane pressure to cells plated on a porous, stiff substrate, or in 2D or 3D by directing compressed air or a column of fluid over a culture of cells [15]. Techniques investigating the mechano-response to tensile stress involve the application of static or cyclic, axial or biaxial strains to monolayers of cells on a deformable membrane, or within a deformable 3D scaffold [156][157]. Additionally, mechanical devices have been used since the 70's to deconstruct the roles of static and dynamic compression in cell growth and metabolism [158].

The second and more recent approach to studying cellular mechanotransduction investigates the response by a single, individual cell to a mechanical stimulus. Sophisticated devices apply pico- or nano-Newton forces to individual cell membranes, receptors or cytoskeletal elements. Particle attachment has been used to apply precise forces to the surface of cells, using small microbeads coated with adhesive ligands or antibodies to a specific receptor and then applying a force to the particle [159, 160]. Different techniques for applying forces include optical trapping, micropipette aspiration and the application of both linear and torsional forces with magnetic manipulation [161-163]. Both atomic force microscopy and traction force microscopy have been used to determine the material properties, as well as the forces generated, by single cells [164-166]. Development of these innovative approaches and tools opens endless possibilities for novel insights into fundamental mechanotransduction mechanisms directing interactions between cells and their surrounding microenvironment.

## CONCLUSION

Stromal-epithelial interactions drive development and maintain tissue homeostasis through a network of both physical and biochemical factors that operate within a 3D mammary tissue. Specifically, mammary gland development, maintenance, and remodeling, as well as epithelial and stromal cellular responses and functions, are modulated by the mechanical environment. These biomechanical cues contribute crucial information to developmental and disease processes, and influence basic cell fate decisions. The cellular and ECM compositions evolve over time, guiding

and responding to changes in the development of the gland. Integral to this process is the complex interplay between soluble factors, cell-cell and cell-ECM interactions and the mechanical environment, which cooperatively drive mammary morphogenesis and differentiation, and regulate tissue homeostasis.

Mechanical force elicits a myriad of biochemical responses in a cell, altering how a cell responds to an exogenous signal, and dramatically influencing differentiation decisions during development. Given that tumorigenesis is associated with drastic changes in the mechanical characteristics of the mammary gland, including the composition and structure of ECM components, intracellular and extracellular tension, interstitial pressure and tissue elastic modulus, altered mechanotransduction and loss of mechanical-homeostasis constitute a plausible mechanism regulating the pathogenesis of breast tumors. While the overall importance of mechanotransduction is generally acknowledged, much remains to be discovered about cell and tissue mechanotransduction, and how such mechanosensory signals guide behavior. The quest to elucidate how mechanical stimulation induces structural, compositional and functional changes at the cellular level, as well as in 3D tissues, is still in its infancy. It will be critical to clarify the molecular basis of mechanotransduction in the development and homeostasis of the mammary gland, as well as in epithelial transformation.

## ACKNOWLEDGEMENTS

We apologize to the many authors whose work is not cited due to space limitations. This work was supported by NIH grant 7R01CA078731-07, DOD grant W81XWH-05-1-330 (BC044791) and DOE grant A107165 to V.M.W., and DOD grant BC062562 to J.K.M.

## REFERENCES

1. S. Moulder and G.N. Hortobagyi, *Clin Pharmacol Ther* 83 (2008) 26-36.
2. S. Huang and D.E. Ingber, *Cancer Cell* 8 (2005) 175-6.
3. C.M. Nelson and M.J. Bissell, *Annu Rev Cell Dev Biol* 22 (2006) 287-309.
4. B.S. Wiseman and Z. Werb, *Science* 296 (2002) 1046-9.
5. S. Lelievre, V.M. Weaver and M.J. Bissell, *Recent Prog Horm Res* 51 (1996) 417-32.
6. E. Farge, *Curr Biol* 13 (2003) 1365-77.
7. R. Keller, L.A. Davidson and D.R. Shook, *Differentiation* 71 (2003) 171-205.
8. G. Helmlinger, P.A. Netti, H.C. Lichtenbeld, R.J. Melder and R.K. Jain, *Nat Biotechnol* 15 (1997) 778-83.

9. M. Brancaccio, E. Hirsch, A. Notte, G. Selvetella, G. Lembo and G. Tarone, *Cardiovasc Res* 70 (2006) 422-33.
10. O.P. Hamill and B. Martinac, *Physiol Rev* 81 (2001) 685-740.
11. M. Tamada, M.P. Sheetz and Y. Sawada, *Dev Cell* 7 (2004) 709-18.
12. M. Chiquet, V. Tunc-Civelek and A. Sarasa-Renedo, *Appl Physiol Nutr Metab* 32 (2007) 967-73.
13. F.H. Silver and L.M. Siperko, *Crit Rev Biomed Eng* 31 (2003) 255-331.
14. M.J. Bissell, H.G. Hall and G. Parry, *Journal of Theoretical Biology* 99 (1982) 31-68.
15. M.J. Paszek and V.M. Weaver, *J Mammary Gland Biol Neoplasia* 9 (2004) 325-42.
16. A. Page-McCaw, A.J. Ewald and Z. Werb, *Nat Rev Mol Cell Biol* 8 (2007) 221-33.
17. P. Lu, M.D. Sternlicht and Z. Werb, *J Mammary Gland Biol Neoplasia* 11 (2006) 213-28.
18. M.D. Sternlicht, M.J. Bissell and Z. Werb, *Oncogene* 19 (2000) 1102-13.
19. V.M. Weaver, O.W. Petersen, F. Wang, C.A. Larabell, P. Briand, C. Damsky and M.J. Bissell, *J Cell Biol* 137 (1997) 231-45.
20. J. de Rooij, A. Kerstens, G. Danuser, M.A. Schwartz and C.M. Waterman-Storer, *J Cell Biol* 171 (2005) 153-64.
21. C.A. Carraway and K.L. Carraway, *Sci STKE* 2007 (2007) re3.
22. C. Dickson, B. Spencer-Dene, C. Dillon and V. Fantl, *Breast Cancer Res* 2 (2000) 191-6.
23. F. Lanigan, D. O'Connor, F. Martin and W.M. Gallagher, *Cell Mol Life Sci* 64 (2007) 3159-84.
24. M.D. Marmor, K.B. Skaria and Y. Yarden, *Int J Radiat Oncol Biol Phys* 58 (2004) 903-13.
25. M.J. Paszek, N. Zahir, K.R. Johnson, J.N. Lakins, G.I. Rozenberg, A. Gefen, C.A. Reinhart-King, S.S. Margulies, M. Dembo, D. Boettiger, D.A. Hammer and V.M. Weaver, *Cancer Cell* 8 (2005) 241-54.
26. A. Samani, J. Zubovits and D. Plewes, *Phys Med Biol* 52 (2007) 1565-76.
27. H.B. Wang, M. Dembo and Y.L. Wang, *Am J Physiol Cell Physiol* 279 (2000) C1345-50.
28. M.A. Wozniak, R. Desai, P.A. Solski, C.J. Der and P.J. Keely, *J Cell Biol* 163 (2003) 583-95.
29. I. Taddei, M.M. Faraldo, J. Teuliere, M.A. Deugnier, J.P. Thiery and M.A. Glukhova, *J Mammary Gland Biol Neoplasia* 8 (2003) 383-94.
30. C.M. Nelson, M.M. Vanduijn, J.L. Inman, D.A. Fletcher and M.J. Bissell, *Science* 314 (2006) 298-300.
31. G.W. Robinson, *Nat Rev Genet* 8 (2007) 963-72.
32. M.A. Chrenek, P. Wong and V.M. Weaver, *Breast Cancer Res* 3 (2001) 224-9.
33. J.R. Hens and J.J. Wysolmerski, *Breast Cancer Res* 7 (2005) 220-4.
34. M.D. Sternlicht, *Breast Cancer Res* 8 (2006) 201.
35. M.D. Sternlicht, H. Kouros-Mehr, P. Lu and Z. Werb, *Differentiation* 74 (2006) 365-81.

36. J.M. Veltmaat, A.A. Mailleux, J.P. Thiery and S. Bellusci, *Differentiation* 71 (2003) 1-17.
37. L. Hinck and G.B. Silberstein, *Breast Cancer Res* 7 (2005) 245-51.
38. J.E. Fata, Z. Werb and M.J. Bissell, *Breast Cancer Res* 6 (2004) 1-11.
39. S.R. Oakes, H.N. Hilton and C.J. Ormandy, *Breast Cancer Res* 8 (2006) 207.
40. S.M. Anderson, M.C. Rudolph, J.L. McManaman and M.C. Neville, *Breast Cancer Res* 9 (2007) 204.
41. C.J. Watson, *Breast Cancer Res* 8 (2006) 203.
42. M.P. Osborne, *Breast development and anatomy*, Lippincott-Raven Publishers, Philadelphia, 1996.
43. J. Russo and I.H. Russo, *Eur J Cancer Prev* 2 Suppl 3 (1993) 85-100.
44. M. Larsen, V.V. Artym, J.A. Green and K.M. Yamada, *Curr Opin Cell Biol* 18 (2006) 463-71.
45. K. Kimata, T. Sakakura, Y. Inaguma, M. Kato and Y. Nishizuka, *J Embryol Exp Morphol* 89 (1985) 243-57.
46. T. Sakakura, Y. Sakagami and Y. Nishizuka, *Dev Biol* 91 (1982) 202-7.
47. B.S. Wiseman, M.D. Sternlicht, L.R. Lund, C.M. Alexander, J. Mott, M.J. Bissell, P. Soloway, S. Itohara and Z. Werb, *J Cell Biol* 162 (2003) 1123-33.
48. H. Kouros-Mehr and Z. Werb, *Dev Dyn* 235 (2006) 3404-12.
49. Z. Werb, J. Ashkenas, A. MacAuley and J.F. Wiesen, *Braz J Med Biol Res* 29 (1996) 1087-97.
50. J.E. Fata, K.J. Leco, R.A. Moorehead, D.C. Martin and R. Khokha, *Dev Biol* 211 (1999) 238-54.
51. W.F. Vogel, A. Aszodi, F. Alves and T. Pawson, *Mol Cell Biol* 21 (2001) 2906-17.
52. F. Berditchevski and E. Odintsova, *J Cell Biol* 146 (1999) 477-92.
53. T.C. Klinowska, C.M. Alexander, E. Georges-Labouesse, R. Van der Neut, J.A. Kreidberg, C.J. Jones, A. Sonnenberg and C.H. Streuli, *Dev Biol* 233 (2001) 449-67.
54. J. Chen, T.G. Diacovo, D.G. Grenache, S.A. Santoro and M.M. Zutter, *Am J Pathol* 161 (2002) 337-44.
55. M.J. Naylor, N. Li, J. Cheung, E.T. Lowe, E. Lambert, R. Marlow, P. Wang, F. Schatzmann, T. Wintermantel, G. Schuetz, A.R. Clarke, U. Mueller, N.E. Hynes and C.H. Streuli, *J Cell Biol* 171 (2005) 717-28.
56. T.L. Woodward, A.S. Mienaltowski, R.R. Modi, J.M. Bennett and S.Z. Haslam, *Endocrinology* 142 (2001) 3214-22.
57. J. Trinkaus, *Cells in organs. The forces that shape the embryo.*, second ed., Prentice-Hall Inc., Englewood Cliffs, NJ, 1984.
58. G.F. Oster, J.D. Murray and A.K. Harris, *J Embryol Exp Morphol* 78 (1983) 83-125.
59. J.Y. Wong, A. Velasco, A. Rajagopalan and Q. Pham, *Langmuir* 19 (2003) 1908-1913.
60. S. Goswami, E. Sahai, J.B. Wyckoff, M. Cammer, D. Cox, F.J. Pixley, E.R. Stanley, J.E. Segall and J.S. Condeelis, *Cancer Res* 65 (2005) 5278-83.
61. A. Czirok, B.J. Rongish and C.D. Little, *Dev Biol* 268 (2004) 111-22.



62. E.Y. Chu, J. Hens, T. Andl, A. Kairo, T.P. Yamaguchi, C. Briskin, A. Glick, J.J. Wysolmerski and S.E. Millar, *Development* 131 (2004) 4819-29.
63. D.E. Ingber, *Ann Med* 35 (2003) 564-77.
64. J.C. Howard, V.M. Varallo, D.C. Ross, J.H. Roth, K.J. Faber, B. Alman and B.S. Gan, *BMC Musculoskelet Disord* 4 (2003) 16.
65. J. Yant, L. Buluwela, B. Niranjana, B. Gusterson and T. Kamalati, *Exp Cell Res* 241 (1998) 476-81.
66. B. Niranjana, L. Buluwela, J. Yant, N. Perusinghe, A. Atherton, D. Phippard, T. Dale, B. Gusterson and T. Kamalati, *Development* 121 (1995) 2897-908.
67. C. Dillon, B. Spencer-Dene and C. Dickson, *J Mammary Gland Biol Neoplasia* 9 (2004) 207-15.
68. V. Fleury and T. Watanabe, *C R Biol* 325 (2002) 571-83.
69. S.R. Lubkin and Z. Li, *Biomech Model Mechanobiol* 1 (2002) 5-16.
70. G. Forgacs, *Biol Bull* 194 (1998) 328-29; discussion 329-30.
71. H. Miao, C.H. Nickel, L.G. Cantley, L.A. Bruggeman, L.N. Bennardo and B. Wang, *J Cell Biol* 162 (2003) 1281-92.
72. K.A. Moore, S. Huang, Y. Kong, M.E. Sunday and D.E. Ingber, *J Surg Res* 104 (2002) 95-100.
73. J.T. Emerman and D.R. Pitelka, *In Vitro* 13 (1977) 316-28.
74. M.H. Barcellos-Hoff, J. Aggeler, T.G. Ram and M.J. Bissell, *Development* 105 (1989) 223-35.
75. C.D. Roskelley, A. Srebrow and M.J. Bissell, *Curr Opin Cell Biol* 7 (1995) 736-47.
76. V.M. Weaver and M.J. Bissell, *J Mammary Gland Biol Neoplasia* 4 (1999) 193-201.
77. T.H. Chun, K.B. Hotary, F. Sabeh, A.R. Saltiel, E.D. Allen and S.J. Weiss, *Cell* 125 (2006) 577-91.
78. S.J. Gunst and D.D. Tang, *Eur Respir J* 15 (2000) 600-16.
79. A. Marti, Z. Feng, H.J. Altermatt and R. Jaggi, *Eur J Cell Biol* 73 (1997) 158-65.
80. D.C. Radisky, P.A. Kenny and M.J. Bissell, *J Cell Biochem* 101 (2007) 830-9.
81. J. Condeelis and J.W. Pollard, *Cell* 124 (2006) 263-6.
82. A.A. Rasmussen and K.J. Cullen, *Breast Cancer Res Treat* 47 (1998) 219-33.
83. C. Kuperwasser, T. Chavarria, M. Wu, G. Magrane, J.W. Gray, L. Carey, A. Richardson and R.A. Weinberg, *Proc Natl Acad Sci U S A* 101 (2004) 4966-71.
84. L.M. Coussens and Z. Werb, *Nature* 420 (2002) 860-7.
85. C. Porta, B. Subhra Kumar, P. Larghi, L. Rubino, A. Mancino and A. Sica, *Adv Exp Med Biol* 604 (2007) 67-86.
86. M.J. Bissell, D.C. Radisky, A. Rizki, V.M. Weaver and O.W. Petersen, *Differentiation* 70 (2002) 537-46.
87. G. Akiri, E. Sabo, H. Dafni, Z. Vadasz, Y. Kartvelishvily, N. Gan, O. Kessler, T. Cohen, M. Resnick, M. Neeman and G. Neufeld, *Cancer Res* 63 (2003) 1657-66.

88. T.Y. Eshchenko, V.I. Rykova, A.E. Chernakov, S.V. Sidorov and E.V. Grigorieva, *Biochemistry (Mosc)* 72 (2007) 1016-20.
89. S. Alowami, S. Troup, S. Al-Haddad, I. Kirkpatrick and P.H. Watson, *Breast Cancer Res* 5 (2003) R129-35.
90. D.C. Jinga, A. Blidaru, I. Condrea, C. Ardeleanu, C. Dragomir, G. Szegli, M. Stefanescu and C. Matache, *J Cell Mol Med* 10 (2006) 499-510.
91. B.S. Garra, *Ultrasound Q* 23 (2007) 255-68.
92. E.I. Deryugina and J.P. Quigley, *Cancer Metastasis Rev* 25 (2006) 9-34.
93. T. Yeung, P.C. Georges, L.A. Flanagan, B. Marg, M. Ortiz, M. Funaki, N. Zahir, W. Ming, V. Weaver and P.A. Janmey, *Cell Motil Cytoskeleton* 60 (2005) 24-34.
94. C.M. Lo, H.B. Wang, M. Dembo and Y.L. Wang, *Biophys J* 79 (2000) 144-52.
95. D.S. Gray, J. Tien and C.S. Chen, *J Biomed Mater Res A* 66 (2003) 605-14.
96. E. Vial, E. Sahai and C.J. Marshall, *Cancer Cell* 4 (2003) 67-79.
97. G. Ferretti, A. Felici, P. Papaldo, A. Fabi and F. Cognetti, *Curr Opin Obstet Gynecol* 19 (2007) 56-62.
98. V.M. Weaver, A.H. Fischer, O.W. Peterson and M.J. Bissell, *Biochem Cell Biol* 74 (1996) 833-51.
99. F.G. Giancotti, *Trends Pharmacol Sci* 28 (2007) 506-11.
100. A. Bertotti, P.M. Comoglio and L. Trusolino, *Cancer Res* 65 (2005) 10674-9.
101. S.K. Muthuswamy, D. Li, S. Lelievre, M.J. Bissell and J.S. Brugge, *Nat Cell Biol* 3 (2001) 785-92.
102. W. Guo, Y. Pylayeva, A. Pepe, T. Yoshioka, W.J. Muller, G. Inghirami and F.G. Giancotti, *Cell* 126 (2006) 489-502.
103. C.C. Park, H. Zhang, M. Pallavicini, J.W. Gray, F. Baehner, C.J. Park and M.J. Bissell, *Cancer Res* 66 (2006) 1526-35.
104. J. Condeelis and J.E. Segall, *Nat Rev Cancer* 3 (2003) 921-30.
105. G. Giannelli, J. Falk-Marzillier, O. Schiraldi, W.G. Stetler-Stevenson and V. Quaranta, *Science* 277 (1997) 225-8.
106. J.P. Thiery, *Cell Differ* 15 (1984) 1-15.
107. M.P. Sheetz, D.P. Felsenfeld and C.G. Galbraith, *Trends Cell Biol* 8 (1998) 51-4.
108. G. Fritz, C. Brachetti, F. Bahlmann, M. Schmidt and B. Kaina, *Br J Cancer* 87 (2002) 635-44.
109. C.G. Kleer, Y. Zhang, Q. Pan, G. Gallagher, M. Wu, Z.F. Wu and S.D. Merajver, *Breast Cancer Res* 6 (2004) R110-5.
110. J.T. Erler and A.J. Giaccia, *Cancer Res* 66 (2006) 10238-41.
111. L.J. Martin and N.F. Boyd, *Breast Cancer Res* 10 (2008) 201.
112. C.M. Vachon, C.H. van Gils, T.A. Sellers, K. Ghosh, S. Pruthi, K.R. Brandt and V.S. Pankratz, *Breast Cancer Res* 9 (2007) 217.
113. N.F. Boyd, J.M. Rommens, K. Vogt, V. Lee, J.L. Hopper, M.J. Yaffe and A.D. Paterson, *Lancet Oncol* 6 (2005) 798-808.
114. G. Ursin, L. Hovanesian-Larsen, Y.R. Parisky, M.C. Pike and A.H. Wu, *Breast Cancer Res* 7 (2005) R605-8.

115. P.P. Provenzano, K.W. Eliceiri, J.M. Campbell, D.R. Inman, J.G. White and P.J. Keely, *BMC Med* 4 (2006) 38.
116. M. Egeblad, L.E. Littlepage and Z. Werb, *Cold Spring Harb Symp Quant Biol* 70 (2005) 383-8.
117. S. Ramaswamy, K.N. Ross, E.S. Lander and T.R. Golub, *Nat Genet* 33 (2003) 49-54.
118. D.A. Kirschmann, E.A. Seftor, S.F. Fong, D.R. Nieva, C.M. Sullivan, E.M. Edwards, P. Sommer, K. Csiszar and M.J. Hendrix, *Cancer Res* 62 (2002) 4478-83.
119. Y.P. Guo, L.J. Martin, W. Hanna, D. Banerjee, N. Miller, E. Fishell, R. Khokha and N.F. Boyd, *Cancer Epidemiol Biomarkers Prev* 10 (2001) 243-8.
120. K.Y. Volokh, *Acta Biomater* 2 (2006) 493-504.
121. H. Axelsson, E. Fredlund, M. Ovenberger, G. Landberg and S. Pahlman, *Semin Cell Dev Biol* 16 (2005) 554-63.
122. L. Holmquist, T. Lofstedt and S. Pahlman, *Adv Exp Med Biol* 587 (2006) 179-93.
123. T.J. Dennerll, H.C. Joshi, V.L. Steel, R.E. Buxbaum and S.R. Heidemann, *J Cell Biol* 107 (1988) 665-74.
124. Y. Muroi, K. Kakudo and K. Nakata, *J Dent Res* 86 (2007) 786-91.
125. H. Ichimiya, T. Takahashi, W. Ariyoshi, H. Takano, T. Matayoshi and T. Nishihara, *Oral Surg Oral Med Oral Pathol Oral Radiol Endod* 103 (2007) 334-41.
126. T.L. Vincent, C.J. McLean, L.E. Full, D. Peston and J. Saklatvala, *Osteoarthritis Cartilage* 15 (2007) 752-63.
127. F. Reno, P. Grazianetti, M. Stella, G. Magliacani, C. Pezzuto and M. Cannas, *Arch Dermatol* 138 (2002) 475-8.
128. F. Reno, M. Sabbatini, M. Stella, G. Magliacani and M. Cannas, *Wound Repair Regen* 13 (2005) 255-61.
129. J.K. Mouw, J.T. Connelly, C.G. Wilson, K.E. Michael and M.E. Levenston, *Stem Cells* 25 (2007) 655-63.
130. S.K. Leivonen and V.M. Kahari, *Int J Cancer* 121 (2007) 2119-24.
131. B.C. Willis and Z. Borok, *Am J Physiol Lung Cell Mol Physiol* 293 (2007) L525-34.
132. D.J. Tschumperlin, G. Dai, I.V. Maly, T. Kikuchi, L.H. Laiho, A.K. McVittie, K.J. Haley, C.M. Lilly, P.T. So, D.A. Lauffenburger, R.D. Kamm and J.M. Drazen, *Nature* 429 (2004) 83-6.
133. A. Katsumi, A.W. Orr, E. Tzima and M.A. Schwartz, *J Biol Chem* 279 (2004) 12001-4.
134. V. Gupta and K.J. Grande-Allen, *Cardiovasc Res* 72 (2006) 375-83.
135. A. Katsumi, T. Naoe, T. Matsushita, K. Kaibuchi and M.A. Schwartz, *J Biol Chem* 280 (2005) 16546-9.
136. T.P. Quinn, M. Schlueter, S.J. Soifer and J.A. Gutierrez, *Am J Physiol Lung Cell Mol Physiol* 282 (2002) L897-903.
137. H.T. Nguyen, R.M. Adam, S.H. Bride, J.M. Park, C.A. Peters and M.R. Freeman, *Am J Physiol Cell Physiol* 279 (2000) C1155-67.

138. R.M. Adam, J.A. Roth, H.L. Cheng, D.C. Rice, J. Khoury, S.B. Bauer, C.A. Peters and M.R. Freeman, *J Urol* 169 (2003) 2388-93.
139. C. Zhong, M.S. Kinch and K. Burridge, *Mol Biol Cell* 8 (1997) 2329-44.
140. D. Sarrio, S.M. Rodriguez-Pinilla, D. Hardisson, A. Cano, G. Moreno-Bueno and J. Palacios, *Cancer Res* 68 (2008) 989-97.
141. M. Lombaerts, T. van Wezel, K. Philippo, J.W. Dierssen, R.M. Zimmerman, J. Oosting, R. van Eijk, P.H. Eilers, B. van de Water, C.J. Cornelisse and A.M. Cleton-Jansen, *Br J Cancer* 94 (2006) 661-71.
142. P.A. Janmey and D.A. Weitz, *Trends Biochem Sci* 29 (2004) 364-70.
143. J.H. Wang and B.P. Thampatty, *Biomech Model Mechanobiol* 5 (2006) 1-16.
144. R. Paul, P. Heil, J.P. Spatz and U.S. Schwarz, *Biophys J* 94 (2008) 1470-82.
145. R.W. Tilghman and J.T. Parsons, *Semin Cancer Biol* 18 (2008) 45-52.
146. C. Hebnar, V.M. Weaver and J. Debnath, *Annu Rev Pathol* (2007).
147. O.W. Petersen, L. Ronnov-Jessen, A.R. Howlett and M.J. Bissell, *Proc Natl Acad Sci U S A* 89 (1992) 9064-8.
148. V.M. Weaver, A.R. Howlett, B. Langton-Webster, O.W. Petersen and M.J. Bissell, *Semin Cancer Biol* 6 (1995) 175-84.
149. J. Debnath, S.K. Muthuswamy and J.S. Brugge, *Methods* 30 (2003) 256-68.
150. T. Gudjonsson, L. Ronnov-Jessen, R. Villadsen, F. Rank, M.J. Bissell and O.W. Petersen, *J Cell Sci* 115 (2002) 39-50.
151. P.A. Kenny, G.Y. Lee, C.A. Myers, R.M. Neve, J.R. Semeiks, P.T. Spellman, K. Lorenz, E.H. Lee, M.H. Barcellos-Hoff, O.W. Petersen, J.W. Gray and M.J. Bissell, 1 (2007) 84-96.
152. J.G.W. Aunins, D.I.C., *Biotechnology Progress* 6 (1990) 54-61.
153. R.J. Pelham, Jr. and Y. Wang, *Proc Natl Acad Sci U S A* 94 (1997) 13661-5.
154. R.H. Schmedlen, K.S. Masters and J.L. West, *Biomaterials* 23 (2002) 4325-32.
155. P.F. Davies, *Physiol Rev* 75 (1995) 519-60.
156. M.E. Wall, P.S. Weinhold, T. Siu, T.D. Brown and A.J. Banes, *J Biomech* 40 (2007) 173-81.
157. E.J. Vanderploeg, S.M. Imler, K.R. Brodtkin, A.J. Garcia and M.E. Levenston, *J Biomech* 37 (2004) 1941-52.
158. M.M. Panjabi, A.A. White, 3rd and J.W. Wolf, Jr., *Acta Orthop Scand* 50 (1979) 653-61.
159. Y. Gan, *Rev Sci Instrum* 78 (2007) 081101.
160. H. Huang, R.D. Kamm and R.T. Lee, *Am J Physiol Cell Physiol* 287 (2004) C1-11.
161. D. Choquet, D.P. Felsenfeld and M.P. Sheetz, *Cell* 88 (1997) 39-48.
162. R.M. Hochmuth, *Journal of Biomechanics* 33 (2000) 15-22.
163. H. Pommerenke, E. Schreiber, F. Durr, B. Nebe, C. Hahnel, W. Moller and J. Rychly, *Eur J Cell Biol* 70 (1996) 157-64.
164. R. Garcia, R. Magerle and R. Perez, *Nat Mater* 6 (2007) 405-11.
165. B. Sabass, M.L. Gardel, C.M. Waterman and U.S. Schwarz, *Biophys J* 94 (2008) 207-20.
166. S. Munevar, Y. Wang and M. Dembo, *Biophys J* 80 (2001) 1744-57.

## **APPENDIX**

### **E.     Patents**

1.     Weaver, V.M., Tsai, K., Methods for predicting and treating drug-, immunotherapy- and/or radiation-resistant tumors. SF2008-034, 2007. Pending.

**PATENT APPLICATION**

**NOVEL METHODS FOR PREDICTING AND TREATING TUMORS  
RESISTANT TO DRUG, IMMUNOTHERAPY, AND RADIATION**

Inventor(s): Valerie M. Weaver, a citizen of Canada, residing at  
661 Moultrie St., San Francisco, Ca 94110

Kun-Chih Kelvin Tsai, a citizen of Taiwan, residing at  
5F, No. 25, Lane 180, Hejiang St., Jhongshan District, Taipei 104, Taiwan

Assignee: REGENTS OF THE UNIVERSITY OF CALIFORNIA  
Office of Technology Transfer, 1111 Franklin St., 5th Floor  
Oakland, CA 94607

Entity: Small

CROSS-REFERENCES TO RELATED APPLICATIONS

[0001] NOT APPLICABLE

5

STATEMENT AS TO RIGHTS TO INVENTIONS MADE UNDER  
FEDERALLY SPONSORED RESEARCH AND DEVELOPMENT

[0002] This invention was made in part with Governmental support under grant no.  
CA078731 awarded by the National Institute of Health and grant no. W81XWH-05-1-330  
10 awarded by the DOD BCRP Program. The Government may have rights in this invention.

REFERENCE TO A "SEQUENCE LISTING," A TABLE, OR A COMPUTER  
PROGRAM LISTING APPENDIX SUBMITTED ON A COMPACT DISK.

[0003] NOT APPLICABLE

15

BACKGROUND OF THE INVENTION

[0004] The development of intrinsic or acquired drug resistance by tumor cells significantly  
limits the efficacy of antineoplastic agents and is the major contributing factor to therapeutic  
failure of human malignancies. Drug resistance refers to progressive disease of the malignant  
20 tumors that occurs at doses associated with manageable toxicity of the drug. It is well known  
in the clinical practice that many malignant tumors are initially sensitive to chemotherapy,  
but the vast majority will eventually recur and develop broad resistance to conventional  
cytotoxic chemotherapeutic agents and radiotherapy (Nat. Rev. Cancer 3:502-516 (2003)).

[0005] Laboratory-based studies have identified a wide variety of genes and molecular  
25 pathways, such as MDR1 (P-glycoprotein) (Cancer Res. 53:747-754 (1993)) and p53 (Cell  
74:957-967 (1993)), that can lead to increased resistance to treatments in malignant tumor  
cells. Nevertheless, significant discrepancies exist between drug resistance identified in  
experimental models and the multidrug resistance (MDR) phenotypes found in human  
malignant tumors (Br. J. Cancer 94:1087-1092 (2006)). For instance, acquisition of p53  
30 mutations and gene amplification of MDR1 are rarely observed following chemotherapy in  
clinical human malignancies and so far there is little evidence demonstrating that single gene-

mediated drug resistance individually correlated with treatment outcome of human malignancies (Nat. Rev. Cancer 3:502-516 (2003)).

[0006] The discrepancy between experimental and clinical drug resistance may partly stem from the distinct multicellular and spatial-dimensional contexts under which tumor drug resistance develops *in vivo*. Most of the current knowledge about the cellular responses to chemicals, toxins or radiation were gathered from studies using unicellular culture models, which lacked consideration of the heterotypic cell-cell interactions in the tumor-host interface (Nature 411:375-379 (2001)). Previously, it has been clearly shown that the drug resistance phenotype of tumor cells for alkylating agents only emerged *in vivo* mainly as a result of host-tumor interactions and could not be detected by unicellular culture models (Science 247:1457-1461 (1990)). The MDR phenotypes of cancers have only be recapitulated by culture models that incorporate elements mimicking *in vivo* tumor or tissue architectures instead of conventional monolayer cell cultures (Proc. Natl. Acad. Sci. U.S.A. 90, 3294-3298 (1993)). For instance, organization of tumor cells into three-dimensional (3D) multicellular spheroids endowed resistance to cytotoxic agents and radiation, which was reversible by disaggregation of the structures (Anticancer Drug Dev. 14:153-168 (1999); Crit. Rev. Oncol. Hematol. 36:193-207 (2000)).

[0007] A variety of mechanisms have been proposed for the development of MDR in tumor cells in 3D multicellular spheroids, including hypoxia, cellular attachment, cell cycle proteins such as KIP1, and cell surface signaling such as the phatidylinositol 3-kinase pathway (Nature Med. 2:1204-1210 (1996); Anticancer Drug Dev. 14:153-168 (1999); Anticancer Drug Dev. 14:169-177 (1999)). When maintained *ex vivo* with preserved tissue architecture, malignant tumors displayed differential sensitivities to cytotoxic drugs similar to those observed *in vivo* (Proc. Natl. Acad. Sci. U.S.A. 84:5029-5033 (1987)). The context-dependency of cell death sensitivity also holds true for non-neoplastic epithelial cells, as organization of mammary epithelial cells into 3D acinar architectures in response to reconstituted basement membrane (rBM) endowed them a MDR phenotype (Cancer Cell 2:205-216 (2002)).

[0008] Cell development and differentiation are governed by the hierarchical order of gene activation and repression controlled at the level of chromatin structures by epigenetic mechanisms. Epigenetic changes are heritable changes in gene expression that do not involve an alteration in the DNA sequence, which commonly involve changes in the patterns of



modifications of DNA and histones, including methylation, acetylation, and phosphorylation, as well as in the architecture of the chromatin conformation (J. Cell Sci. 116:2117-2124 (2003)). Disruptions of the epigenetic regulation of chromatin structure, function, and gene expression therefore leads to the dysregulated of cell growth and differentiation, as well as cancer. Consistent with this view, there is now circumstantial evidence supporting the epigenetic progenitor model in favor of the classical clonal genetic model of cancer (Nat. Rev. Genet. 7:21-33 (2005)). Epigenetic alterations, such as global DNA hypomethylation and chromatin hyperacetylation, are found at very early stages of tumorigenesis. On the other hand, hypermethylation and chromatin hypoacetylation on selective promoters are common strategies which tumor use to silence selective tumor-suppressor genes, such as retinoblastoma 1 (*RBI*), p16 (*CDKN2A*), von Hippel-Lindau tumor suppressor (*VHL*), and MutL protein homologue 1 (*MLH1*).

**[0009]** Histone hypoacetylation can be caused by inactivation of histone acetylase (HAT) activity due to gene mutations, inhibitory action of viral oncoproteins, and chromosomal translocations. For instance, mutations in CBP and P300 are associated with cancer predisposition (Trends Genet. 14:178-183 (1998), Nat. Genet. 24:300-303 (2000)). Fusion proteins involving MLL (mixed-lineage leukemia) or MORF (monocytic-leukemia-zinc-finger-protein related factor) and p300 or CBP have been associated with acute myelogenous leukemia (AML) (Blood 92:2118-2122 (1998), Hum. Mol. Genet. 10:395-404 (2001)).

Histone hypoacetylation and tumorigenesis can also be caused by altered histone deacetylase (HDAC) activities. For instance, chromosomal translocation events in acute promyelocytic leukemia (APL) produce fusion proteins that contain retinoid acid receptor (RAR) $\alpha$  and PML (promyelocytic leukemia protein), and RAR $\alpha$  and PLZF (promyelocytic zinc finger), which recruit HDACs with high affinity and result in constitutive repression of RAR-targeted genes (Oncogene 20:7204-7215 (2001)). Moreover, the fusions proteins AML1-ETO and TEL-AML1, expressed in AML and acute lymphoblastic leukemia, recruit HDACs and repress the AML1 transcriptional factor (Oncogene 20:5660-5679 (2001)). Inappropriate transcriptional repression mediated by HDACs may also operate in the tumorigenesis of solid tumors, although the precise mechanisms remain incompletely understood.

**[0010]** Epigenetic alterations not only play important roles in tumor initiation but may also contribute to malignant progression. Phenotypic plasticity mediated by epigenetic mechanisms has now been recognized as an important source of cancer-cell heterogeneity driving phenotypic evolution of tumors. For example, DNA hypomethylation can drive

genomic instability as a result of decondensation of centromeric heterochromatin and the formation of new centromeres (Hum. Genet. 67:257-263 (1984)). A reduction in heterochromatin-associated protein 1 (*HPI*<sup>HSa</sup>), a nonhistone chromosomal protein that mediates transcriptional repression, is directly associated with breast tumor cell invasion and metastasis (Cancer Res. 60:3359-3363 (2000)). Recently, the polycomb group protein *EZH2*, a histone methyltransferase that causes gene silencing, was found to be overexpressed in metastatic prostate cancer and invasive breast cancer and promotes the proliferation and invasion of tumor cells through its interaction with HDAC2 (Nature 419:624-629 (2002), Proc. Natl. Acad. Sci. USA 100:11606-11611 (2003)). *EZH2* was also found to be an independent predictor of prostate and breast cancer recurrence and death. Moreover, it was reported that the gene expression pathway associated with Bmi-1, a component of the chromatin remodeling complex PRC1 (polycomb repressive complex 1), which mediates ubiquitination of histone H2A, strongly predicts recurrence, metastasis, and death in various types of human cancers (J. Clin. Invest. 115:1503-1521 (2005)). If epigenetic plasticity is a common strategy used by tumor cells to evolve into more advanced malignant states, it's likely that more epigenetic regulators will be identified as contributors to tumor progression.

**[0011]** Epigenetic changes alter the expression of a large number of genes and may lead to a higher and faster phenotypic plasticity, through which tumor cells can adapt to new environments such as cytotoxic drug therapy, than genetic changes. Consistent with this possibility, there is now increasing evidence suggesting that epigenetic changes of malignant tumor cells may be a crucial driving force behind the acquisition of drug resistance (Br. J. Cancer 94:1087-1092 (2006)). For instance, methylation of CpG islands in genes involved in DNA repair, including *BRCA1*, *GSTP1*, and *MGMT*, was associated with increased response to chemotherapy in human ovarian cancers (Cancer Res. 65:8961-8967 (2005); N. Engl. J. Med. 343:1350-1354 (2000)). In contrast, methylation and epigenetic inactivation of the proapoptotic gene *APAF1* is common in metastatic melanoma and confer resistance to conventional chemotherapy (Nature 409:207-211 (2001)). Similarly, a subset of patients with ovarian cancer acquired methylation of the DNA mismatch repair protein hMLH1 during chemotherapy, which was associated with poor overall survival (Clin. Cancer Res. 10:4420-4426 (2004)).

**[0012]** As mentioned, inappropriate transcriptional repression by altered HDAC activities is a common epigenetic mechanism used by oncoproteins and plays a significant role in tumorigenesis (Nat. Rev. Drug Disc. 1:287-299 (2002)). Currently, compounds that bind and

inhibit a broad genus of HDACs are in phase I and II clinical trials for their potentials as anti-tumor agents (Nat. Rev. Cancer 6:38-51 (2006)). These HDAC inhibitors induce histone hyperacetylation, reactivate suppressed genes, and have pleiotropic cellular effects. Most promisingly, HDAC inhibitors has been shown to induce apoptosis in MDR tumor cells and to sensitize them to chemotherapeutic agents or ionizing radiation through activation of both the death-receptor and intrinsic apoptotic pathways (Int. J. Cancer 104:579-586 (2003); Cancer Res. 63:4460-4471 (2003); Oncogene 24:4609-4623 (2005); Nat. Rev. Drug Disc. 1:287-299 (2002)).

**[0013]** HDACs alone or in combination with DNA-demethylating agents have been shown to increase sensitivity to chemotherapeutic agents in cell line models (Anticancer Drugs 13:869-874 (2002)) and are currently being assessed for their potentials as chemosensitizers in clinical trials. However, the key cellular targets of HDAC inhibitors, as well as patients and tumor types that most likely respond to HDAC inhibitors, remain unknown. Moreover, the inhibitors currently in clinical trials do not demonstrate specificity for individual HDACs. This is a significant problem, as individual HDACs have differential substrate specificities and functions. Determining which of these activities most readily effects tumorigenesis is critical for the efficient targeting of individual molecules. Thus, the use of HDAC inhibitors in clinical studies has very limited success to date (Nat. Rev. Drug Disc. 1:287-299 (2002)).

**[0014]** Given the pleiotropic effects of HDAC inhibitors on a wide variety of histone and non-histone substrates (Nat. Rev. Cancer 6:38-51 (2006)), it is unlikely that a single surrogate marker, such as the genomic level of histone acetylation, can serve as a predictor for drug efficacy. As HDAC inhibition can induce alterations in the transcription of a large number (up to 20% of known genes) of genes (Mol. Cancer Ther. 2:151-163 (2003); Proc. Natl. Acad. Sci. USA 101:540-545 (2004); Proc. Natl. Acad. Sci. USA 102:3697-3702 (2005)), transcriptional profiles associated with HDAC mutation or inhibition may show particular promise in the prediction of response to HDAC inhibitors.

**[0015]** The Nuclear Corepressor 2 (N-CoR2) (gene symbol: *NCOR2*; NCBI RefSeq #NM\_006312; UniGene ID Hs.137510) and its paralog N-CoR (gene symbol: *NCOR1*; NCBI RefSeq #NM\_006311; UniGene ID Hs.462323) are epigenetic regulators that mediate transcriptional repression by recruiting and activating various histone deacetylases (HDACs) (Annu. Rev. Physiol. 66:315-360 (2004)). N-CoR2 and N-CoR were originally identified as transcriptional corepressors of unliganded nuclear receptors, such as retinoic acid and

thyroid hormone receptors (Nature 377:454-457 (1995)). It has become increasingly evident that N-CoR2 and N-CoR also mediate repression of a wide array of non-receptor transcriptional factors, including the myogenic specific bHLH protein MyoD (Mol. Endocrinol. 13:1155-1168 (1999)), B-Myb (Mol. Cell. Biol. 22, 3663-3673 (2002)), the Pbx family of homeobox genes (Mol. Cell. Biol. 19:8219-8225 (1999)), the signal transducers and activators of transcription-5 (STAT5) (EMBO J. 20:6836-6844 (2001)), the oncoproteins PLZF-RAR (Nature 391:811-814 (1998)) and LAZ3/BCL6 (Proc. Natl. Acad. Sci. U.S.A. 94:10762-10767 (1997)), serum response factor (SRF), activating protein-1 (AP-1), and nuclear factor- $\kappa$ B (NF $\kappa$ B) (J. Biol. Chem. 275:12470-12474 (2000)).

10 **[0016]** Biochemical purification of the N-CoR2/N-CoR complexes demonstrated that both N-CoR2 and N-CoR exist in large protein complexes comprising GPS2 (G-protein pathway suppressor 2), which mediates inhibition of the JNK pathway (Cell 9:611-623 (2002)), TBL-1 (transducin  $\beta$ -like protein 1) and TBL-R1, which serve as E3 ligases that recruit the ubiquitin conjugating/19S proteasome complex and thereby degrades the N-CoR2/N-CoR complex  
15 (Gene Dev. 14:1048-1057 (2000), Cell 116:511-526 (2004)), and HDAC3, which exhibits histone deacetylase activities. Interestingly, the purified N-CoR2-HDAC3 complex possesses deacetylase activity, whereas HDAC3 alone does not function as a HDAC, suggesting that N-CoR2 or N-CoR not only serves as the adaptor but also the activator of the HDAC3 enzymatic activity (Mol. Cell. Biol. 21:6091-6101 (2001)). Biochemistry studies  
20 have further shown that a particular deacetylase activation domain of N-CoR2 is required for the activation of the otherwise inert HDAC3 (Proc. Natl. Acad. Sci. USA 102:6009-6014 (2005)).

**[0017]** To date, most of the studies on N-CoR or N-CoR2 have been focused on protein biochemistry and their role in hormone receptor signaling and much less was known about  
25 their other biological functions. Recently, aside from its nuclear receptor corepressor functions, N-CoR has been found to play important roles in differentiation (Mol. Endocrinol. 13:1155-1168 (1999)) and stem cell maintenance (Nature 419:934-939 (2002)). Similarly, N-CoR2 was also found to be involved in forebrain development and in maintenance of the neural stem cell state in mice (Nature 450:415-420 (2007)).

30 **[0018]** Recent advances in high-throughput analytical tools that can measure the expression of a large number of genes have enabled molecular profiling of human malignant tumors. This has greatly enhanced tumor classification and allows for prediction of disease

progression and clinical outcome. For instance, unsupervised hierarchical clustering on gene expression data allowed the classification of breast cancers into several distinct subgroups or molecular subtypes (Proc. Natl. Acad. Sci. USA 100:8418-8423 (2003)). In a second study, a 32-gene molecular classifier was used to place human bladder cancers into subclasses with prognostic significance (Nat. Genet. 33:90-96 (2003)). Gene expression profiling in another study allowed the classification of high-grade gliomas with higher accuracy and reproducibility (Cancer Res. 63:1602-1607 (2003)). Molecular profiling of childhood medulloblastomas demonstrated their distinct molecular and clinical features from other types of brain tumors (Nature 415:436-442 (2002)). A 133-gene signature accurately predicted survival among patients with acute myeloid leukemia (N. Engl. J. Med. 350:1605-1616 (2004)). Furthermore, a 70-gene or 76-gene prognostic signature has been developed which successfully predicts survival in patients with breast cancer (N. Engl. J. Med. 347:1999-2009 (2002); Lancet 365:671-679 (2005)). Gene expression signatures have also successfully predicted clinical outcome of prostate cancers (J. Clin. Invest. 113:913-923 (2004)). A more “universal” signature comprising 128 genes have been developed, which could distinguish primary and metastatic adenocarcinomas of diverse origin and primary tumors carrying the signature were associated with metastasis and poor clinical outcome (Nat. Genet. 33:49-54 (2003)).

**[0019]** Aside from the predictive value for long-term disease outcome, it is increasingly recognized that molecular characteristics, such gene expression profiles, of malignant tumors also affect their sensitivity to adjuvant (post-operative) or neo-adjuvant (pre-operative) chemotherapy (Nat. Clin. Pract. Oncol. 3:621-632 (2006)). To this end, several multigene signatures have been developed to predict patient response to preoperative chemotherapy in breast cancers based on the gene expression profiles of tumor biopsies (J. Clin. Oncol. 24:4236-4244 (2006); J. Clin. Oncol. 22:2284-2293 (2004); J. Clin. Oncol. 23:7265-7277 (2005); J. Translational Med. 3:32 (2005)). Of note, these signatures were extracted by combining mathematical and statistical methods and none of them were directly related to a cellular pathway that is involved in the process of cell death, stress response, or drug metabolism. As such, a rationale approach to treat resistant malignant tumors based on the gene expression signatures has been hampered by the lack of biological relevance thereof. Recently, Nevins et al. have developed gene expression signatures that reflect the patterns of oncogeneic pathway deregulation, which can be used to predict the sensitivity to therapeutic agents that target the deregulated pathway identified (Nature 439:353-357 (2006); Nat. Med.

12:1294-1300 (2006)). Conceivably, gene expression signatures that are associated with a particular cellular pathway can offer an opportunity to guide the use of pathway-specific drugs and is of considerable value in a more rationalized design of chemotherapies for human malignancies.

- 5   **[0020]**   The current invention satisfies a need in the art for such a gene expression signature associated with multidrug resistance and HDAC activity in tumor cells.

#### BRIEF SUMMARY OF THE INVENTION

- 10   **[0021]**   The current invention relates to the identification of the epigenetic regulators N-CoR2 and HDAC3 as biomarkers for the diagnosis and prognosis of malignant tumors resistant to anti-tumor therapeutics. Also identified herein are additional marker genes associated with N-CoR2 and HDAC3, which are useful in the diagnosis and prognosis of treatment resistant tumors. The transcript or protein expression levels of the markers identified in the present invention can be used to distinguish malignant tumors with higher  
15   probabilities of not responding to multiple anti-tumor therapeutics, such as chemotherapy, immunotherapy, hormone therapy, and radiotherapy, from those tumors with lower probabilities of treatment resistance.

- 20   **[0022]**   The present invention also provides methods of sensitizing treatment resistant tumors to anti-cancer therapeutics. In one embodiment, these methods comprise the downregulation of N-CoR2 and/or HDAC3 gene expression or inhibition of protein activity or synergy. Also embodied in the current invention are methods of identifying compounds useful for the treatment of treatment resistant tumors. These methods include *in vivo*, *in vitro*, and *ex vivo* identification of compounds that downregulate the expression level of N-CoR2, HDAC3, or associated signature marker genes as well as compounds that inhibit  
25   protein function, activation, or interaction.

**[0023]**   Methods for identifying biomarkers associated with the gene signature of histone deacetylases (HDACs) are also disclosed herein. Marker genes identified by the methods of the invention are useful for the diagnosis and prognosis of multidrug resistant tumors.

- 30   **[0024]**   The invention further provides a method for predicting responsiveness of a malignant tumor to one or more modalities of anti-tumor therapeutics and clinical prognosis comprising steps of: (a) obtaining one or more samples of a tumor from a patient with a

malignant tumor; (b) determining mRNA or protein expression levels of at least one biomarker selected from the group consisting of N-CoR2, HDAC3, and a those listed in Table 1 in said tumor sample; (c) comparing the expression levels of said at least one biomarker in said tumor sample to one or a plurality of threshold reference levels; and (d) assigning the malignant tumor a treatment response or clinical prognosis group based on the comparison(s) in (c). Said threshold reference levels are determined by a method comprising steps of : (e) obtaining samples of tumors from a large number of patients with the same type of said malignant tumor and whose clinical prognosis data are available; (f) determining the expression levels of at least one biomarker in said samples; (g) rank ordering in descending order said large number of patients according to the expression levels of said at least one biomarker; and (h) determining one or a plurality of threshold reference levels wherein said malignant tumor patients whose tumors have expression levels of said at least one biomarker above said threshold reference level(s) are predicted as having a higher risk of non-responsiveness to said anti-tumor therapy and/or a higher risk of poor clinical prognosis than those with expression levels below said threshold reference level(s).

**[0025]** The invention further provides an alternative method for predicting responsiveness of a malignant tumor to one or more modalities of anti-tumor therapy or clinical prognosis comprising steps of: (a) obtaining one or more samples of a tumor from a patient with a malignant tumor, (b) determining expression levels of at least one biomarker selected from the group consisting of N-CoR2, HDAC3, and those found in Table 1 in said tumor samples, (c) determining the similarity levels between the expression levels of said markers in said tumor sample and a multidrug resistance signature, (d) comparing said similarity level in said tumor sample to one or a plurality of threshold similarity level(s), and (e) assigning the malignant tumor a treatment response or clinical prognosis group based on the comparisons in (d).

**[0026]** Threshold similarity levels may be determined by a method comprising steps of: (a) obtaining samples of tumors from a large number of patients with the same type of said malignant tumor and whose clinical follow-up and prognosis data are available; (b) determining expression levels of at least one biomarker selected from the group consisting of N-CoR2, HDAC3, and those found in Table 1, in said samples; (c) determining the similarity levels between expression levels of said markers in said tumor sample from said large number of patients; (d) rank ordering in descending order said large number of patients according to said similarity levels; and (e) determining one or a plurality of said threshold

similarity level(s) wherein said malignant tumor patients whose tumors have similarity levels associated with N-CoR2 HDAC3 above said threshold similarity level(s) are predicted as having a higher risk of non-responsiveness to said anti-tumor therapy and/or a higher risk of poor clinical prognosis than those with similarity levels below said threshold similarity level(s).

[0027] In a specific embodiment of the above method, determining the similarity levels between marker expressions comprises the use of a statistical algorithm, including Pearson's, Spearman's or Kendall's correlation coefficient determination method or the like.

[0028] The invention further provides a method for assessing the ability of a candidate compound to increase the sensitivity of a malignant tumor cell to one or more modalities of anti-tumor therapy comprising steps of: (a) contacting a mammalian cell with a compound; (b) determining the nuclear deacetylase activity of HDAC3 or the mRNA or protein levels of a biomarker selected from the group consisting of N-CoR2, HDAC3, and those listed in Table 1, in said first mammalian cell and in a second mammalian cell that is not contacted with the compound; (c) comparing the deacetylase activity of HDAC3 or the expression levels of said biomarkers in said mammalian cells; (d) classifying the compound as having a ability to increase the sensitivity to an anti-tumor therapy if the deacetylase activity or the expression levels of said biomarkers in said first mammalian cell are different than those in said second mammalian cell.

[0029] In certain embodiments of the invention, the sensitivity of a malignant tumor to anti-tumor therapy is assessed by methods including measuring the size, the number of living tumor cells, or the extent of vascularization of said tumor after said anti-tumor therapy, or evaluating the number and the size of local recurrent tumors or local or distant metastasis thereof at varying lengths of time after said anti-tumor therapy.

[0030] In a particular embodiment of the invention, increasing the sensitivity of a malignant tumor to anti-tumor therapy comprises local or systemic administration of a therapeutically effective amount of a mutant N-CoR2 protein that is deficient in its physical interaction with HDAC3 or unable to activate its deacetylase activity in the host of said malignant tumor.

## BRIEF DESCRIPTION OF THE DRAWINGS

[0031] **FIGURE 1** The probability of remaining relapse-free or survive as a function of time from diagnosis among 295 breast cancer patients in the Netherlands Cancer Institute



database. The patients were grouped into quartiles according to the expression levels of N-CoR2. The patients were further stratified according to their LN status and whether or not they received adjuvant systemic chemotherapy (CT). Patients in each group were stratified according to N-CoR2 gene expression quartiles.

- 5    **[0032]    FIGURE 2** Kaplan-Meier graphs of the probability that a patient would remain relapse-free or survive as a function of time from diagnosis among 295 breast cancer patients in the Netherlands Cancer Institute database. The patients were grouped into quartiles according to the expression levels of HDAC3. The patients were further stratified according to their LN status and whether or not they received adjuvant systemic chemotherapy (CT).  
10    The patients in each group were stratified according to HDAC3 gene expression quartiles.

- [0033]    FIGURE 3** Kaplan-Meier analysis of the probability that patient would remain relapse-free or survive as a function of time from diagnosis among 295 breast cancer patients in the Netherlands Cancer Institute database. The patients were divided into quartiles according to the expression levels of N-CoR2 or HDAC3, respectively, and then further  
15    grouped according to whether their N-CoR2 and HDAC3 gene expressions both fell into respective upper or lower quartile or the Interquartile range. The patients were further stratified according to their LN status and whether or not they received adjuvant systemic chemotherapy (CT). The patients in each group were stratified according to N-CoR2 and HDAC3 gene expression similarly.

- 20    **[0034]    FIGURE 4** The probability that patient would remain survive as a function of time from diagnosis among 50 patients with malignant gliomas (**Figure 4A**) and 60 patients with ovarian cancers (**Figure 4B**). The patients were divided into quartiles according to the expression levels of N-CoR2 or HDAC3, respectively, and then further grouped according to whether their N-CoR2 and HDAC3 gene expressions both fell into respective upper or lower  
25    quartile or the Interquartile range. The patients were further stratified according to their LN status and whether or not they received adjuvant systemic chemotherapy (CT). The patients in each group were stratified according to N-CoR2 and HDAC3 gene expression similarly. P values were determined using the log-rank test comparing the upper and lower quartiles or the interquartile range (\*).

- 30    **[0035]    FIGURE 5** Classification of the 130 breast carcinomas of the M.D. Anderson Cancer Center database into prognostic groups using hierarchical clustering analysis on the 304 N-CoR2 signature genes (represented by 350 Affymetrix probe sets). The tumors were

segregated into two predominant subgroups (subgroup A and subgroup B) based on the first bifurcation in the dendrogram.

[0036] **FIGURE 6** Classification of the 130 breast carcinomas of the M.D. Anderson Cancer Center database into prognostic groups using  $S_{NCOR2}$  as a measure of the N-CoR2-associated transcriptional activities in breast cancer cells. R, responders; NR, non-responders.

[0037] **FIGURE 7** Growth rates and 3D acini formation of HMT3522 S1 cells with stable downregulation of N-CoR2 expression and their control cells. Bar, 500  $\mu$ m.

[0038] **FIGURE 8** Death sensitivity of HMT3522 S1 cells with stable downregulation of N-CoR2 expression and their control cells cultured as 3D acini to TRAIL, Paclitaxel and IR treatments.

[0039] **FIGURE 9** Phase-contrast images and N-CoR2 protein expression of HMT3522 T4-2 cells cultured as 2D monolayers, 3D disorganized and reverted (rev) acinus-like architectures. Bar, 100  $\mu$ m.

[0040] **FIGURE 10** Death sensitivities of HMT3522 T4-2 cells with stable downregulation of N-CoR2 and their control cells to TRAIL (1.0  $\mu$ g/mL) or Paclitaxel (20  $\mu$ M) in different culture models as detailed in **Figure 9**.  $P < 0.05$ , compared with control RNAi in 2D\* or 3D<sup>†</sup>.

[0041] **FIGURE 11** Death sensitivities of HMT3522 T4-2 cells with stable overexpression of N-CoR2, the vector control cells and those with stable downregulation of HDAC3 to TRAIL treatments. \* $P < 0.05$ , compared with vector control cells.

[0042] **FIGURE 12** Nuclear lysates from HEK 293 cells stably expressing myc-tagged N-CoR2, N-CoR2 (K449A) or empty vector were immunoprecipitated with the anti-myc antibody. The precipitates were analyzed by Western blot using anti-myc or anti-HDAC3 antibody. Lamin B1 was used as nuclear loading control.

[0043] **FIGURE 13** Myc-immunoprecipitated N-CoR2, N-CoR2 (K449A) or empty vector complexes from nuclear extracts of HEK 293 cells were analyzed for HDAC activity using a fluorimetric activity assay with or without 5  $\mu$ M of the HDAC inhibitor TSA. Results were repeated in quadruplicate.  $P < 0.05$ , compared with vector\* or N-CoR2<sup>†</sup>.

**[0044] FIGURE 14** Death sensitivities of HMT3522 T4-2 cells with stable overexpression of wild-type N-CoR2, N-CoR2 (K449A) or the control vector to TRAIL treatments. Data are mean  $\pm$  SEM of triplicate experiments; \*P < 0.05, compared with vector.

## 5 DETAILED DESCRIPTION OF THE INVENTION

**[0045]** The present invention relates to methods for diagnosing, predicting, and treating malignant tumors that are resistant to anti-tumor therapeutics including chemotherapy, immunotherapy, hormone therapy, and radiation. The present invention provides novel methods of using the deacetylase activity or expression levels of nuclear co-repressor 2 (“N-CoR2”), histone deacetylases 3 (“HDAC3”), or associated gene expression markers and  
10 profiles to predict or diagnose the presence of multidrug resistant malignant tumors. In addition, the present invention also provides methods of increasing the sensitivity of malignant tumors to anti-tumor therapeutics by inhibiting N-CoR2, HDAC3, or associated gene expression markers or by disrupting the interaction between N-CoR2 and HDAC3.

**[0046]** In one embodiment, the methods of diagnosing or providing a prognosis for multidrug resistant tumors comprise the identification of the differential expression of one or more of the biomarkers identified herein. Methods embraced in the identification of expression levels include RT-PCR, qRT-PCR, microarray hybridization, mass spectroscopy, ELISA, and immunochemistry. In some embodiments, the cancer is breast cancer, malignant  
20 gliomas, ovarian cancer, or any other well known cancer.

**[0047]** The present invention provides kits for the diagnosis or prognosis of multigene resistant tumors. These kits comprise one or more probes for the detection of biomarkers identified by the present invention. In certain embodiments, the kits provided by the current invention comprise probes for the identification of any 1, 2, 3, 4, 5, 10, 15, 20, 25, or more  
25 biomarkers selected from the group consisting of N-CoR2, HDAC3, and those listed in Table 1. In another embodiment, the kit comprises probes for the identification of N-CoR2, HDAC3, and those genes listed in Table 1. In some embodiments, the kit comprises a microarray. In other embodiments, the kit comprises an ELISA assay or cocktail of antibodies. In yet other embodiments, the kit comprises reagents for the RT-PCR or qRT-PCR identification of marker gene expression. In particular embodiments, the diagnosis or  
30 prognosis is further generated by a computer or provided by a computer generated print out.

[0048] Probes useful in the methods and kits of the present invention include nucleic acids, such as oligonucleotides of DNA, RNA, and analogs thereof, as well as antibodies and immuno-reactive fragments thereof.

[0049] This present invention also provides methods of identifying marker genes associated with N-CoR2, HDAC3, or a histone deacetylase, that are useful in the prognosis or diagnosis of malignant tumors resistant to anti-tumor therapeutics. The invention also relates to the identification and use in diagnosis or prognosis of sets of marker genes that are regulated by N-CoR2, HDAC3, a histone deacetylase, or combinations thereof in normal or malignant cells. The transcription or protein expression levels of biomarkers identified herein, or identified by the methods described herein, can further be used to distinguish or classify malignant tumors with high or low probabilities of responding to multiple anti-tumor therapies. In one embodiment, the methods for identifying biomarkers comprise cell growth in a 3D culture matrix. In a particular embodiment, the method comprises cell growth on a reconstituted basement membrane.

[0050] Compounds useful for treating or sensitizing multidrug resistant tumors are provided in the current invention. In one embodiment, these compounds downregulate markers including N-CoR2, HDAC3, and those found in Table 1. In other embodiments, these compounds inhibit the activity, activation, or coordination of N-CoR2, HDAC3, markers listed in Table 1, and combinations thereof. Compounds of the invention include, nucleic acids, antisense oligonucleotides, siRNAs, shRNAs, microRNAs, ribozymes, proteins, peptides, antibodies, immuno-reactive fragments, small organic molecules and the like. The present invention also provides methods of treating multidrug resistant tumors or cancers through use of the compounds identified in the present invention.

[0051] This invention further provides methods for identifying compounds useful in treating or increasing the sensitivity of a tumor cell to anti-tumor therapeutics and methods for increasing the sensitivity of a tumor to an anti-tumor therapeutics by inhibiting the activity of N-CoR2, HDAC3, the N-CoR2/HDAC3 protein complex, or associated biomarkers. In one embodiment, these methods comprise *in vivo*, *in vitro*, or *ex vivo* assays to identify compounds that alter the expression of N-CoR2, HDAC3, or any gene listed in Table 1. In other embodiments, the methods comprise *in vivo*, *in vitro*, or *ex vivo* assays to identify compounds that inhibit the function, activation, or interaction of N-CoR2, HDAC3, or any gene listed in Table 1.

**[0052]** The present invention provides methods of diagnosing a multidrug resistant tumor in a subject. In one embodiment, the method comprises the steps of first analyzing a tumor sample from the subject with an assay that specifically detects a marker selected from the group consisting of N-CoR2, HDAC3, and those listed in Table 1, then determining whether or not the marker is differentially expressed (over or under expressed), and finally determining if the differential expression correlates with a multidrug resistance signature, thereby providing a diagnosis for a multidrug resistant tumor.

**[0053]** Particular embodiments of the present invention provide methods of providing a prognosis for a metastatic cancer. In one embodiment, the method comprises the steps of analyzing a tumor sample from a subject with an assay that specifically detects a marker selected from the group consisting of N-CoR2, HDAC3, and those listed in Table 1, then determining whether or not the marker is differentially expressed (over or under expressed), and finally determining if the differential expression correlates with a multidrug resistance signature, thereby providing a prognosis for a metastatic cancer. In one embodiment, a positive correlation with a multidrug resistance signature indicates a poor prognosis. In another embodiment, the subject is a mammal, such as a rat, mouse, hamster, cow, pig, horse, sheep, or human. In one particular embodiment, the prognosis is expressed as a probability that the patient would remain relapse-free or survive for a given number of years after being diagnosed with cancer.

**[0054]** Methods of identifying a compound useful for the treatment or sensitization of multidrug resistant tumors are embodied by the present invention. In one particular embodiment, the method comprises the steps of first contacting a multidrug resistant tumor cell with a compound and then determining the expression level of N-CoR2 or HDAC3 in said contacted cell relative to the expression level of N-CoR2 or HDAC3 in a reference tumor cell not contacted by said compound, wherein downregulation of N-CoR2 or HDAC3 in the contacted cell relative to the reference cell indicates that the compound is useful for the treatment of multidrug resistant tumors. In other embodiments, the marker or markers being detected comprise one or more genes listed in Table 1.

**[0055]** In another embodiment, the method comprises the steps of contacting a mixture of N-CoR2 and HDAC3 proteins with a compound and then determining the extent of the interaction between N-CoR2 and HDAC3, wherein a reduced interaction between N-CoR2 and HDAC3 after contacting the mixture with the compound indicates that the compound is

useful for the treatment of multidrug resistant tumors. In other embodiments, the method further comprises the use of a biomarker listed in Table 1.

[0056] In yet another embodiment, the method comprises the steps of contacting an HDAC3 protein with a compound and determining the activity of said HDAC3 protein, wherein a reduced activity of said HDAC3 protein indicates that the compound is useful for the treatment of multidrug resistant tumors. In another embodiment, the protein being contacted is selected from the group consisting of N-CoR2, those listed in Table 1, and an HDAC.

[0057] The current invention also provides methods for identifying biomarkers useful for the diagnosis or prognosis of multidrug resistant tumors. In one embodiment, the method comprises the steps of identifying multidrug resistant tumors differentially expressing a histone deacetylase (HDAC), and identifying marker genes differentially expressed in said multidrug resistant tumor, thereby identifying biomarkers useful for the diagnosis or prognosis of multidrug resistant tumors. In one particular embodiment, the HDAC is a class I, class II, class III, or class IV enzyme. In another embodiment, the HDAC is an ATP-dependent or NAD-dependent enzyme.

## DEFINITIONS

[0058] As used herein, "multi-drug resistance" or "multidrug resistant" refers to a classification in which a tumor is not responsive to more than one anti-tumor therapeutic. Anti-tumor therapeutics are well known in the art and include, but are not limited to, cytotoxic drugs, hormone therapy, biologics such as antibodies or fragments thereof, chemotherapy, and radiation therapy.

[0059] A "multidrug resistance signature" or "multidrug resistance gene (or marker or biomarker) signature" refers to the transcriptional profile of one or more associated marker genes as it is differentially expressed in a multidrug resistant cell or tumor. In this fashion, a marker that is overexpressed would correspond to a multidrug resistance signature if said gene was previously shown to be overexpressed in a multidrug resistant tumor or cell.

[0060] Histone deacetylases (HDACs) are enzymes which deacetylate the amino-terminal tails of histones, regulating chromatin assembly, mRNA transcription and other nuclear events. A number of human HDACs are well known in the art and include, but are not limited to, class 1 deacetylases, including HDAC1, HDAC2, HDAC3, and HDAC8, class II

deacetylases, including HDAC4, HDAC5, HDAC6, HDAC7A, HDAC9, and HDAC10, class III deacetylases, including *ScSir2* homologues, SIRT1, SIRT2, SIRT3, SIRT4, SIRT5, SIRT6, and SIRT7, and class IV deacetylases, including HDAC11. HDAC can be NAD-dependent or ATP-dependent enzymes.

5    **[0061]**    “N-CoR2”, “HDAC3”, and other biomarkers recited herein, including those found in Table 1, refer to nucleic acids, e.g., gene, pre-mRNA, mRNA, and polypeptides, polymorphic variants, alleles, mutants, and interspecies homologs that: (1) have an amino acid sequence that has greater than about 60% amino acid sequence identity, 65%, 70%, 75%, 80%, 85%, 90%, preferably 91%, 92%, 93%, 94%, 95%, 96%, 97%, 98% or 99% or greater amino acid  
10    sequence identity, preferably over a region of at least about 25, 50, 100, 200, 500, 1000, or more amino acids, to a polypeptide encoded by a referenced nucleic acid or an amino acid sequence described herein; (2) specifically bind to antibodies, e.g., polyclonal antibodies, raised against an immunogen comprising a referenced amino acid sequence, immunogenic fragments thereof, and conservatively modified variants thereof; (3)  
15    specifically hybridize under stringent hybridization conditions to a nucleic acid encoding a referenced amino acid sequence, and conservatively modified variants thereof; (4) have a nucleic acid sequence that has greater than about 60% nucleotide sequence identity, 65%, 70%, 75%, 80%, 85%, 90%, preferably 91%, 92%, 93%, 94%, 95%, 96%, 97%, 98% or 99% or higher nucleotide sequence identity, preferably over a region of at least about 10, 15, 20,  
20    25, 50, 100, 200, 500, 1000, or more nucleotides, to a reference nucleic acid sequence. A polynucleotide or polypeptide sequence is typically from a mammal including, but not limited to, primate, e.g., human; rodent, e.g., rat, mouse, hamster; cow, pig, horse, sheep, or any mammal. The nucleic acids and proteins of the invention include both naturally occurring or recombinant molecules. Truncated and alternatively spliced forms of these  
25    antigens are included in the definition.

**[0062]**    “Cancer” refers to mammalian cancers, especially human cancers, and carcinomas, sarcomas, adenocarcinomas, lymphomas, leukemias, etc., including solid and lymphoid cancers, kidney, breast, lung, kidney, bladder, colon, ovarian, prostate, pancreas, stomach, brain, head and neck, skin, uterine, testicular, esophagus, and liver cancer, including  
30    hepatocarcinoma, lymphoma, including non-Hodgkin’s lymphomas (*e.g.*, Burkitt’s, Small Cell, and Large Cell lymphomas) and Hodgkin’s lymphoma, leukemia, and multiple myeloma. Cancers embraced in the current application include both metastatic and non-metastatic cancers.

[0063] “Therapeutic treatment” and “cancer therapies” refers to chemotherapy, hormonal therapy, radiotherapy, and immunotherapy.

[0064] “Sensitize” or “sensitizing” refers to the effect of rendering a cell, usually a cancer or multidrug resistant cancer cell or tumor in the context of the present invention, more susceptible to an anti-proliferative or anti-cancer treatment. In this fashion, a sensitizing activity is the effect of use of an agent that if used alone would not demonstrate significant anti-tumor effects but would improve the anti-tumor effects of an anti-proliferative or anti-cancer agent in a more than additive fashion than the use of the anti-proliferative agent by itself.

[0065] By “therapeutically effective amount or dose” or “sufficient amount or dose” herein is meant a dose that produces effects for which it is administered. The exact dose will depend on the purpose of the treatment, and will be ascertainable by one skilled in the art using known techniques (*see, e.g.*, Lieberman, *Pharmaceutical Dosage Forms* (vols. 1-3, 1992); Lloyd, *The Art, Science and Technology of Pharmaceutical Compounding* (1999); Pickar, *Dosage Calculations* (1999); and *Remington: The Science and Practice of Pharmacy*, 20th Edition, 2003, Gennaro, Ed., Lippincott, Williams & Wilkins)

[0066] The terms “overexpress”, “overexpression”, “overexpressed”, “up-regulate”, or “up-regulated” interchangeably refer to a biomarker that is transcribed or translated at a detectably greater level, usually in a cancer cell or a multidrug resistant cancer cell, in comparison to a non-cancer cell or cancer cell that is not multidrug resistant. The term includes overexpression due to transcription, post transcriptional processing, translation, post-translational processing, cellular localization (e.g., organelle, cytoplasm, nucleus, cell surface), and RNA and protein stability, as compared to a non-cancer cell. Overexpression can be detected using conventional techniques for detecting mRNA (*i.e.*, RT-PCR, PCR, hybridization) or proteins (*i.e.*, ELISA, immunohistochemical techniques, mass spectroscopy). Overexpression can be 10%, 20%, 30%, 40%, 50%, 60%, 70%, 80%, 90% or more in comparison to a normal cell. In certain instances, overexpression is 1-fold, 2-fold, 3-fold, 4-fold 5, 6, 7, 8, 9, 10, or 15-fold or more higher levels of transcription or translation in comparison to a non-cancer cell.

[0067] The terms “underexpress,” “underexpression”, “underexpressed” or “downregulated” interchangeably refer to a protein or nucleic acid that is transcribed or translated at a detectably lower level usually in a cancer cell or a multidrug resistant cancer



cell, in comparison to a non-cancer cell or a cancer cell that does not have multidrug resistance. The term includes underexpression due to transcription, post transcriptional processing, translation, post-translational processing, cellular localization (*e.g.*, organelle, cytoplasm, nucleus, cell surface), and RNA and protein stability, as compared to a control.

- 5 Underexpression can be detected using conventional techniques for detecting mRNA (*i.e.*, RT-PCR, PCR, hybridization) or proteins (*i.e.*, ELISA, immunohistochemical techniques). Underexpression can be 10%, 20%, 30%, 40%, 50%, 60%, 70%, 80%, 90% or less in comparison to a control. In certain instances, underexpression is 1-fold, 2-fold, 3-fold, 4-fold or more lower levels of transcription or translation in comparison to a control.
- 10 **[0068]** The term “differentially expressed” or “differentially regulated” refers generally to a protein or nucleic acid that is overexpressed (upregulated) or underexpressed (downregulated) in one sample compared to at least one other sample, generally in a cancer cell that has multidrug resistance, in comparison to a cell or patient without cancer or in a cancer cell that is not multidrug resistant, in the context of the present invention.
- 15 **[0069]** The terms “cancer-associated antigen”, “tumor-specific marker”, “tumor marker”, “maker”, or “biomarker” interchangeably refer to a molecule (typically protein or nucleic acid such as RNA) that is differentially expressed in the cell, expressed on the surface of a cancer cell or secreted by a cancer cell in comparison to a non-cancer cell, and which is useful for the diagnosis of cancer, for providing a prognosis, and for preferential targeting of a
- 20 pharmacological agent to the cancer cell. Oftentimes, a cancer-associated antigen is a molecule that is overexpressed or underexpressed in a cancer cell in comparison to a non-cancer cell, for instance, 1-fold over expression, 2-fold overexpression, 3-fold overexpression or more in comparison to a non-cancer cell or, for instance, 20%, 30%, 40%, 50% or more underexpressed in comparison to a non-cancer cell. Oftentimes, a cancer-associated antigen
- 25 is a molecule that is inappropriately synthesized in the cancer cell, for instance, a molecule that contains deletions, additions or mutations in comparison to the molecule expressed in a non-cancer cell. Oftentimes, a cancer-associated antigen will be expressed exclusively on the cell surface of a cancer cell and not synthesized or expressed on the surface of a normal cell. Exemplified cell surface tumor markers include the proteins c-erbB-2 and human epidermal
- 30 growth factor receptor (HER) for breast cancer, PSMA for prostate cancer, and carbohydrate mucins in numerous cancers, including breast, ovarian and colorectal. Other times, a cancer-associated antigen will be expressed primarily not on the surface of the cancer cell.

[0070] It will be understood by the skilled artisan that markers may be used singly or in combination with other markers for any of the uses, e.g., diagnosis or prognosis of multidrug resistant cancers, disclosed herein.

[0071] "Biological sample" includes sections of tissues such as biopsy and autopsy samples, and frozen sections taken for histologic purposes. Such samples include breast cancer tissues, blood and blood fractions or products (e.g., serum, plasma, platelets, red blood cells, and the like), sputum, tissue, cultured cells, e.g., primary cultures, explants, and transformed cells, stool, urine, etc. A biological sample is typically obtained from a eukaryotic organism, most preferably a mammal such as a primate e.g., chimpanzee or human; cow; dog; cat; a rodent, e.g., guinea pig, rat, Mouse; rabbit; or a bird; reptile; or fish.

[0072] A "biopsy" refers to the process of removing a tissue sample for diagnostic or prognostic evaluation, and to the tissue specimen itself. Any biopsy technique known in the art can be applied to the diagnostic and prognostic methods of the present invention. The biopsy technique applied will depend on the tissue type to be evaluated (e.g., breast, etc.), the size and type of the tumor, among other factors. Representative biopsy techniques include, but are not limited to, excisional biopsy, incisional biopsy, needle biopsy, surgical biopsy, and bone marrow biopsy. An "excisional biopsy" refers to the removal of an entire tumor mass with a small margin of normal tissue surrounding it. An "incisional biopsy" refers to the removal of a wedge of tissue that includes a cross-sectional diameter of the tumor. A diagnosis or prognosis made by endoscopy or fluoroscopy can require a "core-needle biopsy", or a "fine-needle aspiration biopsy" which generally obtains a suspension of cells from within a target tissue. Biopsy techniques are discussed, for example, in *Harrison's Principles of Internal Medicine*, Kasper, et al., eds., 16th ed., 2005, Chapter 70, and throughout Part V.

[0073] The terms "identical" or percent "identity", in the context of two or more nucleic acids or polypeptide sequences, refer to two or more sequences or subsequences that are the same or have a specified percentage of amino acid residues or nucleotides that are the same (i.e., about 60% identity, preferably 65%, 70%, 75%, 80%, 85%, 90%, 91%, 92%, 93%, 94%, 95%, 96%, 97%, 98%, 99%, or higher identity over a specified region, when compared and aligned for maximum correspondence over a comparison window or designated region) as measured using a BLAST or BLAST 2.0 sequence comparison algorithms with default parameters described below, or by manual alignment and visual inspection (see, e.g., NCBI web site <http://www.ncbi.nlm.nih.gov/BLAST/> or the like). Such sequences are then said to

be “substantially identical.” This definition also refers to, or may be applied to, the complement of a test sequence. The definition also includes sequences that have deletions and/or additions, as well as those that have substitutions. As described below, the preferred algorithms can account for gaps and the like. Preferably, identity exists over a region that is at least about 15 amino acids or nucleotides in length, or more preferably over a region that is 20, 25, 50-100 or more amino acids or nucleotides in length.

**[0074]** For sequence comparison, typically one sequence acts as a reference sequence, to which test sequences are compared. When using a sequence comparison algorithm, test and reference sequences are entered into a computer, subsequence coordinates are designated, if necessary, and sequence algorithm program parameters are designated. Preferably, default program parameters can be used, or alternative parameters can be designated. The sequence comparison algorithm then calculates the percent sequence identities for the test sequences relative to the reference sequence, based on the program parameters.

**[0075]** A “comparison window”, as used herein, includes reference to a segment of any one of the number of contiguous positions selected from the group consisting of from 20 to 600, usually about 50 to about 200, more usually about 100 to about 150 in which a sequence may be compared to a reference sequence of the same number of contiguous positions after the two sequences are optimally aligned. Methods of alignment of sequences for comparison are well-known in the art. Optimal alignment of sequences for comparison can be conducted, e.g., by the local homology algorithm of Smith & Waterman, *Adv. Appl. Math.* 2:482 (1981), by the homology alignment algorithm of Needleman & Wunsch, *J. Mol. Biol.* 48:443 (1970), by the search for similarity method of Pearson & Lipman, *Proc. Nat’l. Acad. Sci. USA* 85:2444 (1988), by computerized implementations of these algorithms (GAP, BESTFIT, FASTA, and TFASTA in the Wisconsin Genetics Software Package, Genetics Computer Group, 575 Science Dr., Madison, WI), or by manual alignment and visual inspection (*see, e.g., Current Protocols in Molecular Biology* (Ausubel *et al.*, eds. 1987-2005, Wiley Interscience)).

**[0076]** An example of an algorithm that is suitable for determining percent sequence identity and sequence similarity are the BLAST and BLAST 2.0 algorithms, which are described in Altschul *et al.*, *Nuc. Acids Res.* 25:3389-3402 (1977) and Altschul *et al.*, *J. Mol. Biol.* 215:403-410 (1990), respectively. BLAST and BLAST 2.0 are used, with the parameters described herein, to determine percent sequence identity for the nucleic acids and

proteins of the invention. Software for performing BLAST analyses is publicly available through the National Center for Biotechnology Information (<http://www.ncbi.nlm.nih.gov/>). This algorithm involves first identifying high scoring sequence pairs (HSPs) by identifying short words of length W in the query sequence, which either match or satisfy some positive-valued threshold score T when aligned with a word of the same length in a database  
5 sequence. T is referred to as the neighborhood word score threshold (Altschul *et al.*, *supra*). These initial neighborhood word hits act as seeds for initiating searches to find longer HSPs containing them. The word hits are extended in both directions along each sequence for as far as the cumulative alignment score can be increased. Cumulative scores are calculated  
10 using, for nucleotide sequences, the parameters M (reward score for a pair of matching residues; always > 0) and N (penalty score for mismatching residues; always < 0). For amino acid sequences, a scoring matrix is used to calculate the cumulative score. Extension of the word hits in each direction are halted when: the cumulative alignment score falls off by the quantity X from its maximum achieved value; the cumulative score goes to zero or below,  
15 due to the accumulation of one or more negative-scoring residue alignments; or the end of either sequence is reached. The BLAST algorithm parameters W, T, and X determine the sensitivity and speed of the alignment. The BLASTN program (for nucleotide sequences) uses as defaults a wordlength (W) of 11, an expectation (E) of 10, M=5, N=-4 and a comparison of both strands. For amino acid sequences, the BLASTP program uses as  
20 defaults a wordlength of 3, and expectation (E) of 10, and the BLOSUM62 scoring matrix (*see* Henikoff & Henikoff, *Proc. Natl. Acad. Sci. USA* 89:10915 (1989)) alignments (B) of 50, expectation (E) of 10, M=5, N=-4, and a comparison of both strands.

**[0077]** “Nucleic acid” refers to deoxyribonucleotides or ribonucleotides and polymers thereof in either single- or double-stranded form, and complements thereof. The term  
25 encompasses nucleic acids containing known nucleotide analogs or modified backbone residues or linkages, which are synthetic, naturally occurring, and non-naturally occurring, which have similar binding properties as the reference nucleic acid, and which are metabolized in a manner similar to the reference nucleotides. Examples of such analogs include, without limitation, phosphorothioates, phosphoramidates, methyl phosphonates,  
30 chiral-methyl phosphonates, 2-O-methyl ribonucleotides, peptide-nucleic acids (PNAs).

**[0078]** Unless otherwise indicated, a particular nucleic acid sequence also implicitly encompasses conservatively modified variants thereof (e.g., degenerate codon substitutions) and complementary sequences, as well as the sequence explicitly indicated. Specifically,

degenerate codon substitutions may be achieved by generating sequences in which the third position of one or more selected (or all) codons is substituted with mixed-base and/or deoxyinosine residues (Batzner *et al.*, *Nucleic Acid Res.* 19:5081 (1991); Ohtsuka *et al.*, *J. Biol. Chem.* 260:2605-2608 (1985); Rossolini *et al.*, *Mol. Cell. Probes* 8:91-98 (1994)). The term nucleic acid is used interchangeably with gene, cDNA, mRNA, oligonucleotide, and polynucleotide.

**[0079]** A particular nucleic acid sequence also implicitly encompasses “splice variants” and nucleic acid sequences encoding truncated forms of cancer biomarkers. Similarly, a particular protein encoded by a nucleic acid implicitly encompasses any protein encoded by a splice variant or truncated form of that nucleic acid. “Splice variants,” as the name suggests, are products of alternative splicing of a gene. After transcription, an initial nucleic acid transcript may be spliced such that different (alternate) nucleic acid splice products encode different polypeptides. Mechanisms for the production of splice variants vary, but include alternate splicing of exons. Alternate polypeptides derived from the same nucleic acid by read-through transcription are also encompassed by this definition. Any products of a splicing reaction, including recombinant forms of the splice products, are included in this definition. Nucleic acids can be truncated at the 5’ end or at the 3’ end. Polypeptides can be truncated at the N-terminal end or the C-terminal end. Truncated versions of nucleic acid or polypeptide sequences can be naturally occurring or recombinantly created.

**[0080]** The terms “polypeptide,” “peptide” and “protein” are used interchangeably herein to refer to a polymer of amino acid residues. The terms apply to amino acid polymers in which one or more amino acid residue is an artificial chemical mimetic of a corresponding naturally occurring amino acid, as well as to naturally occurring amino acid polymers and non-naturally occurring amino acid polymer.

**[0081]** The term “amino acid” refers to naturally occurring and synthetic amino acids, as well as amino acid analogs and amino acid mimetics that function in a manner similar to the naturally occurring amino acids. Naturally occurring amino acids are those encoded by the genetic code, as well as those amino acids that are later modified, e.g., hydroxyproline,  $\gamma$ -carboxyglutamate, and O-phosphoserine. Amino acid analogs refers to compounds that have the same basic chemical structure as a naturally occurring amino acid, i.e., an  $\alpha$  carbon that is bound to a hydrogen, a carboxyl group, an amino group, and an R group, e.g., homoserine, norleucine, methionine sulfoxide, methionine methyl sulfonium. Such analogs have modified

R groups (e.g., norleucine) or modified peptide backbones, but retain the same basic chemical structure as a naturally occurring amino acid. Amino acid mimetics refers to chemical compounds that have a structure that is different from the general chemical structure of an amino acid, but that functions in a manner similar to a naturally occurring amino acid.

5   **[0082]**   Amino acids may be referred to herein by either their commonly known three letter symbols or by the one-letter symbols recommended by the IUPAC-IUB Biochemical Nomenclature Commission. Nucleotides, likewise, may be referred to by their commonly accepted single-letter codes.

10   **[0083]**   “Conservatively modified variants” applies to both amino acid and nucleic acid sequences. With respect to particular nucleic acid sequences, conservatively modified variants refers to those nucleic acids which encode identical or essentially identical amino acid sequences, or where the nucleic acid does not encode an amino acid sequence, to essentially identical sequences. Because of the degeneracy of the genetic code, a large number of functionally identical nucleic acids encode any given protein. For instance, the  
15   codons GCA, GCC, GCG and GCU all encode the amino acid alanine. Thus, at every position where an alanine is specified by a codon, the codon can be altered to any of the corresponding codons described without altering the encoded polypeptide. Such nucleic acid variations are “silent variations,” which are one species of conservatively modified variations. Every nucleic acid sequence herein which encodes a polypeptide also describes  
20   every possible silent variation of the nucleic acid. One of skill will recognize that each codon in a nucleic acid (except AUG, which is ordinarily the only codon for methionine, and TGG, which is ordinarily the only codon for tryptophan) can be modified to yield a functionally identical molecule. Accordingly, each silent variation of a nucleic acid which encodes a polypeptide is implicit in each described sequence with respect to the expression product, but  
25   not with respect to actual probe sequences.

30   **[0084]**   As to amino acid sequences, one of skill will recognize that individual substitutions, deletions or additions to a nucleic acid, peptide, polypeptide, or protein sequence which alters, adds or deletes a single amino acid or a small percentage of amino acids in the encoded sequence is a “conservatively modified variant” where the alteration results in the substitution of an amino acid with a chemically similar amino acid. Conservative substitution tables providing functionally similar amino acids are well known in the art. Such conservatively

modified variants are in addition to and do not exclude polymorphic variants, interspecies homologs, and alleles of the invention.

[0085] The following eight groups each contain amino acids that are conservative substitutions for one another: 1) Alanine (A), Glycine (G); 2) Aspartic acid (D), Glutamic acid (E); 3) Asparagine (N), Glutamine (Q); 4) Arginine (R), Lysine (K); 5) Isoleucine (I), Leucine (L), Methionine (M), Valine (V); 6) Phenylalanine (F), Tyrosine (Y), Tryptophan (W); 7) Serine (S), Threonine (T); and 8) Cysteine (C), Methionine (M) (*see, e.g.*, Creighton, *Proteins* (1984)).

[0086] A “label” or a “detectable moiety” is a composition detectable by spectroscopic, photochemical, biochemical, immunochemical, chemical, or other physical means. For example, useful labels include  $^{32}\text{P}$ , fluorescent dyes, electron-dense reagents, enzymes (e.g., as commonly used in an ELISA), biotin, digoxigenin, or haptens and proteins which can be made detectable, e.g., by incorporating a radiolabel into the peptide or used to detect antibodies specifically reactive with the peptide.

[0087] The term “recombinant” when used with reference, e.g., to a cell, or nucleic acid, protein, or vector, indicates that the cell, nucleic acid, protein or vector, has been modified by the introduction of a heterologous nucleic acid or protein or the alteration of a native nucleic acid or protein, or that the cell is derived from a cell so modified. Thus, for example, recombinant cells express genes that are not found within the native (non-recombinant) form of the cell or express native genes that are otherwise abnormally expressed, under expressed or not expressed at all.

[0088] The phrase “stringent hybridization conditions” refers to conditions under which a probe will hybridize to its target subsequence, typically in a complex mixture of nucleic acids, but to no other sequences. Stringent conditions are sequence-dependent and will be different in different circumstances. Longer sequences hybridize specifically at higher temperatures. An extensive guide to the hybridization of nucleic acids is found in Tijssen, *Techniques in Biochemistry and Molecular Biology--Hybridization with Nucleic Probes*, “Overview of principles of hybridization and the strategy of nucleic acid assays” (1993). Generally, stringent conditions are selected to be about 5-10°C lower than the thermal melting point ( $T_m$ ) for the specific sequence at a defined ionic strength pH. The  $T_m$  is the temperature (under defined ionic strength, pH, and nucleic concentration) at which 50% of the probes complementary to the target hybridize to the target sequence at equilibrium (as the

target sequences are present in excess, at  $T_m$ , 50% of the probes are occupied at equilibrium). Stringent conditions may also be achieved with the addition of destabilizing agents such as formamide. For selective or specific hybridization, a positive signal is at least two times background, preferably 10 times background hybridization. Exemplary stringent hybridization conditions can be as following: 50% formamide, 5x SSC, and 1% SDS, incubating at 42°C, or, 5x SSC, 1% SDS, incubating at 65°C, with wash in 0.2x SSC, and 0.1% SDS at 65°C.

[0089] Nucleic acids that do not hybridize to each other under stringent conditions are still substantially identical if the polypeptides which they encode are substantially identical. This occurs, for example, when a copy of a nucleic acid is created using the maximum codon degeneracy permitted by the genetic code. In such cases, the nucleic acids typically hybridize under moderately stringent hybridization conditions. Exemplary “moderately stringent hybridization conditions” include a hybridization in a buffer of 40% formamide, 1 M NaCl, 1% SDS at 37°C, and a wash in 1X SSC at 45°C. A positive hybridization is at least twice background. Those of ordinary skill will readily recognize that alternative hybridization and wash conditions can be utilized to provide conditions of similar stringency. Additional guidelines for determining hybridization parameters are provided in numerous reference, e.g., and *Current Protocols in Molecular Biology*, ed. Ausubel, *et al.*, *supra*.

[0090] For PCR, a temperature of about 36°C is typical for low stringency amplification, although annealing temperatures may vary between about 32°C and 48°C depending on primer length. For high stringency PCR amplification, a temperature of about 62°C is typical, although high stringency annealing temperatures can range from about 50°C to about 65°C, depending on the primer length and specificity. Typical cycle conditions for both high and low stringency amplifications include a denaturation phase of 90°C - 95°C for 30 sec - 2 min., an annealing phase lasting 30 sec. - 2 min., and an extension phase of about 72°C for 1 - 2 min. Protocols and guidelines for low and high stringency amplification reactions are provided, e.g., in Innis *et al.* (1990) *PCR Protocols, A Guide to Methods and Applications*, Academic Press, Inc. N.Y.).

[0091] “Antibody” refers to a polypeptide comprising a framework region from an immunoglobulin gene or fragments thereof that specifically binds and recognizes an antigen. The recognized immunoglobulin genes include the kappa, lambda, alpha, gamma, delta, epsilon, and mu constant region genes, as well as the myriad immunoglobulin variable region



genes. Light chains are classified as either kappa or lambda. Heavy chains are classified as gamma, mu, alpha, delta, or epsilon, which in turn define the immunoglobulin classes, IgG, IgM, IgA, IgD and IgE, respectively. Typically, the antigen-binding region of an antibody will be most critical in specificity and affinity of binding.

5   **[0092]**   An exemplary immunoglobulin (antibody) structural unit comprises a tetramer. Each tetramer is composed of two identical pairs of polypeptide chains, each pair having one “light” (about 25 kD) and one “heavy” chain (about 50-70 kD). The N-terminus of each chain defines a variable region of about 100 to 110 or more amino acids primarily responsible for antigen recognition. The terms variable light chain ( $V_L$ ) and variable heavy chain ( $V_H$ )  
10   refer to these light and heavy chains respectively.

**[0093]**   Antibodies exist, e.g., as intact immunoglobulins or as a number of well-characterized fragments produced by digestion with various peptidases. Thus, for example, pepsin digests an antibody below the disulfide linkages in the hinge region to produce  $F(ab)'_2$ , a dimer of Fab which itself is a light chain joined to  $V_H-C_H1$  by a disulfide bond. The  $F(ab)'_2$   
15   may be reduced under mild conditions to break the disulfide linkage in the hinge region, thereby converting the  $F(ab)'_2$  dimer into an Fab' monomer. The Fab' monomer is essentially Fab with part of the hinge region (*see Fundamental Immunology* (Paul ed., 3d ed. 1993). While various antibody fragments are defined in terms of the digestion of an intact antibody, one of skill will appreciate that such fragments may be synthesized *de novo* either  
20   chemically or by using recombinant DNA methodology. Thus, the term antibody, as used herein, also includes antibody fragments either produced by the modification of whole antibodies, or those synthesized *de novo* using recombinant DNA methodologies (e.g., single chain Fv) or those identified using phage display libraries (*see, e.g., McCafferty et al., Nature* 348:552-554 (1990)).

25   **[0094]**   For preparation of antibodies, e.g., recombinant, monoclonal, or polyclonal antibodies, many technique known in the art can be used (*see, e.g., Kohler & Milstein, Nature* 256:495-497 (1975); Kozbor *et al., Immunology Today* 4: 72 (1983); Cole *et al.*, pp. 77-96 in *Monoclonal Antibodies and Cancer Therapy*, Alan R. Liss, Inc. (1985); Coligan, *Current Protocols in Immunology* (1991); Harlow & Lane, *Antibodies, A Laboratory Manual*  
30   (1988); and Goding, *Monoclonal Antibodies: Principles and Practice* (2d ed. 1986)). The genes encoding the heavy and light chains of an antibody of interest can be cloned from a cell, e.g., the genes encoding a monoclonal antibody can be cloned from a hybridoma and

used to produce a recombinant monoclonal antibody. Gene libraries encoding heavy and light chains of monoclonal antibodies can also be made from hybridoma or plasma cells. Random combinations of the heavy and light chain gene products generate a large pool of antibodies with different antigenic specificity (*see, e.g.,* Kuby, *Immunology* (3<sup>rd</sup> ed. 1997)).

- 5 Techniques for the production of single chain antibodies or recombinant antibodies (U.S. Patent 4,946,778, U.S. Patent No. 4,816,567) can be adapted to produce antibodies to polypeptides of this invention. Also, transgenic mice, or other organisms such as other mammals, may be used to express humanized or human antibodies (*see, e.g.,* U.S. Patent Nos. 5,545,807; 5,545,806; 5,569,825; 5,625,126; 5,633,425; 5,661,016, Marks *et al.*,  
10 *Bio/Technology* 10:779-783 (1992); Lonberg *et al.*, *Nature* 368:856-859 (1994); Morrison, *Nature* 368:812-13 (1994); Fishwild *et al.*, *Nature Biotechnology* 14:845-51 (1996); Neuberger, *Nature Biotechnology* 14:826 (1996); and Lonberg & Huszar, *Intern. Rev. Immunol.* 13:65-93 (1995)). Alternatively, phage display technology can be used to identify antibodies and heteromeric Fab fragments that specifically bind to selected antigens (*see, e.g.,*  
15 McCafferty *et al.*, *Nature* 348:552-554 (1990); Marks *et al.*, *Biotechnology* 10:779-783 (1992)). Antibodies can also be made bispecific, i.e., able to recognize two different antigens (*see, e.g.,* WO 93/08829, Traunecker *et al.*, *EMBO J.* 10:3655-3659 (1991); and Suresh *et al.*, *Methods in Enzymology* 121:210 (1986)). Antibodies can also be heteroconjugates, e.g., two covalently joined antibodies, or immunotoxins (*see, e.g.,* U.S. Patent No. 4,676,980 , WO  
20 91/00360; WO 92/200373; and EP 03089).

**[0095]** Methods for humanizing or primatizing non-human antibodies are well known in the art. Generally, a humanized antibody has one or more amino acid residues introduced into it from a source which is non-human. These non-human amino acid residues are often referred to as import residues, which are typically taken from an import variable domain.

- 25 Humanization can be essentially performed following the method of Winter and co-workers (*see, e.g.,* Jones *et al.*, *Nature* 321:522-525 (1986); Riechmann *et al.*, *Nature* 332:323-327 (1988); Verhoeven *et al.*, *Science* 239:1534-1536 (1988) and Presta, *Curr. Op. Struct. Biol.* 2:593-596 (1992)), by substituting rodent CDRs or CDR sequences for the corresponding sequences of a human antibody. Accordingly, such humanized antibodies are chimeric  
30 antibodies (U.S. Patent No. 4,816,567), wherein substantially less than an intact human variable domain has been substituted by the corresponding sequence from a non-human species. In practice, humanized antibodies are typically human antibodies in which some

CDR residues and possibly some FR residues are substituted by residues from analogous sites in rodent antibodies.

[0096] A “chimeric antibody” is an antibody molecule in which (a) the constant region, or a portion thereof, is altered, replaced or exchanged so that the antigen binding site (variable region) is linked to a constant region of a different or altered class, effector function and/or species, or an entirely different molecule which confers new properties to the chimeric antibody, e.g., an enzyme, toxin, hormone, growth factor, drug, etc.; or (b) the variable region, or a portion thereof, is altered, replaced or exchanged with a variable region having a different or altered antigen specificity.

[0097] In one embodiment, the antibody is conjugated to an “effector” moiety. The effector moiety can be any number of molecules, including labeling moieties such as radioactive labels or fluorescent labels, or can be a therapeutic moiety. In one aspect the antibody modulates the activity of the protein.

[0098] The phrase “specifically (or selectively) binds” to an antibody or “specifically (or selectively) immunoreactive with,” when referring to a protein or peptide, refers to a binding reaction that is determinative of the presence of the protein, often in a heterogeneous population of proteins and other biologics. Thus, under designated immunoassay conditions, the specified antibodies bind to a particular protein at least two times the background and more typically more than 10 to 100 times background. Specific binding to an antibody under such conditions requires an antibody that is selected for its specificity for a particular protein. For example, polyclonal antibodies can be selected to obtain only those polyclonal antibodies that are specifically immunoreactive with the selected antigen and not with other proteins. This selection may be achieved by subtracting out antibodies that cross-react with other molecules. A variety of immunoassay formats may be used to select antibodies specifically immunoreactive with a particular protein. For example, solid-phase ELISA immunoassays are routinely used to select antibodies specifically immunoreactive with a protein (*see, e.g.,* Harlow & Lane, *Antibodies, A Laboratory Manual* (1988) for a description of immunoassay formats and conditions that can be used to determine specific immunoreactivity).

## **PREDICTIVE, DIAGNOSTIC, AND PROGNOSTIC METHODS**

[0099] The present invention provides methods of diagnosing a multidrug resistant cancer by examining cancer biomarkers (either the protein or the RNA encoding the protein) such as

N-CoR2, HDAC3, and those found in Table 1, or a combination thereof in tissues suspected of being or known to be cancerous, *e.g.* breast cancer tissue, including wild-type, truncated or alternatively spliced forms. Diagnosis involves determining the level of a polypeptide or polynucleotide of the invention in a patient and then comparing the level to a baseline or range. Typically, the baseline value is representative of a polypeptide or polynucleotide of the invention in a person or tissue not suffering from multidrug resistant cancer, as measured using a tissue sample or biopsy or other biological sample such as a serum or blood. Variation of levels of a polypeptide or polynucleotide of the invention from the baseline range (either up or down) indicates that the patient has a multidrug resistant cancer or is at risk of developing a multidrug resistant cancer.

**[0100]** As used herein, the term "providing a prognosis" refers to providing a prediction of the probable course or outcome of a cancer such as breast cancer, including prediction of metastasis, multidrug resistance, disease free survival, overall survival, recurrence, etc. The methods can also be used to devise a suitable therapy for cancer treatment, *e.g.*, by indicating whether or not the cancer is still at an early stage or if the cancer had advanced to a stage where aggressive therapy would be ineffective. The methods can also be used to determine whether or not a tumor or cancer will be responsive or unresponsive to a variety of cancer treatments.

**[0101]** Antibody reagents can be used in assays to detect expression levels of N-CoR2, HDAC3, and markers found in Table 1 in patient samples using any of a number of immunoassays known to those skilled in the art. Immunoassay techniques and protocols are generally described in Price and Newman, "Principles and Practice of Immunoassay," 2nd Edition, Grove's Dictionaries, 1997; and Gosling, "Immunoassays: A Practical Approach," Oxford University Press, 2000. A variety of immunoassay techniques, including competitive and non-competitive immunoassays, can be used. *See, e.g., Self et al., Curr. Opin. Biotechnol.*, 7:60-65 (1996). The term immunoassay encompasses techniques including, without limitation, enzyme immunoassays (EIA) such as enzyme multiplied immunoassay technique (EMIT), enzyme-linked immunosorbent assay (ELISA), IgM antibody capture ELISA (MAC ELISA), and microparticle enzyme immunoassay (MEIA); capillary electrophoresis immunoassays (CEIA); radioimmunoassays (RIA); immunoradiometric assays (IRMA); fluorescence polarization immunoassays (FPIA); and chemiluminescence assays (CL). If desired, such immunoassays can be automated. Immunoassays can also be used in conjunction with laser induced fluorescence. *See, e.g., Schmalzing et al.,*

*Electrophoresis*, 18:2184-93 (1997); Bao, *J. Chromatogr. B. Biomed. Sci.*, 699:463-80 (1997). Liposome immunoassays, such as flow-injection liposome immunoassays and liposome immunosensors, are also suitable for use in the present invention. See, e.g., Rongen *et al.*, *J. Immunol. Methods*, 204:105-133 (1997). In addition, nephelometry assays, in which the formation of protein/antibody complexes results in increased light scatter that is converted to a peak rate signal as a function of the marker concentration, are suitable for use in the methods of the present invention. Nephelometry assays are commercially available from Beckman Coulter (Brea, CA; Kit #449430) and can be performed using a Behring Nephelometer Analyzer (Fink *et al.*, *J. Clin. Chem. Clin. Biochem.*, 27:261-276 (1989)).

**[0102]** Specific immunological binding of the antibody to nucleic acids can be detected directly or indirectly. Direct labels include fluorescent or luminescent tags, metals, dyes, radionuclides, and the like, attached to the antibody. An antibody labeled with iodine-125 (<sup>125</sup>I) can be used. A chemiluminescence assay using a chemiluminescent antibody specific for the nucleic acid is suitable for sensitive, non-radioactive detection of protein levels. An antibody labeled with fluorochrome is also suitable. Examples of fluorochromes include, without limitation, DAPI, fluorescein, Hoechst 33258, R-phycoerythrin, B-phycoerythrin, R-phycoerythrin, rhodamine, Texas red, and lissamine. Indirect labels include various enzymes well known in the art, such as horseradish peroxidase (HRP), alkaline phosphatase (AP),  $\beta$ -galactosidase, urease, and the like. A horseradish-peroxidase detection system can be used, for example, with the chromogenic substrate tetramethylbenzidine (TMB), which yields a soluble product in the presence of hydrogen peroxide that is detectable at 450 nm. An alkaline phosphatase detection system can be used with the chromogenic substrate p-nitrophenyl phosphate, for example, which yields a soluble product readily detectable at 405 nm. Similarly, a  $\beta$ -galactosidase detection system can be used with the chromogenic substrate o-nitrophenyl- $\beta$ -D-galactopyranoside (ONPG), which yields a soluble product detectable at 410 nm. An urease detection system can be used with a substrate such as urea-bromocresol purple (Sigma Immunochemicals; St. Louis, MO).

**[0103]** A signal from the direct or indirect label can be analyzed, for example, using a spectrophotometer to detect color from a chromogenic substrate; a radiation counter to detect radiation such as a gamma counter for detection of <sup>125</sup>I; or a fluorometer to detect fluorescence in the presence of light of a certain wavelength. For detection of enzyme-linked antibodies, a quantitative analysis can be made using a spectrophotometer such as an EMAX Microplate Reader (Molecular Devices; Menlo Park, CA) in accordance with the

manufacturer's instructions. If desired, the assays of the present invention can be automated or performed robotically, and the signal from multiple samples can be detected simultaneously.

**[0104]** The antibodies can be immobilized onto a variety of solid supports, such as magnetic or chromatographic matrix particles, the surface of an assay plate (*e.g.*, microtiter wells), pieces of a solid substrate material or membrane (*e.g.*, plastic, nylon, paper), in the physical form of sticks, sponges, papers, wells, and the like. An assay strip can be prepared by coating the antibody or a plurality of antibodies in an array on a solid support. This strip can then be dipped into the test sample and processed quickly through washes and detection steps to generate a measurable signal, such as a colored spot.

**[0105]** Alternatively, nucleic acid binding molecules such as probes, oligonucleotides, oligonucleotide arrays, and primers can be used in assays to detect differential RNA expression of N-CoR2, HDAC3, and markers found in Table 1 in patient samples, *e.g.*, RT-PCR. In one embodiment, RT-PCR is used according to standard methods known in the art. In another embodiment, PCR assays such as Taqman<sup>®</sup> assays available from, *e.g.*, Applied Biosystems, can be used to detect nucleic acids and variants thereof. In other embodiments, qPCR and nucleic acid microarrays can be used to detect nucleic acids. Reagents that bind to selected cancer biomarkers can be prepared according to methods known to those of skill in the art or purchased commercially.

**[0106]** Analysis of nucleic acids can be achieved using routine techniques such as Southern analysis, reverse-transcriptase polymerase chain reaction (RT-PCR), or any other methods based on hybridization to a nucleic acid sequence that is complementary to a portion of the marker coding sequence (*e.g.*, slot blot hybridization) are also within the scope of the present invention. Applicable PCR amplification techniques are described in, *e.g.*, Ausubel *et al.* and Innis *et al.*, *supra*. General nucleic acid hybridization methods are described in Anderson, "Nucleic Acid Hybridization," BIOS Scientific Publishers, 1999. Amplification or hybridization of a plurality of nucleic acid sequences (*e.g.*, genomic DNA, mRNA or cDNA) can also be performed from mRNA or cDNA sequences arranged in a microarray. Microarray methods are generally described in Hardiman, "Microarrays Methods and Applications: Nuts & Bolts," DNA Press, 2003; and Baldi *et al.*, "DNA Microarrays and Gene Expression: From Experiments to Data Analysis and Modeling," Cambridge University Press, 2002.

- [0107] Analysis of nucleic acid markers and their variants can be performed using techniques known in the art including, without limitation, microarrays, polymerase chain reaction (PCR)-based analysis, sequence analysis, and electrophoretic analysis. A non-limiting example of a PCR-based analysis includes a Taqman<sup>®</sup> allelic discrimination assay available from Applied Biosystems. Non-limiting examples of sequence analysis include Maxam-Gilbert sequencing, Sanger sequencing, capillary array DNA sequencing, thermal cycle sequencing (Sears *et al.*, *Biotechniques*, 13:626-633 (1992)), solid-phase sequencing (Zimmerman *et al.*, *Methods Mol. Cell Biol.*, 3:39-42 (1992)), sequencing with mass spectrometry such as matrix-assisted laser desorption/ionization time-of-flight mass spectrometry (MALDI-TOF/MS; Fu *et al.*, *Nat. Biotechnol.*, 16:381-384 (1998)), and sequencing by hybridization. Chee *et al.*, *Science*, 274:610-614 (1996); Drmanac *et al.*, *Science*, 260:1649-1652 (1993); Drmanac *et al.*, *Nat. Biotechnol.*, 16:54-58 (1998). Non-limiting examples of electrophoretic analysis include slab gel electrophoresis such as agarose or polyacrylamide gel electrophoresis, capillary electrophoresis, and denaturing gradient gel electrophoresis. Other methods for detecting nucleic acid variants include, *e.g.*, the INVADER<sup>®</sup> assay from Third Wave Technologies, Inc., restriction fragment length polymorphism (RFLP) analysis, allele-specific oligonucleotide hybridization, a heteroduplex mobility assay, single strand conformational polymorphism (SSCP) analysis, single-nucleotide primer extension (SNUPE) and pyrosequencing.
- [0108] A detectable moiety can be used in the assays described herein. A wide variety of detectable moieties can be used, with the choice of label depending on the sensitivity required, ease of conjugation with the antibody, stability requirements, and available instrumentation and disposal provisions. Suitable detectable moieties include, but are not limited to, radionuclides, fluorescent dyes (*e.g.*, fluorescein, fluorescein isothiocyanate (FITC), Oregon Green<sup>™</sup>, rhodamine, Texas red, tetra-rhodimine isothiocyanate (TRITC), Cy3, Cy5, *etc.*), fluorescent markers (*e.g.*, green fluorescent protein (GFP), phycoerythrin, *etc.*), autoquenched fluorescent compounds that are activated by tumor-associated proteases, enzymes (*e.g.*, luciferase, horseradish peroxidase, alkaline phosphatase, *etc.*), nanoparticles, biotin, digoxigenin, and the like.
- [0109] Useful physical formats comprise surfaces having a plurality of discrete, addressable locations for the detection of a plurality of different markers. Such formats include microarrays and certain capillary devices. *See, e.g.*, Ng *et al.*, *J. Cell Mol. Med.*, 6:329-340 (2002); U.S. Pat. No. 6,019,944. In these embodiments, each discrete surface

location may comprise antibodies to immobilize one or more markers for detection at each location. Surfaces may alternatively comprise one or more discrete particles (*e.g.*, microparticles or nanoparticles) immobilized at discrete locations of a surface, where the microparticles comprise antibodies to immobilize one or more markers for detection. Other  
5 useful physical formats include sticks, wells, sponges, and the like.

[0110] Analysis can be carried out in a variety of physical formats. For example, the use of microtiter plates or automation could be used to facilitate the processing of large numbers of test samples. Alternatively, single sample formats could be developed to facilitate diagnosis or prognosis in a timely fashion.

10 [0111] Alternatively, the antibodies or nucleic acid probes of the invention can be applied to patient samples immobilized on microscope slides. The resulting antibody staining or in situ hybridization pattern can be visualized using any one of a variety of light or fluorescent microscopic methods known in the art.

15 [0112] Analysis of the protein or nucleic acid can also be achieved, for example, by high pressure liquid chromatography (HPLC), alone or in combination with mass spectrometry (*e.g.*, MALDI/MS, MALDI-TOF/MS, tandem MS, *etc.*).

## COMPOSITIONS, KITS AND INTEGRATED SYSTEMS

[0113] The invention provides compositions, kits and integrated systems for practicing the assays described herein using antibodies specific for the polypeptides or nucleic acids  
20 specific for the polynucleotides of the invention.

[0114] Kits for carrying out the diagnostic assays of the invention typically include a probe that comprises an antibody or nucleic acid sequence that specifically binds to polypeptides or polynucleotides of the invention, and a label for detecting the presence of the probe. The kits may include several antibodies or polynucleotide sequences encoding polypeptides of the  
25 invention, *e.g.*, a cocktail of antibodies that recognize N-CoR2, HDAC3, and markers found in Table 1.



## **TREATMENT, COMPOUNDS FOR TREATMENT, AND METHODS OF IDENTIFYING COMPOUNDS EFFECTIVE FOR TREATMENT**

[0115] A variety of methods may be used to identify compounds that prevent, treat, or sensitize multidrug resistant cancers. Typically, an assay that provides a readily measured parameter is adapted to be performed in the wells of multi-well plates in order to facilitate the screening of members of a library of test compounds as described herein. Thus, in one embodiment, an appropriate number of cells can be plated into the cells of a multi-well plate, and the effect of a test compound on the expression of a biomarker can be determined.

[0116] The compounds to be tested can be any small chemical compound, or a macromolecule, such as a protein, sugar, nucleic acid or lipid. Typically, test compounds will be small chemical molecules and peptides. Essentially any chemical compound can be used as a test compound in this aspect of the invention, although most often compounds that can be dissolved in aqueous or organic (especially DMSO-based) solutions are used. The assays are designed to screen large chemical libraries by automating the assay steps and providing compounds from any convenient source to assays, which are typically run in parallel (*e.g.*, in microtiter formats on microtiter plates in robotic assays). It will be appreciated that there are many suppliers of chemical compounds, including Sigma (St. Louis, MO), Aldrich (St. Louis, MO), Sigma-Aldrich (St. Louis, MO), Fluka Chemika-Biochemica Analytika (Buchs Switzerland) and the like.

[0117] In one embodiment, high throughput screening methods are used which involve providing a combinatorial chemical or peptide library containing a large number of potential therapeutic compounds. Such “combinatorial chemical libraries” or “ligand libraries” are then screened in one or more assays, as described herein, to identify those library members (particular chemical species or subclasses) that display a desired characteristic activity. In this instance, such compounds are screened for their ability to reduce or increase the expression of the biomarkers of the invention.

[0118] A combinatorial chemical library is a collection of diverse chemical compounds generated by either chemical synthesis or biological synthesis, by combining a number of chemical “building blocks” such as reagents. For example, a linear combinatorial chemical library such as a polypeptide library is formed by combining a set of chemical building blocks (amino acids) in every possible way for a given compound length (*i.e.*, the number of

amino acids in a polypeptide compound). Millions of chemical compounds can be synthesized through such combinatorial mixing of chemical building blocks.

[0119] Preparation and screening of combinatorial chemical libraries are well known to those of skill in the art. Such combinatorial chemical libraries include, but are not limited to, peptide libraries (*see, e.g.*, U.S. Patent 5,010,175, Furka, *Int. J. Pept. Prot. Res.*, 37:487-493 (1991) and Houghton *et al.*, *Nature*, 354:84-88 (1991)). Other chemistries for generating chemical diversity libraries can also be used. Such chemistries include, but are not limited to: peptoids (*e.g.*, PCT Publication No. WO 91/19735), encoded peptides (*e.g.*, PCT Publication No. WO 93/20242), random bio-oligomers (*e.g.*, PCT Publication No. WO 92/00091), benzodiazepines (*e.g.*, U.S. Patent No. 5,288,514), diversomers such as hydantoins, benzodiazepines and dipeptides (Hobbs *et al.*, *PNAS USA*, 90:6909-6913 (1993)), vinylogous polypeptides (Hagihara *et al.*, *J. Amer. Chem. Soc.*, 114:6568 (1992)), nonpeptidal peptidomimetics with glucose scaffolding (Hirschmann *et al.*, *J. Amer. Chem. Soc.*, 114:9217-9218 (1992)), analogous organic syntheses of small compound libraries (Chen *et al.*, *J. Amer. Chem. Soc.*, 116:2661 (1994)), oligocarbamates (Cho *et al.*, *Science*, 261:1303 (1993)), and/or peptidyl phosphonates (Campbell *et al.*, *J. Org. Chem.*, 59:658 (1994)), nucleic acid libraries (*see* Ausubel, Berger and Sambrook, all *supra*), peptide nucleic acid libraries (*see, e.g.*, U.S. Patent No. 5,539,083), antibody libraries (*see, e.g.*, Vaughn *et al.*, *Nature Biotechnology*, 14(3):309-314 (1996) and PCT/US96/10287), carbohydrate libraries (*see, e.g.*, Liang *et al.*, *Science*, 274:1520-1522 (1996) and U.S. Patent No. 5,593,853), small organic molecule libraries (*see, e.g.*, benzodiazepines, Baum C&EN, Jan 18, page 33 (1993); isoprenoids, U.S. Patent No. 5,569,588; thiazolidinones and metathiazanones, U.S. Patent No. 5,549,974; pyrrolidines, U.S. Patent Nos. 5,525,735 and 5,519,134; morpholino compounds, U.S. Patent No. 5,506,337; benzodiazepines, 5,288,514, and the like).

[0120] Devices for the preparation of combinatorial libraries are commercially available (*see, e.g.*, 357 MPS, 390 MPS, Advanced Chem Tech, Louisville KY, Symphony, Rainin, Woburn, MA, 433A Applied Biosystems, Foster City, CA, 9050 Plus, Millipore, Bedford, MA). In addition, numerous combinatorial libraries are themselves commercially available (*see, e.g.*, ComGenex, Princeton, N.J., Asinex, Moscow, Ru, Tripos, Inc., St. Louis, MO, ChemStar, Ltd, Moscow, RU, 3D Pharmaceuticals, Exton, PA, Martek Biosciences, Columbia, MD, *etc.*).

[0121] In the high throughput assays of the invention, it is possible to screen up to several thousand different modulators or ligands in a single day. In particular, each well of a microtiter plate can be used to run a separate assay against a selected potential modulator, or, if concentration or incubation time effects are to be observed, every 5-10 wells can test a single modulator. Thus, a single standard microtiter plate can assay about 96 modulators. If 1536 well plates are used, then a single plate can easily assay from about 100- about 1500 different compounds. It is possible to assay many plates per day; assay screens for up to about 6,000, 20,000, 50,000, or 100,000 or more different compounds is possible using the integrated systems of the invention.

[0122] The phrase “functional effects” in the context of assays for testing or identifying compounds that modulate a marker protein includes the determination of a parameter that is indirectly or directly under the influence of a biomarker of the invention, e.g., a chemical or phenotypic parameter. A functional effect therefore includes ligand binding activity, histone deacetylation activity, transcriptional activation or repression, the ability of cells to proliferate, the ability to migrate, among others. “Functional effects” include *in vitro*, *in vivo*, and *ex vivo* activities.

[0123] By “determining the functional effect” is meant assaying for a compound that increases or decreases a parameter that is indirectly or directly under the influence of a biomarker of the invention, e.g., measuring physical and chemical or phenotypic effects.

Such functional effects can be measured by any means known to those skilled in the art, e.g., changes in spectroscopic characteristics (e.g., fluorescence, absorbance, refractive index); hydrodynamic (e.g., shape), chromatographic; or solubility properties for the protein; ligand binding assays, e.g., binding to antibodies; measuring inducible markers or transcriptional activation of the marker; measuring changes in enzymatic activity; the ability to increase or decrease cellular proliferation, apoptosis, cell cycle arrest, measuring changes in cell surface markers, measuring histone deacetylation activity, etc. The functional effects can be evaluated by many means known to those skilled in the art, e.g., microscopy for quantitative or qualitative measures of alterations in morphological features, measurement of changes in RNA or protein levels for other genes expressed in placental tissue, measurement of RNA stability, identification of downstream or reporter gene expression (CAT, luciferase,  $\gamma$ -gal, GFP and the like), e.g., via chemiluminescence, fluorescence, colorimetric reactions, antibody binding, inducible markers, measuring histone acetylation, etc.

[0124] “Inhibitors,” “activators,” and “modulators” of the markers are used to refer to activating, inhibitory, or modulating molecules identified using *in vitro* and *in vivo* assays of cancer biomarkers. Inhibitors are compounds that, e.g., bind to, partially or totally block activity, decrease, prevent, delay activation, inactivate, desensitize, or down regulate the activity or expression of cancer biomarkers. “Activators” are compounds that increase, open, activate, facilitate, enhance activation, sensitize, agonize, or up regulate activity of cancer biomarkers, e.g., agonists. Inhibitors, activators, or modulators also include genetically modified versions of cancer biomarkers, e.g., versions with altered activity, as well as naturally occurring and synthetic ligands, antagonists, agonists, antibodies, peptides, cyclic peptides, nucleic acids, antisense molecules, ribozymes, RNAi and siRNA molecules, microRNA, shRNA, small organic molecules and the like. Such assays for inhibitors and activators include, e.g., expressing cancer biomarkers *in vitro*, in cells, or cell extracts, applying putative modulator compounds, and then determining the functional effects on activity, as described above.

[0125] Samples or assays comprising cancer biomarkers that are treated with a potential activator, inhibitor, or modulator are compared to control samples without the inhibitor, activator, or modulator to examine the extent of inhibition. Control samples (untreated with inhibitors) are assigned a relative protein activity value of 100%. Inhibition of cancer biomarkers is achieved when the activity value relative to the control is about 80%, preferably 50%, more preferably 25-0%. Activation of cancer biomarkers is achieved when the activity value relative to the control (untreated with activators) is 110%, more preferably 150%, more preferably 200-500% (i.e., two to five fold higher relative to the control), more preferably 1000-3000% higher.

[0126] The term “test compound” or “drug candidate” or “modulator” or grammatical equivalents as used herein describes any molecule, either naturally occurring or synthetic, e.g., protein, oligopeptide (e.g., from about 5 to about 25 amino acids in length, preferably from about 10 to 20 or 12 to 18 amino acids in length, preferably 12, 15, or 18 amino acids in length), small organic molecule, polysaccharide, peptide, circular peptide, lipid, fatty acid, siRNA, microRNA, polynucleotide, oligonucleotide, etc., to be tested for the capacity to directly or indirectly modulate cancer biomarkers. The test compound can be in the form of a library of test compounds, such as a combinatorial or randomized library that provides a sufficient range of diversity. Test compounds are optionally linked to a fusion partner, e.g., targeting compounds, rescue compounds, dimerization compounds, stabilizing compounds,

addressable compounds, and other functional moieties. Conventionally, new chemical entities with useful properties are generated by identifying a test compound (called a “lead compound”) with some desirable property or activity, e.g., inhibiting activity, creating variants of the lead compound, and evaluating the property and activity of those variant compounds. Often, high throughput screening (HTS) methods are employed for such an analysis.

[0127] A “small organic molecule” refers to an organic molecule, either naturally occurring or synthetic, that has a molecular weight of more than about 50 daltons and less than about 2500 daltons, preferably less than about 2000 daltons, preferably between about 100 to about 1000 daltons, more preferably between about 200 to about 500 daltons.

## **METHODS TO INHIBIT MARKER PROTEIN EXPRESSION USING NUCLEIC ACIDS**

[0128] A variety of nucleic acids, such as antisense nucleic acids, siRNAs, shRNAs, microRNAs, or ribozymes, may be used to inhibit the function of the markers of this invention. Ribozymes that cleave mRNA at site-specific recognition sequences can be used to destroy target mRNAs, particularly through the use of hammerhead ribozymes. Hammerhead ribozymes cleave mRNAs at locations dictated by flanking regions that form complementary base pairs with the target mRNA. Preferably, the target mRNA has the following sequence of two bases: 5'-UG-3'. The construction and production of hammerhead ribozymes is well known in the art.

[0129] Gene targeting ribozymes necessarily contain a hybridizing region complementary to two regions, each of at least 5 and preferably each 6, 7, 8, 9, 10, 11, 12, 13, 14, 15, 16, 17, 18, 19 or 20 contiguous nucleotides in length of a target mRNA. In addition, ribozymes possess highly specific endoribonuclease activity, which autocatalytically cleaves the target sense mRNA.

[0130] With regard to antisense, siRNA, shRNA, microRNA, or ribozyme oligonucleotides, phosphorothioate oligonucleotides can be used. Modifications of the phosphodiester linkage as well as of the heterocycle or the sugar may provide an increase in efficiency. Phosphorothioate is used to modify the phosphodiester linkage. An N3'-P5' phosphoramidate linkage has been described as stabilizing oligonucleotides to nucleases and increasing the binding to RNA. Peptide nucleic acid (PNA) linkage is a complete replacement of the ribose and phosphodiester backbone and is stable to nucleases, increases

the binding affinity to RNA, and does not allow cleavage by RNase H. Its basic structure is also amenable to modifications that may allow its optimization as an antisense component. With respect to modifications of the heterocycle, certain heterocycle modifications have proven to augment antisense effects without interfering with RNase H activity. An example of such modification is C-5 thiazole modification. Finally, modification of the sugar may also be considered. 2'-O-propyl and 2'-methoxyethoxy ribose modifications stabilize oligonucleotides to nucleases in cell culture and *in vivo*.

**[0131]** Inhibitory oligonucleotides can be delivered to a cell by direct transfection or transfection and expression via an expression vector. Appropriate expression vectors include mammalian expression vectors and viral vectors, into which has been cloned an inhibitory oligonucleotide with the appropriate regulatory sequences including a promoter to result in expression of the antisense RNA in a host cell. Suitable promoters can be constitutive or development-specific promoters. Transfection delivery can be achieved by liposomal transfection reagents, known in the art (*e.g.*, Xtreme transfection reagent, Roche, Alameda, CA; Lipofectamine formulations, Invitrogen, Carlsbad, CA). Delivery mediated by cationic liposomes, by retroviral vectors and direct delivery are efficient. Another possible delivery mode is targeting using antibody to cell surface markers for the target cells.

**[0132]** For transfection, a composition comprising one or more nucleic acid molecules (within or without vectors) can comprise a delivery vehicle, including liposomes, for administration to a subject, carriers and diluents and their salts, and/or can be present in pharmaceutically acceptable formulations. Methods for the delivery of nucleic acid molecules are described, for example, in Gilmore, *et al.*, *Curr Drug Delivery* (2006) 3:147-5 and Patil, *et al.*, *AAPS Journal* (2005) 7:E61-E77, each of which are incorporated herein by reference. Delivery of siRNA molecules is also described in several U.S. Patent Publications, including for example, 2006/0019912; 2006/0014289; 2005/0239687; 2005/0222064; and 2004/0204377, the disclosures of each of which are hereby incorporated herein by reference. Nucleic acid molecules can be administered to cells by a variety of methods known to those of skill in the art, including, but not restricted to, encapsulation in liposomes, by iontophoresis, by electroporation, or by incorporation into other vehicles, including biodegradable polymers, hydrogels, cyclodextrins (*see, for example* Gonzalez *et al.*, 1999, *Bioconjugate Chem.*, 10, 1068-1074; Wang *et al.*, International PCT publication Nos. WO 03/47518 and WO 03/46185), poly(lactic-co-glycolic)acid (PLGA) and PLGA microspheres (*see for example* U.S. Pat. No. 6,447,796 and US Patent Application Publication No.

2002/130430), biodegradable nanocapsules, and bioadhesive microspheres, or by proteinaceous vectors (O'Hare and Normand, International PCT Publication No. WO 00/53722). In another embodiment, the nucleic acid molecules of the invention can also be formulated or complexed with polyethyleneimine and derivatives thereof, such as  
5 polyethyleneimine-polyethyleneglycol-N-acetylgalactosamine (PEI-PEG-GAL) or polyethyleneimine-polyethyleneglycol-tri-N-acetylgalactosamine (PEI-PEG-triGAL) derivatives.

[0133] Examples of liposomal transfection reagents of use with this invention include, for example: CellFectin, 1:1.5 (M/M) liposome formulation of the cationic lipid N,N,N,N-tetramethyl-N,N,N,N-tetrapalmit-y-spermine and dioleoyl phosphatidylethanolamine (DOPE) (GIBCO BRL); Cytofectin GSV, 2:1 (M/M) liposome formulation of a cationic lipid and DOPE (Glen Research); DOTAP (N-[1-(2,3-dioleoyloxy)-N,N,N-tri-methyl-ammoniummethylsulfate) (Boehringer Mannheim); Lipofectamine, 3:1 (M/M) liposome  
10 formulation of the polycationic lipid DOSPA and the neutral lipid DOPE (GIBCO BRL); and (5) siPORT (Ambion); HiPerfect (Qiagen); X-treme GENE (Roche); RNAi carrier (Epoch Biolabs) and TransPass (New England Biolabs).

[0134] In some embodiments, antisense, siRNA, shRNAs, microRNA, or ribozyme sequences are delivered into the cell via a mammalian expression vector. For example, mammalian expression vectors suitable for siRNA expression are commercially available, for  
20 example, from Ambion (*e.g.*, pSilencer vectors), Austin, TX; Promega (*e.g.*, GeneClip, siSTRIKE, SiLentGene), Madison, WI; Invitrogen, Carlsbad, CA; InvivoGen, San Diego, CA; and Imgenex, San Diego, CA. Typically, expression vectors for transcribing siRNA molecules will have a U6 promoter.

[0135] In some embodiments, antisense, siRNA, shRNA, microRNA, or ribozyme  
25 sequences are delivered into cells via a viral expression vector. Viral vectors suitable for delivering such molecules to cells include adenoviral vectors, adeno-associated vectors, and retroviral vectors (including lentiviral vectors). For example, viral vectors developed for delivering and expressing siRNA oligonucleotides are commercially available from, for example, GeneDetect, Bradenton, FL; Ambion, Austin, TX; Invitrogen, Carlsbad, CA; Open  
30 BioSystems, Huntsville, AL; and Imgenex, San Diego, CA.

## EXAMPLES

[0136] Example 1

[0137] This example describes the identification of genetic markers associated with N-CoR2.

[0138] HMT3522 T4-2 malignant human breast epithelial cells, developed by Dr. O. W. Peterson (Cancer Res. 52:1210-1217, 1992), were used as a model. HMT3522 T4-2 cells were derived from an epidermal growth factor (EGF)-dependent breast epithelial HMT3522 S-1 cells and an EGF-independent HMT3522 S-2 cells that spontaneously became malignant when injected into nude mice. HMT3522 T4-2 cells were propagated as monolayers on type I collagen-coated plastic surface in chemically defined medium consisting of DMEM:F12 medium (Invitrogen GIBCO), containing 250 ng/ml insulin (Boehringer Mannheim), 10  $\mu$ g/ml transferrin (Sigma, St. Louis, MO), 2.6 ng/ml sodium selenite (Collaborative Research),  $10^{-10}$  M estradiol (Sigma),  $1.4 \times 10^{-6}$  M hydrocortisone (Collaborative Research), and 5  $\mu$ g/ml prolactin (Sigma), as described in J. Cell Biol. 137:231-245 (1997).

[0139] HMT3522 T4-2 cells that stably overexpress N-CoR2 were generated by retrovirus-mediated gene transduction. Briefly, the retroviral construct inducibly expressing HA- and EGFP-epitope tagged N-CoR2 was prepared by subcloning murine *NCOR2* cDNA (e isoform, NCBI RefSeq #NM\_011424) from pCMX-FLAG-NCOR2 (provided by professor M. A. Lazar, University of Pennsylvania) (Proc. Natl. Acad. Sci. USA 96:3519-3524 (1999)) into pBluescriptII KS+ (Stratagene) for the addition of a N-terminal HA-epitope tag and then recloned into a modified hybrid Epstein-Barr virus/retroviral vector pLZRS-MFG-*tet*-EGFP that contains a tetracycline regulated promoter and allows stable multicopy episomal replication in the retroviral packaging lines (Hum. Gene Ther. 7:1405-1413 (1996)) to generate the final expression construct pLZRS-MFG-*tet*-HA-EGFP-NCOR2.

[0140] Amphotropic retrovirus was produced in modified 293 cells or in Phoenix amphi cells (provided by Professor G. Nolan, Stanford Medical Center) with packaging vectors pCgp and pVSVG to boost viral titer. Cells were spin infected with retrovirus carrying N-CoR2 or an empty retroviral vector, followed by infection with a high titer MFG virus expressing the tetracycline-controlled transcriptional transactivator produced in the packaging cell line 293GPG as described (Proc. Natl. Acad. Sci. USA 93:11400-11406 (1996)). To obtain a polyclonal population of cells in which the majority of cells inducibly expressed N-CoR2 or its mutant these transduced cells were first expanded in the presence of tetracycline at 1  $\mu$ g/mL and then N-CoR2 expression was induced by withdrawal of tetracycline for 2 to 4 days, followed by FAC sorting for EGFP positive cells. Sorted cells were expanded again in



the presence of tetracycline. As the overexpressed N-CoR2 protein underwent gradual degradation in monolayer cultures, we did not activate the tetracycline-regulated expression of N-CoR2 in HMT3522 T4-2 cells until being cultured in reconstituted basement membrane.

**[0141]** To profile the gene expressions of HMT3522 T4-2 cells that stably expressed N-

CoR2 or an empty vector, the cells were grown in a reconstituted basement membrane (rBM) culture according to the procedures described in US Patent 6123941 and Nat. Method. 4:359-365 (2007). rBM is a specific 3D culture matrix isolated from mouse Englebreth-Holm-Swarm (EHS) tumors (commercially available as Matrigel, BD Biosciences) and is made of about 80% laminin, about 10% type IV collagen, about 10% proteoglycans and growth factors. To increase the yield of RNA for transcriptional profiling experiments, we grew  $2 \times 10^5$  cells on top of rBM in a 60-mm tissue culture dish. As described, cells grown on top of rBM formed 3D cellular aggregates similar to those embedded in rBM. Four replicate cultures were established for each of the 2 experiment groups, including those using HMT3522 T4-2 cells that stably expressed N-CoR2 (T4-2 N-CoR2 cells) and those expressing the empty vector (T4-2 vector cells). The cultures were maintained for 6 days before the collection of RNA samples.

**[0142]** Total RNA was extracted from monolayer culture or 3D culture by a modified TRI reagent procedure as described (Biotechniques 19:942-945 (1995)) and purified using an RNeasy Mini Kit (Qiagen). Gene expression analysis was performed on an Affymetrix Human Genome U133A 2.0 GeneChip platform containing 22,283 probes according to the manufacturer's protocol (Affymetrix). Twenty micrograms of total RNA from each sample was processed to produce biotinylated cRNA targets. After hybridization, washing and staining arrays were scanned using a confocal scanner (Affymetrix). The hybridization intensity data was processed using the GeneChip Operating software (Affymetrix).

Affymetrix .cel files (probe intensity files) were processed with ArrayAssist Lite (v3.4, Stratagene). The files were imported and processed with the GC-RMA algorithm to yield probe set intensities and additionally, Affymetrix Preset, Absent, Marginal flags were computed. These values were exported in .chp files, which were subsequently imported into the Partek Genomics Suite software (v6.2, Partek). The genes were filtered based on the Affymetrix P/A/M flags to retain only those genes that were present in at least 2 of the 8 samples.

[0143] To select genes in HMT3522 T4-2 cells that are differentially induced or repressed upon overexpression of N-CoR2, the GC-RMA expression values of all the 8 transcriptomes were log2 transformed and pairwise contrasts were performed using Student's *t* test.

[0144] A list of 304 genes (represented by 350 Affymetrix probe sets) were identified from the microarray experiments based on their expression levels significantly different (fold change  $\geq 2$  and a cutoff *P*-value  $< 0.05$  by Student's *t* test) between T4-2 vector cells and T4-2 N-CoR2 cells. These genes are designated as N-CoR2 signature genes as their expressions significantly responded to overexpression of N-CoR2. Functional annotations of these genes suggested that N-CoR2 mainly regulated the transcription of genes involved in extracellular matrix assembly and remodeling (*e.g.*, *FN1*, *SDC2*, *TIMP3*, *MMP1*, *COL4A1*, *THBS1*, *TAGLN*, *TNC*, *COL6A2*, *ITGA6*, *ITGB4*), inflammation (*e.g.*, *IL6*, *TREM1*, *C3AR1*, *FOS*, *MAPK1*, *CXCL3*, *CXCL10*), growth and differentiation (*e.g.*, *SFRP1*, *TGFA*, *CCNG2*, *CNAP1*, *EGFR*, *NOTCH2*, *NRG1*, *EREG*), and cytoskeleton and cell-cell adhesion (*e.g.*, *TPX2*, *SPOCK1*, *ARHGAP1*, *PAK1*, *WASL*, *DSC2*, *DSG3*). Table 1 provides a detailed list of the 304 genes that were differentially expressed in response to N-CoR2 overexpression in HMT3522 T4-2 cells. The genes (probe sets) are ranked in descending order according to the ratio between the mean hybridization intensity of each probe in T4-2 vector cells (*V*) and that in T4-2 N-CoR2 cells (*N*).

**Table 1.** N-CoR2 signature genes that were differentially expressed in response to N-CoR2 overexpression in HMT3522 T4-2 cells.

AFFYMET RIX PROBE SET ID	GENE SYMBOL	REFSEQ TRANSCRIPT ID	MEAN INTENSITY ( <i>V</i> )	MEAN INTENSITY ( <i>N</i> )	RATIO ( <i>V/N</i> )
210119_at	<i>KCNJ15</i>	NM_002243 / NM_170736 / NM_170737	136.33	11.06	12.33
211806_s_at	<i>KCNJ15</i>	NM_002243 / NM_170736 / NM_170737	43.15	4.82	8.94
211719_x_at	<i>FN1</i>	NM_002026 / NM_054034 / NM_212474 / NM_212475 / NM_212476 / NM_212478 / NM_212482	7290.69	1237.54	5.89

216442_x_at	<i>FNI</i>	NM_002026 / NM_054034 / NM_212474 / NM_212475 / NM_212476 / NM_212478 / NM_212482	4490.64	781.95	5.74
214701_s_at	<i>FNI</i>	NM_002026 / NM_054034 / NM_212474 / NM_212475 / NM_212476 / NM_212478 / NM_212482	34.32	6.00	5.72
210495_x_at	<i>FNI</i>	NM_002026 / NM_054034 / NM_212474 / NM_212475 / NM_212476 / NM_212478 / NM_212482	4478.15	790.08	5.67
205207_at	<i>IL6</i>	NM_000600	421.76	79.36	5.31
212464_s_at	<i>FNI</i>	NM_002026 / NM_054034 / NM_212474 / NM_212475 / NM_212476 / NM_212478 / NM_212482	3877.24	730.91	5.30
214336_s_at	<i>COPA</i>	NM_004371	41.88	7.94	5.27
219434_at	<i>TREMI</i>	NM_018643	275.64	54.65	5.04
212154_at	<i>SDC2</i>	NM_002998	517.35	117.88	4.39
211981_at	<i>COL4A1</i>	NM_001845	55.16	13.20	4.18
217859_s_at	<i>SLC39A9</i>	NM_018375	80.47	21.36	3.77
201107_s_at	<i>THBS1</i>	NM_003246	411.89	112.11	3.67
206184_at	<i>CRKL</i>	NM_005207	26.61	7.52	3.54
212158_at	<i>SDC2</i>	NM_002998	88.69	25.07	3.54
209136_s_at	<i>USP10</i>	NM_005153	111.34	32.25	3.45
205547_s_at	<i>TAGLN</i>	NM_001001522 / NM_003186	187.92	54.58	3.44
203925_at	<i>GCLM</i>	NM_002061	469.78	136.88	3.43
200879_s_at	<i>EPAS1</i>	NM_001430	272.67	79.80	3.42
202037_s_at	<i>SFRP1</i>	NM_003012	81.81	24.36	3.36
201150_s_at	<i>TIMP3</i>	NM_000362	64.52	19.75	3.27
212142_at	<i>MCM4</i>	NM_005914 / NM_182746	32.67	10.00	3.27
211559_s_at	<i>CCNG2</i>	NM_004354	16.67	5.11	3.26
209456_s_at	<i>FBXW11</i>	NM_012300 / NM_033644 / NM_033645	66.57	20.42	3.26
210735_s_at	<i>CA12</i>	NM_001218 / NM_206925	190.16	58.46	3.25
210052_s_at	<i>TPX2</i>	NM_012112	691.71	216.33	3.20
204764_at	<i>FNTB</i>	NM_002028	95.95	30.47	3.15
209906_at	<i>C3AR1</i>	NM_004054	23.28	7.46	3.12
201774_s_at	<i>CNAP1</i>	NM_014865	467.66	149.85	3.12

211966_at	<i>COL4A2</i>	NM_001846	52.83	17.44	3.03
201147_s_at	<i>TIMP3</i>	NM_000362	43.90	14.52	3.02
201830_s_at	<i>NET1</i>	NM_005863	122.64	40.69	3.01
206363_at	<i>MAF</i>	NM_001031804 / NM_005360	415.48	137.94	3.01
209401_s_at	<i>SLC12A4</i>	NM_005072	53.10	17.66	3.01
204475_at	<i>MMP1</i>	NM_002421	192.36	64.09	3.00
217445_s_at	<i>GART</i>	NM_000819 / NM_175085	224.08	75.91	2.95
208853_s_at	<i>CANX</i>	NM_001024649 / NM_001746	237.89	81.66	2.91
211519_s_at	<i>KIF2C</i>	NM_006845	97.80	33.68	2.90
211964_at	<i>COL4A2</i>	NM_001846	486.47	167.64	2.90
219213_at	<i>JAM2</i>	NM_021219	15.53	5.45	2.85
211607_x_at	<i>EGFR</i>	NM_005228 / NM_201282 / NM_201283 / NM_201284	463.55	163.46	2.84
210984_x_at	<i>EGFR</i>	NM_005228 / NM_201282 / NM_201283 / NM_201284	475.74	170.80	2.79
210756_s_at	<i>NOTCH2</i>	NM_024408	328.26	118.38	2.77
203798_s_at	<i>VSNL1</i>	NM_003385	90.05	32.73	2.75
209189_at	<i>FOS</i>	NM_005252	1156.59	420.66	2.75
210892_s_at	<i>GTF2I</i>	NM_001518 / NM_032999 / NM_033000 / NM_033001	95.29	34.75	2.74
205729_at	<i>OSMR</i>	NM_003999	89.57	32.83	2.73
203967_at	<i>CDC6</i>	NM_001254	14.73	5.41	2.72
202240_at	<i>PLK1</i>	NM_005030	367.26	134.92	2.72
221530_s_at	<i>BHLHB3</i>	NM_030762	66.58	24.51	2.72
211249_at	<i>GPR68</i>	NM_003485	16.79	6.20	2.71
202363_at	<i>SPOCK1</i>	NM_004598	55.22	20.40	2.71
218115_at	<i>ASF1B</i>	NM_018154	123.19	45.68	2.70
212022_s_at	<i>MKI67</i>	NM_002417	383.86	143.95	2.67
211980_at	<i>COL4A1</i>	NM_001845	550.91	206.88	2.66
212190_at	<i>SERPINE2</i>	NM_006216	668.64	252.62	2.65
202444_s_at	<i>SPFH1</i>	NM_006459	102.12	38.60	2.65
208351_s_at	<i>MAPK1</i>	NM_002745 / NM_138957	92.19	35.08	2.63
201755_at	<i>MCM5</i>	NM_006739	93.87	36.11	2.60
221901_at	<i>KIAA1644</i>	XM_376018 / XM_936510	111.78	43.02	2.60
204318_s_at	<i>GTSE1</i>	NM_016426	114.61	44.39	2.58
52837_at	<i>KIAA1644</i>	XM_376018 / XM_936510	69.64	27.20	2.56
209098_s_at	<i>JAG1</i>	NM_000214	212.90	83.59	2.55
209347_s_at	<i>MAF</i>	NM_001031804 / NM_005360	24.86	9.79	2.54
204879_at	<i>PDPN</i>	NM_001006624 / NM_001006625 / NM_006474 / NM_198389	329.72	129.96	2.54

207357_s_at	<i>GALNT10</i>	NM_017540 / NM_198321	212.98	84.03	2.53
208852_s_at	<i>CANX</i>	NM_001024649 / NM_001746	333.80	131.78	2.53
40837_at	<i>TLE2</i>	NM_003260	107.13	42.69	2.51
221520_s_at	<i>CDCA8</i>	NM_018101	200.88	80.78	2.49
205015_s_at	<i>TGFA</i>	NM_003236	34.75	14.02	2.48
210543_s_at	<i>PRKDC</i>	NM_006904	157.63	63.61	2.48
219093_at	<i>FLJ20701</i>	NM_017933	403.42	162.82	2.48
209758_s_at	<i>MFAP5</i>	NM_003480	44.75	18.23	2.45
204962_s_at	<i>CENPA</i>	NM_001809	219.28	90.09	2.43
210082_at	<i>ABCA4</i>	NM_000350	11.46	4.77	2.40
214686_at	<i>ZNF266</i>	NM_006631 / NM_198058	17.77	7.41	2.40
206429_at	<i>F2RL1</i>	NM_005242	38.12	16.02	2.38
210105_s_at	<i>FYN</i>	NM_002037 / NM_153047 / NM_153048	35.10	14.78	2.37
218073_s_at	<i>TMEM48</i>	NM_018087	76.98	33.03	2.33
218365_s_at	<i>DARS2</i>	NM_018122	56.42	24.32	2.32
204147_s_at	<i>TFDP1</i>	NM_007111	108.10	46.74	2.31
218717_s_at	<i>LEPREL1</i>	NM_018192	196.30	85.17	2.30
212372_at	<i>MYH10</i>	NM_005964	80.32	34.96	2.30
202954_at	<i>UBE2C</i>	NM_007019 / NM_181799 / NM_181800 / NM_181801 / NM_181802 / NM_181803	3038.31	1325.26	2.29
221004_s_at	<i>ITM2C</i>	NM_001012514 / NM_001012516 / NM_030926	96.07	42.05	2.28
217010_s_at	<i>CDC25C</i>	NM_001790 / NM_022809	15.92	6.98	2.28
209408_at	<i>KIF2C</i>	NM_006845	270.75	119.13	2.27
216033_s_at	<i>FYN</i>	NM_002037 / NM_153047 / NM_153048	11.66	5.15	2.27
202779_s_at	<i>UBE2S</i>	NM_014501 / XM_941060	2736.53	1214.09	2.25
207850_at	<i>CXCL3</i>	NM_002090	106.06	47.22	2.25
215253_s_at	<i>DSCR1</i>	NM_004414 / NM_203417 / NM_203418	25.11	11.19	2.24
201645_at	<i>TNC</i>	NM_002160	304.33	136.18	2.23
215942_s_at	<i>GTSE1</i>	NM_016426	36.42	16.31	2.23
202479_s_at	<i>TRIB2</i>	NM_021643	77.65	34.81	2.23
204033_at	<i>TRIP13</i>	NM_004237	286.45	128.65	2.23
202870_s_at	<i>CDC20</i>	NM_001255	2583.94	1160.70	2.23
219928_s_at	<i>CABYR</i>	NM_012189 / NM_138643 / NM_138644 / NM_153768 / NM_153769 / NM_153770	58.24	26.32	2.21

217080_s_at	<i>HOMER2</i>	NM_004839 / NM_199330 / NM_199331 / NM_199332	107.14	48.48	2.21
212016_s_at	<i>PTBP1</i>	NM_002819 / NM_031990 / NM_031991 / NM_175847	763.83	348.48	2.19
209156_s_at	<i>COL6A2</i>	NM_001849 / NM_058174 / NM_058175	12.80	5.88	2.18
211194_s_at	<i>TP73L</i>	NM_003722	65.03	29.89	2.18
200641_s_at	<i>YWHAZ</i>	NM_003406 / NM_145690	1891.11	870.58	2.17
201529_s_at	<i>RPA1</i>	NM_002945	112.68	51.92	2.17
217173_s_at	<i>LDLR</i>	NM_000527	332.27	153.20	2.17
215177_s_at	<i>ITGA6</i>	NM_000210	806.65	372.47	2.17
204768_s_at	<i>FEN1</i>	NM_004111	205.73	95.00	2.17
218755_at	<i>KIF20A</i>	NM_005733	341.77	158.10	2.16
203865_s_at	<i>ADARB1</i>	NM_001033049 / NM_001112 / NM_015833 / NM_015834	177.68	82.32	2.16
209395_at	<i>CHI3L1</i>	NM_001276	145.15	67.32	2.16
212021_s_at	<i>MKI67</i>	NM_002417	181.65	84.26	2.16
203676_at	<i>GNS</i>	NM_002076	15.58	7.23	2.15
213562_s_at	<i>SOLE</i>	NM_003129	492.91	229.04	2.15
209645_s_at	<i>ALDH1B1</i>	NM_000692	116.91	54.64	2.14
216969_s_at	<i>KIF22</i>	NM_007317	158.72	74.29	2.14
209278_s_at	<i>TFPI2</i>	NM_006528	50.76	23.81	2.13
214536_at	<i>SLURP1</i>	NM_020427	38.09	17.87	2.13
202718_at	<i>IGFBP2</i>	NM_000597	201.29	94.69	2.13
221436_s_at	<i>CDCA3</i>	NM_031299	195.39	91.95	2.12
209896_s_at	<i>PTPN11</i>	NM_002834	17.55	8.26	2.12
208782_at	<i>FSTL1</i>	NM_007085	210.15	98.97	2.12
215357_s_at	<i>POLDIP3</i>	NM_032311 / NM_178136	116.88	55.07	2.12
217202_s_at	<i>GLUL</i>	NM_001033044 / NM_001033056 / NM_002065	79.13	37.34	2.12
200900_s_at	<i>M6PR</i>	NM_002355	316.05	149.12	2.12
204589_at	<i>NUAK1</i>	NM_014840	194.88	92.30	2.11
218009_s_at	<i>PRC1</i>	NM_003981 / NM_199413 / NM_199414	337.52	159.87	2.11
201984_s_at	<i>EGFR</i>	NM_005228 / NM_201282 / NM_201283 / NM_201284	2124.37	1007.51	2.11
210935_s_at	<i>WDR1</i>	NM_005112 / NM_017491	559.44	265.33	2.11
211905_s_at	<i>ITGB4</i>	NM_000213 / NM_001005619 / NM_001005731	1052.93	500.01	2.11
216689_x_at	<i>ARHGAP1</i>	NM_004308	222.84	106.03	2.10

201801_s_at	<i>SLC29A1</i>	NM_004955	64.64	30.82	2.10
203145_at	<i>SPAG5</i>	NM_006461	99.59	47.51	2.10
214710_s_at	<i>CCNB1</i>	NM_031966	1404.09	670.35	2.09
209615_s_at	<i>PAK1</i>	NM_002576	78.62	37.63	2.09
218726_at	<i>DKFZp762E1312</i>	NM_018410	60.36	28.91	2.09
211804_s_at	<i>CDK2</i>	NM_001798 / NM_052827	103.89	50.00	2.08
203976_s_at	<i>CHAF1A</i>	NM_005483	38.07	18.35	2.07
211162_x_at	<i>SCD</i>	NM_005063	1184.84	572.31	2.07
58916_at	<i>KCTD14</i>	NM_023930	28.95	14.00	2.07
218308_at	<i>TACC3</i>	NM_006342	202.69	98.40	2.06
200796_s_at	<i>MCL1</i>	NM_021960 / NM_182763	34.79	16.94	2.05
209624_s_at	<i>MCCC2</i>	NM_022132	26.63	13.00	2.05
209396_s_at	<i>CHI3L1</i>	NM_001276	100.75	49.24	2.05
212614_at	<i>ARID5B</i>	NM_032199	18.89	9.26	2.04
204140_at	<i>TPST1</i>	NM_003596	164.97	80.90	2.04
215739_s_at	<i>TUBGCP3</i>	NM_006322	94.67	46.43	2.04
201555_at	<i>MCM3</i>	NM_002388	304.81	149.69	2.04
204508_s_at	<i>CA12</i>	NM_001218 / NM_206925	121.17	59.66	2.03
210301_at	<i>XDH</i>	NM_000379	245.51	120.99	2.03
207821_s_at	<i>PTK2</i>	NM_005607 / NM_153831	283.60	140.15	2.02
200644_at	<i>MARCKSL1</i>	NM_023009	166.24	82.36	2.02
212949_at	<i>BRRN1</i>	NM_015341	28.66	14.21	2.02
202095_s_at	<i>BIRC5</i>	NM_001012270 / NM_001012271 / NM_001168	473.20	235.27	2.01
202058_s_at	<i>KPNA1</i>	NM_002264	187.66	93.38	2.01
221029_s_at	<i>WNT5B</i>	NM_030775 / NM_032642	47.71	23.74	2.01
203963_at	<i>CA12</i>	NM_001218 / NM_206925	1086.47	540.99	2.01
208539_x_at	<i>SPRR2B</i>	NM_001017418	5343.04	2670.07	2.00
207655_s_at	<i>BLNK</i>	NM_013314	122.03	244.59	0.50
209533_s_at	<i>PLAA</i>	NM_001031689 / NM_004253	63.38	127.13	0.50
202219_at	<i>SLC6A8</i>	NM_005629	356.75	718.43	0.50
213510_x_at	<i>LOC220594</i>	NM_145809	12.83	25.89	0.50
221568_s_at	<i>LIN7C</i>	NM_018362	21.41	43.29	0.49
213082_s_at	<i>SLC35D2</i>	NM_007001	79.26	160.33	0.49
210580_x_at	<i>SULT1A3</i>	NM_001017387 / NM_001017389 / NM_001017390 / NM_001017391 / NM_003166 / NM_177552	53.48	108.19	0.49
205660_at	<i>OASL</i>	NM_003733 / NM_198213	193.82	393.43	0.49
202357_s_at	<i>CFB</i>	NM_001710	94.01	191.29	0.49
212989_at	<i>TMEM23</i>	NM_147156	40.03	81.72	0.49

204686_at	<i>IRSI</i>	NM_005544	118.07	241.06	0.49
214329_x_at	<i>TNFSF10</i>	NM_003810	44.20	90.28	0.49
209422_at	<i>PHF20</i>	NM_016436	77.62	158.60	0.49
202869_at	<i>OAS1</i>	NM_001032409 / NM_002534 / NM_016816	126.11	258.43	0.49
218446_s_at	<i>FAM18B</i>	NM_016078	47.24	96.87	0.49
219424_at	<i>EBI3</i>	NM_005755	19.66	40.35	0.49
208841_s_at	<i>G3BP2</i>	NM_012297 / NM_203504 / NM_203505	81.38	167.15	0.49
204454_at	<i>LDOC1</i>	NM_012317	953.41	1959.60	0.49
203909_at	<i>SLC9A6</i>	NM_006359	35.79	73.82	0.48
222158_s_at	<i>C1orf121</i>	NM_016076	14.79	30.54	0.48
208801_at	<i>SRP72</i>	NM_006947	57.96	119.73	0.48
49452_at	<i>ACACB</i>	NM_001093	29.49	60.95	0.48
200994_at	<i>IPO7</i>	NM_006391	39.24	81.14	0.48
203247_s_at	<i>ZNF24</i>	NM_006965	12.43	25.73	0.48
203446_s_at	<i>OCRL</i>	NM_000276 / NM_001587	51.08	105.81	0.48
201828_x_at	<i>CXX1</i>	NM_003928	1810.05	3750.20	0.48
219503_s_at	<i>TMEM40</i>	NM_018306	20.04	41.54	0.48
219628_at	<i>WIG1</i>	NM_022470 / NM_152240	26.58	55.17	0.48
218042_at	<i>COPS4</i>	NM_016129	19.22	39.94	0.48
202854_at	<i>HPRT1</i>	NM_000194	409.07	851.08	0.48
209565_at	<i>RNF113A</i>	NM_006978	158.91	330.99	0.48
201904_s_at	<i>CTDSPL</i>	NM_001008392 / NM_005808	167.47	349.18	0.48
205483_s_at	<i>ISG15</i>	NM_005101	469.58	979.50	0.48
204897_at	<i>PTGER4</i>	NM_000958	15.27	31.87	0.48
204014_at	<i>DUSP4</i>	NM_001394 / NM_057158	78.05	162.95	0.48
221514_at	<i>UTP14A</i>	NM_006649	156.08	326.84	0.48
203007_x_at	<i>LYPLA1</i>	NM_006330	48.47	101.55	0.48
213883_s_at	<i>TM2D1</i>	NM_032027	46.96	98.40	0.48
201921_at	<i>GNG10</i>	NM_001017998 / NM_004125 / XM_929619 / XM_940579	368.56	775.54	0.48
207847_s_at	<i>MUC1</i>	NM_001018016 / NM_001018017 / NM_001018021 / NM_002456	41.04	86.42	0.47
203108_at	<i>GPRC5A</i>	NM_003979	208.08	438.12	0.47
213587_s_at	<i>ATP6V0E2L</i>	NM_145230	25.27	53.41	0.47
218952_at	<i>PCSKIN</i>	NM_013271	169.94	359.28	0.47
221931_s_at	<i>SEHIL</i>	NM_001013437 / NM_031216	43.80	92.68	0.47



221989_at	<i>RPL10</i>	NM_006013 / XM_209178 / XM_209500 / XM_371781 / XM_497357 / XM_926723 / XM_929431 / XM_930080 / XM_931512 / XM_931519 / XM_931525 / XM_931532 / XM_931535 / XM_934704 / XM_934705 / XM_934706 / XM_937850 / XM_939745 / XM_941543 / XM_941661 / XM_942217 / XM_944311 / XM_944319 / XM_944324 / XM_945797 / XM_945798 / XM_945799 / XM_945800	4.90	10.38	0.47
205145_s_at	<i>MYL5</i>	NM_002477 / XM_938923	12.55	26.56	0.47
201238_s_at	<i>CAPZA2</i>	NM_006136	89.77	191.02	0.47
210645_s_at	<i>TTC3</i>	NM_001001894 / NM_003316	24.14	51.41	0.47
210136_at	<i>MBP</i>	NM_001025081 / NM_001025090 / NM_001025092 / NM_001025094 / NM_001025098 / NM_001025100 / NM_001025101 / NM_002385	8.49	18.08	0.47
201358_s_at	<i>COPB</i>	NM_016451	142.12	304.25	0.47
210511_s_at	<i>INHBA</i>	NM_002192	129.36	276.98	0.47
201888_s_at	<i>IL13RA1</i>	NM_001560	23.61	50.66	0.47
209115_at	<i>UBE1C</i>	NM_003968 / NM_198195 / NM_198197	27.53	59.10	0.47
217739_s_at	<i>PBEF1</i>	NM_005746 / NM_182790 / XM_929247	30.38	65.23	0.47
213361_at	<i>TDRD7</i>	NM_014290	8.68	18.65	0.47
210663_s_at	<i>KYNU</i>	NM_001032998 / NM_003937	104.25	224.59	0.46
204698_at	<i>ISG20</i>	NM_002201	383.20	826.64	0.46
204415_at	<i>IFI6</i>	NM_002038 / NM_022872 / NM_022873	34.19	73.79	0.46

218053_at	<i>PRPF40A</i>	XM_371575 / XM_931099 / XM_938514 / XM_943711	61.31	132.43	0.46
207719_x_at	<i>CEP170</i>	NM_014812	10.04	21.69	0.46
206295_at	<i>IL18</i>	NM_001562	86.99	188.27	0.46
33304_at	<i>ISG20</i>	NM_002201	222.58	482.12	0.46
214112_s_at	<i>CXorf40A</i>	NM_001013845 / NM_178124	219.43	479.14	0.46
205315_s_at	<i>SNTB2</i>	NM_006750 / NM_130845	40.07	87.78	0.46
217948_at	---	---	322.08	706.40	0.46
214022_s_at	<i>IFITM1</i>	NM_003641	1869.34	4135.74	0.45
211122_s_at	<i>CXCL11</i>	NM_005409	5.81	12.87	0.45
212510_at	<i>GPD1L</i>	NM_015141	10.17	22.53	0.45
205595_at	<i>DSG3</i>	NM_001944	80.07	177.64	0.45
202923_s_at	<i>GCLC</i>	NM_001498	75.00	167.13	0.45
202169_s_at	<i>AASDHPPT</i>	NM_015423	11.33	25.30	0.45
202351_at	<i>ITGAV</i>	NM_002210	228.62	510.51	0.45
219356_s_at	<i>CHMP5</i>	NM_016410	108.75	242.88	0.45
201864_at	<i>GDII</i>	NM_001493	160.21	358.31	0.45
222266_at	<i>C19orf2</i>	NM_003796 / NM_134447	11.46	25.69	0.45
204020_at	<i>PURA</i>	NM_005859	89.35	200.32	0.45
218086_at	<i>NPDC1</i>	NM_015392	147.25	330.55	0.45
209028_s_at	<i>ABII</i>	NM_001012750 / NM_001012751 / NM_001012752 / NM_005470	48.80	109.59	0.45
218237_s_at	<i>SLC38A1</i>	NM_030674	269.77	608.07	0.44
202437_s_at	<i>CYP11B1</i>	NM_000104	27.81	62.70	0.44
213016_at	---	---	15.13	34.12	0.44
201996_s_at	<i>SPEN</i>	NM_015001	32.11	72.47	0.44
217388_s_at	<i>KYNU</i>	NM_001032998 / NM_003937	280.28	634.02	0.44
212640_at	<i>PTPLB</i>	NM_198402	202.85	459.88	0.44
219010_at	<i>C1orf106</i>	NM_018265	257.64	585.64	0.44
219351_at	<i>TRAPPC2</i>	NM_001011658 / NM_014563	31.50	71.62	0.44
213083_at	<i>SLC35D2</i>	NM_007001	103.19	234.84	0.44
218163_at	<i>MCTS1</i>	NM_014060	228.29	521.74	0.44
207941_s_at	<i>RNPC2</i>	NM_004902 / NM_184234 / NM_184237 / NM_184241 / NM_184244	34.40	78.71	0.44
214722_at	<i>NOTCH2NL</i>	NM_203458	69.57	159.38	0.44
209726_at	<i>CA11</i>	NM_001217	45.82	105.08	0.44
203917_at	<i>CXADR</i>	NM_001338	31.01	71.25	0.44
38043_at	<i>FAM3A</i>	NM_021806	29.77	68.61	0.43
218986_s_at	<i>FLJ20035</i>	NM_017631	12.73	29.34	0.43
222242_s_at	<i>KLK5</i>	NM_012427	11.35	26.38	0.43
53991_at	<i>DENND2A</i>	NM_015689	8.82	20.60	0.43
209289_at	<i>NFIB</i>	NM_005596	27.75	64.90	0.43
201540_at	<i>FHL1</i>	NM_001449	451.06	1059.88	0.43

204097_s_at	<i>RBMX2</i>	NM_016024	9.32	21.99	0.42
202602_s_at	<i>HTATSF1</i>	NM_014500	33.73	79.70	0.42
204981_at	<i>SLC22A18</i>	NM_002555 / NM_183233	86.64	205.14	0.42
200696_s_at	<i>GSN</i>	NM_000177 / NM_198252	385.91	914.82	0.42
221841_s_at	<i>KLF4</i>	NM_004235	111.47	264.55	0.42
205709_s_at	<i>CDS1</i>	NM_001263	18.03	42.93	0.42
216942_s_at	<i>CD58</i>	NM_001779	14.54	34.65	0.42
213294_at	---	---	7.66	18.29	0.42
212415_at	<i>SEPT6</i>	NM_015129 / NM_145799 / NM_145800 / NM_145802	4.62	11.03	0.42
212616_at	<i>CHD9</i>	NM_025134	7.23	17.34	0.42
217947_at	<i>CMTM6</i>	NM_017801	206.54	498.31	0.41
211612_s_at	<i>IL13RA1</i>	NM_001560	43.45	104.96	0.41
212531_at	<i>LCN2</i>	NM_005564	174.02	420.45	0.41
201661_s_at	<i>ACSL3</i>	NM_004457 / NM_203372	10.17	24.61	0.41
213729_at	<i>PRPF40A</i>	XM_371575 / XM_931099 / XM_938514 / XM_943711	6.42	15.54	0.41
205220_at	<i>GPR109B</i>	NM_006018	266.95	645.95	0.41
203186_s_at	<i>S100A4</i>	NM_002961 / NM_019554	94.02	227.62	0.41
203821_at	<i>HBEGF</i>	NM_001945	403.66	977.38	0.41
221766_s_at	<i>FAM46A</i>	NM_017633	10.35	25.10	0.41
215813_s_at	<i>PTGS1</i>	NM_000962 / NM_080591	31.23	76.88	0.41
202277_at	<i>SPTLC1</i>	NM_006415 / NM_178324	44.77	110.99	0.40
202829_s_at	<i>SYBL1</i>	NM_005638	15.37	38.13	0.40
201887_at	<i>IL13RA1</i>	NM_001560	37.84	93.97	0.40
216095_x_a t	<i>MTMR1</i>	NM_003828	128.02	318.26	0.40
217813_s_at	<i>SPIN</i>	NM_006717	23.85	59.32	0.40
205428_s_at	<i>CALB2</i>	NM_001740 / NM_007087 / NM_007088	57.31	143.13	0.40
204343_at	<i>ABCA3</i>	NM_001089	15.33	38.38	0.40
38037_at	<i>HBEGF</i>	NM_001945	144.05	361.24	0.40
209194_at	<i>CETN2</i>	NM_004344	74.08	187.44	0.40
202371_at	<i>TCEAL4</i>	NM_001006935 / NM_001006936 / NM_001006937 / NM_024863	105.84	269.43	0.39
206645_s_at	<i>NR0B1</i>	NM_000475	42.07	107.59	0.39
221829_s_at	<i>TNPO1</i>	NM_002270 / NM_153188	83.30	213.54	0.39
219045_at	<i>RHOF</i>	NM_019034	210.67	540.25	0.39

211343_s_at	<i>COL13A1</i>	NM_005203 / NM_080798 / NM_080799 / NM_080800 / NM_080801 / NM_080802 / NM_080803 / NM_080804 / NM_080805 / NM_080806 / NM_080807 / NM_080808 / NM_080809 / NM_080810 / NM_080811 / NM_080812 / NM_080813 / NM_080814 / NM_080815	34.51	88.75	0.39
205900_at	<i>KRT1</i>	NM_006121	37.24	95.82	0.39
203156_at	<i>AKAP11</i>	NM_016248 / NM_144490	8.20	21.24	0.39
215245_x_at	<i>FMR1</i>	NM_002024	30.13	78.43	0.38
201215_at	<i>PLS3</i>	NM_005032	155.28	411.68	0.38
221553_at	<i>RP11- 217H1.1</i>	NM_032121 / XM_927839	34.17	90.64	0.38
203042_at	<i>LAMP2</i>	NM_002294 / NM_013995	237.56	638.66	0.37
201132_at	<i>HNRPH2</i>	NM_001032393 / NM_019597	52.45	143.04	0.37
221581_s_at	<i>LAT2</i>	NM_014146 / NM_022040 / NM_032463	59.56	163.24	0.36
201865_x_at	<i>NR3C1</i>	NM_000176 / NM_001018074 / NM_001018075 / NM_001018076 / NM_001018077 / NM_001020825 / NM_001024094	120.48	332.55	0.36
213593_s_at	<i>TRA2A</i>	NM_013293	12.37	34.25	0.36
210367_s_at	<i>PTGES</i>	NM_004878	88.52	246.35	0.36
212007_at	<i>UBXD2</i>	NM_014607	41.95	117.00	0.36
205767_at	<i>EREG</i>	NM_001432	65.08	183.71	0.35
200914_x_at	<i>KTN1</i>	NM_182926	118.02	343.43	0.34
210387_at	<i>HIST1H2BG</i>	NM_003518	198.74	579.17	0.34
202378_s_at	<i>LEPROT</i>	NM_017526	78.41	228.55	0.34
203780_at	<i>EVA1</i>	NM_005797 / NM_144765	45.59	133.29	0.34
202435_s_at	<i>CYP11B1</i>	NM_000104	15.25	44.59	0.34
221844_x_at	---	---	32.98	96.74	0.34
212622_at	<i>TMEM41B</i>	NM_015012	8.86	26.02	0.34
201472_at	<i>VBPI</i>	NM_003372	54.92	161.81	0.34
203303_at	<i>DYNLT3</i>	NM_006520	15.03	44.35	0.34

204533_at	<i>CXCL10</i>	NM_001565	8.07	24.04	0.34
212605_s_at	---	---	13.86	41.36	0.34
214718_at	<i>GATAD1</i>	NM_021167	11.00	33.09	0.33
209022_at	<i>STAG2</i>	NM_006603	7.90	24.13	0.33
205623_at	<i>ALDH3A1</i>	NM_000691	24.99	77.90	0.32
219956_at	<i>GALNT6</i>	NM_007210	47.43	147.85	0.32
205128_x_at	<i>PTGS1</i>	NM_000962 / NM_080591	39.76	125.00	0.32
202376_at	<i>SERPINA3</i>	NM_001085	62.35	196.67	0.32
213229_at	<i>DICER1</i>	NM_030621 / NM_177438	146.36	464.53	0.32
212223_at	<i>IDS</i>	NM_000202 / NM_006123	58.68	186.65	0.31
204584_at	<i>LICAM</i>	NM_000425 / NM_024003	102.94	327.45	0.31
219995_s_at	<i>FLJ13841</i>	NM_024702	245.82	795.33	0.31
219001_s_at	<i>WDR32</i>	NM_024345	8.09	26.25	0.31
208241_at	<i>NRG1</i>	NM_004495 / NM_013956 / NM_013957 / NM_013958 / NM_013959 / NM_013960 / NM_013961 / NM_013962 / NM_013964	5.57	18.19	0.31
211671_s_at	<i>NR3C1</i>	NM_000176 / NM_001018074 / NM_001018075 / NM_001018076 / NM_001018077 / NM_001020825 / NM_001024094	78.44	263.10	0.30
204602_at	<i>DKK1</i>	NM_012242	76.05	259.47	0.29
213135_at	<i>TIAM1</i>	NM_003253	7.06	24.42	0.29
204881_s_at	<i>UGCG</i>	NM_003358	34.89	120.86	0.29
206342_x_at	<i>IDS</i>	NM_000202 / NM_006123	77.09	267.58	0.29
218085_at	<i>CHMP5</i>	NM_016410	23.89	84.03	0.28
212414_s_at	<i>SEPT6</i>	NM_015129 / NM_032569 / NM_145799 / NM_145800 / NM_145802	19.17	68.28	0.28
215206_at	<i>EXT1</i>	NM_000127	29.69	106.70	0.28
205097_at	<i>SLC26A2</i>	NM_000112	23.64	85.76	0.28
204976_s_at	<i>AMMECR1</i>	NM_001025580 / NM_015365	9.92	36.28	0.27
204351_at	<i>S100P</i>	NM_005980	48.68	180.28	0.27
217975_at	<i>WBP5</i>	NM_001006612 / NM_001006613 / NM_001006614 / NM_016303	108.30	441.28	0.25
205363_at	<i>BBOX1</i>	NM_003986	29.13	120.76	0.24
209792_s_at	<i>KLK10</i>	NM_002776 / NM_145888	120.93	505.96	0.24

202439_s_at	<i>IDS</i>	NM_000202 / NM_006123	64.34	270.52	0.24
212221_x_at	<i>IDS</i>	NM_000202 / NM_006123	133.36	571.11	0.23
200821_at	<i>LAMP2</i>	NM_002294 / NM_013995	81.15	347.91	0.23
201917_s_at	<i>SLC25A36</i>	NM_018155	6.22	28.72	0.22
205569_at	<i>LAMP3</i>	NM_014398	13.64	64.51	0.21
204750_s_at	<i>DSC2</i>	NM_004949 / NM_024422	33.27	159.80	0.21
218668_s_at	<i>RAP2C</i>	NM_021183	11.22	54.25	0.21
205809_s_at	<i>WASL</i>	NM_003941	15.28	77.44	0.20
201007_at	<i>HADHB</i>	NM_000183	1389.06	7136.54	0.19
203453_at	<i>SCNN1A</i>	NM_001038	14.92	142.26	0.10
202411_at	<i>IFI27</i>	NM_005532	13.86	155.11	0.09

## [0145] Example 2

[0146] This example demonstrates that N-CoR2 and HDAC3 expression is prognostic of the clinical outcome in breast cancer patients.

5 [0147] The transcriptional expression levels of N-CoR2, HDAC3, and associated clinical information, including therapeutic outcome and survival, were obtained from several publicly available tumor transcriptome data sets, including 295 patients with primary breast carcinomas (N. Engl. J. Med. 347:1999-2009 (2002)), 50 patients with malignant gliomas (Cancer Res. 63:1602-1607 (2003)), and 60 patients with ovarian carcinomas (J. Clin. Oncol. 10 22:4700-4710 (2004)). The patient survival data from the ovarian cancer data set was provided by D. Spentzos (Beth Israel Deaconess Medical Center and Harvard Medical School, Boston, MA). We searched the probe hybridization ratio (for two-color cDNA arrays) or the probe signal intensity (for Affymetrix arrays) of N-CoR2 (*NCOR2*) and HDAC3 (*HDAC3*) in each data set. If *NCOR2* was represented by more than one probe set, 15 the one that displayed the highest hybridization intensity in respective array platforms (*e.g.*, 207760\_s\_at in Affymetrix HG-U133A 2.0 array; 39358\_at in Affymetrix HG-U95 array; IMAGE:80772 for cDNA array) were chosen for the analysis.

[0148] The patients were grouped into quartiles based on the relative (untransformed) expression levels of N-CoR2 or HDAC3 in respective data sets. For the breast cancer data 20 sets, patients were stratified according to their lymph node (LN), positive or negative, and chemotherapy (CT) status. The probability of remaining relapse-free or overall survival was computed using the method of Kaplan and Meier(reference). The curves were plotted and compared using the log-rank test with the software packages SPSS 15.0 (SPSS Inc.) and

GraphPad Prism 3.02 (GraphPad Software). The log-rank test was used to calculate the *P* values. Multivariate analysis of survival with the use of the Cox proportional hazard method was performed with the software package SPSS 15.0 (SPSS Inc.).

[0149] In **Figure 1**, a 295 breast cancer patient database from the Netherlands Cancer Institute (N. Engl. J. Med. 347:1999-2009 (2002)) was divided into the following three groups according to the expression quartiles of N-CoR2: (1) upper quartile, (2) Interquartile range, and (3) lower quartile. The probability of remaining free of post-therapeutic disease relapse (**Figure. 1A**) or overall survival (**Figure 1B**) was plotted over a 20-year period of follow-up. The Kaplan-Meier curves shows that patients with the expression levels of N-CoR2 in the upper quartile had significantly higher probability of post-therapeutic disease relapse and mortality than those with expression levels in the lower quartile. The association of N-CoR2 with clinical outcomes was most prominent and significant in patients with LN-positive disease and those who had received adjuvant systemic CT.

[0150] **Figure 2** shows a similar analysis of the clinical outcome of the 295 breast cancer patients in the Netherlands Cancer Institute database with respect to the expression quartiles of HDAC3. Similar to N-CoR2, the patients with the expression levels of HDAC3 in the upper quartile had significantly higher probability of post-therapeutic disease relapse (**Figure 2A**) and mortality (**Figure 2B**) than those with expression levels in the lower quartile, and the association was most prominent and significant in patients with LN-positive disease and those who had received adjuvant systemic CT.

[0151] **Figure 3** shows a similar analysis of the clinical outcome of the 295 breast cancer patients of the Netherlands Cancer Institute database according to whether their expression levels of N-CoR2 and HDAC3 both fall in respective upper or lower quartiles. In patients with LN-positive disease or those who had received adjuvant systemic CT, those with expression levels of both N-CoR2 and HDAC3 in the upper quartiles had remarkably high probabilities of relapse (**Figure 3A**) and mortality (**Figure 3B**) and around two-thirds of the patients developed disease progression within 5 years. In contrast, the patients expression levels of both N-CoR2 and HDAC3 in the lower quartiles had a low probability of disease relapse or mortality.

[0152] Table 2 shows a multivariate Cox proportional-hazards analysis on the association of the expression levels of N-CoR2 and HDAC3 with clinical outcome of the 295 breast cancer patients from the Netherlands Cancer Institute database who were stratified according

to clinical characteristics including age, tumor size, LN and ER status, histological grade, molecular subtypes (Proc. Natl. Acad. Sci. USA 100:8418-8423 (2003)), and CT status. N-CoR2 but not HDAC3 was an independent predictive factor of the relapse-free and overall survival. The association between N-CoR2 expression and death or relapse was independent of age, tumor size and differentiation. Of all the independent predictive factors, N-CoR2 was the strongest predictor of the likelihood of disease relapse and mortality, with a hazard ratio of 1.96 ( $P = 0.007$ ) and 1.87 ( $P = 0.005$ ), respectively.

Table 2. Multivariable Cox proportional-hazards analysis on the association of the expression levels of N-CoR2 and HDAC3 with clinical outcome of the 295 breast cancer patients from the Netherlands Cancer Institute database who were stratified according to clinical characteristics including age, tumor size, LN and ER status, histological grade, molecular subtypes, and CT status.

Variable	Death		Relapse	
	Hazard Ratio (95% CI)	P Value	Hazard Ratio (95% CI)	P Value
N-CoR2	1.96 (1.2-3.18)	0.007	1.87 (1.21-2.9)	0.005
HDAC3	1.56 (0.76-3.19)	0.221	0.99 (0.5-1.95)	0.97
Age (per 10-yr increment)	0.7 (0.47-1.05)	0.087	0.6 (0.42-0.85)	0.005
Tumor size (per cm)	1.26 (0.98-1.63)	0.07	1.26 (1.00-1.57)	0.047
Tumor grade		0.011		0.017
Grade 2 vs. grade 1	3.94 (1.35-11.47)		2.24 (1.12-4.48)	
Grade 3 vs. grade 1	5.18 (1.77-15.14)		2.81 (1.38-5.7)	
Positive LN status vs. negative status	1.5 (0.75-2.97)	0.249	1.56 (0.86-2.85)	0.146
Positive ER status vs. negative status	0.66 (0.33-1.31)	0.232	0.97 (0.52-1.82)	0.927
Chemotherapy vs. no chemotherapy	0.59 (0.29-1.23)	0.16	0.54 (0.29-1.02)	0.056
Hormonal treatment vs. no treatment	0.83 (0.34-2.06)	0.693	0.7 (0.32-1.53)	0.372
Mastectomy vs. breast-conserving therapy	0.97 (0.6-1.57)	0.886	0.9 (0.59-1.38)	0.628
Molecular subtype		0.075		0.182
Normal-like & luminal B vs. luminal A	1.72 (0.81-3.66)		1.47 (0.82-2.62)	
Basal & ERBB2+ vs. luminal A	2.74 (1.15-6.53)		1.92 (0.96-3.85)	

**[0153]** Table 3 shows a multivariate Cox proportional-hazards analysis on the association of the expression levels of N-CoR2 and HDAC3 with clinical outcome of the 110 breast cancer patients who had received adjuvant (postoperative) systemic CT identified from the 293 breast cancer patients of the Netherlands Cancer Institute database. The patients were stratified according to age, tumor size, LN and ER status, histological grade and molecular subtypes. In this subgroup of the patients, both N-CoR2 and HDAC3 were independent predictive factors of the risk of mortality, while only N-CoR2 was independently associated with death and relapse ( $P < 0.001$ ). Compared with clinical characteristics and molecular classification of breast cancers, N-CoR2 was the strongest predictor of the likelihood of



disease relapse and mortality with hazard ratios of 9.64 ( $P < 0.001$ ) and 5.45 ( $P < 0.001$ ), respectively.

Table 3. Multivariate Cox proportional-hazards analysis on the association of the expression levels of N-CoR2 and HDAC3 with clinical outcome of the 110 breast cancer patients who had received adjuvant (postoperative) systemic CT.

Variable	Death		Relapse	
	Hazard Ratio (95% CI)	P Value	Hazard Ratio (95% CI)	P Value
N-CoR2	9.64 (3.27-28.43)	<0.001	5.45 (2.31-12.85)	<0.001
HDAC3	6.67 (1.67-26.65)	0.007	1.89 (0.5-7.11)	0.348
Age (per 10-yr increment)	0.57 (0.24-1.35)	0.199	0.69 (0.38-1.41)	0.305
Tumor size (per cm)	1.60 (1.0-2.57)	0.05	1.43 (0.97-1.21)	0.068
Tumor grade		0.12		0.18
Grade 2 vs. grade 1	1.82 (0.33-9.96)		1.2 (0.38-3.76)	
Grade 3 vs. grade 1	4.3 (0.84-22.11)		2.45 (0.79-7.58)	
Positive LN status vs. negative status	0.46 (0.09-2.28)	0.339	0.85 (0.19-3.87)	0.831
Positive ER status vs. negative status	0.09 (0.02-0.41)	0.002	0.23 (0.06-0.85)	0.027
Hormonal treatment vs. no treatment	0.24 (0.03-1.91)	0.176	0.53 (0.16-1.82)	0.315
Mastectomy vs. breast-conserving therapy	0.81 (0.32-2.04)	0.653	0.81 (0.38-1.75)	0.591
Molecular subtype		0.314		0.53
Normal-like & luminal B vs. luminal A	3.77 (0.63-22.64)		1.59 (0.51-4.95)	
Basal & ERBB2+ vs. luminal A	1.93 (0.3-12.41)		0.88 (0.22-3.58)	

**[0154]** Table 4 shows a multivariate Cox proportional-hazards analysis on the association of the expression levels of N-CoR2 and HDAC3 with clinical outcome of the 185 breast cancer patients who did not received adjuvant (postoperative) systemic CT identified from the 293 breast cancer patients of the Netherlands Cancer Institute database. Unlike the patients who had received adjuvant systemic CT, the molecular subtypes of breast cancers was the strongest predictor of the risk of death ( $P = 0.005$ ) and disease relapse ( $P = 0.025$ ) in the patients who did not receive adjuvant CT, whereas neither N-CoR2 nor HDAC3 was independent predictive factor of clinical outcome in this subgroup of the patients.

Table 4. Multivariate Cox proportional-hazards analysis on the association of the expression levels of N-CoR2 and HDAC3 with clinical outcome of the 185 breast cancer patients who did not received adjuvant (postoperative) systemic CT.

Variable	Death		Relapse	
	Hazard Ratio (95% CI)	P Value	Hazard Ratio (95% CI)	P Value
N-CoR2	1.12 (0.54-2.31)	0.761	1.25 (0.69-2.28)	0.46
HDAC3	1.15 (0.46-2.88)	0.761	0.92 (0.39-2.15)	0.841
Age (per 10-yr increment)	0.71 (0.44-1.16)	0.177	0.58 (0.38-0.91)	0.018
Tumor size (per cm)	1.35 (0.94-1.85)	0.115	1.21 (0.89-1.65)	0.22
Tumor grade		0.057		0.047
Grade 2 vs. grade 1	5.28 (1.18-23.55)		2.81 (1.1-7.15)	
Grade 3 vs. grade 1	6.25 (1.4-28.0)		3.35 (1.27-8.83)	

Positive LN status vs. negative status	1.48 (0.69-3.15)	0.316	1.62 (0.84-3.12)	0.147
Positive ER status vs. negative status	1.48 (0.62-3.55)	0.375	1.87 (0.85-4.12)	0.123
Hormonal treatment vs. no treatment	1.16 (0.37-3.62)	0.8	0.75 (0.25-2.23)	0.604
Mastectomy vs. breast-conserving therapy	1.48 (0.81-2.71)	0.201	1.61 (0.93-2.78)	0.088
Molecular subtype		0.005		0.025
Normal-like & luminal B vs. luminal A	1.88 (0.76-4.64)		1.45 (0.71-2.95)	
Basal & ERBB2+ vs. luminal A	5.65 (1.93-16.52)		3.2 (1.35-7.55)	

[0155] In **Figure 4**, 50 patients with malignant gliomas (Cancer Res. 63:1602-1607 (2003)) (**Figure 4A**) and 60 patients with ovarian cancers (J. Clin. Oncol. 22:4700-4710 (2004)) (**Figure 4B**) were divided into quartiles according to their expression levels of N-CoR2 and/or HDAC3, respectively. Kaplan Meier survival analysis shows that higher N-CoR2 and/or HDAC3 expressions were associated with higher probability of mortality in both types of human malignancies. Tumors stratified according to their expression levels of N-CoR2 and HDAC3 displayed trends of mortality similar to those stratified using the expression levels of N-CoR2 or HDAC3 alone, suggesting that N-CoR2 and HDAC3 may play synergistic roles in mediating unfavorable clinical outcome in human malignancies.

#### [0156] Example 3

[0157] This example demonstrates that biomarkers associated with N-CoR2 are prognostic markers for the response to preoperative combinational chemotherapy in breast cancers.

[0158] To further show that the N-CoR2 signature genes are associated with increased resistance to systemic chemotherapy independent of other therapeutic interventions, the tumor transcriptome from a cohort of 133 breast cancer patients who received pre-operative (neoadjuvant) combination chemotherapy, including paclitaxel and fluorouracil-doxorubicin-cyclophosphamide, wherein the treatment responses were pathologically defined (J. Clin. Oncol. 24:4236-4244 (2006)), were analyzed. Gene expression profiles of the pre-treatment breast cancer tissues from the 133 breast cancer patients were provided by Professor L. Pusztai (University of Texas M.D. Anderson Cancer Center, Houston, TX). The patients who did not have residual cancer cells in the breast by pathological examinations following chemotherapy were considered as having clinically beneficial responses (*i.e.*, “responders”) and those having residual cancer cells in the breast as “non-responders”. Three patients without available information on the post-treatment breast pathological data from the original data set were excluded, leaving a total of 130 cases for the analysis.

**[0159]** The 304 N-CoR2 signature genes (represented by 350 Affymetrix probe sets) were identified based on their expression levels (on a  $\log_2$  base) significantly different (fold change  $\geq 2$  and a cutoff  $P$ -value  $< 0.05$  by Student's  $t$  test) between T4-2 vector cells and T4-2 N-CoR2 cells as shown in Example 1. These genes were extracted from the gene expression profiles of the 130 patients and their respective probe signal intensity data were median-centered. Average linkage clustering was carried out using the Cluster and TreeView software (Proc. Natl. Acad. Sci. USA 95:14863-14868 (1998)).

**[0160]** We further determined whether expression profiles of genes altered by N-CoR2 in 3D tissue cultures would recapitulate the expression profiles of N-CoR2-regulated genes in tumors, which could be quantified by measuring their similarities to each other. We measured the degree of resemblance between the average expression levels (on a  $\log_2$  scale) of the 304 N-CoR2 signature genes (350 probe sets) in T4-2 vector cells or T4-2 N-CoR2 cells and the levels of the corresponding genes in the tumor transcriptome data sets using Spearman's rank correlation ( $\rho$ ). We computed the correlations based on transcript abundance rank order of the 350 probe sets instead of their absolute expression levels. We then determined the relative similarities of the expression profiles of the 350 probe sets from the 130 breast tumors with those in T4-2 N-CoR2 cells and T4-2 vectors cells, respectively, by comparing their Spearman's  $\rho$ , which was designated as a "N-CoR2 similarity score ( $S_{NCOR2}$ )",  $S_{NCOR2} = \rho_{NCOR2}^2 \times \rho_{vector}^{-2}$ , where  $\rho_{NCOR2}$  represents the Spearman's correlation coefficient between the expression profile of the 350 probe sets in a given tumor sample and those in T4-2 N-CoR2 cells, and  $\rho_{vector}$  is the coefficient between those in the tumor and in T4-2 vector cells. Tumors with higher  $S_{NCOR2}$  are considered to have higher N-CoR2 associated transcriptional activities.

**[0161]** As shown in Table 5, the breast tumors with higher expression levels of N-CoR2 had an increase in the odds (2.2-fold) of unresponsiveness to pre-operative CT compared with those with lower expression levels. This finding was statistically significant,  $p = 0.029$ .

Table 5. Results from the analysis of N-CoR2 expression in a cohort of 130 patients with breast cancer.

Predictor	Group	Responder (%)	Non-responder (%)	Odds ratio (95% Confidence Interval)	P value
N-CoR2	High	15 (23.1)	50 (76.9)	2.2 (1.0 - 4.8)	0.029*
	Low	26 (40)	39 (60)	1	

\*P values were calculated with use of Fisher's exact test.

**[0162]** In **Figure 5**, a hierarchical clustering analysis on the 304 N-CoR2 signature genes (represented by 350 Affymetrix probe sets) segregated the 130 breast carcinomas into two predominant subgroups (subgroup A and subgroup B) based on the first bifurcation in the dendrogram. Table 6 shows that the breast tumors that were allocated in subgroup A by average linkage clustering analysis had a 3.5-fold increase in the odds ratio of unresponsiveness (*i.e.*, nonresponders) to pre-operative systemic CT than those allocated in subgroup B.

Table 6. Results from the analysis of the transcriptional expression of 304 N-CoR2 signature genes in a cohort of 130 patients with breast cancer.

Predictor	Group	Responder (%)	Non-responder (%)	Odds ratio (95% Confidence Interval)	P value
Average Lineage Clustering	Subgroup A	13 (19.1)	55 (80.9)	3.5 (1.6 - 7.6)	0.001*
	Subgroup B	28 (45.2)	34 (54.8)	1	

\*P values were calculated with use of Fisher's exact test.

**[0163]** In **Figure 6**  $S_{NCOR2}$  was used as a measure of the N-CoR2-associated transcriptional activities in breast cancer cells. Patients were separated into two groups according to the median value of  $S_{NCOR2}$  across all tumors. The tumors with higher  $S_{NCOR2}$  values had higher correlations ( $\rho_{NCOR2}$ ) with respect to the expression of the 304 N-CoR2 associated genes with T4-2 N-CoR2 cells and lower correlations with T4-2 vector cells ( $\rho_{vector}$ ). Consistent with this, the tumors with lower  $S_{NCOR2}$  values had lower correlations with respect to the expression of the 304 N-CoR signature genes with T4-2 N-CoR2 cells and higher correlations with T4-2 vector cells.

**[0164]** As shown in Table 7, the breast tumors with higher  $S_{NCOR2}$  values had a 5-fold higher odds ratio of unresponsiveness to chemotherapy compared with those with lower  $S_{NCOR2}$  values ( $p = <0.001$ ).

Table 7.  $S_{NCOR2}$  analysis of the transcriptional profile of 304 N-CoR2 signature genes in a cohort of 130 patients with breast cancer.

Predictor	Group	Responder (%)	Non-responder (%)	Odds ratio (95% Confidence Interval)	P value
$S_{NCOR2}$	High	10 (15.4)	55 (84.6)	5.0 (2.2 - 11.5)	< 0.001*
	Low	31 (47.7)	34 (52.3)	1	

\*P values were calculated with use of Fisher's exact test.

**[0165]** As shown in Table 8, the likelihood of unresponsiveness to pre-operative CT of the 130 breast cancer patients of the M.D. Anderson Cancer Center database was analyzed using

a logistic regression model including age, tumor size, nuclear grade, LN, ER and HER2 status as predictors. Of all the clinical characteristics, only ER status ( $P = 0.003$ ) and age ( $P = 0.037$ ) are significantly predictors. Patient stratification by hierarchical clustering analysis on the N-CoR2 signature genes was also an independent predictor of the likelihood of resistance to pre-operative CT with an odds ratio of 2.71 ( $P = 0.038$ ). In Table 9, a similar logistic regression model including  $S_{NCOR2}$  and clinical characteristics of the patients shows that  $S_{NCOR2}$  also independently provides a strong prognostic measure of the likelihood of unresponsiveness to pre-operative CT (Odds ratio 3.85;  $P = 0.005$ ). Moreover, as shown in Table 10, when all the three predictors (N-CoR2 expression, hierarchical clustering and  $S_{NCOR2}$ ) were included in the logistic regression model,  $S_{NCOR2}$  remained an independent predictor of chemotherapy resistance with an odds ratio of 3.26 ( $P = 0.03$ ).

Table 8. Analysis of prognostic methods in a cohort of 130 breast cancer patients.

Variable	Odds Ratio (95% Confidence Interval)	P value
Hierarchical clustering based on N-CoR2 signature (subgroup A vs. subgroup B)	2.71 (1.06-6.96)	0.038
Age (per 10-yr increment)	1.60 (1.00-1.01)	0.037
Tumor size ( $\geq 5$ cm vs. $< 5$ cm)	1.71 (0.64-4.54)	0.284
Tumor grade ( $\geq$ grade 3 vs. $<$ grade 3)	1.23 (0.42-3.63)	0.71
Positive LN status vs. negative status	0.37 (0.13-1.05)	0.061
Positive ER status vs. negative status	4.46 (1.66-12.01)	0.003
Positive HER2 vs. negative HER2	0.49 (0.18-1.33)	0.162

Table 9. Analysis of prognostic methods in a cohort of 130 breast cancer patients.

Variable	Odds Ratio (95% Confidence Interval)	P value
High $S_{NCOR2}$ vs. low $S_{NCOR2}$	3.85 (1.5-9.89)	0.005
Age (per 10-yr increment)	1.60 (1.00-1.1)	0.047
Tumor size ( $\geq 5$ cm vs. $< 5$ cm)	1.86 (0.68-5.11)	0.227
Tumor grade ( $\geq$ grade 3 vs. $<$ grade 3)	1.19 (0.40-3.53)	0.754
Positive LN status vs. negative status	0.39 (0.14-1.13)	0.084
Positive ER status vs. negative status	4.68 (1.73-12.65)	0.002
Positive HER2 vs. negative HER2	0.45 (0.16-1.25)	0.127

Table 10. Analysis of prognostic methods in a cohort of 130 breast cancer patients.

Variable	Odds Ratio (95% Confidence Interval)	P value
N-CoR2	1.48 (0.58-3.83)	0.414
Hierarchical clustering based on N-CoR2 signature (subgroup A vs. subgroup B)	1.41 (0.46-4.27)	0.547
High $S_{NCOR2}$ vs. low $S_{NCOR2}$	3.26 (1.12-9.49)	0.03
Age (per 10-yr increment)	1.60 (1.00-1.1)	0.045

Tumor size ( $\geq 5$ cm vs. $< 5$ cm)	1.93 (0.7-5.33)	0.206
Tumor grade ( $\geq$ grade 3 vs. $<$ grade 3)	1.26 (0.42-3.79)	0.678
Positive LN status vs. negative status	0.41 (0.14-1.21)	0.105
Positive ER status vs. negative status	4.12 (1.48-11.44)	0.007
Positive HER2 vs. negative HER2	0.43 (0.15-1.22)	0.113

**[0166]** Table 11 shows that N-CoR2 expression, hierarchical clustering and  $S_{NCOR2}$  provide a prognostic measure of resistant tumors with high specificities and positive predictive values and relatively lower negative predictive values.

5 Table 11. Analysis of prognostic methods in a cohort of 130 breast cancer patients.

	Predictor		
	N-CoR2	Average Linkage Clustering	$S_{NCOR2}$
Sensitivity	56.2 (49.8-61.9)*	61.8 (55.4-67.2)	61.8 (55.5-66.7)
Specificity	63.4 (49.5-75.9)	68.3 (54.5-80.1)	75.6 (62.0-86.3)
Positive predictive value	76.9 (68.2-84.8)	80.9 (72.5-88.0)	84.6 (76.0-91.3)
Negative predictive value	40.0 (31.2-47.9)	45.2 (36.0-53.0)	47.7 (39.1-54.4)

\*Data in parenthesis are 95% confidence intervals.

**[0167]** Example 4

**[0168]** This example demonstrates an increase in the sensitivity of breast cancer cells to death stimuli and anti-cancer therapy by downregulation of N-CoR2 or HDAC3.

10 **[0169]** In order to investigate whether N-CoR2 and/or HDAC3 contribute to the resistance to death stimuli in breast epithelial cells and to determine if these cells can be sensitized by reducing N-CoR2 and/or HDAC3 expression, retroviral-mediated RNA interference (RNAi) was employed to stably downregulate N-CoR2 or HDAC3 expression in breast epithelial cells using siRNA oligonucleotide sequences (5'-AAGGGTATCATCACCGCTGTG-3' (SEQ  
15 ID NO:1) for N-CoR2 and 5'-AAGATGCTGAACCATGCACCT-3' (SEQ ID NO:2) for HDAC3) (Mol. Cell. Biol. 23:5122-5131 (2003)). The oligonucleotides specifying the small hairpin RNAs (shRNAs) were subcloned from pSilencer-H1 into pLZRS-MFG-CMV-Neo-U6, a recombinant self-inactivating retroviral vector constructed from the backbone of an MFG provirus (Proc. Natl. Acad. Sci. USA 85:6460-6464 (1988); Proc. Natl. Acad. Sci. USA  
20 90:3539-3543 (1993)), which directs the expression of shRNA under the control of the U6 promoter. Amphotropic retrovirus was produced in Phoenix amphi cells (provided by Professor G. Nolan, Stanford Medical Center) with packaging vectors pCgp and pVSVG to boost viral titer. S1 cells or T4-2 cells, maintained in monolayer cultures, were then spin infected with retrovirus carrying the various RNAi constructs and infected cell populations  
25 were selected using 300  $\mu$ g/ml G418 (Invitrogen). The effect of shRNA-dependent

knockdown of N-CoR2 or HDAC3 expressions was verified by real-time PCR (RT-PCR) and immunoblotting.

[0170] Non-neoplastic HMT3522 S1 breast epithelial cells or neoplastic HMT3522 T4-2 cells were embedded ( $8.5 \times 10^5/\text{ml}$ ) within reconstituted basement membrane (rBM) gel (Matrigel, BD Biosciences) in chamber slides (Lab-Tek chamber slides, Nunc) according to the procedures described in US Patent 6123941 and Nat. Method. 4:359-365 (2007). The three dimensional cultures were maintained for 12 days before induction of cell death. Phenotypic reversion of HMT3522 T4-2 cells in three dimensional rBM cultures was performed using an epidermal growth factor receptor (EGFR) specific tyrosine kinase inhibitor tyrphostin AG 1478 (100 nM) (Calbiochem), as previously described (Proc. Natl. Acad. Sci. USA 95:14821-14826 (1998))

[0171] Apoptotic cell death of the breast epithelial cells cultured in three dimensional rBM was initiated by treatment with recombinant, purified human tumor necrosis factor-related apoptosis-inducing ligand (TRAIL) peptides (BIOMOL) or Paclitaxel (Sigma-Aldrich) as described (Cancer Cell 2:205-216 (2002)). DNA damage-induced cell death was initiated by ionizing radiation (IR) using a Mark I Cesium 137 irradiator (JL Shepherd & Associates). Percent cell death induced by TRAIL or Paclitaxel was quantified using detection of active caspase 3 (Cell Signaling) by indirect immunofluorescence as described (J. Cell Biol. 163:1397-1407 (2003)). Percent cell death induced by IR was quantified using Live/Dead Viability/Cytotoxicity Assay (Molecular Probes). For both methods, cells were counterstained with 4',6-diamidino-2-phenylindole (DAPI) to label cell nuclei present at different focal planes in the 3D architectures. Percent death was calculated as cells positive for ethidium bromide or active caspase 3 expressed as a percentage of the total number of cells scored by the nuclear staining.

[0172] For the comparison of cell growth rates, cells were seeded on culture plastics and the cell number was determined at indicated time points. Population doublings were calculated as  $\ln(\text{cell number at day } n / \text{cell number at day } 0) / \ln 2$ . Data were shown as mean  $\pm$  SEM of triplicate experiments.

[0173] To compare the three dimensional acinar morphogenetic capacity of breast epithelial cells, HMT3522 S1 cells stably transfected with N-CoR2 shRNA or control shRNA were grown in 3D rBM as described above for 10 days. To illustrate the basal surfaces and the intercellular junctions of the polarized acinar structures, the cultures were directly fixed

with 2% paraformaldehyde and then incubated with primary antibodies toward  $\beta$ 4-integrin and  $\beta$ -catenin, followed by FITC- (green) or Texas red- (red) conjugated secondary antibodies, respectively. Phase contrast images or immunofluorescence images were taken using a scanning confocal laser (model 2000-MP, Bio-Rad Laboratories) attached to a  
5 fluorescence microscope (model Eclipse TE-300, Nikon).

[0174] For immunoblot analysis, cell colonies (S1 acini or T4-2 cellular aggregates) in 3D rBM were isolated using ice-cold PBS/EDTA. Total cell lysates from monolayered cells or isolated colonies were prepared in Laemmli lysing buffer containing protease inhibitors and immunoblot analysis was performed as described (Exp. Cell Res. 298:122-132 (2004)).

10 [0175] **Figure 7** shows that stable downregulation of N-CoR2 expression by RNAi in HMT3522 S1 cells does not significantly alter their growth on culture plastics or the integrity and polarization of acini in 3D rBM, compared with cells stably transfected with control shRNA. However, as shown in **Figure 8**, downregulation of N-CoR2 rendered the  
15 HMT3522 S1 cell acini much more sensitive to multiple death stimuli, including the death receptor ligand TRAIL, the cytotoxic drug Paclitaxel, and IR, than the acini formed by control cells across a wide range of drug concentrations or IR doses.

[0176] In **Figure 9**, the neoplastic HMT3522 T4-2 cells grew as disorganized cellular aggregates in 3D rBM. Inhibiting EGFR activity by inclusion of an EGFR inhibitor tyrphostin AG 1478 resulted in the phenotypic reversion of the cellular aggregates into  
20 organized spheroid-like structures, which was consistent with previous results (Proc. Natl. Acad. Sci. USA 95:14821-14826 (1998); Cancer Cell 2:205-216 (2002)). Compared with HMT3522 T4-2 cells that were grown as cell monolayer on culture plastics, the protein abundance of N-CoR2 increased slightly when the same cells were grown as disorganized cellular aggregates in 3D rBM. Structural reversion of HMT3522 T4-2 cellular aggregates  
25 into organized spheroids by EGFR inhibition was accompanied with a further increase in the protein abundance of N-CoR2.

[0177] As shown in **Figure 10**, HMT3522 T4-2 cells cultured in 3D rBM displayed decreased sensitivity (i.e., increased resistance) to different death stimuli, including TRAIL and Paclitaxel treatments. Structurally reverted HMT3522 T4-2 spheroids displayed a further  
30 decrease in the sensitivity to TRAIL and Paclitaxel treatments. The increased resistance of the spheroidal structures to death stimuli was completely reversed by downregulation of N-



CoR2 expression, suggesting that N-CoR2 also mediates architecture-dependent death resistance in neoplastic breast epithelial cells.

[0178] **Figure 11** shows that stable overexpression of N-CoR2 in HMT3522 T4-2 cells by retrovirus-mediated gene transduction render them markedly resistant to TRAIL treatments.

5 However, when HDAC3 expression was simultaneously downregulated by retrovirus-mediated RNAi in the N-CoR2-overexpressed cells, their sensitivity to the TRAIL treatment could be restored to an extent comparable to that of vehicle-treated cells, suggesting that the ability of N-CoR2 to suppress cell death is HDAC3-dependent and the death resistance can be reversed by HDAC3 downregulation.

10 [0179] The results of this example show that multidrug resistant breast cancer cells can be sensitized by the downregulation of N-CoR2 and/or HDAC3 gene expression. In this fashion, multidrug resistant tumors should also be sensitized *in vivo* by these and equivalent methods.

[0180] Example 5

15 [0181] This example demonstrates that cancer cells can be sensitized to death stimuli and anticancer therapy by abrogating the N-CoR2-dependent activation of HDAC3.

[0182] The nuclear deacetylase activity of HDAC3 requires its stoichiometric interaction with N-CoR2. It has been shown previously that mutation of the lysine 449 residue on N-CoR2 to alanine does not influence the interaction between N-CoR2 and HDAC3 but

20 abolishes the activation of HDAC3 (Proc. Natl. Acad. Sci. USA 102:6009-6014 (2005)). Based on this finding, to abrogate the N-CoR2-dependent activation of HDAC3, the lysine 449 residue on N-CoR2 was mutated to alanine using the QuickChange Site-Directed Mutagenesis kit (Stratagene) using pMFG-*tet*-HA-EGFP-NCOR2 as a template. The retroviral construct carrying N-CoR2 (K449A) then was stably incorporated into the genomic  
25 DNA of HMT3522 T4-2 cells by retrovirus-mediated gene transduction as described in Example 1. The resultant HMT3522 T4-2 N-CoR2 (K449A) cells were maintained and propagated on collagen I-coated culture dishes as described in Example 1.

[0183] To confirm the ability of the mutant N-CoR2 (K449A) to abrogate the deacetylase activity of HDAC3, HEK 293 cells were transduced with retroviral constructs inducibly  
30 expressing myc-tagged N-CoR2, N-CoR2 (K449A), or a control EGFP construct (pLZRS-MFG-*tet*-myc(4)-EGFP-N-CoR2, pLZRS-MFG-*tet*-myc(4)-EGFP-N-CoR2 (K449A), or

pLZRS-MFG-*tet*-myc(4)-EGFP). Cells were treated with 1 µg/mL of doxycycline for 16 hours to induce expressions of myc tagged proteins and nuclear protein extracts were prepared as described previously (Nucleic Acid Res. 11:1475-1489 (1983)). Nuclear lysates was transferred and incubated at 4°C for 3 hours with 50 µL of equilibrated protein G agarose beads (Invitrogen) and 5 µg of purified hybridoma mouse anti-myc antibody. Beads were washed with wash buffer (diluent buffer with 0.5 M KCl) three times and with diluent once. Washed conjugated beads were used in the Fluor de Lys<sup>TM</sup> Assay System (BioMol) per kit instructions to determine HDAC activity associated with the immunoprecipitation. Fluorescence was determined using a Spectra Max M5 fluorimetric plate reader (Molecular Devices). The HDAC activity assay was performed with or without 5 µM of the HDAC inhibitor trichostatin A (TSA) (as a negative control). Results were repeated in quadruplicate.  $P < 0.05$ , compared with vector\* or N-CoR2<sup>†</sup>.

**[0184]** To examine the interaction between the wild-type or mutant N-CoR2 and HDAC3, nuclear lysates from HEK 293 cells stably expressing myc-tagged N-CoR2, N-CoR2 (K449A), or empty vector were immunoprecipitated with the anti-myc antibody as described above. The precipitates were then analyzed by Western blot using anti-myc or anti-HDAC3 antibody (Santa Cruz). Lamin B1 was used as nuclear loading control.

**[0185]** HMT3522 T4-2 cells stably overexpressing the mutant N-CoR2 (K449A) were embedded within rBM gel and cultured for 5 days, after which the 3D culture was treated with recombinant, purified human TRAIL peptides (BIOMOL). Percent cell death induced by TRAIL was quantified using detection of active caspase 3 as described in Example 4.

**[0186]** **Figure 12** shows that the mutant N-CoR2 (K449A) protein, when transfected into cells, retained the ability to bind to HDACs3 in the cell nuclear extracts similar to the wild type N-CoR2 protein.

**[0187]** As shown in **Figure 13**, the overexpression of wild type N-CoR2 protein in cells significantly enhanced the deacetylase activity of the immunoprecipitated HDAC3 from the nuclear extracts. Conversely, the overexpressed mutant N-CoR2 (K449A) protein failed to do so, as such, the deacetylase activity of HDAC3 remained unaltered compared with the wild-type protein.

**[0188]** As shown in **Figure 14**, stable overexpression of wild-type N-CoR2 in HMT3522 T4-2 cells rendered them less sensitive to death induction by TRAIL treatments. However,

when the mutant N-CoR2 (K449A) was transduced into HMT3522 T4-2 cells, they were rendered hypersensitive to death induction to an extent even greater than that of the vector control cells. This result shows that the deacetylase activity of HDAC3 is crucial to the N-CoR2-mediated death resistance in breast epithelial cells. Thus, targeting the interaction  
5 between N-CoR2 and HDAC3 is a valid approach to sensitize neoplastic cells to death stimuli and anticancer treatments.

**[0189]** It is understood that the examples and embodiments described herein are for illustrative purposes only and that various modifications or changes in light thereof will be suggested to persons skilled in the art and are to be included within the spirit and purview of  
10 this application and scope of the appended claims. All publications, patents, and patent applications cited herein are hereby incorporated by reference in their entirety for all purposes.

WHAT IS CLAIMED IS:

- 1                   1.       A method of diagnosing a treatment resistant tumor in a subject, the  
2 method comprising the steps of:
  - 3                   (a) analyzing a tumor sample from the subject with an assay that specifically  
4 detects a marker selected from the group consisting of N-CoR2, HDAC3, and those listed in  
5 Table 1;
  - 6                   (b) determining whether or not the marker is differentially expressed (over or  
7 under expressed); and
  - 8                   (c) determining if the differential expression correlates with a multidrug  
9 resistance signature, thereby providing a diagnosis for a treatment resistant tumor.
- 1                   2.       The method of claim 1, wherein the assay detects protein.
- 1                   3.       The method of claim 2, wherein the assay is selected from the group  
2 consisting of ELISA, Western Blotting, flow cytometry, immunofluorescence,  
3 immunohistochemistry, mass spectrometry, and protein, tissue or cell microarray.
- 1                   4.       The method of claim 1, wherein the assay detects nucleic acid.
- 1                   5.       The method of claim 4, wherein the assay comprises a technique  
2 selected from the group consisting of mass spectroscopy, PCR, RT-PCR, microarray  
3 hybridization, thermal cycle sequencing, capillary array sequencing, and solid phase  
4 sequencing.
- 1                   6.       The method of claim 1, wherein the assay comprises a reagent that  
2 binds to a protein.
- 1                   7.       The method of claim 6, wherein the reagent is an antibody or fragment  
2 thereof.
- 1                   8.       The method of claim 1, wherein the assay comprises a reagent that  
2 binds to a nucleic acid.
- 1                   9.       The method of claim 8, wherein the reagent is a nucleic acid.

1                   10.     The method of claim 1, wherein the method comprises detecting N-  
2     CoR2, HDAC3 and/or any three or more than three of the markers selected from those listed  
3     in Table 1.

1                   11.     The method of claim 10, wherein the method comprises microarray  
2     hybridization.

1                   12.     A method of providing a prognosis for a malignant tumor after  
2     treatments, the method comprising the steps of:  
3                   (a) analyzing a tumor sample from a subject with an assay that specifically  
4     detects a marker selected from the group consisting of N-CoR2, HDAC3, and those listed in  
5     Table 1;  
6                   (b) determining whether or not the marker is differentially expressed (over or  
7     under expressed); and  
8                   (c) determining if the differential expression correlates with a multidrug  
9     resistance signature, thereby providing a prognosis for a malignant tumor.

1                   13

1                   14.     The method of claim 12, wherein the assay comprises microarray  
2     hybridization, RT-PCR, protein microarray or any assay described in claims 3 and 5.

1                   15.     The method of claim 14, wherein the method comprises detecting N-  
2     CoR2, HDAC3 and/or any three markers selected from those listed in Table 1.

1                   16.     A method of providing a prognosis for the response of a malignant  
2     tumor to preoperative anti-tumor therapeutics, the method comprising the steps of:  
3                   (a) analyzing a tumor sample from the subject with an assay that specifically  
4     detects a marker selected from the group consisting of N-CoR2, HDAC3, and those listed in  
5     Table 1;  
6                   (b) determining whether or not the marker is differentially expressed (over or  
7     under expressed); and

8 (c) determining if the differential expression correlates with a multidrug  
9 resistance signature, thereby providing a prognosis for the response of a tumor to  
10 preoperative anti-tumor therapeutics.

1 17. The method of claim 16, wherein said anti-tumor therapeutics  
2 comprises chemotherapy, immunotherapy and/or radiation therapy.

1 18. The method of claim 16, wherein the assay comprises microarray  
2 hybridization, RT-PCR, protein microarray or any assay described in claims 3 and 5.

1 19. The method of claim 18, wherein the method comprises detecting N-  
2 CoR2, HDAC3 and/or any three markers selected from those listed in Table 1.

1 20. A method of increasing the treatment responsiveness of a malignant  
2 tumor in an individual, the method comprising downregulating the expression of N-CoR2 or  
3 HDAC3 or inhibiting the activity thereof in said tumor.

1 21. The method of claim 20, wherein said method comprises administering  
2 to said individual a nucleic acid complimentary to a N-CoR2 or HDAC3 mRNA.

1 22. The method of claim 21, wherein said nucleic acid is an siRNA,  
2 shRNA, microRNA, or antisense oligonucleotide.

1 23. The method of claim 20, wherein said method further comprises  
2 administering to said individual a mutant N-CoR2 protein that fails to interact with or activate  
3 HDAC3 or a polypeptide mimic of the interaction regions of N-CoR2 and HDAC3 or an antibody that  
4 binds to N-CoR2 or HDAC3 and inhibit their interaction or the activity thereof.

1

2 24. A method of identifying a compound useful for the treatment of  
3 treatment resistant tumors, the method comprising the steps of:

4 (a) contacting a multidrug resistant tumor cell with a compound; and

5 (b) determining the expression level of N-CoR2 or HDAC3 in said contacted  
6 cell relative to the expression level of N-CoR2 or HDAC3 in a reference tumor cell not  
7 contacted by said compound;

wherein downregulation of N-CoR2 or HDAC3 in the contacted cell relative to the reference cell indicates that the compound is useful for the treatment of treatment resistant tumors.

25. The method of claim 24, wherein said compound is selected from the group consisting of small molecules, proteins, antibodies, and nucleic acids.

26. The method of claim 24, wherein the compound is a nucleic acid.

27. A method of identifying a compound useful for the treatment of treatment resistant tumors, the method comprising the steps of:

(a) contacting a mixture of N-CoR2 and HDAC3 proteins with a compound;  
and

(b) determining the extent of the interaction between N-CoR2 and HDAC3;  
wherein a reduced interaction between N-CoR2 and HDAC3 after contacting the mixture with the compound indicates that the compound is useful for the treatment of multidrug resistant tumors.

28. The method of claim 27, wherein determining the extent of the interaction comprises an assay selected from the group consisting of ELISA, immunoprecipitation, glutathione-S-transferase fusion protein pull-down, yeast or mammalian two-hybrid system, Western blotting, fluorescence anisotropy, fluorescence polarization, FRET, and analytical ultracentrifugation.

29. A method for identifying a compound useful for the treatment of treatment resistant tumors, the method comprising the steps of:

(a) contacting a mixture of N-CoR2 and HDAC3 proteins with a compound;  
and

(b) determining the activity of said HDAC3 protein;  
wherein a reduced activity of said HDAC3 protein indicates that the compound is useful for the treatment of treatment resistant tumors.

30. .

31. A method of treating a mammal with a treatment resistant tumor, the method comprising the step of administering to said mammal a compound identified in any one of claims 24, 27, or 29.

1                    32.     A method for identifying biomarkers useful for the diagnosis or  
2     prognosis of treatment resistant tumors, the method comprising the steps of:  
3                    (a) establishing cells or identifying malignant tumors differentially expressing  
4     N-CoR2 and/or HDAC3 or the activity thereof; and  
5                    (b) identifying marker genes differentially expressed in said cells or tumors,  
6     thereby identifying biomarkers useful for the diagnosis or prognosis of treatment resistant  
7     tumors.



ABSTRACT OF THE DISCLOSURE

The present invention relates to methods for prognosis, diagnosis, and treatment of malignant tumors that were treatment resistant. The present invention provides methods of prognosis and diagnosis of multidrug resistant tumors through detection of the expression levels of nuclear co-repressor 2 (“N-CoR2”), histone deacetylases 3 (“HDAC3”), and their associated gene expression biomarkers. The present invention also provides methods of sensitizing tumors to anti-tumor therapeutics by disrupting HDAC3 activation, abrogating the N-CoR2-HDAC3 interaction, inhibiting the activity of either protein, or by downregulating the expression of either protein.

61350054 v1

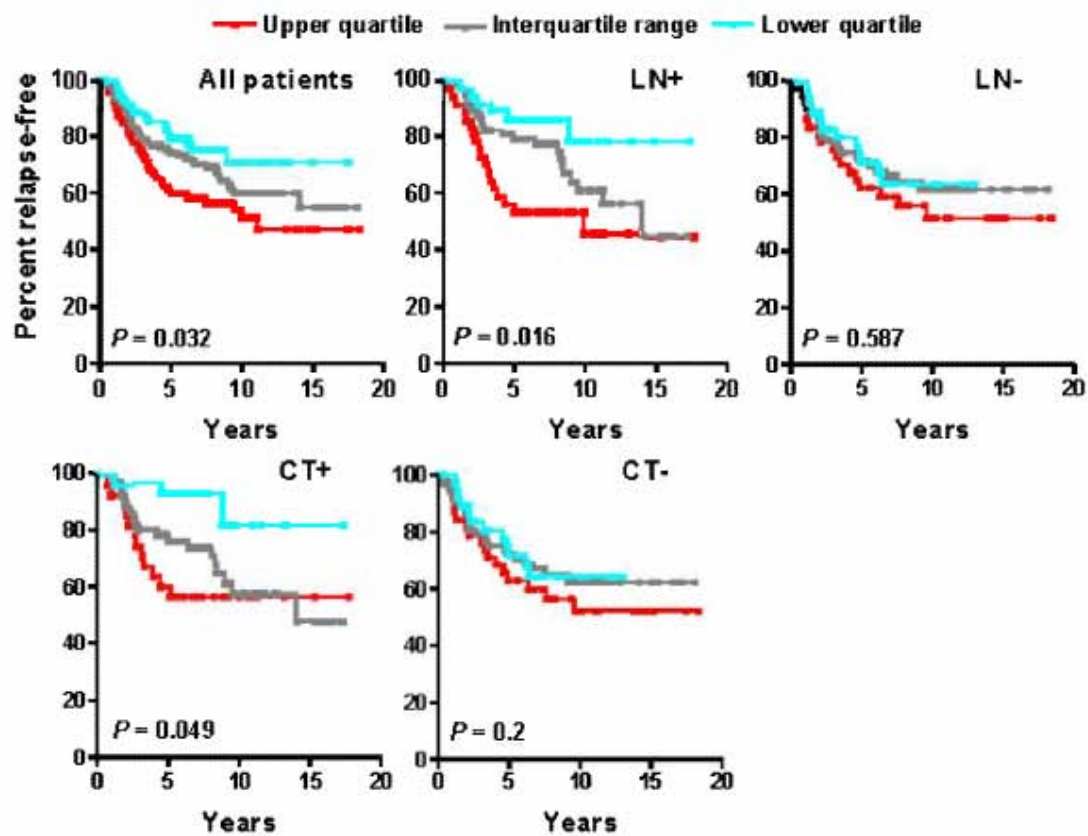


FIG. 1A

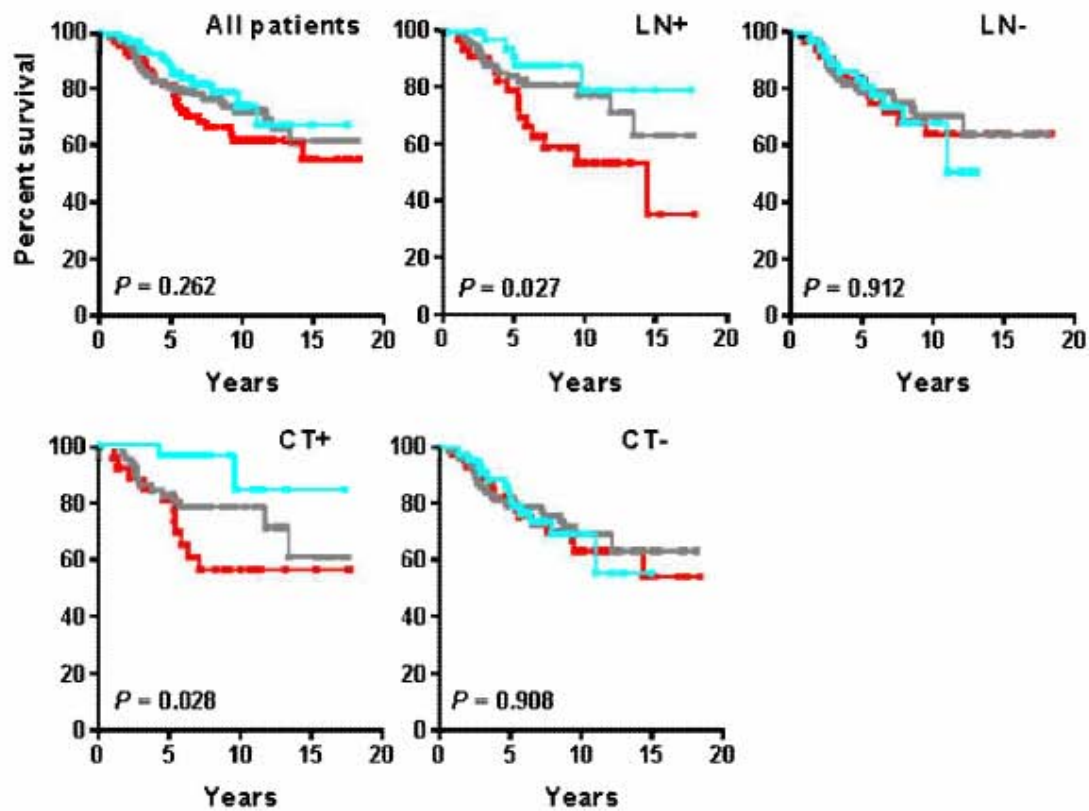


FIG 1R

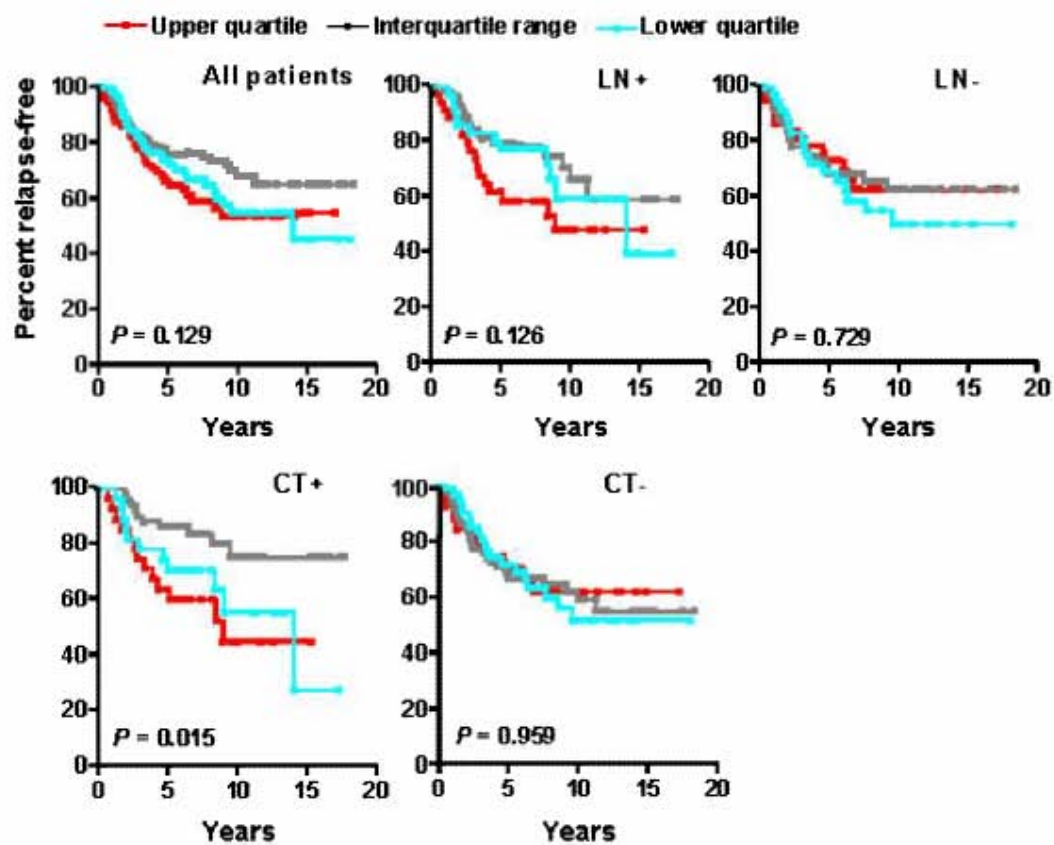


FIG. 2A

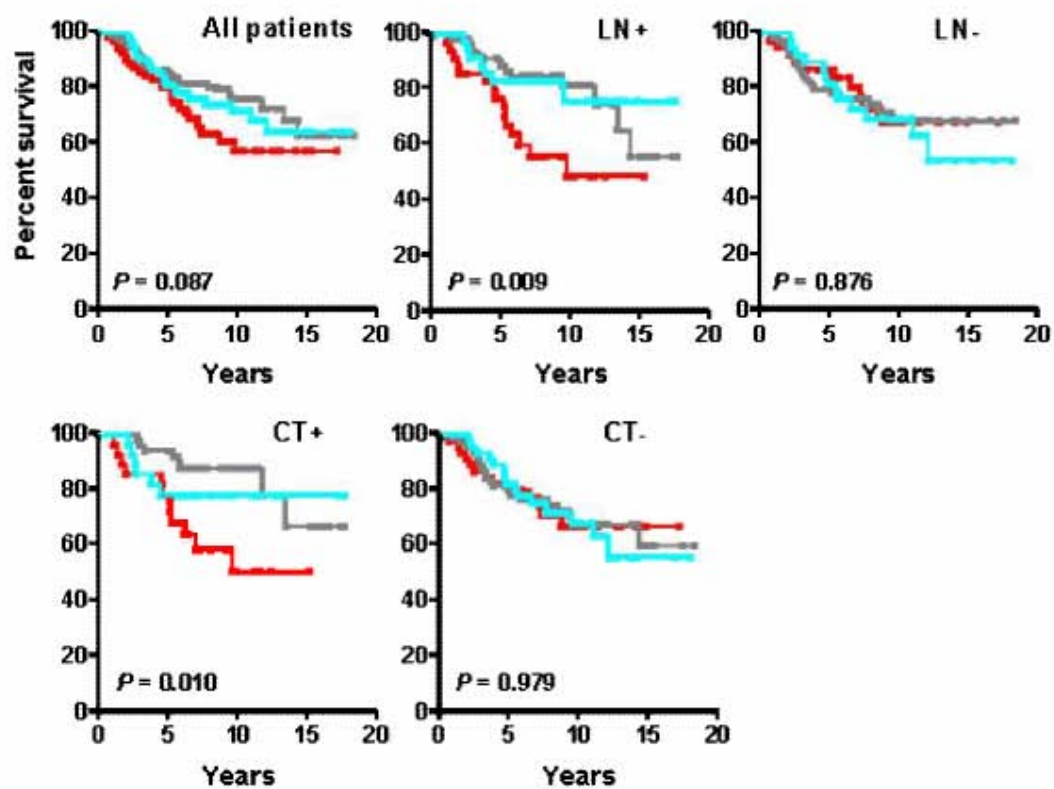


FIG 2B

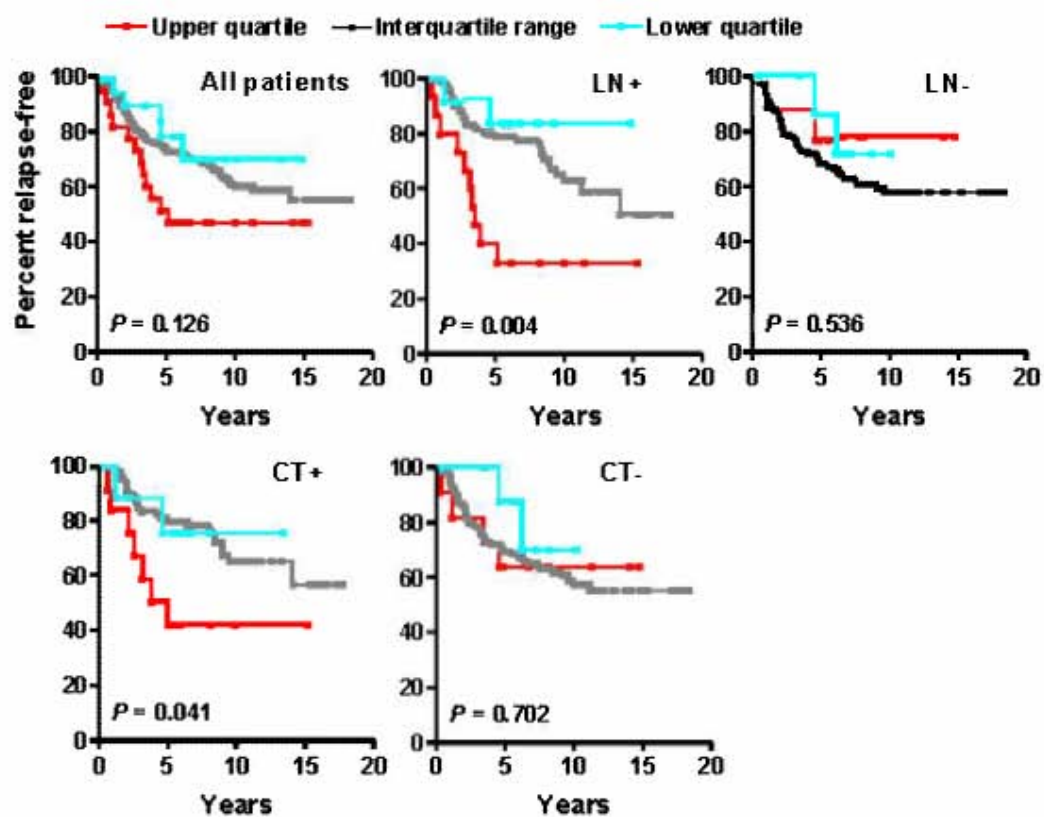


FIG. 3A

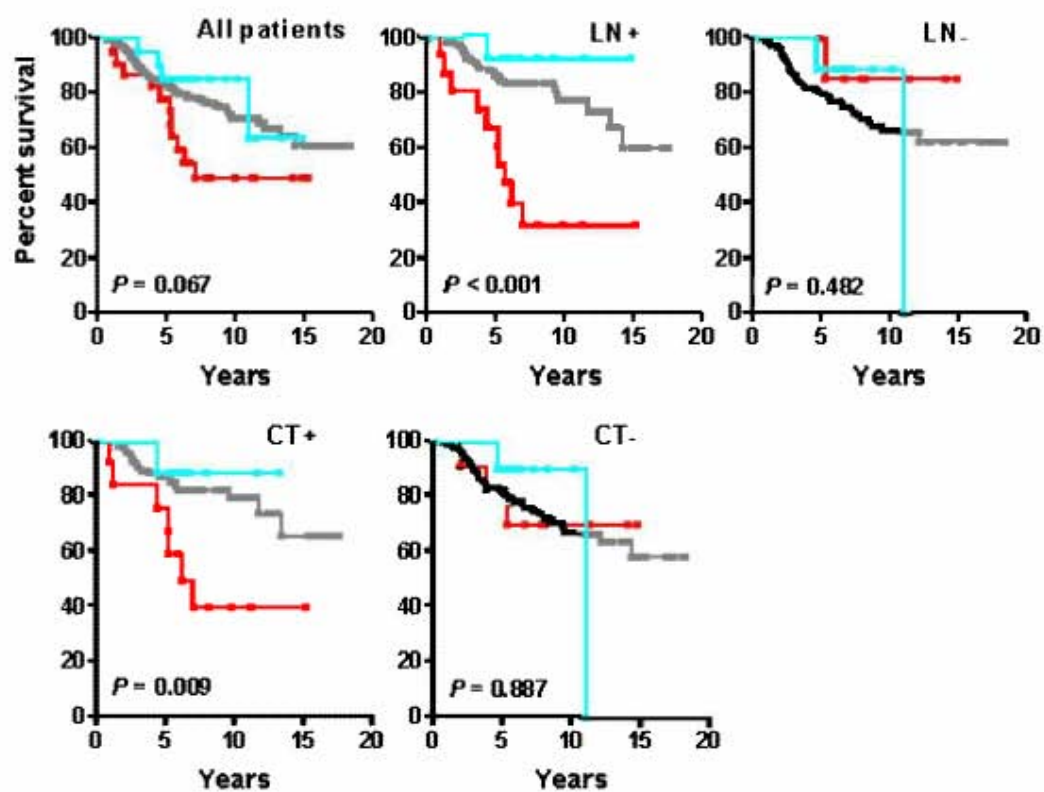


FIG 3B

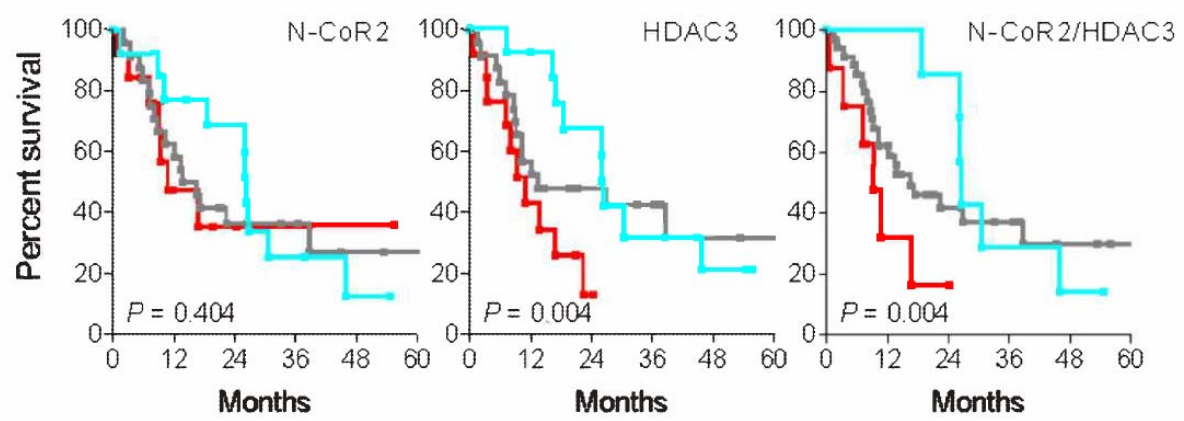


FIG. 4A

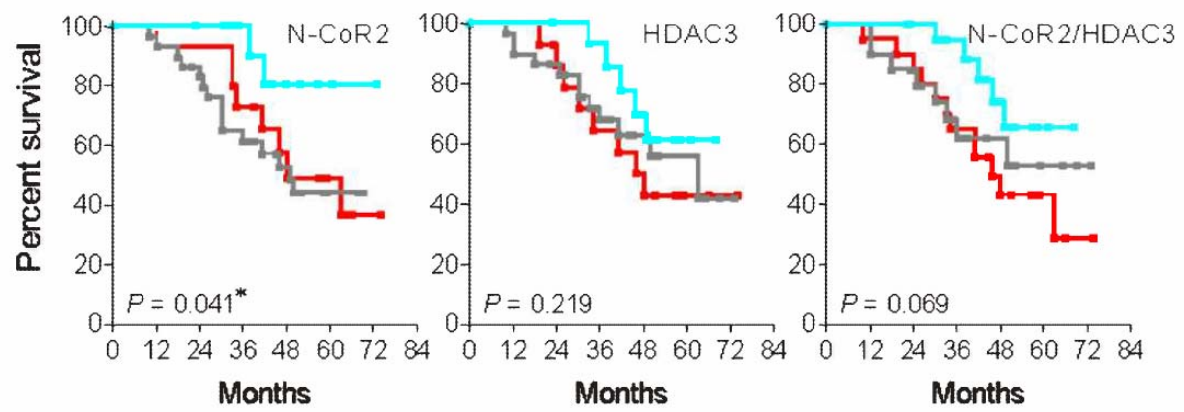


FIG. 4B



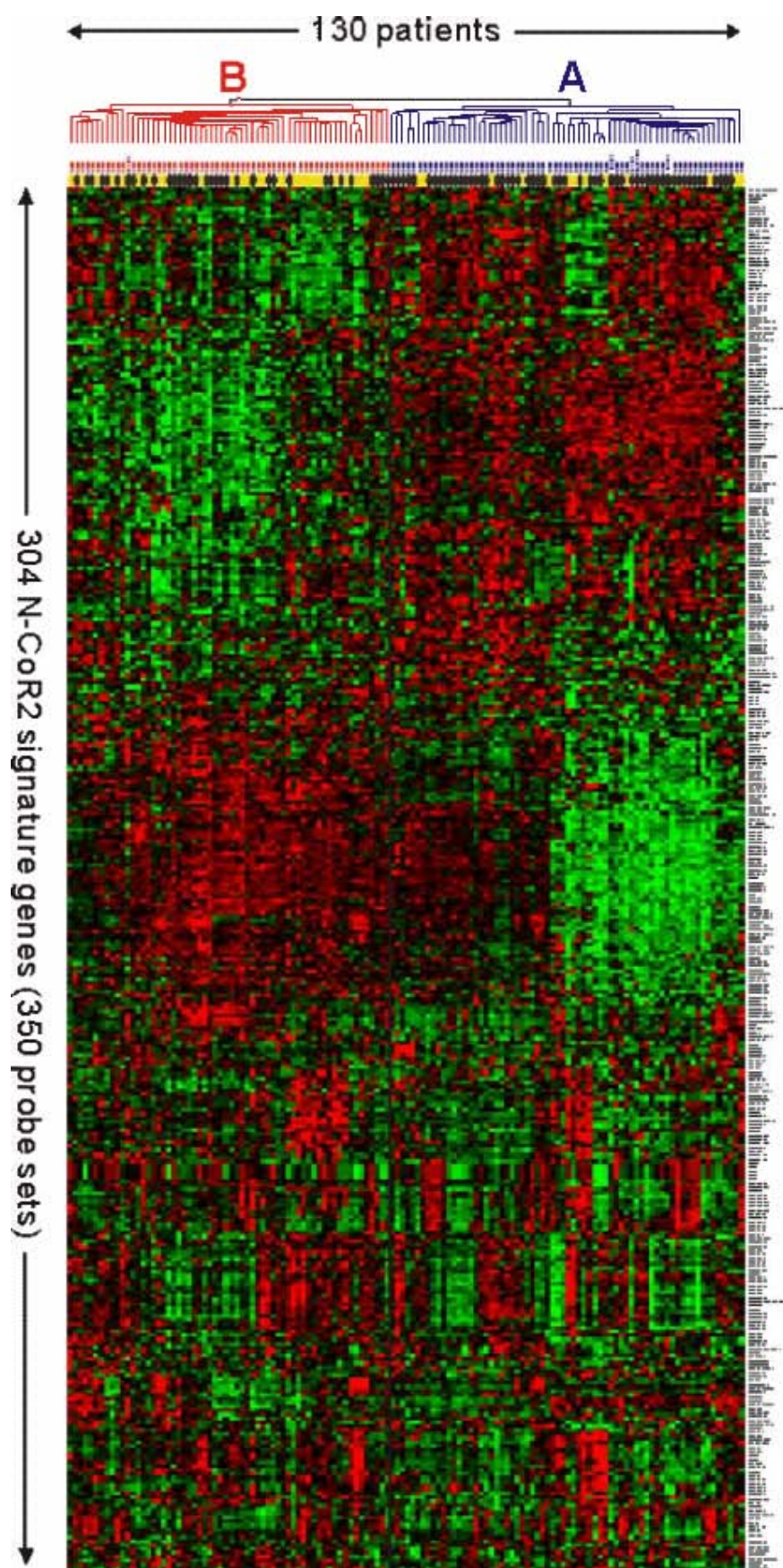


FIG. 5

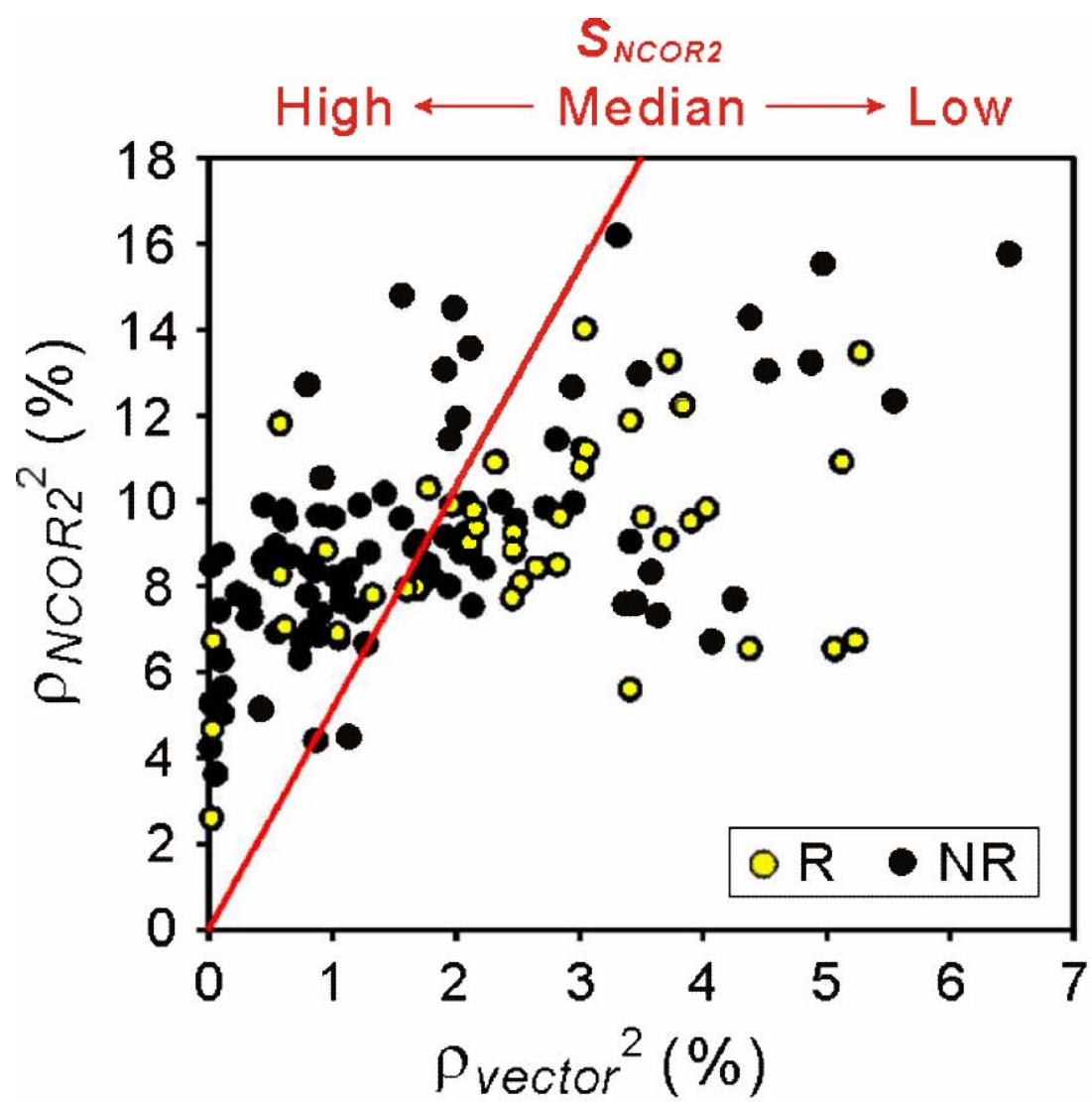
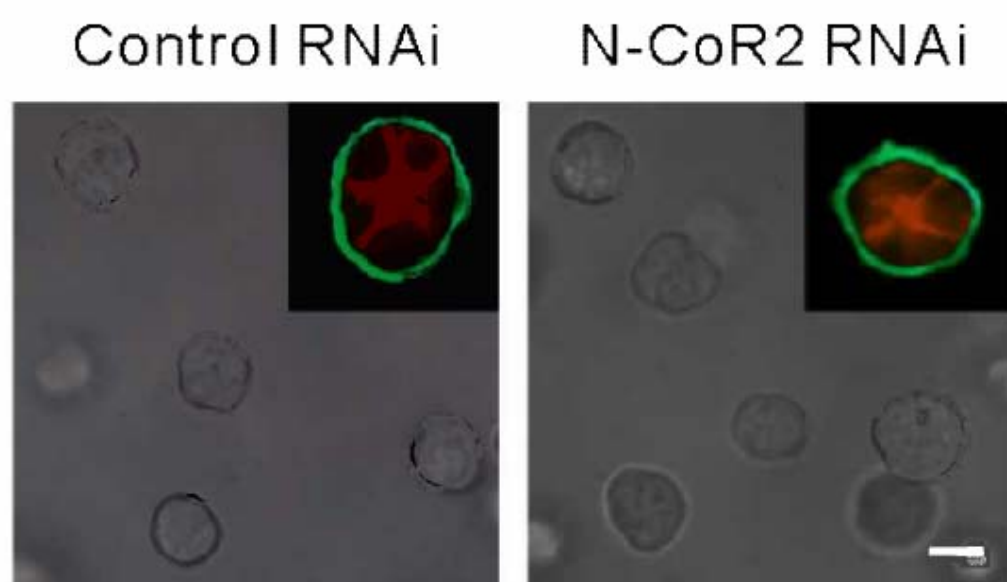
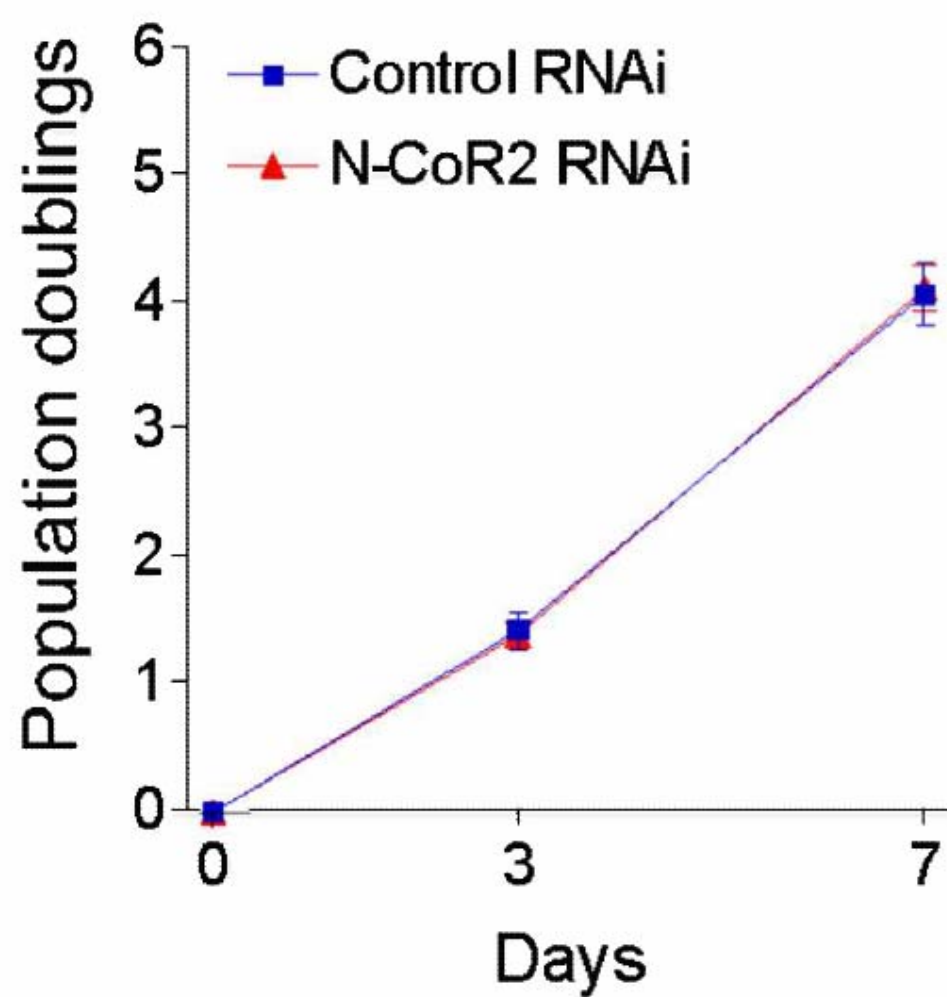


FIG. 6



**FIG 7**



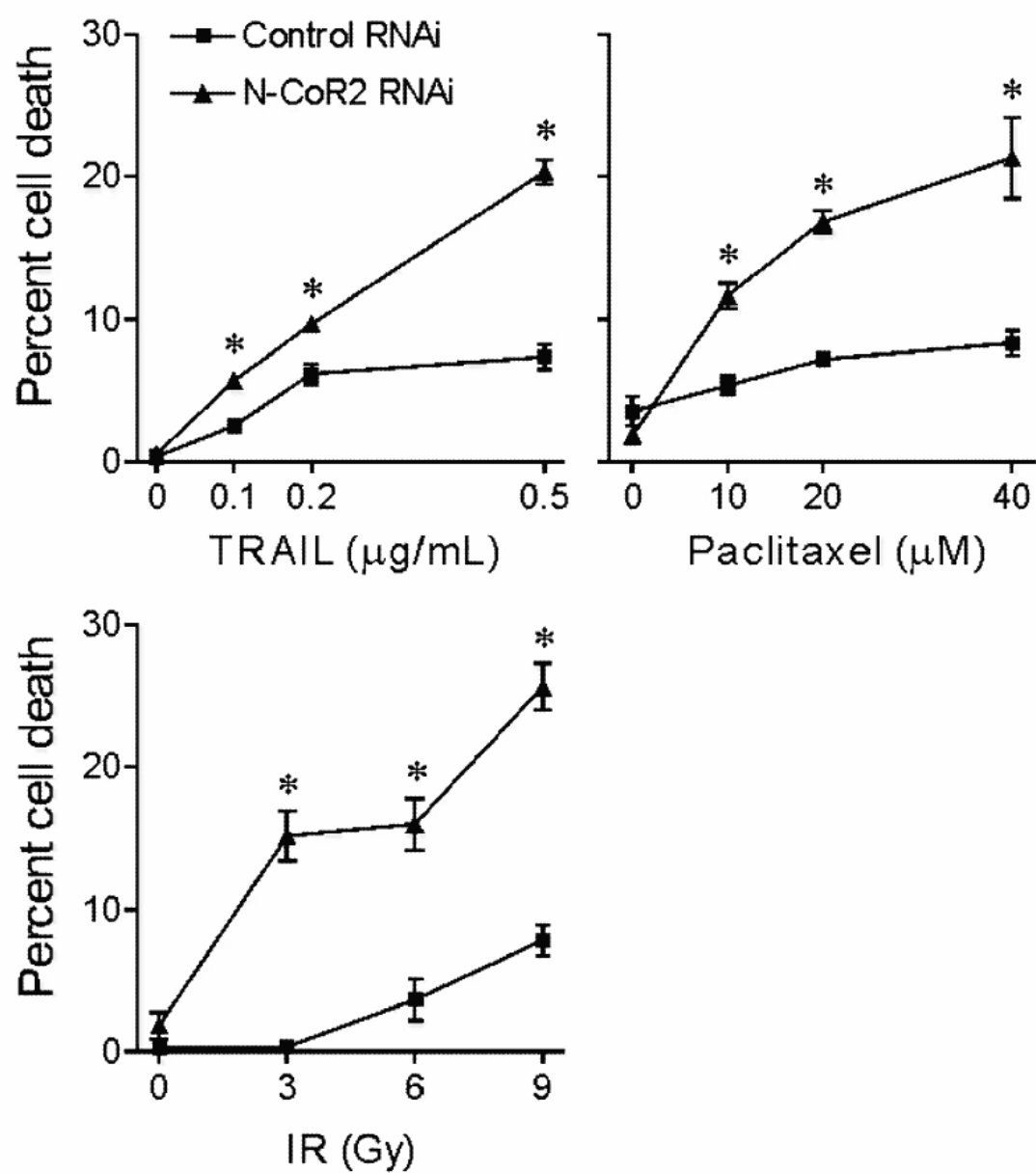
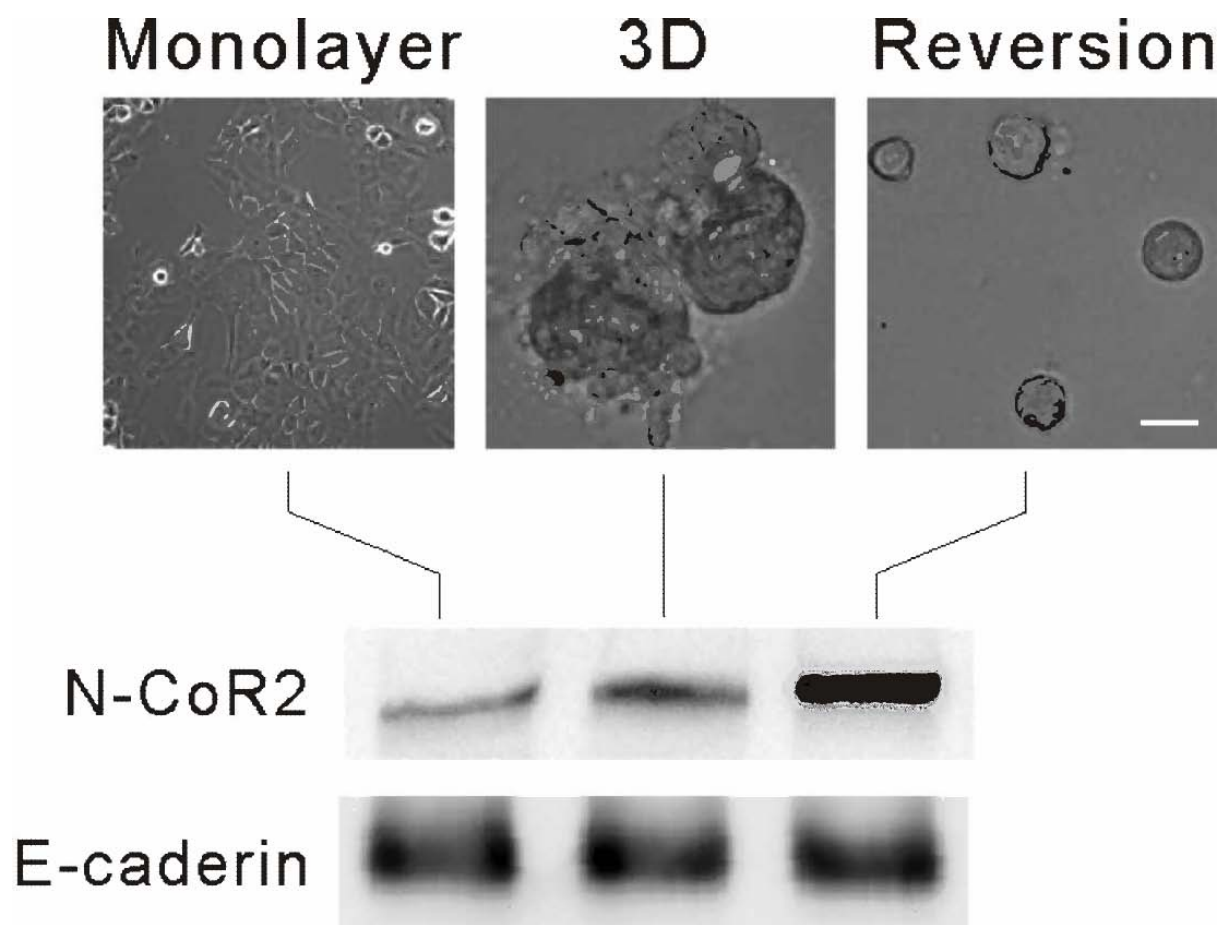
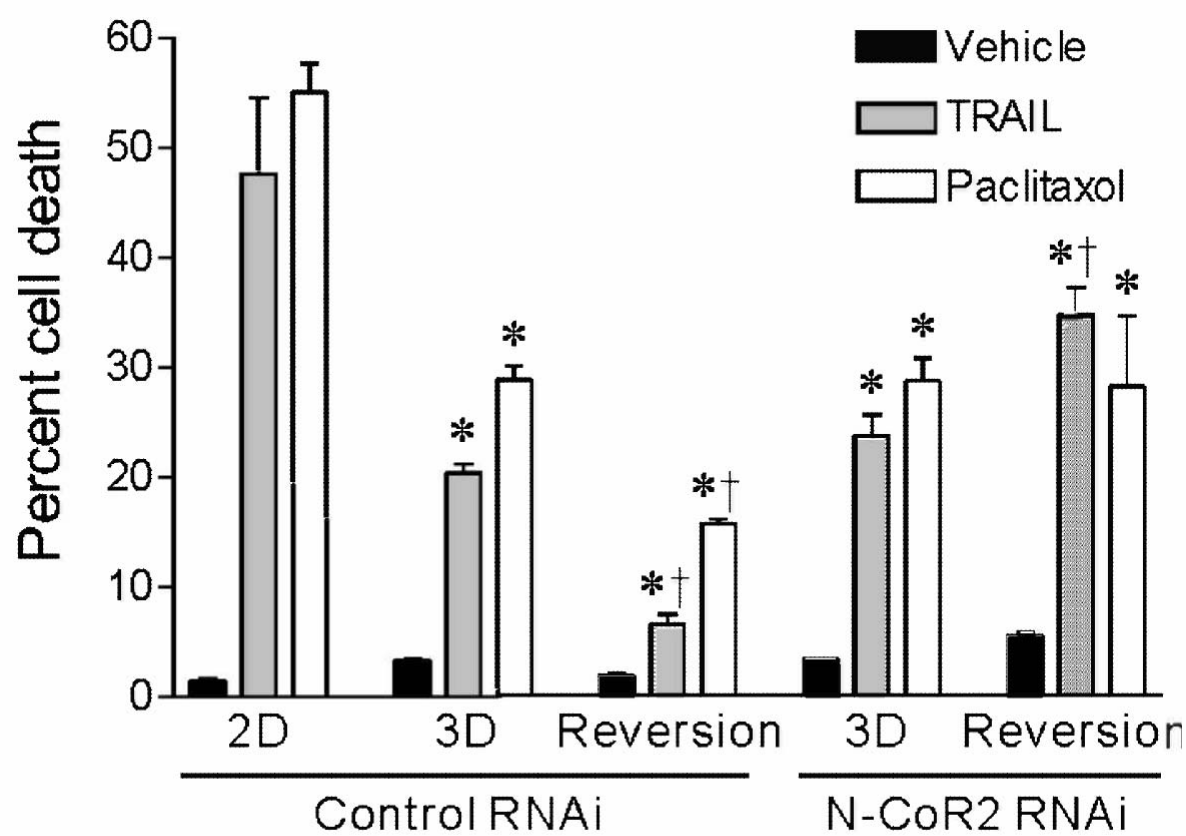


FIG. 8



**FIG. 9**



**FIG. 10**

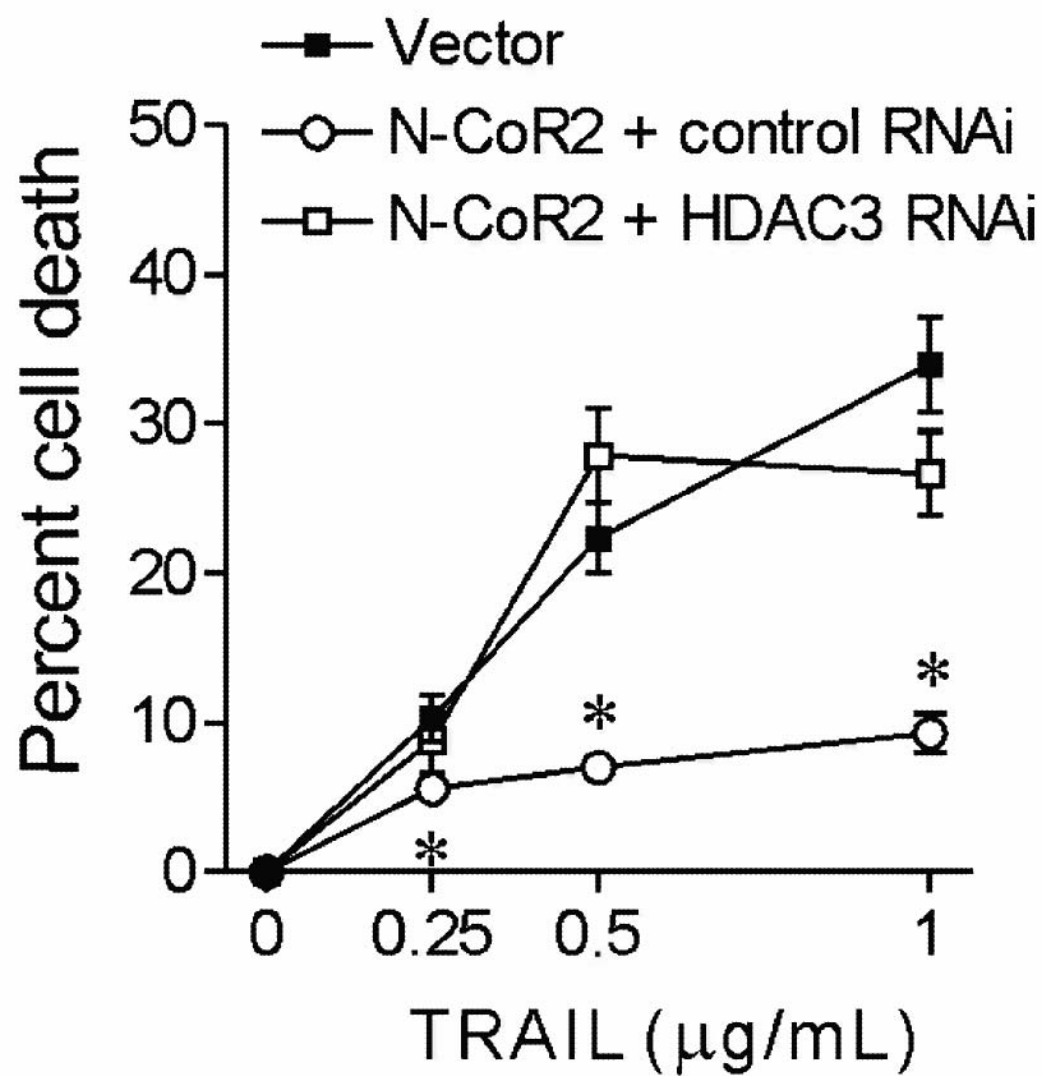


FIG. 11

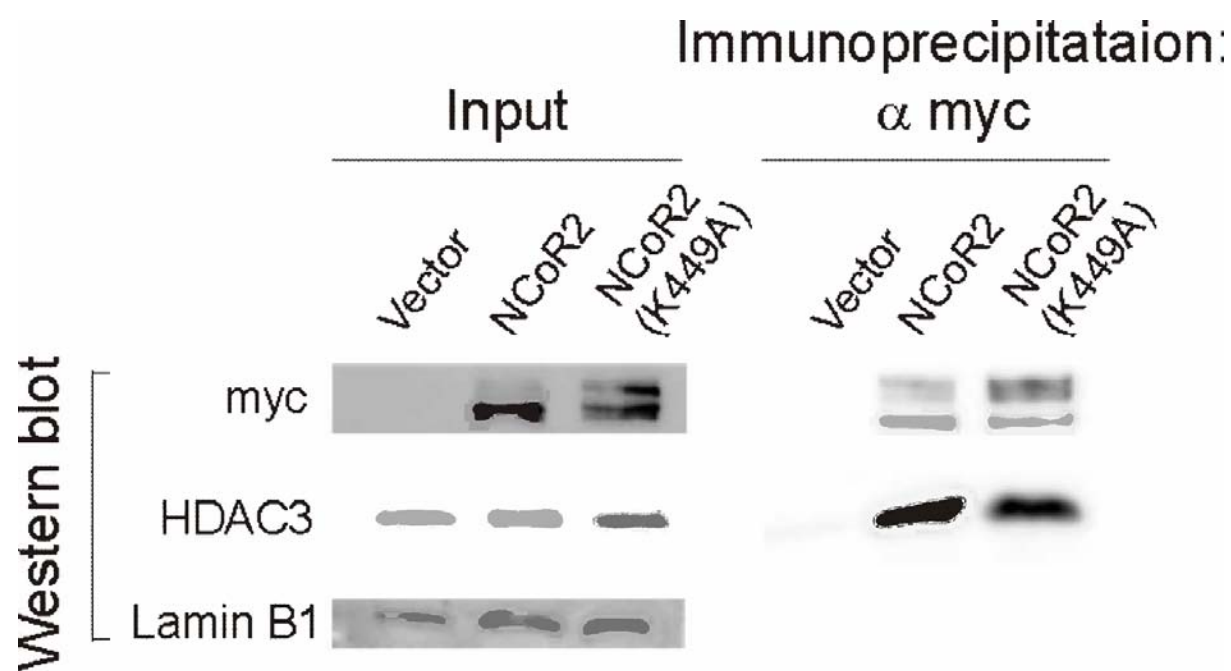


FIG. 12

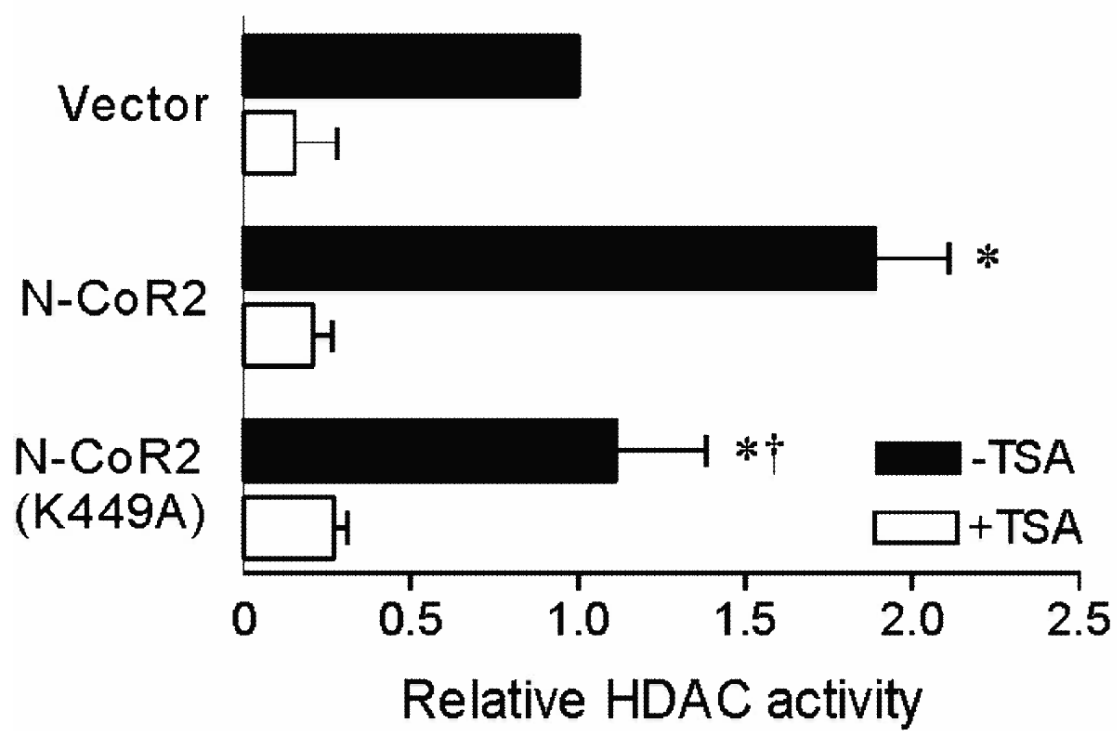


FIG. 13

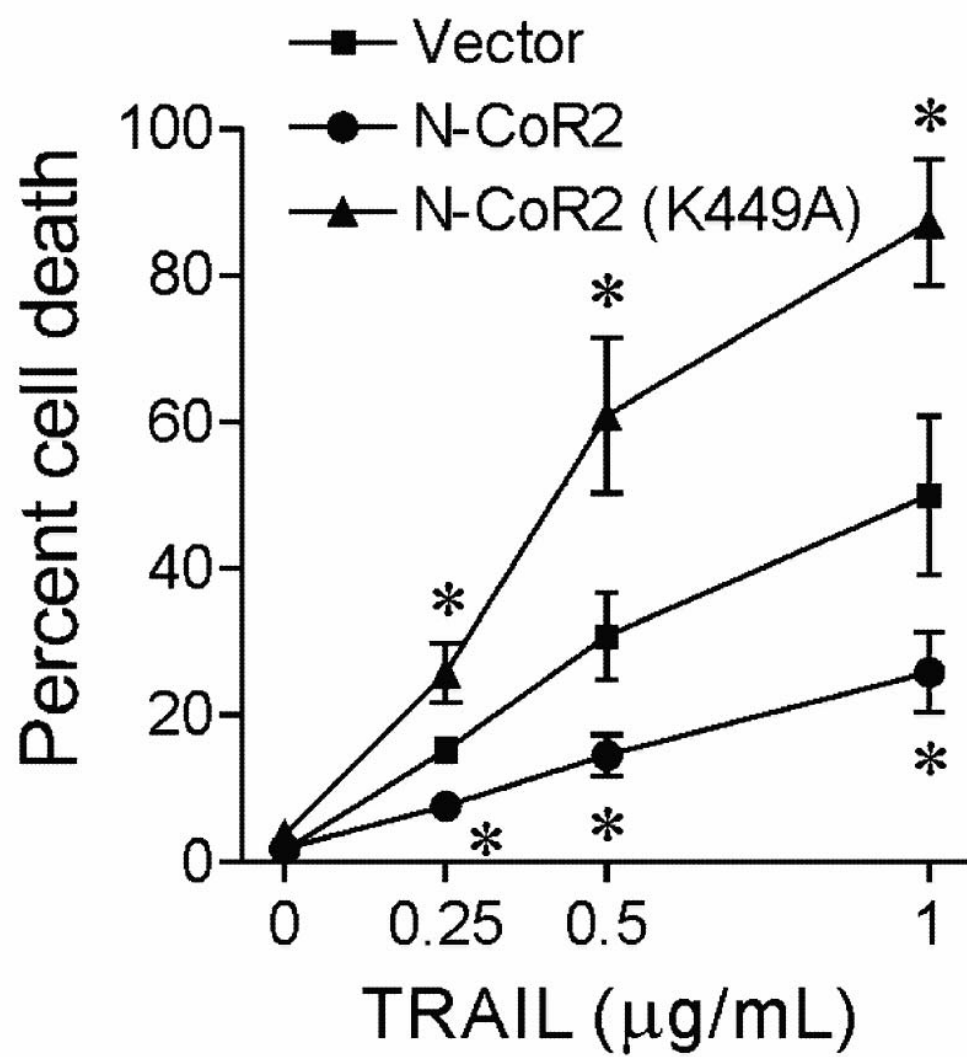


FIG. 14

# INFORMAL SEQUENCE LISTING

<210> 1  
 <211> 21  
 <212> DNA  
 <213> Artificial Sequence

<220>  
 <223> Synthetic N-CoR2 siRNA oligonucleotide

<400> 1  
 aagggtatca tcaccgctgt g 21

<210> 2  
 <211> 21  
 <212> DNA  
 <213> Artificial Sequence

<220>  
 <223> Synthetic HDAC3 siRNA oligonucleotide

<400> 2  
 aagatgctga accatgcacc t 21



## APPENDIX

### B. Abstracts

1. Gilbert, P.M., Mouw, J.K., Gbegnon, M.K., Lakins, J.N., and Weaver, V.M. "The Breast Tumor Modulator HoxA9 Regulates BRCA1 and Integrin-Mediated Adhesion." ASCB 46th annual meeting, San Diego, CA, 2006.
2. Leight, J., Zahir, N., Lakins, J.N., Wong, J., and Weaver, V.M. "Force-dependent apoptosis resistance and breast tumorigenesis." ASCB 46th annual meeting, San Diego. 2006.
3. Nestor, K.M., Lakins, J.N., Imbalzano, A.N., Nickerson, J.A., and Weaver, V.M. "Loss of SWI/SNF Activity Alters Mammary Epithelial Cell Morphogenesis and Adhesion Dynamics." ASCB 46th annual meeting, San Diego, CA. 2006.
4. Tsai, K.C., Chatterjee, C., Lakins, J.N., and Weaver, V.M. "The SMRT Way to Resist Death." ASCB 46th annual meeting, San Diego, CA. 2006.
5. Leach JB, S Petrova, JN Lakins, K Johnson, J Leight, V Weaver. "Force-Dependent Mammary Morphogenesis and Malignancy in a Tunable 3D Model System." (Poster) American Society for Cell Biology Annual Meeting, San Diego, CA, Dec 2006 .
6. Zahir, N., Leight, J.L., Lakins, J.N., Alston-Mills, B., Tsai, K.C., and Weaver, V.M. "Force-dependent JNK activation promotes therapeutic responsiveness of a mammary epithelium." ASCB 46th annual meeting, San Diego, CA, 2006
7. Butcher, D.T., Friedland, J.C., Nuth, M., Dow, L.E., Bojadziewa, J., Humbert, P., and Weaver, V.M. "Force-dependent disruption of scribble/Dgl5-dependent tissue polarity." AACR Annual Meeting, Los Angeles, CA. 2007.
8. Nestor, K.M., Lakins, J.N., Imbalzano, A.N., Nickerson, J.A., and Weaver, V.M. "The Influence of Chromatin Remodeling on Mammary Epithelial Cell Behavior." University of California, San Francisco Graduate Students' Association Career & Research Days, San Francisco, CA. 2007.
9. Nestor, K.M., Lakins, J.N., Cohet, N., Ohkawa, Y., Nickerson, J.A., Imbalzano, A.N., and Weaver, V.M. "Flipping the SWI/SNF Switch: Chromatin Remodeling Alters the Adhesion-Dependent Phenotype of Mammary Epithelial Cells." AACR Annual Meeting, Los Angeles, CA. 2007.
10. Johnson, K.R., Kass, L., Zahir, N., Mrass, P., Erler, J.T., Weninger, W., Gasser, D., Wells, R.G., and Weaver, V.M. "Force dependent malignant transformation." Engineering Cell Bio II conference. 2007.
11. Kelvin K.C. Tsai, Chandrima Chatterjee, Jonathan N. Lakins, Manunya Nuth, Michael E. Werner, I. Saira Mian, Valerie M. Weaver, "Tissue Architecture Linked to Epigenetic Control of Therapeutic Response." Cambridge Healthtech Institute's Fourth Annual Stem Cell and 3D Models for Therapeutic Screening, Boston, MA, 2007

12. Kandice R. Levental, Laura Kass, Janine T. Erler, Paulus M. Rass, Amato Giaccia, Wolfgang Weninger, David Gasser, Valerie M. Weaver, "Force-dependent malignant transformation", The 47th Annual Meeting of the American Society for Cell Biology, Washington, DC, 2007
13. I. Kang, J. Friedland, J. Lakins, W. Liu, J. Chernoff, M. Schwartz, C. Chen, D. Boettiger, V. Weaver, "Arf6 Restricts Rac Signaling to Promote Cell Survival in the 3<sup>rd</sup> Dimension", The 47th Annual Meeting of the American Society for Cell Biology, Washington, DC, 2007
14. Michael E. Werner, Nastaran Zahir, Kelvin Tsai, Chandrima Chatterjee, Johnathan N. Lakins and Valerie M. Weaver, "Matrix stiffness differentially regulates Jun Kinase and SMRT to modulate the apoptosis responsiveness of a 3D mammary epithelium", The 47th Annual Meeting of the American Society for Cell Biology, Washington, DC, 2007
15. Janna K. Mouw, Penney M. Gilbert, Mawuse K. Gbegnon, Jonathan N. Lakins, and Valerie M. Weaver, "Biophysical Regulation of The Breast Tumor Modulator HoxA9 Through Integrin-Mediated Adhesion" The 47th Annual Meeting of the American Society for Cell Biology, Washington, DC, 2007.
16. K. R. Johnson, S. J. Desai, J. N. Lakins, V. M. Weaver, "The Role of PTP-MEG1 in Mammary Epithelial Cell Morphogenesis" The 47th Annual Meeting of the American Society for Cell Biology, Washington, DC, 2007.
17. Kaiser, C., G Rozenberg, G., M Paszek, M., M Dembo, M., D Hammer, D. and Weaver, V.M. Force,  $\alpha 5\beta 1$ -integrin and breast cancer metastasis., ASCB 47<sup>th</sup> Annual Meeting, Washington, D.C. 2007
18. Inkyung Kang, Kandice Levantal, Laura Kass, Hongmei Yu, David Gasser, Rebecca Wells and Valerie M. Weaver 1 "Remodeling of extracellular matrix in mammary tissues via lysyl oxidase drives tumorigenesis by enhancing PI3K signaling", Keystone, Taos, NM. 2008.

### **C. Oral Meetings Presentations:**

1. Johnson, K.R., Kass, L., Zahir, N., Rass, P., Weninger, W., Gasser, D., Margulies, S.S., Janmey, P.A., and Weaver, V.M. "Tissue Stiffness Promotes Mammary Tumorigenesis Through Enhanced PI3 Kinase Activation." Mini Symposium Speaker ASCB 46th annual meeting, San Diego, CA. 2006.
2. Manunya Nuth, M., Friedland, J.C., Lakins, J.N., Chernoff, J., Kennedy, A., and Weaver, V.M. Rac1, Matrix Force and Tissue Architecture: the Oxidative Effect. Mini Symposium Speaker ASCB 46<sup>th</sup> annual meeting, San Diego, CA, December 2006.
3. Weaver, V.M. Symposium speaker, "Tensional Stress". Special AACR Conference 'In the Forefront of Basic and Translational Cancer Research', Hilton Waikoloa Resort, Kona, Hawaii, 01/24/07
4. Weaver V.M. Symposium speaker, "Spatial-Mechanical Regulation of Malignant Transformation and Treatment Response", 4th International Conference on Tumor Microenvironment, Florence, Italy, 03/07/07

5. Weaver V.M. Symposium speaker, "Force, Dimensionality and Integrin – Dependent Survival", Fibronectin, Integrins and Related Molecules Gordon Conference, Lucca (Barga), Italy, 04/23/07
6. Weaver V.M. Symposium speaker "Force, Dimensionality and Tissue Morphogenesis and Malignancy", American Association of Anatomists, Plenary Symposium, FASEB, Washington, DC, 04/29/07
7. Tsai, K.C., Chatterjee, C., Lakins, J.N., Nuth, M., Werner, M.E., Mian, I.S., and Weaver, V.M. "Tissue Architecture Linked to Epigenetic Control of Therapeutic Response." Invited Symposium Speaker Fourth Annual Stem Cell and 3D Models for Therapeutic Screening conference. August 2007.
8. Weaver V.M. Symposium speaker, "Mechanics Meets Morphogenesis in Mammary Biology." Engineering Cell Biology -- The Cell in Context, Massachusetts Institute of Technology- Cambridge, Massachusetts, 08/06/07
9. Weaver V.M. Symposium speaker, "Forcing form in the Third Dimension", Mechanisms of Cell Signaling Gordon Conference, Oxford, United Kingdom, 09/16/07
10. Weaver V.M. Mini Symposium Speaker, Forcing form and function, Biomedical Sciences Graduate Student Retreat, Lake Tahoe, CA, October 13, 2007
11. Weaver V.M. Symposium speaker and Chair, "Spatial-Mechanical Cues from the Microenvironment Modulate Malignant Transformation and Treatment Efficacy." [AACR-NCI-EORTC International Conference on Molecular Targets and Cancer Therapeutics: Discovery, Biology, and Clinical Applications](#), San Francisco, California, 10/24/07
12. Weaver V.M. Symposium speaker, "Spatial-Mechanical Cues from the Microenvironment Modulate Malignant Transformation and Treatment Efficacy." UC Davis BreastCancer Symposium, Sacramento, California, 10/25/07
13. Weaver V.M. Mini Symposium speaker "Forcing Transformation" UC Berkeley UCSF BioEngineering Graduate Retreat, Lake Tahoe, CA October 26, 2007
14. Weaver V.M. Major Symposium speaker, "Transformation: A Force To Resist" Force and Form in Cell Biology, ASCB 47th Annual Meeting, Washington, D.C. 12/02/07
15. Tsai, K.C., Chatterjee, C., Lakins, J.N., Nuth, M., Werner, M.E., Mian, I.S., and Weaver, V.M. Mini Symposium Speaker "Tissue Architecture Linked to Epigenetic Control of Therapeutic Response." ASCB 47th annual meeting. Washington, D.C. 2007.
16. Weaver V.M. Plenary presentation and chair, "Forcing Form and Function" AACR Special Interest Conference on Cytoskeleton Signaling in Cancer, San Diego, California. 02/04/08
17. Weaver V.M. Symposium Speaker, "Tension Contractility and the Microenvironment", for Protrusion, Adhesion and Contractility session, in the Keystone Meeting on Cell Migration in Invasion and Inflammation (B7), Taos, New Mexico. 02/13/08

18. Kelvin K.C. Tsai, Chandrima Chatterjee, Michael E. Werner, I. Saira Mian, Manunya Nuth, Jonathan N. Lakins, John Tobias, Valerie M. Weaver  
Invited speaker, “Three Dimensional Dissection of Therapeutic Resistance in Breast Cancer.”  
The 6th Timberline Symposium: “3D Tissue Biology: Human Stem Cells, Cancer and the Microenvironment”, Mt. Hood, Oregon, USA (2008).

**D. Invited Institutional Presentations:**

1. Wong J.Y, Biomaterials for Early Detection and Treatment of Cardiovascular Disease, Invited Seminar Speaker, Dept of Chemistry, University of Calgary, December 2006, Calgary, CANADA.
2. Weaver V.M. Invited Lecture, "Form, Force and Mammary Morphogenesis: Implications for Stem Cell Function", NIH Mammary Gland Biology Group, Bethesda, Maryland, 05/01/07
3. Weaver V.M. Invited Speaker, "Force and Tumorigenesis", MRC, London, United Kingdom, 09/13/07
4. Weaver V.M. Seminar, “Forcing Tumorigenesis.” Advances in Molecular and Cellular Pathology Seminar, Departments of Pathology and Genomics and Pathobiology, University of Alabama, Birmingham, Alabama, 09/27/07
5. Weaver V.M. Seminar, “Force, Dimensionality and Tissue Morphogenesis and Malignancy.” Louisiana State University Health Science Center, New Orleans, Louisiana 11/08/07
6. Weaver V.M. Seminar, “Transformation: A Force to Resist” – Investigative Pathology Department, Seminar Series in Pathology, Vanderbilt University, Nashville, Tennessee, 02/24/08

## **The Breast Tumor Modulator HoxA9 Regulates BRCA1 and Integrin-Mediated Adhesion**

Penney M. Gilbert, Janna K. Mouw, Mawuse K. Gbegnon, Jonathan N. Lakins, and Valerie M. Weaver

Institute for Medicine and Engineering/Department of Pathology and Lab Medicine, University of Pennsylvania, Philadelphia, PA 19104

Stromal-epithelial interactions drive development and maintain tissue homeostasis through a network of soluble and insoluble factors that operate within a three-dimensional (3D) tissue. Genetic and epigenetic changes in mammary epithelial cells (MECs) cooperate with a modified tissue microenvironment to drive malignant transformation of the breast. We have been studying how altered expression of developmental regulators contributes to breast tumorigenesis and have specifically focused on investigating their influence on integrin expression and/or activity. Homeobox genes play a critical role in tissue development, are frequently lost in tumors, and can regulate integrin and ECM expression. We showed that HoxA9 is lost in invasive human breast tumors and that re-expressing HoxA9 in breast cancer cells decreases migration, invasion, and anchorage independent growth in culture. Additionally, HoxA9 re-expression reduces proliferation and drives phenotypic reversion of breast tumor cells grown within a 3D reconstituted basement membrane (rBM), but not on tissue culture plastic. HoxA9 represses the malignant phenotype of breast cancer cells *in vivo* as well as in 3D rBM and this reversion is coincident with BRCA1 induction and normalization of adhesion and integrin expression. Ablating BRCA1 function through expression of the delta exon-11b BRCA1 mutant or a BRCA1 RNAi disrupts rBM morphogenesis in normal MECs and inhibits reversion of HoxA9 re-expressing breast cancer cells. Accordingly, we are exploring functional and mechanistic links between HoxA9, BRCA1 and integrin dependent tissue behavior. In addition, we are studying the effects of altered HoxA9 expression on the biophysical properties of the stroma and how in turn, changes in the mechanical properties of the extracellular matrix during normal development and mammary tumorigenesis can influence HoxA9 expression. (Support: DISS0402407, DODW81XWH-05-1-330, NCI CA078731 and DAMD17-01-1-0368).

## **Force-dependent apoptosis resistance and breast tumorigenesis**

Jennifer Leight, Nas Zahir, Johnathon Lakins, Joyce Wong, and Valerie M. Weaver

Apoptosis resistance plays a key role in malignant transformation and metastasis of the breast. Because cell-extracellular matrix (ECM) interactions regulate mammary epithelial cell (MEC) survival, we have been studying how the ECM could influence malignant transformation and treatment responsiveness of breast tumors. Previously we identified  $\alpha 6 \beta 4$  integrin dependent activation of NF $\kappa$  B as a key apoptosis resistance mechanism that is up regulated in breast cancers. We showed that the efficacy of NF $\kappa$  B-mediated breast cancer survival is greatly enhanced when MECs are grown within a compliant ECM to form a three-dimensional (3D) tissue-like structure. To test the hypothesis that three dimensionality and matrix compliance regulate apoptosis resistance and to delineate the underlying mechanisms, we used reconstituted basement membrane-cross-linked poly acrylamide gels of defined elastic moduli onto which we grew MECs as 3D structures. Here we report that MECs form organized acini-like structures on a compliant matrix (140 Pa) and exhibit a markedly enhanced survival phenotype to chemotherapy agents and immune receptor activators within 4-5 days. In contrast, on a stiff matrix (60 kPa) MECs fail to undergo morphogenesis and undergo apoptosis readily in response to exogenous death stimuli even after several days of culturing to form multi-cellular structures. 3D compliant MEC structures acquire apoptosis resistance coincident with tissue polarity and a blunted ability to stimulate AP-1 and SRE activity. Because we showed that compliance-dependent apoptosis resistance correlates with decreased stress gene expression and a failure to induce stress-gene in response to apoptotic insults we conclude that matrix compliance regulates stress-dependent gene expression. Using synthetic 2D and 3D gels of calibrated stiffness we are currently exploring the mechanism whereby matrix compliance and three-dimensionality could regulate stress gene expression to modulate tissue polarity and apoptosis resistance. Supp. DOD W81XWH-05-1-330, HL6438801A1 & CA078731.

Leach JB, S Petrova, JN Lakins, K Johnson, J Leight, V Weaver. "Force-Dependent Mammary Morphogenesis and Malignancy in a Tunable 3D Model System." (Poster) American Society for Cell Biology Annual Meeting, San Diego, CA, Dec 2006.

Epithelial morphogenesis proceeds within a 3D tissue in which soluble, cellular and physical cues cooperate to direct tissue form and function. Although we understand much about the role of soluble factors and cell interactions in homeostasis and tumorigenesis, we know little about the role of spatial organization and mechanical force in these processes. Key to understanding tissue behavior is the availability of tractable model systems in which biochemical, spatial and mechanical variables can be independently manipulated. Here we report the development, analysis and morphogenetic assessment of 2D and 3D gels for the study of mammary epithelial cell (MEC) behavior including: collagen I/reconstituted basement membrane (COL/rBM-gel), rBM-polyacrylamide (rBM-PA-gels), self-assembling peptide/rBM (SAP/rBM-gel), and peptide-conjugated polyethyleneglycol (PEG-conj-gels). MEC morphogenesis can be recapitulated using rBM-gels, COL/rBM-gels, and rBM-PA-gels with elastic moduli similar to that of normal mammary gland. However, 3D models employing natural biomaterials (rBM-gels, COL/rBM-gels) are biochemically and mechanically non-uniform; thus, in these undefined systems it is difficult to derive definitive conclusions relating force, ligand density and epithelial behavior. Additionally, while synthetic biomaterials, e.g., rBM-PA-gels, permit precise control of matrix stiffness and ligand density, PA gels are incompatible 3D and in vivo. SAP/rBM-gels offer a versatile 3D matrix with calibrated stiffness and ligand presentation. Unfortunately SAP gels are not easily adapted for studies directed at 3D epithelial morphogenesis and migration/invasion because matrix stiffening depends upon increasing matrix density and the peptide backbone is not easily remodeled by embedded cells. Although PEG gels that can be mechanically and biochemically modified offer an attractive alternative, traditional chemistry has been optimized for relatively stiff materials, e.g., cartilage and muscle. Accordingly, we are investigating soft PEG-conj-gels with adhesive laminin-derived ligands and collagenase-digestible linkers by testing their suitability as a tractable biomaterial for reconstituted multi-cellular epithelial morphogenesis studies. Here we will summarize our synthesis strategy and biological characterization.

## **#1711 Regulation of JNK Activity by Matrix Stiffness Mediates Apoptosis Induction in a Mammary Epithelium**

Nastaran Zahir, Jennifer L. Leight, Johnathon L. Lakins, Brenda Alston-Mills, Kelvin K.C. Tsai and Valerie M. Weaver

The composition and spatial organization (3D) of the extracellular matrix (ECM) influence apoptosis responsiveness of mammary epithelial cells (MECs) to cancer therapeutics (Weaver et al., Cancer Cell, 2002). Because the 3D organization of the ECM determines its mechanical properties, the question of whether and how matrix stiffness could modify therapeutic efficacy in a mammary epithelium was investigated. Distinct microenvironments were established by utilizing basement membrane (BM) crosslinked polyacrylamide gels of calibrated stiffness (elastic modulus, E). Similar to normal mammary acini residing within a soft tissue *in vivo* (E = 170 Pascals), MECs grown on soft 3D-BM-gels (E = 140 Pascals) formed polarized acini and exhibited resistance to Taxol, TRAIL and gamma radiation. In contrast, MECs grown on a 3D-BM-gel with a similar stiffness to mammary tumors (E = 5000 Pascals) formed disorganized structures and displayed a marked sensitivity to exogenous apoptotic cues, despite growth rates similar to MEC acini. Matrix stiffness resulted in an increase in the magnitude and duration of JNK activation. Moreover, JNK activity was necessary for cancer therapy-dependent apoptosis induction in 3D MEC tissues. Whether JNK activity is sufficient for apoptosis induction in 3D MEC tissues is now under investigation. These data illustrate how the mechanical properties of the tissue microenvironment could alter the efficacy of anti-cancer treatments through by modulating adhesion-dependent growth and survival signaling. (Funding: W81XWH-05-1-330 & CA078731 to V.M.W. & T32CA09677-13 to N.Z.)



**The American Society for Cell Biology  
San Diego, CA December 2006**

**Force and Malignant Transformation**

**Author Block:** L. Kass,<sup>1</sup> K. R. Johnson,<sup>2</sup> N. Zahir,<sup>2</sup> J. N. Lakins,<sup>1</sup> D. Gasser,<sup>3</sup> V. M. Weaver<sup>1</sup>; <sup>1</sup>Institute for Medicine and Engineering & Pathology, University of Pennsylvania, Philadelphia, PA, <sup>2</sup>Bioengineering & Institute for Medicine and Engineering, University of Pennsylvania, Philadelphia, PA, <sup>3</sup>Genetics, University of Pennsylvania, Philadelphia, PA

Stromal-epithelial interactions regulate tissue homeostasis and are altered in tumors, and modifying extracellular matrix-integrin interactions can profoundly influence expression of the malignant phenotype in culture and in vivo. However, the molecular mechanisms whereby altered stromal-epithelial interactions regulate tumorigenesis are not well defined. We found that malignant transformation is associated with a significant increase in mammary gland stiffness and mature focal adhesions. We showed that matrix stiffness and/or exogenous force independently induce cell contractility to promote focal adhesion maturation and enhance integrin-dependent signaling to compromise multi-cellular tissue morphogenesis and promote a tumor-like behavior in mammary tissues. Because force-dependent integrin aggregation preceded FA assembly, we generated  $\beta 1$  integrin mutants with increased transmembrane molecular associations (V737N, G744N) and used these mutants to show that forcing focal adhesion maturation increased integrin/growth factor-dependent signaling that compromised multi-cellular tissue morphogenesis and promoted tumorigenic behavior. We now report that force-dependent focal adhesion maturation drives tumorigenic behavior by enhancing cell survival, disrupting cell-cell junctional integrity and promoting growth factor-dependent cell invasion in nonmalignant mammary tissue-like structures within 3D hydrogels. We also found that forcing focal adhesion maturation through ectopic  $\beta 1$  integrin (V737N) expression in pre-malignant MCF10DCIS.com MECs promotes their malignant transformation in 3D rBM culture and in vivo. Results showed that xenografts of pre-neoplastic MCF10DCIS MECs with increased numbers of mature focal adhesions formed larger palpable tumor masses of significantly increased mass as compared to their DCIS controls. Histologically forced focal adhesion maturation promoted malignant transformation evidenced by tumor invasion, increased angiogenesis and enhanced tumor cell survival. Studies are currently underway to explore effects on tumor metastasis and to delineate molecular mechanisms for these effects. (Supp: NIH T32HL00795404 to KRJ; DOD W81XWH-05-1-330 and NIH CA078731 to VMW).

**Control/Tracking Number:** 06-A-2235-ASCB

**Activity:** Abstract Submission

**Tissue Stiffness Promotes Mammary Tumorigenesis Through Enhanced PI3 Kinase Activation**

**Author Block:** K. R. Johnson,<sup>1</sup> L. Kass,<sup>2</sup> N. Zahir,<sup>1</sup> P. Mrass,<sup>3</sup> W. Weninger,<sup>3</sup> D. Gasser,<sup>4</sup> S. S. Margulies,<sup>1</sup> P. A. Janmey,<sup>1</sup> V. M. Weaver<sup>2</sup>;

<sup>1</sup>Bioengineering, University of Pennsylvania, Philadelphia, PA, <sup>2</sup>Pathology and Laboratory Medicine, University of Pennsylvania, Philadelphia, PA, <sup>3</sup>Immunology, Wistar Institute, Philadelphia, PA, <sup>4</sup>Genetics, University of Pennsylvania, Philadelphia, PA

Malignant transformation is associated with profound changes in the tissue microenvironment, and although inducing a reactive stroma in a tissue can enhance malignant transformation, the mechanism is poorly understood. We are using MMTV-Her2/neu mice and organotypic mammary epithelial cell (MEC) three-dimensional tissue models to study how alterations in the physical properties of the extracellular matrix (ECM) could modulate mammary tumorigenesis. Using compression and shear analysis, we show that malignant transformation is preceded by and associated with a progressive stiffening of the tissue. Biochemical, immunological, and polarization microscopy analysis indicate that gland stiffness, altered tissue morphology, and tumor invasiveness are functionally linked to increased collagen deposition, bundling, and crosslinking. We examined the relevance and molecular mechanisms whereby ECM stiffness might influence normal breast epithelia and breast tumor behavior. Studies combining MECs expressing an inducible homodimerizing ErbB2 construct (p75.B2) with ribose-induced crosslinked collagen gels demonstrated that ECM stiffness can cooperate with oncogene activation to drive MEC transformation and invasion. Results indicate that ECM stiffness perturbs tissue morphogenesis by altering polarity, disrupting cell-cell interactions, and increasing growth and proliferation. Moreover, we show that matrix stiffness enhances epidermal growth factor (EGF) receptor-dependent PI3 kinase activity and PI3 kinase enhances tumor invasion. We are currently investigating whether matrix stiffness promotes tumor progression by altering EGFR signaling through PI3 kinase and if so how. (Supp: NIH T32HL00795404 to KRJ; DOD W81XWH-05-1-330 and NIH CA078731 to VMW)

**Author Disclosure Block:** K.R. Johnson, None.

**General Info (Complete):**

**Student :** Yes

**Are you a current member (paid through 12/31/2006) or did you already apply for membership this year? :** Yes

**Presentation Preference (Complete):**

**Presentation Preference :** Minisymposium or Poster

**Minisymposium :** Cancer Mechanisms

**Category (Complete):** C04 Extracellular Matrix and Cell Behavior ; C05 Extracellular Matrix and Cell Signaling

**Payment (Complete):** Your credit card order has been processed on Tuesday 1 August 2006 at 10:07 AM.

**Status:** Complete

Darci T. Butcher<sup>1</sup>, Julie C. Friedland<sup>2</sup>, Manunya Nuth<sup>2</sup>, Lukas E. Dow<sup>3</sup>, Jasmina Bojadzieva<sup>3</sup>, Patrick Humbert<sup>3</sup> and Valerie M. Weaver<sup>1</sup>.

<sup>1</sup>University of California San Francisco, Department of Surgery, 513 Parnassus Ave S-1364 San Francisco, CA 94143.

<sup>2</sup>University of Pennsylvania, Department of Pathology, 422 Curie Blvd., 415 Stellar-Chance Building, PA 19104.

<sup>3</sup>Cell Cycle & Cancer Genetics Laboratory, Peter MacCallum Cancer Centre, Melbourne, VIC 3002, Department of Biochemistry & Molecular Biology, Department of Pathology, University of Melbourne, Parkville, VIC 3010, Australia

### Force-dependent disruption of scribble/Dlg5-dependent tissue polarity

Extracellular matrix (ECM) cues regulate cell fate through biochemical and biophysical signaling cascades. Although we know much about how various ECMs' activate transmembrane cell receptors to alter cell behavior via biochemical mechanisms, we know relatively little about how physical cues from the ECM modulate cell function. Recently, we reported that a progressive increase in ECM stiffness perturbs mammary epithelial tissue morphogenesis by promoting the maturation of focal adhesions to stimulate cell contractility. We also showed that breast tumors *in vivo* are characterized by a loss of tissue organization and a sustained increase in ECM stiffness. We also found that malignantly transformed mammary epithelial cells (MECs) are more contractile than their non-transformed counterparts and that inhibiting cell-generated force through ectopic expression of N19Rho or via treatment with a Rock or myosin II inhibitor induces a phenotypic reversion of the malignant tissue. Because normal tissue structure and behavior are functionally linked to tissue polarity, we have begun studying the effect of force on a key regulator of tissue polarity, scribble/discs large junctional complex assembly and stability to clarify the molecular basis by which force could alter tissue function. Here we report that elevated matrix stiffness increases scribble expression and concomitantly disrupts scribble localization from apical/lateral junctions to perturb junctional integrity in nonmalignant MEC tissue-like structures (acini), suggesting mechanical force disrupts mammary tissue polarity by destabilizing scribble-like junctions. Indeed, perturbing adherens junctions through ectopic expression of a dominant negative E cadherin compromised mammary morphogenesis in association with altered scribble junction integrity. Consistently, gene expression microarray analysis of nonmalignant (HMT-3522 S1), premalignant (HMT-3522 S3) and malignant transformed (HMT-3522 T4-2) three dimensional reconstituted basement membrane MEC tissues revealed that there is a progressive decrease in discs large 5 (Dlg5) mRNA expression associated with malignant transformation of these cells, and that Dlg5 is subsequently re expressed following phenotypic reversion and reduced cell-generated force in the T4-2 cells. Furthermore, expression of a shRNA to Dlg5 disrupted MEC tissue morphogenesis. Because highly contractile breast tumor cells expressed lower levels of inappropriately localized scribble protein, we are exploring the possibility that force disrupts mammary tissue integrity to modify MEC behavior by enhancing scribble turnover and reducing Dlg5 expression.

**Control/Tracking Number:** 07-AB-7463-AACR

**Activity:** Abstract Submission

**Current Date/Time:** 12/11/2006 4:31:22 PM

**Flipping the SWI/SNF switch: The influence of chromatin remodeling on mammary epithelial cell behavior.**

**Short Title:**

hBrm alters breast cell homeostasis

**Author Block:** *Kathleen M. Nestor, Jonathon N. Lakins, Nathalie Cohet, Yasuyuki Ohkawa, Jeffrey A. Nickerson, Anthony N. Imbalzano, Valerie M. Weaver.* University of California, San Francisco, San Francisco, CA, University of Massachusetts Medical School, Worcester, MA

*Abstract:*

SWI/SNF chromatin remodeling proteins, such as hBrm and BRG-1, are reduced or completely lost in expression in a variety of cancer cell lines and primary tumors such as breast, prostate and lung cancers. The consequence of these losses remains poorly defined, although it is known that these proteins interact and regulate the expression of a myriad of cellular homeostatic genes. Recent evidence has demonstrated that loss of one of the interchangeable catalytic subunits, BRG-1, promotes the aggressive metastatic behavior in human fibroblasts via enhanced migration and increased expression of  $\alpha 5$  and  $\alpha V$  integrin. Here we investigated the functional consequences of altering SWI/SNF protein function on mammary epithelial cell behavior through the ectopic expression of an ATPase-null, dominant negative hBrm (dn hBrm) in non-transformed MCF-10A mammary epithelial cells (MECs) and the application of two and three dimensional reconstituted basement membrane (2D and 3D rBM) culture assays. Data showed that reducing the ATPase catalytic activity of hBrm enhanced cell growth and adhesion and promoted cell migration in MECs cultured on 2D extracellular substrata. Compromising hBrm function additionally disrupted tissue morphogenesis of MECs grown within rBM reflected by a significant increase in colony size, loss of lumen formation, disruption of basal polarity and absence of endogenous basement membrane deposition. Preliminary studies show similar effects on MEC behavior induced through shRNA knockdown of hBrm expression implying that hBrm proteins may play a critical role in MEC morphogenesis by regulating cell-extracellular matrix interactions. Consistently, the aberrant behavior elicited in MECs through the absence of hBrm ATPase activity was associated with elevated total and membrane expression of  $\alpha 3$  and  $\alpha 6$  integrin, suggesting hBrm may modulate MEC-ECM interactions to alter behavior by modulating integrin expression. Supported by NIH grant CA078731 and DOD grants DAMD1701-1-0368, 1703-1-0496, and W81XWH-05-1-330.

## Forcing malignant transformation

**Author Block:** V.M. Weaver<sup>1</sup>, K.R. Johnson<sup>2</sup>, L. Kass<sup>1</sup>, N. Zahir<sup>2</sup>, P. Mrass<sup>3</sup>, J.T. Erler<sup>4</sup>, W. Weninger<sup>3</sup>, and D. Gasser<sup>5</sup>

<sup>1</sup>Departments of Surgery and Anatomy and Center for Bioengineering and Tissue Regeneration, University of California-San Francisco, San Francisco, CA, <sup>2</sup>Bioengineering Department, University of Pennsylvania, Philadelphia, PA, <sup>3</sup>Immunology Group, Wistar Institute, Philadelphia, PA, <sup>4</sup>Department of Radiation Oncology, Stanford University School of Medicine, Stanford, CA, <sup>5</sup>Department of Genetics, University of Pennsylvania, Philadelphia, PA, University of Pennsylvania School of Medicine, Philadelphia, PA

Malignant transformation is associated with profound biochemical and biophysical changes in the tissue microenvironment and a progressive tissue stiffening. However, the molecular mechanisms that induce tissue stiffening and the role of mechanics in malignant progression remains essentially undefined. We are using MMTV-Her2/neu transgenic mice and organotypic mammary epithelial cell (MEC)-fibroblast three-dimensional (3D) tissue models to study how alterations in the physical properties of the extracellular matrix (ECM) arise and to determine whether these changes could modulate mammary tumorigenesis. Using compression and shear analysis, we found that malignant transformation is preceded by and associated with a progressive increase in mammary gland rigidity that is associated with an incremental reorganization and stiffening. Because we found that gland stiffness, altered tissue morphology, and tumor invasiveness are functionally linked to increased collagen deposition, bundling, and crosslinking, we examined the relevance and molecular mechanisms whereby ECM stiffness might influence normal breast epithelia and breast tumor behavior. 3D organotypic MEC studies and xenograft manipulations illustrated that increasing collagen cross-linking, reoriented the collagen stroma and stiffened the tissue and that these changes synergistically promoted tumor invasion and angiogenesis in cooperation with expression of oncogenes including activated Erb2 and Ras. Moreover, either pharmacological inhibition or function blocking antibodies directed towards the collagen cross linker lysyl oxidase normalized the organization and compliance of the breast stroma and repressed breast transformation in MMTV-Her2/neu mice. By way of clarifying potential molecular mechanisms we determined that matrix stiffness enhances epidermal growth factor (EGF) receptor-dependent PI3 kinase activity through modulation of PTEN expression and activity. We further determined that matrix stiffness modulates ErbB2 signaling and PI3kinase activity by modulating integrin adhesions and that forcing integrin adhesion maturation drives malignant transformation of pre neoplastic breast lesions in vivo. We are now exploring the underlying mechanisms whereby force could alter growth factor receptor signaling by modulating integrin adhesions and signaling. (Supp: DOD W81XWH-05-1-330, NIH CA078731 to VMW).

## Forcing malignant transformation

**Author Block:** V.M. Weaver<sup>1</sup>, K.R. Johnson<sup>2</sup>, L. Kass<sup>1</sup>, N. Zahir<sup>2</sup>, P. Mrass<sup>3</sup>, J.T. Erler<sup>4</sup>, W. Weninger<sup>3</sup>, and D. Gasser<sup>5</sup>

<sup>1</sup>Departments of Surgery and Anatomy and Center for Bioengineering and Tissue Regeneration, University of California-San Francisco, San Francisco, CA, <sup>2</sup>Bioengineering Department, University of Pennsylvania, Philadelphia, PA, <sup>3</sup>Immunology Group, Wistar Institute, Philadelphia, PA, <sup>4</sup>Department of Radiation Oncology, Stanford University School of Medicine, Stanford, CA, <sup>5</sup>Department of Genetics, University of Pennsylvania, Philadelphia, PA, University of Pennsylvania School of Medicine, Philadelphia, PA

Malignant transformation is associated with profound biochemical and biophysical changes in the tissue microenvironment and a progressive tissue stiffening. However, the molecular mechanisms that induce tissue stiffening and the role of mechanics in malignant progression remains essentially undefined. We are using MMTV-Her2/neu transgenic mice and organotypic mammary epithelial cell (MEC)-fibroblast three-dimensional (3D) tissue models to study how alterations in the physical properties of the extracellular matrix (ECM) arise and to determine whether these changes could modulate mammary tumorigenesis. Using compression and shear analysis, we found that malignant transformation is preceded by and associated with a progressive increase in mammary gland rigidity that is associated with an incremental reorganization and stiffening. Because we found that gland stiffness, altered tissue morphology, and tumor invasiveness are functionally linked to increased collagen deposition, bundling, and crosslinking, we examined the relevance and molecular mechanisms whereby ECM stiffness might influence normal breast epithelia and breast tumor behavior. 3D organotypic MEC studies and xenograft manipulations illustrated that increasing collagen cross-linking, reoriented the collagen stroma and stiffened the tissue and that these changes synergistically promoted tumor invasion and angiogenesis in cooperation with expression of oncogenes including activated Erb2 and Ras. Moreover, either pharmacological inhibition or function blocking antibodies directed towards the collagen cross linker lysyl oxidase normalized the organization and compliance of the breast stroma and repressed breast transformation in MMTV-Her2/neu mice. By way of clarifying potential molecular mechanisms we determined that matrix stiffness enhances epidermal growth factor (EGF) receptor-dependent PI3 kinase activity through modulation of PTEN expression and activity. We further determined that matrix stiffness modulates ErbB2 signaling and PI3kinase activity by modulating integrin adhesions and that forcing integrin adhesion maturation drives malignant transformation of pre neoplastic breast lesions in vivo. We are now exploring the underlying mechanisms whereby force could alter growth factor receptor signaling by modulating integrin adhesions and signaling. (Supp: DOD W81XWH-05-1-330, NIH CA078731 to VMW).

## **Tissue Architecture Linked to Epigenetic Control of Therapeutic Response**

Kelvin K.C. Tsai\*, Chandrima Chatterjee<sup>†</sup>, Jonathan N. Lakins\*, Manunya Nuth<sup>‡</sup>,  
Michael E. Werner\*, I. Saira Mian<sup>‡</sup>, Valerie M. Weaver\*

\*Department of Surgery and Center for Bioengineering and Tissue Regeneration,  
University of California, San Francisco, CA; <sup>†</sup>Department of Pathology, University of  
Pennsylvania, Philadelphia, PA; <sup>‡</sup>Life Sciences Division, Lawrence Berkeley National  
Laboratory, Berkeley, CA

Using three-dimensional tissue culture as a model system, we report that tissue organization is associated with profound resistance to multiple death inducers due to transcriptional reprogramming of cellular pro-apoptotic/anti-apoptotic pathways by the nuclear receptor corepressor *SMRT* (silencing mediator of retinoic acid and thyroid hormone receptor). The SMRT-mediated death resistance was found to be functionally-linked to chromatin remodelling-mediated transcriptional regulation through activation of the histone deacetylase-3 and is usurped by malignant tumor cells during their phenotypic evolution of multi-drug resistance. Our findings provide a novel example in which tissue architecture and microenvironmental heterogeneity are tied to *in vivo* selection of drug resistance. (Supported by DOD BCRP W81XWH-05-1-330 and NIH CA078731 to VMW).

ASCB 2007

### Arf6 Restricts Rac Signaling to Promote Cell Survival in the 3<sup>rd</sup> Dimension

I. Kang,<sup>1</sup> J. Friedland,<sup>2</sup> J. Lakins,<sup>1</sup> W. Liu,<sup>2</sup> J. Chernoff,<sup>2</sup> M. Schwartz,<sup>3</sup> C. Chen,<sup>2</sup> D. Boettiger,<sup>2</sup> V. Weaver<sup>1</sup>; <sup>1</sup>Surgery, University of California, San Francisco, CA, <sup>2</sup>Institute for Medicine and Engineering, University of Pennsylvania, Philadelphia, PA, <sup>3</sup>Biochemistry, University of Virginia, Charlottesville, VA

Rac modulates reactive oxygen species generation, actin cytoskeleton-dependent migration, and cell survival by activating a repertoire of signaling effectors. The molecular mechanisms that specify Rac-GTPase targeting, however, remain unclear. Our data shows that Rac activates reactive oxygen species leading to downstream activation of MMPs, which compromises the viability of mammary epithelial cells grown on a two dimensional laminin matrix. When mammary epithelial cells are grown in a three dimensional laminin matrix, the specific activity of GTP-Rac increases dramatically and is essential for mammary epithelial cell survival. The specific activity of Arf6 is significantly elevated in mammary epithelial cells cultured within a three dimensional matrix, and Arf6 promotes survival of mammary epithelial cells grown on 2D laminin matrix by enhancing Rac-Pak signaling and restricting Rac-dependent reactive oxygen species production. Our findings suggest that matrix presentation alters cell fate by influencing Arf6-regulated membrane trafficking to limit Rac target selection.

(Supported by W81XWH-05-1-330 and DE-FG02-07ER64420)



Michael E. Werner, Nastaran Zahir, Kelvin Tsai, Chandrima Chatterjee, Johnathan N. Lakins and Valerie M. Weaver

### **Matrix stiffness differentially regulates Jun Kinase and SMRT to modulate the apoptosis responsiveness of a 3D mammary epithelium**

The apoptotic responsiveness of mammary epithelial cells (MECs) is strongly influenced by biochemical and biophysical cues from the extracellular matrix (ECM). Although we know much about how the ECM regulates cell survival through biochemical signaling we know little about how matrix mechanics could regulate cell death. Here we studied the role of matrix stiffness in mammary tissue survival. We assembled 3D MEC tissue-like structures on basement-membrane-cross-linked-polyacrylamide gels of calibrated stiffness (elastic modulus, E) supplemented with a basement membrane overlay (3D-BM-gel). MECs on soft 3D-BM-gels (E=140 Pascals) formed polarized acini that were highly resistant to Taxol, TRAIL and  $\gamma$ -radiation-mediated apoptosis whereas MECs grown on stiff 3D-BM-gels (E=5000 Pascals) formed disorganized colonies sensitive to apoptotic stimuli. We found that matrix stiffness enhances Jun Kinase expression (JNK) and activity and that inhibiting JNK through pharmacological treatment or via expression of dominant negative JNK1/2 enhanced MEC survival. Expression of an inducible active MEKK elevated JNK activity and sensitized mammary tissues within a compliant matrix to apoptotic stimuli. Consistent with the idea that matrix stiffness sensitizes mammary tissues to apoptosis by enhancing RhoGTPase-actomyosin contractility to promote focal adhesion maturation and JNK signaling we found that MECs expressing V14Rho assembled focal adhesions, had elevated JNK activity and were more responsive to death stimuli, and that death could be repressed using a JNK inhibitor. Recently we determined that a compliant ECM up-regulates the co-repressor SMRT to confer apoptosis resistance to mammary tissues because it inhibits pro-apoptotic gene expression. Intriguingly, force can induce stress signaling and MEKK can phosphorylate and inhibit SMRT-dependent stress gene repression (Hong, S.H. et al., Mol Cell Biol, 2000). Accordingly, we are testing whether matrix stiffness could regulate MEC survival by influencing acto-myosin contractility to alter integrin-dependent stress signaling and epigenetically modulate the expression of apoptosis pathway genes. (Supp: W81XWH-05-1-330 and NCI CA078731 to VMW).

**Control/Tracking Number:** 06-A-2235-ASCB

**Activity:** Abstract Submission

### **Force dependent malignant transformation**

**Author Block:** K.R. Johnson,<sup>1</sup> L. Kass,<sup>2</sup> N. Zahir,<sup>1</sup> P. Mrass,<sup>3</sup> J.T. Erler,<sup>5</sup> W. Weninger,<sup>3</sup> D. Gasser,<sup>4</sup> R.G. Wells,<sup>6</sup> V.M. Weaver<sup>2</sup>;

<sup>1</sup>Bioengineering, University of Pennsylvania, Philadelphia, PA, <sup>2</sup>Surgery, University of California-San Francisco, San Francisco, CA, <sup>3</sup>Immunology, Wistar Institute, Philadelphia, PA, <sup>4</sup>Genetics, University of Pennsylvania, Philadelphia, PA, <sup>5</sup>Radiation Oncology, Stanford University School of Medicine, Stanford, CA, <sup>6</sup>Medicine (Gastroenterology), University of Pennsylvania School of Medicine, Philadelphia, PA

Malignant transformation is associated with profound biochemical and biophysical changes in the tissue microenvironment, which lead to tissue stiffening. However, the role of tissue mechanics in malignant transformation remains essentially undefined. We are using MMTV-Her2/neu transgenic mice and organotypic mammary epithelial cell (MEC)-fibroblast three-dimensional (3D) tissue models to study how alterations in the physical properties of the extracellular matrix (ECM) could modulate mammary tumorigenesis. Using compression and shear analysis, we found that malignant transformation is preceded by and associated with a progressive increase in mammary gland stiffness. Because we found that gland stiffness, altered tissue morphology, and tumor invasiveness are functionally linked to increased collagen deposition, bundling, and crosslinking, we examined the relevance and molecular mechanisms whereby ECM stiffness might influence normal breast epithelia and breast tumor behavior. 3D organotypic MEC studies and xenograft manipulations illustrated that increasing collagen cross-linking to stiffen the tissue synergistically promoted tumor invasion in cooperation with expression of oncogenes including activated Erb2 and Ras. Consistently, pharmacological inhibition of collagen cross-linking repressed breast transformation in MMTV-Her2/neu mice. By way of clarifying potential molecular mechanisms we determined that matrix stiffness enhances epidermal growth factor (EGF) receptor-dependent PI3 kinase activity. Accordingly, we are testing if matrix stiffness promotes transformation by altering EGFR-dependent PI3 kinase signaling and if so how. (Supp: NIH T32HL00795404 to KRJ; DOD W81XWH-05-1-330 and NIH CA078731 to VMW).

**Revised 05-15-06**

**Force,  $\alpha 5 \beta 1$ -integrin and breast cancer metastasis**

C Kaiser, G Rozenberg, M Paszek, M Dembo, D Hammer and VM Weaver

The extracellular matrix (ECM) is a key regulator of tumor progression and metastasis. We have been studying how altered mammary epithelial cell (MEC)-ECM interactions could mediate breast tumor metastasis. We showed that matrix stiffness disrupts mammary tissue polarity, destabilizes adherens junctions, and promotes cell invasion. Stiffness leads to elevated  $\alpha 5$  integrin expression and promotes maturation of adhesions to enhance integrin and growth factor-dependent signaling, modify RhoGTPases, and elevate myosin-dependent cell contractility.  $\alpha 5$  integrin is often over-expressed in metastatic breast cancers and we showed that  $\alpha 5$  integrin disrupts tissue architecture, enhances tumor growth and promotes uPA-uPAR-dependent invasion and drives tumor angiogenesis. Here, we asked whether functional links exist between  $\alpha 5$  integrin-uPA/uPAR and the force-dependent, invasive pro-angiogenic phenotype. We used Traction Force Microscopy (TFM) to show that ectopic expression of  $\alpha 5$  integrin, which perturbs mammary morphogenesis and increases uPAR expression, also increases total cell force in nonmalignant MECs. We also determined that invasive tumors that endogenously over-express  $\alpha 5$  integrin and uPAR exert higher total force, and that inhibiting uPA/uPAR activity reverts the tumor phenotype, inhibits invasion and reduces cell force. Studies are now underway to explore the molecular mechanisms linking  $\alpha 5$  integrins, uPA/uPAR, and cell-generated contractility linked to the invasive breast tumor phenotype. Suppt by: BRP HL6438801A1 to VMW & DAH and DOD W81XWH-05-1-330 to VMW.

Invited speaker, “*Tissue Architecture Linked to Epigenetic Control of Therapeutic Response.*” Cambridge Healthtech Institute’s **Fourth Annual Stem Cell and 3D Models for Therapeutic Screening**, Boston, MA, USA (2007).

## **Tissue Architecture Linked to Epigenetic Control of Therapeutic Response**

Kelvin K.C. Tsai\*, Chandrima Chatterjee<sup>†</sup>, Jonathan N. Lakins\*, Manunya Nuth<sup>‡</sup>,  
Michael E. Werner\*, I. Saira Mian<sup>‡</sup>, Valerie M. Weaver\*

\*Department of Surgery and Center for Bioengineering and Tissue Regeneration,  
University of California, San Francisco, CA; <sup>†</sup>Department of Pathology, University of  
Pennsylvania, Philadelphia, PA; <sup>‡</sup>Life Sciences Division, Lawrence Berkeley National  
Laboratory, Berkeley, CA

Using three-dimensional tissue culture as a model system, we report that tissue organization is associated with profound resistance to multiple death inducers due to transcriptional reprogramming of cellular pro-apoptotic/anti-apoptotic pathways by the nuclear receptor corepressor *SMRT* (silencing mediator of retinoic acid and thyroid hormone receptor). The *SMRT*-mediated death resistance was found to be functionally-linked to chromatin remodelling-mediated transcriptional regulation through activation of the histone deacetylase-3 and is usurped by malignant tumor cells during their phenotypic evolution of multi-drug resistance. Our findings provide a novel example in which tissue architecture and microenvironmental heterogeneity are tied to *in vivo* selection of drug resistance. (Supported by DOD BCRP W81XWH-05-1-330 and NIH CA078731 to VMW).

Invited speaker, “*Three Dimensional Dissection of Therapeutic Resistance in Breast Cancer.*” **The 6th Timberline Symposium: “3D Tissue Biology: Human Stem Cells, Cancer and the Microenvironment”**, Mt. Hood, Oregon, USA (2008).

## **Three Dimensional Dissection of Therapeutic Resistance in Breast Cancer**

Kelvin K.C. Tsai\*, Chandrima Chatterjee<sup>†</sup>, Michael E. Werner\*, I. Saira Mian<sup>‡</sup>, Manunya Nuth<sup>†</sup>, Jonathan N. Lakins\*, John Tobias<sup>†</sup>, Valerie M. Weaver\*

\*Department of Surgery and Center for Bioengineering and Tissue Regeneration, University of California, San Francisco, CA; <sup>†</sup>Department of Pathology and Penn Bioinformatics Core, University of Pennsylvania, Philadelphia, PA; <sup>‡</sup>Life Sciences Division, Lawrence Berkeley National Laboratory, Berkeley, CA

The three-dimensional context under which multidrug resistance develops *in vivo* in chemorefractory tumors likely plays a critical role in its pathogenesis. Here we show that, using culture models that recapitulate the *in vivo* context, the epigenetic regulator nuclear receptor corepressor 2 (N-CoR2) was both necessary and sufficient for a MDR phenotype developed by mammary epithelial cells (MECs) driven by tissue organization in three dimensions. Overexpression of N-CoR can override its context dependency and permitted acquisition of death resistance in 3D tumor tissues and isolated tumor cells. The N-CoR2-mediated death resistance was found to be functionally-linked to chromatin remodeling-mediated gene silencing through activation of histone deacetylase 3 (HDAC3). Gene expression profiling demonstrated that N-CoR2 conferred death resistance to MECs by repressing the induction of multiple apoptotic mediators, including *TNFSF10*, *STAT1* and various caspases, in response to death stimuli. Transcriptome analysis on human breast cancers provides compelling evidence that N-CoR2/HDAC3-mediated death resistance can be usurped by chemo-refractory tumors and contributes to poor therapeutic outcome (Supported by DOD BCRP W81XWH-05-1-330 and NIH CA078731 to VMW).

Remodeling of extracellular matrix in mammary tissues via lysyl oxidase drives tumorigenesis by enhancing PI3K signaling

Inkyung Kang<sup>1\*</sup>, Kandice Levantal<sup>2\*</sup>, Laura Kass<sup>1,3</sup>, Hongmei Yu<sup>1</sup>, David Gasser<sup>4</sup>, Rebecca Wells<sup>5</sup> and Valerie M. Weaver<sup>1</sup> 1. Dept of Surgery, UCSF, San Francisco, CA, 2. Institute for Medicine and Engineering, Univ Penn, Philadelphia, PA, 3. Dept of Physiology, Universidad Nacional del Litoral, Santa Fe, Argentina, 4. Dept of Genetics, Univ Penn, Philadelphia, PA, 5. Depts of Medicine, Univ Penn, Philadelphia, PA (\*: co-first authors)

Breast tumorigenesis is associated with matrix metalloproteinase-dependent extracellular matrix (ECM) remodeling accompanied by a progressive stiffening of the stroma that is characterized by elevated lysyl oxidase expression, linear reorientation and bundling of collagen fibrils. Previously we reported that excessive ECM stiffness enhances cell proliferation and survival and disrupts mammary tissue morphogenesis by promoting integrin clustering, focal adhesion maturation, integrin-dependent signaling through ERK, and cell-generated force (Paszek et al., Cancer Cell 2005). Since lysyl oxidase (LOX) crosslinks and strengthens collagen fibrils, we predict that excessive LOX activity promotes breast transformation by increasing ECM stiffness to promote integrin adhesions, integrin-dependent signaling, and cell-generated force and that inhibiting LOX activity would temper tumor progression by reducing matrix stiffness. To test this hypothesis, we monitored the effect of reducing LOX activity by studying mammary tumor formation in MMTV-neu mice treated with a LOX pharmacological inhibitor (BAPN) or a functionally blocking monoclonal antibody against LOX. We then assessed the effect of inducing LOX activity in a xenograft NOD SCID model through co-injection of fibroblasts expressing activated LOX with MCF10AT mammary epithelial cells (a model of human ductal carcinoma in situ) as compared to control fibroblasts with MCF10AT into cleared mammary fat pads. Data revealed that LOX inhibition tempered breast tumor progression and incidence in association with a reduction in the presence of linearized thick bundles of collagen fibrils and in the stiffness of mammary tissues. Consistently, elevated LOX activity induced collagen linearization and breast tissue stiffening and promoted breast tumor growth and progression. Studies are now underway to explore the molecular mechanisms whereby LOX-dependent collagen crosslinking could alter matrix stiffness to modulate breast tumor progression. To this end we have determined that LOX-dependent breast transformation was associated with increased focal adhesions, elevated PI3Kinase activity and reduced PTEN expression and activity. Upon further investigation we could show that PTEN expression and integrin activity correlate with LOX-dependent breast tumorigenesis. (Supported by: DE-FG02-07ER64420, W81XWH-05-1-330, and CA078731A2 from DOD, DOE, and NIH, respectively. Keystone 2008, Taos, NM